

CCIS 2014



3RD CONFERENCE OF COMPUTATIONAL INTERDISCIPLINARY SCIENCES

3RD CONFERENCE OF COMPUTATIONAL INTERDISCIPLINARY SCIENCES

Christian E. Schaerer César A. Caretta (Eds.)



Pan-American Association
of Computational
Interdisciplinary Sciences

CCIS 2014 IS A PACIS PUBLICATION

Copyright ©2014 by Pan American Association of Computational Interdisciplinary Sciences
PACIS. All rights reserved.

Published by PACIS, Av. dos Astronautas, 1758 - Jd. Granja
CEP 12227-010 Sao José dos Campos, SP, Brasil
Phone: 55-12-3945-6534 / 6554
Fax: 55 - 12 - 3945 - 6375

ISBN 978-85-68888-00-1

No part of this publication may be reproduced, stored in a retrieval system, or transmitted in any form or by any means, electronic, mechanical, photocopying, recording, scanning, or otherwise, except with the prior written permission of the Publisher, or authorization through payment of the appropriate per-copy fee to PACIS. Requests to the Publisher for permission should be addressed to PACIS, Av. dos Astronautas, 1758 - Jd. Granja CEP 12227-010 Sao José dos Campos, SP, Brasil.

For general information on our other products and services please contact to PACIS
Web page: <http://www.epacis.net/epacis/index.php>
Email: contact@epacis.net

PACIS also publishes the Journal of Computational Interdisciplinary Sciences - JCIS

Production: Cristian Cappelletti, NIDTEC, Polytechnic School,
National University of Asuncion, Paraguay. P.O.Box: 2111 SL.
San Lorenzo, Central, Paraguay. Email: ccappo@pol.una.py

Ordering Article Reprints: <http://www.epacis.net/epacis/index.php>
You can place your order for reprints of an article published in this proceedings
by visiting the above website. This service is provided by PACIS.
Printed in Brazil.

Preface

The Conference on Computational Interdisciplinary Science (CCIS) aims to be a meeting place of researchers and students working in areas of science that use scientific computing in their research projects. It is an initiative of the Pan-American Association on Computational Interdisciplinary Sciences (PACIS) (<http://epacis.net/epacis/>) and has a periodicity of 2 years. Although there are other forums that discuss related topics, such as Applied Computing, Bioinformatics and Computational Physics, the CCIS seeks, in an innovative way, a broader dialog, which is inherently inter and multi-disciplinary, where researchers from different areas can share their experiences and find solutions to their computational problems.

The program of the 3rd. CCIS consisted of keynote lectures, contributed sessions and tutorials on Computational Mathematics, Computational Physics and Astronomy, Computational Chemistry and Computational Biology. Topics like computational methods applied in Space and Environmental Sciences, Technology, Innovation and Economy are also in the conference scope. Contributions can be oriented toward applications of computational methods, algorithms, numerical simulations and high-performance computing (HPC) in Science and Technology.

CCIS 2014 was focused on the following topics:

GPU/GPGPU scientific computing; Computational Grid Applications; Cloud Computing and e-Science; Fuzzy and Quantum Computing; Frontiers of Computational Physics and Fluid Dynamics; Frontiers of Computational Chemistry & Biology; Computational Data Analysis, Simulation and Modeling; Validation in Astrophysics and Cosmology; Scientific Computing in Computer Science; Environmental Sciences and Geography Modeling; Image processing; Big Data and Data Mining; Parallel Numerical Algorithms; Libraries for Numerical Computations; Languages, Tools and Environments for Programming Numerical Algorithms; Applications of Numerical Algorithms in Science and Technology; Scientific Computing in Science and Engineering; Software Engineering for Scientific Applications; Applications of Computer Science; Optimization; Engineering; Computer Science; Telecommunications; Electrical Engineering

September 2014.

Christian E. Schaerer, César A. Caretta
Conference Chairs
CCIS 2014

Organization

CCIS 2014 is organized by the Polytechnic School of the National University of Asunción (FPUNA), the Autonomous University of Asunción (UAA) and the Pan-American Association on Computational Interdisciplinary Sciences (PACIS).

Steering Committee

Benjamín Barán (UNA, Paraguay)
Esteban W. G. Clua (UFF, Brazil)
Marcus Hauser (IEP, Germany)
José da Rocha M. Pontes (UFRJ, Brazil)
Reinaldo R. Rosa (INPE, Brazil)
Sandra Ap. Sandri (INPE, Brazil)

Executive Committee

Program Chair: Benjamín Barán (UNA, Paraguay)
Organizing Chair: Hugo Correa (UAA, Paraguay)
Informatics Chair: Maria Elena Garcia (UNA, Paraguay)
Institutional Communication: Liduvina Vega (UNA, Paraguay)
Contact point with PACIS: Mariano Bordas Urquhart (UNA, Paraguay)
ETyC coordination: Nubia Acosta (UNA, Paraguay)
Accounting: Asunción Vera (UNA, Paraguay)
Liz Cano (UAA, Paraguay)
Secretary: Delia Cohenca (UNA, Paraguay)
Johana Pineda (UNA, Paraguay)
Academic Coordination: Mirta Benítez (UNA, Paraguay)
Inter-intitutional Coordination: Gonzalo Martín (UAA, Paraguay)
Blanca de Báez (UAA, Paraguay)
Protocol Coordination: Lucía Calderon (UNA, Paraguay)

International Advisory Committee

José Aguilar (ULA, Venezuela)
Paulo M. Bisch (UFRJ, Brasil)

3rd Conference of Computational Interdisciplinary Sciences

Carlos Brizuela (CICESE, Mexico)
Haroldo Fraga de Campos Velho (INPE, Brazil)
Esteban W. G. Clua (UFF, Brazil)
Patricia Corbo (UORT, Uruguay)
Alvaro L. G. A. Coutinho (UFRJ, Brasil)
Ernesto Cuadros-Vargas (SPCU, Peru)
Fátima Dolz (UMSA, Bolivia)
Yezid Donoso (UA, Colombia)
Jacques Facon (PUCPR, Brazil)
Carlos Juiz (UIB, Spain)
Marcus Hauser (IEP, Germany)
Francisco J. Mata (UNCR, Costa Rica)
Reinaldo R. Rosa (INPE, Brasil)
José da Rocha M. Pontes (UFRJ, Brazil)
Sandra Ap. Sandry (INPE, Brasil)
Rodrigo Santos (UNS, Argentina)

Local Advisory Committee

Gerardo Alejandro Blanco Bogado (UNA, Paraguay)
José Bogarín (IB, Paraguay)
Luca Cernuzzi (UCA, Paraguay)
María José Fernández De Nestosa (UNA, Paraguay)
Pedro Esteban Gardel Sotomayor (UNA, Paraguay)
Susana López de Martín (UAA, Paraguay)
Sergio Daniel Lukoski (UAA, Paraguay)
Jorge Molina (UNA, Paraguay)
Magna Monteiro (UNA, Paraguay)
Juan Pablo Nogués (UPA, Paraguay)
Carlos Nuñez (UNA, Paraguay)
Diego Pinto (UNA, Paraguay)
Gregor Recalde (UNA, Paraguay)
José Riveros Insfrán (UNA, Paraguay)
Juan Carlos Rolón (UNA, Paraguay)
Daniel Romero (UNA, Paraguay)
Miki Saito (CONATEL, Paraguay)
Enrique Vargas (UCA, Paraguay)
Cynthia Villalba (UNA, Paraguay)

Sponsoring Institutions

Consejo Nacional de Ciencia y Tecnología (CONACyT, Paraguay).

Supporting Institutions

Sociedad Matemática Paraguaya (SMP, Paraguay).

Sociedad Científica del Paraguay (SCP, Paraguay).

Plenary Speakers

Luiz Bevilacqua (UFRJ, Brazil)

Paul Bourgine (UPS, France)

Anne De Wit (ULB, Belgium)

Geneviève Dupont (ULB, Belgium)

Flavio Fenton (GIT, USA)

David Laroze (UT, Chile)

Alberto Paccanaro (UL, United Kingdom)

Invited Speakers

Raul Ceretta Nunes (UFSM, Brazil)

Carlos Juiz (UIB, Spain)

Fernando A. Oliveira (UNB, Brazil)

Dario Rodriguez Aseretto (JRC, European Commission)

Álvaro Ruiz de Mendarozqueta (UNC, Argentina)

Lecturers

Benjamín Barán (UNA, Paraguay)

Esteban W. G. Clua (UFF, Brazil)

Reinaldo R. Rosa (INPE, Brazil)

Contents

Part I : Plenary and Invited Talks

Plenary Talks

Influence of chemical reactions on convective dissolution 2
Anne De Wit

A new model for single-particle diffusion processes under multiple excitation states 3
Luiz Bevilacqua

Models for intracellular Ca^{2+} signalling 4
Geneviève Dupont

Complex dynamics of parametrically driven magnetic systems 5
David Laroze

Inference and structure discovery in biological networks 8
Alberto Paccanaro

From computational interdisciplinary sciences to integrative transdisciplinary sciences: the Complex Systems Digital Campus UNESCO UniTwin 9
Paul Bourguine

High-performance-computing for heart simulations and its complex spatiotemporal dynamics 11
Flavio Fenton

Invited Talks

Building security situational awareness 12
Raul Ceretta Nunes

Environmental risk models and applications 13
Dario Rodriguez Aseretto

El impacto de la filosofía ágil (Agile) en las organizaciones que desarrollan software 14
Álvaro Ruiz de Mendarozqueta

Opportunities and challenges for green HPC	15
<i>Carlos Juiz</i>	

Upper critical dimension Galilean Invariance and exact solution for the etching model	16
<i>Fernando A. Oliveira</i>	

Part II: Paper Session

Numerical Methods I

A Survey of results concerning steady solutions and the stability of a class of rotating flows . . .	18
<i>José Pontes, Norberto Mangiavacchi, Gustavo Anjos, Gustavo Oliveira, Rachel Lucena and Davi Ferreira</i>	

Finite element simulation of fingering in convective dissolution in porous media	21
<i>Rachel Lucena, Norberto Mangiavacchi, José Pontes, Anne De Wit and Gustavo Anjos</i>	

Comparative CFD simulations of gas transport in slug flow from periodic arrays with single or multiple bubbles	25
<i>Gustavo Oliveira, Norberto Mangiavacchi, Gustavo Anjos, José Pontes and John Richard Thome</i>	

Study of local equilibrium models of suspended sediment using Point-Particle direct numerical simulation	34
<i>Hyun Ho Shin, Christian E. Schaerer, Norberto Mangiavacchi and Luis M Portela</i>	

Reconstruction of the Langevin Equation from some Non-Markovian Time Series	41
<i>Zbigniew Czechowski</i>	

Architecture of Environmental Risk Modelling: for a faster and more robust response to natural disasters	46
<i>Dario Rodriguez Aseretto, Christian E. Schaerer and Daniele de Rigo</i>	

Computer Science in Biology and Image Processing.

Computer Vision: Identification, Classification and Tracking of Objects	58
<i>Alcides David Cantero Alonso and Eustaquio Alcides Martínez Jara</i>	

Automated early detection of diabetic retinopathy based on digital image processing techniques	70
<i>Humberto Chamorro Torres, José S. Encina Melgarejo, José L. Vázquez Noguera, Horacio Legal Ayala and Diego P. Pinto Roa</i>	

Gaps in the knowledge of behavioral biology of Chagas disease vectors. Challenges for control .	81
<i>Antonieta Rojas de Arias</i>	

Phage display in protein engineering	87
<i>Pablo Hernán Sotelo Torres</i>	

Simulation of the Electrophoretic Mobility of Supercoiled and Catenated DNA Molecules	90
<i>Maridian J. Kadomatsu-Hermosa, Alicia Castán, Jorge Cebrián, Victor Martínez, Cristina Parra, María José Fernández-Nestosa, Christian E. Schaerer, Jorge B. Schwartzman, Dora B. Krimer and Pablo Hernández</i>	
Using infrared photoelectric sensors for automatic detection of reinfestation by <i>Triatoma infestans</i>	96
<i>Federico Augusto Gaona Verón, Adolfo J. Jara C., Jorge Martín Vera, Silvia Maria Aquino, Christian E. Schaerer, Magna Monteiro, Carlos Juiz, Tomeu Serra, Maria Celeste Vega Gomez and Antonieta Rojas de Arias</i>	
Numerical Methods II	
Chaotic dynamics of a magnetic particle at finite temperature	108
<i>Omar Suarez, David Laroze, Javier Martinez-Mardones, Dora Altbir and Harald Pleiner</i>	
Parabolic optimal control constrained optimization using active restriction method	111
<i>Juan José Cáceres Díaz, Roberto Andrés Viveros Vera, Miki Saito and Christian E. Schaerer</i>	
A Parallel-in-time solution for a Parabolic Differential Control Problem with PETSc	121
<i>Juan José Cáceres Silva, Benjamín Barán and Christian E. Schaerer</i>	
Harmonic Ritz control strategy for restarting GMRES(m)	133
<i>Juan Carlos Cabral Figueredo and Christian E. Schaerer</i>	
Neural networks in the study of climate patterns seasonal	139
<i>Juliana Anochi, Haroldo F. de Campos Velho and Jose Demisio Simoes Da Silva</i>	
Optimization	
Particle Swarm Optimization Algorithms for solving many-objective problems	143
<i>Mateo Fernando Torres Bobadilla, Benjamín Barán Cegla and Uri Pablo Yael Rozenworcel</i>	
Experimental Comparison of Many-objective Evolutionary Preference-based Methods in a Parallel Framework	155
<i>Christian von Lücken, Carlos Brizuela and Benjamín Barán</i>	
Particle Swarm Optimization applied to parameter tuning of CLAHE based on Entropy and Structural Similarity Index	167
<i>Luis G. Moré, Marcos A. Brizuela, José L. Vázquez, Horacio Legal Ayala and Diego P. Pinto Roa</i>	
Solving Many Objective Optimisation Problems with Harmony Search	179
<i>Daniel Brassel, Osmar Brassel, Benjamín Barán and Joaquín Lima</i>	
Ant Colony Multi-objective Optimization Algorithms applied to the Reactive Power Compensation Problem	189

3rd Conference of Computational Interdisciplinary Sciences

Hugo R. Benítez Vega, Rodolfo Paez, Diego Pedro Pinto Roa, Pedro Esteban Gardel Sotomayor and Benjamín Barán

A Survey on Virtual Optical Network Embedding 200
Enrique Davalos, Benjamín Barán and Diego Pedro Pinto Roa

Computer Science and Applications

Databases Integration in Grid Computing Applications 212
Paulo Ruiz, Haroldo F. de Campos Velho, Renata Ruiz and Elton Oliveira

Entrepreneurial Ecosystem: An Entrepreneurial Thematic Geoportal and Data Warehouse . . . 219
Esther Hochsztain, Andrómaca Tasistro and María Messina

Simulation of Quantum Walks using HPC 230
Pedro Lara, Aaron Leão and Renato Portugal

An Innovation Cellular Automata for Traffic Simulation 243
Marcelo Zamith, Regina Leal-Toledo and Esteban Clua

Multifactor Transparent Authentication 255
Alcides Rivarola and Cristian Cappo

Iterative Estimation for Flight Dynamic Helicopter Simulator 264
Ivana Yoshie Sumida, Haroldo F. de Campos Velho, Eduardo F. P. Luz, Ronaldo Vieira Cruz and Luiz Carlos Goes

Engineering and Computer Science in Medicine

Pervasive Monitoring of Ambulatory Hypertensive Patients and Diagnosis Support 267
Jorge Cespedes and Cynthia Villalba

CHIEM: A Centralized Health Information Exchange Model 279
Jesús María Romero Riveros, Pablo José López Estigarribia, Cynthia Emilia Villalba Cardozo, José Luis Vázquez Noguera and Diego Pedro Pinto Roa

A Novel Pulse Width Modulation Algorithm Based on Time Space Model 291
José Riveros

Measurement and Monitoring System Water Level for Inland Navigation 303
Ignacio Andrés Villamayor Benítez and Norma Graciela Silva Ortiz

Energy policies in the residential sector of the Republic of Paraguay 315
Diana Valdez, Karen Balbuena and Gerardo Blanco

Marginal Abatement Costs for Greenhouse Gas Emissions Reduction in Paraguay's Energy Sector: An Analysis under Uncertainty 329
Juan P. Nogués P.

Part III: Poster Session

Neuro-Fuzzy Classifier for Deforestation Estimation in a Citizen Science Project	334
<i>Marilyn Menecucci Ibanez Dos Reis, Fernando Manuel Ramos, Adenilson Carvalho and Eduardo Fávero Pacheco Da Luz</i>	
Characterization of the Cosmological Nonlinear Path of Single Galaxies in N-Body Simulations	336
<i>Diego H. Stalder D., Reinaldo Rosa and Esteban Clua</i>	
Automated Coronary Artery Segmentation in CTA	337
<i>Federico Lopez Bertoni and Horacio Legal Ayala</i>	
Integrated system of data acquisition and monitoring of intra and peridomestic infestation of vector of Chagas disease	344
<i>Luis Rodríguez, Marcio Duarte, Santiago Gómez, Christian E. Schaerer and Antonieta Rojas de Arias</i>	
Grooming-Hierarchical WDM Network Design	346
<i>Alberto Amadeo and Diego Pinto</i>	
Applying Seasonality to a discrete form of the Bass Model	347
<i>Claudia Montaña, Santiago Gómez and Christian E. Schaerer</i>	
Automated Monitoring of Electrical Conductivity , Humidity and Temperature of Agricultural Soil	348
<i>Richard González and Israel Caceres</i>	
Applying a wire plate Electrostatic Precipitator for collection of particulate matter from burning coconut pit	354
<i>Edgar Marcial Maqueda Acuña, Alfredo Renault López and Norma Graciela Silva Ortiz</i>	
A numerical implementation of the 2-D incompressible Navier-Stokes equation using stream function-vorticity formulation	362
<i>Laura Oporto and Christian E. Schaerer</i>	
Stability command of a Tilt-rotor vehicle with a Fuzzy Logic controller	365
<i>Eduardo Coronel and Adolfo J. Jara C.</i>	
Multiresolution analysis and robustness of a Contour-Point Signature-based human postures recognition system	377
<i>Gabriela Gaona, Javier Pérez, Christian E. Schaerer and Waldemar Villamayor Venialbo</i>	
Implementing the Parareal method as a PETSc function	380
<i>Juan José Cáceres Silva, Benjamín Barán and Christian E. Schaerer</i>	

3rd Conference of Computational Interdisciplinary Sciences

Sensitivity Analysis of a Chromium-Iron redox reaction in a batch system using PHREEQC	382
<i>Luis Salgueiro, Juan Pablo Nogués Pea, Magna Monteiro and Christian E. Schaerer</i>	
A new variant of MOACS for many-objective TSP	384
<i>Francisco Riveros, Nestor Benitez, Julio Paciolo and Benjamín Barán</i>	
Viscous fingering instabilities in rectilinear porous media flow	395
<i>Juan Zena and Christian E. Schaerer</i>	
Superlinear Convergence for Block Conjugate Gradient using Variable Block Size Strategies	400
<i>Pedro Torres and Christian E. Schaerer</i>	
Allocation algorithms for dynamic partial reconfiguration on reconfigurable hardware	402
<i>Federico Fernández and Juan Carlos Fabero</i>	
Monitoring Vital Signs Using Biomedical Technologies based devices Reconfigurable	405
<i>Federico Fernández, Jose Nuñez and Lucas Frutos</i>	
Web Geographic Information System to visualize the Patio Aquifer vulnerabilitiy to contami- nation	408
<i>Liz Báez, Juan Pablo Nogués and Cynthia Villalba</i>	
A quasi-classical trajectory study of the OH + SO reaction: the role of ro-vibrational energy	410
<i>J. D. Garrido, W. A. D. Pires, M. A. C. Nascimento and M. Y. Ballesterb</i>	
Application of the Hydrus model to simulate Redox reactions in a ZVI Filter.	411
<i>Cristhel Leguizamón, Juan P. Nogués, Christian E. Schaerer and Magna Monteiro</i>	
Mechanism of reduction of Cr(VI) in presence of iron filings	413
<i>Andrés Aquino Valdovinos, Magna Monteiro and Silvia Aquino</i>	
Using the Kinect Sensor with Open Source Tools for the Development of Educational Games for Kids in Pre-school Age	415
<i>Christian von Lücken and Romina Fernández</i>	
Mutual Information Based Medical Image Registration using Clever Optimization Algorithms	418
<i>Pedro Cespedes, Horacio Legal and Christian E. Schaerer</i>	
Ant Colony Optimization applied to Micro uidic Routing 2 Problem in DMFB	421
<i>Carlos Mendoza, Eduardo Szaran, Diego Pedro Pinto Roa and Carlos A. Brizuela</i>	
ILP-based Mathematical Model for node failure protection in Optical Multicast Network	422
<i>Miguel Angel Britez and Diego Pedro Pinto Roa</i>	

3rd Conference of Computational Interdisciplinary Sciences

Role of type II topoisomerases in regulation of supercoiling and pre-catenation in replication intermediates of DNA	423
<i>Victor Martínez, Jorge Cebrián, Maridian J. Kadomatsu-Hermosa, Cristina Parra, Alicia Castán, María José Fernández-Nestosa, Christian E. Schaerer, Pablo Hernández, Dora B. Krimer and Jorge B. Schwartzman</i>	
Measurement of the Education Mobility between Generations Using Goal Programming: A Cased Applied to Paraguay	425
<i>Jorge L. Recalde and María M. López</i>	
A Quantitative Paradigm for Quality of Protection in WDM networks	427
<i>Marcelo Rodas and Diego Pedro Pinto Roa</i>	
Design of a Mixed-Integer Linear Programming Model for Cooperative Agricultural Production Planning Including Inventariables Resources Managing	429
<i>María M. López and Jorge L. Recalde</i>	
Real Time Locating System using Wi-Fi	431
<i>Alberto Capli, Nora Gonzalez Nuñez, Claudio Barua and Cynthia Villalba</i>	
Theoretical study of Pirimetanil and their transformation products	434
<i>Gisselle Morinigo, Alba Bisgarra, Carla Sirtori and Norma Caballero</i>	
Theoretical Study Of Permethrin	436
<i>Francisco Arias, Viviana Lopéz Aca and Norma Caballero</i>	
A Multi-objective Study of Cooperative vs Selfish Routing in WDM Networks	438
<i>Baudelio Báez, José Colbes and Diego Pedro Pinto Roa</i>	
Voronoi Tessellation for calculationg local 3D densities on the environment of clusters of galaxies	440
<i>Marcel Chow-Martínez and César A. Caretta</i>	
Two-Phase Flow Including Capillary Pressure And Buoyancy Effects: A Two- Dimensional Model To Study The Carbon Sequestration Process	441
<i>Jhabriel Varela, Juan Pablo Nogués and Christian E. Schaerer</i>	
HTTP-WS-AD: Anomaly detector for web applications and web Services	443
<i>José Giménez and Cristian Cappel</i>	
Energy planning in terms of useful energy for the Republic of Paraguay	446
<i>Enrique Buzarquis, Javier Amatte, Gerardo Blanco and Benjamín Barán</i>	
Neuro-fuzzy Approach Addressing Predictability	448
<i>Pettras L. B. Santos, Sandra Sandri and Haroldo F. de Campos Velho</i>	
Application of Artificial Neural Networks to Vocational Guidance	453

3rd Conference of Computational Interdisciplinary Sciences

Nelson Romero, Eustaquio Alcides Martínez Jara and Alejandro Benítez

Numerical simulation of plane mixing layer with exothermic chemical reaction using FEniCS libraries 465

Diego René González Weiberlen, Hyun Ho Shin and Christian E. Schaerer

Facial Recognition based on Indexed Metric Spaces 470

Liz J. González and Christian von Lücken

Analysis of the key parameters involved in the method of crystallization from a mixture of sucrose and steviol glycosides from *Stevia rebaudiana* Bertoni paraguayana origin. 473

Shirley Duarte, Fátima Díaz and María Peláez

Influence of the Temperature of carbonization on the characteristic and efficiency of material carbonized obtained from care coconut *Acrocomia aculeata* (Arecaceae) 475

Shirley Duarte, Maria Sarubbi, Jorge Lin and Pedro Torres

Biodiesel production by reactive distillation: Evaluation of operating parameters using dynamic simulation 476

Ruth Lucinda Garbini León and Carlos D. Mendez

Wireless Sensor Network for Aerosol Measurement 479

Lucas Frutos and Federico Fernández

Kaolin Pellets Processing For Slow Release Pheromone Applied To *Triatoma infestans* Capture 480

Silvia Aquino, María Vega, Marize Varella de Oliveira, Alexandre Antunes Riveiro and Magna Monteiro

Describing the role of space-dependent bistability for the phenomenon of morphogenesis 482

Francisco J.P. Lopes, Vilarinho, Eric Y. Otomo and Paulo M. Bisch

Part I : Plenary and Invited Talks

Influence of chemical reactions on convective dissolution

Anne De Wit

Nonlinear Physical Chemistry, Unit Université libre de Bruxelles, Belgium

Abstract

When one liquid partially dissolves in another denser one beneath it in the gravity field, buoyancy-driven convective fingering can appear which enhances the further mixing of the two partially miscible liquids. This is typically observed during CO₂ sequestration when injected less dense CO₂ is dissolving into saline aquifers. Upon dissolution, the CO₂ forms a denser boundary layer at the top of the aqueous solution which next starts to sink with fingering convective flows. We investigate both experimentally and theoretically the influence of chemical reactions on the properties of such buoyancy-driven instability. We show that a chemical reaction can either enhance or decrease the amplitude of the convective dissolution depending on the type of density profile building up in time in the lower reactive solution. On the basis of a reaction-diffusion-convection model, we classify the various possible cases as a function of the Rayleigh numbers of the problem. Using a laboratory-scale system, we experimentally demonstrate the possibility to enhance convective dissolution of CO₂ in aqueous solutions by simple reactions.

A new model for single-particle diffusion processes under multiple excitation states

Luiz Bevilacqua

A.L.Coimbra Institute COPPE/UFRJ, Brazil

Abstract

The bi-flux phenomenon occurring in a single component diffusion process may be triggered by the presence of two distinct energy states, say E_1 and E_2 . Starting from a discrete approach considering partial and temporary retention it was possible to derive the governing equation for this diffusion problem. For a one-dimensional flux in an isotropic

$$p_t = D\beta p_{xx} - R\beta(1 - \beta)p_{xxxx} \quad (1)$$

medium the governing equation reads represents the fraction of particles in primary excitation state E_1 and $(1-\beta)$ represents the fraction of particles scattering in the subsidiary excitation state E_2 . The primary flux, that is particles in excitation state E_1 follow the classical Fick's law. The velocity of the secondary $\mathbf{\Psi}_2 = \beta R p_{xxx} \mathbf{e}_1$ flux is given by flux velocity for the secondary flow. We present the evolution of the concentration $p(x, t)$ for cases where β is constant compared with the evolution of the concentration for cases where β varies in time. Singular behaviours leading to negative values of the concentration as function of R are presented. The influence of the boundary conditions is shown to be critical for the concentration evolution. The bi-flux theory is extended to a multi-flux process. Comments on the applications in the mathematical and computational modelling of particular systems are introduced.

Models for intracellular Ca^{2+} signalling

Geneviève Dupont

Unité de Chronobiologie Théorique, Faculté des Sciences, Université Libre de
Bruxelles, Belgium

Abstract

In cellular physiology, Ca^{2+} acts as a universal second messenger responsible for a variety of responses, ranging from gene expression to apoptosis. In most cases, the type of response is encoded in the spatio-temporal organization of the Ca^{2+} increases. Since the experimental discovery of Ca^{2+} oscillations and waves, modelling has been extensively used to investigate how these auto-organized phenomena are brought about. After reviewing the general mechanisms common to most cell types, I will focus on the atypical Ca^{2+} responses that are generated when *Shigella*, a widespread bacterium responsible for dysentery, invades epithelial cells. *Shigella* usurps the Ca^{2+} signaling machinery of the host cells to favour its development. In particular, by creating a dense actin network at the invasion site, the bacterium generates a localized Ca^{2+} response allowing the production of ATP, which can in turn fuel further invasion processes. A computational approach of this phenomenon, taking into account the reduced diffusivity of signaling molecules in the actin network as well as the interplay between Ca^{2+} and mitochondrial metabolism will be described.

Complex dynamics of parametrically driven magnetic systems

David Laroze

Instituto de Alta Investigación, Universidad de Tarapacá, Arica, Chile

Abstract

The world of nanometric scale is becoming increasingly accessible due to the remarkable development of experimental techniques. The technological applications of nanostructures can be found in many different areas such as biomedicine or high-precision instrumentation. In material science, one significant application of magnetic particles and clusters is in the area of recording media [1] and so the magnetization reversal is one of the fundamental features of data storage. Therefore, a detailed study of simple magnetic systems is really important and will be presented here.

Nonlinear time-dependent problems in magnetism have already been studied in numerous cases. The standard approaches to modeling the classical magnetic systems are the Landau-Lifshitz or Landau-Lifshitz- Gilbert (LLG) equation. Recent accounts of developments can be found in Refs. [2-3]. In this seminar we present theoretical and numerical results on deterministic spin dynamics of anisotropic magnetic systems in the presence of a time dependent magnetic field using the Landau-Lifshitz- Gilbert equation. In particular, we study the case when the magnetic field consists in two terms. One has time dependence, while the other is constant. We analyze different configurations of the magnetic field orientation respect to the anisotropy direction. We focus on zero-, one- and two-spatial dimensional systems, which correspond to a particle, a wire and a magnetic plane, respectively.

In the magnetic particle case, we numerically characterize the dynamical behavior of the system by monitoring the Lyapunov exponents, and by calculating Poincaré sections and Fourier spectra [4-5]. In addition, we calculate analytically the corresponding Melnikov function, which gives us the bifurcations of the homoclinic orbits. We find a rather complicated landscape of sometimes closely intermingled chaotic and non-chaotic areas in parameters space. Finally, we show that when the magnetic forcing is quasi-periodic the system exhibits strange nonchaotic attractors [6]. In the continuum case the pattern formation is studied. In particular, we show that depending

on the parameters the spatio-temporal magnetization field can exhibit localized precession [7-8], propagative and non-propagative front solutions [9-10], localized waves [11], two-soliton bound state solutions [12], breather soliton solutions [13], as well as chaotic patterns [14]. Close to the parametric resonance instability, an amplitude equation allows us to understand and characterize these states.

The author acknowledges partial financial support from FONDECYT 1120764, Millennium Scientific Initiative, P10-061-F, Basal Program Center for Development of Nanoscience and Nanotechnology (CEDENNA) and UTA-project 8750-12.

References

- [1] C. Ross, Annual Review of Materials Research 31, 203 (2001).
- [2] P. E. Wigen (Ed.), Nonlinear Phenomena and Chaos In: Magnetic Materials (World Scientific, Singapore, 1994).
- [3] I. D. Mayergoyz, G. Bertotti, and C. Serpico, Nonlinear Magnetization Dynamics in Nanosystems (Elsevier, Dordrecht, 2009).
- [4] J. Bragard, H. Pleiner, O. J. Suarez, P. Vargas, J. A. C. Gallas, D. Laroze, Physical Review E, 84, 037202 (2011).
- [5] D. Laroze, J. Bragard, O. J. Suarez, H. Pleiner, IEEE Transaction on-Magnetics, 47, 3032 (2011).
- [6] D. Laroze, D. Becerra-Alonso, J. A. C. Gallas, and H. Pleiner, IEEE-Transactions on Magnetics 48, 3567 (2012).
- [7] M. G. Clerc, S. Coulibaly and D. Laroze, Physical Review E 77, 056209(2008).
- [8] M. G. Clerc. S. Coulibaly, D. Laroze, EPL 90, 38005 (2010).
- [9] M. G. Clerc. S. Coulibaly, D. Laroze, Physica D 239, 72 (2010).
- [10] M. G. Clerc. S. Coulibaly, D. Laroze, International Journal of Bifurcation and Chaos 19, 2717 (2009); *ibid* 19, 3525 (2009).
- [11] M. G. Clerc. S. Coulibaly, D. Laroze, EPL 97, 30006 (2012).

- [12] D. Urzagasti, D. Laroze, M. G. Clerc, S. Coulibaly, H. Pleiner, Journal of Applied Physics, 111, 07D111 (2012).
- [13] D. Urzagasti, D. Laroze, M. G. Clerc, H. Pleiner, EPL 104, 40001 (2013).
- [14] D. Urzagasti, D. Laroze, H. Pleiner, European Physical Journal S.T. 223,141 (2014).

Inference and structure discovery in biological networks

Alberto Paccanaro

Department of Computer Science at Royal Holloway, University of London,
United Kingdom

Abstract

An important idea that has emerged recently is that a cell can be viewed as a complex network of interrelating proteins, nucleic acids and other bio- molecules. At the same time, data generated by large-scale experiments often have a natural representation as networks such as protein-protein interaction networks, genetic interaction networks, co-expression networks. From a computational point of view, a central objective for systems biology is therefore the development of methods for making inferences and discovering structure in biological networks possibly using data which are also in the form of networks. In this talk, I'll present novel computational methods for solving biological problems which can all be phrased in terms of inference and structure discovery in large scale networks. These methods are based and extend recent developments in the areas of machine learning (particularly semi-supervised learning), graph theory and network science.

I will show how these computational techniques can provide effective solutions for biological problems such as: detecting protein complexes from protein-protein interaction data; de-noising large scale protein-protein interaction experiments; selecting genes which can be used as biomarkers for biological processes. Finally I will describe how these ideas could be applied to problems in the area of Network Medicine, such as disease gene prediction and drug repositioning.

From computational interdisciplinary sciences to integrative transdisciplinary sciences: the Complex Systems Digital Campus UNESCO UniTwin.

Paul Bourgin

Université Paris Saclay, École Polytechnique, Paris, France

Abstract

The aim of computational interdisciplinary sciences, like computational physics, chemistry or biology, is to simulate systems when a model has been proposed by an interdisciplinary team. Such model is generally a prototype in standard conditions and the distance with phenomenological data is generally essentially qualitative.

The aim of integrative transdisciplinary sciences, like condensed matter physics, integrative biology or ecology, territorial intelligence, integrative social science, is to construct predictive multi-level models of complex systems in vivo and in natura. The prediction paradigm has to shift from predicting not what will happen in certainty but what can happen in probability. Indeed this shift is necessary like in quantum mechanics because the causality is entangled at all distances in space between internal and environmental levels of organization and at all distance in time through individuated history and individuation processes. The criterium of success is thus well defined by the distance between empirical and theoretical probability laws on their multi-level dynamics like in quantum mechanics.

Peirce epistemological triangle provides another equivalent way to present integrative transdisciplinary sciences. The triangle starts from some surprising facts by abduction of new hypotheses in integrated models. It continues by deduction of some expected facts from such model change. And the triangle becomes closed by induction when asking such expected facts to Nature .. but producing new surprises. Such epistemological triangle is nothing else than assimilation of data by models, as done by the brain at each sensorimotor cycle. Each integrative science needs a new transdisciplinary scientific community sharing the protocols (i) for producing its multi-scale dynamical data in vivo and in Natura and (ii) for assimilating these multi-scale data by its multi-levels integrated models. Here the Peirce epistemological triangle abduction-deduction-induction holds at the social cognitive level of scientific communities.

3rd Conference of Computational Interdisciplinary Sciences

The main objective of the Complex Systems Digital Campus (CS-DC) is to organize the shift between computational interdisciplinary sciences toward integrative transdisciplinary sciences. The CS-DC is launching international e- laboratories and e-departments for helping the new transdisciplinary communities to share all the research and educational resources for facing their scientific and societal challenges in the complex systems roadmap. The CS-DC is recognized in 2014 as an UNESCO UniTwin, twining a network of hundred universities in the world, continuously increasing.

High-performance-computing for heart simulations and its complex spatiotemporal dynamics

Flavio Fenton

Physics Department, Georgia Institute of Technology, Atlanta, USA

Abstract

The heart is an electro-mechanical system in which, under normal conditions, electrical waves propagate in a coordinated manner to initiate an efficient contraction. In pathologic states, propagation can destabilize and exhibit chaotic dynamics mostly produced by single or multiple rapidly rotating spiral/scroll waves that generate complex spatiotemporal patterns of activation that inhibit contraction and can be lethal if untreated. Despite much study, little is known about the actual mechanisms that initiate, perpetuate, and terminate spiral waves in cardiac tissue. In this talk, I will motivate the problem with some experimental examples and then discuss how we study the problem from a computational point of view, from the numerical models derived to represent the dynamics of single cells to the coupling of millions of cells to represent the three-dimensional structure of a working heart. Some of the major difficulties of computer simulations for these kinds of systems include: i) Different orders of magnitude in time scales, from milliseconds to seconds; ii) millions of degrees of freedom over millions of integration steps within irregular domains; and iii) the need for near-real-time simulations. Advances in these areas will be discussed as well as the use of GPUs over the web using webGL.

Building security situational awareness

Raul Ceretta Nunes

Federal University of Santa Maria, Brazil

Abstract

Nowadays people and organizations are constant vulnerable to new threats in cyberspace and protecting their network-available critical information is a challenge. To detect threats in an effective and early way we depend on the Early Warning Systems (EWS). These systems help to build a security situational awareness from the monitored environment to allow early reactions to malicious events, improving control and monitoring of involved resources.

A security situational awareness system splits into four levels: (i) perception of malicious events; (ii) comprehension of information; (iii) ability to build projections based on historical data and (iv) resolution, where countermeasures are needed to address the identified risks. This talk will discuss how we can build each of these levels and why each one depends on the efficient computational methods and interdisciplinary knowledge.

Environmental Risk Models and Applications

Dario Rodriguez Aseretto

Joint Research Centre, European Commission

Abstract

Demands on the disaster response capacity of the European Union are likely to increase, as the impacts of disasters continue to grow both in size and frequency. This has resulted in intensive research predominantly on issues concerning spatially-explicit information, modelling and map accuracy and their multiple sources of uncertainty. There have been several recent catastrophic events including floods in Central Europe, and severe forest fires in Sweden and Portugal. Furthermore, South America is also highly exposed to natural disasters such as landslides, earthquakes and tsunamis. Floods and droughts are recurrent in the region and cause severe losses. These events highlight the increasing need to develop activities that support Disaster Management. When a disaster happens, the main needs of the affected population are temporary shelter, food, clean water, primary health care, household items or clothes.

Advances in computing have enabled a data centred revolution in science that has been significant: now we can develop and implement very complex models in order to reproduce the physics of the natural phenomena in an accurate, timely and effective manner. These approaches should help to enhance the power of community resilience; i.e., improving the community's capacity to resist, adapt or change in order to achieve a new level of functioning or structure in the occurrence of extreme events and disasters. In this talk, we give an overview of models and applications used for environmental risk assessment in Europe. We focus on environmental data analysis, modelling, and visualization. In general, environmental phenomena must be considered in a high dimensional feature space. They are also nonlinear and highly variable at several spatial and temporal scales.

This presentation discusses several fundamental problems of primary importance in environmental risk models. Simulated and real data case studies, including topo-climatic modelling, environmental risks, natural hazards and renewable resources, are considered to illustrate the most recent achievements and to highlight new challenges.

El impacto de la filosofía ágil (Agile) en las organizaciones que desarrollan software

Álvaro Ruiz de Mendarozqueta

Universidad Nacional de Córdoba, Argentina

Abstract

Las organizaciones de desarrollo de software que han ido introduciendo métodos y prácticas ágiles, no sólo han cambiado los procesos sino que afectaron los paradigmas en que se basan los procesos de desarrollo de software. Aquellas organizaciones que han mejorado sus resultados por el empleo de métodos ágiles, se encuentran con que sus proyectos aplican una filosofía de trabajo (basada en el manifiesto ágil) que parece oponerse a la que se usa en el resto de la organización. A su vez el cambio de paradigma afecta a los roles y a las maneras de comunicarse en los proyectos de desarrollo de software. El objetivo es mostrar los posibles impactos y un enfoque para poder minimizarlos.

Opportunities and Challenges for Green HPC

Carlos Juiz

Departamento de Ciencias de la Computación,
Universitat de les Illes Balears, Spain

Abstract

Recognizing the unsustainability in designing power hungry HPC systems, in the recent years an effort towards an energy and performance efficient HPC design is on the rise. Based on the available data on top green HPC systems, in this paper we analyze the main components of the HPC system with the attempt to provide an insight into the green efficiency in line with the technology development. Using global scale measurements, our goal is to discover the most promising designs and pinpoint on the existing main challenges that should direct future research efforts.

Upper critical dimension, Galilean Invariance, and exact solution for the etching model

Fernando Oliveira

International Center for Condensed Matter Physics,
CP 04455, 70919-970, Brasília DF, Brazil.

Abstract

We generalise the etching model [1] from $1+1$ to $d+1$ dimensions. The dynamic exponents of this model are compatible with those of the KPZ universality class. We investigate the roughness dynamics with surfaces up to $d = 6$. We show that the data from all substrate lengths and for all dimension can be collapsed into one common curve. We determine the dynamic exponents as a function of the dimension. Our results suggest that $d = 4$ is not an upper critical dimension for the etching model, and that it fulfills the Galilean Invariance [2]. Moreover for $d = 1$ we obtain the exact exponents for the model and we show that they belong to the KPZ universality class [3].

References

- [1] B. A. Mello, A. S. Chaves, and F. A. Oliveira, Phys. Rev. E 63, 041113 (2001)
- [2] E. A. Rodrigues, B. A. Mello, and F. A. Oliveira to be published
- [3] W. S. Alves, F. A. Oliveira and I. V. L. Costa, to be published

Part II : Paper Session

A Survey of Results Concerning Steady Solutions and the Stability of a Class of Rotating Flows

José Pontes^{a1}, Norberto Mangiavacchi^a, Gustavo Rabello dos Anjos^a, Rachel Manhães de Lucena^a, Gustavo C. P. Oliveira^a and Davi V. A. Ferreira^b
^aGroup of Environmental Studies of Hydropower Reservoirs GESAR/UERJ, State University of Rio de Janeiro,
R. Fonseca Telles 121 Rio de Janeiro, RJ, 20550-013 Brazil ^b Graduate Program in Civil Engineering - Federal University of Rio de Janeiro
P.O. Box 68506, Rio de Janeiro, RJ, 21941-972 Brazil

Abstract

We review the key points concerning the linear stability of the classical von Kármán's solution of rotating disk flow, modified by the coupling, through the fluid viscosity, with concentration field of a chemical species. The results were published by Mangiavacchi et al. (Phys. Fluids, **19**: 114109, 2007) and refer to electrochemical cells employing iron rotating disk electrodes, which dissolve in the 1 M H_2SO_4 solution of the electrolyte. Polarization curves obtained in such cells present a current instability at the beginning of the region where the current is controlled by the hydrodynamics. The onset of the instability occurs in a range of potentials applied to the cell and disappear above and below this range. Dissolution of the iron electrode gives rise to a thin concentration boundary layer. The concentration boundary layer increases the interfacial fluid viscosity, diminishes the diffusion coefficient and couples both fields, with a net result of affecting the hydrodynamic of the problem. Since the current is proportional to the interfacial concentration gradient of the chemical species responsible by the ions transport, the instability of the coupled fields can lead to the current instability observed in the experimental setups. This work reviews the results of the linear stability analysis of the coupled fields and the first results concerning the Direct Numerical Simulation, currently undertaken in our group. We also address the steady flow developed between two coaxial counterrotating disks and close to a semi-spherical rotating electrode in electrochemical cells.

Keywords: Rotating disk flow, rotating semi-sphere flow, hydrodynamic stability, finite element method

¹E-mail Corresponding Author: jopontes@metalmat.ufrj.br

1. STABILITY OF ROTATING DISK FLOW IN ELECTRO-CHEMICAL CELLS

We review the problem of the stability other linear stability of the classical von Kármán's solution of rotating disk flow, modified by the coupling, through the fluid viscosity, with concentration field of a chemical species, as found in electrochemical cells using rotating disk electrodes. A constitutive equation relating the electrode viscosity to the concentration of the iron ions generated by the dissolution of the electrode, is assumed. We show that the coupling hydrodynamic field, to the iron concentration, which carries the current changes the stability properties of the purely hydrodynamic field, reducing the critical Reynolds number to the range of values attained in electrochemical setups. Our results support also the hypothesis that oscillations of the interfacial concentration gradient are strong enough to drive the current oscillations experimentally observed [5]. A brief review of a Finite Element Code developed at our group and numerical results concerning the base flow and some patterns emerging from the instability of the base flow are also presented.

2. THE FLOW BETWEEN COAXIAL ROTATING DISKS

The flow between coaxial rotating admits steady solutions which are governed by a generalization of von Kármán's nonlinear time independent ODE equations for a single rotating disk, that take into account pressure variations along the radial direction. Families of solutions qualitatively similar exist for variable distances between the disks. We present some families of solutions obtained by integration of the generalized von Kármán's ODEs equations and some results of the numerical integration of the three dimensional time dependent hydrodynamic equations, also including some solutions with pattern formation beyond the stability limit of the azimuthal angle independent [1].

3. THE CONCENTRATION AND HYDRODYNAMIC FIELDS CLOSE TO A ROTATING SEMI-SPHERE ELECTRODE

Rotating disk electrodes, regularly used in electrochemical cells present the weakness of rapidly loosing the at shape due to the dissolution of the iron electrode in the acid solution of the electrolyte. To overcome the problem rotating semi-spherical electrodes have been used. In this setup the electrode

maintains the original form, though losing mass. The flow close to a rotating semi-spherical electrode present some characteristics also found in rotating disk flow and, at the same time, those found in boundary layers. A solution in power series of the polar multiplying the functions which describe the velocity profiles in the radial direction found by Howarth (1951) is well known [4, 3]. In the present work we generalize Howarth's solution by coupling the hydrodynamic and the concentration fields through the same constitutive equation assumed in the case of rotating disk flow. We present The coupled solution of the boundary layer equations and the first numerical simulations of the three dimensional time dependent equations using the Finite Element Method [2].

References

- [1] Davi Vaz de Andrade Ferreira. Estudo do campo hidrodinâmico entre dois discos rotatórios. Master's thesis, Instituto Alberto Luiz Coimbra de Pós-Graduação em Engenharia COPPE - Universidade Federal do Rio de Janeiro, 2013.
- [2] Rachel Manhães de Lucena. Hidrodinâmica de células eletroquímicas com eletrodo de disco rotatório. Master's thesis, Instituto Alberto Luiz Coimbra de Pós-Graduação em Engenharia COPPE - Universidade Federal do Rio de Janeiro, 2013.
- [3] J. G. S. Godinez. *Eletrodo Semi-esférico rotatório: teoria para o estado estacionário*. PhD thesis, Instituto Alberto Luiz Coimbra de Pós graduação e Pesquisa em Engenharia, Universidade Federal do Rio de Janeiro, Brasil, Rio de Janeiro, 1996.
- [4] L. Howarth. Note on the boundary layer of a rotating sphere. *Phil. Mag.*, 42:1308-1315, 1951.
- [5] N. Mangiavacchi, J. Pontes, O. E. Barcia, O. E. Mattos, and B. Tribollet. Rotating disk flow stability in electrochemical cells: Effect of the transport of a chemical species. *Phys. Fluids*, 19:114109, 2007. DOI:10.1063/1.2805844.

Finite Element Simulation of Fingering in Convective Dissolution in Porous Media

Rachel M. Lucena^{a1}, Norberto Mangiavacchi^a, José Pontes^a,
Anne De Wit^b, and Gustavo Anjos^a

^aGroup of Environmental Studies for Water Reservoirs - GESAR, State University of Rio de Janeiro, Rio de Janeiro, RJ, Brazil

^bNonlinear Physical Chemistry Unit, CP 231, Faculté des Sciences, Université Libre de Bruxelles (ULB), Brussels, Belgium.

Abstract

We address the problem of buoyancy-driven fingering generated in porous media by the instability of a partially miscible fluid layer dissolving in another denser fluid placed below it. A 2D time dependent numerical simulation is performed, assuming that the flow is governed by Darcy's law, along with the Boussinesq approximation to account for buoyancy effects introduced by concentration dependent densities. The velocity field is modeled by a vorticity-stream function formulation. The resulting equations are solved through the finite element method, with the material derivative of the concentrations numerically represented by a Semi-Lagrangian Scheme.

Keywords: fingering, instability, finite element method.

1. FINITE ELEMENT METHOD

Fingering refers to hydrodynamic instabilities of deforming interfaces into fingers during the displacement of fluids in porous media. These instabilities are closely linked to changes in viscosity or density between the different layers or within a single phase containing a solute invariable concentration that affects the fluid density or viscosity[1].

Fingering occurs in a variety of applications, including CO_2 sequestration techniques, secondary and tertiary crude oil recovery, fixed bed regeneration chemical processing, hydrology, filtration, liquid chromatography, and medical applications, among others. In fact, the phenomena are expected to occur

¹E-mail Corresponding Author: rachel.lucena@uerj.br

in different fields of science and technology, in which flows in porous media are present.

We consider the problem of buoyancy-driven fingering generated in porous media by the dissolution of a fluid layer initially placed over a less dense one in which it is partially miscible. The focus is on the lower layer only where the convective dissolution dynamics takes place.

A 2D time dependent numerical simulation is performed, assuming that the flow is governed by Darcy's law, along with the Boussinesq approximation to account for buoyancy effects introduced by a concentration dependent density. The viscosity is assumed as constant. A vorticity-stream function formulation is adopted to solve the hydrodynamic field [2, 3]. The resulting equations are solved through the finite element method, with the material derivative of the concentrations numerically represented by a semi-lagrangian scheme[4].

Boundary conditions for the velocity field are prescribed as no slip at the upper and lower walls and periodic at the sidewalls. For the dimensionless concentration field, we prescribe as boundary conditions no flux at the lower wall, periodic boundary conditions at the sidewalls and at the top we set a constant value equal to 1. The upper boundary is assumed as flat and horizontal. The onset of fingering is induced by the numerical grid.

Darcy's law and the advective-diffusion equation of the transport of the relevant chemical species are solved in the weak form (also called variational form). The variational form of the governing equations are obtained by properly weighting the equations with weighting functions. The global system, with discrete representation of the derivatives and written in matrix form reads:

$$\begin{aligned} \mathbf{K}\psi + \mathbf{M}\omega &= 0 \\ \mathbf{M}\omega &= R\mathbf{D}_x c \\ (\mathbf{M} + \Delta t\mathbf{K})c^{n+1} - \mathbf{M}c_d^n &= 0. \end{aligned} \tag{1}$$

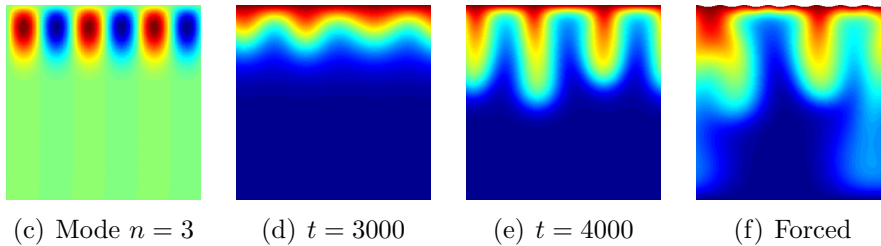
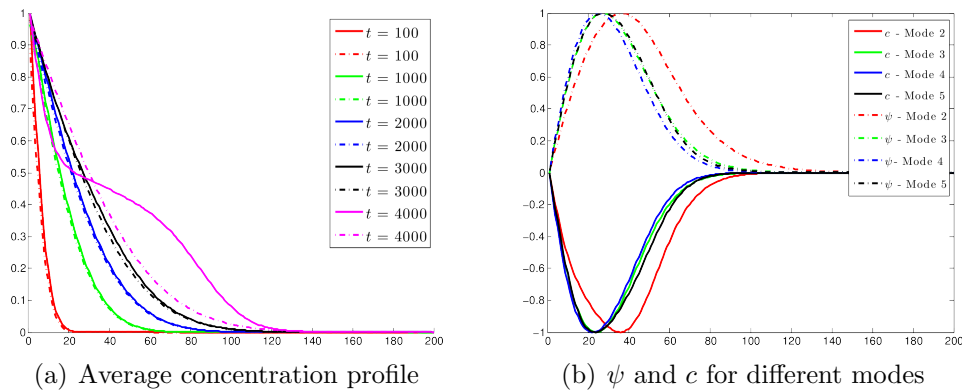
where Eq. 1 are the stream function, vorticity equation (Darcy's Law) and concentration transport equation, respectively, \mathbf{K} is the stiffness matrix, \mathbf{M} is the mass matrix, \mathbf{D}_x is the gradient matrix, c_d is the concentration at the departure points of the lagrangian trajectories.

The system of equations is solved in two steps. In the first one we obtain the stream function and vorticity. Velocity components are then obtained and introduced in the transport equation of c , which is subsequently solved.

An incomplete LU pre-conditioner is applied to the matrices and the linear systems are then solved with the use of GMRES (Generalized Minimal Residual) solver. Preconditioned conjugate gradients methods were also used to obtain the velocity field from the stream function solutions.

2. NUMERICAL RESULTS

Figure (a) shows average concentration profiles c for different times, where the dashed curves refer to the analytical solution related to the numerical profile shown by the continuous curve of the same color. We can observe that for $t = 4000$ a sharp distortion due to the perturbation growth, can be observed in the nonlinear evolution regime of c (see Fig. (e)). Fig. (b) shows the amplitude of perturbation modes of concentration and stream function obtained from the solution of the governing equations using Fourier analysis, at $t = 3000$.



3. CONCLUSIONS

Solutions obtained up to now are in accordance with those found in the literature [5]. The evolution strongly depends on the initial condition. We are

currently investigating the nonlinear evolution of instabilities developed with either a flat upper surface or forced by a deformed upper surface (Figs. 1(e) and 1(f)).

ACKNOWLEDGMENTS: The authors R.L., N.M., J.P. and G.A. acknowledge financial support from the Brazilian agencies FAPERJ, CAPES and CNPq. A.D. acknowledges financial support from FNRS Forecast programme.

References

- [1] HOMSY, GM, 1987. Viscous fingering in porous media, *Annu. Rev. Fluid Mech.* 19: 271-311.
- [2] ALMARCHA, C, TREVELYAN, PMJ, GROSFILS, P, DE WIT, A, 2010. Chemically driven hydrodynamics instabilities, *Physical Review Letters*, 104: 044501-(1-4).
- [3] BUDRONI, MA, RIOLFO, LA, LEMAIGRE, L, ROSSI, F, RUSTICI, M, DE WIT, A, 2014. Chemical control of hydrodynamic instabilities in partially miscible two-layer systems. *Journal Physical Chemistry Letters* 5: 875-881.
- [4] ANJOS, G, MANGIAVACCHI, N, CARVALHO, LM, PONTES, J, SOARES, CBP, 2007. Aproximação Semi-lagrangeana para as Equações de Navier-Stokes acopladas ao transporte de espécie química, *XXX CN-MAC*, 672.
- [5] LOODTS, V, RONGY, L, DE WIT, A, 2014. Convective dissolution of carbon dioxide in salted water: linear stability analysis and effect of control parameters, *Chaos*, in press.

Comparative CFD Simulations of Gas Transport in Slug Flow from Periodic Arrays with Single or Multiple Bubbles

G. P. Oliveira^{a,1}, N. Mangiavacchi^a, G. Anjos^a,
J. Pontes^a, J. R. Thome^b

^aGroup of Environmental Studies in Water Reservoirs - GESAR, State University of Rio de Janeiro, Rio de Janeiro, Brazil

^bHeat and Mass Transfer Laboratory - LTCM, École Polytechnique Fédérale de Lausanne, Lausanne, Switzerland

Received on June 6, 2014 / accepted on August 21, 2014

Abstract

This paper presents a comparative study of transport effects in slug flows through numerical models settled upon volume-preserving periodic arrays of bubbles. The behaviour of the flow is investigated under an adiabatic laminar regime as usually found in microchannels, as well as in microscale fluid applications. Full 3D Direct Numerical Simulations (DNS) are performed for three different cases of setups containing both single and multiple bubbles. Profiles of the bubbles' centroidal velocity are compared, as with the average mass flow rates calculated over the periodic boundaries of the domain.

Keywords: Finite element, slug flow, periodic boundary conditions, bubble.

1. INTRODUCTION

Slug flow (or Taylor flow) is a two-phase flow regime recognizable by capsule-shaped elongated bubbles that separate portions of liquid forming a scenario of high void fraction and large surface-area-to-volume ratio [1], [2]. The mutual and quasi-periodic interaction among the bubbles occurring in this regime impacts directly mass transfer processes taking place mainly in gas-liquid flows. Consequently, several applications of slug flows have been developed in fields such as nuclear, biological and chemical engineering [3], [4], [5].

In the leading edge of the recent technologies applied to efficient cooling of microdevices, slug flows come up mainly due to the improved heat transfer properties reached in this regime. Such quest for operative mechanisms

¹E-mail Corresponding Author: gustavo.oliveira@uerj.br

of high performance in heat dissipation uplifts interests to understand the dynamics of multiple bubbles inside microchannels. For this reason, different sights regarding both numerical and experimental methods are in promising development [6], [7], [8]. The study of elongated bubbles and their heat transfer effects were investigated numerically in recent papers [9] [10], reporting the necessity of simulations containing several bubbles.

The present paper focuses on an adiabatic low-Reynolds modelling to study the gas transport effects of the slug flow from distinctive configurations of periodic arrays of bubbles conserving the same void fraction. Finite element techniques are implemented via an Arbitrary Lagrangian-Eulerian [11], [12] description coupled with periodic boundary conditions and pressure-driven flow as numerical strategies to represent the hydrodynamics of bubble trains occurring inside a microchannel.

2. MODELLING OF BUBBLES IN PERIODIC ARRAYS

To represent mathematically the problems studied here, the model begins from a primal base configuration of periodic array \mathcal{A}_1 which is formed by a cylindrical domain of diameter D , length of period L and periodic boundaries Γ_L, Γ_R encircling a Taylor bubble of volume V_g represented by a convex region Ω_1 . Operating as a branching process, two more configurations of arrays \mathcal{A}_2 and \mathcal{A}_3 are obtained by sectioning the longest bubble into two or three bubbles as depicted in Fig. 1. The length of the periodic cell is defined as a function of the diameter and preserves the total volume regardless of the configuration studied, as with the regions Ω_2 and Ω_3 that also keep the fractioned volume. Moreover, a moving frame technique is applied in the models by which the bubbles are kept fixed, while the cylindrical wall moves backwards with velocity equal to the average velocity of the bubbles' centroids. Furthermore, a negative pressure gradient is applied on the streamwise direction of the flow given by the positive x -axis so producing motion from the left side to the right one. Clearly, the average centroidal velocity is reduced to the centroidal velocity only for the case of a unique bubble.

The two-phase system aforementioned is governed by the dimensionless ALE/FE incompressible Navier-Stokes equations embedded with additional terms to take the contributions of the periodic pressure and interface force

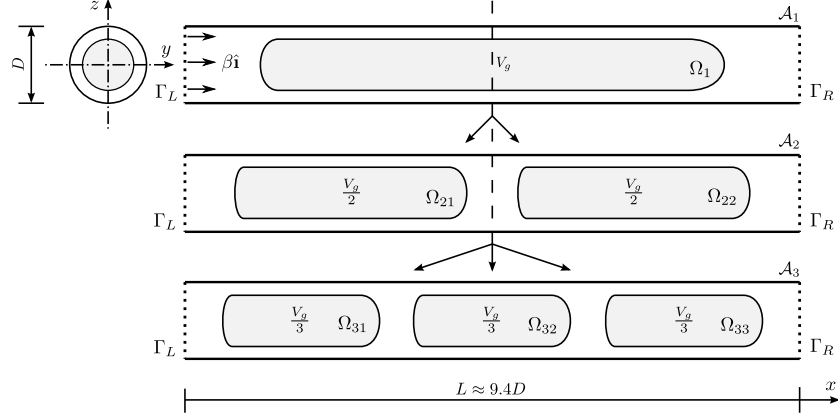


Figure 1: Diagram displaying the branch of a volume-preserving model into three periodic arrays of Taylor bubbles in a cartesian system.

into account, being written, subsequently as

$$\frac{D(\rho \mathbf{u})}{Dt} = \beta \hat{\mathbf{i}} - \nabla P + \frac{1}{Re} \nabla \cdot [\mu(\nabla \mathbf{u} + \nabla \mathbf{u}^T)] + \frac{1}{We} \mathbf{f} + \frac{1}{Fr^2} \rho \mathbf{g} \quad (1)$$

$$\nabla \cdot \mathbf{u} = 0 \quad (2)$$

with

$$\frac{D(\rho \mathbf{u})}{Dt} = \frac{\partial(\rho \mathbf{u})}{\partial t} + (\mathbf{u} - \hat{\mathbf{u}}) \cdot \nabla(\rho \mathbf{u}), \quad (3)$$

where \mathbf{u} is the velocity field, ρ , μ , are the reference density and viscosity of the fluid, respectively, $\hat{\mathbf{u}}$ is the *mesh velocity* [13], \mathbf{g} the vector of standard constant gravity g , Re the Reynolds number, We the Weber number, and Fr the Froude number. Furthermore, the term $-\beta \hat{\mathbf{i}}$ is a vector with constant value β , which is responsible for the mass flow. In turn, the original pressure is replaced by the counterpart periodic P through a decomposition [12], thus rendering the unknown to be found. Finally, the force field \mathbf{f} amounts to the jump conditions existing on the interface in accordance with the “one-fluid” formulation and σ is the surface tension of the liquid assumed as constant.

3. NUMERICAL RESULTS

Analyses of full 3D direct numerical simulations (DNS) performed for each model of array are displayed in this section for an air-water duo. To single out the ability of the numerical method to track the interfacial region of the

bubbles, Fig. 2 depicts the computational representation of the periodic array \mathcal{A}_1 through a marker function separating the internal gas phase from the external liquid phase. As can be seen through the inclined cut plane on the bubble body, inner and outer element layers meet at the bubble body so as to assure the propriety of thin thickness for the interface.

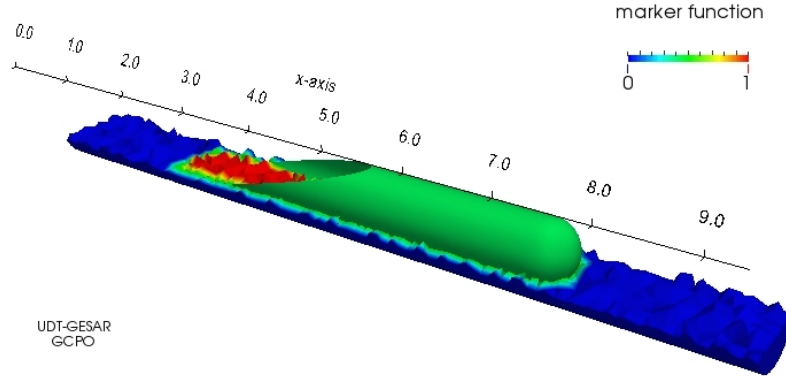


Figure 2: Overview of the gas-liquid periodic array for a single bubble highlighted by a marker function.

Figure 3 depicts the profiles of the bubbles' centroidal x -velocity versus the dimensionless time for each setup of array, whereas Fig. 4 plots the element-averaged mass flows calculated in the periodic boundaries in each case. From these figures, it can be inferred that breaking the longest bubble in two or three smaller bubbles reduces both their average velocity and respective average flow rates for the same value of the pressure gradient, thus supporting that these flow properties depend slightly on the array configuration.

Although the velocity profiles develop monotonically similar in each case, the acceleration experienced by the longest bubble in the array \mathcal{A}_1 is higher than those achieved in the other configurations. Furthermore, as depicted in Fig. 5, the overall behaviour of the velocity for both the bubbles of \mathcal{A}_2 and \mathcal{A}_3 is an identical motion within an equivalent simulation time.

Qualitative images of the pressure field of the periodic flows at a time step far from the initial condition are organized in Figs. (5-7). Since the pressure gradient affects the flow from left to right, higher pressures are felt by the trailing bubble of \mathcal{A}_2 and outermost bubble of the train in \mathcal{A}_3 . Equally verified are the high pressure regions around the trailing bubbles' cap due to

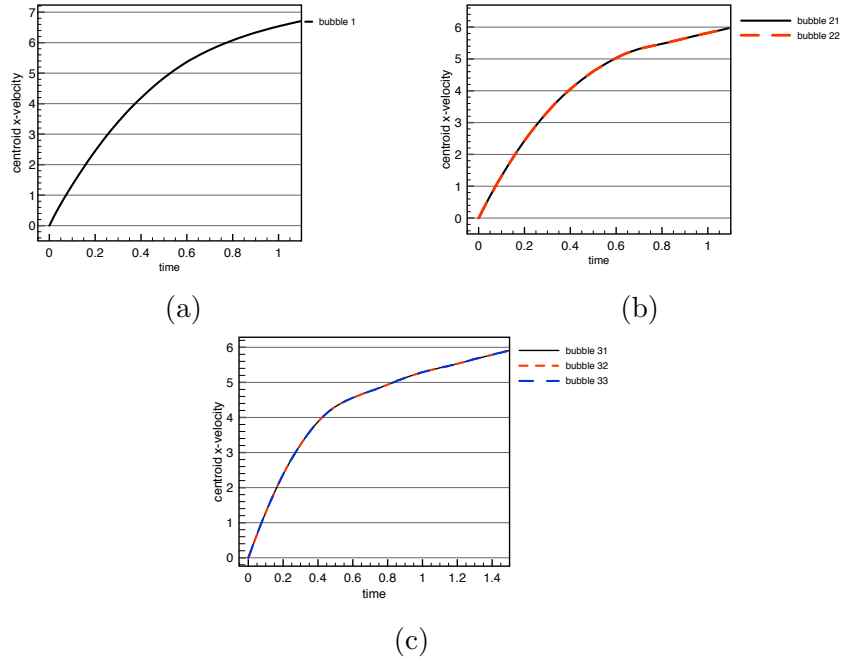


Figure 3: Bubbles' centroidal x-velocity profiles for the periodic arrays. (a) array 1; (b) array 2; (c) array 3.

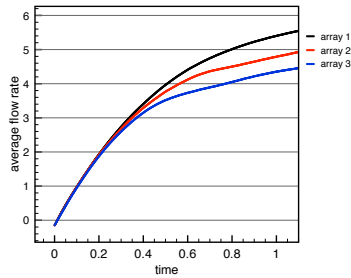


Figure 4: Element-average flow rates for the periodic arrays obtained by weighting of the mean velocity on the periodic boundaries.

a cumulative effect of wake interactions coming from the leading bubbles. In the liquid portion, emphasis was given to the mesh construction only, since the velocity field showed in the simulations was well uniform. By defining subscripts a, w to stand for *air*, *water*, respectively, the physical properties settled for the computations are specified in Table 1, from which $Re \approx 14.58$, $We \approx 0.20$, and $Fr \approx 13, 22$ are obtained.

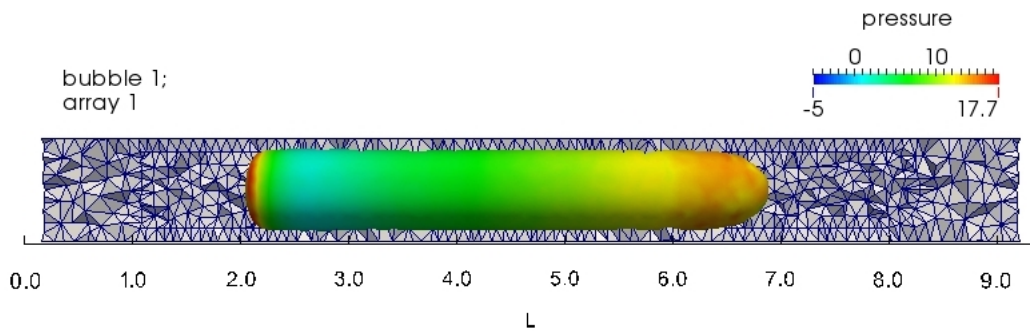


Figure 5: Pressure fields on the bubble's interface for the array 1 (single bubble).

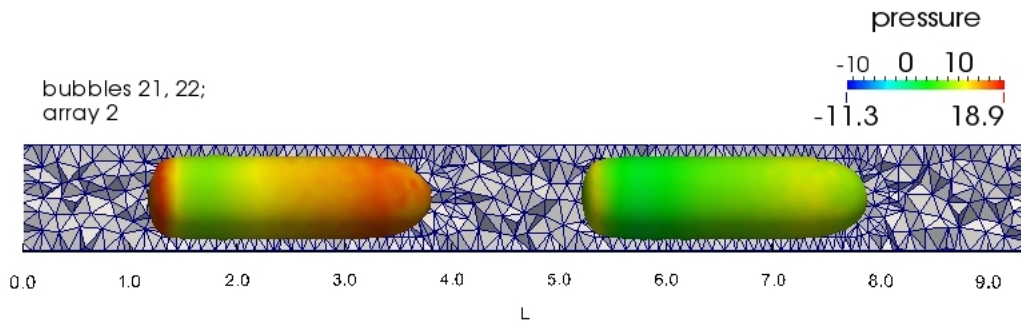


Figure 6: Pressure fields on the bubbles' interface for the array 2 (leading and sequential bubble).

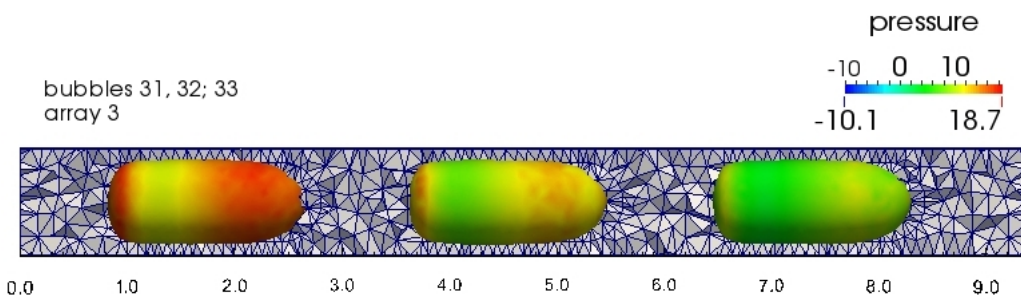


Figure 7: Pressure fields on the bubbles' interface for the array 3 (train of three bubbles).

Physical property	a	w
density (ρ)	1.205	998.63
viscosity (μ)	1.820×10^{-5}	1.002×10^{-3}
surface tension (σ)	-	0.0728

Table 1: Physical properties used in the air-water simulation setups (in S.I. units).

4. CONCLUSION

This paper was intended to analyze comparatively the gas transport in microchannel slug flows through periodic domains. The effect of the imposition of a pressure gradient along with a moving frame technique allowed the settlement of economic simulation setups to assess the overall phenomena taking place inside a confined microchannel. Average quantities of the bubble velocity profiles and mass flow rates gave an insight about the transport of the fractioned gas and it was verified that the change of such quantities are slightly dependent on the array configuration.

By survey of the high pressure zones, we concluded that the trailing bubbles undergo cumulative influence both in the rear and cap regions, due to the forcing of the pressure gradient and the wake interaction of the front bubbles. Since the flow parameters characterized a laminar regime, considerable bubble asymmetries were not observed.

For future study, the inclusion of heat transfer sources as well as more accurate analyses of the gas fractioning through bubble trains is suggested, mainly for different pairs of substances, such as refrigerant fluids or even more viscous liquids.

ACKNOWLEDGMENTS

G.C.P.O and N.M thank to the following Brazilian agencies for the sponsoring of this research: CNPq/Science Without Borders Program, CAPES and FAPERJ.

References

- [1] Davies, RM, Taylor, G, 1950. The mechanics of large bubbles rising through extended liquids and through liquids in tubes, Proceedings of the Royal Society of London. Series A. Mathematical and Physical Sciences 200(1062): 375–390.
- [2] Griffith, P, Wallis, GB, 1961. Two-phase slug flow, Journal of Heat Transfer 83(3): 307–318.
- [3] Fabre, J, Lin, A, 1992. Modeling of two-phase slug flow, Annual Review of Fluid Mechanics 24(1): 21–46.
- [4] Taha, T, Cui, ZF, 2004. Hydrodynamics of slug flow inside capillaries, Chemical Engineering Science 59(6): 1181–1190.
- [5] Kashid, MN, Agar, DW, Turek, S, 2007. CFD modelling of mass transfer with and without chemical reaction in the liquidliquid slug flow microreactor, Chemical Engineering Science 62(18): 5102–5109.
- [6] Cheng, L., Ribatski, G, Thome, JR, 2008. Two-phase flow patterns and flow-pattern maps: fundamentals and applications, Applied Mechanics Reviews 61(5): 050802.
- [7] Gupta, R., Fletcher, DF, Haynes, BS, 2009. On the CFD modelling of Taylor flow in microchannels, Chemical Engineering Science 64(12): 2941–2950.
- [8] Chen, Y, Kulenovic, R, Mertz, R 2009. Numerical study on the formation of Taylor bubbles in capillary tubes, International Journal of Thermal Sciences 48(2): 234–242.
- [9] Talimi, V, Muzychka, YS, Kocabiyik, S 2012. A review on numerical studies of slug flow hydrodynamics and heat transfer in microtubes and microchannels, International Journal of Multiphase Flow 39: 88–104.
- [10] Magnini, M, Pulvirenti, B, Thome, JR 2013. Numerical investigation of the influence of leading and sequential bubbles on slug flow boiling within a microchannel, International Journal of Thermal Sciences 71:36–52.

- [11] Anjos, GR, Borhani, N, Mangiavacchi, N, Thome, JR 2014. A 3D moving mesh Finite Element Method for two-phase flows, *Journal of Computational Physics* 270: 366–377.
- [12] Mangiavacchi, N, Oliveira, GCP., Anjos, G, Thome, JR 2013. Numerical simulation of a periodic array of bubbles in a channel, *Mecánica Computacional XXXII* (21):1813–1824.
- [13] Donea, J, Huerta, A, Ponthot, J-Ph, Rodríguez-Ferran, A 2004. Arbitrary Lagrangian–Eulerian methods, *Encyclopedia of computational mechanics*, John Wiley & Sons.

Study of Local Equilibrium Models of Suspended Sediment using Point-Particle Direct Numerical Simulation

Hyun Ho Shin^{a1}, Christian E. Schaerer^a,
Norberto Mangiavacchi^b and Luis M. Portela^c

^aScientific and Applied Computing Laboratory, Polytechnic School, National University of Asuncion, San Lorenzo, Paraguay

^bDepartment of Mechanical Engineering, State University of Rio de Janeiro, Rio de Janeiro, Brazil

^cDepartment of Chemical Engineering, Delft University of Technology, Delft, The Netherlands

Abstract

Local-equilibrium model for the closure of two-fluid models to be used in the suspended sediment transport simulation is evaluated using the point-particle direct numerical simulation.

Keywords: Suspended sediment transport, point-particle, direct numerical simulation, local-equilibrium.

1. INTRODUCTION

The transport of sand-like suspended sediment in turbulent open channel flow is important in many environmental and engineering applications [1, 2]. Complex physics, such as the sediment particles interactions with the fluid turbulence and the near-wall effects, are involved in these phenomena.

The Eulerian-Eulerian (two-fluid) approach can be suitable for the computer simulation of suspended sediment transport, but it requires large amount of modelling in order to represent accurately the complex physics [3]. An approach less restrictive in terms of modelling is Eulerian-Lagrangian (particle-tracking) Direct Numerical Simulation (DNS), which becomes costly to be applied in engineering applications, but a validated Eulerian-Lagrangian DNS can be used as a research tool in order to obtain better physical understanding and for the systematic parametric studies for the two-fluid models [3].

Most engineering simulations in hydraulic is done using convection-diffusion models: Reynolds-Averaged Navier-Stokes (RANS) equations with mixing-length or $k - \varepsilon$ models for the turbulence closure and convection-diffusion

¹E-mail Corresponding Author: hhs82528@gmail.com

transport equations for the sediment. In these models, some important parameters, like the fluid-particle settling velocity have to be determined using empirical ad-hoc models.

In two-fluid models, two sets of averaged equations, one for each phase (continuous: fluid flow, dispersed: sediment particles), coupled through the interfacial stresses, are solved. The two-fluid models are more general and rigorous than convection-diffusion models and allow a systematic development and testing of different physical-based models. Although, two-fluid models are commonly used for solid particles in a gas flow, they usually were not used for sediment transport (solid particle in a liquid flow). Only recently, some works had applied two-fluid models to study some fundamental issues, such as diffusion processes, or velocity lag of sediment [4, 5, 6].

In this work, we evaluate the two-fluid model for sediment transport using particle-tracking DNS, specifically the term named kinetic stresses or particle Reynolds stresses. This term accounts for the particle velocity fluctuations. In order to solve the particle motion using two-fluid models, it is necessary to close the set of equations providing a model for the particle Reynolds stresses. The local-equilibrium model is commonly used for this purpose, and it was initially presented by Tchen [7] and Hinze [8] for homogeneous and steady turbulence. The author of [9] extended it taking into account the “effect of crossing trajectories” and the “continuity effect” on the particles dispersion, and the authors of [10] analysed the extended local-equilibrium model for particles motion in stationary homogeneous fluid turbulence using Large-Eddy Simulation.

For the particle-tracking DNS, the forces of the drag, gravity and surrounding fluid stresses are considered acting on the particle in the center of the particle, considering the size of the particle negligible. This method is known as point-particle, and it was largely used in the particle-tracking DNS and tested with experimental data [3]. The simulation is performed assuming a dilute situation, hence one-way coupling is applicable. Only close to the wall, the motion of the particles is influenced by the size of particles when the particles are touching the bottom wall. We use a virtual bouncing wall to ensure the particle resuspension; the authors of [11, 12] showed that this simple approach gives accurate results.

We compute the ratio of particle to fluid Reynolds stresses for solid sediment particles in liquid fluid flow using point-particle DNS in order to evaluate the local equilibrium model presented by [10].

The next section, equations of motion for the point-particle DNS with

simulations parameters and a brief model descriptions are presented. Then, the last section presents results and concluding remarks.

2. EQUATION OF MOTION FOR PP-DNS AND MODEL DESCRIPTION

The continuous phase is represented by the incompressible Navier-Stokes equations given by:

$$\begin{aligned} \nabla \cdot u_1, \\ \frac{Du_1}{Dt} = -\frac{\nabla p}{\rho_1} + \nu \nabla^2 u_1, \end{aligned}$$

where, u_1 is the fluid velocity, p the pressure, ρ_1 the fluid density, and ν the fluid kinematic viscosity. In this work, we consider particle laden flow in a dilute situation, so, it can be assumed one-way coupling, *i.e.*, the effect of the particle on the fluid flow and particle collision can be neglected.

The motion of the dispersed phase is given by:

$$\frac{du_2}{dt} = \frac{1}{\tau_p}(u_1 - u_2) + \frac{\beta - 1}{\beta}g + \frac{1}{\beta} \frac{Du_1}{Dt},$$

where, $\beta = \rho_2/\rho_1$ (with ρ_2 particle density) is the particle-fluid density ratio, $\tau_p = \beta \frac{d_p^2}{18\nu}$ is the particle relaxation time with d_p particle diameter and g is the gravity acceleration.

We performed DNS simulations of particle laden open channel flow driven by a constant streamwise pressure gradient. The solution of the continuous-phase uses a standard finite volume code on staggered grid for incompressible flows, using a two-step predictor-corrector solver, with second-order Adams-Bashforth scheme. The time step is determined by the Courant stability criterion. Free-slip boundary condition at the top of the channel, and no-slip condition at the bottom-wall are imposed. In the stream and span-wise directions we used periodic boundary conditions. For the discrete phase, we integrated the particle equation of motion using an explicit method with point-particle approach. The motion of the particles is calculated using second order Runge-Kutta scheme and a tri-linear interpolation is employed to calculate the fluid velocity at the particle position. The top and bottom wall is considered as particle bouncing wall. More details of the code can be found in [13].

The shear Reynolds number based on the wall-shear velocity u_τ and channel height H is equal to $Re_\tau = 500$. This gives a bulk Reynolds number, based on the channel height and centreline velocity, of around $Re_b \approx 10,000$. The simulation is performed on a computational domain of size $6H \times 3H \times H$, corresponding to $3,000 \times 1,500 \times 500$ in wall units in the stream (x), span (y) and normal-wise direction (z), respectively. We use a grid of $192 \times 192 \times 192$ nodes. For the stream and span-wise directions, we use a uniform grid spacing, with $\Delta x^+ \approx 15.6$ and $\Delta y^+ \approx 7.8$, and for the wall-normal direction, non-uniform grid spacing with a hyperbolic-tangent stretching: stretching factor used was 1.7 that gives the smallest spacing at the wall ($\Delta z^+ \approx 0.6$) and the largest spacing in the middle of the channel ($\Delta z^+ \approx 4.73$).

The same parameters of the flow and particle used in [11] are chosen:

$$\beta = 1.0367; \quad d_p^+ = 3.47; \quad \tau_p^+ = 0.693; \quad v_t^+ = -0.236.$$

where v_t is the particle terminal velocity. In [11], these parameters are chosen in order to mimic as much as possible the experimental conditions of [14]. Total number of particle tracked is $N_p = 1 \times 10^5$.

The local-equilibrium model for the particle dispersion proposed by [7] and [8] neglecting the added mass and Basset forces is:

$$\langle u'_{2i} u'_{2j} \rangle = \frac{1 + b^2 St_L}{1 + St_L} \langle u'_{1i} u'_{1j} \rangle \quad i, j = x, y, z, \quad (1)$$

where, $b = 1/\beta$, St_L is the Stokes number, and the variables with prime symbol are the fluctuating part of the velocity. The Stokes number St_L relates the ratio of particle relaxation time to the some fluid time scale. The authors of [10] used the eddy-particle interaction time τ_{12} for the fluid time scale:

$$St_L = \frac{\tau_p}{\tau_{12}} \quad (2)$$

The eddy-particle interaction time τ_{12} takes into account the fluid Lagrangian turbulent time scale τ_1 and the crossing trajectories effects proposed by [9]:

$$\tau_{12} = \tau_1 \left[1 + \frac{\beta^2 U_r^2}{\frac{2}{3} k_1} \right]^{-1/2} \quad (3)$$

where, $\beta^2 = 0.45$, U_r is the averaged value of the local relative velocity and k_1 is the fluid turbulent kinetic energy.

3. RESULTS AND CONCLUDING REMARKS

Initially, the particles are released uniformly distributed in the channel. In the initial stage, large amount of particles are deposited on the bottom wall due to the gravity effects, until the particle diffusion balances it. After this, the statistically steady concentration is reached at approximately $t^+ = 5,000$. The results is obtained using data from $t^+ = 12,750$ to $t^+ = 25,000$.

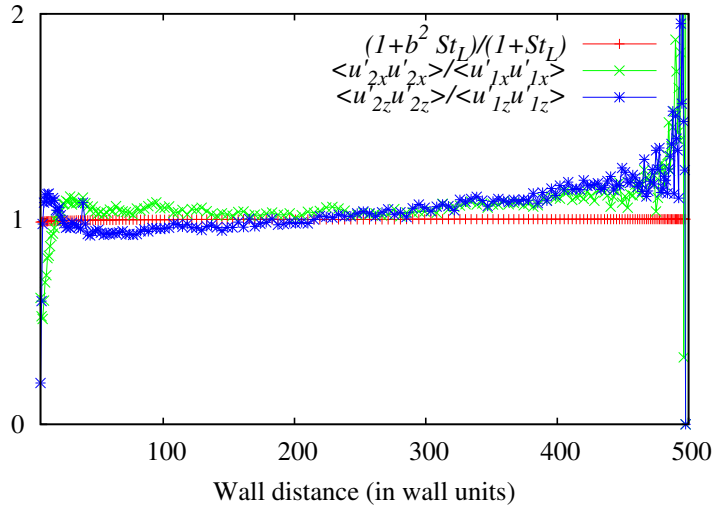


Figure 1 - Evaluation of the local-equilibrium model.

The Figure 1 shows the values of the coefficient of the local-equilibrium model, $(1 + b^2 St_L)/(1 + St_L)$ from the equation (1), and the ratios of particle Reynolds stresses to the fluid Reynolds stresses. The wall distance zero is the bottom wall, and 500 is top free surface. The values of the Reynolds stresses ratios computed are roughly constant with value about 1. Slight variation near the bottom wall could be a consequence of the near wall effect, and the variations near free surface is not clear, but it seems that there are not enough particles to compute an accurate statistics, this because of the gravity. From the figure, it can be observed that the value of $(1 + b^2 St_L)/(1 + St_L)$ is almost constant. Taking this result into consideration, it seems that the introduction of the quite complicated formulation for the particle Reynolds

stresses is not necessary, and a simple model for particle Reynolds stresses being equal to the fluid Reynolds stresses, or at least proportional to some constant ranging from 1 to 1.1 could be reasonable.

Further research for the closure of others terms in the two-fluid models, like drift velocity model, can be evaluated and analysed using point-particle DNS.

References

- [1] MacArthur, RC, Neill, CR, Hall, BR, Galay, VJ, Shvidchenko, AB, 2008. Overview of sedimentation engineering. *Sedimentation Engineering: Processes, Measurement, Modeling, and Practice*, ASCE Manuals and Reports on Engineering Practice 110: 1-20.
- [2] Chanson, H, 2004. *Hydraulics of open channel flow: An introduction*. 2nd Edition. Butterworth-Heinemann: Oxford.
- [3] Portela, LM, Oliemans, RVA, 2006. Possibilities and limitations of computer simulations of industrial turbulent dispersed multiphase flows, *Flow Turbulence Combust* 77: 381-403.
- [4] Greimann, B, Muste, M, Holly, F, 1999. Two-phase formulation of suspended sediment transport, *Journal of Hydraulic Research* 43 (4): 479-500.
- [5] Jiang, J, Law, AWK, Cheng, NS, 2004. Two-phase modeling of suspended sediment distribution in open channel flows, *Journal of Hydraulic Research* 42 (3): 273-281.
- [6] Toorman, EA, 2008. Vertical mixing in the fully developed turbulent layer of sediment-laden open-channel flow, *Journal of Hydraulic Engineering* 134 (9): 1225-1235.
- [7] Tchen, CM, 1947. Mean value and correlation problems connected with the motion of small particles suspended in a turbulent fluid, Martinus Nijhoff: The Hague.
- [8] Hinze, JO, 1959. *Turbulence: An introduction to its mechanism and theory*, McGraw-Hill: New York.

- [9] Csanady, GT, 1963. Turbulent diffusion of heavy particles in the atmosphere, *Journal of the Atmospheric Sciences* 20 (3): 201-208.
- [10] Deutsch, E, Simonin, O, 1991. Large eddy simulation applied to the motion of particles in stationary homogeneous fluid turbulence, *Proc. of ASME-FED* 110: 35-42
- [11] Cargnelutti, M, Portela, LM, 2007. In influence of the resuspension on the particle sedimentation in wall-bounded turbulent flows. In *Sixth International Conference on Multiphase Flow 2007*, Leipzig, Germany.
- [12] Soldati, A, Marchioli, C, 2012. Sedimentation transport in steady turbulent boundary layers: Potentials, limitations, and perspectives for Lagrangian tracking in DNS and LES, *Advances in Water Resources* 48: 18-30.
- [13] Portela, LM, Oliemans, R, 2003. Eulerian-Lagrangian DNS/LES of particle-turbulence interactions in wall-bounded flows, *International Journal for Numerical Methods in Fluids* 43 (9): 1045-1065.
- [14] Breugem, WA, Uijtewaal, WSJ, 2006. In A PIV/PTV experiment on sediment transport in a horizontal open channel flow, *River Flow* 1: 789-798.

Reconstruction of the Langevin Equation from some Non-Markovian Time Series

Zbigniew Czechowski^{a1}

^aInstitute of Geophysics Polish Academy of Sciences, Warsaw, Poland

Abstract

The Langevin equation for some non-Markov processes was introduced as a macroscopic model of various phenomena. The numerical Modified Histogram Procedure (MHP) of reconstruction of the equation from time series was proposed. An efficiency of MHP was tested on simulated time series (with short and long-tail distributions) generated by different Langevin equations. For exemplary geophysical time series' appropriate Langevin equations were reconstructed.

Keywords: Stochastic processes, non-Markov processes, nonlinear time series modeling, persistence, Ito equation, Fokker-Planck equation.

1. INTRODUCTION

The main task of time series analysis is to understand the underlying mechanism that generates the observed data and, in turn, to forecast future values. In this paper we focus on a stochastic approach, therefore we assume that generating mechanism is probabilistic and that the observed series is a realization of a stochastic process. For example, many geophysical phenomena, because of their complexity and our ignorance about details of internal mechanisms and boundary conditions, should be described by using stochastic processes. Geophysical time series show features like: fractal patterns, long-tail inverse-power tails of distribution functions, long correlations and persistence, which cannot be described by linear stochastic models. Investigation of these phenomena requires using of some nonlinear methods of stochastic modeling.

Modeling lies at the heart of time series analysis. In a linear case, well known modeling procedures were elaborated (ARMA, ARIMA, SARIMA, etc.). However, methods of nonlinear time series modeling are much less understood than classical methods for linear cases. The Langevin equation introduces a nonlinearity in drift and diffusion terms and leads to a wide

¹E-mail Corresponding Author: zczech@igf.edu.pl

class of distributions (from Gaussian up to long tail). Therefore, using the Langevin equation may provide some progress in the field of effective methods of constructing nonlinear models from time series data.

A numerical procedure of reconstructing the Langevin equation from time series was proposed in [1]. This direct procedure, based on the histogram of joined distribution function, leads to approximation of terms in the equation. However, the procedure was derived only for stationary Markov processes.

In this paper we extend the approach to stationary non-Markov stochastic processes. A novel Langevin-type dynamics with non-Markovian features is introduced and an associated Fokker-Planck-like equation for distribution function is derived. Then, the numerical histogram procedure must be considerably modified in order to be able to reconstruct the Langevin-type equation for non-Markov time series. We propose the Modified Histogram Procedure. The performance of the new reconstruction procedure is analyzed on simulated time series which are generated by different Langevin equations with memory.

2. THE LANGEVIN EQUATION FOR SOME NON-MARKOV PROCESSES

Discrete Langevin equation has the form:

$$y(t + \Delta t) = y(t) + a(y(t))\Delta t + \sqrt{b(y(t))}\sqrt{\Delta t}R_t \quad (1)$$

and describes an evolution of Markov process $y(t)$ of order 1. Function $a(y)$ corresponds to deterministic force (drift) and $b(y)$ to the stochastic force (diffusion), R_t are independent random variables with normal density.

For non-Markov processes memory or non-local effects must be taken into account. In this paper, for simplicity, we assume that the next state $y(t + \Delta t)$ of the process is dependent not only on the present state $y(t)$ but also on the previous state $y(t - \tau)$ with a fixed lag τ . In order to introduce the dependence on the past, we modify the Langevin equation by introducing to the diffusion term an additional random function $c(\Delta^L y, d, r_t)$ which determines the sign of the diffusion term i.e.,

$$y(t + \Delta t) = y(t) + a(y(t))\Delta t + c(y(t) - y(t - \tau), d, r_t)\sqrt{b(y(t))}\sqrt{\Delta t}|R_t|, \quad (2)$$

where the parameter d and random variable r_t will be explained later. The modification enables to describe persistent processes and seasonal effects.

For persistent processes the function $c(\Delta^L y, d, r_t)$ has the following form:

$$c(\Delta y, d, r_t) = \begin{cases} 1 & \text{if } (\Delta y \geq 0 \wedge r_t \geq d) \vee (\Delta y < 0 \wedge r_t < d) \\ -1 & \text{if } (\Delta y < 0 \wedge r_t \geq d) \vee (\Delta y \geq 0 \wedge r_t < d) \end{cases} \quad (3)$$

where $\Delta y(t) = y(t) - y(t - \Delta t)$, r_t is a random variable with uniform distribution in $[0, 1]$ and d is the persistence parameter ($0 \leq d \leq 1$). The function is keeping the tendency of increase of $y(t)$ in the next step with probability $1 - d$ (tendency of decrease in the next step with probability $1 - d$). For $d = 0$ we have the full persistence, $d = 1/2$ leads to the Langevin equation without the modification, for $1/2 < d < 1$ the process is antipersistent.

For the case of time series with periodical correlation function, the function $c(\Delta^L y, d, r_t)$ is defined as follows:

$$c(\Delta^L y, d, r_t) = \begin{cases} 1 & \text{if } (\Delta^L y < 0 \wedge r_t > d) \vee (\Delta^L y \geq 0 \wedge r_t \leq d) \\ -1 & \text{if } (\Delta^L y < 0 \wedge r_t \leq d) \vee (\Delta^L y \geq 0 \wedge r_t > d) \end{cases} \quad (4)$$

and depends on the sign of the difference $\Delta^L y(t) = y(t) - y(t - (L - 1)\Delta t)$, where τ is equal to the period $L\Delta t$. Here the function $c(\Delta^L y, d, r_t)$ represents a relationship between the values of $y(t - (L - 1)\Delta t)$ and those of $y(t + \Delta t)$, which are separated by the interval $L\Delta t$. For $d = 0$ the interrelation is maximal. The condition $d = 1$ leads to the Langevin equation without the modification.

3. THE RECONSTRUCTION PROCEDURE

The idea of the reconstruction procedure arises from a correspondence of the Langevin equation with the Fokker-Planck equation and bases on numerical estimations of joint distribution function. The histogram procedure (HP) [1] fails in the case of Langevin equation with memory, because it leads to a wrong reconstruction of the function $a(y)$. However, the procedure estimates the function $b(y)$ correctly.

In the case of non-Markov processes $y(t)$ the following equation describing an evolution of distribution function $p(y, t)$ can be derived [2]:

$$\frac{\partial}{\partial t} p(y, t) = -\frac{\partial}{\partial y} [a(y)p(y, t) + E(y)p(y, t)] + \frac{1}{2} \frac{\partial^2}{\partial y^2} [b(y)p(y, t)] \quad (5)$$

The function $E(y)$ which modifies the drift term contains a contribution of memory effects. However, basing on assumptions concerning the function

$c(\Delta^L y, d, r_t)$, it is difficult to derive an analytical form of the function. For reconstruction of Eq. (2) from time series we propose the Modified Histogram Procedure (MHP) in which the contribution given by function $E(y)$ can be estimated. The MHP algorithm used in our work is summarized in three steps as follows:

1. First, from the time series under investigation we estimate the parameter d . For persistent processes it corresponds to the Hurst exponent H , which can be found by using the Detrended Fluctuation Analysis. For processes with periodical correlation function the interdependence parameter d can be deduced from a sum of products $sign(\Delta^L y(i))$ and $sign(\Delta y(i + 1))$.
2. Next, we apply the histogram procedure (HP) which leads to a first reconstruction $a_1(y)$ of function $a(y)$ and $b_1(y)$ of function $b(y)$. In the procedure an appropriate method of estimation of joint distribution function is crucial. Various methods can be applied, for example: the histogram estimate or for the smooth function - the kernel density estimation (KDE) for bivariate data. According to Eq. (5) the reconstructed function $a_1(y)$ differs from $a(y)$ for a deviation $E(y)$, but $b_1(y)$ should be a good estimator of function $b(y)$.
3. In the third step a magnitude of the deviation is estimated. To this end, the time series generated by the Langevin equation (2) with the parameter d estimated in step 1 and reconstructed functions $a_1(y)$ and $b_1(y)$ is treated as the input to the second use of the histogram procedure. At the result, functions $a_2(y)$ and $b_2(y)$ are reconstructed. According to our assumption that the deviation of function $a(y)$ is similar in the first and the second use of the histogram procedure, we calculate the difference $a_2(y) - a_1(y)$ and subtract it from the first reconstruction $a_1(y)$, i.e., the proper reconstruction should be $a_R(y) = a_1(y) - [a_2(y) - a_1(y)]$. Both reconstructions of $b(y)$ are similar, therefore we can put $b_R(y) = (b_1(y) + b_2(y))/2$.

The reconstructed Langevin equation has a form Eq. (2) with $a(y) = a_R(y)$, $b(y) = b_R(y)$ and the parameter d estimated in step 1.

4. TESTING OF THE MODIFIED HISTOGRAM PROCEDURE

For testing of the modified histogram method (MHP) we use the Langevin equation (2) with different functions $a(y)$ and $b(y)$ and different values of the parameter d . This makes it possible to compare reconstructed functions to the input ones. We choose four examples which represent different stochastic processes with short and long-tail stationary distribution functions (Gaussian, exponential, lognormal and inverse-gamma) to show that the MHP is an effective procedure for reconstruction of the Langevin equation from many kinds of time series.

The similar procedure was applied to two examples of geophysical time series: the persistent one [3] and that with a periodical correlation function [4]. The reconstructed Langevin equations constitute macroscopic models of these phenomena.

ACKNOWLEDGMENTS: This work was financed by the project of the National Science Centre (contract no. DEC-2012/05/B/ST10/00598).

References

- [1] SIEGERT, S, FRIEDRICH, R, PEINKE ,J, 1998. Analysis of data sets of stochastic systems, *Physics Letters A* 243: 275-280.
- [2] GARDINER CW, 1985. *Handbook of Stochastic Methods for Physics, Chemistry and the Natural Sciences*, Springer-Verlag, Berlin Heidelberg.
- [3] CZECHOWSKI, Z, 2013. On reconstruction of the Ito-like equation from persistent time series, *Acta Geophysica* 61: 1504-1521.
- [4] CZECHOWSKI, Z, TELESKA, L, 2013. Construction of a Langevin model from time series with a periodical correlation function: Application to wind speed data, *Physica A* 392: 55925603.

3rd Conference of Computational Interdisciplinary Sciences
**Architecture of Environmental Risk Modelling: for a faster
and more robust response to natural disasters**

Dario Rodriguez-Aseretto ^{a,1}, Christian Schaerer ^b, Daniele de Rigo ^{a,c}

^a European Commission, Joint Research Centre, Institute for Environment and Sustainability, Ispra (VA), Italy.

^b Polytechnic School, National University of Asuncion, San Lorenzo, Central, Paraguay.

^c Politecnico di Milano, Dipartimento di Elettronica, Informazione e Bioingegneria, Milano, Italy.

Abstract

Demands on the disaster response capacity of the European Union are likely to increase, as the impacts of disasters continue to grow both in size and frequency. This has resulted in intensive research on issues concerning spatially-explicit information and modelling and their multiple sources of uncertainty. Geospatial support is one of the forms of assistance frequently required by emergency response centres along with hazard forecast and event management assessment. Robust modelling of natural hazards requires dynamic simulations under an array of multiple inputs from different sources. Uncertainty is associated with meteorological forecast and calibration of the model parameters. Software uncertainty also derives from the data transformation models (D-TM) needed for predicting hazard behaviour and its consequences. On the other hand, social contributions have recently been recognized as valuable in raw-data collection and mapping efforts traditionally dominated by professional organizations. Here an architecture overview is proposed for adaptive and robust modelling of natural hazards, following the *Semantic Array Programming* paradigm to also include the distributed array of social contributors called *Citizen Sensor* in a semantically-enhanced strategy for D-TM modelling. The modelling architecture proposes a multi-criteria approach for assessing the array of potential impacts with qualitative rapid assessment methods based on a *Partial Open Loop Feedback Control* (POLFC) schema and complementing more traditional and accurate a-posteriori assessment. We discuss the computational aspect of environmental risk modelling using array-based parallel paradigms on *High Performance Computing* (HPC) platforms, in order for the implications of urgency to be introduced into the systems (Urgent-HPC).

Keywords: Geospatial, Integrated Natural Resources Modelling and Management, Semantic Array Programming, Warning System, Remote Sensing, Parallel Application, High Performance Computing, Partial Open Loop Feedback Control

¹E-mail Corresponding Author: dario.rodriquez@jrc.ec.europa.eu

1. INTRODUCTION: CONTEXT, PITFALLS AND THE SCIENCE-POLICY INTERFACE

Europe experienced a series of particularly severe disasters in the recent years [1, 2], with worrying potential impacts of similar disasters under future projected scenarios of economy, society and climate change [3, 4]. They range from flash floods [5, 6, 7] and severe storms in Western Europe with an expected increasing intensity trend [8], large-scale floods in Central Europe [9], volcanic ash clouds [10, 11, 12] (e.g. after the Eyjafjallajkull eruption), large forest fires in Portugal and Mediterranean countries [13, 14]. Biological invasions such as emerging plant pests and diseases have the potential to further interact e.g. with wildfires [15] and to impact on ecosystem services [16] and economy with substantial uncertainties [17].

It should be underlined that these recent highlights are set in the context of systemic changes in key sectors [18, 19, 20] which overall may be expected to at least persist in the next decades. As a general trend, demands on the EU's resilience in preparedness and disaster response capacity are likely to increase, as the impacts of disasters continue to grow both in size and frequency, even considering only the growing exposure (societal factors) [21, 22]. The aforementioned examples of disturbances are often characterised by non-local system feedbacks and off-site impacts which may connect multiple natural resources (system of systems) [23, 24, 25]. In this particular multifaceted context [26, 27, 28], landscape [29] and ecosystem dynamics show intense interactions with disturbances [30].

As a consequence, classical disciplinary and domain-specific approaches which might be perfectly suitable at local-scale may easily result in unacceptable simplifications within a broader context. A broad perspective is also vital for investigating future natural-hazard patterns at regional/continental scale and adapting preparedness planning [31, 32, 33]. The complexity and uncertainty associated with these interactions – along with the severity and variety of the involved impacts [34] – urge robust, holistic coordinated [35] and transparent approaches [36, 37]. At the same time, the very complexity itself of the control-system problems involved [38, 39, 40] may force the analysis to enter into the region of deep-uncertainty [41].

The mathematization of systems in this context as a formal control problem should be able to establish an effective science-policy interface, which is *not* a trivial aspect. This is easily recognised even just considering the peculiarities – which have been well known for a long time – of geospatially-aware environmental data [42] and decision support systems [43, 44, 45], their entanglement with growingly complex ICT aspects [46, 47] and their not infrequent cross-sectoral characterisation. Several pitfalls may degrade the real-world usefulness of the mathematization/implementation process. While it is relatively intuitive how a poor mathematization with a too simplistic approach might result in a failure, subtle pitfalls may lie even where an “appropriately advanced” theoretical approach is proposed.

Mathematization should resist *silo thinking* [48, 49] temptations such as academic solution-driven pressures [37, 50] to force the problem into fashionable “hot topics” of control theory: robust approximations of the real-world broad complexity may serve egregiously instead of state-of-art solutions of oversimplified problems.

Other long-lasting academic claims are “towards” fully automated scientific workflows in computational science, maybe including self-healing and self-adapting capabilities of the computational models implementing the mathematization. These kinds of claims might easily prompt some irony [51] among experienced practitioners in wide-scale transdisciplinary modelling for environment (WSTMe, [52]) as a never-ending research Pandora’s box with doubtful net advantages [53]. Complex, highly uncertain and sensitive problems for policy and society, as WSTMe problems typically are, will possibly never be suitable for full automation: even in this family of problems, “humans will always be part of the computational process” [54] also for vital accountability aspects [55].

While a certain level of autonomic computing [56] capabilities might be essential for the evolvability and robustness of WSTMe (in particular, perhaps, a higher level of semantic awareness in computational models and a self-adapting ability to scale up to the multiple dimensions of the arrays of data/parameters; see next section), here the potential pitfall is the illusion of *fully automating* WSTMe. The domain of applicability of this puristic academic *silo* – although promising for relatively simple, well-defined (and not too policy-sensitive) case studies – might be intrinsically too narrow for climbing up to deal with the *wicked problems* typical of complex environmental systems [57, 58, 59].

The discussed pitfalls might deserve a brief summary. First, perhaps, is the risk of “solving the wrong problem precisely” [60] by neglecting key sources of uncertainty – e.g. unsuitable to be modelled within the “warmly supported” solution of a given research group. During emergency operations, the risks of providing a “myopic decision support” should be emphasised; i.e. suggesting inappropriate actions [61] – e.g. inaction or missing precaution – due to the potential overwhelming lack of information [62] or the oversimplification/underestimation of potential chains of impacts due to the lack of computational resources for a decent (perhaps even qualitative and approximate) rapid assessment of them.

Overcoming these pitfalls is still an open issue. Here, we would like to contribute to the debate by proposing the integrated use of some mitigation approaches. We focus on some general aspects of the *modelling architecture* for the computational science support, in order for emergency-operators, decision-makers, stakeholders and citizens to be involved in a participatory [63] information and decision support system which assimilates uncertainty and precaution [64, 57]. Since no silver bullet seems to be available for mitigating the intrinsic wide-extent of complexity and uncertainty in environmental risk modelling, an array of approaches is

integrated and the computational aspects are explicitly connected with the supervision and distributed interaction of human expertise. This follows the idea that the boundary between classical control-theory management strategies for natural resources and hazards (driven by automatic control problem formulations – “minimize the risk score function”) and scenario modelling under deep-uncertainty (by e.g. merely supporting emergency-operators, decision-makers and risk-assessors with understandable information – “sorry, no such thing as a risk score function can be precisely defined”) is fuzzy. Both modelling and management aspects may be computationally intensive and their integration is a transdisciplinary problem (*integrated natural resources modelling and management*, INRMM [65]).

2. ENVIRONMENTAL RISK MODELLING - ARCHITECTURE

Figure 1 illustrates a general modelling conceptualization where the interactions among natural hazard behaviour, related transdisciplinary impacts, risk management and control strategies are taken into account. The special focus on the many sources of uncertainty [36] leads to a robust semantically-enhanced modelling architecture based on the paradigm of Semantic Array Programming (SemAP) [66, 67], with an emphasis on the array of input, intermediate and output data/parameters and the array of data-transformation modules (D-TM) dealing with them.

Arrays of hazard models $h_j^{\zeta_f}(\cdot)$, dynamic information forecasts X^{ζ_x} (i.e. meteorology) and static parametrisation θ^{ζ_θ} (i.e. spatial distribution of land cover) are considered. Their multiplicity derives from the many sources on uncertainty $\zeta = \{\zeta_f, \zeta_x, \zeta_\theta\}$ which affect their estimation (or implementation, for the D-TM software modules $f_i^{\zeta_f}(\cdot)$ which are the building blocks of the hazard models $h_j^{\zeta_f}(\cdot)$).

Furthermore, during emergency modelling support the lack of timely and accurate monitoring systems over large spatial extents (e.g. at the continental scale) may imply a noticeable level of uncertainty to affect possibly even the location of natural hazards (*geoparsing* [68] uncertainty). This peculiar information gap may be mitigated by integrating remote sensing (e.g. satellite imagery) with a distributed array of social contributors (Citizen Sensor [69, 70, 71]), exploiting mobile applications (Apps) and online social networks [72]. Remote sensing and the Citizen Sensor are here designed to cooperate by complementing accurate (but often less timely) geospatial information with distributed alert notifications from citizens, which might be timely but not necessarily accurate. Their safe integration implies the supervision of human expertise, even if the task may be supported by automatic tools [73]. Assessing the evolution in the timespan $\mathcal{U}^t = [t_{\text{begin}}, t_{\text{end}}]$ of a certain hazard event for the associated array of impacts $C^{k,t}$ may be also complex (e.g. [41, 74, 75]). In particular, the array of impacts is often irreducible to a unidimensional quantity (e.g. monetary cost) [76, 77].

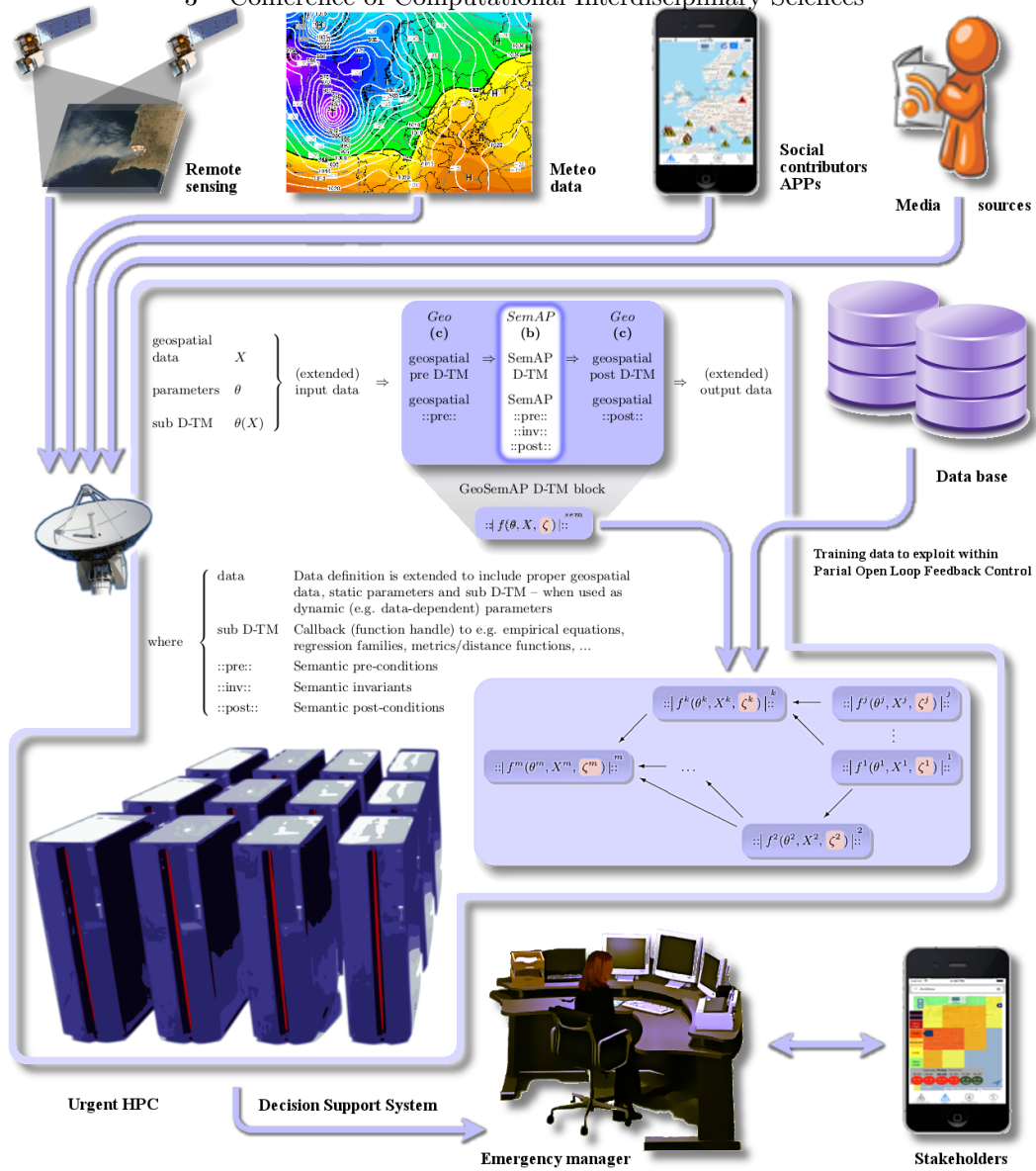


Figure 1 - Modular architecture for environmental risk modelling. Based on Urgent HPC, it follows the Semantic Array Programming paradigm (image adapted from [36, 52]) integrating as inputs remote sensing, meteo data and the Citizen Sensor.

The analysis of non-trivial systems subject to environmental risk and natural resources management may naturally lead to multi-objective (multi criteria) control problems, which might benefit from advanced machine learning techniques for

mitigating the involved huge computational costs [78]. Indeed, the multiplicity of modelling dimensions (states; controls; uncertainty-driven arrays of parameters and scenarios; arrays of D-TM modules to account for software uncertainty) may easily lead to an exponential increase of the required computational processes (the so called “curse of dimensionality”). A viable mitigation strategy might be offered by HPC tools (such as Urgent HPC [79, 80, 81]) in order to sample high-dimensional modelling space with a proper method.

Box 1 – In a nutshell.

Context Demands on the EU’s resilience in preparedness and disaster response capacity are likely to increase, as the impacts of disasters continue to grow.

- Classical disciplinary and domain-specific approaches which might be perfectly suitable at local-scale may result in unacceptable simplifications in a broader context.

Pitfalls Mathematization of systems in this context as a formal control problem should be able to establish an *effective* science-policy interface. Academic *silo thinking* should stop advertising solution-driven oversimplification to fit control theory “hot topics”.

- Although in this family of problems “humans will always be part of the computational process” (despite any academic potential illusion of fashionable *full automation*),
- evolvability (for adapting models to new emerging needs and knowledge) and robustness (for supporting uncertainty-aware decision processes) would still need
 - ▷ a higher level of semantic awareness in computational models and
 - ▷ a self-adapting ability to scale up to the multiple dimensions of the arrays of data/parameters.

Multiplicity: uncertainty and complexity In this context, the boundary between classical control-theory management strategies for natural resources and hazards and scenario modelling under deep-uncertainty is fuzzy (INRMM).

- A key aspect of soundness relies on explicitly considering the multiple dimensions of the problem and the array of uncertainties involved.
- As no silver bullet seems to be available for reliably attacking this amount of uncertainty and complexity, an integration of methods is proposed.

Mitigating with an integrated approach Array programming is well-suited for easily managing a multiplicity of arrays of hazard models, dynamic input information, static parametrisation and the distribute array of social contributions (Citizen Sensor).

- *Array-based abstract* – thus better scalable – *modularisation* of the data-transformations (D-TM), and a *semantically-enhanced* design of the D-TM structure and interactions (Semantic Array Programming) is proposed to consider also the array of uncertainties (data, modelling, geoparsing, software uncertainty) and the array of criteria to assess the potential impacts associated with the hazard scenarios.
- The unevenly available information during an emergency event may be efficiently exploited by means of a POLFC schema.
- Its demanding computations may become affordable during an emergency event with an appropriate array-based parallelisation strategy within Urgent-HPC.

SemAP can simplify WSTMe modelling of nontrivial static [82, 83] and dynamic [41, 75, 84] geospatial quantities. Under the SemAP paradigm, the generic i -th D-TM module $Y_i = f_i(\theta_i, X_i)$ is subject to the semantic checks sem_i as pre-, post-conditions and invariants on the inputs θ_i, X_i , outputs Y_i and the D-TM itself $f_i(\cdot)$. The control problem is associated with the unevenly available dynamic updates of field measurements and other data related to an on-going hazard emergency. An *Emergency Manager* may thus be interested in assessing the best control strategy $u^t(\cdot)$ given a set of impacts and their associated costs as they can be approximately estimated (rapid assessment) with the currently available data. This data-driven approach can be implemented as Partial Open Loop Feedback Control (POLFC) approach [85] for minimizing the overall costs associated with the natural hazard event, from the time $t \in \mathcal{U}^t$ onwards:

$$u^t(\cdot) = \arg \min_{u \in U_{t, t_{end}}^u} [\mathcal{C}^{1,t} \mathcal{C}^{2,t} \dots \mathcal{C}^{k,t} \dots \mathcal{C}^{n,t}] \quad (1)$$

where the k -th cost $\mathcal{C}^{k,t}$ is linked to the corresponding impact assessment criterion. This POLFC schema within the SemAP paradigm may be considered a semantically-enhanced dynamic data-driven application system (DDDAS) [41, 75, 84]. Finally, the Emergency Manager may communicate the updated scenarios of the emergency evolution (by means of geospatial maps and other executive summary information) in order for decision-makers and stakeholders to be able to assess the updated multi-criteria pattern of costs and the preferred control options. This critical communication constitutes the science-policy interface and must be as supportive as possible. It is designed to exploit web map services (WMS) [86, 87] (on top of the underpinning free software for WSTMe, e.g. [88]) which may be accessed in a normal browser or with specific Apps for smart-phones [73].

3. CONCLUDING REMARKS

NSF Cyberinfrastructure Council report reads: *While hardware performance has been growing exponentially - with gate density doubling every 18 months, storage capacity every 12 months, and network capability every 9 months - it has become clear that increasingly capable hardware is not the only requirement for computation-enabled discovery. Sophisticated software, visualization tools, middleware and scientific applications created and used by interdisciplinary teams are critical to turning flops, bytes and bits into scientific breakthroughs* [89]. Transdisciplinary environmental problems such as the ones dealing with complexity and deep-uncertainty in supporting natural-hazard emergency might appear as seemingly intractable [90]. Nevertheless, approximate rapid-assessment based on computationally intensive modelling may offer a new perspective at least able to support emergency operations and decision-making with qualitative or semi-

quantitative scenarios. Even a partial approximate but timely investigation on the potential interactions of the many sources of uncertainty might help emergency managers and decision-makers to base control strategies on the best available – although typically incomplete – sound scientific information. In this context, a key aspect of soundness relies on explicitly considering the multiple dimensions of the problem and the array of uncertainties involved. As no silver bullet seems to be available for reliably attacking this amount of uncertainty and complexity, an integration of methods is proposed, inspired by their promising synergy. Array programming is perfectly suited for easily managing a multiplicity of arrays of hazard models, dynamic input information, static parametrisation and the distribute array of social contributions (Citizen Sensor). The transdisciplinary nature of complex natural hazards – their need for an unpredictably broad and multifaceted readiness to robust scalability – may benefit (1) from a disciplined *abstract modularisation* of the data-transformations which compose the models (D-TM), and (2) from a *semantically-enhanced* design of the D-TM structure and interactions. These two aspects define the Semantic Array Programming (SemAP, [66, 67]) paradigm whose application – extended to geospatial aspects [52] – is proposed to consider also the array of uncertainties (data, modelling, geoparsing, software uncertainty) and the array of criteria to assess the potential impacts associated with the hazard scenarios. The unevenly available information during an emergency event may be efficiently exploited by means of a partial open loop feedback control (POLFC, [85]) schema, already successfully tested in this integrated approach [41, 75, 84] as a promising evolution of adaptive data-driven strategies [91]. Its demanding computations may become affordable during an emergency event with an appropriate array-based parallelisation strategy within Urgent-HPC.

References

- [1] SIPPEL, S., OTTO, F.E.L., 2014. [Beyond climatological extremes - assessing how the odds of hydrometeorological extreme events in South-East Europe change in a warming climate](#). *Climatic Change*: 1-18.
- [2] CIRELLA, G.T., et al, 2014. [Natural hazard risk assessment and management methodologies review: Europe](#). In: Linkov, I. (Ed.), *Sustainable Cities and Military Installations*. NATO Science for Peace and Security Series C: Environmental Security. Springer Netherlands, pp. 329-358.
- [3] CISCAR, J. C., et al, 2013. [Climate impacts in Europe: an integrated economic assessment](#). In: *Impacts World 2013 - International Conference on Climate Change Effects*. Potsdam Institute for Climate Impact Research (PIK) e. V., pp. 87-96.
- [4] CISCAR, J. C., et al, 2014. [Climate Impacts in Europe - The JRC PESETA II project](#). Vol. 26586 of EUR - Scientific and Technical Research. Publ. Off. Eur. Union, 155 pp.
- [5] DANKERS, R., FEYEN, L., 2008. [Climate change impact on flood hazard in Europe: An assessment based on high-resolution climate simulations](#). *J. Geophys. Res.* 113(D19):D19105+.
- [6] GAUME, E., et al, 2009. [A compilation of data on European flash floods](#). *Journal of Hydrology* 367(1-2): 70-78.

- [7] MARCHI, L., et al, 2010. [Characterisation of selected extreme flash floods in Europe and implications for flood risk management](#). Journal of Hydrology 394(1-2): 118-133.
- [8] FESER, F., et al, 2014. [Storminess over the North Atlantic and Northwestern Europe - a review](#). Quarterly Journal of the Royal Meteorological Society.
- [9] JONGMAN, B., et al, 2014. [Increasing stress on disaster-risk finance due to large floods](#). Nature Climate Change 4 (4): 264-268.
- [10] SELF, S., 2006. [The effects and consequences of very large explosive volcanic eruptions](#). Philosophical Transactions of the Royal Society A: Mathematical, Physical and Engineering Sciences 364(1845): 2073-2097.
- [11] SWINDLES, G. T., et al, 2011. [A 7000 yr perspective on volcanic ash clouds affecting northern Europe](#). Geology 39(9): 887-890.
- [12] GRAMLING, C., 2014. [As volcano rumbles, scientists plan for aviation alerts](#). Science 345(6200): 990.
- [13] ALLARD, G., et al, 2013. [State of Mediterranean forests 2013](#). FAO, 177 pp.
- [14] SCHMUCK, G., et al, 2014. [Forest Fires in Europe, Middle East and North Africa 2013](#). Publications Office of the European Union. 107 pp.
- [15] NIJHUIS, M., 2012. [Forest fires: Burn out](#). Nature 489 (7416), 352-354.
- [16] BOYD, I.L., et al, 2013. [The consequence of tree pests and diseases for ecosystem services](#). Science 342 (6160): 1235773+.
- [17] VENETTE, R.C., et al, 2012. [Summary of the international pest risk mapping workgroup meeting sponsored by the cooperative research program on biological resource management for sustainable agricultural systems](#). In: 6th International Pest Risk Mapping Workgroup Meeting: "Advancing risk assessment models for invasive alien species in the food chain: contending with climate change, economics and uncertainty". Organisation for Economic Co-operation and Development (OECD), pp. 1-2.
- [18] MAES, J., et al, 2013. [Mapping and Assessment of Ecosystems and their Services - An analytical framework for ecosystem assessments under action 5 of the EU biodiversity strategy to 2020](#). Publications office of the European Union, 57 pp.
- [19] EUROPEAN COMMISSION, 2013. [Communication from the commission to the European Parliament, the Council, the European Economic and Social Committee and the Committee of the Regions - A new EU forest strategy: for forests and the forest-based sector](#). No. COM(2013) 659 final. Communication from the Commission to the Council and the European Parliament.
- [20] EUROPEAN COMMISSION, 2013. [Commission staff working document accompanying the document: Communication from the commission to the European Parliament, the Council, the European Economic and Social Committee and the Committee of the Regions - a new EU forest strategy: for forests and the forest-based sector](#). Commission Staff Working Document 2013 (SWD/2013/0342 final), 98pp.
- [21] BARREDO, J. I., 2007. [Major flood disasters in Europe: 1950-2005](#). Natural Hazards 42(1): 125-148.
- [22] BARREDO, J. I., 2010. [No upward trend in normalised windstorm losses in Europe: 1970-2008](#). Natural Hazards and Earth System Science 10(1): 97-104.
- [23] EVANS, M. R., et al, 2012. [Predictive ecology: systems approaches](#). Philosophical transactions of the Royal Society of London. Series B, Biological sciences 367(1586): 163-169.
- [24] PHILLIS, Y. A., KOUIKOGLU, V. S., 2012. [System-of-Systems hierarchy of biodiversity conservation problems](#). Ecological Modelling 235-236: 36-48.
- [25] LANGMANN, B., 2014. [On the role of climate forcing by volcanic sulphate and volcanic ash](#). Advances in Meteorology 2014: 1-17.
- [26] GOTCRET, M. V., WHITE, D., 2001. [Assessing the impact of integrated natural resource management: Challenges and experiences](#). Ecology and Society 5 (2): 17+

- [27] HAGMANN, J., et al, 2001. [Success factors in integrated natural resource management R&D: Lessons from practice](#). Ecology and Society 5 (2), 29+.
- [28] ZHANG, X., et al, 2004. [Scaling issues in environmental modelling](#). In: Wainwright, J., Mulligan, M. (Eds.), Environmental modelling : finding simplicity in complexity. Wiley.
- [29] ESTREGUIL, C., et al, 2013. [Forest landscape in Europe: Pattern, fragmentation and connectivity](#). EUR - Scientific and Technical Research 25717 (JRC 77295), 18 pp.
- [30] TURNER, R., 2010, [Disturbance and landscape dynamics in a changing world](#). Ecology, 91 10: 2833-2849.
- [31] Van WESTEN, C.J., 2013. [Remote sensing and GIS for natural hazards assessment and disaster risk management](#). In: Bishop, M. P. (Ed.), Remote Sensing and GIScience in Geomorphology. Vol. 3 of Treatise on Geomorphology. Elsevier, pp. 259-298.
- [32] URBAN, M.C., et al, 2012. [A crucial step toward realism: responses to climate change from an evolving metacommunity perspective](#). Evolutionary Applications 5 (2): 154-167.
- [33] BAKLANOV, A., 2007. [Environmental risk and assessment modelling - scientific needs and expected advancements](#). In: Ebel, A., Davitashvili, T. (Eds.), Air, Water and Soil Quality Modelling for Risk and Impact Assessment. NATO Security Through Science Series. Springer Netherlands, pp. 29-44.
- [34] STEFFEN, W., et al, 2011. [The anthropocene: From global change to planetary stewardship](#). AMBIO 40 (7): 739-761.
- [35] WHITE, C., et al, 2012. [The value of coordinated management of interacting ecosystem services](#). Ecology Letters 15 (6): 509-519.
- [36] de RIGO, D., 2013, [Software Uncertainty in Integrated Environmental Modelling: the role of Semantics and Open Science](#). Geophys. Res. Abstr. 15: 13292+.
- [37] de RIGO, D., (exp.) 2014. Behind the horizon of reproducible integrated environmental modelling at European scale: ethics and practice of scientific knowledge freedom. F1000 Research, submitted.
- [38] LEMPERT, R. J., May 2002. [A new decision sciences for complex systems](#). Proceedings of the National Academy of Sciences 99 (suppl 3): 7309-7313.
- [39] RAMMEL, C., et al, 2007. [Managing complex adaptive systems - a co-evolutionary perspective on natural resource management](#). Ecological Economics 63 (1): 9-21.
- [40] van der SLUIJS 2012, J. P., 2012. [Uncertainty and dissent in climate risk assessment: A Post-Normal perspective](#). Nature and Culture 7 (2): 174-195.
- [41] de RIGO, D., et al, 2013. [An architecture for adaptive robust modelling of wildfire behaviour under deep uncertainty](#). IFIP Adv. Inf. Commun. Technol. 413: 367-380.
- [42] GUARISO, G., et al, 2000. A map-based web server for the collection and distribution of environmental data. In: Kosmatin Fras, M., Mussio, L., Crosilla, F., Podobnikar, T. (Eds.), Bridging the gap: ISPRS WG VI/3 and IV/3 Workshop, Ljubljana, February 2-5, 2000 : Collection of Abstracts. Ljubljana.
- [43] GUARISO, G., WERTHNER, H., 1989. Environmental decision support systems. E. Horwood; Halsted Press.
- [44] GUARISO, G., et al, 1985. [Decision support systems for water management: The lake Como case study](#). European Journal of Operational Research 21(3): 295-306.
- [45] SONCINI-SESSA, R., et al, 2007. Integrated and participatory water resources management theory. Elsevier.
- [46] GUARISO, G., PAGE, B. (Eds), 1994. Computer support for environmental impact assessment: proceedings of the IFIP TC5/WG5.11 Working Conference on Computer Support for Environmental Impact Assessment, CSEIA 93, Como, Italy, 6-8 October, 1993. North-Holland.
- [47] CASAGRANDE, R., GUARISO, G., 2009. [Impact of ICT in environmental sciences: A citation analysis 1990-2007](#). Environmental Modelling & Software 24 (7): 865-871.

- [48] COLE, J., 2010. [Interoperability in a crisis 2: Human factors and organisational processes](#). Tech. rep., Royal United Services Institute.
- [49] STERMAN, J.D., 2002. [All models are wrong: reflections on becoming a systems scientist](#). *System Dynamics Review* 18 (4): 501-531.
- [50] WEICHSELGARTNER, J., KASPERSON, R., 2010. [Barriers in the science-policy-practice interface: Toward a knowledge-action-system in global environmental change research](#). *Global Environmental Change* 20 (2): 266-277.
- [51] BAINBRIDGE, L., 1983. [Ironies of automation](#). *Automatica* 19(6): 775-779.
- [52] de RIGO, D., et al, 2013. [Toward open science at the European scale: Geospatial Semantic Array Programming for integrated environmental modelling](#). *Geophysical Research Abstracts* 15: 13245+.
- [53] STENSSON, P., JANSSON, A., 2013. [Autonomous technology - sources of confusion: a model for explanation and prediction of conceptual shifts](#). *Ergonomics* 57 (3): 455-470.
- [54] RUSSELL, D. M., et al, 2003. [Dealing with ghosts: Managing the user experience of autonomic computing](#). *IBM Systems Journal* 42 (1): 177-188.
- [55] ANDERSON, S., et al, 2003. [Making autonomic computing systems accountable: the problem of human computer interaction](#). In: *Database and Expert Systems Applications, 2003. Proceedings. 14th International Workshop on. IEEE*, pp. 718-724.
- [56] KEPHART, J. O., CHESS, D. M. 2003. [The vision of autonomic computing](#). *Computer* 36 (1): 41-50.
- [57] van der SLUIJS, J.P., 2005. [Uncertainty as a monster in the science-policy interface: four coping strategies](#). *Water Science & Technology* 52 (6): 87-92.
- [58] FRAME, B., 2008. ['Wicked', 'messy', and 'clumsy': long-term frameworks for sustainability](#). *Environment and Planning C: Government and Policy* 26 (6): 1113-1128.
- [59] MCGUIRE, M., SILVIA, C., 2010. [The effect of problem severity, managerial and organizational capacity, and agency structure on intergovernmental collaboration: Evidence from local emergency management](#). *Public Administration Review* 70(2): 279-288.
- [60] BEA, R., et al, 2009. [A new approach to risk: The implications of e3](#). *Risk Management* 11 (1): 30-43.
- [61] ADAMS, K.M., HESTER, P.T., 2012. [Errors in systems approaches](#). *International Journal of System of Systems Engineering* 3 (3/4): 233+.
- [62] LARSSON, A., et al, 2010. [Decision evaluation of response strategies in emergency management using imprecise assessments](#). *Journal of Homeland Security and Emergency Management* 7 (1).
- [63] INNOCENTI, D., ALBRITO, P., 2011. [Reducing the risks posed by natural hazards and climate change: the need for a participatory dialogue between the scientific community and policy makers](#). *Environmental Science & Policy* 14 (7): 730-733.
- [64] RAVETZ, J., 2004. [The post-normal science of precaution](#). *Futures* 36 (3): 347-357.
- [65] de RIGO, D., 2012. [Integrated Natural Resources Modelling and Management: minimal redefinition of a known challenge for environmental modelling](#). Excerpt from the Call for a shared research agenda toward scientific knowledge freedom, Maieutike Research Initiative
- [66] de RIGO, D., 2012, [Semantic Array Programming for Environmental Modelling: Application of the Mastrave Library](#). *Int. Congress on Environmental Modelling and Software. Managing Resources of a Limited Planet*, 1167-1176.
- [67] de RIGO, D., 2012. [Semantic Array Programming with Mastrave - Introduction to Semantic Computational Modelling](#).
- [68] CORTI, P., et al, 2012. [Fire news management in the context of the european forest fire information system \(EFFIS\)](#). In: *proceedings of "Quinta conferenza italiana sul software geografico e sui dati geografici liberi" (GFOSS DAY 2012)*.
- [69] SHETH, A., 2009. [Citizen sensing, social signals, and enriching human experience](#). *Internet Computing, IEEE* 13 (4): 87-92.

- [70] ZHANG, D., et al, 2011. [The emergence of social and community intelligence](#). Computer 44 (7): 21-28.
- [71] ADAM, N.R., et al, 2012. [Spatial computing and social media in the context of disaster management](#). Intelligent Systems, IEEE 27 (6): 90-96.
- [72] FRATERNALI, P., et al, 2012. [Putting humans in the loop: Social computing for water resources management](#). Environmental Modelling & Software 37: 68-77.
- [73] RODRIGUEZ-ASERETTO, D., et al, (exp.) 2014. Daily forest fire progression map using MODIS active fire observation. IEEE Earthzine 7(2). Submitted.
- [74] BOSCO, C., et al, 2013. [Multi-Scale Robust Modelling of Landslide Susceptibility: Regional Rapid Assessment and Catchment Robust Fuzzy Ensemble](#). IFIP Adv. Inf. Commun. Technol. 413: 321-335.
- [75] DI LEO, M., et al, 2013. [Dynamic data driven ensemble for wildfire behaviour assessment: a case study](#). IFIP Adv. Inf. Commun. Technol. 413: 11-22.
- [76] ACKERMAN, F., HEINZERLING, L., 2002. [Pricing the priceless: Cost-Benefit analysis of environmental protection](#). University of Pennsylvania Law Review 150 (5): 1553-1584.
- [77] GASPARATOS, A., 2010. [Embedded value systems in sustainability assessment tools and their implications](#). Journal of Environmental Management 91 (8): 1613-1622.
- [78] de RIGO, D., et al, 2001. [Neuro-dynamic programming for the efficient management of reservoir networks](#). In: Proceedings of MODSIM 2001, International Congress on Modelling and Simulation. Vol. 4. Model. Simul. Soc. Australia and New Zealand, pp. 1949-1954.
- [79] RODRIGUEZ-ASERETTO, D., et al, 2009. [Injecting dynamic Real-Time data into a DDDAS for forest fire behavior prediction](#). Lecture Notes in Computer Science 5545: 489-499.
- [80] CENCERRADO, A., et al, 2009. [Support for urgent computing based on resource virtualization](#). Lecture Notes in Computer Science 5544: 227-236.
- [81] JOSHIMOTO, K, K, et al, 2012. [Implementations of Urgent Computing on Production HPC Systems](#). Procedia Computer Science 9: 1687-1693.
- [82] de RIGO, D., BOSCO, C., 2011. [Architecture of a Pan-European framework for integrated soil water erosion assessment](#). IFIP Adv. Inf. Commun. Technol. 359: 310-318.
- [83] de RIGO, D., et al, 2013. [Continental-Scale Living Forest Biomass and Carbon Stock: A Robust Fuzzy Ensemble of IPCC Tier 1 Maps for Europe](#). IFIP Adv. Inf. Commun. Technol. 359: 271-284.
- [84] RODRIGUEZ-ASERETTO, D., et al, 2013. [A data-driven model for large wildfire behaviour prediction in Europe](#). Procedia Computer Science 18: 1861-1870.
- [85] CASTELLETTI, A., et al, [On-Line design of water reservoir policies based on inflow prediction](#). IFAC-PapersOnLine 17: 14540-14545.
- [86] MCINERNEY, D., et al, 2012. [Developing a forest data portal to support Multi-Scale decision making](#). IEEE J. Sel. Top. Appl. Earth Obs. Remote Sens. 5(6): 1692-1699.
- [87] BASTIN, et al, 2012. [Web services for forest data, analysis and monitoring: Developments from EuroGEOSS](#). IEEE Earthzine 5(2): 389531+.
- [88] RODRIGUEZ-ASERETTO, D., et al, 2013. [Free and open source software underpinning the European Forest Data Centre](#). Geophysical Research Abstracts 15: 12101+.
- [89] NATIONAL SCIENCE FOUNDATION, CYBERINFRASTRUCTURE COUNCIL, 2007. [Cyberinfrastructure vision for 21st century discovery](#). Tech. Rep. NSF 07-28, National Science Foundation.
- [90] ALTAY, N., GREEN, W.G., 2006. [OR/MS research in disaster operations management](#). European Journal of Operational Research 175 (1): 475-493.
- [91] RODRIGUEZ-ASERETTO, D., et al, 2008. [An adaptive system for forest fire behavior prediction](#). In: Computational Science and Engineering, 2008. CSE '08. 11th IEEE International Conference on. IEEE, pp. 275-282.

Computer Vision: Identification, Classification and Tracking Objects

Alcides David Cantero Alonso^{a1}, Eustaquio Alcides Martínez ^a

^aFacultad Politécnica, Universidad Nacional del Este
Ciudad del Este - Paraguay

Abstract

Recognition is a basic, fundamental and complex function of computer vision, where by a computing system is able to learn to recognize shapes for later correctly classifying them. This paper involves the development and implementation of a computer vision system, which is able to perform the identification of a certain object group previously "taught" to the system for subsequent classification and tracking. The system is developed using digital image processing techniques and artificial neural networks in different stages according to a previously designed architecture. The first step is training the artificial neural network, for which are previously necessary the extracting of object patterns, being this process accomplished through techniques of digital image processing, among which stands out the segmentation technique called Mean Shift. The neural network used is the multilayer perceptron type, having its configuration two hidden layers, besides the input and output layers; it applies Levenberg-Marquardt algorithm as its training algorithm. In a second stage, two processes are performed: classification and tracking the objects under study. The results, when testing with two different object sets, are quite satisfactory. The identification and classification analysis of the artificial neural network, yields an accuracy above 98%; while for the tracking process there are very good results for scenes in which there are no occlusions.

Keywords: computer vision, artificial neural network, digital image processing, pattern recognition, heuristic algorithm.

1. INTRODUCTION

Visual perception is the activity that most humans are able to perform all day long. One of the biggest challenges that human faces, is to understand

¹E-mail Corresponding Author: davidcantero.99@gmail.com

image recognition organ function, in order to subsequently try to imitate such operation through existing technologies, looking for solution to real world problems. Computer vision arises inspired by human visual system [1], which could be said to be the largest source of information for people, it suggests processing information by different techniques, which are dependent on the goals sought. The goal of computer vision is to model and automate the visual recognition process, i.e., to distinguish between different objects. Object recognition is one of the most fascinating abilities a human has since childhood. A child is able to define and identify an object at glance, or even to tell its category, despite variations in appearance due to different reasons.

1.1. Importance and Motivation

Computer vision is a relatively new technological area compared to others, and despite being very complex and difficult, it is constantly developing with the emergence of new technologies over the years [1]. Recognition is a basic, fundamental and complex computer vision function; whereby the system is able to learn to recognize shapes for a later correct classification [2]; while object tracking allows the analysis and observation of the trajectories and behavior of them.

1.2. Objectives

1.2.1. General Objective

To identify and classify objects using Artificial Neural Networks and to track their movements

1.2.2. Specific Objectives

- To process images captured by an optical sensor.
- To obtain object patterns.
- To identify the most appropriate neural networks model for the problem stated.
- To train the neural network with the obtained patterns.

- To classify objects captured by the optical sensor.
- To keep track of the studied object moving.

2. THEORETICAL FRAMEWORK

2.1. Computer Vision

Computer vision, also called artificial vision [3], is considered a branch of classical Artificial Intelligence [4]. This includes a number of stages required to give the computer the ability to capture and identify an image, so imitating the process performed by humans. While the architecture and the stages of a vision system are application dependent, some stages are found in most applications, these latter are shown in Figure 1.

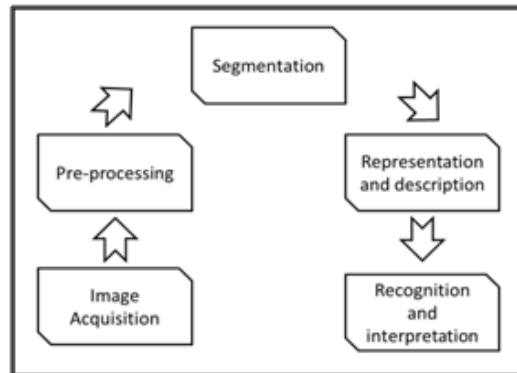


Figure 1 - Stages of an Artificial Vision System.

The artificial vision systems have different types of applications: measurement, flaw detection, correction and recognition, which can be used in areas such as industry, medicine and robotics.

2.1.1. Vision for Object Recognition

It is possible to consider two types of recognition [5], if a particular or known object is looked for in the image, an object detection is performed;

however if different instances of a generic object class are sought, an instance detection is performed. The last type is the process that divides objects into different classes; for example, to recognize two different vehicle brands and models, and according to certain shared characteristics, locate them in the car class. Object recognition is based on assigning a class to different objects, and the tool that makes this process is called a classifier [6].

2.1.2. Pattern Recognition

One feature is the basic unit used in representing objects [7]. These objects are represented by regions in a segmented image, they can be divided into different sets, which from the classification view point is given according to certain common characteristics. Some of these are measures of intensity, color measurement, corners, texture, among others. These characteristics are elementary numerical descriptions used by statistical object description. The measured object according to its characteristics is called a pattern. The pattern $x = (x_1, x_2, \dots, x_n)$ that describes an object is a feature vector, and the set of all forms of possible patterns is called feature space X . The classifiers are unable to recognize objects, but they can do it with the patterns presented to them. The steps followed in pattern recognition are shown in Figure 2.

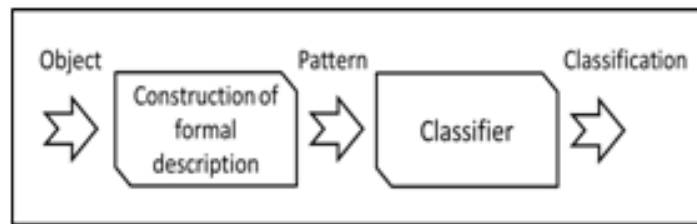


Figure 2 - Steps to pattern recognition.

2.1.3. Tracking objects in real time

Much of the tracking techniques or algorithms are based on scene change detection in an image sequence [8]. Tracking may be simply defined as the problem of estimating the trajectory of an object in the image plane as it moves along, for that, the follower system assigns fixed labels to the object or

objects to be followed during the image sequence. Difficulties in movement monitoring include [8] abrupt changes in motion, changes in pattern appearance, both: in the scene and in the object itself, and occlusions between objects.

2.2. Digital Image Processing

Digital image processing (Figure 3) is described as the set of techniques that generally have three main objectives [1]: enhancement, compression and extracting a digital image measures so as to improve its visual interpretation process by humans or by an autonomous machine system in a next stage.

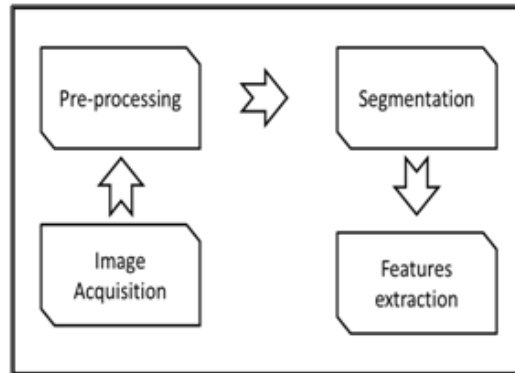


Figure 3 - Steps to pattern recognition.

In the acquisition phase of the digital image, the image can be acquired directly in that format, or by performing the sampling and quantification thereof (the image). Preprocessing produces images with minimal unwanted noise so as to facilitate the work of the following stages. At this stage the operations are made on the images. Segmentation is the process by which the scene object is analyzed isolately. Finally, in the phase of feature extraction, data are converted in edges or points of the image so that they are readable by computer.

2.3. Artificial Neural Networks

Artificial Neural Networks are those used in order to mimic human brain behavior, giving an unthinking object an approach to the information processing capacity that people have. They can be used to solve problems individually or in combination with other techniques. They are able to solve problems of identification, optimization, prediction and classification. The elements which comprise an artificial neural network are (Figure 4): neuron, where calculations are carried out, usually a weighted sum of the inputs provided. Plus an activation function that generates an output. This basic structure was proposed by McCulloch and Pitts [9].

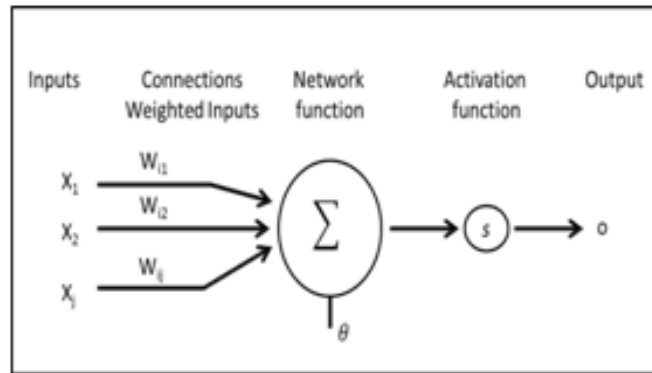


Figure 4 - Basic structure of a neural network.

There are two phases in a neural network: training phase, where a set of input data is used to determine the weights which define the network. These are calculated iteratively with the aim of minimizing the error up until getting an output close to the desired one. The other phase is called test phase or information retrieval, in which a different set of data is used, from which outputs are obtained. There are several artificial neural networks models, among which may be mentioned: Perceptron, Multilayer Perceptron, Hopfield networks, networks of radial basis neurons, Back propagation, among others.

Multilayer Perceptron

The multilayer perceptron or MLP is a supervised neural network that can take as input continuous or discrete values (binary), usually consisting of a set of sensory units (input layer), one or more hidden layers and an output layer as shown in Figure 5.

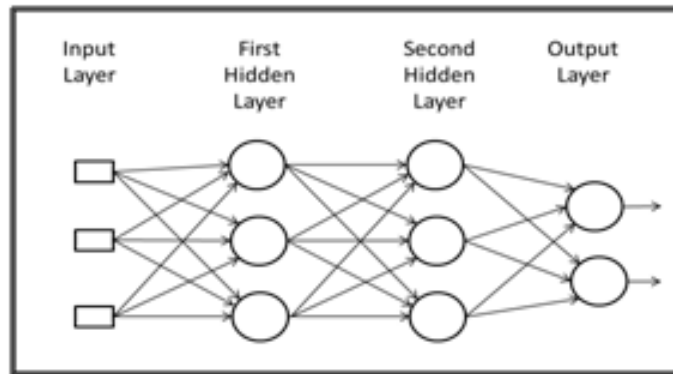


Figure 5 - Structure of a Multilayer Perceptron.

Having the network intermediate layers, the challenge was to find a learning algorithm to update the weights. Undoubtedly, the appearance of the back propagation algorithm was the cornerstone for the interest resurgence in neural networks, being since then one of the most studied and used algorithms in learning process [10].

3. MATERIALS AND METHODS

3.1. Resources Used

Hardware: Webcam, Notebook: 16 GB memory, Intel i7processor

Software: Technical programming language, Others, Lighting device.

3.2. System Architecture

The system architecture is defined as in Figure 6.

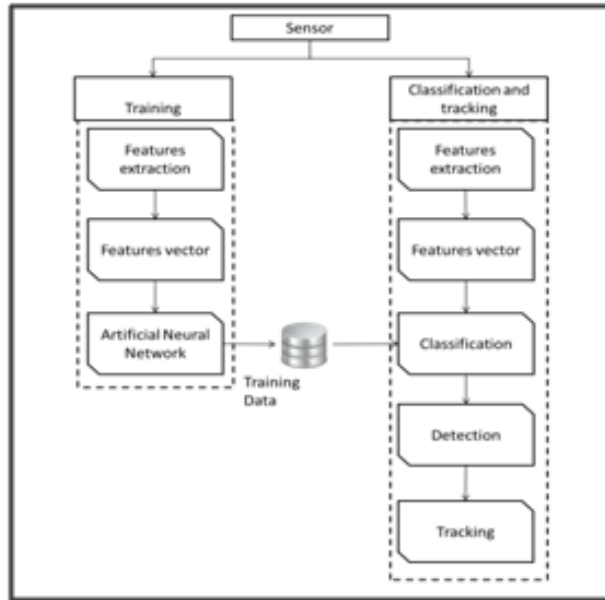


Figure 6 - System Architecture.

3.2.1. Feature Extraction Module

In order to achieve this goal, tasks operations covering digital image processing are performed. For object segmentation, it was used the technique of moving average. A total of 18 distinctive object characteristics are extracted from the objects, which are stored in an array, with their respective outputs in another array. Average value of the Red component, Average value of the Green component, Average value of the Blue component, Hue, Saturation, Brightness or Value, Compactness, Entropy, Object statistics moments, totaling 10.

3.2.2. Training Module

The type of ANN chosen for use in the application is the Multilayer Perceptron (18 inputs nodes, 5 outputs nodes, 2 hidden layers with 10 nodes each one), due to its ability to successfully solve many problems. The training role chosen is the one using the Levenberg-Marquardt method, having the mean square error as a performance parameter.

For training the ANN, 60% of the samples are allocated to the training set and 40% to the test set, so as to use them in the recognition step.

3.2.3. Classification and Tracking Module

Run the whole process done in previous stages, but with the network trained beforeh and so as to classify the objects in the scene sent by the web camera and then to keep track of them.

4. TESTS AND RESULTS

In order to check the system operation, tests were carried out with two sets of objects, divided into five classes. The first set of objects, called C1, comprises the classes: Pencil, Compact Disc (CD), Notebook, Sharpener, Eraser. Objects set C2 were used for the following tests, which consists of 5 kinds of fruits: Banana, Red apple, Green apple, Pear, Orange. Mean error squared with a value of 10^{-9} is used as stopping criterion of the neural network.

4.1. Set C1 recognition

The set is composed of 105 samples, which were divided: 60% for the training set and 40% for the test set, i.e. 63 and 42 samples respectively. The training process stops after 26 iterations when the error parameter is minimized to the desired value.

4.2. Set C2 recognition

The set has 114 samples, which were divided into 60% for the training process and 40% for the test set, i.e. 68 and 46 samples respectively. The training process stops after 16 iterations (epochs) when the error parameter reaches the desired minimum

4.3. Analysis of results

In order to perform the result analysis for the identification and classification tests, confusion matrices were used, in order to obtain the sensitivity, the ratio of false positives, the specificity and the accuracy of the ANN. From

these matrices the total number of true positives, false negatives, false positives and true negatives are calculated, which are necessary for evaluating the network. For Set C1, the network yields 40 true positives, 2 false positives, 2 false negatives and 166 true negatives. The results according to the criteria presented above are exposed in Table 1.

Criterion	Formula	Percentage
Sensitivity	$VPR = \frac{40}{(40 + 2)} = 0,952$	95,2%
False Positive Rate	$FPR = \frac{2}{(2 + 166)} = 0,012$	1,2%
Specificity	$SPC = 1 - 0,012 = 0,988$	98,8%
Accuracy	$ACC = \frac{40 + 166}{42 + 168} = 0,981$	98,1%

Table 1 - Analysis of the results for the set C1

For Set C2, the network yields 44 true positives, 2 false positives, 2 false negatives and 182 true negatives. The results, according to criteria presented above, are exposed in Table 2.

Criterion	Formula	Percentage
Sensitivity	$VPR = \frac{44}{(44 + 2)} = 0,957$	95,7%
False Positive Rate	$FPR = \frac{2}{(2 + 182)} = 0,011$	1,1%
Specificity	$SPC = 1 - 0,011 = 0,989$	98,9%
Accuracy	$ACC = \frac{44 + 182}{46 + 184} = 0,983$	98,3%

Table 2 - Analysis of the results for the set C2

Tracking tests

The mean shift tracking algorithm produced good results when the scene is clean, without occlusion of the object. Occlusion is understood as the partial or complete disappearance of the object under analysis. In cases where there are object occlusions or when the object is in part out of the scene, tracking is lost. For fast moving object, the algorithm takes time to resume tracking it, but finds it again

5. CONCLUSIONS

A computer vision application was developed, with the capability to identify, classify and track certain objects. After analyzing the results, it is possible to state that the system has a very high efficiency and effectiveness. Regarding the implementation of the artificial neural network, with the values obtained for both data sets, it is possible to express that it works quite accurately for classifying objects presented, considering that obtaining classifiers effectiveness of 100% is very difficult to achieve. One aspect to improve is the tracking module, mainly for the occlusion problem which generated the monitoring losing by the system. Another major problem presented was the scene lighting, since a small change in it, critically affects the entire process. Algorithms used for both tracking and segmentation, in this case the mean shift algorithm, very effectively respond to the problem posed proving to be robust algorithms for problems in this area.

ACKNOWLEDGMENTS: Our thanks to Prof. Alberto Rojas for his help in the translation of the article into English.

References

- [1] Sucar, L. E. and Gmez, G. Instituto Nacional de astrofísica, óptica y electrónica, <http://ccc.inaoep.mx/esucar/Libros/vision-sucar-gomez.pdf> 07/11/2013.
- [2] Munoz, D. J. Proceso de reconocimiento de objetos, asistido por computador (Visión artificial), aplicando gases neuronales y técnicas de minería de datos, *Scientia et Technica*, n 30, 2006.

- [3] Platero, C. Introducción a la Visión Artificial, http://www.elai.upm.es/webantigua/spain/Asignaturas/MIP_VisionArtificial/ApuntesVA/cap1IntroVA.pdf 16/11/2013.
- [4] Schierwagen, A. Vision as computation, or: Does a computer vision system really assign meaning to images?, <http://www.informatik.uni-leipzig.de/schierwa/vision.pdf> 11/11/13.
- [5] Grauman, K. and Leibe, B. Visual Object Recognition, <http://cs.gmu.edu/kosecka/cs482/grauman-recognition-draft-27-01-11.pdf> 15/11/13.
- [6] Sonka, M., Vaclav, H. and Boyle, R. Image Processing, Analysis, and Machine Vision, Toronto: Thomson, 2008.
- [7] Marr, D. and Nishihara, H. K. Representation and Recognition of the Spatial Organization of Three-Dimensional Shapes, Proceedings of the Royal Society of London, vol. 200, n 1140, 1978.
- [8] Yilmaz, A., Javed, O. and Shah, M. Object Tracking: A Survey, ACM Computing Surveys, vol. 38, n 4, p. 45, 2006.
- [9] Haykin, S. Neural Networks: A comprehensive Foundation, New Jersey: Prentice Hall International, Inc., 1999.
- [10] Rojas, R. Neural Networks. A systematic Introduction, Berlin: Springer, 1996.

Automated early detection of diabetic retinopathy based on digital image processing techniques

Humberto Chamorro Torres, José S. Encina Melgarejo, José L. Vázquez Noguera,
Horacio Legal Ayala, Diego P. Pinto-Roa
Polytechnic School, National University of Asuncion, Paraguay

Abstract

Diabetic retinopathy is a condition occurring in persons with diabetes, which causes progressive damage to the retina and ultimately case of blindness. Its detection in its early stage with proper and vigilant treatment and monitoring of the eyes can reduce the risks. In this work, a novel automatic detection of diabetic retinopathy is proposed based on the combination of image segmentation, feature extraction and Support Vector Machine classifier. The proposed approach gives in 95% accuracy, resulting in a valid diabetic retinopathy detector.

Keywords: Retinal Images, Diabetic Retinopathy, Image segmentation, Feature extraction, Blood Vessels, Hard Exudates, Microaneurysms, Support Vector Machine.

1. INTRODUCTION

Diabetic retinopathy (DR) often has no early warning signs. Even macular edema, which may cause vision loss more rapidly, may not have any warning signs until an advanced stage. Cataracts, glaucoma, and most importantly, damage to blood vessels inside the eye, is a condition known as diabetic retinopathy. The screening of diabetic patients for the development of DR can reduce the risk of blindness in these patients by 50% [1].

Retinal image classification has been done by various methods [4], [8] and [10]. These approaches are based on features extraction from the retinal images using image processing techniques. Many works [11–15] describe distribution of exudates, count, size and the distribution of the hemorrhages and microaneurysms considered for segmentation, an algorithm to grade the level of retinopathy in retinal image and multiple classifiers for the classification process.

Diabetes UK guidelines [6] establishes that any procedure used for screening sight diabetic retinopathy should have at least 80% sensitivity and 95% specificity.

The retinal blood vessels are derived from the central retinal artery and vein, which lie in the optic nerve. The hard exudates (HE) are found in diverse sizes from puny blots to booming tracts with clear peripheries and the microaneurysms (MA) are the vital symptoms of Diabetic Retinopathy and a tiny area of blood protruding from an artery or vein in the back of the eye.

Blood vessels, hard exudates and microaneurysms segmentation is done on retinal images because these are the best indicators of DR. The features used include the areas of these segmented structures. By using Support Vector Machine, we propose an automatic system which classifies as normal or DR images, based on the features extracted.

The rest of this article is organized as follows: Section 2 provides more detailed information about the proposed methodology; the first part of the method includes retinal structures and pathologies segmentation algorithms and sequences of images generated by applying those algorithms. The second part corresponds to feature extraction; here the input data is transformed into the set of features. In the last part, the classification process is proposed, which analyzes the numerical properties of various image features and organizes data into categories. In Section 3 experimental tests are described, including the the characteristics of the images used, quantities of training and test images and it is exposed the results in terms of sensitivity, specificity and accuracy metrics. Finally, Section 4 concludes and evaluate the overall performance obtained in this work by the proposed methodology.

2. PROPOSED METHODOLOGY

The scheme for the proposed methodology is given in Figure 1. As a first step, it segments blood vessels, hard exudates and microaneurysms separately from input retinal images. Then as second step, the blood vessels, HE and MA areas are extracted, so they can be used in third step for classification by SVM classifier.

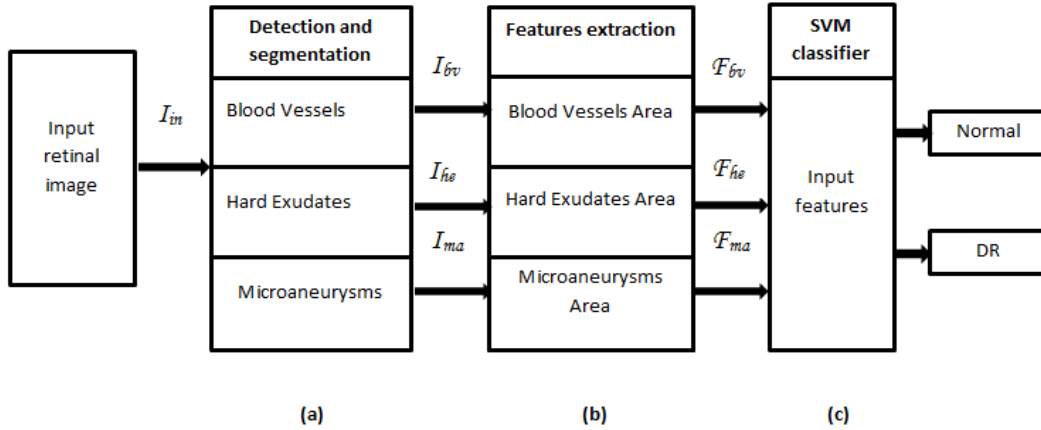


Figure 1 Proposed Methodology, Steps: (a) Detection and segmentation, (b) Feature extraction and (c) SVM classifier.

2.1 Detection and Segmentation

Segmentation is the process of assigning a label to every pixel in an image such that pixels with the same label share certain visual characteristics. The goal of segmentation is to simplify and change the representation of an image into something that is more meaningful and easier to analyze [2], [3]. Image segmentation is used to locate structures of the eyes like blood vessels and retinal eye abnormalities like hard exudates and microaneurysms.

Detection of Blood Vessels: This first part involves the extraction of the green channel from image I_{in} because blood containing features appears most contrasted in this channel. Over the green channel image is applied a contrast limited adaptive histogram equalization (CLAHE) [17] to smoothen the background and intensity normalization such that it spreads pixel intensities more evenly over the intensity range. After that, it is applied a median filtering resulting in image I_{mf} to remove noise, and then I_{mf} with the enhanced image to obtain highlighted blood vessels. This image is thresholded in intensity to yield a new image. It is then applied a closing operator from Mathematical morphology with a line structuring element to highlight the vessels in the image; after that we delete small connected elements to remove

noise in the binary image, the result image is the final I_{bv} image. The proposed method can be seen in Figure 2, and the sequence of generated images is shown in Figure 5.

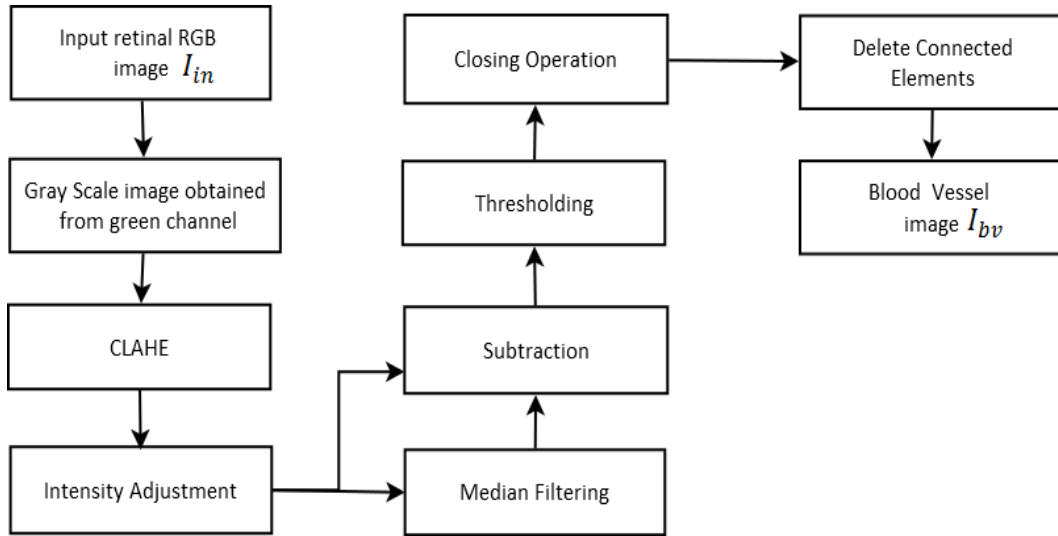


Figure 2 Blood Vessels detection block diagram.

Detection of Hard Exudates: HE are bright lesions, it is easier to detect them in the intensity channel. As a first step of the algorithm the intensity channel is obtained from the original RGB image I_{in} , then this image is closed by a disk structuring element. After that, we obtain the bright component applying Top-hat transform by a disk structuring element, the resulting image is thresholded to yield a new image. From this new image it is extracted the remaining parts of blood vessels. Because in some retinal images circular edges are brighter, they can be recognized as hard exudates, the morphological gradient is calculated and the circular edge is extracted from the image. Also, the optic disc can be confused as hard exudate, to solve this problem optic disc is identified and removed by method based on [7] to get a final image I_{he} . The proposed method can be seen in Figure 3, and the sequence of generated images is shown in Figure 6.

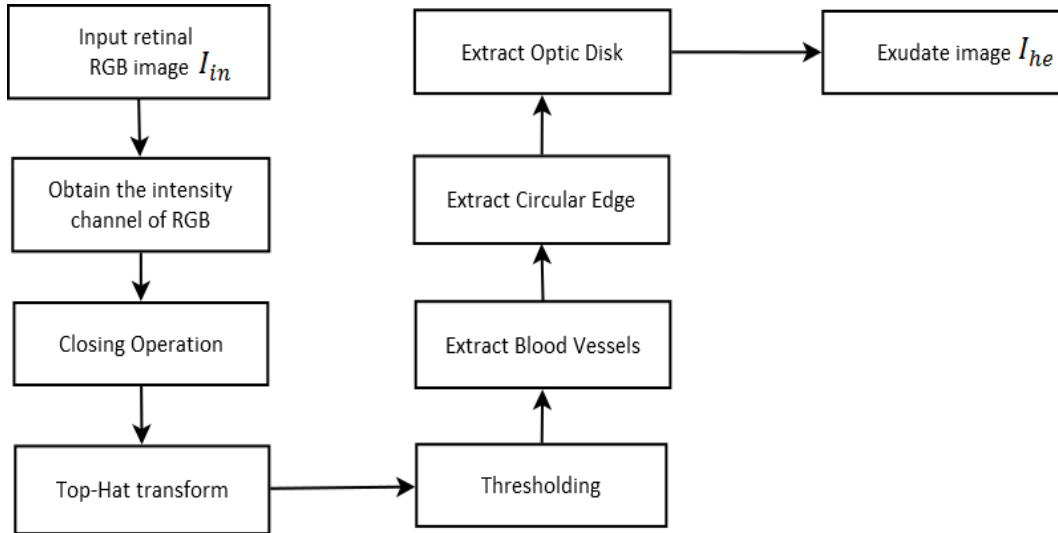


Figure 3 Hard Exudates detection block diagram.

Detection of Microaneurysms: MA are difficult to detect in retinal images. First, median filtering is performed on the green channel I_{in} to reduce noise in the image; then it is applied intensity normalization and CLAHE for image enhancement. Over the enhanced image is then applied a morphological erosion by a disk structuring element. After that, it is obtained the internal border by calculating the difference between the enhanced image and the eroded one. This image is thresholded in intensity to yield an image with MA patches. From this image, connected elements between minimum and maximum pixels are extracted to obtain the possibles MA. Finally, a closing operator by a disk structuring element is applied to highlight circle shaped elements, obtaining a new image from which the circle shaped connected elements are the MA detected I_{ma} . The proposed method can be seen in Figure 4, and the sequence of generated images is shown in Figure 7.

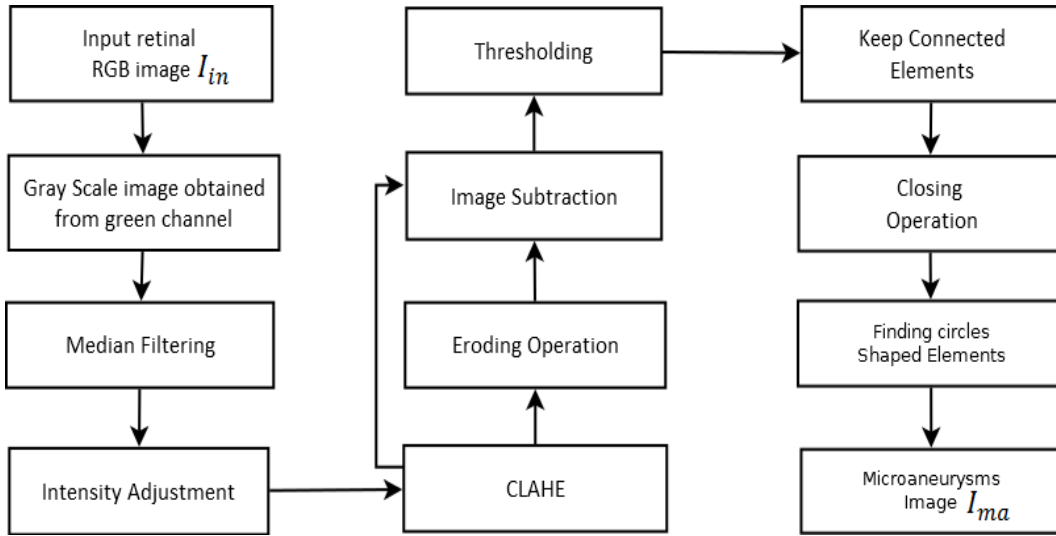


Figure 4 MA detection block diagram.

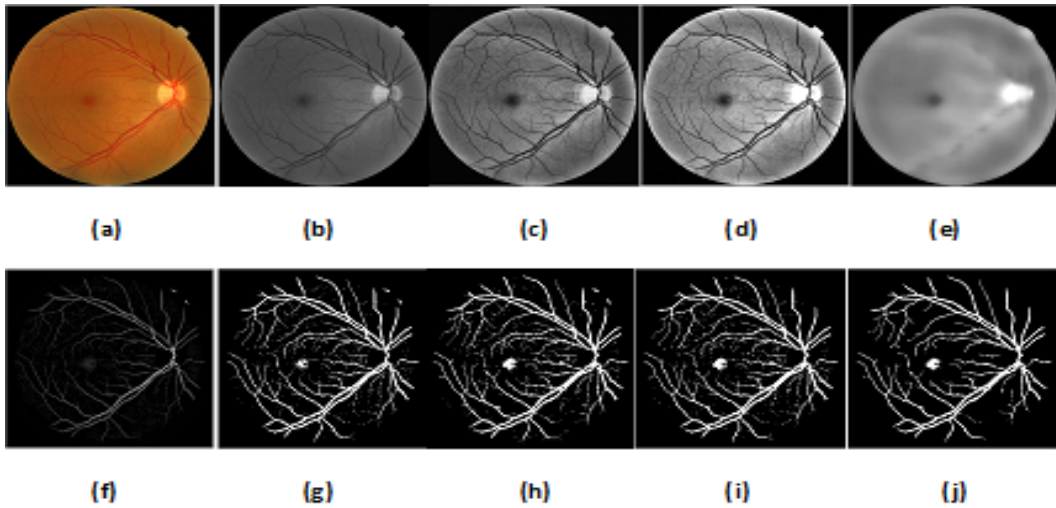


Figure 5 Blood Vessels segmentation images sequence (a) Retinal image, (b) Green Channel image, (c) Equalized image, (d) Intensity adjusted image, (e) Median filtered image, (f) Subtracted image, (g) Thresholded image, (h) Closed image, (i) Image with deleted connected elements, (j) Blood Vessels Segemented Image I_{bv} .

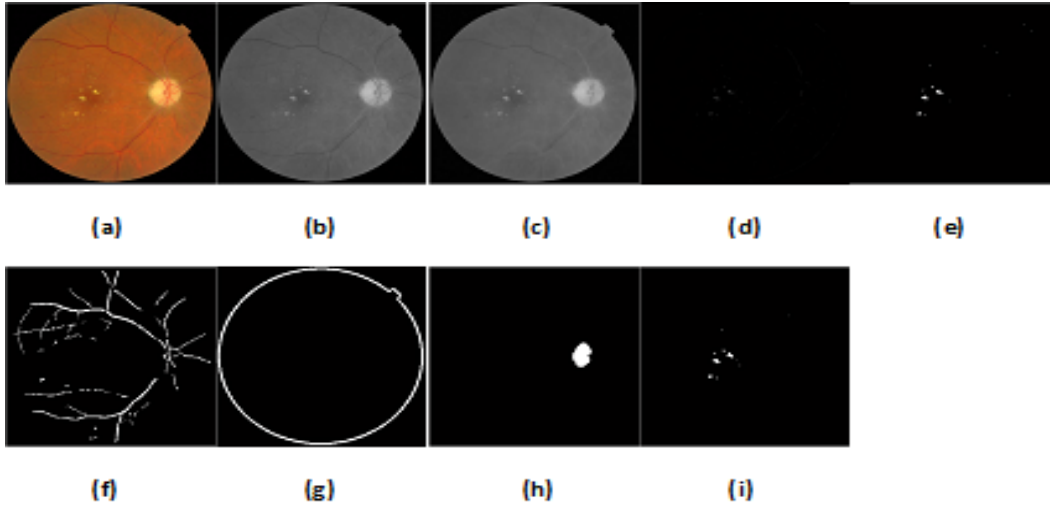


Figure 6 Hard Exudates segmentation images sequence (a) Retinal image, (b) Intensity channel image, (c) Closed image, (d) Top-Hat transformed image, (e) Thresholded image, (f) Blood Vessels image, (g) Circular edge image, (h) Optic disc image and (i) HE segmented image I_{he} .

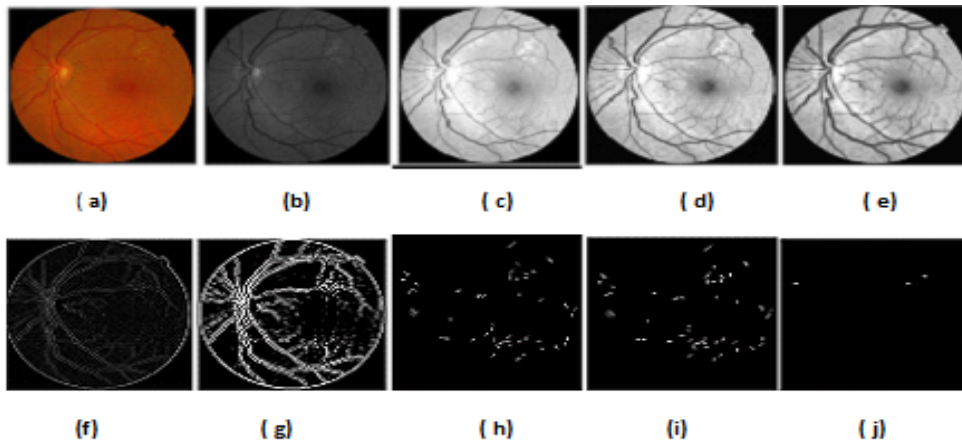


Figure 7 Microaneurysms segmentation images sequence (a) Retinal image, (b) Green Channel image, (c) Median filtered image, (d) Intensity adjusted image, (e) Equalized image, (f) Eroded image, (g) Subtracted image, (h) Thresholded image, (i) Image with deleted connected components and (j) Image with circle shaped components I_{ma} .

2.2 Feature Extraction

The feature vector used for classification consists of three features obtained from segmentation of retinal structures. These features are the area of blood vessels (F_{bv}), hard exudates (F_{he}) and microaneurysms (F_{ma}). These features are determined by finding the total number of white pixels in I_{bv} , I_{he} and I_{ma} images respectively.

2.3 Classification

The classification is performed by a well known binary classifier called Support Vector Machines (SVM) [16]. It achieves a significantly higher search accuracy in image classification than traditional query refinement schemes after just three to four rounds of relevance feedback. SVM receives a set of training features, each marked as belonging to one of two categories, 0 if it is a healthy retina and 1 if it is a retina with DR; this allows to construct a model that assigns one or another category of features to be classified.

3. EXPERIMENTAL TESTS

For these experiments, 100 images from MESSIDOR database have been used. The resolution of these images are 2240 x 1488 pixels. For further information about the database see in [5]. The images selected for testing include blurry and low lighted images so as to test the robustness. The diagnoses have been provided by medical experts for each image.

For MA and blood vessels segmentation, it was used a threshold value of 30 and for HE segmentation the threshold value was 20; these values were chosen empirically based on previous tests performed on a subset of the database.

The metrics used to evaluate the performance of the classification are sensitivity, specificity and accuracy. Sensitivity means the percentage of abnormal retinal images classified as abnormal, specificity means the percentage of normal retinal images classified as normal and accuracy is percentage of correctly diagnosed images of total quantity of images. As training images,

Table 1: Classification rates results

Metrics	Training images	Test images	Correctly classified	Classification Accuracy
Sensitivity	10	38	35	92.11
Specificity	10	42	41	97.67
Accuracy	20	80	76	95

twenty images (10 normal and 10 DR images) along with their corresponding ground truths were used. For testing, a set of eighty images (42 normal images and 38 DR images) were taken and their features were calculated.

From Table 1, it is observed that 1 from 42 normal images was not correctly classified, giving a 97.67 % specificity rate whereas 3 from 38 DR images were misdiagnosed, that is 92.11% sensitivity rate, that will be a total of 76 correctly diagnosed images from 80 test images obtaining 95% accuracy rate.

During the experimental tests, when we increased the accuracy in the detection of DR, it was perceived a decrease of the number of correctly identified as normal.

4. CONCLUSION AND FURTHERWORK

In this work, the detection and segmentation process is done by using Mathematical Morphology and image enhancement techniques. This first part performs image segmentation which includes the isolation of blood vessels, HE and MA, after that the SVM classifier is trained through supervised learning for the features extracted to classify the retinal images.

We achieved our goal of overcoming 80% of sensitivity and 95% specificity. As furtherwork, we can add more features (such as soft exudates and hemorrhages) to increase the accuracy, use other retinal images databases, extend the functionality by classifying the retinopathy grade by using a non-binary classifier and compare the obtained results with the state of art.

References

- [1] SHAYA, FT, ALJAWADI, M, 2007. Diabetic retinopathy, *Clin Ophthalmol* 1(3): 259265.
- [2] SHAPIRO, LG, STOCKMAN, GC, 2001. *Computer Vision*, 279-325, New Jersey, Prentice-Hall, ISBN 0-13-030796-3.
- [3] BARGHOUT, L, LEE, LW, 2003. Perceptual information processing system.
- [4] SOPHARAK, A, UYYANONVARA, B, BARMAN, S, WILLIAMSON, TH, 2008. Automatic detection of diabetic retinopathy exudates from non-dilated retinal images using mathematical morphology methods. *Computerized Medical Imaging and Graphics*, 32(8), 720-727.
- [5] MESSIDOR DATABASE, <http://messidor.crihan.fr/download.php>.
- [6] KUIVALAINEN, M, 2005. Retinal image analyzing machine vision, Master's thesis.
- [7] HANSKOVÁ, V, PAVLOVIČOVA, J, ORAVEC, M, BLAŠKO, R, 2013. Diabetic retinopathy screening by bright lesions extraction from fundus images. *Journal of Electrical Engineering*, 64(5), 311-316.
- [8] NAYAK, J, BHAT PS, ACHARYA, R, LIM, CM, KAGATHI, M, 2008, Automated identification of diabetic retinopathy stages using digital fundus images. *Journal of medical systems*, 32(2), 107-115.
- [9] NIEMEIJER, M, 2006. Automatic detection of diabetic retinopathy in digital fundus photographs.
- [10] ZHANG, X, FAN, G, 2006. Retinal spot lesion detection using adaptive multiscale morphological processing. In *Advances in Visual Computing*, 490-501.
- [11] OSAREH, A, 2004. Automated Identification of diabetic retinal exudates and the optic disc. PhD thesis, Univ. of Bristol.
- [12] WALTER, T, KLEIN, JC, 2001, Segmentation of color fundus images of the human retina: Detection of the optic disc and the vascular tree using morphological techniques. In *Medical Data Analysis*, 282-287.

- [13] BASHA, SS, PRASAD, KS, 2008. Automatic detection of hard exudates in diabetic retinopathy using morphological segmentation and fuzzy logic. *International Journal of Computer Science and Network Security*, 8(12), 211-8.
- [14] KUMARI, VV, NARAYANAN, NS, 2010. Diabetic retinopathy-early detection using image processing techniques. *International Journal on Computer Science and Engineering*, 2(2).
- [15] ZOHRA, BF, MOHAMED, B, 2009. Automated diagnosis of retinal images using the Support Vector Machine (SVM). *Faculte des Science. Department of Informatique, USTO, Algerie*.
- [16] CORTES, C, VAPNIK, V, 1995. Support-vector networks. *Machine learning*, 20(3), 273-297.
- [17] ZUIDERVELD, K, 1994. Contrast limited adaptive histogram equalization. In *Graphics gems IV*, 474-485. *Academic Press Professional, Inc.*5

Gaps in the knowledge of behavioral biology of Chagas disease Vectors. Challenges for control

Antonieta Rojas de Arias^{a1}

^aCentro para el Desarrollo de la Investigación Científica (CEDIC/Díaz Gill
Medicina Laboratorial/FMB)

Manduvirá 635 entre 15 de agosto y O'leary. Asunción,Paraguay

Abstract

Triatomines are vectors of Chagas, a neglected disease and a health problem in 27 countries in Latin America. Although the burden caused by Chagas disease decreased significantly between 1990 and 2001, currently is still greater than that produced by malaria, leishmaniasis, leprosy and schistosomiasis [1]. The main mode of transmission is through the vector, thus the importance of contributing with tools for vector control and eventual elimination of the disease as a public health problem. The main control strategy is focused on the chemical spraying in infested dwellings with these insects, however quickly reinfestation of houses and the restoration of the transmission cycle are observed. Early detection of this process of reinfestation contributes to the monitoring of these insects and prevents domestic vector transmission. The purpose of this dissertation is to show the progress in the understanding of the biological behavior of these insects in order to open a window to the interdisciplinary audience, to promote the innovation in new systems or tools that contribute to its control.

Keywords: Chagas disease, behavioral biology, vector, challenges to control, new tools

1 Introduction

Triatomines are hemimetabolous insects. Before reaching adult stage, triatomines progress through 5 larval instars, all of them obligatory hematophagous. Nymphs require blood to achieve the molting process, while adults to keep energy consumption during their activities. These insects live in sylvatic, peridomestic and domestic habitats and their movement between these areas

¹E-mail Corresponding Author: rojasdearias@gmail.com

depends on the time of year, weather conditions, time of day and the physiological condition of individuals [10]. It has been found that their movement can be by flying or walking, mainly observed in females with fertile eggs [2]. There are several paradoxes related to their behavior. Like other nocturnal insects are attracted by artificial light, however it has been reported that are markedly photophobic. Currently, mechanisms of attraction to artificial light have not been elucidated [9]. Other characteristic of these insects is their immobility during the day, which is governed by the circadian clock. Physical contact with the surface and with other triatomines allows a mechanic-sensorial stimulus that activates thigmotaxis. Triatomines are selective with respect to humidity rather than temperature. After feeding triatomines move towards places of lower temperature and decreases metabolism if access to new sources of blood are not possible. Therefore, the selection of a shelter depends of the multimodal integration of external stimuli and endogenous signals [9].

2 How triatomines select their hiding places

Refuges are strategically selected in search of more suitable microclimate. To reach them volatiles emitted by feces of triatomines distributed into the environment in the proximities of their refuges are the main feature. The feces emit pheromones, however to avoid empty sites attract triatomines, the duration of the lure of feces is about 10 days. Taking into consideration both phenomenon, it is therefore important to note that the attraction to light is not similar when aggregation pheromones are present or absent [13, 9].

3 How triatomines locate their food sources

Host odors stimulate triatomines to leave their refuges when it detects at the distance, the olfactory impulses indicate the direction but insects usually are encourage moving against the current of air (anemotaxis). Like most sucking insects carbon dioxide modifies the behavior of triatomines associated with the endogenous circadian rhythm, stimulating the insects at early hours of the scotophase. Carbon dioxide is not a specific attractant in triatomines, in contrast are attracted by others like nonanal, isobutyric acid, and ammonia present in the sweat of vertebrates. However, the insects are exposed to

mixtures of odors, usually present in a synergistic way. Triatomines respond to CO₂ when concentration is around 300 ppm above the atmospheric concentration; however when lactic acid or fatty acids are exposed alone they do not cause attraction. When CO₂ is combined with lactic acid and fatty acids could resemble a host [3, 4, 7, 5, 14]. The physical evidence that relates to more attracting triatomines is heat and oriented towards the insect host's body, however little is known about how this system works. It has been determined that *Triatoma infestans* detects heat of a face host up to 2 meters away and the body of a dog by several feet. Triatomines also detect infrared rays; this is very important cue because the issue is not interrupted by air currents or by the position of the insect. Remarkably triatomines are exposed to multiple signals simultaneously, not only heat, so synergism can be observed, so the response to the presence of a potential host depends on the multimodal integration of a variety of evidences, the physiological state of the insect and the individual experience [8, 11, 9].

4 How triatomines communicate with others

These insects use two systems for communication: a vibrating mechanism and by other chemicals. The stridulation is used for sexual communication and defense, while pheromones are used for different contexts. Stridulation consists in a vibration that occurs when the insect rubs the tip of its rostrum against a prosternal groove. This phenomenon occurs with alternate back and forth movements. This vibration beeps, but since triatomines have not auditory organs this vibration plays a fundamental role. Stridulation occurs during mating, but is also used by females when are not receptive for copulation. The vibration signals differ for each case (for matching or as alarm for the defense) [15, 9]. Triatomines feces are sources of aggregation and arresting pheromones, these are not species - specific and can therefore attract other species. There is however hydrocarbons of cuticle origin, those insects require physical contact with them, and generally correspond to arresting pheromones [9]. Other pheromones are released during copulation, the origin of these volatiles has been controversial since it has been found butyric acid (BA) from Brindley glands that is released when are disturbed and not with sexual purposes; others suggest that sex pheromones are released by metasternal glands of the female where there is no BA [6, 12].

5 New advances in the understanding of the biological behavior of triatomines

It is now known that insects are not small machines that respond to stimuli, but rather have small brains that are capable of complex learning including the acquisition of rules and concepts. However in Chagas vectors little information is known about mainly capability of learning due to weaknesses in the proposed experimental designs. Nevertheless, this is a huge field for experimentation due to triatomines are considered good models to measure cognitive abilities as they can be bred in laboratory conditions, their sizes are easier to handle and are easily stimulated by heat [17, 16]. Several triatomine biology behaviors have been used to investigate control strategies as capture traps and artificial refuges. Originally traps have been used with live animals as hosts to attract triatomines, but are unusable for long periods, for other cases have been used Baker's yeast that produces CO₂, or synthetic pheromones and their synergism capacities. The biggest problem with these traps is the limited persistence of attractants. Many issues in these assays are unknown and required more research [14, 9]. Regarding triatomines dispersion, there are two issues: the role of signals for dispersion to look for a host (this signal includes odors) and the second, orientation of triatomines based on the light that is still widely discussed. Specifically it is necessary to know if triatomines are really attracted to light or is an erroneous menotaxis. In relation to the behavior of infected insect with *Trypanosoma cruzi* nothing is known [9]. The genome sequence of *Rhodnius prolixus* has been elucidated, giving the chance to open a new window for control research based in studies of the molecular bases of their behavior. It is necessary more research in their sensory capacities, how these insects access to information or localize resources and communication, mainly how they use the multimodal sensory inputs as well as how modulatory process of feeding are affected by insect physiological processes and if these changes are induced by peripheral or central components of the nervous system [9]. More work needs to be done in different behavioral biology aspects of these insects; however, the own vector is considered as one of the most fascinating models in insect science to carry out experimentations in order to contribute to the knowledge to control main vectors of Chagas diseases, which causes higher disabilities in Latin America population.

ACKNOWLEDGMENTS: This material is based upon work supported by the Project 03/11 "Investigación Educación y Biotecnología Aplicada a la Salud". Fondos Estructurales del MERCOSUR-FOCEM. Programa Nacional de Incentivo a Investigadores (PRONII). This summary has been prepared based on the excellent review carried out by Lazzari et al 2013.

References

- [1] Panamerican Health Organization (PAHO). 2013. La enfermedad de Chagas en las Américas. Factsheet-chagas-spa.
- [2] Abrahan LB, Gorla DE, Catala SS 2011. Dispersal of *Triatoma infestans* and other Triatominae species in the arid Chaco of Argentina - Flying, walking or passive carriage? The importance of walking females. Mem Inst Oswaldo Cruz 106: 232-239.
- [3] Barrozo RB, Lazzari CR 2004. The response of the blood-sucking bug *Triatoma infestans* to carbon dioxide and other host odours. Chem Senses 29: 319-329.
- [4] Barrozo RB, Lazzari CR 2004. Orientation behaviour of the bloodsucking bug *Triatoma infestans* to short-chain fatty acids: synergistic effect of L-lactic acid and carbon dioxide. Chem Senses 29: 833-841.
- [5] Cork A, Park KC 1996. Identification of electrophysiologically-active compounds for the malaria mosquito, *Anopheles gambiae*, in human sweat extracts. Med Vet Entomol 10: 269-276.
- [6] Fontan A, Audino PG, Martinez A, Alzogaray RA, Zerb EN, Camps F, Cork A 2002. Attractant volatiles released by female and male *Triatoma infestans* (Hemiptera: Reduviidae), a vector of Chagas disease: chemical analysis and behavioral bioassay. J Med Entomol 39: 191-197.
- [7] Guerenstein PG, Guerin PM 2001. Olfactory and behavioural responses of the blood-sucking bug *Triatoma infestans* to odours of vertebrate hosts. J Exp Biol 204: 585-597.
- [8] Lazzari CR, Núñez JA 1989. Blood temperature and feeding behavior in *Triatoma infestans* (Heteroptera, Reduviidae). Entomol Gener 14: 183-188.

- [9] Lazzari CR, Pereira MH, Lorenzo MG. 2013. behavioral biology of Chagas Disease vectors. Mem Inst Oswaldo Cruz, Rio de Janeiro, Vol. 108(Suppl. I): 34-47, 2013
- [10] Lent H and Wygodzinsky P. 1979. Revision of the Triatominae (Hemiptera, Reduviidae) and their significance as vectors of Chagas' disease. Bull Am Mus Nat Hist 163: 123-520.
- [11] Lorenzo MG and Lazzari CR 1999. Temperature and relative humidity affect the selection of shelters by *Triatoma infestans*, vector of Chagas disease. Acta Trop 72: 241-249.
- [12] Manrique G, Vitta AC, Ferreira RA, Zani CL, Unelius CR, Lazzari CR, Diotaiuti L, Lorenzo MG 2006. Chemical communication in Chagas disease vectors. Source, identity and potential function of volatiles released by the metasternal and Brindley's glands of *Triatoma infestans* adults. J. Chem Ecol 32: 2035-2052.
- [13] Reisenman CE, Figueiras ANL, Giurfa M, Lazzari CR 2000. Interaction of visual and olfactory cues in the aggregation behavior of the haematophagous bug *Triatoma infestans*. J Comp Physiol A 186: 961-968.
- [14] Rojas de Arias A, Abad-Franch F, Acosta N, López E, González N, Zerba E, Tarelli G, Masuh H 2012. Post-control surveillance of *Triatoma infestans* and *Triatoma sordida* with chemically-baited sticky traps. PLoS Negl Trop Dis 6: e1822.
- [15] Schofield CJ 1977. Sound production in some triatominae bugs. Physiol Entomol 2: 43-52.
- [16] Vinauger C, Lallement H, Lazzari CR 2013. Learning and memory in *Rhodnius prolixus*: habituation and aversive operant conditioning of the proboscis extension response (PER). J Exp Biol 216: 892-900.
- [17] Vinauger C, Pereira MH, Lazzari CR 2012. Learned host preference in a Chagas disease vector, *Rhodnius prolixus*. Acta Trop. 122: 24-28.

Phage display in protein engineering

Pablo H. Sotelo^{a1}

^aBiotechnology Department, Chemistry Faculty, Universidad Nacional de Asunción, Paraguay

Abstract

Phage display technology has been developed and improved by researchers from different fields, and its applications have extended from protein engineering to biomaterial development. Phage display technology has been widely used in basic research such as studying the sites and the networks of protein-protein interactions, and in applied research such as developing new diagnostics tools, therapeutics and vaccines and biomaterial. During this lecture, it will discuss how this technology complements bioinformatics tools in the study of protein interactions. Also it will explore the role of bioinformatics in the development of new biotechnological products using filamentous phages.

Phages, also known as bacteriophages, are viruses that infect bacterial cells. Many phages such as M13 and fd are good protein expression vectors. In 1985, George P. Smith displayed foreign peptides on the virion surface by inserting the foreign DNA fragments into the filamentous phage gene III [1]. During this work, it was demonstrated that foreign peptides in fusion proteins on the virion surface were accessible and could be expressed in a functional form. Also in that paper, Smith inferred that desired clones could be isolated from a phage library of random inserts in a fusion-phage vector by one or more rounds of selection. This allowed a direct correlation between a genotype (gene sequence) with a phenotype (protein interaction).

By cloning large numbers of different DNA sequences into the phage, is possible to produce display with a repertoire of many billions of unique displayed proteins. A phage display library is, in fact, an ensemble of up to about 10 billion recombinant phage clones, each harboring a different foreign coding sequence, and therefore displaying a different guest peptide on the virion surface. This is called phage display libraries.

Using phage display libraries is possible identify proteins able interact to a specific target. The target of interest (could be a small

¹Email Corresponding Author: phsotelo@qui.una.py

molecule, protein or organism) is immobilized on a surface and exposed to the phage display library. The bacteriophage particles displaying on their surface a molecule with affinity for the immobilized target will therefore bind and the rest of the library will be washed away. The bound fraction can be eluted and amplified resulting in a mixture of bacteriophage particles displaying the relevant molecule. This procedure is repeated in a process called biopanning and allows the identification of molecules with high binding affinity to the target of interest.

Using mutagenesis techniques, is possible to produce a phage display library with multiple variants of the same protein; coupling this with a directed biopanning is possible to identify mutants with higher affinities to the selected target, this procedure is called Directed Evolution [2]. This method enables the relatively rapid engineering of protein without requiring an in-depth understanding of structure/function relationships.

The other procedure to produce engineered proteins is the rational design, in this method proteins are modified and assayed using computational tools. After that, mutations are made in the protein and its function analyzed. However this approach requires an in-depth knowledge of the structural features of the protein, and the complexity of the structure/function relationship in enzymes has proven to be the factor limiting the general application of rational design active site and their contribution to function.

Since both methods, rational design and directed evolution, produce different kind of information, a complementary approach in which both methods collaborate in the improvement of protein function was developed. In this approach directed evolution brings information to rational design about the effect of changing a position, and rational design brings information of which sites could be of interest to modify by directed evolution. Examples using this approach for the analysis of proteins structure and function will be discussed.

Since both methods, rational design and directed evolution, produce different kind of information, a complementary approach in which both methods collaborate in the improvement of protein function was developed. In this approach directed evolution brings information to rational design about the effect of changing a position, and rational design brings information of which sites could be of interest to modify by directed evolution. Examples using this approach for the analysis of proteins structure and function will be discussed.

In other terms, the capacity to transport peptides allowed the use of this phage in the development of new diagnostics tools, therapeutics and vaccines and biomaterial. Since the structure of the virus is known, a rational design of recombinant virus using bioinformatics tools, could be used in the development of biotechnological products. During this presentation, it will analyze some examples of recombinant phages developed using computational tools.

Keywords: Phage display, protein interactions, directed evolution.

ACKNOWLEDGMENTS: We thank the Instituto de Biotecnología (INBIO) for financial support.

References

- [1] SMITH, G.P.,1985. Filamentous fusion phage: novel expression vectors that display cloned antigens on the virion surface, *Science* 228(4705): p. 1315-7.
- [2] FERNANDEZ-GACIO, A., M. UGUEN, AND J. FASTREZ, 2003. Phage display as a tool for the directed evolution of enzymes, *Trends Biotechnol*, 21(9): p. 408-14.

Simulation of the Electrophoretic Mobility of Supercoiled and Catenated DNA Molecules

Maridian J. Kadomatsu-Hermosa^a, Jorge Cebrián^b, Alicia Castán^b,
Cristina Parra^a, Víctor Martínez^a, María José Fernández-Nestosa^a,
Christian E. Schaerer^a, María-Luisa Martínez- Robles^b, Pablo Hernández^b,
Dora B. Krimer^b and Jorge B. Schwartzman^b

^aScientific and Applied Computing Laboratory. Polytechnic School. National University of Asunción. P. O. Box 2111 SL, San Lorenzo, PARAGUAY.

^bDepartment of Cellular and Molecular Biology. Centro de Investigaciones Biológicas (CSIC), Ramiro de Maeztu 9, 28040, Madrid, SPAIN.

Abstract

In this work we demonstrated that the electrophoretic mobility of DNA in agarose gel can be mathematically simulated by using Maxwell-Stefan equations of mass transport as the constitutive equation of the mass conservation. Finite Different Lax-Friedrich approximation scheme was employed to approximate the resulting nonlinear hyperbolic partial differential equation. Here we used two-dimensional agarose gel electrophoresis (2Dgels) to compare the electrophoretic mobility of supercoiled Dimers. Comparison between experimental 2Dgels and numerical simulations showed a significant agreement between both results, a fact that validate the approximation.

Keywords: DNA topoisomers, electrophoresis, 2Dgels, electrophoretic mobility, Maxwell-Stefan equations, Finite Difference Method, Lax - Friedrich scheme.

1. INTRODUCTION

Bidimensional gel electrophoresis is one of the best methods to separate molecules with different masses and shapes [1]. The DNA is a double stranded molecule composed by so called nucleotides (Thymine, Cytosine, Adenine and Guanine). It has been demonstrated that the electrophoretic mobility of the DNA molecules is a function of the degree of supercoiling presented; in this way, the different types are readily separated and identified [3, 4, 5]. Using mathematical simulations, we were able to predict and reproduce the mobility of DNA molecules subject to the electrophoretical variables (electrostatic potential, agarose gel concentration and the DNA and buffer concentration).

To better understand the contribution of DNA supercoiling to the electrophoretic mobility we considered DNA molecules in the gel as a two-phase fluid model in a porous media. Hence conservation law models are used for the mass and the Maxwell-Stefan equation as a constitutive relation between the mobility of topoisomers and the electrostatic gradient of the 2D agarose gel electrophoresis. These equations correlate the mass transport of a multicomponent system to a series of driving forces like chemical activity, pressure gradient and the electrostatic potential [7]. Based on this model, we obtain a nonlinear hyperbolic partial differential equation, which is subsequently solved using a Lax-Friedrich finite difference scheme [8].

2. Numerical simulation of the electrophoretic mobility

In this section we considered that the porous media (gel) is homogeneous, and rigid enough in order to neglect any modification in its structure and form, also we assumed that the buffer ions are absorbed in the diffusion term and it is determined experimentally. Finally, we considered the DNA as a fluid. The DNA is denoted by subindex α while the buffer corresponds to the β component. Hence the constitutive the Maxwell - Stefan equations for species α and β are:

$$\frac{x_\alpha x_\beta}{D_{\alpha\beta}}(v_\alpha - v_\beta) + \frac{x_\alpha v_\alpha}{D_{\alpha g}^*} = -x_\alpha z_\alpha \left(\frac{F}{RT} \right) \nabla \phi \quad (1)$$

$$\frac{x_\beta x_\alpha}{D_{\alpha\beta}}(v_\beta - v_\alpha) + \frac{x_\beta v_\beta}{D_{\beta g}^*} = -x_\beta z_\beta \left(\frac{F}{RT} \right) \nabla \phi \quad (2)$$

where x represents the molar fraction (saturation), v_α the velocity of one component, z_α the elemental charge of the components considered, $D_{\alpha\beta}$ the diffusivity of α referred to β , F the Faraday constant, R the ideal gas constant, T the absolute temperature and $\nabla \phi$ the electrostatic potential applied. Equations (1) and (2) can be reduced to the following expression for the velocity of

$$v_\alpha = - \left(\frac{F}{RT} \nabla \phi \right) D_{\alpha g} \left(z_\alpha - z_\beta + \frac{z_\beta}{x_\alpha} \right) + \frac{v_\beta D_{\alpha g}}{D_{\beta g}} \left(\frac{x_\alpha - 1}{x_\alpha} \right), \quad (3)$$

The value of v_α was determined experimentally calculating the final position of the topoisomers in the immunotections and dividing it by the time required for the electrophoresis. This value was employed to determine the experimental value of $D_{\alpha g}$ and it was used to calculate the simulated value of v_α in equation 3; it was not possible to determine experimentally the value of v_β , so it was set as proportional of the v_α value.

The conservation law for continuity of fluid α gives

$$\partial_t x_\alpha - \partial_r(v^* x_\alpha) = 0, \quad (4)$$

where v^* is mean fluid velocity given by $v^* := x_\alpha v_\alpha + x_\beta v_\beta$ and ∂_r denotes the partial derivative with respect to the space variable, and t is the electrophoresis running time. This equation was completed with the constitutive equations introduced earlier. Combining the equations (3) and (4) we obtained the final equation that must be approximate in order to simulate the electrophoretic mobility. So combining and neglecting some terms, we obtained the following non-linear hyperbolic partial differential equation:

$$\partial_t x_\alpha + \partial_r f(x_\alpha, v_\alpha, v_\beta) = 0, \quad (5)$$

where $f(x_\alpha, v_\alpha, v_\beta) := (x_\alpha^2(v_\alpha - v_\beta) + x_\alpha v_\beta)$.

Discretization of model equations. For simplicity in this section we redefined $x_\alpha(t, r)$ by $u(t, r)$. We considered a spatial temporal dimensionless domain for equation (5) of the form $\hat{\Omega} \times [t_0, t_f]$ where $\hat{\Omega} = \Omega \cup \partial\Omega$ with $\Omega = (r_0, r_f)$. In addition, a partition of the space in N intervals such as $h = (r_f - r_0)/N$ and $r_i = hi$ for all $i = 0, \dots, N$. Analogously, the time was partitioned in M intervals such as $t_j = \tau j$ with $\tau = (t_f - t_0)/M$ for all $i = 0, \dots, M$. The discrete approximation of $u(\tau j, hi) \approx u_i^j$. Then we discretized equation (5) using a finite difference approximation, the conservative nonlinear Lax-Friedrich method taking the form:

$$u_i^{j+1} = u_i^j - \frac{\tau}{h} \left(\hat{f}_{i+1/2}^n - \hat{f}_{i-1/2}^n \right), \quad (6)$$

where $\hat{f}_{i-1/2}^n = \frac{1}{2}(f_{i-1} + f_i) - \frac{h}{2\tau}(u_i^n - u_{i-1}^n)$. It is important to emphasize the necessity to satisfy the stability CFL condition $\max |\partial_u f(u, v_\alpha, v_\beta)| \leq h/\tau$. The value of $\max |\partial_u f(u, v_\alpha, v_\beta)|$ was determined from the Equation

$$\begin{aligned} \max |\partial_u f(u, v_\alpha, v_\beta)| &= \left| 2x_\alpha \left(-CD_{\alpha g} \left(z_\alpha - z_\beta + \frac{z_\beta}{x_\alpha} \right) + v_\beta D_{\alpha g} \frac{x_\alpha - 1}{D_{\beta g} x_\alpha} - v_\beta \right) \right. \\ &\quad \left. + x_\alpha^2 \left(\frac{CD_{\alpha g} z_\beta}{x_\alpha^2} + \frac{v_\beta D_\alpha}{D_{\beta g} x_\alpha} - \frac{v_\beta D_{\alpha g} (x_\alpha - 1)}{D_{\beta g} x_\alpha^2} \right) + v_\beta \right| \quad (7) \end{aligned}$$

where $C = FE/(RT)$ a constant for the conditions of simulated.

3. Comparison of experimental and numerical results.

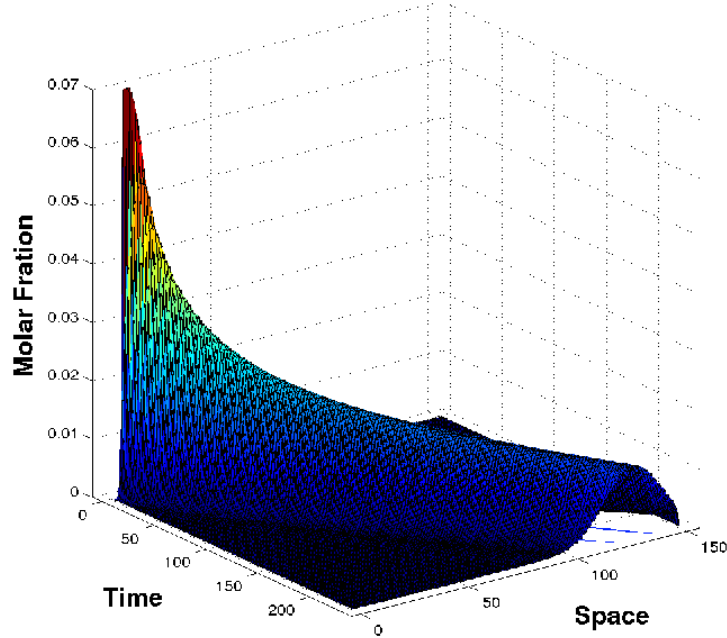


Figure 1: Plot of the mathematical approximation of the Maxwell-Stefan equation.

For numerical resolution we considered the following of the constants: Faraday constant $F = 96485.34C/mol$, electrical constant $E = 100V/m$, universal constant of gas $R = 8.314472J/mol.K$, working temperature $T = 293.16K$, $z_\alpha = -38$, $z_\alpha = -3$ and $v_\beta = 1.92v_\alpha$. The value of v_α at each step is obtained by

$$v_\alpha = -3.5393e^{-11}\Delta Lk^3 + 1.2629e^{-10}\Delta Lk^2 + 2.6538e^{-8}\Delta Lk + 8.4757e^{-7}, \quad (8)$$

where ΔLk is the supercoiling degree of each topoisomer.

In Figure 2 is shown the difference mobility as a function of the ΔLk for supercoiled dimers for 1D and 2D electrophoresis immunodetections. Observe that the strong superposition of both results: simulation and experimental (electrophoresis). In fact, the largest error was about $1.4mm$, which can be considered a very good agreement between both results. This results validate the model and the numerical method implemented.

4. Conclusions

The numerical simulation showed very good approximation to the experimental results. The results obtained so far encouraged us to improve the modeling as

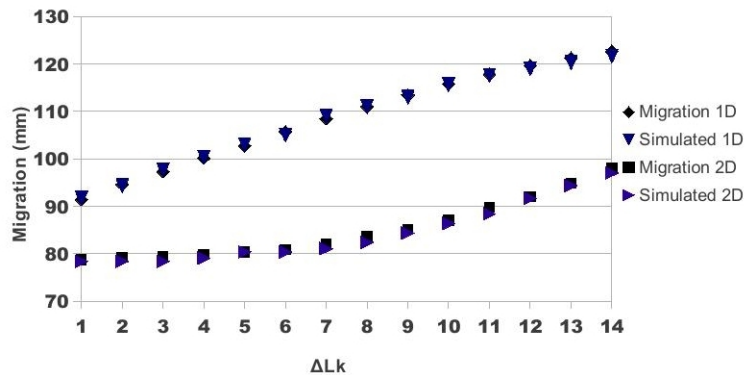


Figure 2: Comparison of the experimental and the simulation data. Graphic representation of the final position of dimeric topoisomers during the 1st and the 2nd dimensions.

well as to develop faster numerical schemes.

ACKNOWLEDGMENTS: This work was supported by grants BFU2011-22489 from the Spanish Ministerio de Economía y Competitividad, AP/038170/11 from the AECL, Agencia Española de Cooperación Internacional and I-COOP0009 from the Agencia Estatal CSIC. MJ Kadomatsu was a recipient of a fellowship from the CONACYT, Paraguay. We thank ML Martínez for technical assistance.

References

- [1] STELLWAGEN NC, 2009. Electrophoresis of DNA in agarose gels, polyacrylamide gels and in free solution, *Electrophoresis* 30(Suppl 1): S188S195.
- [2] LOPEZ, V, MARTINEZ-ROBLES, ML, HERNANDEZ, P, KRIMER, DB, SCHVARTZMAN, JB, 2012. Topo IV is the topoisomerase that knots and unknots sister duplexes during DNA replication, *Nucleic Acids Res* 40: 35633573.
- [3] MARTINEZ-ROBLES, ML, WITZ, G, HERNANDEZ, P, SCHVARTZMAN, JB, STASIAK, A, KRIMER, DB, 2009. Interplay of DNA supercoiling and catenation during the segregation of sister duplexes, *Nucleic Acids Res* 37: 51265137.

- [4] BAXTER, J, SEN, N, MARTINEZ, VL, DE CARANDINI, ME, SCHVARTZMAN, JB, DIFFLEY, JF, ARAGON, L, 2011. Positive supercoiling of mitotic DNA drives decatenation by topoisomerase II in eukaryotes, *Science* 331: 13281332.
- [5] LOPEZ, V, MARTINEZ-ROBLES, ML, HERNANDEZ, P, KRIMER, DB, SCHVARTZMAN, JB, 2012. Topo IV is the topoisomerase that knots and unknots sister duplexes during DNA replication, *Nucleic Acids Res.* 40: 35633573.
- [6] STASIAK, A, KATRITCH, V, BEDNAR, J, MICHOD, D, DUBOCHET, J, 1996. Electrophoretic mobility of DNA knots, *Nature* 384: 122.
- [7] KADOMATSU, J., SCHAEERER, C, 2010. Pervaporation simulation using Maxwell - Stefan equations. Graduate degree thesis. Chemistries Sciences Faculty and Politechnic Faculty, National University of Asuncion.
- [8] STRIKWERDA, J. C.; *Finite Difference Schemes and Partial Differential Equations*, 2nd edition. SIAM

Using infrared photoelectric sensors for automatic detection of reinfestation by *Triatoma infestans*

Federico Gaona^{a1}, Adolfo Jara ^a, Martin Vera^a, Silvia Aquino ^a,
Christian Schaerer^a, Magna Monteiro^a, Carlos Juiz ^c, Bartomeu Serra^c,
Celeste Vega^b and Antonieta Rojas de Arias ^b.

^aPolytechnic School, National University of Asuncion,
San Lorenzo, Paraguay. P.O.Box: 2111 SL.

^bCentro para el Desarrollo de la Investigación Científica - CEDIC,
Asunción, Paraguay.

^cUniversidad de las Islas Baleares - UIB, Islas Baleares, Spain.

Abstract

This work involves the design and implementation of a device, electronic sensor, capable of detecting the entry of *Triatoma infestans* bugs (commonly known as vinchucas) into a trap, in order to study the efficiency and effectiveness of kaolin porous tablets, produced to promote slow release of the attractant pheromone, in this case the benzaldehyde, to be applied during the vector control transmitter of Chagas disease. Paperboard boxes are used as traps in which the porous tablets impregnated with pheromone are placed. In addition, optical methods are used, i.e., infrared photoelectric sensors (LEDs senders and receivers) and a computer with a new software able to record, filter and discriminate analog signals occurring with unexpected movement of bugs. With this new software it is possible to analyze the applicability of the electronic system and the effectiveness of the pheromone. The biggest challenge of this implementation is to ensure the detection of the insect when it enters in the trap. These photoelectric sensors are strategically placed at all entrances of the traps. The system, sensor and pills are thoroughly tested in laboratory with controlled bugs (coming from CEDIC facilities) in different states and sexes (nymphs and adults, males and females) for more than 60 days. The results are considered satisfactory, since they exceeded the results generated by traditional systems through manual detection.

Keywords: Infrared sensing, *Triatoma infestans*.

¹E-mail Corresponding Author: federico.gaona@pol.una.py

1. INTRODUCTION

In Paraguay, as well as in other Latin American countries, Chagas disease is one of the pressing issues in the area of public health [1]. This disease is caused by the parasite *Trypanosoma cruzi*, being *Triatoma infestans* insect, or commonly called vinchuca, the main vector of South America [2]. Currently, it also comes to be a growing concern in European countries and the United States, due to the growing eco-tourism to South American countries, where Chagas disease is referred to as an exotic disease.

There are enough development of techniques to control bugs by pheromones [3] in the literature. Thus, studies have been performed using different materials release pheromones attract way to control insect pests in agriculture [4]. Lately, there were new systems for the particular detection of *Triatoma infestans*. One of the instruments built by the CEDIC (Centre for the Development of Scientific Research - Paraguay) in collaboration with the Polytechnic School of the National University of Asuncion is a system with sensors primed with preexisting pheromones [6], to which they incorporate slow-release tablets of the most attractive pheromones identified as most attractive [7].

Because these new tablets are attractive by slow release of pheromones over 90 days [7], monitoring or manual verification vinchucas presence could be inefficient, especially if the traps are placed in remote areas of the cities. This is the main motivation for the research of an automated detection of vinchucas, and consequently, the reason for the design and development the electronic device that present in this paper.

Therefore, the structure of the paper is as follows: first, we depict the lab facilities on which were carried out the tests with controlled live vinchucas strategically placing traps. Then the electronic and computer system for the automated detection (physical configuration circuit, sensor locations and programs involved) are described. Finally the results and the conclusions are presented.

2. DESCRIPTION OF TEST FACILITY

In order to avoid the possibility of vinchucas infestation, we built a cage of nylon mesh, as Figure 1 shows. The cage had got two traps, one including a tablet (T1) and the other without it (T2), both for the automated

detection by sensors. The bugs were released in the center of the cage, so they dispersed throughout the cage, slipping quickly into the darkest and tight places. Afterwards, we observe that the vinchucas tended toward the traps either T1 or T2, in order to verify the efficiency and effectiveness of kaolin porous tablets. During the experiment, our electronic system would be monitoring all the time the presence or absence of insect events in each trap box.

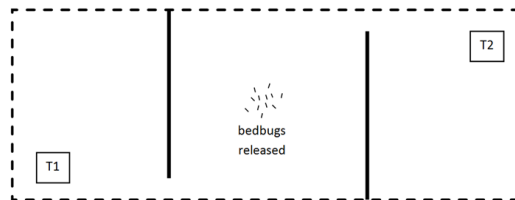


Figure 1 - Test facility (cage) plan in top view.

We decided to place traps in the farthest the cage in order to discriminate possible coincidences and observe clearly where the vinchucas were addressed. Each trap had double-sided tape, so that any object should be stuck entering the box, also trapping vinchucas.

3. DESCRIPTION OF ELECTRONIC-COMPUTER SYSTEM

Each trap consists of a cardboard box with a small electronic circuit board for each entrance into the box. Figure 2 shows each electronic board of each entry containing two embedded photosensors (LTH1550 model) [5].

The central hub has a series of analog inputs, six channels in this case, to receive signals from the photosensors. This centralized circuit communicates with a computer on which runs an application that plots and records the events of each trap. The whole detection system is outlined in Figure 3.

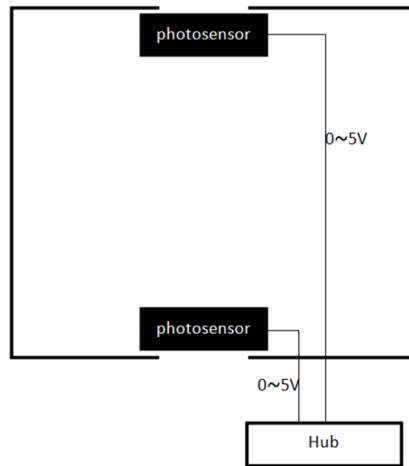


Figure 2 - Schema of a box (trap) in top view.

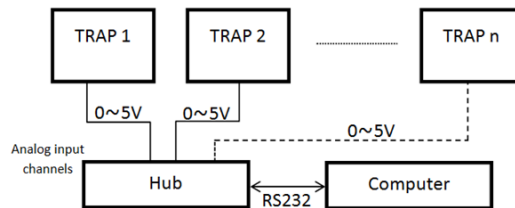


Figure 3 - Overview of automated detection system.

Central Hub of sensors. The central hub is fully designed and assembled exclusively for laboratory tests. It is based on a general purpose microcontroller PIC16F1825. This microcontroller is a 8-bit processor RISC, which contains an integrated analog-to-digital converter (A-D) of 10-bit resolution, with 12 input channels and a automatic acquisition module; plus many other features [8].

In our experiments, only six input channels are used, (named as AI1 to AI6). There are wires to board terminal blocks for easy installation, connecting the analog signal coming from the sensors and fed with 5V to the board photo sensors. This power is used by the microcontroller itself, and therefore used by a module of internal A-D conversion, so that the voltage ranges are suitable for the entire system.

Digital communication with the computer. In order to connect the electronic sensors to the computer, an UART standard RS232 protocol with a computer compatible port is used. The hub module incorporates controller hardware UART protocol, which facilitates programming by setting all required parameters, which in this case are: baud to 9600 bits / s, no parity, 1 stop bit, 8 data bits and no flow control.

Embedded Photosensor LTH1550. LTH1550 photo sensors are mounted on small printed circuit boards to connect the necessary resistors for driving the LED emitter (resistor 1[kohm]) and for excitation of the collector of the phototransistor (resistor 100[kohm]) embedded encapsulation LTH1550 such as shown in the diagram of Figure 4.

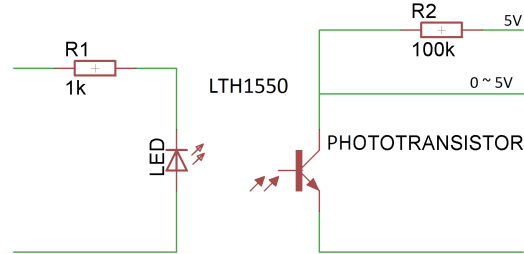


Figure 4 - Schema of the electronic light sensor plate for a LTH1550 module.

The phototransistor produces a LTH1550 variation proportional to the intensity of light reflected at the same current through its own infrared LED transmitter. This current change is directly related to Ohms law with variation of voltage for the AD converter through resistor 100[kohm] that goes directly to the analog input channel of the microcontroller which converts it to a variation of digital values given by Equation 1.

$$digital_value = \frac{V \times (2^{10} - 1)}{V_{cc}}, \quad (1)$$

where V is proportional to the light intensity and it is multiplied by the number of values that can take the AD converter which in this case, is 10 bits, so you can have 1024 possible values, from 0 to 1023. V_{cc} is the power converter which is the same as the microcontroller and equal to 5[V].

Due to the environmental infrared light in the laboratory plus those emitted by the LTH1550 photosensor by its own, the maximum variation of clarity

and darkness is about 1[V] voltage, ranging from 3,5[V] to 4,5[V], corresponding to maximum clarity and maximum darkness, respectively. The maximum clarity reaches at a clear reflection of white paper in front of the sensor, at a distance of 1[cm]., and the maximum darkness reaches at dark pad (simulating an adult bug) closer than the thickness of the pad (approximate height of an adult vinchuca). This test was performed in order to calibrate and to estimate the voltage variation when the vinchucas pass under the optical sensor.

Tests with adult vinchucas produced a similar voltage variation, but not reaching to the maximum intensity of the pad. This can be explained considering that the color of the insect vector is not completely black. Therefore, this proves that the maximum variation in voltage is about 1[V].

Considering equation (1) above, the maximum variation in voltage of 1[V] corresponds to a maximum variation of a digital value of 206 units, enough to plot by the corresponding algorithm in the computer.

Location of sensors. In order to detect the vinchucas, we use the lighter color of the box floor and the darker color of the insect vector to detect the variation of light in the box trap. Thus, the LTH1550 photosensor can detect this variation of dark and light when bug enters passing under the sensor, located above each entrance to the trap.

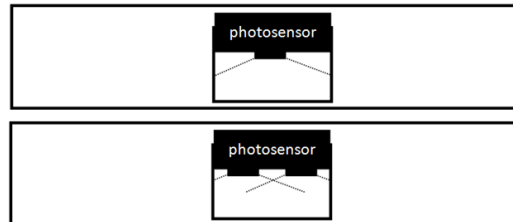


Figure 5 - Front view of an entrance to the trap. Top: plate with a light sensing LTH1550 and down two sensors. Dashed lines show the approximate area of detection.

Finally, there are two LTH1550 per plate, and a plate for each entry. This implies that we have 2 analog signal voltage variation per entry to the trap that should go to the microcontroller analog channels at the central hub. Since this set has 6 channels, we may cover up to 3 entries to the trap in our laboratory cage.

Programming the microcontroller. The logic programmed into the microcontroller simply involves reading six analog channels, applying a filter by averaging 25 samples of each channel and send a packet of data via UART from ASCII to a connected computer. Figure 6 shows the flowchart of the function of an analog read channel and average filter application. This flow is repeated for each channel whose result will be sent to the computer.

For this application the average filter is appropriate and sufficient for the computational requirements needed for this digital process is low (and the microcontroller used is low-end), because the input signal changes slowly when entering the insect and the same is relatively slow moving as tested.

The number of samples was determined by the latency testing main operating cycle, which should at least read all channels about 5 times per second to get a sense of real-time acquisition and subsequent plotting of the signal from the sensors.

The reason why it is necessary the filter is simply to prevent outside interference by occasional sudden changes in the signal, so that these are not reflected in the computer and the algorithm does not detect it incorrectly.

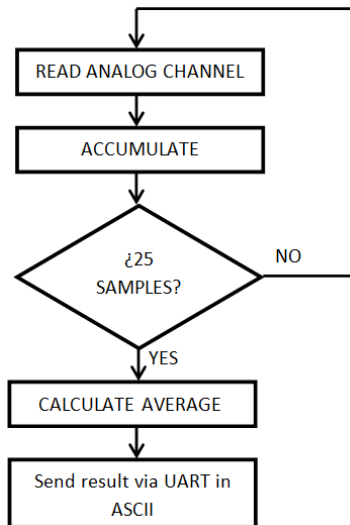


Figure 6 - Flowchart of the acquisition and application of average filter for each analog input channel of the microcontroller.

Computer Programming. The desktop application for Microsoft Windows developed in Visual Studio Express 2010 capture the analog data filtered by

the microcontroller and graphics via a GUI component called PictureBox. Given that each light sensing plate includes two LTH1550 photo sensors, this application first finds the average value of these two signals for a single graph for light sensing plate or entrance to the trap.

When a dark object passes under the sensor, the voltage rises and delivery photo sensor therefore accentuated curve upward enough to set a detection algorithm, Figure 7 shows a dark object entering the box, it can be any object the very dark or insect vector, and the curve shows along its width in time throughout the entering process of the insect, from head to tail.

Through numerous laboratory tests, it has been verified that vinchucas normally enter (or come close) to the trap slowly, but this process lasting more than 1 minute. That is why the logic of counting takes a delay of 1 minute, so that if after detecting the first signal variation that exceeds the upper threshold, a margin of safety time in which the bug can be taken, is added shake their income, causing many changes in the signal, but inhibiting their inaccurate count due to the delay (false positives).

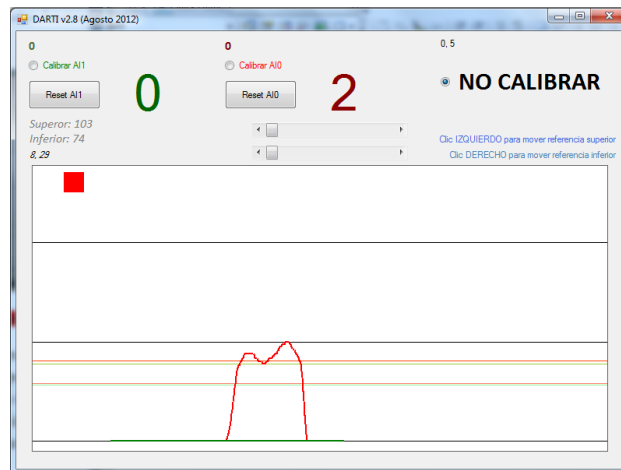


Figure 7 - Screenshot of the graph generated by the computer software when you enter a dark object. The red color represents the average value of channel 0 and 1 (AI0). Green to the average value of channel 2 and 3 (AI2). So that two entrances are monitored with 4 channels.

Obviously the location of the reference lines will depend on the ambient light, the color of the insect vector, the stability of the signal or electrical

noise present on the power supply or the environment itself, among other external factors unforeseen. That is why we developed the program provides the option to calibrate, which is nothing more than eye locate references lines or thresholds to be considered for the Schmitt trigger type behavior. This calibration should be done whenever the sensors change of environment. This is the main disadvantage of this method of optical detection, since it depends pretty lighting and color work environment (or reflectivity of light) of the object mentioned above.

The variation of digital values of 206 units found by equation (1) above is what is represented in the graph of computer software and directly related to the pixels on the screen (and GUI picture box object) and a scale factor, but could relate also voltage or even better, with light intensity.

Surprisingly, despite stability in the signal observed during the day and record all changes, the experiment provided the next day dawned, the algorithm counted some vinchucas, but none of them caught in the trap. Because of this, we decided to perform the experiments with night footage of more than 10 hours straight, using cameras that capture infrared lights (having a powerful transmitter) to film in the dark. This allowed also to show that that despite the strong infrared light source there was vinchucas activity in the cage.

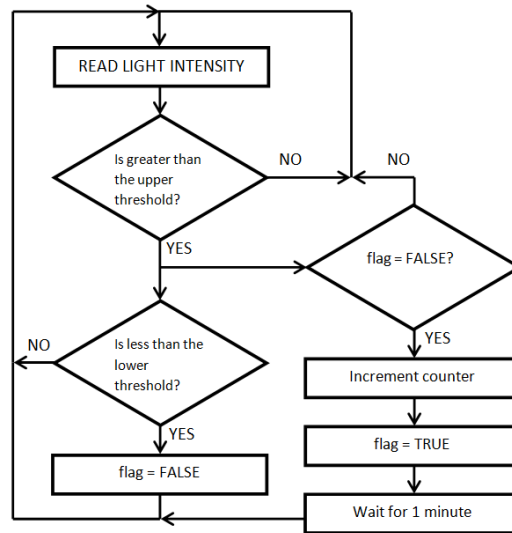


Figure 8 - Flowchart counting logic in the computer software.

4. RESULTS

Table 1 shows the results of 52 hours of system testing is at a controlled temperature of about 25 C, employing 6 vinchucas adult females in the cage, and a cam capable of recording 13 hours maximum continued, and night using infrared film.

Test number	August-September	Number of adult female vinchucas	Automatic Detection through our system	Detection by observation of film	Success (%)
1	28 al 29 (13hs)	6	8	8	100%
2	29 al 30 (13hs)	6	7	7	100%
3	30 al 31 (13hs)	6	0	0	100%
4	31 al 1 (13hs)	6	3	3	100%

Table 1 - Summary of studies with automatic and manual detection, proving the effectiveness of the system.

5. CONCLUSIONS AND OPEN PROBLEMS

This work contributes to several important issues for further research and improvements related to the investigation in the field. On one hand, the developed system collaborated with a parallel work of checking the efficiency and effectiveness of kaolin porous tablets, produced to promote the slow release of the pheromone, in this case the benzaldehyde.

On the other hand, the effectiveness of a cheap and simple electronic system for detection of dark objects (like a bug) entering a box is also shown. Simple algorithms were developed based on the observed natural reaction of these bugs. We have to point out the advantage of the automation of miniaturized embedded systems and their low energy consumption. Moreover, the electronic system is not complex also provides deployment in harsh environments. Furthermore it was also found that the presence of infrared light in the environment does not prevent the normal activity of these bugs, which was in strong doubt in the course of this work, which mostly operate at night or in the dark.

It is noteworthy that the main disadvantages of this method of detection has to do with the optical sensor itself, which when infrared is strongly affected by sunlight and by recognizing any dark object by reflection not only detect vinchucas but any other insect or similar object. Therefore, it is a challenge for the future work to be able to identify the object entering the trap (not covered in this paper), in order to discriminate and avoid making false positives in field, e.g. counting other species of bugs.

ACKNOWLEDGMENTS: This work has been partially supported by the Detección Automatizada de Reinfestación por Triatoma Infestans project funded by the University of the Balearic Islands, programs of VIII, IX and X Convocatoria de Ayudas para Proyectos de Cooperación Universitaria al Desarrollo.

References

- [1] ACOSTA, N.; LPEZ, E.; GONZLEZ, N.; FERNNDEZ, M.J.; ROJAS DE ARIAS, A. 2002. Perfiles isoenzimaticos de poblaciones de Triatoma infestans de la Regin Oriental y Occidental del Paraguay. Memorias del Instituto de Investigaciones en Ciencias de la Salud (PY). 1 (1): 58-62.
- [2] BRENER, Z.; ANDRADE, Z.; BARRAL-NETTO, M. 2000. A Tripanossomase Americana e seu Impacto na Sade Pblica das Amricas. In: Trypanosoma cruzi e Doen?a de Chagas. 2a ed. Rio de Janeiro, BR: Guanabara Koogan S.A. 1-15.
- [3] SALAS, J. 2008. Capacidad de captura de Neoleucinodes elegantalis (Lepidoptera: Pyralidae) en dos tipos de trampa provistas con su feromona sexual. Bioagro (VE). 20 (2): 135-139.
- [4] TAKAHASHI, R. M.; ASSIS, O. B. G. Obten?o de vidros porosos para uso como dispositivo de libera?o de feromnios. 2008. Cermica (BR). 54 (332): 462-465.
- [5] Hoja de datos t?cnica del fabricante LITEON. Reflective Photointerrupters. LTH-209-01/LTH-1550-01/LTH-1650-01. Disponible en: <http://pdf1.alldatasheet.com/datasheet-pdf/view/194716/LITEON/LTH-1550-01.html>.

- [6] ROJAS DE ARIAS A, ABAD-FRANCH F, ACOSTA N, LPEZ E, GONZLEZ N, et al. (2012) Post-Control Surveillance of *Triatoma infestans* and *Triatoma sordida* with Chemically-Baited Sticky Traps. PLoS Negl Trop Dis 6(9): e1822. doi:10.1371/journal.pntd.0001822
- [7] AQUINO, S.(2012). Producción y caracterización de pastillas cerámicas porosas para la utilización como emisor de feromonas de *T. infestans*. tesis de maestria. Universidad Nacional de Asunción. Facultad Politécnica.
- [8] Hoja de datos técnica del fabricante MICROCHIP. Microcontrollers. PIC16F/LF1825/1829. Disponible en: ww1.microchip.com/downloads/en/DeviceDoc/41440A.pdf

Chaotic dynamics of a magnetic particle at finite temperature

Omar J. Suarez^{a1}, David Laroze^a, Javier Martínez-Mardones^b, Dora Altbir^c and Harald Pleiner^d

^a Instituto de Alta Investigación, Universidad de Tarapacá, Casilla 7D, Arica, Chile

^b Instituto de Física, Pontificia Universidad Católica de Valparaíso, Casilla 4059, Valparaíso, Chile

^c Departamento de Física, CEDENNA, Universidad de Santiago de Chile, Av. Ecuador 3493, Santiago, Chile

^d Max Planck Institute for Polymer Research, D55021 Mainz, Germany

Abstract

We study the deterministic spin dynamics of an anisotropic magnetic particle at

finite temperature using the Landau-Lifshitz-Bloch equation. We assume that the external magnetic field is comprised with a constant and a time dependent term. We focus our study for temperatures below of the Curie temperature. We characterize the dynamical behavior of the system through calculation of the Lyapunov exponents, bifurcation diagrams, and Fourier power spectra. We find that the system presents multiple transitions between regular and chaotic behavior when we varied the magnitude and frequency of the applied magnetic field, and the temperature.

Keywords: Chaotic dynamics, Lyapunov spectrum, magnetization dynamics

The dynamical behavior of magnetic media in the femto-second and pico-second regime can be possible due to the advances in the ultra-fast pulsed laser experiments. Some of the experimental observations, near to the Curie temperature, are in agreement with the dynamics based on the Landau-Lifshitz-Bloch (LLB) equation [1]. This equation was derived for classical ferromagnetic system by Garanin [2]. Recently, it was applied to micromagnetic models at high temperatures [3]. In this work, we characterize the dynamical behavior an anisotropic magnetic particle at finite temperature

¹E-mail Corresponding Author: ojsuarez1@yahoo.com

under the presence of a time dependent magnetic field using the LLB equation. We characterize this system through calculation of the Lyapunov exponents (LEs) [4, 5]. When the largest Lyapunov exponent (LLE) becomes positive the system is a chaotic regime, while for LLE is zero or negative the system exhibits regular states (quasi-periodic, periodic or fixed point). Here, we explore the LEs as a function of the temperature, magnitude and frequency of the applied magnetic field.

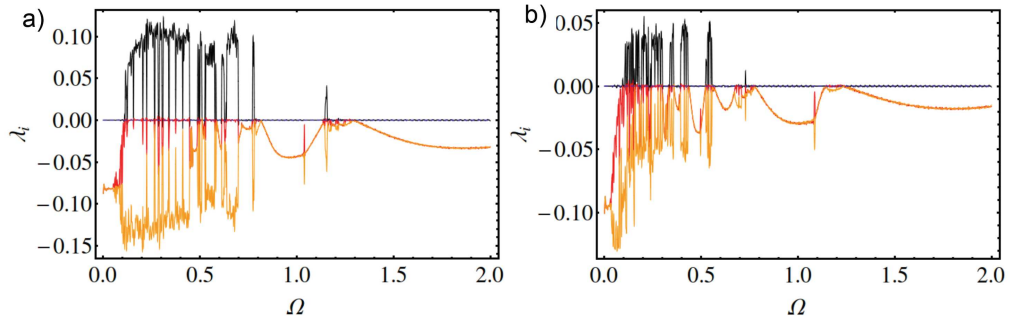


Figure 1 - Lyapunov exponent as a function of the frequency Ω for two different temperatures: $T = 0$ (a) and $T = 0.6T_C$ (b).

Figure 1 shows the LEs as a function of the frequency, at the two different temperatures: $T = 0$ (a), and $T = 0.6T_C$ (b). In the frame (a) we observe that the regular states are presented for low frequencies ($\Omega < 0.11$) or for high frequencies ($\Omega > 1.17$), whereas the chaotic regimes occur for certain values of Ω . Also, we observe alternation between chaotic and regular domains. When the temperature is increased, higher amount of chaotic domains appear at low frequencies as it is shown in the panel (b). At $T = 0.6T_C$ the threshold in which the states become purely regulars is $\Omega = 0.732$. Let us comment that for higher temperatures we observe that chaos is vanished for lower thresholds.

ACKNOWLEDGMENTS: D. L. acknowledges partial financial support from FONDECYT 1120764, Millennium Scientific Initiative, P10-061-F, Basal Program Center for Development of Nanoscience and Nanotechnology (CEDENNA) and UTA-project 8750-12. O.J.S. acknowledges the financial support from CONICYT FONDECYT Postdoctoral program fellowship under grant 3130678.

References

- [1] MENDIL, J, et. al, 2014. Resolving the role of femtosecond heated electrons in ultrafast spin dynamics, *Sci. Rep.* 4:3980.
- [2] GARANIN, DA, 1991. Generalized equation of motion for a ferromagnet, *Physica A* 172:470-491.
- [3] ATXITIA, U, et. al, 2007. Micromagnetic modeling of laser-induced magnetization dynamics using the Landau-Lifshitz-Bloch equation, *Appl. Phys. Lett.* 91:232507.
- [4] BRAGARD, J, et. al, 2011. Chaotic dynamics of a magnetic nanoparticle, *Phys. Rev. E* 84:037202.
- [5] LAROZE, D, et. al, 2011. Characterization of the Chaotic Magnetic Particle Dynamics, *IEEE Trans. Mag.* 47:3032-3035.

Parabolic optimal control constrained optimization using active restriction method

Juan José Cáceres^{a1}, Roberto A. Viveros^{a2}, Miki Saíto^a, Christian E. Schaerer^b

^a Engineering School, National University of Asuncion, San Lorenzo, Paraguay.

^b Polytechnic School, National University of Asuncion, San Lorenzo, Paraguay.

P.O.Box: 2111 SL. Email: chris.schaerer@gmail.com

Abstract

In this work we use quadratic programming in order to simulate and control the heat distribution on an electronic circuit board. The controller acts on the board in both transient and steady states, driving the temperature values from a given distribution to another desired one. The control variable is subject to equality and inequality constraints. The incorporation of inequality constraints in the synthesis of the controller allows a better representation of the physical conditions of the system model. A quadratic cost function is defined to penalize the error between the reference value and the measured value of the temperature, which is represented by the state variable y . The energy employed by the control variable v is also included in the cost function. So we have three weight factors (α, β, γ) associated to each one of the terms of the cost function. The goal of this work is to find the appropriate tuning of the mentioned weight factors so the controller acts optimally over the circuit, keeping the control variable v within the limits of the constraints. The results help to evaluate the necessary constraints to obtain an optimal heat controller.

Keywords: Quadratic programming, Active Constraints Method, Optimal Control.

1. INTRODUCTION

In this work, we are interested in solving a parabolic constrained optimization problem of the form:

$$\begin{aligned} & \min \mathcal{J}(y, v) \\ & \text{subject to} \quad \begin{cases} \mathcal{H}(y, v) = 0 \\ \mathcal{G}(y, v) \leq 0, \end{cases} \end{aligned} \quad (1)$$

¹E-mail Corresponding Author: jjcaceres@copaco.com.py

²E-mail Corresponding Author: viveros.01@gmail.com

where $\mathcal{J}(y, v)$ is a cost function to be minimized establishing the performance of the system, $\mathcal{H}(y, v) = 0$ are the equality constraints representing the system that corresponds to a parabolic state equation including the boundary and initial conditions of the system, and $\mathcal{G}(y, v) \leq 0$ are the inequality constraints that are considered to model the restrictions on the control variables.

Parabolic optimal control problems model several processes in electronics engineering that had an increasing interest in the last decade. Computational aspects, when only equality constraints are considered, have been discussed previously in [6,9], nonlinear aspects in [7] and parallel numerical implementations have been proposed in [8].

In this work we explore a numerical optimal solution of a heat distribution in a 2D electronic circuit [5,9] subject to inequality restrictions on the control variable v . The distribution of the temperature y on the circuit Ω is modeled through a dimensionless heat equation with f modeling the internal circuit sources terms. In problem (1) the dimensionless heat equation is represented by $\mathcal{H}(y, v) = 0$ and it is given by:

$$\partial_t y = \Delta y + v + f \quad \text{in } \Omega \quad (2)$$

where y and v are the state and control variables, respectively. In addition, the initial condition $z(\cdot, t) = z_0$ at $t_0 = 0$ and the boundary condition $z(x, t) = 0$ on $\partial\Omega$ for $t_0 < t \leq t_f$ are specified. To simplify the notation the dimensionless variables incorporate the properties of the circuit.

The performance functional $\mathcal{J}(y, v)$ is given by

$$\begin{aligned} \mathcal{J}(y, v) = & \frac{\alpha}{2} \int_{\Omega} \int_{t_0}^{t_f} \|y - \tilde{y}\|_2^2 + \frac{\beta}{2} \int_{\Omega} \|y(t_f) - \tilde{y}\|_2^2 + \\ & + \frac{\gamma}{2} \int_{\Omega} \int_{t_0}^{t_f} \|v\|_2^2 \end{aligned} \quad (3)$$

where \tilde{y} is the target function that the system has to follow or reach in t_f . The constants α , β and γ are the tuning parameters which affect directly to the solution of the system. Finally, the inequality constraints are denoted in (1) as $\mathcal{G}(y, v) \leq 0$ and take the form $\eta \leq v \leq \theta$ for all $t \in (t_0, t_f]$.

To solve numerically the optimization with the constraints problem presented above, either the objective function and the constraints are first discretized and then optimized or they are first optimized and then discretized.

In the context of this work, following [9] we use the first discretize then optimize approach, and an all-at-once approach. The rest of this paper is organized as follows. In Section 2, the discrete optimization problem is introduced. In Section 3, the active restriction method and its algorithm are presented, the numerical results are discussed in Section 4 and the Conclusions in Section 5. The results present the sensibility of the method to the constraints, and they show that the more restrictive the constraint is, the more iterations are needed for the convergence of the algorithm, resulting in more computational time.

2. DISCRETE PROBLEM

The discretization of problem (1) is performed using a standard finite difference scheme for the space and a backward Euler for the time resulting:

$$\mathcal{J}(\mathbf{z}, \mathbf{v}) = \frac{1}{2}(\mathbf{z} - \tilde{\mathbf{y}})^T \mathbf{K}(\mathbf{z} - \tilde{\mathbf{y}}) + \frac{1}{2} \mathbf{v}^T \mathbf{G} \mathbf{v} + (\mathbf{y} - \tilde{\mathbf{y}})^T \mathbf{g} \quad (4)$$

and

$$\begin{cases} \mathbf{E} \mathbf{z} + \mathbf{N} \mathbf{v} = \mathbf{f} \\ \eta \leq \mathbf{v} \leq \theta \end{cases} \quad (5)$$

where \mathbf{z} is state variable vector and \mathbf{v} is the vector control variable. To simplify the notation in the algorithm we define vector $\mathbf{x} := [\mathbf{z}^T, \mathbf{u}^T]^T$. The problem (1) with respect to the discrete expressions (4) and (5) takes the form:

$$\text{Minimize } f(\mathbf{x}) = \frac{1}{2} \mathbf{x}^T \mathbf{Q} \mathbf{x} + \mathbf{x}^T \mathbf{p} \quad (6a)$$

$$\text{Subject to } \begin{cases} \mathbf{a}_i \mathbf{x} = \mathbf{b}_i, & i \in \mathcal{E} \\ \mathbf{a}_j \mathbf{x} \leq \mathbf{b}_j, & j \in \mathcal{I} \end{cases} \quad (6b)$$

where $\mathbf{Q} \in \mathbb{R}^{n \times n}$ is symmetric positive definite and $\mathbf{x}, \mathbf{p}, \mathbf{a}_i \in \mathbb{R}^n$. Vectors \mathbf{b}_i and \mathbf{b}_j are appropriate vectors that model the equality and inequality constraints. The sets \mathcal{E} and \mathcal{I} are index sets associated to the feasibility region denoted by \mathcal{S} and defined as:

$$\mathcal{S} = \{\mathbf{x} \in \mathbb{R}^n, \mathbf{a}_i \mathbf{x} = \mathbf{b}_i \forall i \in \mathcal{E}, \mathbf{a}_j \mathbf{x} \leq \mathbf{b}_j \forall j \in \mathcal{I}\}. \quad (7)$$

The restrictions associated to indexes $i \in \mathcal{E}$ are specified as active, since they establish equality constraints, while the restrictions associated to indexes $j \in \mathcal{I}$ are denoted as inactive.

3. ACTIVE RESTRICTION METHOD

In the active restriction method, given an estimation $\mathbf{x}^k \in \mathcal{S}$, a minimization subproblem is defined with active restrictions associated to \mathbf{x}^k . The active restrictions define a working set $\mathcal{W}_k := \{i \in \mathcal{E} + \mathcal{I}, \mathbf{a}_i \mathbf{x} = \mathbf{b}_i\}$. If \mathbf{x}^k is not the optimal solution, meaning that it does not minimize the quadratic form, then a new direction and a new solution \mathbf{x}_{k+2} has to be found, starting a new iteration of the method. It is important to remark that when a new solution \mathbf{x}_{k+1} is found the working set \mathcal{W}_k can be modified, since any restriction defined initially as active, can be now inactive and viceversa. The new feasible direction \mathbf{d}^k is found by considering that $\tilde{\mathbf{x}}_k = \mathbf{x}_k + \mathbf{d}_k$ is the solution of the following minimization problem:

$$\text{Minimize } f(\mathbf{x}) = \frac{1}{2} \mathbf{x}^T \mathbf{Q} \mathbf{x} + \mathbf{x}^T \mathbf{p} \quad (8a)$$

$$\text{sujeito a } \{\mathbf{a}_i^T \mathbf{x} = b_i, \quad i \in \mathcal{W}_k \quad (8b)$$

and the feasible direction is $\mathbf{d}_k = \tilde{\mathbf{x}}_k - \mathbf{x}_k$ and a new \mathbf{x}^{k+1} solution is obtained by:

$$\mathbf{x}_{k+1} = \mathbf{x}_k + \alpha_k \mathbf{d}_k, \quad (9)$$

where α_k is chosen in order to assure that the new solution remains in the feasible region \mathcal{S} as follows

$$\alpha_k = \min \left(1, \min_{\substack{j \notin \mathcal{W}_k, \\ \mathbf{a}_j^T \mathbf{d}_k > 0}} \frac{b_j - \mathbf{a}_j^T \mathbf{x}_k}{\mathbf{a}_j^T \mathbf{d}_k} \right). \quad (10)$$

If $\alpha_k < 1$ there is a restriction which does not belong to \mathcal{W}_k that intersects with the direction \mathbf{d}_k . In this case, this restriction must be included into \mathcal{W}_k obtaining a new $\mathcal{W}_{k+1} \neq \mathcal{W}_k$. The method proceeds performing a new iteration (computing a new (9)) and including new restrictions until \mathbf{x}^{k+1} is optimal (being a local minimizer), i.e. it is the minimizer in the polytope defined by the active restrictions that belongs to \mathcal{S} . This means that $\tilde{\mathbf{x}}^{k+1}$ is a candidate for local minimizer in its working set \mathcal{W}_{k+1} and since $\mathbf{x}^{k+1} = \tilde{\mathbf{x}}^k$, then $\mathbf{d}^k = 0$.

Given a initial feasible solution \mathbf{x}_0 ;
 Set \mathcal{W}_0 as a subset with the active restrictions associated to \mathbf{x}_0
for $k = 0, 1, 2, \dots$ **do**
 Find the solution \mathbf{x}^* of the problem (8) below

$$\begin{aligned} \text{Minimize } f(\mathbf{x}) &= \frac{1}{2} \mathbf{x}^T \mathbf{Q} \mathbf{x} + \mathbf{x}^T \mathbf{p} \\ \text{subject to } \mathbf{a}_i^T \mathbf{x} &= b_i, \quad i \in \mathcal{W}_k \end{aligned}$$

 Compute $\mathbf{d}_k = \mathbf{x}^* - \mathbf{x}_k$.

if $\mathbf{d}_k = 0$ **then**

 Compute λ_i satisfying (12)

$$\sum_{i \in \mathcal{W}} \lambda_i \mathbf{a}_i = \mathbf{Q} \mathbf{x}_k + \mathbf{p}$$

 and set $\mathcal{W} = \mathcal{W}_k$;

if $\lambda_i \leq 0, \forall i \in \mathcal{W}_k \cap \mathcal{I}$ **then**

STOP. The desired solution is \mathbf{x}_k ;

else

 Take $j = \max_{j \in \mathcal{W}_k \cap \mathcal{I}} \lambda_j$, $x_{k+1} = x_k$; and $\mathcal{W}_{k+1} \leftarrow \mathcal{W}_k \setminus j$;

end if

else if ($\mathbf{d}_k \neq 0$) **then**

 Compute α_k , and $\mathbf{x}_{k+1} = \mathbf{x}_k + \alpha_k \mathbf{d}_k$.

if $\alpha_k < 1$ **then**

 (some restrictions must be included),

 obtain \mathcal{W}_{k+1} including new restrictions to \mathcal{W}_k ;

else

$\mathcal{W}_{k+1} \leftarrow \mathcal{W}_k$

end if

end if

end for

To verify if a candidate solution \mathbf{x}^{k+1} with $\mathbf{d}^k = 0$ is a local minimizer, the Lagrange multiplier λ_i of the following expression are computed [1]:

$$\sum_{i \in \mathcal{W}} \lambda_i \mathbf{a}_i = \nabla f(\hat{\mathbf{x}}) = \mathbf{Q} \hat{\mathbf{x}} + \mathbf{p}. \quad (12)$$

If all $\lambda_j, j \in \mathcal{W} \cap \mathcal{I}$ are negatives or zero, then \mathbf{x} is a local minimizer for problem 6 and it can be considered as its solution. On the other hand, if some Lagrange multipliers λ_j are positive meaning that there is a feasible minimizing direction, then the restriction associated to those Lagrange multipliers

must be included to the working set, so the new working set $\mathcal{W}_k \subset \mathcal{W}_{k+1}$ and the iteration continues. Details about the stopping criterion, as well as the convergence criterion of the algorithm can be seen in [1]. The algorithm is summarized as follows:

4. NUMERICAL RESULTS

In this section the numerical results of the following optimal distribute parabolic control problem are presented:

$$\begin{cases} z_t + z_{xx} = v, & x \in \Omega, t \geq 0, \\ z(x, 0) = 0, & x \in \Omega, t = 0, \\ z(x, t) = 0, & x \in \partial\Omega, t \geq 0 \\ \eta \leq v \leq \theta, & \eta, \theta \in \mathbb{R} \end{cases} \quad (13)$$

where $\Omega = [0, 1] \times [0, 1]$. The target function is chosen as *target* $y^*(x) = x_1(1 - x_1)e^{-x_1}x_2(1 - x_2)e^{-x_2}$. The functional to be minimized is given by the expression (3).

The spatial domain Ω is discretized using a uniform grid with grid spacing $h = (1 - 0)/N_x$. $N_x = N_y$ are the number of grid points in the direction x and y , respectively. The time domain $[t_0, t_f]$ is discretized in N_t points with $\tau = (1 - 0)/N_t$. The internal tolerance for the iterative method is $tol = 10^{-6}$.

Experiment 1. In this experiment we analyze the influence of the tuning parameters α , β and γ in the quality of the solution. To this end, we consider values of $\eta = -100$ and $\theta = 100$. These values are high enough to decouple the influence of α , β and γ in the solution of the influence of η and θ . This means that the inequality restrictions are not active.

The solution is for two values of α , leaving β and γ as constants is presented at Figures 1 (a) and (b). The Figure 1 presents the temperature at the middle point of the circuit. Observe that increasing the value of α the difference between the solution obtained by the algorithm \mathbf{y} and the target function $\tilde{\mathbf{y}}$ is minimized. The optimal value of α is 33.81. The influence of β is important to deal with the boundary layer in the neighborhood of t_f . The optimal value is found around $\beta = 100$.

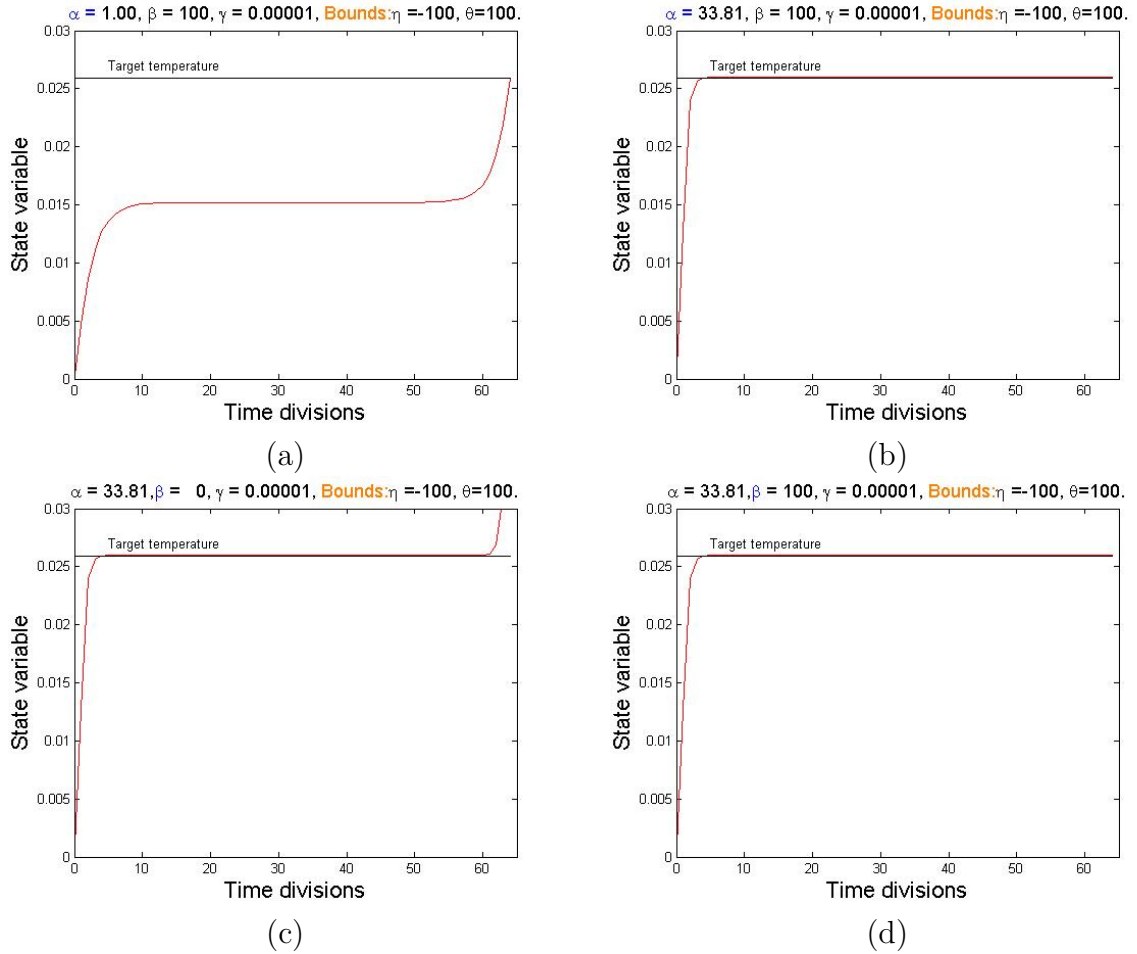


Figure 1: Numerical solution and reference target function at the middle point of the circuit. (a) $\alpha = 1$, $\beta = 100$ and $\gamma = 0.00001$; (b) $\alpha = 33.81$, $\beta = 100$ and $\gamma = 0.00001$; (c) $\alpha = 33.81$, $\beta = 0$ and $\gamma = 0.00001$; (d) $\alpha = 33.81$, $\beta = 100$ and $\gamma = 0.00001$; (e) $\alpha = 33.81$, $\beta = 100$ and $\gamma = 0.001$; (f) $\alpha = 33.81$, $\beta = 100$ and $\gamma = 0.00001$;

When the value of γ varies leaving α and β as constants, a better solution \mathbf{y} is obtained when γ is decreased, and in fact it can be observed a stronger influence of γ in the solution than the other two parameters. The optimal value of γ is found at $1e-5$.

Experiment 2. In this experiment, the sensibility of the methods is analyzed, in terms of number of iterations as a function of the parameters η and θ , that defines the constraints (5). For this experiment it is considered $\alpha = 33.81$, $\beta = 100$ and $\gamma = 0.00001$, $N_x = 10$ and $N_t = 257$.

In Tables 1 and 2 the number of iterations and constraints required by the Algorithm 1 are shown as a function of η and θ , respectively. Observe that the algorithm is more sensible to θ (upper bound) than η (lower bound). In

		upper bound θ						
		10	6	4	3.5	3	2.5	2
lower bound η	-10	1 (0)	13	83	150	283	607	1058
	-6	1	13	83	150	283	607	1058
	-2	1	13	83	150	292	638	1159
	-1	1	13	83	153	289	806	1223
	0	1	13	91	185	312	802	1205
	1	1279	1287	1347	1358	1437	1851	2142

Table 1: Number of iterations of the algorithm as a function of η and θ .

		upper bound θ						
		10	6	4	3.5	3	2.5	2
lower bound η	-10	0	24	164	298	564	1216	2134
	-6	0	24	164	298	564	1216	2134
	-2	0	24	164	298	568	1224	2140
	-1	0	24	164	304	576	1222	2140
	0	0	24	180	368	622	1228	2144
	1	2716	2734	2852	2882	2978	3270	3956

Table 2: Number of active restrictions depending on the values of η and θ .

Table 1 can be observed that the number of iterations needed by the algo-

rithm to obtain a solution is increased when the upper bound θ is tighter. A similar behavior can be observed with respect to the lower bound η , although for this case, the behavior is much smoother.

The behavior observed at Table 1 can be understood better observing the Table 2. Notice that when the distance between θ and η are decreased, the number of active restrictions is increased. Then the algorithm has a necessity to increase the number of iterations for seeking a solution.

5. CONCLUDING REMARKS

In this article a tool for analyzing the distribution of temperature in a circuit board was presented. The problem of optimal distribution was modeled using an optimization with constraints approach where the performance functional was quadratic and the constraints were equality and inequality, associated to the differential equation and the restriction on the controller. The active restriction method was used for solving this optimization problem. The results help to understand the value of the restriction in the inequality constraints in order to have a physical relevant solution, as well as the desired response (solution) of the distribution of temperature in the board. In addition, it was observed that the more restrictive the inequalities are, it is more difficult (it takes more iterations) to obtain the convergence of the algorithm. As a consequence, the algorithm has more computational cost in terms of running time.

Acknowledgement. CES acknowledges the partial support given by the CONACYT for this work thorough the PRONII program.

References

- [1] NOCEDAL, J, WRIGHT, S, 1999. Numerical Optimization, Springer-Verlag New York, Inc., 175 Fifth Avenue, New York, NY 10010, USA.
- [2] FRIEDLANDER, A, 2009. Elementos de Programação não-linear, Wiley, IEEE PRESS, USA - New Jersey.
- [3] LUENBERGER, D, 1986. Linear and nonlinear programming. 2nd ed., New York, Addison – Wesley Publishing Company.

- [4] JANICKI, M, NAPIERALSKI, A, 2000. Modelling electronic circuit radiation cooling using analytical thermal model, *Microelectronics Journal* 31: 781-785.
- [5] JANICKI, M, DE MEY, G, NAPIERALSKY, A, 2002. Transient thermal analysis of multilayered structures using Green's functions, *Microelectronics Reliability Journal* 42: 1059-1064.
- [6] FLEITAS FIGUEREDO, J, STALDER, J, 2010. Una aplicación paralela en el tiempo para la simulación y control de ecuaciones diferenciales parciales parabólicas, Bachelor Thesis, Engineering School, FIUNA - National University of Asuncion.
- [7] TIBA, D, NEITTAANMÄKI, P, 1994. Optimal Control of Nonlinear Parabolic System, Marcel Dekker Inc.
- [8] DU, X, SARKIS, M, SCHAERER, CE, SZYLD, DB, 2013. Inexact and truncated Parallel in Time Krylov subspace methods for Parabolic Optimal Control Problems, *Electronic Transactions on Numerical Analysis*, V. 40: 36-57.
- [9] MATHEW, T, SARKIS, M, SCHAERER, CE, 2010. Analysis of block parareal preconditioners for parabolic control problems, *SIAM Journal on Computing*, V. 32: 1180-1200.

A Parallel-in-time solution for a Parabolic Differential Control Problem with PETSc

Juan José Cáceres^{ab}, Benjamín Barán^{abc}, Christian Schaerer^a

^aLaboratorio de Computación Científica y Aplicada, Facultad Politécnica,
Universidad Nacional de Asunción, Paraguay

^bFacultad de Ciencias y Tecnología, Universidad Católica - Nuestra Señora de la
Asunción, Paraguay

^cFacultad Politécnica, Universidad Nacional del Este, Paraguay

Abstract

An optimal control problem for parabolic differential equations can be solved using numerical methods when there is no known algebraic solution. This can be done using time and space discretizations and finding an approximate solution. When the solution needed is not just the last instant of the evolution, but every modeled instant, some memory problems arise in the problem discretization, due to the huge size achieved from the involved matrices.

This work presents a parallel solution scheme on Portable Extensible Toolkit for Scientific Computation (PETSc) for an Optimal Control Problem for Parabolic Differential Equations using a dual layer KSP solvers that uses the Multiple-Shooting method to overcome the memory problems presented.

Keywords: Parabolic control, multiple-shooting, PETSc, Parallel computing

1. INTRODUCTION

A large amount physical phenomenons are modeled by partial differential equations (PDE) [2]. Some of those phenomenons studied in engineering are diffusion processes such as the heat dissipation, polyphasic fluid diffusion, diffraction tomography among others, are modeled by parabolic partial differential equations. Furthermore, in order to interact with the processes, a control function is introduced to the equations, so that the process can reach some desired target value.

The optimal control problem rises when the usage of the control function and the target process value are conflicting variables [16]. In this work, a cost function $J(y, v)$ is defined that relates the modeled process y and the usage of the control variable v .

$$\begin{cases} \text{minimize} & J(y, v) \\ \text{s.t.} & \nabla_t y = \Delta_x y + v \end{cases} \quad (1)$$

The solution of the control problem is to find v in order to satisfy (1).

This work presents theoretical bases used to solve (1), then discusses the construction of a dual layer Krylov Subspace Problem (KSP) [2] solver in PETSc. An example of this method was used in a previous work [1], where execution results are shown, because this work focuses on general concepts about using the dual layer KSP approach, no time results are presented.

2. PROBLEM MODEL

To solve the optimal control problem (1) the discretization proposed in [7] is used, that uses the finite differences method for the time discretization and finite elements method for the spatial discretization. This approach transforms the problem into the linear system:

$$\begin{bmatrix} \mathbf{Q} & 0 & \mathbf{E}^T \\ 0 & \mathbf{G} & \mathbf{N}^T \\ \mathbf{E} & \mathbf{N} & 0 \end{bmatrix} \begin{bmatrix} \mathbf{z} \\ \mathbf{u} \\ \mathbf{q} \end{bmatrix} = \begin{bmatrix} \mathbf{f}_1 \\ \mathbf{0} \\ \mathbf{f}_3 \end{bmatrix} \quad (2)$$

The system (2) can be solved in terms of the discrete control variable \mathbf{u} as shown in [11, 12, 1]:

$$\mathbf{H}\mathbf{u} = \mathbf{b} \quad (3)$$

where $\mathbf{H} = \mathbf{G} + \mathbf{N}^T \mathbf{E}^{-T} \mathbf{Q} \mathbf{E}^{-1} \mathbf{N}$ and $\mathbf{b} = \mathbf{N}^T \mathbf{E}^{-T} (\mathbf{Q} \mathbf{E}^{-1} \mathbf{f}_3 - \mathbf{f}_1)$. This is a parabolic linear system and there are many solutions for this type of problem in the literature [3]. The usual PDE solution involves building the input matrix \mathbf{H} and the right hand side vector \mathbf{b} [2, 4, 10].

In this case, the input matrix \mathbf{H} is dense because it involves an operation with \mathbf{E}^{-1} , the inverse of the sparse matrix \mathbf{E} [18, 17, 20] and this is very expensive in computational resources [9, 19].

3. SOLUTION MODEL

The solution implemented in PETSc is a dual layer KSP scheme, to avoid building matrix \mathbf{H} [8]. The outer solver is used to solve equation (3) and the inner solver is used to calculate the product of \mathbf{E}^{-1} and a vector.

To aid in the speed of the solution [1], the inner solver used finds a coarse approximation with the Parareal method [14] using a multiple-shooting [6] approach.

This work presents a way to build the fine and coarse matrices needed for the parallel implementation of the dual layer scheme, then describes a way to edit the standard Conjugate Gradient method (used as the outer solver) to use the coarse inner solver. This inner solver is not included as a PETSc routine [5], therefore the coarse inner solver functions are also described.

The main issues to build a functional solver is to address the locality of the data structures. This is very important, because each processor can only access its local data structures and its portion of the calculated solution. In this type of data distribution, the full problem and solution are held among the different processors.

For the coming subsections, the following naming conventions are used: \hat{q} is the size of the space discretization of the state function, \hat{p} is the size of the space discretization of the controller, \hat{l} is the size of the time discretization (considered as the fine time discretization), \hat{k} is the size of the coarse time discretization (for the inner solver). Notice that \hat{k} must divide \hat{l} to have proper decomposition from the whole problem, for the approximation in each processor, and let $\hat{m} = \hat{k}/\hat{l}$ be the amount of fine intervals for each coarse interval.

3-A. Local Data Structures

The local data structures used are available in all the processors, as this structures are replicated its size should be small to avoid memory complications.

Using the method proposed in [1], the problem (1) is first discretized in space and second in time. The space discretization is therefore considered as a basic structure for both fine and coarse time discretizations.

All of the resulting matrices of the finite elements method [2] will be included as local. This is:

$$M\dot{\underline{z}} = K\underline{z} + B\underline{u} \quad (4)$$

$$\begin{aligned}
J_h(\underline{z}, \underline{u}) &= \frac{\alpha}{2} \int_{t_0}^{t_f} (\underline{z} - \underline{z}^*)^T M (\underline{z} - \underline{z}^*) dt \\
&+ \frac{\beta}{2} \{ [\underline{z}(t_f) - \underline{z}^*(t_f)]^T M [\underline{z}(t_f) - \underline{z}^*(t_f)] \} + \frac{\gamma}{2} \int_{t_0}^{t_f} \underline{u}^T R \underline{u} dt
\end{aligned} \tag{5}$$

Equations (4) and (5) are the results of the discretization of Equation (1) [8]. The matrices $F_0 = M$ and $F_1 = M + \tau K$ are also stored and they are used as auxiliary in this approach.

3-B. Parallel Data Structures

This work is centered in the time parallelization of the problem, so the parallel data structures used are the resulting matrices of the time discretizations and the solution of the problem.

The smallest size of the parallelization so that this approach can be used is that each process holds at least one coarse time interval. To allow the coarse approximation, the process should have the fine time intervals that makes up the coarse time interval, so it holds at least \hat{l}/\hat{m} fine time intervals. The problem is divided in a way that the coarse time intervals belong to just one process, in other words, each process has an integer amount of coarse time intervals.

3-C. Algorithms

The outer KSP layer is just a slight variation of a standard solver. As an example, the Conjugate Gradient method can be used for the outer layer because the matrix \mathbf{H} of Equation (3) is positive semidefinite [3, 8]. The algorithm used for the Conjugate Gradient method [4], where A is the data matrix, b is the right hand side vector, x_0 is the initial solution guess, max_i is the iteration limit for convergence and ε is the error tolerance for the solution, is presented in Algorithm 1.

The function used to avoid building matrix \mathbf{H} is presented in Algorithm 2, where \mathbf{G} , \mathbf{N} , \mathbf{E} , \mathbf{Q} are the matrices presented in Section 2 and \mathbf{s} is the vector \mathbf{H} must be multiplied with. All the operations used are standard sparse matrix-vector operations, that result in a vector. Notice that this function doesn't create a dense matrix, since matrix \mathbf{H} is not created and every matrix used is sparse [1], which is the main advantage of this approach.

Algorithm 1 Conjugate Gradient

Input: $A, b, \varepsilon, x_0, max_i$

Output: x

```

1:  $r_0 \leftarrow b - Ax_0$ 
2:  $p_0 \leftarrow r_0$ 
3:  $i \leftarrow 0$ 
4: while  $r_{i+1} \geq \varepsilon \wedge i < max_i$  do
5:    $\alpha_i \leftarrow \frac{r_i^T r_i}{p_i^T A p_i}$  ▷  $A p_i$  is calculated by the Algorithm 2
6:    $x_{i+1} \leftarrow x_i + \alpha_i p_i$ 
7:    $r_{i+1} \leftarrow r_i - \alpha_i A p_i$  ▷  $A p_i$  is calculated by the Algorithm 2
8:    $\beta_i \leftarrow \frac{r_{i+1}^T r_i}{r_i^T r_i}$ 
9:    $p_{i+1} \leftarrow r_{i+1} + \beta_i p_i$ 
10:   $i \leftarrow i + 1$ 
11: end while
12: if  $r_{i+1} < \varepsilon$  then
13:   return  $x_i$  ▷ Convergent
14: else
15:   return n.c. ▷ Non-Convergent
16: end if

```

Because Algorithm 2 is called in every iteration of the outer solver, although its possible to introduce a second standard iterative solver (not using an approximation) would result in squaring the computational complexity of the solution [1].

Algorithm 2 Matrix-Vector product $\mathbf{H}\mathbf{s}$

Input: $\mathbf{G}, \mathbf{N}, \mathbf{E}, \mathbf{Q}, \mathbf{s}$

Output: \mathbf{x} ▷ $\mathbf{x} = \mathbf{H}\mathbf{s} = \mathbf{G}\mathbf{s} + \mathbf{N}^T \mathbf{E}^{-T} \mathbf{Q} \mathbf{E}^{-1} \mathbf{N}\mathbf{s}$

```

1:  $\mathbf{s}_1 \leftarrow \mathbf{G}\mathbf{s}$ 
2:  $\mathbf{s}_2 \leftarrow \mathbf{N}\mathbf{s}$ 
3:  $\mathbf{s}_3 \leftarrow \mathbf{E}^{-1} \mathbf{s}_2$  ▷  $\mathbf{E}\mathbf{s}_3 = \mathbf{N}\mathbf{s}$  is approximated by the Algorithm 3
4:  $\mathbf{s}_4 \leftarrow \mathbf{Q}\mathbf{s}_3$  ▷  $\mathbf{s}_4 = \mathbf{Q}\mathbf{E}^{-1} \mathbf{s}_2$ 
5:  $\mathbf{s}_5 \leftarrow \mathbf{E}^{-T} \mathbf{s}_4$  ▷  $\mathbf{E}^T \mathbf{s}_5 = \mathbf{Q}\mathbf{s}_3$  is approximated by the Algorithm 3
6:  $\mathbf{x} \leftarrow \mathbf{s}_1 + \mathbf{N}^T \mathbf{s}_5$  ▷  $\mathbf{x} = \mathbf{G}\mathbf{s} + \mathbf{N}^T \mathbf{s}_5$ 

```

The Parareal method implemented for the approximation is given by Al-

gorithm 3, where b is the right hand side vector, E_g is the coarse preconditioning matrix, C is the coarse state matrix, Z^0 is the initial coarse guess, \hat{k} is the amount of coarse intervals, \hat{m} is the amount of fine intervals per coarse interval and ε the error tolerance of the solution.

Algorithm 3 Parallel in time Parareal

Input: $b, E_g, C, Z^0, \hat{k}, \hat{m}, \varepsilon$

Output: y

```

1:  $S \leftarrow \text{fineSolver}(b, \hat{k}, \hat{m})$  ▷ Call to Algorithm 4
2:  $Z \leftarrow Z^0$ 
3:  $R \leftarrow S - C \times Z$  ▷  $\mathbf{R}^1 \leftarrow \mathbf{S} - \mathbf{CZ}^0$ , communicates  $S^k$  to the next process
4:  $\varepsilon_0 \leftarrow \|R\|$ 
5: while  $\|R\|/\varepsilon_0 > \varepsilon$  do
6:    $\text{coarse} \leftarrow E_g^{-1}R$  ▷  $aux \leftarrow \mathbf{E}_g^{-1}\mathbf{R}^i$ 
7:    $Z \leftarrow Z + \text{coarse}$  ▷  $\mathbf{Z}^{i+1} \leftarrow \mathbf{Z}^i + aux$ 
8:    $R \leftarrow S - C \times Z$  ▷  $\mathbf{R}^{i+1} \leftarrow \mathbf{S} - \mathbf{CZ}^i$ 
9: end while
10:  $y \leftarrow \text{marching}(b, x_{i-1}, \hat{k}, \hat{m})$  ▷ Call to Algorithm5
11: return  $y$ 

```

In this implementation, the only explicit call for data communication between different processes is in Step 3 of Algorithm 3. The function `fineSolver` acts as a preconditioner for the coarse system, and it is defined in the Algorithm 4, while the function `marching` extends the coarse approximation to the fine intervals.

Algorithm 4 fineSolver

Input: b, \hat{k}, \hat{m}

Output: S

```

1: for all  $k < \hat{k}$  do ▷ parallel loop, distributed in  $\hat{k}$  processes
2:    $s \leftarrow \vec{0}$ 
3:   for all  $i < \hat{m}$  do ▷ local loop
4:      $s \leftarrow F_1^{-1}(F_0s - b(k, i))$  ▷  $sum_{i+1} = F_1^{-1}[F_0sum_i - \underline{b}(j_{k-1} + i)]$ 
5:   end for
6:    $S(k) = s$ 
7: end for
8: return  $S$ 

```

Algorithms 4 and 5 are similar, but while Algorithm 4 is used to get a coarse grid starting point from a fine grid, Algorithm 5 is used to get a fine grid from the processed coarse grid.

Algorithm 5 marching

Input: $b, coarse, \hat{k}, \hat{m}$

Output: y

```

1: for all  $k < \hat{k}$  do                                ▷ parallel loop, distributed in  $\hat{k}$  processes
2:    $z \leftarrow coarse(k)$ 
3:   for all  $i < \hat{m}$  do                                ▷ local loop
4:      $z \leftarrow F_1^{-1}(F_0 z - b(i, k))$            ▷  $z_{i+1} = F_1^{-1}[F_0 z_i - \underline{b}(j_{k-1} + i)]$ 
5:      $y(k, i) = z_i$ 
6:   end for
7: end for
8: return  $y$ 

```

The next section will analyze the PETSc functions needed to implement the Algorithms.

4. PETSc

This section describes how to implement in PETSc the solution proposed following the order of section 3.

The first definition needed is the data locality. PETSc needs to establish the context in which each task will be launched and the context for each data structure. The context `SELF` is used for local tasks and data structures and the context `WORLD` is used for parallel tasks and data structures.

To build a local PETSc matrix `mat` from a standard C array `M`, of `rows` count of rows and `cols` count of columns, the following code can be used:

Local Matrix Creation

```

MatCreate(PETSC_COMM_SELF,&mat);
MatSetSizes(mat,PETSC_DECIDE,PETSC_DECIDE,rows,cols);
MatSetType(mat,MATAIJ);
for (i=0; i<rows; i++) {
    for (j=0; j<cols; j++) {
        if (val=M[i][j]) {
            MatSetValues(mat,1,&i,1,&j,&val,INSERT_VALUES);
        }
    }
}

```

To build a parallel PETSc matrix `pmat`, this creation statement includes the number of rows of the whole matrix `rows` and number of columns `cols`, the expected non-zero values per row of the diagonal `dnz` and the off-diagonal `onz` [5], and it leaves PETSc to decide the amount of rows per process from the amount of launched processes (the number rows per process can be forced to ensure the correct functioning of the application).

During the insertion each parallel process should only access the rows it owns, and the insertion uses the same `MatSetValues` function as in the local matrix case:

Parallel Matrix Creation

```

MatCreateMPIAIJ(PETSC_COMM_WORLD,PETSC_DECIDE,PETSC_DECIDE,
rows,cols,dnz,PETSC_NULL,onz,PETSC_NULL,&pmat);
MatGetOwnershipRange(pmat,&rstart,&rend);
for (i=rstart; i<rend; i++) {
    for (j=0; j<cols; j++) {
        ...
        MatSetValues(pmat,1,&i,1,&j,&val,INSERT_VALUES);
        ...
    }
}

```

The basic operations used on this work are the matrix-vector product and the vector-vector linear combination. Let `pmat` be a parallel PETSc matrix of `rows` rows and `cols` columns and `pvec`, `pvec2` parallel PETSc vectors of `cols` elements, then the following operations can be used:

 Basic Operations

```

\\ Matrix-Vector product
VecCreate(PETSC_COMM_WORLD,&result);
VecSetSizes(result,PETSC_DECIDE,rows);
VecSetFromOptions(result);
MatMult(pmat,pvec,result);
\\ Vector-Vector linear combination
VecAXPBY(pvec2,a,b,pvec); \\pvec2=a*pvec+b*pvec2

```

The context operations used in this work are a linear system solver and the communication between processes. For the linear system, let $Ax = b$ be the problem where the matrix A is stored in the PETSc array `pmat` and the right hand side vector b is stored in the PETSc vector `pvec`. For the communication between processes, suppose that you want to copy the vector elements stored in the index `C` vector `ix` of the PETSc parallel vector `source`, to the respective `ix2` index positions of the PETSc parallel vector `dest`.

 Advanced Operations

```

\\ Ax=b solver
KSPCreate(PETSC_COMM_WORLD,&ksp);
KSPSetOperators(ksp,pmat,pmat,SAME_NONZERO_PATTERN);
KSPSetUp(ksp);
KSPSolve(ksp,pvec,result);
\\ Process communication
ISCreateGeneral(PETSC_COMM_SELF,size,ix,PETSC_COPY_VALUES,&from);
ISCreateGeneral(PETSC_COMM_SELF,size,ix2,PETSC_COPY_VALUES,&to);
VecScatterCreate(source,from,dest,to,&scat);
VecScatterBegin(scat,source,dest,INSERT_VALUES,SCATTER_FORWARD);
VecScatterEnd(scat,source,dest,INSERT_VALUES,SCATTER_FORWARD);

```

With this operations the steps required in the presented algorithms can be built, therefore a program can be built in PETSc to solve a parabolic differential control system.

5. Results

As this paper focuses on a general way to implement a dual layer KSP solver, the results prove that the approach works without considering time

investments, since they depend on the solvers used (both outer and inner solver). Furthermore the infrastructure on which the application is run could affect the resolution times of the different approaches.

Table 1: Outer iterations(Inner iterations)

ε_i	IFOM	pCG(1)	pCG(2)
10^{-12}	16(586)	16(586)	16(580)
10^{-10}	17(510)	17(510)	17(502)
10^{-8}	18(442)	18(442)	18(414)
10^{-7}	18(362)	18(362)	18(364)
10^{-6}	21(338)	21(338)	21(342)
10^{-5}	24(274)	24(274)	24(280)
10^{-4}	28(220)	28(220)	63(312)

Table 1 shows the iterations used for the resolution in the single process reference paper [8] labeled as IFOM and iterations of different amount of processes in the proposal labeled as pCG(p). Since columns IFOM and pCG(1) are the same, the implementation is validated. This shows that the dual KSP layer approach is a viable alternative to a traditional single KSP layer approach and that it increases problem sizes that can be solved by each hardware configuration, because no dense matrixes are built.

6. CONCLUDING REMARKS

This work presents details of the PETSc routines developed to implement the temporal marching of evolution equations in the context of an in-time parallelization scheme. The implemented routines can be used independently of the number of processes launched in the computing platform, or the number of nodes and processors in which those processes are executed. This allows an efficient implementation of evolution problems or more complex ones such as the optimal control problems faced in this work.

In the Solution Model a suitable set of known methods are presented, to find a solution using a double KSP layer approach. This selection of methods should be taken as a guide to solve the problem, as there are more methods that can be exchanged in either layer of the solution.

The most important PETSc functions needed for the implementation are described, and some examples are presented that should give insight to make

a working C program. The time advantages of the implementation presented (using CG as the outer layer and Parareal in the inner layer) are discussed in [1].

ACKNOWLEDGMENTS: C.S. acknowledges the support given by CONACyT through the PRONII program.

References

- [1] CÁCERES J., 2014. Implementación de un esquema de paralelización temporal utilizando PETSc. Engineering Thesis, Universidad Católica - Nuestra Señora de la Asunción
- [2] GOCKENBACH M., 2002. Partial differential equations: analytical and numerical methods. SIAM.
- [3] STRANG G., 1998. Introduction to Linear Algebra. Wellesley-Cambridge Press.
- [4] AXELSSON O., 1996. Iterative Solution Methods, Cambridge University Press.
- [5] BALAY S., BROWN J., BUSCHELMAN K., EIJKHOUT V., GROPP W., KAUSHIK D., KNEPLEY M., CURFMAN MCINNES L., SMITH B., ZHANG H., 2012. PETSc users manual. Technical Report ANL-95/11 - Revision 3.3, Argonne National Laboratory.
- [6] SCHAERER C., KASZKUREWICZ E., 2001. The shooting method for the solution of ordinary differential equations: A control-theoretical perspective. International Journal of Systems Science, 32(8).
- [7] KASZKUREWICZ E., SCHAERER C., MANGIAVACCHI N., 2007. A multilevel schwarz shooting method for the solution of the poisson equation in two dimensional incompressible flow simulations. Applied Mathematics and Computation, 153(3):803-831.
- [8] DU X., SARKIS M., SCHAERER C., SZYLD D., 2013. Inexact and truncated parareal-in-time Krylov subspace methods for parabolic optimal control problems. Electronic Transactions on Numerical Analysis.

- [9] FALGOUT R., MEIER YANG U., 2002. hypre: a library of high performance preconditioners. Numerical Solution of Partial Differential Equations on Parallel Computers.
- [10] FRITZ J., 1982. Partial Differential Equations. Springer.
- [11] GALLIER J., 2010. Schur complement and symmetric positive semidefnite (and defnite) matrices. Penn Engineering.
- [12] ZHANG F., 2005. Schur complement and its applications. Springer.
- [13] HAZEWINDEL M., 2001. Encyclopedia of Mathematics. Springer.
- [14] MADAY Y., LIONS J.L., TURINICI G., 2001. Résolution d'edp par un schéma en temps "pararéel". C. R. Acad. Sci. Paris Sér. I Math., 332(7):661-668.
- [15] HUNG-LIN LIU E., 2006. Fundamental methods of numerical extrapolation with applications. MIT Open Course Ware.
- [16] TIBA D., NEITTAANMÄKI P., 1994. Optimal Control of Nonlinear Parabolic Systems. Marcel Dekker, Inc.
- [17] SAAD Y., 2003. Iterative methods for sparse linear systems. SIAM.
- [18] STOER J., BULIRSCH R., 2002. Introduction to Numerical Analysis. Springer-Verlag, third edition.
- [19] VOGEL C., 2002. Computational Methods for Inverse Problems. SIAM.
- [20] WATKINS D., 2007. The Matrix Eigenvalue Problem. SIAM.

Harmonic Ritz control strategy for restarting GMRES(m)

Juan Carlos Cabral Figueredo¹, Christian Schaerer¹

¹ LCCA, Polytechnic School, National University of Asuncion, Paraguay.
P.O.Box: 2111 SL. Email: jccabral19@gmail.com, cschaer@pol.una.py

Abstract

The Generalized Minimal Residual (GMRES) method is normally used for the solution of large, sparse and non-symmetric linear systems of equations $Ax = b$. Due to the high computational cost of the construction of an orthogonal basis for a Krylov subspace, in practice, the restarted GMRES method (denoted as GMRES(m)) is used, since it constructs a Krylov subspace of dimension m . However, if an appropriate m is not chosen, the convergence of the GMRES algorithm is not guaranteed thus the method may experience stagnation or slow convergence. In the restarting strategy, important information is lost, and the resulting subspace may not be rich enough to guarantee the quality of the solution.

In this work we propose the appropriate combination of two techniques. Firstly, we enrich the subspace using approximate harmonic Ritz eigenvectors associated with the smallest harmonic Ritz eigenvalues. Secondly, to choose an appropriate parameter m , we consider the GMRES(m) method as a control problem, in which the parameter m is the controlled variable and chooses adaptively at each cycle. Numerical experiments show that the control inspired Ritz - GMRES(m) has good convergence and robustness than others adaptive method.

Keywords: GMRES, Krylov subspace, adaptive GMRES(m), control strategy, Harmonic Ritz eigenvectors controller

1. INTRODUCTION

The GMRES(m) is a popular iterative method for solving the large non-symmetric system of linear equations

$$Ax = b \tag{1}$$

At the j th cycle finds a solution of the form

$$x_j = x_{j-1} + V_m y_j, \tag{2}$$

where x_{j-1} is the previous approximate solution of x , and the residual is $r_{j-1} = b - Ax_{j-1}$; then V_m is a $n \times m$ matrix where its columns form an orthogonal basis of the Krylov Subspace $\mathcal{K}_m(A, r_{j-1}) \equiv \text{span}\{r_{j-1}, Ar_{j-1}, A^2r_{j-1}, \dots, A^{m-1}r_{j-1}\}$. Using the Arnoldi's relation $AV_m = V_{m+1}\tilde{H}_m$, y_j minimize the l_2 -norm of the residual $\|r_j\|_2 = \|b - A(x_{j-1} + V_m y_j)\|_2 = \|\beta e_1 - \tilde{H}_m y_j\|_2$.

The GMRES(m) consists in setting a fixed a maximum m , hence when the maximum m is reach, a new residual and a new Krylov subspace are computed, performing a new cycle. GMRES(m) is framed in the control formulation as follows:

$$\begin{aligned} z_j &= \text{GMRES}(A, r_{j-1}, m) \\ x_j &= x_{j-1} + z_j \\ r_j &= b - Ax_j \end{aligned} \tag{3}$$

where x_j is the state variable, and r_{j-1} and the parameter m are the control variables. To improve z_j (and consequently x_j), it is possible to modify r_{j-1} or m or both, where m is directly associated to computational cost of the method.

Properties of GMRES(m) are: 1) if m is not appropriate \rightarrow GMRES(m) converges slowly; and 2) important information of $\mathcal{K}_m(A, r_{j-1})$ is lost at the restarting $\rightarrow \mathcal{K}_m(A, r_{j-1})$, hence the new Krylov subspace may not be rich enough to maintain the rate of convergence.

2. HPD-GMRES(m)

We propose the combination of two techniques: *First Strategy*: Modify m at each iteration [5]. We use an updating law for m named discrete Proportional-Derivative controller with the form [1]:

$$m_j = m_{j-1} + \left[\alpha \frac{\|r_{j-1}\|}{\|r_{j-2}\|} + \gamma \frac{\|r_{j-1}\| - \|r_{j-3}\|}{2\|r_{j-2}\|} \right]. \tag{4}$$

where $\alpha, \gamma \in \mathbb{R}$.

- If GMRES(m) has poor convergence $\rightarrow \frac{\|r_{j-1}\|}{\|r_{j-2}\|} \approx 1$, if $\alpha > 0$, then m_j is increased.
- If GMRES(m) has a good convergence $\rightarrow \frac{\|r_{j-1}\|}{\|r_{j-2}\|} \approx 0$ and $\frac{\|r_{j-1}\| - \|r_{j-3}\|}{2\|r_{j-2}\|} < 0$. If γ is positive, the derivative part decrease the value of m_j .

Second Strategy: Enrich the Krylov subspace with Harmonic-Ritz vectors. A harmonic Ritz value $\tilde{\lambda}_i$ with harmonic Ritz vector $\varphi_i = Wg_i$, $g_i \in \mathbb{C}^{s \times 1}$, with respect to the subspace $AK_s(A, r_0)$ satisfies

$$(A\varphi_i - \tilde{\lambda}_i\varphi_i) \perp AK_s(A, r_0) \iff (AW)^H(AWg_i - \tilde{\lambda}_iWg_i) = 0. \quad (5)$$

Then the reduced eigenvalue problem is the $s \times s$ generalized eigenvalue problem

$$W^H A^H AWg_i = \tilde{\lambda}_i W^H A^H Wg_i \quad (6)$$

where W is a $n \times s$ matrix (its first m columns are Arnoldi's vectors and the last d corresponds to the approximate eigenvectors φ). Some g_i associated with the smallest λ_i are needed. An approximate eigenvector is $\varphi_i = Wg_i$, this deflates the smallest eigenvalues and thus improves the convergence.

At the end of j th restart cycle, HPD-GMRES(m, d) seeks the approximate solution x_j of the form

$$x_j = x_{j-1} + z_j \quad \text{with} \quad z_j \in \mathcal{K}_m(A, r_{j-1}) + \{\varphi_i\}_{i=1}^d \quad (7)$$

where $\{\varphi_i\}_{i=1}^d$ is a group of vectors constituted by d harmonic Ritz vectors associated with the smallest d (in magnitude) harmonic Ritz values. The pseudocode of the HPD-GMRES(m) is:

Algorithm

1. Given $A, x_{j-1}, r_{j-1}, m_{j-1}, \varphi_i$.
2. Compute m_j from Control strategy PD, do $s_j = m_j + d$.
3. Compute $AW_s = Q_{s+1}\tilde{H}$ using Arnoldi's iterations.
4. Compute $y = \arg \min_{y \in \mathbb{C}^s} \|\beta e_1 - \tilde{H}_s y\|$, if $\|r_j\| < \textit{tolerance}$, then stop, else compute the harmonic vectors φ_i and go to 1.

3. NUMERICAL RESULTS

Here it is reported some numerical results tested on a variety of matrices from Matrix Market Collection [10]), in particular the attention it is concentrated in two benchmark problems: *Sherman 5* and *Sherman 3*. Algorithms configurations are: the initial solution is $x_0 = 0$, stopping criterion is $\frac{\|r_j\|}{\|r_0\|} < 10^{-9}$ and the maximum number of iterations is 1000.

Table 1: Numerical results for Sherman 5 and Sherman 3.

Algorithms	Sherman 5		Sherman 3	
	Time (sec)	Iteration	Time (sec)	Iteration
LGMRES(27,3)	23,76	1000	7,06	289
GMRES-E(27,3)	8,35	275,6	38,14	1000
LGMRES-E(27,2,1)	33,55	665,2	8,37	220,2
HPD-GMRES(27,3)	14,94	74,6	17,84	72,6

For comparison purpose $Ax = b$ was solved using: LGMRES(m, l) (obtained from [11]) GMRES-E(m, d) (obtained from [4]), LGMRES-E(m, d, l) (obtained from [12]). The following values are considered for each method: LGMRES(m, l), $m = 27, l = 3$; GMRES-E(m, d), $m = 27, d = 3$; LGMRES-E(m, l, d), $m = 27, d = 3, l = 3$; HPD-GMRES(m, d), $m_{initial} = 27, m_{step} = 3, m_{min} = 3, m_{max} = 200, \alpha = 2, \gamma = 1$. To evaluate the algorithms were carried five runs and the results are averaged. For running the controller parameters α and γ , it is considered $\alpha = 2$ and $\gamma = 1$. This increase the value of m when have slows down convergence, and decrease it when have good convergence.

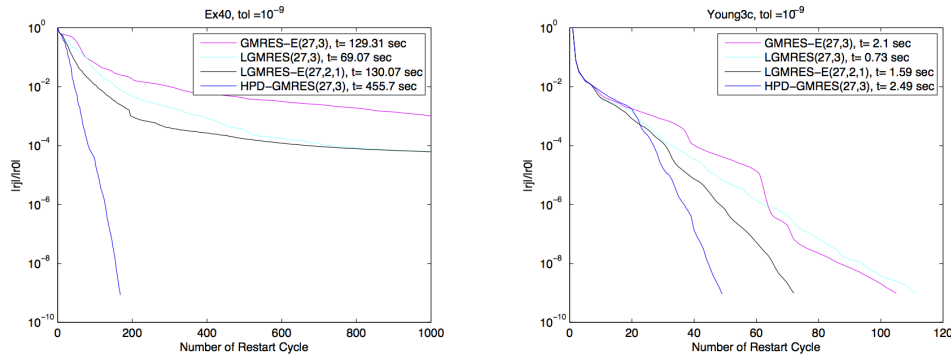


Figure 1: Relative residual norm Vs. Number of Restart Cycle.

Comparing in Figure 1 the behavior of the residual of the methods implemented, it is possible to observe that in all cases the HPD converges with a appropriate rate of convergence. However, this improvement has a cost in terms of timing (see Table 1) since the algorithm needs to compute Ritz eigenvalues.

4. CONCLUSION

In this work, we introduce the appropriate combination of two techniques for restarting GMRES. Firstly, we enrich the subspace using harmonic Ritz eigenvectors associated with the smallest harmonic Ritz eigenvalues. Secondly, we consider the GMRES(m) method as a control problem, in which the parameter m is the controlled variable chosen adaptively in each cycle. The advantage of this control strategy method is that only a few additional vectors need to be stored and the controller has the capability to increase the dimension of the Krylov subspace if any convergence problem is detected. Numerical experiments in classical problems [5] show that the control inspired HPD-GMRES(m) has good convergence properties in comparison to other adaptive methods.

ACKNOWLEDGMENTS: CES acknowledges the financial support given by CONACyT-PRONII. JCC acknowledges the schoollarship given by the ITAIPU-Binacional.

References

- [1] ROLANDO CUEVAS, CHRISTIAN E. SCHAERER AND AMIT BHAYA, *A control inspired strategy for varying the restart parameter m of GMRES(m)*, Congresso Nacional de Matemtica Aplicada e Computacional - CNMAC XXXIII, pp. 1000-1001, 2010.
- [2] M. EMBREÉ, *The tortoise and the hare restart GMRES*, SIAM J. on Num. Analysis, 2003.
- [3] R. B. MORGAN, *Computing interior eigenvalues of large matrices*, Linear Algebra Appl., 154- 156 (1991), pp. 289-309.

- [4] R. B. MORGAN, *A restarted GMRES methods augmented with eigenvectors*, SIAM J. MATRIX ANAL. APPL. Vol. 16, No. 4, pp. 1154-1171, October 1995.
- [5] A. H. BAKER, E. R. JESSUP, AND TZ. V. KOLEV, *A simple strategy for varying the restart parameter in GMRES(m)*, J. Comput. Appl. Math. pp. 751761, 2009.
- [6] QIANG NIU, AND LINZHANG LU, *Restarted GMRES method Augmented with the Combination of Harmonic Ritz Vectors and Error Approximations*, International Journal of Mathematical and Computational Sciences 6, 2012.
- [7] Y.SAAD, M.H. SCHULTZ, *GMRES: A generalized minimal residual method for solving nonsymmetric linear systems*, SIAM J. Sci. Statist. Comput., 7 (1986), pp. 856–869.
- [8] YOUSEF SAAD, *Iterative Methods for Sparse Linear Systems.*, Philadelphia, SIAM, (2003),
- [9] V. SIMONCINI AND D. B. SZYLD, *Recent computational developments in Krylov subspace methods for linear systems*, Numer. Linear Algebra Appl. 2007; 14:159.
- [10] T. DAVIS AND Y. HU, *The University of Florida Matrix Collection. Univ. of Florida and ATT Research.* Sitio web: <http://www.cise.ufl.edu/research/sparse/matrices/>.
- [11] A. H. BAKER, E. R. JESSUP, AND T. MANTEUFFEL, *A technique for accelerating the convergence of restarted GMRES*, SIAM J. Matrix Anal. Appl., pp. 962-984, 2005.
- [12] QIANG NIU, AND LINZHANG LU, *Restarted GMRES method Augmented with the Combination of Harmonic Ritz Vectors and Error Approximations*, International Journal of Mathematical and Computational Sciences 6, 2012.

Neural networks in the study of climate patterns seasonal

Juliana A. Anochi^{a c1}, Haroldo F. de Campos Velho^{b c}, José Demisio S. da Silva†

^aApplied Computing Graduate Program (CAP)

^bAssociated Laboratory for Computing and Applied Mathematics (LAC)

^cNational Institute for Space Research, São José dos Campos, SP, Brazil

Abstract

This work describes an Artificial Intelligence based technique to prepare data for constructing a climate prediction empirical model from reanalysis data in the South region of Brazil using Artificial Neural Network (ANN). The method uses Rough Sets Theory (RST) to reduce the amount of variables. The input of ANN there is two kinds of data: the variables chosen by the RST and full variables data to learn the seasonal behavior of the variable precipitation.

Keywords: Climate Prediction, Neural Networks, Rough Sets Theory.

1. CLIMATE PRECIPITATION PREDICTION BY ANN

The development of regional climate models from data considers the hypothesis that it is possible to extract information from historical data on the behavior of climatic conditions. Accordingly, development methodology needs to have a large number of data to ensure that the model considers a wide range of situations. However, despite able to ensure, in principle, greater robustness to the derived models, the handling of large volumes of data may require much computational. In this paper considered the use of Rough Sets Theory principles in extracting relevant information from the available data to achieve the reduction among the variables used for forecasting purposes.

Artificial Neural Networks (ANN) have emerged as excellent tools for deriving data oriented models because of their inherent characteristic of plasticity that permits the adaptation of the learning task when data is provided. In this regards, the use of an ANN is adequate to derive the forecasting model proposed in this paper. For the problem of building prediction models, as proposed in this paper, are used Multilayer Perceptron and models of recurrent Elman and Jordan [2].

¹E-mail Corresponding Author: juliana.anochi@lac.inpe.br

1.1 Rough Sets Theory

Rough Sets Theory was proposed in 1982 by Zdzislaw Pawlak as a mathematical theory to treat uncertain and imprecise information, by deriving approximations of a data set [4]. Rough Sets are based on the similarities among objects measured by an indiscernibility relation, which establish that a set of objects are similar (indiscernible) if they hold the same values for all of their attributes.

Rough Sets Theory uses the concept of Information Systems in which the available data are represented in a table in which the objects are displayed in the rows and the attributes in the columns [3]. Formally, an information system is composed of a finite non-empty set U (Universe) of objects and a finite non-empty set A of attributes, $IS = (U, A)$, so that, for each $a \in A$, $a : U \rightarrow V_a$. The set V_a is the set of values of a , that is, the domain of a .

A Decision System is an IS augmented with a decision attribute $d \notin A$. Formally, $DS = (U, A \cup \{d\})$, where $d \notin A$ is the decision attribute [3].

The indiscernibility relation is used as a measure of similarity among objects. Thus, a set of objects with the same attributes are indiscernible if only if their attributes hold the same values from their corresponding domains. This is an equivalence relation that may be used to treat problems as redundancy of attributes or the existence of irrelevant attributes in the data assigned to only one representative of a class.

The attribute reduction procedure is performed by the discernibility function $f_A(B)$ derived from the discernibility matrix which is a symmetric matrix constructed by comparing the attribute values that discern the objects. The attribute representing discernible values are inserted into the matrix. Each entry in the matrix consists of a set of attributes that distinguish a pair of objects x_i and x_j expressed by [3]:

$$M_{i,j} = \{a \in A \mid a(x_i) \neq a(x_j)\} \quad (1)$$

where $1 \leq i, j \leq n$ and $n = |U/IND_A(B)|$

2. EXPERIMENTS AND RESULTS

In the dimensionality reduction process the relevant attributes are those that mostly occur in the data, in terms of the indiscernibility relation. The data was downloaded from the reanalysis data repository from NCEP/NCAR. The data consists of monthly means from January 2000 to December 2009.

The geographic coordinates (Lat 35S, 22.5S) to (Lon 60W, 45W) with a spatial resolution of $2.5^\circ \times 2.5^\circ$.

The available variables are: air temperature (airt), Zonal Wind Components at vertical levels: 300hPa (v300), 500hPa (v500) and 850hPa (v850), Meridional Wind Components at vertical levels: 300hPa (u300), 500hPa (u500) and 850hPa (u850), Surface pressure (spres), Specific humidity (shum) and Precipitation (prec).

The variables that were reduced by the use of RST are: airt (77%), u300 (79%), u850 (80%), v300 (77%), v500 (79%), v850 (70%) and spres (78%). It is to be noticed that the variables that form the reducts have a presence greater than 70% in the discernibility function.

It is observed that of 7 variables out of 10, were considered relevant for South. Figure 1 shows the results for season winter of 2007 in the South region of Brazil.

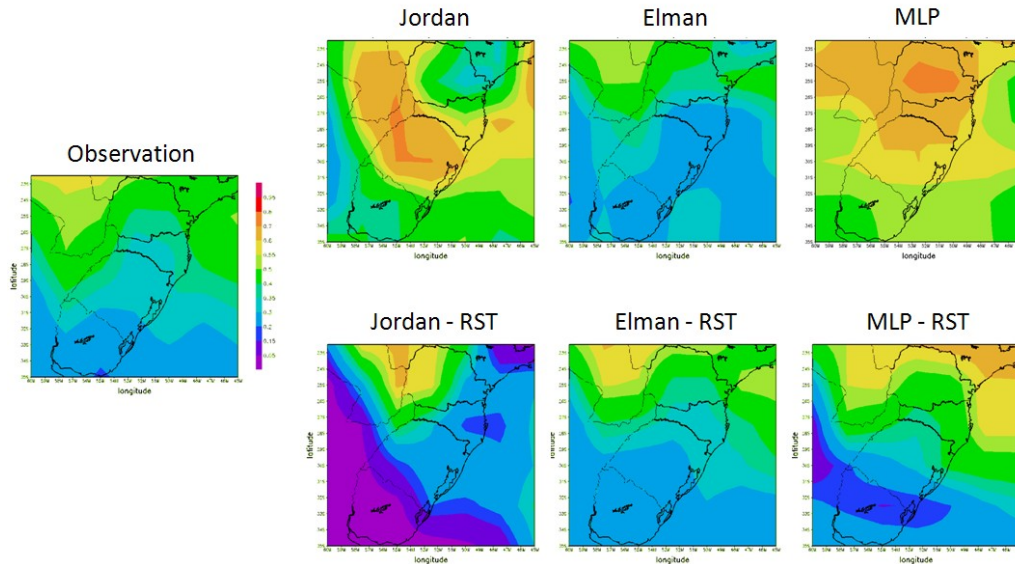


Figure 1 - Estimation of precipitation in the winter of 2007 in the South.

3. FINAL REMARKS

The proposed methodology works well with Elman-ANN using RST. The data reduction approach allows the derivation of smaller data sets derived from the resulting reducts for the training phase of the neural network without losing data expressiveness for forecasting purposes. Thus, the rough sets technique used in the data reduction process allows the identification of relevant information of the data for climate prediction. In addition, it is a technique that approaches the problem of dealing with huge amounts of data which is a characteristic of the processes in meteorology.

ACKNOWLEDGMENTS: The authors would like to thank CNPq for the financial support.

References

- [1] Elman L., 1990. Finding Structure in Time, *Cognitive Science*, 14:179-211.
- [2] Haykin, S, 1998, *Neural networks principles and practices*, 2 ed., Prentice Hall, Canada.
- [3] Komorowski, J., Pawlak, Z., Polkowski, L., Skowron, A., 1999. Rough sets: A tutorial. Rough fuzzy hybridization: A new trend in decision-making, 3-98.
- [4] Pawlak, Z, 1982, Rough sets, *International Journal of Computer and Information Sciences*, Poland, 1:341–356.

Particle Swarm Optimisation Algorithms for solving many-objective problems

Mateo Torres ^a, Benjamín Barán ^{a b}, Uri Yael^a

^a Universidad Católica “Nuestra Señora de la Asunción” - UCA

^b Universidad Nacional de Asunción - UNA

Abstract

As the number of conflicting objectives increases, multi-objective optimisation problems (MOPs) become harder to solve; reflecting this difficulty, they even receive the name of *many-objective* problems. Today, these difficult problems are mainly solved with evolutionary algorithms as the Non-dominated Sorting Genetic Algorithm (NSGA). This paper proposes the use of Particle Swarm Optimisation based algorithms for solving many-objective problems presenting evidence regarding the feasibility of the proposal.

Keywords: Multi-objective optimisation problems, Many-objective optimisation, Particle Swarm Optimisation, Non-dominated Sorting Genetic Algorithm.

1. INTRODUCTION

In multi-objective optimisation problems (MOPs), conflicts among objectives usually prevent from having a single optimal solution but rather a set of trade-off solutions known as Pareto optimal set [1, 2].

In the last years, it has been pointed out that the difficulty of MOPs increases for many-objective problems, i.e. problems having 4 or more objectives [1, 3]. In Pareto-based algorithms, these difficulties are intrinsically related to the fact that as the number of objectives increases, the proportion of non-dominated elements in the populations grows, being increasingly difficult to distinguish among solutions using only the dominance relation [2, 4]. Additionally, several algorithms are based on data structures with complexities that grow exponentially in the number of objectives and other factors [3, 5].

Once an algorithm finds a Pareto set, a decision maker selects a solution from this optimal set. This decision making is beyond the scope of this paper, which is limited to the steps required to obtain a good approximation

to the Pareto optimal set. At this stage, visualization of solution alternatives becomes very important. Although several methods have been proposed to this aim [6], there is a lack of a simple and intuitive way to represent solutions in objective space with more than three objectives [1].

As the number of objectives grows, the following phenomena becomes evident:

- Pareto-based algorithms as the well established NSGA are unable to provide the required selection pressure towards better solutions in order to conduct an efficient evolutionary search [1, 2].
- For a given set of solutions, as the number of objectives m increases, the expected growing of the domain space proportion e containing the points that the Pareto dominance classifies as non-comparable is given by the following expression:

$$e = \frac{2^m - 2}{2^m} \quad (1)$$

Note that $\lim_{m \rightarrow \infty} e = 1$. This phenomena indicates that Pareto dominance may be inadequate to discriminate among solutions in many-objective problems [1, 4].

In the following sections important concepts for understanding of MOPs are introduced. Also, this work illustrates the feasibility of using MOPSO for solving many-objective problems. Therefore, two multi-objective algorithms are described, first NSGA-II [7] and then, two variants of MOPSO [5, 8]. In Section 5, a complexity analysis on the mentioned algorithms is shown while in Section 6 our experimental tests are described and results are presented. Finally, in Section 7, conclusions and future work are depicted.

2. MULTI OBJECTIVE OPTIMISATION

Problems addressed in this paper are mainly many-objective. Usually, these problems have conflicting objectives and solving them is not a trivial task. Often, when dealing with more than one objective, the need of selecting a solution among a set of non-comparable solutions arises, because a single optimal solution may not exist.

Definition 1 *Multi-objective optimisation problem* [1]: Let F be a set of m objective functions $\{f_1, f_2, \dots, f_m\}$, $f_i : \mathbb{R}^n \Rightarrow \mathbb{R}$, a MOP is defined as:

$$\begin{aligned} \text{Optimise (Maximise/Minimise)} \quad y = F(x) &= (f_1(x), f_2(x), \dots, f_m(x)) \\ x &= (x_1, x_2, \dots, x_n) \in \mathcal{X} \subseteq \mathbb{R}^n \\ y &= (y_1, y_2, \dots, y_m) \in \mathcal{Y} \subseteq \mathbb{R}^m \end{aligned} \quad (2)$$

subject to

$$x_i^{(L)} \leq x_i \leq x_i^{(U)} \quad \forall i \in \{1, 2, \dots, n\} \quad (3)$$

$$g(x) = (g_1(x), g_2(x), \dots, g_k(x)) \leq 0 \quad (4)$$

x is a vector of n decision variables, while y represents an m -dimensional objective vector. Constraints (3) represent $2n$ variable bounds that help to define the decision variable space or decision space \mathcal{X} . Objective functions constitute a multi-dimensional space called the objective space, termed as \mathcal{Y} . Vector g is composed of k constraint functions (4) which shape the feasible region. Solutions that do not satisfy constraint functions and/or variable bounds are called infeasible solutions, while solutions that meet all constraints (3) and (4) are feasible solutions. The set of all feasible solutions \mathcal{X}_f is known as the feasible region. The domain of each f_i is \mathcal{X}_f . For each solution $x \in \mathcal{X}_f$ there exists a point y in the objective space. This \mathcal{X}_f defines the feasible objective space \mathcal{Y}_f :

$$\mathcal{Y}_f = F(\mathcal{X}_f) = \bigcup_{x \in \mathcal{X}_f} \{F(x)\} \quad (5)$$

As previously stated, problems with $m \geq 4$ are called many-objective; otherwise, they are simply referred to as multi-objective optimisation problems.

In a feasible set of solutions \mathcal{X}_f , given 2 solutions $u, v \in \mathcal{X}_f$, It is said that u Pareto dominates, or simply dominates v (denoted as $u \succ v$) if it is not worse in any objective and it is strictly better in at least one objective [1, 2].

Definition 2 *Pareto Optimal set*. For a given MOP the Pareto Optimal set, denoted as \mathcal{P}^* , is defined as the set of non-dominated feasible solutions, i.e.:

$$\mathcal{P}^* = \{x \in \mathcal{X}_f \mid \nexists x' \in \mathcal{X}_f \text{ such as } x' \succ x\}$$

Definition 3 *Pareto Optimal Front.* For a given MOP the Pareto Optimal Front, denoted as \mathcal{PF}^* , is defined as the image in objective space of the Pareto set \mathcal{P}^* , i.e.:

$$\mathcal{PF}^* = \{y = F(x) \in \mathcal{Y}_f | x \in \mathcal{P}^*\}$$

3. NSGA-II

The reference algorithm in current literature for solving MOPs with evolutionary algorithms is undoubtedly the Non-dominated Sorting Genetic Algorithm II (NSGA-II) [1, 7]. This algorithm depicts a fast non-dominated sort procedure to classify individuals in a set of candidate solutions called population in several non-dominated fronts (Algorithm 1).

Algorithm 1: Fast Non-dominated Sort, responsible of the $m(2N)^2$ complexity of the algorithm.

```

input : P
foreach p ∈ P do
  Sp = ∅; np = 0;
  foreach q ∈ P do
    if p ≻ q then
      | Add q to set Sp of solutions dominated by p;
    else if q ≻ p then np = np + 1;
  if np = 0 then prank = 1; F1 = F1 ∪ {p};
i = 1;
while Fi ≠ ∅ do
  Q = ∅ // Used to store members of the next front;
  foreach p ∈ Fi do
    foreach q ∈ Sp do
      | nq = nq - 1;
      | if nq = 0 then qrank = i + 1; Q = Q ∪ {q};
  i = i + 1; Fi = Q;

```

Additionally, NSGA-II presents a crowding distance value d_i to preserve diversity. It implements a crowded-comparison approach using another method called *crowding distance assignment*. It depends in a new operator called *crowded-comparison operator* (\prec_n) which defines a partial order as follows:

$$i \prec_n j \iff (\mathcal{F}_i < \mathcal{F}_j) \vee (\mathcal{F}_i = \mathcal{F}_j \wedge d_i > d_j) \quad (6)$$

where \mathcal{F}_i is the front containing solution i [7].

In evolutionary algorithms as NSGA-II, a set of candidate solutions is known as *population*. In the main loop of NSGA-II, a parent population P_t and another offspring population are combined into a set R_t and then

separated in several non-dominated fronts \mathcal{F}_i . Afterwards, every generated front is assigned a crowding distance until the new population P_{t+1} grows to the population size limit N . Eventually, elements of the next unused front are sorted to complete the population. Finally, a new offspring population Q_{t+1} is generated [7].

Regarding complexity, according to the analysis given in by Deb et al. [7], the complexity of the operations in one iteration are:

1. *non-dominated sorting*: time complexity on the order of $m(2N)^2$ because of the two nested loops used to divide the population in non-dominated fronts, and the comparison of solutions (Algorithm 1).
2. *crowding distance assignment*: since it has to sort m times, and the complexity is given by the sorting algorithm, the overall time complexity is on the order of $m(2N) \log(2N)$.
3. *sorting on \prec_n* : time complexity on the order of $2N \log(2N)$. Each sort produced in a front is given by the sorting algorithm.

The overall complexity of the algorithm is therefore on the order of $m(2N)^2$, which is governed by the non-dominating sorting part of the algorithm. It is shown in Sections 5 and 6 that iterating over a population of $2N$ has considerable impact on execution time.

4. MOPSO

4.1. Particle Swarm Optimisation

The *Particle Swarm Optimisation* meta-heuristic (PSO), developed by Kennedy and Eberhart in 1995 [9], is inspired in social behaviour of individuals like bees and birds, which perform a collective zone exploration looking for food or guiding the swarm or flock to desirable locations. PSO basically consists in an iterative algorithm having a group of individuals called *swarm*, in which each individual called *particle* explores the decision space looking for optimal solutions.

In a n -dimensional decision space, each particle i in the swarm knows its current position $x_i = [x_{i_1}, x_{i_2}, \dots, x_{i_n}]$, its current velocity $v_i = [v_{i_1}, v_{i_2}, \dots, v_{i_n}]$ which led it to its current position, and the best position it has been $p_i = [p_{i_1}, p_{i_2}, \dots, p_{i_n}]$ called *best personal position*. Additionally, all other particles

are aware of the best position found by the entire swarm $g = [g_1, g_2, \dots, g_n]$ called *global best position*.

At every iteration t , every component j of the position and the velocity is updated for each particle i as follows:

$$v_{ij}^{t+1} = \omega \times v_{ij}^t + C_1 \times \text{rand}() \times (p_{ij}^t - xv_{ij}^t) + C_2 \times \text{rand}() \times (g_{ij}^t - x_{ij}^t) \quad (7)$$

$$x_{ij}^{t+1} = x_{ij}^t + v_{ij}^{t+1} \quad (8)$$

where ω is the *inertia* parameter, C_1 is called the *cognitive* parameter, C_2 is the *social* parameter and $\text{rand}()$ is a procedure that returns a random value in $[0, 1]$.

Equation (7) is used to update the velocity of the i -th particle from its current velocity, the euclidean distance to its best personal position, and the euclidean distance to the best global position.

In (8), position vector components belonging to the i -th particle are updated using the updated velocity. The use of distances in (7) is to achieve an “attraction” for the particle towards both its personal best position and the global best position. These distances are called *cognitive factor* and *social factor* respectively. Parameters C_1 and C_2 are constants that determine how accelerated is the particle towards the mentioned factors [9], defining the maximum influence of these factors in (7). In a similar fashion, $\text{rand}()$ is used to define the real influence of such factors. The final outcome is the preservation of diversity.

The inertia parameter ω introduced by Eberhart and Shi [10] is used to command the impact of the previous velocities in the calculations for the next value. ω manages the balance between the global and personal decision space exploration [11]. Big values of ω lean toward exploring new areas (*exploration*), but small values are in favour of searching areas close to the current position (*exploitation*). It is usual to limit the growth of the velocity by defining a maximum value v_{\max} [11]. After calculating the new velocity, it is moderated:

$$\begin{aligned} &\mathbf{if} \ v_{ij} > v_{\max} \ \mathbf{then} \ v_{ij} = v_{\max} \\ &\mathbf{else \ if} \ v_{ij} < -v_{\max} \ \mathbf{then} \ v_{ij} = -v_{\max} \end{aligned} \quad (9)$$

Finally, if the position reaches the limit of the feasible decision space \mathcal{X}_f , it is normally “bounced” in the opposite direction on the component that reached the limit. This ensures that every solution found in the iteration process will be inside the feasible set of solutions.

4.2. Particle Swarm Optimisation in Multi-Objective Problems

Adapting the PSO algorithm to optimize a multi-objective problem requires a modification of the concept of better personal position and best global position. Since having conflicting objectives result in non-comparable solutions, now the algorithm must handle a best personal *repository* for every particle and a global best *repository* as well. An adaptation to the PSO algorithm to solve MOPs is known as *Multi Objective Particle Swarm Optimisation* (MOPSO) [12]. In this Section two variants of MOPSO are briefly presented.

4.2.1 Moore and Chapman (1999)

Moore and Chapman [5] introduced a method in which every particle stores a best personal repository for every non-dominated positions it has visited. This version is simply referred to as MOPSO in this work. A global best repository is maintained as well, storing the non-dominated positions visited by the entire swarm. To calculate a new velocity, every particle selects a random element from its personal repository to use in (7) as best personal position. Similarly, a random element of the global repository is selected to use as global best position.

Algorithm 2: Moore y Chapman’s MOPSO with complexity on the order of mN^2 .

```

input :  $\omega, C_1, C_2, v_{\max}, N$ 
for  $i = 1$  to  $N$  do
    Initialize the  $i$ -th particle with a random velocity and position;
    eval( $i$ );
    Update the personal repository if the  $i$ -th particle ( $P_i$ );
    Update the global repository ( $G$ );
while not stop.condition() do
    for  $i = 1$  to  $N$  do
        Select best personal position (random element in  $P_i$ );
        Select best global position (random element in  $G$ );
        Calculate new velocity for the  $i$ -th particle (eq. 7);
        Limit velocity components to  $v_{\max}$  (eq. 9);
        Calculate a new position for the  $i$ -th particle (eq. 8);
        Update position to constraints if necessary;
    for  $i = 1$  to  $N$  do
        eval( $i$ );
        Update the personal repository if the  $i$ -th particle ( $P_i$ );
        Update the global repository ( $G$ );
Return non.dominated.solutions( $G$ );

```

As complexity is concerned, it is clear that, for every iteration, going through every component on the decision space to calculate in the first loop drives on the order of N^2 complexity. Also, comparing non-domination in the best particle selection is on the order of M . Therefore, the overall complexity

is MN^2 . Note that spatial complexity (or memory needs) increases due to storing a personal repository for each particle resulting in an overall spatial complexity on the order of $nN(N + 1)$ (Algorithm 2).

4.2.2 Coello and Lechuga (2002)

Coello and Lechuga [8] presented a version of MOPSO in which a fixed size repository stores every non-dominated solution found by the swarm in the exploration process. That repository employs an *adaptive mesh* scheme in which the explored space is represented in bounded regions called *hypercubes*. In this work, this version is referred to as MOPSO_CL.

Each hypercube is given a score equal to dividing a constant number like 10 by the total number of non-dominated solutions contained by it [12]. Such score is later used to select the best global position from the repository, which is updated in every iteration, inserting every non-dominated solution found by the swarm and removing the ones that prove to be dominated by the new solution. If the repository is full while inserting a new solution, a solution is removed from the hypercube containing the largest number of solutions. In Algorithm 3 the procedure for assigning solutions to hypercubes is shown.

Algorithm 3: Assign Solutions to Hypercubes using MOPSO_CL, with complexity on the order of n_{div}^m .

```

input : G, ndiv, m
qtyHypercubes = ndivM;
H = initialize.hypercubes(qtyHypercubes);
for i = 1 to m do
    maxi = 1 get.max( Gi );
    mini = 1 get.min( Gi );
for i = 1 to m do
    ampi =  $\frac{\text{max}_i - \text{min}_i}{n_{\text{div}} - 1}$ ;
    inii =  $\frac{\text{min}_i - \text{amp}_i}{2}$ ;
for i = 1 to |G| do
    for i = 1 to |G| do
        j = Calculate index for particle i;
        insert.particle.in.hypercube(H[j], G[i]);
for i = 1 to qtyHypercubes do update.calif(H[i]);

```

Regarding the complexity of this version, it is clear from the last loop that it is on the order of n_{div}^m .

5. COMPLEXITY ANALYSIS

The complexity analysis was performed taking into account the original definition of the algorithms [5, 7, 8]. In what follows, a summary based on

algorithms presented in Sections 3 and 4 are illustrated. These results are completely congruent with the ones proposed by the authors:

- NSGA-II: On the order of $m(2N)^2$, as stated in Section 3.
- MOPSO: On the order of mN^2 , as stated in Section 4.2.1.
- MOPSO_CL: On the order of n_{div}^m , as stated in Section 4.2.2.

Considering that this work is mainly interested in many-objective problems (m may be very large), experiments with MOPSO_CL are not presented due to its exponential growth in m . However, it is worth noting that this complexity is given by the hypercube administration (see Algorithm 3). Therefore, an adaptation of MOPSO_CL is suggested to take advantage of a sparse matrix representation for many-objective problems.

Let the relation \mathcal{U} be:

$$\mathcal{U} = \frac{\text{complexity}(\text{NSGA})}{\text{complexity}(\text{MOPSO})} = \frac{m(2N)^2}{mN^2} = 4 \quad (10)$$

It is clearly expected that MOPSO's execution time be around 4 times faster than NSGA-II's; therefore, it may be a good idea to use MOPSO to solve many-objective problems. To validate this statement, in the following section our experimental tests are shown.

6. EXPERIMENTAL RESULTS

To validate the complexity analysis presented in Section 5, the following experiments was performed: varying m (dimension of objective space), n (dimension of decision space), N (population size limit) and E (evaluation limit), execution time is compared.

Being t_{MOPSO} and t_{NSGA} execution times for NSGA-II and MOPSO respectively, the improvement ratio τ is calculated as follows:

$$\tau = \frac{t_{\text{NSGA}}}{t_{\text{MOPSO}}} \quad (11)$$

This clearly means that, for a given configuration, if $\tau > 1$, MOPSO is faster than NSGA-II.

6.1. Environment

3.000 parameter combinations were executed: $N \in \{100, 200, \dots, 1000\}$ for population size limit, $m \in \{4, 6, 8, 10, 12\}$ for number of objectives, $n \in \{14, 15, 16, 17, 18, 19\}$ for decision space dimension, and finally $E \in \{1000, 2000, \dots, 10000\}$ for number of executions of the objective functions, used as stop criteria.

Both algorithms were used to solve the same problem: DTLZ1 [13]. Once these executions were finished, correlations for every parameter of the mentioned variables and τ were calculated.

6.3. Execution Times

Table 1: Average execution times with 3.000 executions.

algorithms	Execution time (seconds)
NSGA-II	35.087
MOPSO	3.063
τ	11.455

As expected, $\tau > 1$ in every performed test, proving the feasibility of using MOPSO with many-objective problems.

The hardware used in this experiments is an Intel® Core™i7 CPU 970 @ 3.20 GHz with 12 GB RAM and running Fedora 20.

In the rest of this section, correlations for each variable are presented to show the impact of each variable in execution times.

6.3. Correlations

The influence that each variable has over execution times are studied by analyzing the correlations between τ and each variable. Correlations are shown in Table 2.

From the calculations, it is clear that increasing N , m and E lean towards using MOPSO for solving many-objective problems. However, when increasing n NSGA-II still looks as a right choice, although it is worth noticing that large values of n naturally increases E .

Table 2: Experimental Correlations

Variable	Correlation	Comment	favoured algorithm
$\rho_{\tau,N}$	0.796	Strong influence of N	MOPSO
$\rho_{\tau,m}$	0.257	Weak influence of m	MOPSO
$\rho_{\tau,n}$	-0.912	Strong influence of n	NSGA-II
$\rho_{\tau,E}$	0.787	Strong influence of E	MOPSO

7. Conclusions and future work

With the presented evidence, it is clear that MOPSO is a feasible alternative for solving many-objective problems. Given the considerable difference in execution times in the studied algorithms, it does not seem reasonable to limit the number of executions of the objective function as stop condition.

As future work, authors are working on performing quality measurements (not presented in this work); analysing the complexity of other algorithms; and correlating other variables' impact in quality of the generated approximation solution set.

References

- [1] C. von Lüken, B. Barán, and C. Brizuela, “A survey on multi-objective evolutionary algorithms for many-objective problems,” *Computational Optimization and Applications*, pp. 1–50, 2014.
- [2] K. Deb and D. Kalyanmoy, *Multi-Objective Optimization Using Evolutionary Algorithms*. New York, NY, USA: John Wiley & Sons, Inc., 2001.
- [3] D. W. Corne, J. D. Knowles, and M. J. Oates, “The pareto envelope-based selection algorithm for multiobjective optimization,” in *Proceedings of the Parallel Problem Solving from Nature VI Conference*, pp. 839–848, Springer, 2000.
- [4] M. Farina and P. Amato, “On the optimal solution definition for many-criteria optimization problems,” in *Fuzzy Information Processing Society, 2002. Proceedings. NAFIPS. 2002 Annual Meeting of the North American*, pp. 233–238, 2002.

- [5] J. Moore and R. Chapman, “Application of particle swarm to multiobjective optimization,” *Department of Computer Science and Software Engineering, Auburn University*, 1999.
- [6] D. Walker, R. Everson, and J. Fieldsend, “Visualisation and ordering of many-objective populations,” in *Evolutionary Computation (CEC), 2010 IEEE Congress on*, pp. 1–8, July 2010.
- [7] K. Deb, A. Pratap, S. Agarwal, and T. Meyarivan, “A fast and elitist multiobjective genetic algorithm: Nsga-ii,” *Evolutionary Computation, IEEE Transactions on*, vol. 6, pp. 182–197, Apr 2002.
- [8] C. A. Coello Coello and M. Lechuga, “Mopso: a proposal for multiple objective particle swarm optimization,” in *Evolutionary Computation, 2002. CEC '02. Proceedings of the 2002 Congress on*, vol. 2, pp. 1051–1056, 2002.
- [9] J. Kennedy and R. Eberhart, “Particle swarm optimization,” in *Neural Networks, 1995. Proceedings., IEEE International Conference on*, vol. 4, pp. 1942–1948 vol.4, Nov 1995.
- [10] Y. Shi and R. Eberhart, “A modified particle swarm optimizer,” in *Evolutionary Computation Proceedings, 1998. IEEE World Congress on Computational Intelligence., The 1998 IEEE International Conference on*, pp. 69–73, May 1998.
- [11] Y. Shi and R. Eberhart, “Parameter selection in particle swarm optimization,” in *Evolutionary Programming VII* (V. Porto, N. Saravanan, D. Waagen, and A. Eiben, eds.), vol. 1447 of *Lecture Notes in Computer Science*, pp. 591–600, Springer Berlin Heidelberg, 1998.
- [12] J. Lima and B. Barán, “Optimización de enjambre de partículas aplicada al problema del cajero viajante bi-objetivo,” *Revista Iberoamericana de Inteligencia Artificial*, 2006.
- [13] K. Deb, L. Thiele, M. Laumanns, and E. Zitzler, “Scalable Multi-Objective Optimization Test Problems,” in *Congress on Evolutionary Computation (CEC 2002)*, pp. 825–830, IEEE Press, 2002.

Experimental Comparison of Many-objective Evolutionary Preference-based Methods in a Parallel Framework

Christian von Lücken^{a1}, Carlos Brizuela^b, Benjamin Barán^a

^a Universidad Nacional de Asunción, Facultad Politécnica, Paraguay

^b CICESE Research Center, Ensenada, México

Abstract

Multi-objective Evolutionary Algorithms (MOEA) are used to solve complex multi-objective problems. As the number of objectives increases, Pareto-based MOEAs are unable to reproduce the same effectiveness showed for two or three objectives. Thus, several authors proposed preference-based methods as an alternative. On the other hand, parallelization has shown to be useful in evolutionary optimizations. This paper combines for the first time seven preference-based methods for many objective optimization in a multi-threading parallelization framework. Preference-based methods were used to replace the elitism procedure of the Non-dominated Sorting Genetic Algorithm II. Executions of each alternative were carried-out for the DTLZ-2 problem in a commodity multi-core platform. Obtained solutions were compared by different criteria, providing some insights into the improvements that the proposed combination may offer in many-objective optimization.

Keywords: Multi-objective Evolutionary Algorithms, Many-objective Optimization, Parallel Evolutionary Algorithms

1. Introduction

Multi-objective optimization problems (MOPs) have several, possibly conflicting, objectives to optimize. Conflicts between objectives lead to a set of solutions called the Pareto set, denoted as \mathcal{P}^* , while these solutions mapped to the objective space form the Pareto Front (\mathcal{PF}^*). In most practical cases, it is difficult to obtain a complete and exact Pareto set of a MOP. Multi-objective Evolutionary Algorithms (MOEAs) have proven to be very effective to provide near optimal approximations in complex multi-objective problems having two or three optimization objectives [2].

A solution is said to be dominate another one if it is not worse in any objective and it is strictly better in at least one objective, thus, Pareto

¹E-mail Corresponding Author: clucken@pol.una.py

set is formed with solutions that are non-dominated with respect to the whole search space [4, 2]. As the number of objectives increases, so does the number of solutions that dominance operator classifies as equivalent (or non-comparable) leading to a reduction of the search ability of Pareto-based MOEAs [9].

Improving MOEAs' performance to solve the so-called many-objective problems, i.e. problems having more than 4 objectives, is an important research area and different alternatives were proposed [18]. Among these alternatives are comparison relations with preference information for solutions [9, 8, 9, 14, 7, 11].

On the other hand, parallel MOEAs (pMOEAs) are able to use larger populations and to reduce the execution time [2]. The literature reports various parallel MOEAs (pMOEAs) that have been used to solve diverse problems [15]. These pMOEAs were mainly developed and tested in distributed memory parallel systems; however, nowadays availability of lower cost shared memory multi-core platform requires a review of the parallelization methods in the new existing environment in order to leverage the computational power that these platforms may offer.

Parallel Pareto-based MOEAs has been extensively studied for a small number of objectives [2], and some works compare preference relations for many-objective problems [3, 11, 10]; however, to the best of our knowledge they were not tried in a parallel framework. Therefore, this paper presents for the first time a comparison of two parallelization approaches for the Non-dominated Sorting Genetic Algorithm II (NSGA-II) [5], using seven ranking methods proposed for many-objective optimization problems [9, 8, 7, 14, 11].

This paper is organized as follows: Section 2 presents the methods and the parallel MOEA framework considered in this work. Section 3 presents the experimental setup and obtained results. Finally, Section 4 presents conclusions and future works.

2. Methods considered in this work

2.1. MOEAs considered for parallelization

Several modifications of the NSGA-II [5] ranking method were proposed to be used in many-objective optimization [18]. Also, in this paper the NSGA-II algorithm is used as test bed. With NSGA-II, the fitness of a solution is based on two values: its non-dominance ranking and its crowding distance. At each

generation, an elitism procedure based on these values is used to ensure that the best elements survive from one generation to the next. Details of the NSGA-II can be found in [5].

In this paper, the following operators and ranking methods are used to modify the fitness assignment procedure of the NSGA-II, for space reason the details are not explained here but we refer the interested reader to the corresponding references:

1. **Favour relation [8]:** this relation counts the objectives in which a given solution outperforms another. Given \mathbf{x} and $\mathbf{x}' \in \mathcal{X}_f$, where \mathcal{X}_f represents the feasible solution space, it is said that \mathbf{x} is favoured than \mathbf{x}' , denoted as $\mathbf{x} \prec_{favour} \mathbf{x}'$, if and only if

$$n_b(\mathbf{F}(\mathbf{x}), \mathbf{F}(\mathbf{x}')) > n_b(\mathbf{F}(\mathbf{x}'), \mathbf{F}(\mathbf{x})) \quad (1)$$

$$n_b(\mathbf{F}(\mathbf{x}), \mathbf{F}(\mathbf{x}')) = |\{f_i(\mathbf{x}) \text{ s.t. } f_i(\mathbf{x}) < f_i(\mathbf{x}')\}| \quad (2)$$

In [8], the favour relation is proposed to be used with the Satisfiability Class Ordering classification (SCO) procedure [8] to sort solutions.

2. **ϵ -Preferred Relation [14]:** the ϵ -Preferred relation compares solutions by counting the number of times a solution exceeds user defined ϵ_i limits for each dimension and, in case of a tie, it uses the favour relation. Given two solutions \mathbf{x} and $\mathbf{x}' \in \mathcal{X}_f$, it is said that \mathbf{x} is ϵ -preferred than \mathbf{x}' , denoted as $\mathbf{x} \prec_{\epsilon\text{-preferred}} \mathbf{x}'$, iff: $\mathbf{x} \prec_{\epsilon\text{-exceed}} \mathbf{x}' \vee (\mathbf{x}' \not\prec_{\epsilon\text{-exceed}} \mathbf{x} \wedge \mathbf{x} \prec_{favour} \mathbf{x}')$, where $\mathbf{x} \prec_{\epsilon\text{-exceed}} \mathbf{x}'$ implies that:

$$|\{i : y_i < y'_i \wedge |y_i - y'_i| > \epsilon_i\}| > |\{i : y'_i < y_i \wedge |y'_i - y_i| > \epsilon_i\}|$$

As in [8], in [14] the SCO algorithm is used to rank solutions.

3. **Preference Ordering based on order of efficiency (PO_k) [7]:** a solution \mathbf{x} is considered to be efficient of order k if it is Pareto optimal in the $\binom{m}{k}$ subspaces of the objective space taking into account only k objectives at a time. The order of efficiency of a solution \mathbf{x} , denoted by $K(\mathbf{x})$ is the minimum k value for which \mathbf{x} is efficient. Based on the order of efficiency a ranking procedure is proposed in [7].
4. **Preference Ordering based on efficiency degree ($PO_{k,z}$) [7]:** this method refines the ranking based on PO_k when several solutions share the same best order of efficiency. A solution \mathbf{x} is efficient of order k with degree z if $\mathbf{F}(\mathbf{x})$ is not dominated by any member of the Pareto Front

for exactly z out of the possible $\binom{m}{k}$ k -element subsets of the objectives. Details of the ranking method based on efficiency degree are in [7].

5. **$-\epsilon$ -DOM ranking [11]:** the $-\epsilon$ -DOM distance replaces the NSGA-II crowding distance. The $-\epsilon$ -DOM distance of a solution \mathbf{x} is:

$$\max\{f_i(\mathbf{x}') - f_i(\mathbf{x}) : f_i(\mathbf{x}) < f_i(\mathbf{x}') , i \in \{1, \dots, m\}\} , \text{ or} \\ 0 \text{ if } \nexists i \text{ such that } f_i(\mathbf{x}) < f_i(\mathbf{x}') , i \in \{1, \dots, m\}$$

Therefore, given solutions \mathbf{x} and \mathbf{x}' , *mepsd* reflects the smallest ϵ value such that if subtracted from all objectives of $\mathbf{F}(\mathbf{x}')$, \mathbf{x}' dominates \mathbf{x} , while the $-\epsilon$ -DOM rank value is the minimum of such values.

6. **Crisp $(1 - k)$ -dominance relation [9]:** this relation counts the objectives in which a solution is better or equal than another. Let \mathbf{x} and $\mathbf{x}' \in \mathcal{X}_f$, $\mathbf{F}(\mathbf{x}) = \mathbf{y}$, $\mathbf{F}(\mathbf{x}') = \mathbf{y}'$, it is said that \mathbf{x} $(1 - k)$ -dominates \mathbf{x}' iff : $n_e(\mathbf{y}, \mathbf{y}') < m$ and $n_b(\mathbf{y}, \mathbf{y}') \geq \frac{m - n_e}{k + 1}$, where m is the number of objectives, $0 \leq k \leq 1$, n_b is as in Eq. (2), and $n_e(\mathbf{F}(\mathbf{x}), \mathbf{F}(\mathbf{x}'))$ is $|\{f_i(\mathbf{x}) \text{ s.t. } f_i(\mathbf{x}) = f_i(\mathbf{x}')\}|$. The $(1 - k)$ -dominance relation serves as a new definition of optima, called k -optimality, as well as the corresponding optimal set of solutions [9].
7. **Fuzzy $(1 - k_F)$ -dominance relation [9]:** the fuzzy extension of $(1 - k)$ -dominance is defined by determining membership functions μ_b^i , μ_e^i and μ_w^i for each objective function i . There are several membership functions that can be used. In case of a trapezoidal function four parameters (a, b, c, d) are required to represent a meaning of equality and difference.

2.2. Parallel Multi-objective Evolutionary Algorithms

This section introduces the island-based parallel framework considered in this paper. The island model is the most popular parallelization paradigm for MOEAs [2], it consists of a number of subpopulations or islands evolving independently which are provided with a mechanism to interchange individuals exploring for global optima. As the goal here is not to provide a full pMOEAs' survey, readers are kindly referred to [15, 16, 2] for further reading.

There are several alternatives to develop a pMOEA [16]. However, most pMOEAs are based on the parallelization of a current MOEA; particularly, the NSGA-II [5] is a good option for parallelization [17]. Therefore, this work considers NSGA-II as foundation for parallel implementations that differ in

at least one of the following features: the way in which the ranking of individuals is produced, i.e. how fitness is assigned; the number of subpopulations and the process used to form subpopulations. Regarding the ranking of solutions, this work uses the original NSGA-II method and the seven alternatives presented in Section 2.1. While, considering how pMOEAs divide the main population, this work considers a random distributed population pMOEA (RND) and a K-means based distributed population pMOEA (KM) [13].

In the RND distribution, the population is randomly divided into a number of equal size partitions. While, the KM distribution is based on the original proposal of Streichert et al. [13] which used K-means to divide the search space of a given optimization problem in suitable partitions without a priori knowledge of its search space. In [13], zone constraints are implemented to limit subpopulations to their specific region. In this paper, K-means is used to divide the population; however, zone constraints are not considered.

An evolutionary iteration comprises the procedures of fitness assignment, selection, crossover, mutation and elitism that are carried out by a MOEA to produce a new offspring from the current population. As a mechanism to search for global optima, some methods, as in [12], combine subpopulation evolutions with iterations where the whole set of solutions is considered to be subject of the evolutionary process. In a parallel multicore platform, the aforementioned approach can be efficiently applied for interchange information between subpopulations; therefore, it is considered in this work.

Algorithm 1 presents the basic framework for the parallel implementation of the NSGA-II and its variants used in this work. First, the algorithm reads and set its parameters; besides the usual MOEA parameters, also, the total number of evolutionary steps (it_g), the number of single thread iterations (it_s), and the number of parallel iterations (it_p) must be given. Then, the global number of iterations t is set to 0, and the global population P_t is created at random. Thereafter, it_s evolutionary iterations are executed in a single thread considering the evolutionary population as a whole. The next step is to split $P(t)$ using the procedure PM in τ subpopulations ($P_t^1 \dots, P_t^\tau$). Once the global population was partitioned, τ threads are created, one for each island. Each thread has an identifier Id , thus at each thread Id , evolution of P_t^{Id} occurs during it_p iterations. When running parallel iterations in all the threads end, the global count of iterations t is updated to $t + it_p$. The procedure continues until t reaches the maximum number of iterations. Finally, the final set of solutions is saved.

Algorithm 1 Basic framework for parallel implementations used in this work

Read parameters: population size (N), selection, crossover and mutation probability. Set the ranking method RM and its parameters. Set the population partition method PM, the number of islands to be used τ . Read it_g, it_s, it_p : the maximum number of iterations, the number of single thread iterations and the number of parallel thread iterations.

Set $t = 0$

Create an initial random global evolutionary population P_t

while $t < it_g$ **do** $\triangleright it_g$ is the total number of evolutionary steps performed

while $(t + 1) \bmod it_s \neq 0$ **do** $\triangleright it_s$: iterations considering the evolutionary population as a whole

Evolve P_t in P_{t+1} using the NSGA-II with a given ranking method

$t = t + 1$

end while

Split P_t in P_t^1, \dots, P_t^τ using a given population partition method PM

In τ **parallel threads**

for $t' = 0$ **to** it_p **do** $\triangleright it_p$: iterations considering the population as subpopulations in parallel

Evolve $P_{t+t'}^{Id}$ in $P_{t+t'+1}^{Id}$ using the NSGA-II with a given ranking method

$t' = t' + 1$

end for

End parallel

$t = t + it_p$

end while

Save non-dominated solutions from P_t

3. Experimental comparison

3.1. Experimental setup and metrics

In order to determine if, in a many-objective optimization problem, the original NSGA-II and its seven variants (presented in Subsection 2.1) can improve their results by parallelization, this paper compares the results obtained by their parallel and sequential implementations. The parallel versions are based on the framework presented in Subsection 2.2 using the RND and the KM distribution. The test problem used in this work is the DTLZ-2 with 8 objectives [6].

Parallel methods were executed using 2 and 4 threads. Thus, a total of 40 different combinations of number of threads, ranking and distribution methods were executed. For each combination, 10 runs were performed using the same set of 10 initial populations. Executions were executed using the following common parameters: population size: 400, stopping criterion 400 iteration, binary coding of 32 bits per variable, one point crossover probability: 0.8, mutation probability: 0.002. For the ϵ -Preferred relation, the ϵ value is 0.0001; for the $(1 - k)$ -dominance relation, k is 0.5; and, for the $(1 - k_F)$ -dominance relation, k is also 0.5 and a fuzzy trapezoidal rule is used ($a = -0.001, b = 0, c = 0, d = 0.001$). No fine tuning of the above parameters was considered. For parallel methods subpopulation iteration is

set to 5, followed by another 5 iterations of the whole population until the stop criterion is reached.

Sequential and parallel programs were programmed in the C language. Parallel methods were implemented for execution in Sharing Memory Platforms using the OpenMP library [1]. The experimental computational platform was a machine provided with two Intel Xeon quad-core Processors E5640 (12M Cache, 2.66 GHz, 5.86 GT/s) and 16 GB of main memory running the GNU/Linux operating system.

To evaluate a given set of non-dominated solutions \mathcal{S}_t in a population P_t , different aspects of it may be measured as the proximity to the true Pareto Front and the distribution or the extend of solutions. Therefore, the following metrics are considered in this work [4]:

1. Number of solutions in \mathcal{PF}^* (N): this metric counts the obtained solutions that are in the true Pareto set. In DTLZ-2 the Pareto Front is composed by those solutions having $\sum_{i=1}^m f_i(\mathbf{x})^2 = 1$ [6]. The N metric is expected to be maximized.
2. Generational Distance (GD): this metric measure the average distance between obtained solutions in objective space and the true Pareto Front of the problem. Thus, this metric should be minimized. Since GD requires a reference \mathcal{PF}^* to be computed, and equations to produce \mathcal{PF}^* are known, a set of a set of 2000 optimal solutions was determined analytically.
3. Spread (Δ): this metric measures the extent of the Pareto Front that the obtained set of solutions covers. The spread metric is expected to be minimized.
4. Spacing (S): this metric measures if the obtained non-dominated solutions are uniformly distributed. The metric is the average distance of each point from its nearest neighbour, thus, if solutions are uniformly distributed the value of this metric approaches zero. Then, the value of this metric is expected to be minimized.

3.2. Experimental results

Table 1 shows average values and standard deviation of the considered metrics evaluated over the final result of the 10 runs performed for each implemented combination. In this table, each row corresponds to a given ranking method, while columns are for the execution type. Besides the metrics values

Number of solutions in the Pareto Set (N)					
Part	Sequential	2-RND	2-KM	4-RND	4-KM
NSGAI	0.0(0.0)	0.0(0.0)	0.1(0.3)	0.1(0.3)	0.0(0.0)
ϵ -DOM	342.5(6.576)	337.9(5.262)	346.4(11.706)	340.8(8.328)	358.0(9.529)
ϵ -Preferred	72.6(83.493)	120.7(57.331)	67.5(38.792)	151.0(77.062)	100.9(44.7)
$(1 - k)$ -dom.	264.2(104.945)	349.4(86.165)	233.2(88.933)	339.7(60.402)	235.3(76.013)
$(1 - k_F)$ -dom.	388.3(35.1)	399.5(0.671)	399.3(0.9)	398.8(0.980)	399.2(0.980)
Favour	143.0(101.444)	155.2(59.499)	167.1(52.922)	229.4(105.428)	132.4(60.622)
PO_k	385.8(5.192)	384.2(3.572)	390.7(6.357)	381.3(4.124)	393.4(2.107)
$PO_{k,z}$	390.3(3.226)	383.7(2.648)	391.0(1.897)	385.9(3.961)	393.0(2.608)
Generational Distance (GD)					
Part	Sequential	2-RND	2-KM	4-RND	4-KM
NSGAI	2.69E-02(1.40E-03)	2.74E-02(6.50E-04)	2.59E-02(8.64E-04)	2.69E-02(1.11E-03)	2.50E-02(9.60E-04)
ϵ -DOM	7.06E-03(5.26E-04)	7.02E-03(7.44E-04)	6.70E-03(9.12E-04)	6.37E-03(6.31E-04)	5.20E-03(5.76E-04)
ϵ -Preferred	2.04E-05(9.98E-06)	1.11E-05(4.14E-06)	1.51E-05(5.24E-06)	9.46E-06(2.35E-06)	1.15E-05(3.11E-06)
$(1 - k)$ -dom.	7.07E-06(1.90E-06)	5.96E-06(1.55E-06)	7.47E-06(1.99E-06)	5.81E-06(5.65E-07)	7.18E-06(1.21E-06)
$(1 - k_F)$ -dom.	1.39E-03(8.97E-04)	1.10E-03(6.46E-05)	1.09E-03(6.74E-05)	1.12E-03(9.24E-05)	1.12E-03(8.13E-05)
Favour	1.14E-05(5.98E-06)	9.49E-06(3.57E-06)	8.52E-06(1.45E-06)	7.58E-06(1.79E-06)	1.15E-05(6.60E-06)
PO_k	6.00E-03(1.36E-03)	5.02E-03(5.19E-04)	4.64E-03(1.70E-03)	4.17E-03(9.55E-04)	1.90E-03(8.24E-04)
$PO_{k,z}$	5.39E-03(1.11E-03)	5.17E-03(8.94E-04)	5.49E-03(1.81E-03)	4.29E-03(8.19E-04)	2.22E-03(7.52E-04)
Spread (Δ)					
Part	Sequential	2-RND	2-KM	4-RND	4-KM
NSGAI	3.19E-01(1.77E-02)	3.09E-01(1.55E-02)	2.98E-01(1.25E-02)	2.96E-01(1.73E-02)	2.70E-01(1.05E-02)
ϵ -DOM	5.21E-01(4.00E-02)	5.45E-01(3.10E-02)	5.03E-01(3.15E-02)	5.84E-01(3.69E-02)	5.15E-01(4.51E-02)
ϵ -Preferred	1.00E+00(1.15E-06)	1.00E+00(9.41E-09)	1.00E+00(2.21E-07)	1.00E+00(4.90E-12)	1.00E+00(1.80E-08)
$(1 - k)$ -dom.	1.00E+00(2.84E-11)	1.00E+00(0.00E+00)	1.00E+00(1.61E-13)	1.00E+00(0.00E+00)	1.00E+00(6.49E-13)
$(1 - k_F)$ -dom.	8.03E-01(1.23E-01)	7.43E-01(3.78E-02)	7.72E-01(4.02E-02)	7.42E-01(3.00E-02)	7.83E-01(6.25E-02)
Favour	1.00E+00(5.52E-11)	1.00E+00(1.62E-13)	1.00E+00(5.16E-11)	1.00E+00(7.28E-14)	1.00E+00(2.12E-09)
PO_k	7.10E-01(3.24E-02)	7.36E-01(5.28E-02)	8.45E-01(7.34E-02)	9.32E-01(1.18E-01)	9.66E-01(1.25E-01)
$PO_{k,z}$	7.14E-01(3.95E-02)	8.10E-01(1.60E-01)	8.28E-01(4.37E-02)	8.68E-01(7.02E-02)	9.43E-01(6.97E-02)
Spacing (S)					
Part	Sequential	2-RND	2-KM	4-RND	4-KM
NSGAI	3.41E-01(1.45E-02)	3.24E-01(1.20E-02)	3.16E-01(1.04E-02)	3.05E-01(1.36E-02)	2.97E-01(1.66E-02)
ϵ -DOM	3.29E-01(2.80E-02)	3.36E-01(2.58E-02)	3.09E-01(3.25E-02)	3.27E-01(2.55E-02)	2.48E-01(1.72E-02)
ϵ -Preferred	2.04E-07(5.17E-07)	1.45E-09(3.02E-09)	2.56E-08(7.58E-08)	4.57E-13(1.11E-12)	4.92E-10(1.35E-09)
$(1 - k)$ -dom.	1.83E-14(5.46E-14)	4.30E-18(9.51E-18)	1.40E-14(3.70E-14)	5.55E-18(1.31E-17)	3.28E-14(9.83E-14)
$(1 - k_F)$ -dom.	8.32E-03(1.64E-03)	8.14E-03(1.83E-03)	7.67E-03(1.57E-03)	8.17E-03(2.09E-03)	8.04E-03(1.40E-03)
Favour	2.03E-12(5.46E-12)	6.64E-15(1.23E-14)	2.69E-13(7.10E-13)	1.51E-15(4.24E-15)	7.73E-11(2.31E-10)
PO_k	1.39E-01(2.24E-02)	1.24E-01(2.01E-02)	9.75E-02(2.71E-02)	1.00E-01(2.70E-02)	4.14E-02(1.34E-02)
$PO_{k,z}$	1.33E-01(3.53E-02)	1.29E-01(2.74E-02)	9.88E-02(2.69E-02)	1.05E-01(2.69E-02)	5.16E-02(2.72E-02)
Execution Time (seconds)					
Part	Sequential	2-RND	2-KM	4-RND	4-KM
NSGAI	76.1(0.294)	62.6(1.42)	67.5(0.866)	50.4(0.685)	56.0(0.588)
ϵ -DOM	108.8(0.902)	89.7(0.389)	90.5(1.62)	73.6(0.568)	78.6(1.14)
ϵ -Preferred	134.4(2.13)	106.0(0.624)	118.4(2.37)	87.4(0.676)	102.5(2.69)
$(1 - k)$ -dom.	92.3(0.451)	78.2(0.676)	86.3(2.85)	62.8(0.782)	75.7(2.18)
FAFuzzy	232.0(8.18)	165.6(3.19)	182.8(3.59)	142.7(1.06)	156.1(6.11)
Favour	116.5(2.71)	92.8(1.23)	104.4(2.27)	78.2(1.88)	91.1(1.86)
PO_k	81.0(0.696)	70.9(0.536)	74.2(1.52)	58.0(0.709)	67.0(1.60)
$PO_{k,z}$	81.3(0.788)	71.0(0.738)	74.1(0.99)	57.7(0.898)	66.3(2.30)

Table 1: Average values of metrics N, GD, Spread, Spacing, and execution time for the methods considered in this work solving the DTLZ2 problem with 8 objectives

of the obtained solutions, Table 1 also shows the average and standard deviation of the execution time in seconds of each implementation as an additional metric. The column label Sequential shows the values for sequential executions; the columns 2-RND and 2-KM are for the values for parallel executions using the random and K-means population distribution methods with two threads, respectively. Similarly, 4-RND and 4-KM are for parallel executions using the random and K-means population distribution methods with threads.

To analyse the results in Table 1, for each metric, the best metric value for each row (ranking method) is boldfaced, while, the best value for each

column (execution method) is in gray. Thus, a cell that is in boldface and gray is for the solution set with best metric value. In this way, it is easier to note that for most of the considered metrics, at least one parallel implementation obtains a solution set that is better than its corresponding sequential counterparts in convergence or diversity. The result is remarkable since parallel and sequential implementations were executed using the same number of iterations, and, therefore, the same number of objective function evaluations. Moreover, parallel implementations obtain better results with improved execution times.

As it is expected, regarding the metrics related to convergence (GD and N) executions of the original NSGA-II with the considered parameters obtain worse values than the alternatives that were proposed for many-objective problems. However, considering the Spread of solutions NSGA-II obtains the best values.

The implementations of $(1 - k_F)$ -dominance relation obtain the best convergence values, but they cover a small portion of the Pareto Front as their Spread metric indicate. In fact, with the exception of ϵ -DOM, the alternatives to the original NSGA-II ranking procedures obtain solutions concentrated into a region with Spread values greater than 0.7. Spacing values shows that in spite that solutions provided by $(1 - k)$ -dominance and Favour concentrate in a small area their solutions are better distributed than in the case of the other alternatives.

Regarding the number of solutions in the Pareto Front, results of the ϵ -DOM sequential and parallel implementations ranks 4 or 5 to eight, with an average value of more than 340; while, regarding the Spread metric these implementations receive the second position. Thus, ϵ -DOM implementations obtain many solutions covering a larger portion of the Pareto Front than the other alternatives. In spite of an analysis of the ϵ -DOM spacing metric results show that solutions in the covered region are not well distributed, we consider that this method offers the best trade-off between convergence and diversity among the considered ranking methods.

Between the population distribution methods considered in this work, the results show that the best parallelization choice (and the number of subpopulations considered) depends on the ranking method to be used. As an example, for the N metric and the ϵ -DOM ranking, the KM with 4 subpopulations obtains the best value; for the ϵ -Preferred the best value is for RND using 4 partitions, while, in case of the $(1 - k)$ -dominance the best result also is for the Random partitioning, but with two subpopulations. Other exper-

iments are needed to determine the relation that exist between the metric results and the ranking and partition methods with varying population size and number of subpopulations.

4. Conclusions and future work

The increasing availability of multi-core platforms made necessary to adapt existing serial and parallel algorithms, as well to assess them in this new computing platform. Also, development of newer algorithms for many-objective problems is needed. A first step for this development is to analyse the current existing alternatives.

In this work, sequential and parallel versions of the NSGA-II using different ranking methods that have been developed for many objective problems were evaluated over a set of performance metrics. Comparison between the various considered methods was executed using a single parallel framework in order to combine the different methods that have been considered.

The obtained results have shown that in most of the studied cases parallel MOEAs outperform their sequential counterparts. Comparison results have also shown that, for the considered experimental setting and metrics, the best serial ranking method is, in general, the best in parallel executions. Among the considered ranking methods, the ϵ -DOM ranking appears to provide the best trade-off between convergence and diversity. The obtained results, also indicates that different methods may be useful at different moments of the search of solutions. Thus, the algorithm choice must consider if the desition maker is interested into obtain a solution set with a large diversity or if it is interested in emphasizing convergence to a given region.

Future works include, among others: to extend the comparison to other problems; to test the proposed parallel approach with different thread numbers and parameters; to analyse the relations among population sizes, number of subpopulations, and partition and ranking methods; to improve the partition techniques; and, to analyse optimized parallelization schemes. Additionally, the development of new metrics for many-objective problems is needed to evaluate the convergence and diversity properties of the obtained solution sets.

References

- [1] B. Chapman, G. Jost, R. Van Der Pas, and D.J. Kuck. *Using OpenMP: portable shared memory parallel programming*. The MIT Press, 2007.
- [2] C. Coello Coello, G. Lamont, and D. Van Veldhuizen. *Evolutionary Algorithms for Solving Multi-Objective Problems*. Springer, New York, second edition, 2007. ISBN 978-0-387-33254-3.
- [3] D. Corne and J. Knowles. Techniques for highly multiobjective optimization: some nondominated points are better than others. In *Proc. of the 9th Ann. Conf. on Genetic and Evol. Comput.*, GECCO '07, pages 773–780. ACM Press, 2007.
- [4] K. Deb. *Multi-objective optimization using evolutionary algorithms*. Wiley, 2001.
- [5] K. Deb, A. Pratap, S. Agarwal, and T. Meyarivan. A fast and elitist multiobjective genetic algorithm: NSGA-II. *IEEE Trans. on Evol. Comput.*, 2002. doi: 10.1109/4235.996017.
- [6] K. Deb, L. Thiele, M. Laumanns, and E. Zitzler. Scalable multi-objective optimization test problems. In *Proc. of the 2002 Congr. on Evol. Comput.*, 2002. doi: 10.1109/CEC.2002.1007032.
- [7] F. di Pierro, S. Khu, and D. Savić. An investigation on Preference Order ranking scheme for multiobjective evolutionary optimization. *IEEE Trans. on Evol. Comput.*, 2007. doi: 10.1109/TEVC.2006.876362.
- [8] N. Drechsler, R. Drechsler, and B. Becker. Multi-objective optimisation based on relation favour. In *First Int. Conf. on Evol. Multi-Criterion Optim.* 2001. doi: 10.1007/3-540-44719-9_11.
- [9] M. Farina and P. Amato. On the Optimal Solution Definition for Many-criteria Optimization Problems. In *Proceedings of the NAFIPS-FLINT International Conference'2002*, pages 233–238, Piscataway, New Jersey, June 2002. IEEE Service Center.
- [10] H. Ishibuchi, N. Tsukamoto, and Y. Nojima. Evolutionary many-objective optimization: A short review. In *2008 IEEE Congr. on Evol. Comput.*, 2008. doi: 10.1109/CEC.2008.4631121.
- [11] M. Köppen and K. Yoshida. Substitute distance assignments in NSGA-II for handling many-objective optimization problems. In *Proc. of the*

- 4th Int. Conf. on Evol. Multi-Criterion Optim. EMO 2007*, 2007. doi: 10.1007/978-3-540-70928-2_55.
- [12] F. de Toro Negro, J. Ortega, E. Ros, S. Mota, B. Paechter, and J. M. Martín. PSFGA: parallel processing and evolutionary comput. for multiobjective optim. *Parallel Comput.*, 2004. doi: 10.1016/j.parco.2003.12.012.
- [13] F. Streichert, H. Ulmer, and A. Zell. Parallelization of Multi-objective Evolutionary Algorithms Using Clustering Algorithms. In *Proc. of the 3th Int. Conf. on Evol. Multi-Criterion Optim. EMO 2005*, 2005. doi: 10.1007/978-3-540-31880-4_7.
- [14] A. Sülflow, N. Drechsler, and R. Drechsler. Robust Multi-objective Optimization in High Dimensional Spaces. In *Proc. of the 4th Int. Conf. on Evol. Multi-Criterion Optim. EMO 2007*, 2007. doi: 10.1007/978-3-540-70928-2_54.
- [15] E. Talbi, S. Mostaghim, T. Okabe, H. Ishibuchi, G. Rudolph, and C. Coello Coello. Parallel approaches for multiobjective optimization. In *Multiobjective Optimization*, 2008. doi: 10.1007/978-3-540-88908-3_13.
- [16] D. van Veldhuizen, J. Zydallis, and G. Lamont. Considerations in Engineering Parallel Multiobjective Evolutionary Algorithms. *IEEE Trans. on Evol. Comput.*, 7(2):144–173, April 2003.
- [17] C. von Lüken. Algoritmos evolutivos para optimización multiobjetivo: Un estudio comparativo en un ambiente paralelo asíncrono. Master’s thesis, Universidad Nacional de Asunción, Paraguay, 2003. (In Spanish).
- [18] C. von Lüken, B. Barán, and C. Brizuela. A survey on multi-objective evolutionary algorithms for many-objective problems. *Comput. Optimization and Applications*, 1(1):1–50, 2014. doi: 10.1007/s10589-014-9644-1.

Particle Swarm Optimization applied to parameter tuning of CLAHE based on Entropy and Structural Similarity Index

Marcos Andrés Brizuela Núñez, Luis Guillermo Moré Rodríguez, José Luis Vázquez Noguera, Horacio Legal Ayala, Diego P. Pinto-Roa
Facultad Politécnica, Universidad Nacional de Asunción (FP-UNA)
San Lorenzo - Paraguay

Abstract

Contrast enhancement is fundamental in image processing, as a preprocessing step for other high level applications. Capturing images sometimes results in poor details of the scene. Transforming the image to improve details is essential to any contrast enhancement operation. Contrast enhancement can be divided into two approaches: global and local. In global approach, a transformation function is applied to the image at once, while in local approach a function is applied to blocks of pixels. Contrast Limited Adaptive Histogram Equalization(CLAHE) is an algorithm that improves image contrast locally, but requires 2 parameters to be determined; to address this complex tuning problem, we propose a method to find optimal parameters using PSO, evaluating two metrics: Entropy, which maximizes the amount of information, and SSIM, which evaluates the image distortion level of the resultant image. Experimental results show that CLAHE gives a good level of contrast enhancement for general images and the parameters are not the same for each one.

Keywords: Contrast enhancement, particle swarm optimization, structural similarity index, entropy, contrast limited adaptive histogram equalization.

1. INTRODUCTION

Images captured by any device may not reflect properly the fine details of the captured scene because they may contain some areas brighter than others or shadows that hides image details [1]. Contrast Enhancement is a technique which tries to reveal hidden or barely perceptible details. It consists in the expansion of the range of gray levels by modifying the histogram of the image [2]. Besides providing a better view of the details of the image, contrast enhancement is normally used as a form of preprocessing, serving as an input to more complex applications (e.g. feature detection, pattern recognition, monitoring images, medical images, and others) [3].

One contrast enhancement method is the Histogram Equalization (HE), which consists in transforming the distribution of gray levels. HE is very popular due to its simplicity and effectiveness [4]. However, it often does not give the best visual results. Various techniques have been developed based in HE [5], [6], [7]. For our work, we have chosen a technique called Contrast Limited Adaptive Histogram Equalization (CLAHE) [9]. This algorithm is an extension of the Adaptive Histogram Equalization (AHE) [8]. Also, we will use Particle Swarm Optimization (PSO) algorithm in order to find the appropriate parameters for CLAHE. To assess the quality of the solutions, we will use two evaluation metrics: Entropy, and Structural Similarity Index (SSIM)[12]. In [11] a method is proposed, which finds the optimal parameters of CLAHE, but unlike our approach, the image degradation is not taken into account as a metric for evaluation. We compare our results with the results of this method and we noted that the use of the image degradation as a metric marked a noticeable difference between the results.

The rest of the paper is organized as follows: Section 2 describes the Histogram Equalization. The CLAHE algorithm is briefly described in Section 3. In Section 4 we define the evaluation metrics. Section 5 presents the PSO applied in this work; while in Section 6 the obtained results are presented and discussed. Finally, Section 7 states our conclusion.

2. HISTOGRAM EQUALIZATION

The Histogram is a distribution of the gray levels of an image. Histogram Equalization(HE) consists in applying a transformation function of the cumulative distribution of gray levels in order to obtain a new distribution that approximates an uniform distribution, this is, the same amount of pixels for each gray level. However, HE has some drawbacks, such as noise amplification, contrast over-stretching, or it can change the overall brightness [4], [11], [14]. For these reasons, HE based methods are divided into two major categories: global and local methods [15] to be explained in the next section.

2.1. Global Histogram Equalization

Global HE uses the histogram information of the entire input image in its transformation function [15]. In this approach, the contrast stretching is limited to the gray levels with high frequencies. That is, the high frequency gray levels dominate the low frequency gray levels. In this situation, the global approach transforms the gray levels and the dominating gray levels

that have higher frequency gain contrast stretching, which causes a significant contrast loss for the gray levels with less occurrence. Additionally, in most cases, the neighboring pixels may not get captured and transformed with precision.

2.2. Local Histogram Equalization

Local HE tries to resolve the issues associated with global HE. It divides the image into sub images and equalizes them independently. There are many ways to divide an image into blocks of windows. One simple way is by dividing the image in two windows. Another way is to slide the window pixel by pixel on the entire image sequentially, but only the pixels that fall into the window are considered for the equalization. This gives an equalization centered in the window and only the gray levels within the window are allowed to get better enhancement of the portion of the image that is hidden or difficult to visualize with a global equalization. However, local HE is computationally expensive, and sometimes causes over-enhancement.

To address the issues showed before, one of the local methods, Contrast Limited AHE (CLAHE) will be explained on the next section.

3. CONTRAST LIMITED AHE

The natural behavior of the human eye is to assess the information contained in an image, based on its local components. Hence, it might be relevant to perform a contrast enhancement based on the local region approach. For AHE, it is implemented by optimizing contrast within rectangular regions of the image, so called *contextual regions* [9], with the region dimensions defined as $(\mathcal{R}_x, \mathcal{R}_y)$. Then, the histogram equalization is performed within the contextual regions. A bi-linear interpolation function is executed on contextual regions boundaries to correct inconsistencies between them. One of the characteristics of AHE is that is capable to enhance contrast information of the image [10].

AHE is associated with noise amplification, particularly visible in areas where there are homogeneous gray levels. This problem can be solved by limiting the contrast enhancement in such areas. The idea behind CLAHE is to limit the amount of pixels that can reach a certain gray level, thus correcting the gray level peak associated to the homogeneous regions. The pixels are redistributed in order to clip the peak, and are equally redistributed across the histogram of the contextual region. We can define the clip limit \mathcal{C}

as a factor associated with the average of the histogram contents. When we define a low coefficient, the local histograms will not show heights associated to homogeneous areas, thus giving a narrow enhancement. When we choose a higher \mathcal{C} , we get a behavior of CLAHE that turns out to be equivalent to the AHE algorithm. In Figures 1(a) and 1(b), we see an example of directly applying CLAHE using arbitrary parameters: contextual region $(\mathcal{R}_x, \mathcal{R}_y) = (8, 8)$ and $\mathcal{C} = 3$.



Figure 1: An example of applying CLAHE.

We need to define certain comparison metrics in order to determine the quality of the results obtained. Those metrics are described briefly in the subsequent section.

4. COMPARISON METRICS

4.1. Entropy

Information entropy is a coefficient that gives a quantitative measure of the randomness found within the signal carried by the image[16]. When we measure entropy of two qualitatively similar images, we have in our hands an instrument to evaluate if there is an improvement in the amount of information carried by the images. The information found within gray scale images is defined as a coefficient which shows how much of the enabled gray levels are effectively used to construct the image [17].

In order to formulate the information entropy, it is fundamental to define the histogram of an image, as shown in (1):

$$\mathcal{H} = \{h_i \in [0 \dots N] \mid i = 0, 1, \dots, L - 1\} \quad (1)$$

where h_i is the counting of occurrences of the i -th gray level composing in the image; N is the total number of pixels of the image, note that $N = \sum_{i=0}^{L-1} h_i$; L is the maximum gray level defined to represent gray scales of the image. For a 8-bit scale, the maximum gray level is $2^8 = 256$ possible gray levels. Then, the normal distribution of the gray scales of the histogram is defined as:

$$\mathcal{P}_i = \frac{h_i}{N} \quad (2)$$

finally, we can formulate the entropy of a given image as (3):

$$\mathcal{H} = - \sum_{i=0}^{L-1} \mathcal{P}_i \log_2(\mathcal{P}_i) [\text{bits}] \quad (3)$$

It is desirable to measure the entropy of an image because it is directly related to the brightness homogeneity [18]. Another important feature is that it is directly related to an efficient usage of the available gray levels of the image.

For the preservation of the structural characteristics of the enhanced image, the SSIM is defined in the next section.

4.2. Structural Similarity Index

Structural Similarity Index (SSIM) is a coefficient that is capable of assessing the structural information changes, giving a good measure of the image distortion. SSIM lies on the idea that there is a strong dependency between pixels that are close to each other [12]. Traditional methods like Peak Signal to Noise Ratio (PSNR), and Mean Squared Error (MSE), are inconsistent with human eye perception [13]. SSIM is calculated across several windows that are defined within the image.

Let x and y be two windows at equal cartesian coordinates, for the original image and the resultant image, respectively; then, we can formulate SSIM as in (4):

$$SSIM(x, y) = \frac{(2\mu_x\mu_y + c_1)(2\sigma_{xy} + c_2)}{(\mu_x^2 + \mu_y^2 + c_1)(\sigma_x^2 + \sigma_y^2 + c_2)} \quad (4)$$

where μ_x is the average of x ; μ_y is the average of y ; σ_x^2 is the variance of x ; σ_y^2 is the variance of y ; σ_{xy} is the covariance of x and y ; $c_1 = (K_1L)^2$ where L is the dynamic range for the pixel values (255 for a 8 bit grayscale

image) and $K_1 \ll 1$ is a small constant; $c_2 = (K_2L)^2$, and $K_2 \ll 1$. c_1 and c_2 are constants to stabilize the division when the denominator tends to zero.

When it comes into practice, a single coefficient is taken to assess the entire resultant image quality, hence the Mean of SSIM (MSSIM) is defined as measuring the image quality as a whole. It is defined in (5):

$$MMSIM(x, y) = \frac{1}{M} \sum_{j=1}^M SSIM(x_j, y_j) \quad (5)$$

where x and y are the original and resultant images respectively; x_j and y_j are the image pixels at the j -th window; and M stands for the total of windows that were used to process the original image.

5. PARTICLE SWARM OPTIMIZATION

Particle Swarm Optimization (PSO) is a metaheuristic which has been applied successfully in several optimization problems, in a broad range of scientific research fields[19]. We define PSO as follows[20]: Let i be a complete cycle of execution of the algorithm, denominated *iteration*, and a \mathcal{D} -dimensional search space; then, each particle of the swarm is composed by a series of vectors, where \vec{x}_i is the current position of a particle within the search space; \vec{p}_i is its previous best position, and \vec{v}_i is its velocity. We can describe \vec{x}_i as an array of coordinates, in which a point of the solution space is completely defined. When a particle evaluates this solution against the best solution it has found so far, the solution is stored in \vec{p}_i ; similarly, the best position achieved by the whole swarm is stored in \vec{p}_g . A single particle moves towards a new point to the next evaluation, adding \vec{v}_i coordinates to \vec{x}_i , and the algorithm adjusts a new \vec{v}_i , which can be seen as a movement pace. Taking this description into account, we might be able to formulate the PSO algorithm as showed in (6):

$$\begin{cases} \vec{v}_i = \omega \vec{v}_i + U(0, \phi_1) \otimes (\vec{p}_i - \vec{x}_i) + U(0, \phi_2) \otimes (\vec{p}_g - \vec{x}_i), \\ \vec{x}_i = \vec{v}_i + \vec{x}_i \end{cases} \quad (6)$$

where ω is the *inertia weight*; $U(0, \phi_i)$ represents a function of random numbers between $[0, \phi_i]$, generated on every iteration for each particle, and \otimes is a scalar-vector multiplication. In Algorithm 1, the PSO-CLAHE pseudo-code used in this work is shown.

```

initialize inputImage, numIterations, numParticles, w, i,  $\phi_1$ ,  $\phi_2$ ;
for each particle  $x_i$  do
    initialize  $x_i$  randomly and set the velocity  $\vec{v}_i$  to 0;
    outputImage = runCLAHE( $x_i$ , inputImage);
     $A_i$  = calculateFitness(outputImage, inputImage);
    set the local best  $\vec{p}_i$  of the particle to its initial position;
    set the global best particle  $\vec{p}_g$  if the current particle is better;
end
while  $i = 0$ ,  $i < numIterations$  do
    for each particle  $x_i$  do
        calculate the new velocity  $\vec{v}_i$  according to Eq. (6);
        calculate the new position  $\vec{x}_i$  according to Eq. (6);
        outputImage = runCLAHE( $x_i$ , inputImage);
         $A_i$  = calculateFitness(outputImage, inputImage);
        actualize the local best  $\vec{p}_i$  if the current particle is better;
        actualize the global best  $\vec{p}_g$  if the current particle is better;
    end
end
return  $\vec{p}_g$ ;

```

Algorithm 1: PSO-CLAHE proposed pseudo-code

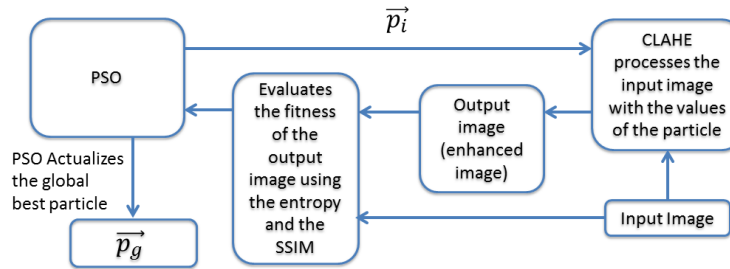


Figure 2: PSO-CLAHE relationship

In the context of the problem being addressed, a particle is composed by the input coefficients for CLAHE, this is $\vec{x}_i = ((\mathcal{R}_x, \mathcal{R}_y), \mathcal{C})$, where $(\mathcal{R}_x, \mathcal{R}_y)$ is the contextual region in which the local histogram equalization is performed, and \mathcal{C} is the coefficient of clip limit applied by the particle. The inertia weight value ω is set to 0.1, and $\vec{U}(0, \phi_i)$ takes values between 1.5 and 2.5 for every iteration.

To evaluate the quality of the results achieved by the particle, a fitness function is defined: Let \mathcal{A} be such function, and given Entropy (3) and MSSIM (5) which are obtained from the resultant image, we can formulate \mathcal{A} as showed in (7):

$$\mathcal{A} = \mathcal{H} \times MSSIM \quad (7)$$

PSO stores a new \vec{p}_i every time $\mathcal{A}_{\vec{p}_i} < \mathcal{A}_{x_i}$, and stores a new \vec{p}_g whenever $\mathcal{A}_{\vec{p}_g} < \mathcal{A}_{x_i}$. This comparison series occurs until a stop criterion is reached. In Figure 2 is presented the relationship between PSO and CLAHE algorithms.

6. RESULTS AND DISCUSSION

Six images were chosen to test the PSO, see Figures 3(a), 3(b), 3(c) and 5(a), 5(b), 5(c). For every image, 10 tests were run; the population was configured with 100 particles and 50 iterations as stop criterion. The best fitness (the best result in terms of gain of entropy and loss of Structural Similarity) from the tests for PSO-CLAHE was taken for every image, and results are listed in Table 1. In Table 2, we show the results we obtained using a state-of-the-art method for Contrast Enhancement [11], for comparison purposes.

Image Name	Normalized Coefficients			Fitness Best \mathcal{A}	Parameters applied		
	Original \mathcal{H}	\mathcal{H}	$MSSIM$		\mathcal{R}_x	\mathcal{R}_y	\mathcal{C}
Lenna	0.9306	0.9813	0.9246	0.9073	2	3	1.1604
Flowers	0.8748	0.9201	0.9103	0.8375	42	6	0.5590
Mammogram	0.8217	0.8732	0.9052	0.7904	7	3	1.5883
Giraffe	0.6724	0.8127	0.7984	0.6489	72	5	2.1555
Trees	0.7675	0.8382	0.8187	0.6862	17	17	2.4977
Woman	0.6685	0.9327	0.7296	0.6804	5	2	8.0793

Table 1: Summary of Results for PSO-CLAHE

Image Name	Normalized Coefficients			Fitness Best \mathcal{A}	Parameters applied		
	Original \mathcal{H}	\mathcal{H}	$MSSIM$		\mathcal{R}_x	\mathcal{R}_y	\mathcal{C}
Lenna	0.9306	0.9948	0.8208	0.7639	2	2	0.030
Flowers	0.8748	0.9906	0.631	0.5519	2	2	0.044
Mammogram	0.8217	0.9564	0.6215	0.5107	2	2	0.051
Giraffe	0.6724	0.9754	0.3169	0.2131	2	2	0.056
Trees	0.7675	0.9842	0.5735	0.4402	2	2	0.063
Woman	0.6685	0.7936	0.5735	0.3834	32	32	0.042

Table 2: Summary of Results for the method proposed on [11]

When comparing Table 2 against Table 1, it is seen for all rows that resulting entropy coefficients from the method proposed in [11] are higher for every row listed, than the ones obtained from PSO-CLAHE; this is because

in Table 2, entropy was maximized, without setting a explicit constraint that prevents image quality degradation. Therefore, the fitness coefficients resulted lower for every row in Table 2, when compared with the same values in Table 1. Finally, we can state that images obtained with our method show better image quality, and less amplified noise when compared with resultant images obtained from the method in [11].

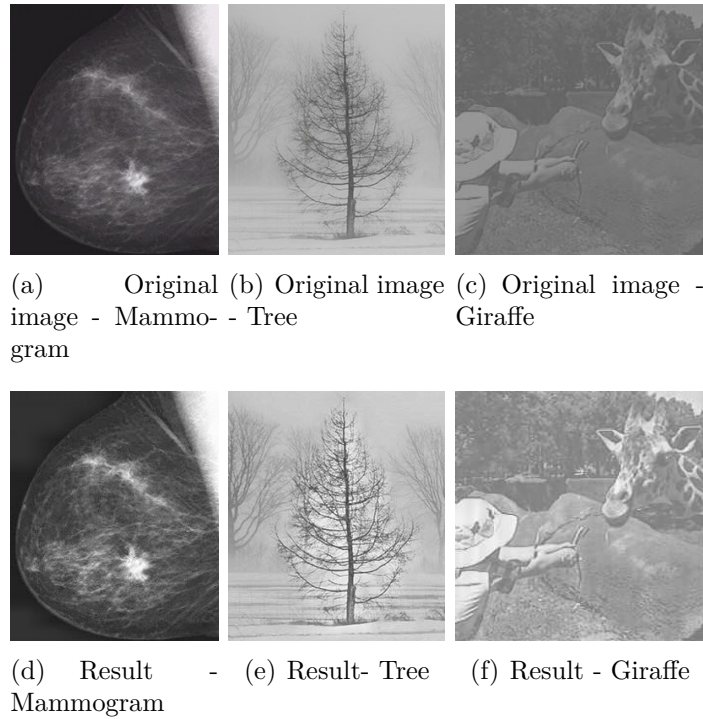


Figure 3: Original images and best solutions for PSO-CLAHE



Figure 4: Image results for the method proposed on [11]

The enhanced images are shown in Figure 3(d), 3(e), 3(f) and Figure 5(d), 5(e), 5(f). It is remarkable that there was a perceptible enhancement of contrast in every image in Figures 3 and 5, and that there was no amplified noise. In Figures 3(d), 3(f) and 5(f), we obtained better appreciation of image details. Meanwhile, in Figures 5(d) and 5(e), strong contrast was achieved. It is clearly shown that, in Figure 5(d) there is little noise amplification, when comparing with Figure 1(b).

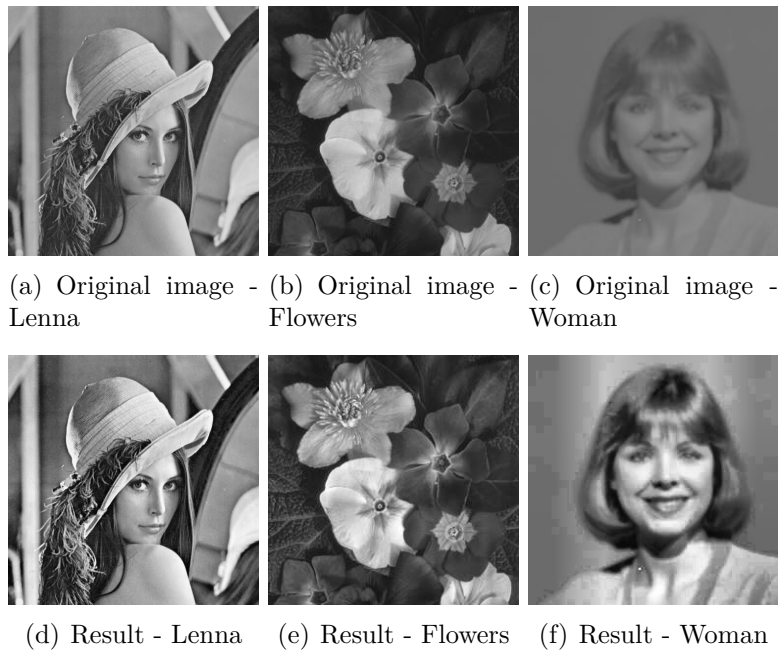


Figure 5: Original images and best solutions for PSO-CLAHE

7. CONCLUSION

This paper states a promissory approach for Contrast Enhancement. We proposed the use of PSO to find the optimal parameters of CLAHE, a local HE method, regardless of the nature and size of the image, based on Entropy and SSIM as the metrics that determine which parameters are optimal. The results indicated that our method can be applied to any type of gray level images, gives good results in terms of visual assessment, and it is not limited to a particular type of image. Using Entropy and SSIM yields images with a good natural appearance, and without amplifying noise, which is a serious drawback of AHE-based techniques. As a future work, it might be interesting

to apply PSO-CLAHE in order to perform Contrast Enhancement on HDR images [21] .

References

- [1] LEE, LEE, KIM, 2013. Enhancement Based on Layered Difference Representation of 2D Histograms. *IEEE Transactions on Image Processing*, Vol 22, No 12.
- [2] SHOME, KRISHNA, 2011. Enhancement of Diabetic Retinopathy Imagery Using Contrast Limited Adaptive Histogram Equalization. *International Journal of Computer Science and Information Technologies*, Vol. 2.
- [3] KWOK, WANG, HA, FANG, CHEN, 2013. Locally-Equalized Image Contrast Enhancement Using PSO-Tuned Sectorized Equalization. *Computational Intelligence in Image Processing*. Chatterjee, A; Siarry, P. (Eds.).
- [4] GARG, MITTAL, GARG, 2011. Histogram Equalization Techniques For Image Enhancement. *IJECT* Vol. 2, Issue 1.
- [5] KIM, 1997. Contrast enhancement using brightness preserving bi-histogram equalization. *IEEE Trans. Consumer Electron.*, Vol 43, no.1.
- [6] CHEN, RAMLI, 2003. Minimum mean brightness error bi-histogram equalization in contrast enhancement. *IEEE Transactions on Consumer Electronics*, vol 49, issue 4.
- [7] WAN, CHEN, ZHANG, 1999. Image enhancement based on equal area dualistic sub-image histogram equalization method. *IEEE Transactions on Consumer Electronics*, vol. 45, no. 1.
- [8] PIZER, AMBURN, AUSTIN, CROMARTIE, GESELOWITZ, HAAR, ZIMMERMAN, ZUIDERVELD, 1987. Adaptive histogram equalization and its variations. *Computer Vision, Graphics, and Image Processing*, 39:355-368.
- [9] ZUIDERVELD, 1994. Contrast Limited Adaptive Histogram Equalization. *Graphic Gems IV* IBM.
- [10] ZIMMERMAN, PIZER, STAAB, PERRY, MCCARTNEY, BRENTON, 1988. An Evaluation of the Effectiveness of Adaptive Histogram

- Equalization for Contrast Enhancement. IEEE Transactions on Medical Imaging, Vol. 7. No. 4.
- [11] MIN, LIM, KIM, LEE. A Novel Method of Determining Parameters of CLAHE Based on Image Entropy. International Journal of Software Engineering and Its Applications.
 - [12] WANG, BOVIK, SHEIK, SIMONCELLI, 2004. Image Quality Assessment: From Error Visibility to Structural Similarity. IEEE Transactions on Image Processing, Vol. 13, No. 4.
 - [13] NARASIMHAN, SUDARSHAN, RAJU, 2011. A Comparison of Contrast Enhancement Techniques in Poor Illuminated Gray Level and Color Images. International Journal of Computer Applications (0975 – 8887). Volume 25– No.2.
 - [14] VIJ, SINGH. Enhancement of Images Using Histogram Processing Techniques. Int. J. Comp. Tech. Appl., Vol 2.
 - [15] HASHEMI, KIANI, NOROOZI, MOGHADDAM, 2010. An image contrast enhancement method based on genetic algorithm. Pattern Recognition Letters 31.
 - [16] TSAI, LEE, MATSUYAMA, 2008. Information Entropy Measure for Evaluation of Image Quality. J Digit Imaging 21(3): 338–347.
 - [17] KWOK, HA, LIU, FANG, 2006. Intensity-Preserving Contrast Enhancement for Gray-Level Images using Multi-objective Particle Swarm Optimization. IEEE International Conference on Automation Science and Engineering.
 - [18] KHELLAF, BEGHADADI, DOPOISOT, 1991. Entropic Contrast Enhancement. IEEE Transactions on Medical Imaging. Vol. 10, No. 4.
 - [19] POLI, 2007. An Analysis of Publications on Particle Swarm Optimisation Applications. Department of Computer Science, University of Essex. Technical Report CSM-469. ISSN: 1744-8050.
 - [20] POLI, KENNEDY, BLACKWELL, 2007. Particle swarm optimization - An overview. Swarm Intell 1: 33–57.
 - [21] REINHARD, HEIDRICH, DEBEVEC, PATTANAIK, WARD, MYSZKOWSKI, 2010. High Dynamic Range Imaging: Acquisition, Display, and Image-Based Lighting. Morgan Kaufmann. ISBN: 978-0-12-374914-7.

Solving Many Objective Optimization Problems with Harmony Search

Daniel Brassel¹, Osmar Brassel², Benjamín Barán³ and Joaquín Lima⁴
Universidad Nacional de Asunción, UNA

Abstract

Multiobjective optimization problems (MOP) with more than three objectives in conflict are known as Many Objectives and generally are more difficult to solve than MOPs with two or three objectives. The literature reports that algorithms for solving MOPs, such as NSGA-II, have difficulty to converge when the number of objectives scale to four or more. In searching of approaches to efficiently solve MOPs cataloged as Many Objectives, this paper explores the application of alternative algorithms based on Harmony Search (HS).

Experimental results up to sixteen objectives in test problems widely accepted, DTLZ1 and DTLZ2, are reported and compared with performance metrics such as hypervolumen and error. Experimental results demonstrate the viability of Harmony Search based algorithms to effectively solve Many Objective Optimization Problems.

Keywords: Multi-objective optimization, Many Objective Optimization, Harmony Search, Non-dominated Sorting Genetic Algorithm

1. INTRODUCTION

In many Multiobjective Optimization Problems (MOPs), obtaining a complete and accurate set of solutions may become pretty difficult. Multi Objective Evolutionary Algorithms (MOEAs) have demonstrated ability in obtaining approximations or a complete solutions sets in MOPs with 2 and 3 objectives. However, in recent years, several researchers have reported difficulties in convergence when applying MOEAs in solving problems with 4 or more objectives, known as Many Objectives Optimization Problems [9].

¹dbrassel@gmail.com

²osmarbb@gmail.com

³bbaran@pol.una.py

⁴joaquin.lima@pol.una.py

Moreover, Farina [2] presents the following equation:

$$e = \frac{2^M - 2}{2^M} \quad (1)$$

where e is the proportion of a M -dimensional space in which its components certainly could be in the solution set of a given MOP. Clearly, when the number of objectives M tends to infinity ($M \rightarrow \infty$), e turns equal to 1, or what is the same, any solution in the objective space could be considered as a feasible solution of the MOP. Then, we can conclude that MOEAs and any other approach based only in Pareto optimality may be inadequate to determine appropriate solutions of Many Objective Optimization Problems.

Another difficulty for some MOEAs are data structures and subroutines whose computational costs increases exponentially when the objective number grows. Finally, also occurs that the number of candidate individuals required for approximating the entire solution set increases as the dimensionality of the objective space grows [9].

The next sections are as follows. Section 2 gives a brief introduction to multiobjective optimization and the concept of Many Objective. In sections 3 and 4, both NSGA-II algorithm and Multiobjective HS algorithms are briefly described. Then, performance metrics and obtained experimental results are presented in Section 5. Finally, in Section 6 conclusions of this work are shared.

2. MULTIOBJECTIVE OPTIMIZATION AND MANY OBJECTIVE OPTIMIZATION PROBLEMS

Assuming that all objectives should be minimized, and that all are equally important and independent, a MOP is expressed as follows:

$$\begin{aligned} \text{Minimize } y &= F(x_i) = (f_1(x_i), f_2(x_i), \dots, f_M(x_i)) \in Y_f \\ \text{Subject to } x_i &\in X_f \end{aligned} \quad (2)$$

where x_i is a decision vector in the feasible decision space X_f , y is an M -dimensional solution in the feasible solutions space Y_f , $f_m(x_i)$ is the m -th objective function, and M is the number of objectives in the problem.

Given two solutions x_i and x_j both belong to X_f , is said that x_i Pareto-dominates x_j (denoted as $x_i \succ x_j$) if and only if:

$$\begin{aligned} \forall m \in \{1, 2, \dots, M\} &: f_m(x_i) \leq f_m(x_j) \wedge \\ \exists m \in \{1, 2, \dots, M\} &: f_m(x_i) < f_m(x_j) \end{aligned} \quad (3)$$

Otherwise x_i and x_j are non-dominated solutions, resulting both equally feasible.

Finally, Fleming et. al. [3] introduced the notion of Many Objective in cataloging MOPs with a number of objectives in conflict or in competition of four or more ($M \geq 4$). Several authors [2, 3, 6, 9] concluded that Many Objective Optimization Problems are difficult to solve compared to standard MOPs with two or three objectives because of the following reasons.

- The increase of an M -dimensional space proportion in which solutions certainly could be in the solution set is given by equation 1. Clearly when M tends to infinity, e turns equal to 1, or what is the same, the whole objective space.
- Data structures and subroutines whose computational costs increases exponentially with the objectives number.
- The number of candidate individuals required for approximating the entire solution set increases as the dimensionality of the objective space grows.

3. NSGA-II: Non-dominated Sorting Genetic Algorithm II

NSGA-II is an MOEA of reference for solving MOPS [9]. This algorithm has two main methods which respectively allow the fast classification of solutions into a set on several non-dominated fronts and preserve diversification of solutions. These methods are the fast non-dominated sorting and the crowding distance.

In most MOEAs, such as NSGA-II, a set of candidate individuals called population is repeatedly evolving until to find a solution, or a set of them in case of MOPs (Pareto solutions set). In the main loop of NSGA-II, Algorithm 1, a parent population P_t and a new generated population Q_t , both of size N , are combined into a new set $R_t = P_t \cup Q_t$ of size $2N$. R_t is separated into several non-dominated fronts \mathcal{F}_i and next, the crowding distance operator is applicated to each front \mathcal{F}_i , until selecting a new population P_{t+1} of size N [1].

4. MULTIOBJECTIVE HARMONY SEARCH

Algorithm 1: NSGA-II Algorithm

```

t ← 0;
Generate random population Pt;
Apply fast-nondominated-sort to Pt;
Assign to each solution in Pt an adaptability value equals to its dominance level;
Generate a population Qt from Pt;
while stopping criterion not meet do
    Rt ← Pt ∪ Qt;
    F ← fast-nondominated-sort(Rt);
    i ← 1;
    Pt+1 ← ∅;
    while |Pt+1| < N do
        crowding-distance-assignment(Fi);
        Pt+1 ← Pt+1 ∪ Fi;
        i ← i + 1;
    Sort Pt+1 according to crowding distance operator;
    Keep in Pt+1 the first N solutions;
    Generate a population Qt+1 from Pt+1;
    t ← t + 1;

```

Harmony Search (HS), first introduced in 2000 [5], is a metaheuristic optimization technique based on the principles of musical improvisation and correctly applied to MOPs by Ricart et. al. [8] in 2011.

The main aggregation proposed by Ricart et. al. [8] to Harmony Search to solving MOPs is a ranking assignment to solutions based in a propose by Fonseca and Fleming [4], where the ranking of a solution x_i in an iteration t is defined by follow equation:

$$\text{rank}(x_i, t) = 1 + p_i^{(t)} \quad (4)$$

where $p_i^{(t)}$ is the number of solutions in the current iteration that dominate the current solution in question.

In [8] two multiobjective harmony search proposal are introduced which are described below.

4.1 MOHS1: MULTIOBJECTIVE HARMONY SEARCH, 1ST PROPOSAL

This multiobjective variant does not introduce significant changes in the original HS algorithm [8]. The main idea is the use of the Harmony Memory (HM) as repository for the best trade-off solutions found, specifying a ranking for them according to the Fonseca-Fleming method. The pseudocode for this proposal is shown in algorithm 2.

The algorithm begins by reading initialization parameters and populating HM with random solutions. Next, at each iteration, the algorithm tries to find a new trade-off solution using the decision variables of the solutions in

Algorithm 2: Pseudocode for MOHS1

Input: $F(x)$, HMCR, PAR, HMS, MI, FW
Output: P extracted from HM
 Randomly initialize HM;
while *stopping criterion is not satisfied* **do**
 Improvise a new solution x_i ;
 Calculate the Pareto ranking of x_i considering HM;
 if x_i *has a better ranking than the worst solution in HM* **then**
 Update HM with x_i ;

HM. The new generated solution is ranked with respect to HM. If its ranking turns better than the worst ranked solution in HM, the new solution is stored in HM replacing the worst one [8].

At each iteration, the non-dominated solutions stored in HM represent an approximation to the Pareto set. When the stopping criterion is met, the solutions with ranking equal to one (nondominated solutions) stored in HM are returned as the best approximation to the Pareto optimum decision set for the MOP.

4.2 MOHS2: MULTIOBJECTIVE HARMONY SEARCH, 2ND PROPOSAL

The main idea of this proposal is to generate a new memory HM_2 at each iteration with the same size as the original memory, HM_1 . From the union of both memories ($HM_u \leftarrow HM_1 \cup HM_2$) only half the number of solutions are admitted as components of the memory for the next iteration.

Algorithm 3: Pseudocode for MOHS2

Input: $F(x)$, HMCR, PAR, HMS, MI, FW
Output: P extracted from HM_1
 Randomly initialize HM;
while *stopping criterion is not satisfied* **do**
 Empty HM_2 ;
 while HM_2 *is not filled* **do**
 Improvise a new solution x_i from HM_1 ;
 Store x_i in HM_2 ;
 $HM_u \leftarrow HM_1 \cup HM_2$;
 Calculate Pareto ranking of HM_u using Fonseca-Fleming;
 Empty HM_1 ; $R \leftarrow 1$;
 $F \leftarrow$ Extract all solutions from HM_u with ranking R ;
 while HM_1 *has space* $\geq |F|$ **do**
 Move all solutions from F to HM_1 ;
 $R \leftarrow R + 1$;
 $F \leftarrow$ Extract all solutions from HM_u with ranking R ;
 $T \leftarrow$ Space left in HM_1 ;
 if $T > 0$ **then**
 Truncate F to size T ;
 Move every solution F to HM_1 ;

As shown in algorithm 3, MOHS2 begins generating random solutions until HM_1 is filled. Next, at each iteration, solutions for HM_2 are improvised using values of decision variables contained in HM_1 . Once all solutions for HM_2 are generated, HM_u is calculated as $HM_1 \cup HM_2$, and then the Fonseca-Fleming ranking of HM_u is calculated.

Once the ranking assignment is finished, solutions in HM_u are group in several fronts according to their ranking. Then solutions from this fronts are transferred to a new HM_1 in ascending order, i.e. solutions in the front with the lowest ranking first, and then those fronts with successively higher rankings. When the number of solutions in a front exceeds the available space in HM_1 , a truncating procedure is applied until the size of the front is equal to the space available in HM_1 . Finally, having completed the transfer of solutions, HM_1 has a new set of solutions for the next iteration.

5. COMPARISON EXPERIMENT

A comparison experiment was made between MOHS Algorithms and NSGA-II for solving Many Objective Optimization Problems DTLZ1 and DTLZ2 with 2, 3, 4, 8 and 16 objectives for each problem, based on the following metrics

- **Error.** DTLZ problems have the peculiarity that the error of approximation of solutions can be simply calculated by the following formulas [6]

$$\text{DTLZ1} \rightarrow E = 1/N \sum_{j=1}^N (\sum_{i=1}^M f_i - 0.5) \quad (5)$$

$$\text{DTLZ2} \rightarrow E = 1/N \sum_{j=1}^N (\sum_{i=1}^M f_i^2 - 1) \quad (6)$$

- **Hypervolumen.** It is a generally accepted metric of comparison that evaluates both diversity and convergence and is calculated based on a common point of reference in order to obtain a scalar value representing the space covered by each approximation set. We used the implementation of the metric developed by Fonseca et al. [7].

Each problem was solved 10 times for each algorithm in 2, 3, 4, 8 and 16 objectives. For each result the values for error and hypervolume metrics were calculated. Then the metrics results were normalized and averaged. Also for each problem in each algorithm were taken samples of the

approximate solutions in time instants determined by the following geometric series $100ms, 200ms, 400ms, \dots, 102.400ms$. For the tables below, the algorithm names are abbreviated as follow. NSGA-II as N2, MOHS1 as HS1 and MOHS2 as HS2.

Tables 1 and 2 show the values obtained at each instant for the error metric observed for DTLZ1 and DTLZ2 problems respectively and finally the best obtained value in each number of objectives considered is highlighted in bold. MOHS1 clearly obtains better values than MOHS2 and NSGA-II in both DTLZ1 and DTLZ2 problems.

Time ms.	2 Objectives			3 Objectives			4 Objectives			8 Objectives			16 Objectives		
	N2	HS1	HS2	N2	HS1	HS2	N2	HS1	HS2	N2	HS1	HS2	N2	HS1	HS2
0.1k	1E-2	8E-1	6E-1	1E+1	1E+0	2E+0	2E+2	2E+0	4E+0	3E+2	9E+0	1E+2	4E+2	8E+0	4E+2
0.2k	2E-3	2E-1	5E-1	6E-2	7E-1	9E-1	1E+2	7E-1	9E-1	4E+2	3E+0	1E+2	4E+2	3E+0	4E+2
0.4k	1E-3	1E-4	3E-1	1E-2	3E-1	9E-1	7E+1	2E-1	7E-1	4E+2	1E+0	2E+2	4E+2	2E+0	5E+2
0.8k	4E-5	2E-5	3E-1	5E-4	2E-3	4E-1	4E+1	1E-2	6E-1	4E+2	6E-1	3E+2	4E+2	8E-1	5E+2
1.6k	1E-5	4E-6	2E-1	4E-4	2E-4	3E-1	7E+1	2E-3	2E-1	4E+2	2E-1	4E+2	4E+2	3E-1	5E+2
3.2k	9E-6	8E-7	1E-1	2E-4	3E-5	5E-2	8E-1	7E-4	3E-2	4E+2	1E-1	5E+2	5E+2	6E-2	5E+2
6.4k	3E-6	3E-7	4E-5	4E-4	9E-6	1E-3	2E-1	2E-4	2E-2	4E+2	5E-3	5E+2	4E+2	7E-3	5E+2
10.2k	5E-6	5E-8	2E-5	5E-4	3E-6	3E-4	4E-1	7E-5	3E-3	4E+2	2E-3	5E+2	4E+2	8E-3	5E+2
25.6k	2E-5	2E-8	4E-6	3E-4	5E-7	1E-4	6E-1	2E-5	3E-3	4E+2	9E-4	5E+2	4E+2	3E-3	5E+2
51.2k	8E-6	5E-9	1E-6	7E-4	1E-7	3E-4	1E+0	2E-6	2E-3	4E+2	5E-4	5E+2	4E+2	2E-3	5E+2
102.4k	2E-5	6E-10	4E-7	3E-4	3E-6	2E-4	1E+0	3E-5	3E-3	4E+2	2E-3	5E+2	4E+2	2E-3	5E+2

Table 1: Error metric result for test problem DTLZ1

Time ms.	2 Objectives			3 Objectives			4 Objectives			8 Objectives			16 Objectives		
	N2	HS1	HS2	N2	HS1	HS2									
0.1k	2E-3	2E-3	6E-3	3E-2	2E-2	1E-1	2E-1	8E-2	7E-1	7E+0	6E-1	2E+0	6E+0	6E-1	3E+0
0.2k	1E-3	8E-5	1E-3	2E-2	9E-3	9E-2	9E-2	4E-2	4E-1	8E+0	4E-1	3E+0	8E+0	4E-1	5E+0
0.4k	1E-3	2E-6	1E-4	2E-2	2E-3	5E-2	8E-2	1E-2	3E-1	8E+0	3E-1	4E+0	9E+0	3E-1	6E+0
0.8k	1E-3	6E-7	1E-5	2E-2	2E-4	2E-2	8E-2	4E-3	2E-1	9E+0	2E-1	5E+0	8E+0	2E-1	8E+0
1.6k	1E-3	6E-7	3E-6	1E-2	8E-5	1E-2	8E-2	1E-3	1E-1	9E+0	1E-1	7E+0	8E+0	2E-1	8E+0
3.2k	1E-3	5E-7	8E-6	1E-2	4E-5	8E-3	7E-2	3E-4	7E-2	8E+0	1E-1	9E+0	7E+0	1E-1	9E+0
6.4k	1E-3	3E-5	1E-5	2E-2	9E-5	6E-3	7E-2	4E-4	6E-2	7E+0	7E-2	9E+0	6E+0	1E-1	9E+0
10.2k	1E-3	4E-7	4E-6	2E-2	7E-7	3E-3	7E-2	4E-6	6E-2	7E+0	6E-2	1E+1	7E+0	9E-2	9E+0
25.6k	1E-3	2E-6	9E-6	2E-2	9E-6	4E-3	6E-2	4E-4	5E-2	8E+0	4E-2	1E+1	7E+0	7E-2	9E+0
51.2k	1E-3	9E-7	3E-6	2E-2	4E-5	7E-3	6E-2	6E-5	5E-2	8E+0	3E-2	1E+1	7E+0	6E-2	9E+0
102.4k	1E-3	4E-7	3E-6	2E-2	3E-7	5E-3	7E-2	4E-4	5E-2	8E+0	2E-2	1E+1	8E+0	5E-2	9E+0

Table 2: Error metric result for test problem DTLZ2

In addition, Figures 1 and 2 respectively show the behavior of the three algorithms in problems DTLZ1 and DTLZ2 with 4 and 16 objectives.

Next, the obtained values for Hipervolumen metric are presented in Tables 3 and 4. MOHS2 slightly obtains better values than MOHS1 and NSGA-II in both DTLZ1 and DTLZ2 problems for low number of objectives. For high number of objectives MOHS1 obtains better values than MOHS2 and NSGA-II algorithms.

6. CONCLUSION

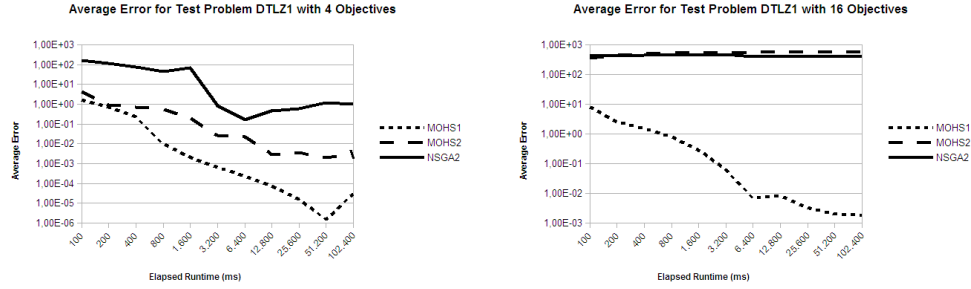


Figure 1: DTLZ1 with 4 and 16 objectives



Figure 2: DTLZ2 with 4 and 16 objectives

The experimental results presented in this work confirm that difficulties in solving MOPs increases when the objectives number grows, such as reported in the literature.

Also, the results show that Multiobjective HS proposals are equally competitive that traditional algorithms for MOPs, such as NSGA-II.

In respect to the error metric, is seen that MOHS1 algorithm is superior to the other algorithms in all test problems and in all considered objectives numbers. Also, is noted that MOHS2 has a performance comparable to

M →	2 Obj.		3 Obj.		4 Obj.		8 Obj.		16 Obj.	
Alg. ↓	HV	SD								
MOHS1	0.9888	0.4529%	0.9644	1.8770%	0.9999	0.0023%	1.0000	0.0000%	1.0000	0.0000%
MOHS2	1.0000	0.0050%	1.0000	0.0362%	1.0000	0.0000%	0.9957	0.1388%	0.9836	0.5147%
NSGA-II	0.9965	0.0444%	0.9707	0.6070%	0.9999	0.0128%	0.9899	0.0007%	0.9889	0.0003%

Table 3: Hypervolume metric values and Standard Deviation for DTLZ1 problem.

M →	2 Obj.		3 Obj.		4 Obj.		8 Obj.		16 Obj.	
Alg. ↓	HV	SD								
MOHS1	0.9932	0.1356%	0.9932	0.2891%	1.0000	0.2672%	1.0000	0.5257%	1.0000	0.4124%
MOHS2	1.0000	0.0091%	1.0000	0.1959%	0.9956	0.2478%	0.8504	1.2346%	0.7499	1.8342%
NSGA-II	0.9969	0.0482%	0.9596	0.5085%	0.9445	0.5147%	0.8222	8.9635%	0.9892	0.5303%

Table 4: Hypervolume metric values and Standard Deviation for DTLZ2 problem.

NSGA-II.

Regarding to the Hypervolume metric, is noted that MOHS2 slightly outperforms the other algorithms in a low number of objectives, $M \geq 4$, and that MOHS1 has slightly better results in high number of objectives. However, no major differences are observed between all considered algorithms, which suggests that all they have good performance in terms of diversity of solutions.

In general, algorithms with a logic that try to find at same time optimal and diverse solutions, such as NSGA-II and MOHS2, lose the ability to converge when the objectives number increases. in contrast for MOHS1 algorithm, whose logic is based only in enhance solutions after each iteration, is apparently unaffected by the increase of objectives number, but in lack of a solutions conservation strategy is subject to the fluctuation of the approximations calculated, as shown in graphs.

As final conclusion is demonstrated the need of study and development of alternative mechanisms that must be applied to traditional algorithms in order to overcome the current difficulties of lack of convergence and fluctuation in approximation when solving Many Objective Optimization Problems. Investigation of such alternatives will be the subject of future works.

References

- [1] DEB, K., A. PRATAP, S. AGARWAL and T. MEYARIVAN, A Fast and Elitist Multiobjective Genetic Algorithm: NSGA-II, *Evolutionary Computation*, *IEEE Transactions on* 6 (2002), pp. 182–197.
- [2] M. FARINA and P. AMATO, “On the optimal solution definition for many-criteria optimization problems,” in *Fuzzy Information Processing Society, 2002. Proceedings. NAFIPS. 2002 Annual Meeting of the North American*, pp. 233-238, 2002.

- [3] PETER FLEMING, ROBIN C. PURSHOUSE, and ROBERT J. LYGOE. Many-Objective Optimization: An Engineering Design Perspective. In Carlos A. Coello Coello, Arturo Hernández Aguirre, and Eckart Zitzler, editors, *Evolutionary Multi-Criterion Optimization. Third International Conference, EMO 2005*, pages 14–32, Guanajuato, México, March 2005. Springer. Lecture Notes in Computer Science Vol. 3410.
- [4] FONSECA, C. and P. FLEMING, *Genetic Algorithms for Multiobjective Optimization: Formulation, Discussion and Generalization*, , 423, Citeseer, 1993, pp. 416-423.
- [5] GEEM, Z. W., *Optimal Design of Water Distribution Networks using Harmony Search*, 2000, Phd thesis, Korea University.
- [6] KUKKONEN, SAKU, and JOUNI LAMPINEN. Ranking-dominance and many-objective optimization. *Evolutionary Computation, 2007. CEC 2007. IEEE Congress on. IEEE*, 2007.
- [7] CARLOS M. FONSECA, LUÍS PAQUETE, and MANUEL LÓPEZ-IBÁÑEZ. An improved dimension - sweep algorithm for the hypervolume indicator. In *Proceedings of the 2006 Congress on Evolutionary Computation (CEC06)*, pages 1157–1163. IEEE Press, Piscataway, NJ, July 2006.
- [8] RICART, J., HÜTTEMANN, G., LIMA, J., and BARÁN, B. (2011). Multiobjective harmony search algorithm proposals. *Electronic Notes in Theoretical Computer Science*, 281, 51-67.
- [9] C. VON LÜCKEN, B. BARÁN, and C. BRIZUELA, “A survey on multi-objective evolutionary algorithms for many-objective problems,” *Computational Optimization and Applications*, pp. 1-50, 2014.

Ant Colony Multi-objective Optimization Algorithms applied to the Reactive Power Compensation Problem

Hugo R. Benítez Vega ^a, Rodolfo Páez ^a,
Diego Pinto ^{a1}, Pedro Gardel-Sotomayor ^{a b}, Benjamín Barán. ^a
^a Polytechnic School, National University of Asuncion, Paraguay
^b University of Valladolid, Spain

Abstract

The reactive power compensation (RPC) problem is formulated as a combinatorial optimization problem involving nonlinear objective function with multiple local minima. In this paper, as a new approach, different multi-objective ant colony optimization (MOACO) algorithms are applied to the reactive power compensation problem. The objectives selected for this study were minimizing the investment of reactive compensation devices, minimizing the average voltage deviation and minimizing the maximum voltage deviation, in this paper employs six MOACOs algorithms which differ primarily in how they use the criterion of the information obtained during the construction of a solution, how to update this information, the number of colonies used and how they are treated information for optimal solutions from the standpoint of multi-objectives. To analyse the efficiency and effectiveness of these modern search algorithms, the proposed methods are applied to the IEEE 118-bus standardized system and the results are compared with each other, using comparison metrics.

Keywords: Multi-objective Ant Colony Optimization, Reactive Power Compensation, Comparison metrics.

1. INTRODUCTION

Nowadays, it is extremely important to operate Electric Power Systems, EPS, as efficiently and reliable as possible. A way to increase EPS reliability simultaneously reducing electric power losses is by Reactive Power Compensation, RPC. In an EPS, the main goal related to the RPC is to determine the adequate size and the physical distribution of capacitive or inductive compensation devices . This optimization task generally involves several factors

¹E-mail Corresponding Author: dpinto@pol.una.py

such as investment or transmission losses, that are subject to operational constraints such as reliability and voltage profile. These factors, considered as the optimization objectives, usually are contradictory, therefore, in the last years this problem has been treated as a Multi-objective Optimization Problem, MOP[1]. Multi-objective Ant Colony Optimization algorithms, MOACO, have shown excellent results solving complex MOP [2], therefore, it is an interesting task to apply different MOACOs to the RPC and analysis which one presents the best performance.

2. MULTI-OBJECTIVE OPTIMIZATION

A Multi-objective Optimization Problem, MOP, [3] generally consist in a set of n parameters or decision variables, a set of k objective functions and a set of m constraints. The objective functions and the constraints are functions of the decision variables. A MOP can be defined as:

Optimise

$$y = f(x) = (f_1(x), f_2(x), \dots, f_k(x)) \quad (1)$$

subject to:

$$e(x) = (e_1(x), e_2(x), \dots, e_m(x)) \geq 0 \quad (2)$$

where:

x n -dimensional decision vector, X denotes the decision space, y is a k -dimensional objective vector, and Y denotes the objective space. Optimize, depending on the problem, may mean minimize or maximize. The constraints set $e(x) \geq 0$ defines the feasible solutions set X_f and its corresponding feasible objective vectors set Y_f . Each solution of the MOP is represented by a n -tuple $x = (x_1, x_2, \dots, x_n)$, which defines a objective vector $y = (f_1(x), f_2(x), \dots, f_k(x))$, where each x must satisfy the constraints set $e(x) \geq 0$.

In a single objective optimization problem the feasible decision vectors are completely sorted by the objective function. This is, when two feasible solutions, u and v , are compared only one of the three following options is satisfied: $f(u) > f(v)$, $f(u) = f(v)$ or $f(u) < f(v)$. However, in a multi-objective context there is not a single best solution, but a set of best trade

off solutions. In this set, no solution can be consider better than the others if all objectives are considered simultaneously. Usually, there are conflicting objectives, this is, the optimization of a objective implies the degradation of some other objective. Therefore, a new concept of optimality must be define for a multi-objective context.

Before explaining the Pareto dominance, some mathematical relations must be defined. Given two decision vectors $u, v \in X$.

$$f(u) = f(v) \text{ if and only if } f_i(u) = f_i(v) \forall i \in 1, 2, \dots, k \quad (3)$$

Considering a minimization context, given two decision vectors $u, v \in X$, u dominates v (denoted as $u \succ v$) if u is better or equal than v in every objective and strictly better in, at lest, one objective. This is:

$$\forall i \in \{1, 2, \dots, k\} : f_i(u) \text{ is better or equal than } f_i(v) \quad (4)$$

Note that the above definition of Pareto dominance is independent of whether the problem is a minimization problem, maximization problem or a combination of both. The vector u is non-comparable to the vector v , denoted as $u \sim v$, if and only if, $u \not\succeq v \wedge v \not\succeq u \wedge u \neq v$. Alternatively, $u \triangleright v$ denotes that u dominates or is non-comparable to v . If $x \in X_f$, x is non-dominated respect to a set $Q \subseteq X_f$ if and only if:

$$\forall v \in Q : (x \triangleright v) \quad (5)$$

If x is non-dominated respect to the set X_f , and only in that case, x is a optimal Pareto solution P^* and can be defined as the set of decision vectors non-dominated with respect to X_f , this is:

$$P^* = \{x \in X_f \mid x \text{ is non-dominated with respecto to } X_f\} \quad (6)$$

Therefore, the corresponding objective vectors set $P_{true} = f(P^*)$ is the optimal Pareto front.

3. PROBLEM FORMULATION

The RPC problem is considered for this paper as a MOP with three objectives to be minimized as follows:

1) Investment in reactive power compensation devices. This optimization objective is related to the resources optimization.

2) Average voltage deviation. This objective measures the general quality of the solution.

3) Maximal voltage deviation. This objective indicates the quality of the solution for each busbar, it is designed to avoid large voltage deviation at any busbar.

4. ANT COLONY OPTIMIZATION

Ant Colony Optimization, ACO, is a meta-heuristic inspired by the behaviour of real ants colony [4]. It has been shown that ants are able to find shortest path from their nest to food sources. These ants choose the way forward with a probabilistic decision biased by the amount of pheromone: the more stronger the pheromone trail, the greater the chance of choose a path [2]. The meta-heuristic ACO uses simple agents called ants and a pheromone matrix $\tau_{i,j}$, it also take in consideration heuristic information by a parameter $\eta_{i,j}$ known as visibility, ants do not modify this heuristic information during the algorithm execution. The relative influence between heuristic information and pheromone level is define by the parameters β and α . The ant k located in the node i employs a decision rule based on the pheromone trail $\tau_{i,j}$ and the heuristic information $\eta_{i,j}$ to determinate the probability of choosing node $j \in J_i$ as next node to visit, where J_i is the set of nodes in the neighbourhood of i . This decision rule is defined by:

$$P_{i,j} = \begin{cases} \frac{\tau_{i,j}^\alpha \cdot \eta_{i,j}^\beta}{\sum_{x \in J_i} \tau_{i,x}^\alpha \cdot \eta_{i,x}^\beta}, & \text{si } j \in J_i \\ 0, & \text{otherwise} \end{cases} \quad (7)$$

Upon completion of a solution, the ant evaluates the solution and modifies the pheromone trails on the pheromone matrix $\tau = \{\tau_{i,x}\}$, to keep the knowledge of areas already explored. This information saved on the pheromone matrix will guide the search for future ants. The algorithm can also include a process of pheromone trails evaporation after each iteration. The update and evaporation pheromone process is performed according to the equation [2]:

$$\tau_{ij} = (1 - \rho) \cdot \tau_{ij} + \rho \cdot \Delta\tau \quad (8)$$

where ρ represents the evaporation coefficient, and $\Delta\tau$, in a minimization context is calculated as:

$$\Delta\tau = \frac{1}{f_k(x)} \quad (9)$$

with $k \in \{1, 2, \dots, b\}$ considering an update based on a single objective. In case b objectives are optimized simultaneously the next equation can be considered [10]:

$$\Delta\tau = \sum_{k=1}^b \frac{1}{f_k(x)} \quad (10)$$

to normalisation purposes the f_k values are divided by a maximum value predefined. Therefore, the pheromone trail update is proportional to the solution performance considering all the problem objectives.

5. MOACO ALGORITHMS

A total of six MOACOs were selected for this paper as follows:

1) Multiple Objective Ant Q Algorithm (MOAQ): this algorithm was proposed by Mariano and Morales in [5], based on the Ant-Q algorithm [6]. An ant colony is dedicated to each objective. Therefore, a problem with b objectives will have b ant colonies, each colony optimizing a different objective. The transition rule is based on the pheromone matrix τ , and the visibility η , for the transition each colony employs a rule denominated pseudo-random-proportional, according to equation 7. The update of τ_{ij} is based on the equation 8. The expression $\gamma \cdot \max_{z \in J_j} \tau_{jz}$ is added to $\Delta\tau_{ij}$, where γ represents the learning step [6] and denotes the quality of the path according to the information learned in the past.

2) Pareto Ant Colony Optimization (PACO): this algorithm proposed in [7] employs b pheromones tables (τ^b), one for each objective. In every iteration an ant determines a set of weights, in [7] these weights were randomly selected, $\delta = (\delta_1, \delta_2, \dots, \delta_b)$, and uses then to evaluate the transition rule. Considering the ant in the i state, the j state is selected according to:

$$j = \begin{cases} \max_{j \in J_i} \left\{ (\sum_{k=1}^b \delta_k \cdot \tau_{i,j}^k)^\alpha \cdot \eta_{i,j}^\beta \right\}, & \text{if } q \leq q_0 \\ \hat{i}, & \text{otherwise} \end{cases} \quad (11)$$

where \hat{i} is a random variable selected according to the probability distribution generated by the equation:

$$p_{i,j} = \begin{cases} \frac{(\sum_{k=1}^b \delta_k \cdot \tau_{i,j}^k)^\alpha \cdot \eta_{i,j}^\beta}{\sum_{x \in J_i} \left\{ (\sum_{k=1}^b \delta_k \cdot \tau_{i,x}^k)^\alpha \cdot \eta_{i,x}^\beta \right\}}, & \text{if } j \in J_i \\ 0, & \text{otherwise} \end{cases} \quad (12)$$

The two best ant for each objective update the corresponding pheromone matrix according to the equation 8, employing an elitist update process. Every time an ant moves to a new state, a local step by step update process is perform. This update process is apply to the b pheromone matrices according to 8, considering a constant value for $\Delta\tau = \tau_0$, this represents the initial value of the pheromone trails, defined *a priori*.

3) Multi-objective Ant Colony System (MOACS): proposed by Baran and Schaerer en [8] as an extension of the MACS-VRPTW [9]. The MOACS gives the same importance to all objective, this is the main difference with the original algorithm [8]. Originally it was implemented with three objectives, with a unique pheromone matrix to minimize simultaneously the three objectives. Therefore, the information of good solutions is equally important for each objective function in the Pareto Front. This algorithm uses the pseudo-random-proportional rule and selects the state j as next state to visit, considering the ant in state i , by the equation:

$$j = \begin{cases} \max_{j \in J_i} \left\{ \lambda_{i,j} \cdot [\eta'_{i,j}]^{\lambda\beta} \cdot [\eta''_{i,j}]^{(1-\lambda)\beta} \right\}, & \text{if } q < q_0 \\ \hat{i}, & \text{otherwise} \end{cases} \quad (13)$$

where \hat{i} is a random variable selected according to the probability distribution generated by the equation:

$$p_{i,j} = \begin{cases} \frac{\lambda_{i,j} \cdot [\eta'_{i,j}]^{\lambda\beta} \cdot [\eta''_{i,j}]^{(1-\lambda)\beta}}{\sum_{x \in J_i} \lambda_{i,x} \cdot [\eta'_{i,x}]^{\lambda\beta} \cdot [\eta''_{i,x}]^{(1-\lambda)\beta}}, & \text{if } j \in J_i \\ 0, & \text{otherwise} \end{cases} \quad (14)$$

Every time an ant moves from state i to state j , performs a local pheromone update according to equation 8, with $\Delta\tau = \tau_0$, the initial value of pheromones. When a non-dominated solution is found, the Pareto Set is updated and the pheromone matrix is reinitialized because the information was learned with dominated solutions [8]. If a dominated solution is found, the pheromone update is made according to 8, with $\Delta\tau$ defined by the multi-objective expression 10.

4) Multi-objective Max-Min Ant System (M3AS): proposed in [10] as an multi-objective version of the Max-Min Ant System [11]. The original algorithm considered four objective functions. A global pheromone matrix keeps the information of pheromones for all the objectives. An ant in state i chose the next state to visit according to the probability p given by the equation 14 of the MOACS.

The non-dominated solutions update the pheromone matrix according to 8 with a $\Delta\tau$ calculated by 10. If $\tau_{ij} > \tau_{max}$, then $\tau_{ij} = \tau_{max}$, with $\tau_{max} = \frac{\Delta\tau}{(1-\rho)}$, and if $\tau_{ij} < \tau_{min}$, then $\tau_{ij} = \tau_{min}$, with $\tau_{min} = \frac{\Delta\tau}{2m \cdot (1-\rho)}$. Therefore, a lower and upper bound is imposed to the pheromone level.

5) Multi-objective Omicron ACO (MOA): algorithm initially proposed as a bi-objective MOACO in [1], based in the OA by Gomez and Baran [12]. In this paper the MOA was modified for three objectives, for this, a single pheromone matrix and three different visibilities, one for each objective, are employed. The MOA uses a population, P, of non-dominated solutions to update the pheromone matrix. As transition rule the multi-objective extension of the MOACS, equation 14, was employed. In the pheromone update process a constant pheromone value is added to all

La actualización de feromonas se basa en depositar una cantidad constante en todos los arcos que componen todas las soluciones de la población P. La regla se basa en el parámetro O (*Omicron*) al igual que en el OA. De esta manera, se mantiene el nivel de feromonas con una cota inferior y otra superior, como se muestra en la sección dedicada al OA.

6) Multi-objective Ant System (MAS): proposed by Paciello et all. in [2] as an multi-objective extension of the Ant System [4]. The modifications

are focus on the selection of the next state and in the pheromone update process. The stochastic selection of the next state to visit uses the expression 14, based on the MOACS. The MAS uses a single pheromone matrix with a visibility for each optimization objective and the ants are spread in different decision space regions according to a $\lambda = m$ value.

λ takes discrete values equally spaced between 1 and the number m of ants, this is $\lambda \in \{1, 2, \dots, m\}$. Thus, a distribution is obtained in the solution space of the problem, where for example, in the bi-objective context, the ant with $\lambda = 1$ is specialized in the second objective and an ant with a λ value of M is specialized in the first objective. Clearly the other values of λ represent intermediate degrees of specialization between these two extremes.

The pheromone update is done after all solutions of the iteration are finished, and only the non-dominated solutions found during the iteration update the pheromone matrix. The update rule uses the expression 8 with $\Delta\tau$ according to 9, therefore, the update process depends on the evaluation of the solution according to all objective functions.

A mechanism to control the algorithm convergence is introduce. The pheromone matrix is reinitialized if during K' generations, with K' defined *a priori*, no new non-dominated solutions are found. This encourages the exploration of new paths. This mechanism helps to avoid local optima convergence.

These algorithms were selected considering the good performance they have exhibited solving complex MOP. It is important to remark that all of the MOACOs had to be specially formulated to be applied for the multi-objective RPC problem.

6. EXPERIMENTAL STUDY AND RESULT ANALYSIS

To validate the algorithms the well known IEEE 118 Bus Power System was employed, and ten different executions of each MOACO was performed. As aforementioned, a multi-objective algorithm generates a set of tradeoff solutions, none of which can is better that other consider all objective, this is, a set of non-dominated solution. This set of solution is denoted as Pareto Front of the algorithm, *FP*.

To analysis the performance of the MOACOs applied to the RPC problem a set of comparison metrics was selected. These metrics evaluate the solution in

different ways considering the characteristics of a MOP. The metrics selected for this paper are:

1) Distance M_1 : calculates the average distance between each point of the calculated Pareto Front, FP , and the nearest point of the Optimal Pareto Front, $PTrue$.

$$M_1(FP) = \frac{1}{|FP|} \sum_{p \in FP} \min \{d(p, q) | q \in PTrue\} \quad (15)$$

where $PTrue$ was considered as the set of all non-dominated solutions found by all algorithms in all executions.

2) Distribution M_2 : is the average of solutions in a FP that are separated by a distance bigger than a σ predefined.

$$M_2(FP) = \frac{1}{|FP| - 1} \sum_{p \in FP} q \in FP | d(p, q) > \sigma \quad (16)$$

3) Extension M_3 : indicates the distance between the extreme solutions in FP .

$$M_3(FP) = \sqrt{\sum_{i=1}^k \max(|p_i - q_i|) | p, q \in FP} \quad (17)$$

Metrics M_1 , M_2 and M_3 are defined in [13]. The set $PTrue$ considered to evaluate these metrics is the set of all non-dominated solutions found by the six algorithms in all executions. In all cases the distance metric employed is the standard euclidean distance between two point, denoted as $d(p, q)$.

The comparison metrics for the six MOACOs are shown in Table I. Analysing Table I it can be notice than MOACS algorithm presents very good performance, showing it capability to obtain a set of solutions very close to those considered as optimal. Considering metric M_2 , MOACS obtained the best distribution of FP , in metric M_1 and M_3 MOACS generated the second FP closer to the $PTrue$ and with the second largest extension. PACO algorithm also obtained good M_2 and M_3 metrics, it has the second best distribution and the largest FP , but it had the worse results in M_1 metric, this is, it generated the FP farthest from $PTrue$.

ALG	M_1	ALG	M_2	ALG	M_3
M3AS	0,055	MOACS	41,66	PACO	2,453
MOACS	0,072	PACO	36,94	MOACS	2,441
MAS	0,075	MOA	26,39	M3AS	1,381
MOA	0,076	MOAQ	24,31	MOA	0,177
MOAQ	0,081	M3AS	17,63	MOAQ	0,156
PACO	0,088	MAS	15,76	MAS	0,151

Table 1: M_1 , M_2 and M_3 comparison metrics.

7. CONCLUSIONS AND FUTURE WORK

This paper presents for the first time, to the authors knowledge, a comparative study of six different MOACOs applied to the RPC problem with three different objectives. To analysis the algorithms performance, three well known performance metrics were employed. Analysing these metrics it can be concluded that MOACS algorithm shows the most promising results for the problem in study. It is propose, as future work, to: *i*) apply more MOACOs to the MORPC problem, *ii*) consider more comparison metrics and *iii*) perform a statistical analysis of the results.

References

- [1] GARDEL, P, BARAN, B, FERNANDEZ, U, ESTIGARRIBIA, H, DUARTE, S, 2006. Multi-objective Reactive Power Compensation with an Ant Colony Optimization Algorithm, The 8th IEE International Conference on AC and DC Power Transmission, London, England.
- [2] PACIELLO, J, MARTINEZ, H, BARAN, B, 2006. Team algorithms for ant colony based multi-objective problems, ASAI 2006, Mendoza, Argentina.
- [3] VANVELDHUIZEN, D, Multi-objective evolutionary algorithms: Classifications, analyses, and new innovations, Ph.D. dissertation, Graduate School of Engineering. Air Force Institute of Technology, Wright-Patterson AFB, Ohio.

- [4] DORIGO, M, MANIEZZO, V, COLORNI, A, 1996. The ant system: Optimization by a colony of co-operating agents. IEEE Trans. systems Man and Cybernetics, vol. 26, pp. 2941.
- [5] MARIANO, C, MORALES, E, 1999. A Multiple Objective Ant-Q Algorithm for the Design of Water Distribution Irrigation Networks, Technical Report HC-9904, Instituto Mexicano de Tecnologia del Agua.
- [6] GAMBARDELLA, D M L, Ed., Ant-Q: A reinforcement Learning approach to the traveling salesman problem. Morgan Kaufmann, 1995.
- [7] DOERNER, K, GUTJAHR, W, HARTL, R, STRAUSS, C, 2002. Eds., Pareto Ant Colony Optimization: A Metaheuristic Approach to Multi-objective Portfolio Selection.
- [8] SCHAERER, M, BARAN, B, 2003. A multi-objective Ant Colony System for Vehicle Routing Problems with Time Windows. Twenty first IASTED International Conference on Applied Informatics, pg. 97-102. Innsbruck, Austria.
- [9] GAMBARDELLA, L, 1999. MACS-VRPTW: A Multiple Ant Colony System for Vehicle Routing Problems with Time Windows, In D. Corne, M. Dorigo, F. Glover (Eds.), New Ideas in Optimization, McGraw-Hill, pp. 7376.
- [10] PINTO, D, BARAN, B, 2005. Multi-objective Multicast Routing Problem with a new Ant Colony Optimization approach. Proceedings of the 3rd international IFIP/ACM Latin American conference on Networking.
- [11] STUZLE, T, 2000. Max-min ant system. Future Generation Computer Systems.
- [12] GOMEZ, O, BARAN, B, Omicron ACO, proceedings of clei-2004. latin-american conference on informatics (clei). arequipa. peru, 2004.
- [13] ZITZLER, E, DEB, K, THIELE, L, 2000. Comparison of multi-objective evolutionary algorithms: Empirical Result. Evolutionary Computation.

A Survey on Virtual Optical Network Embedding

Enrique Dávalos^{a1}, Benjamín Barán^{a2}, Diego P. Pinto-Roa^{a3}

^aNational University of Asunción

Abstract

Network virtualization is a key component of the Future Internet. A central problem in Network Virtualization is the process of mapping virtual networks over a substrate or physical infrastructure. Due to its special characteristics, optical networks scenarios require different approaches for this problem named Virtual Optical Network Embedding (VONE). This paper presents a survey of current research in the VONE problem. Their main features are provided and some aspects of related important topics are presented.

Keywords: Optical Networks, Network Virtualization, Virtual Optical Network Embedding.

1. INTRODUCTION

The term Network Virtualization is used to describe the technologies that creates logically isolated network partitions over shared physical (or substrate) network infrastructures, so that multiple virtual networks can simultaneously coexist over the shared infrastructures [1]. In that sense, network virtualization covers both node and link virtualization, which are the fundamental components of a network. Although a broad set of commercial solutions was developed for node and link virtualization for years, e.g. Layer 2 Virtual LAN (VLAN), Virtualized Private Networks (VPN), Software-enabled NIC virtualization, TDM/FDM, etc. [2], in recent years virtualized networks have attracted the attention of research and industry communities. One of the first objectives of research in this area was to implement platforms to test novel or proposed Internet architectures and protocols (testbeds), as VINI/Trellis, G-Lab and OneLab [3,4]. Furthermore, several research projects were driven to explore the various aspects of network virtualization addressed by these projects, as OpenFlow and GEYSERS [6,7]. These projects have left clear that Network Virtualization will constitute a

¹edavalos@pol.una.py

²bbaran@pol.una.py

³dpinto@pol.una.py

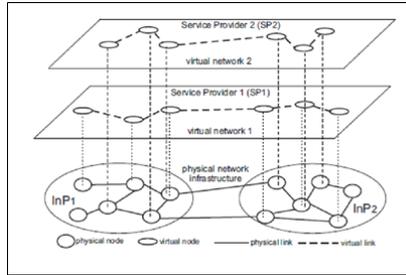


Figure 1: An example of Network Virtualization

key component of future Internet [5] One of the main challenges in network virtualization is the problem of how to allocate or map virtual networks in a substrate or physical network. This problem is named Virtual Network Embedding (VNE). Nowadays, we can find surveys as [8,9] that are related to the VNE problem for generic networks (packet switched) or L2-L3 virtualization networks. In Figure 1, taken from [9], a network virtualization environment is showed, in which two Network Infrastructure providers (InP) coexist. Two Virtual Network requirements, coming from different Service Providers (SP) have been mapped or embedded, assigning physical network resources to virtual nodes and links.

In optical networks, this process is named Virtual Optical Network Embedding (VONE). Optical network virtualization is still under initial study [12]. This is because of its analogue nature, diverse optical transmission technologies and the complexity of the virtualization approach suitable for optical networks. It causes that these specific features need to be taken into consideration, and contributes for the need of research on specific algorithms for the VONE problem. In this work we present a survey on the main proposed approaches about the VONE problem. We also propose a way to classify them and enumerate some aspects on special topics related to them.

2. VIRTUAL OPTICAL NETWORK EMBEDDING (VONE) PROBLEM

The Virtual Optical Network Embedding (VONE) problem, often referred also as Virtual Optical Network Assignment (VONA) problem, deals with the efficient allocation of Virtual Optical Network (VON) requests over a substrate (or physical) optical network owned by one or more Infrastructure Providers. This problem can be treated as two separated sub-problems: 1)

The assignment of virtual optical nodes to physical nodes, or Virtual Optical Node Mapping, and 2) the assignment of paths formed by consecutive links in the substrate network (lightpaths) to virtual links (Virtual Optical Link Mapping). To find a way to classify the different approaches for the study of VONE problem, we focus on its following aspects:

1. Online vs offline problem [8]: In the VONE on-line (dynamic) problem, the VON requirements can come and leave dynamically and are not known before their arrivals. They must be mapped as they are arriving. In the VONE off-line or static problem, all the requirements are known in advance.
2. Types of optical infrastructure networks: Depending on the technology in the substrate nodes, we can classify the networks using two points of view: a) SLR/MLR/Elastic networks, and b) Transparent/ Opaque networks.

Single Line Rate (SLR), Multi Line Rate (MLR) and Elastic optical networks. In conventional Wavelength Division Multiplexing (WDM), the fiber bandwidth is divided in sub-carriers of 50 or 100 GHz. There is just one type of transponder, with transmission rate of 10, 40 or 100 Gbps in each sub-carrier. This kind of network are also named Single-Line-Rate (SLR) optical networks. Mixed-Line-Rate (MLR) optical networks provide an extra degree of flexibility for bandwidth provision, allowing different kinds of transponders in the same optical network. Different modulation technologies are also coexisting, appearing undesired effects of some modulation format over each other in contiguous transponders, named non-linear Physical Layer Impairments (PLI). Recently, the development of optical orthogonal frequency division multiplexing (OOFDM) as a viable modulation for optical transmission [10] permits fiber bandwidth to be divided into slots with a finer granularity, with frequency slots (FS) of a few GHz. OOFDM variable-bandwidth transponders can use more than one spectrally contiguous FS if needed, to allocate efficiently the traffic on the fiber. Such optical networks have therefore been called Elastic optical networks or Flexible-grid optical networks [11].

Transparent vs Opaque Networks. In Transparent networks there are no all-optical or optical-electrical-optical (O/E/O) spectrum converters in the substrate network. All connections in a individual VON must be

using the same spectrum, and the Wavelength Continuity Restriction (WCR) must be applied in all the VON. In opaque networks, only applies the WCR to each virtual optical link (different links in the same VON can be using different spectrum).

3. Metrics: The most used metrics to evaluate the quality of an embedding simulation in VONE approaches are blocking ratio and Number of used links or number of used wavelengths. In the on-line version, blocking ratio evaluates the relation between the blocked or rejected requests (which could not be mapped) with the accepted requests. In the off-line version of the problem, its analogue is the Number of installed networks. These metrics have a strong relation with the capacity of the algorithm to find the most load balanced solution. On the other hand, number of used links or number of used wavelengths evaluates the capacity to find the solution with least cost of network resources.

It is very important to note that in most papers only one metric is used. In the literature it have been proposed several possible parameters[8], considering the various aspects to evaluate in the performance of a single VNE approach.

4. Node mapping: Many proposed schemes leads only with the virtual link mapping, considering the virtual nodes already mapped, using geographical restrictions. Only a few works lead with virtual node and link mapping, most of them taking into account a CPU capacity of data centers attached to substrate nodes, which have to be shared with the VON. [30,31] make an one-to-one virtual node mapping, i.e. only one virtual node is allowed to be mapped on a substrate node.

Taking this into account, in Figure 2 we present a list of VONE approaches, with their most important contribution and features.

3. RELATED RESEARCH AREAS TO VONE PROBLEM

VN Reconfiguration. In the on-line scenario of VNE problem, the requests are mapped in the infrastructure network as they arrive, and must be retired when their life time expires. This process causes that the mapping of currently mapped VN stayed non-optimal. This situation can increase the blocking probability of incoming requests. Therefore, the Virtual Network Reconfiguration problem (VNR) leads on re-allocating or migrating virtual

resources (nodes and links) to improve the resource utilization of the infrastructure network. The VNR problem can be classified as proactive when it is realized in order to avoid future rejections, and as reactive, when the VNE strategy rejects a VN request.

The VNR has not been much studied yet. Only a few works can be found in the literature. In [32] the authors propose path migration but not node migration, to improve the utilization of bandwidth assigned to virtual networks. [33] presents a reactive approach with an ILP formulation and a heuristic, taking into account the cost incurred by the disrupted services. For optical network environments, in our best knowledge only the work in [34] presents an optical VNR approach, which is a reactive process that attempts and tries to migrate a subset of VN nodes to relieve congestion on overloaded optical substrate links.

Survivable VNE. The Survivable Virtual Network Embedding (SVNE) problem assigns resources to virtual network requirements, in presence of arbitrary node and link failures. The survivability of optical networks has been extensively studied [35,36]. In virtual networks environments, the scheme must guarantee the survivability of all virtual nodes and links, and not only the connectivity of nodes as other type of environments.

The approaches differs mainly in the type of failure (multiple/single failure of links/nodes), and whether backup resources are reserved in advance or not (restoration/protection schemes). Several works on SVNE are applicable to optical networks, or are specific for this technology. [37] defines content connectivity and provides an ILP formulation to maintain content connectivity in optical networks. Rahman and Boutaba in [38] present a formulation of the SVNE problem and propose a heuristic to solve single substrate link failures in VNE. [39] analyses adaptive virtual optical networks planning considering requirements such as service resilience. Finally, Meixner et al in [40] presents a study of the disaster-resilient and post-disaster-survivable VN mapping problem using a probabilistic model to reduce the expected VN disconnections.

4. CONCLUSION

This paper presented a survey of current works on Virtual Optical Network Embedding (VONE) problem, which leads on optimizing the mapping process of multiple virtual optical networks on one substrate optical network. Important aspects of this problem were discussed and taken into account

to propose a classification of the VONE problem (online/offline problem, SLR/MLR/elastic transparent/opaque substrate network, metrics used to evaluate the efficiency of the approach, whether node mapping is considered or not). We also discuss some research areas strongly related to VONE problem, as Virtual Network Reconfiguration (VNR) and Survivability of VNE.

It is to be noted that only a few works optimizes both node mapping and link mapping. In node mapping it is necessary to clearly define the resources to share with virtual nodes. Some works define the switching capabilities, while others focus on CPU capabilities of attached data centers to substrate networks. It would be interesting to increase the range of metrics used to evaluate the efficiency of the proposed solution. Almost every work propose the blocking rate or number of mapped networks as unique parameter. Other possible metrics could be the revenue/cost ratio, the utilization of network resources or the total length of virtual links. The process or Virtual Network Reconfiguration has not been much studied yet and it would be a good opportunity to future works.

References

- [1] S. Jeong and H. Otsuki, Framework of Network Virtualization, 2009, FG-FN OD-17
- [2] Anjing Wang; Iyer, M.; Dutta, R.; Rouskas, G.N.; Baldine, I., Network Virtualization: Technologies, Perspectives, and Frontiers, Light-wave Technology, Journal of , vol.31, no.4, pp.523,537, Feb.15, 2013
- [3] A. Bavier, N. Feamster, M. Huang, L. Peterson, and J. Rexford, In VINI veritas: Realistic and controlled network experimentation, in Proc. ACM SIGCOMM Computer Commun. Rev., Pisa, Italy, Oct.2006
- [4] D. Schwerdel, D. Hock, D. Gnther, B. Reuther, P. Mller, and P. Tran-Gia, ToMaToA network experimentation tool, in Proc. 7th Int. ICST Conf. Testbeds Research Infrastructures for the Development of Networks and Communities (TridentCom 2011), Shanghai, China, Apr. 2011.
- [5] N. Feamster, L. Gao, and J. Rexford, How to lease the internet in your spare time, Computer Communication Review, vol. 37, no. 1,2007.

Reference	Type of Network	online / offline	Node Mapping	Optimization	Performance Metrics	Contribution
[13] Wei, Wan,Hu, Wang (2009)	SLR/Opaque	offline	Yes	Heuristic/ILP	blocking ratio	Considers a physical node defined by its packet-forward rate and ROADM capability. Includes traffic grooming.
[14] Peng, Nejabati, Azodolmolky, Escalona, Simeonidou (2011)	SLR/Opaque	online	No	Heuristic	blocking ratio	Presents a 3-layer reference model for an PLI-aware IaaS
[15] Zhang, Shi, Vadrevu, Mukherjee (2011)	SLR/Opaque	offline	Yes	MILP, Heuristic	Number of used links / Installed VON	Each node attached to a Datacenter with a CPU capacity. Includes path splitting and traffic grooming.
[16] Abedifar, Eshghi (2012)	SLR/ Transparent	online	No	RWA algorithm	blocking ratio	Adapts a RWA algorithm for link mapping. Tries to minimize the number of used wavelengths in each optical link.
[17] De Leenher, Buysse, Devellder, Mukherjee (2012)	SLR/Opaque	offline	Yes	ILP, 2 heuristics	Number of wavelengths	Proposes clusters with groups of VON requests. In each cluster there is no isolation among the VON. Based on GMPLS. Part of GEYSERS project.
[18] Pages et al (2012)	SLR- Elastic/ Opaque	offline	No	ILP	Number of installed VON	Two approaches: Fixed-VONA (SLR) and Flex-VONA(elastic).
[19] Peng et al (2012)	SLR/ Opaque	online	No	ILP / K-shortest path	blocking ratio	Proposes quality check of mapping considering PLI. If a ILP solution dont pass, it applies K shortest paths.
[20] Peng et al (2012)	SLR/ Elastic	online	No	MILP / Heuristics	blocking ratio	Extension of previous work
[21] Pages, Perelló, Spadaro (2012)	SLR / Elastic	offline	Yes	ILP based Heuristic	Optical and IT resources usage	Planning of IT resources (distributed datacenters) with network virtualization.
[22] Pages, Perelló,Spadaro, Junyent (2012)	SLR / Transparent - Opaque	offline	No	ILP, GRASP	Number of installed VON	Use of GRASP meta-heuristic. Presents a comparison between run times of ILP, GRASP and k-shortest path
[23] Pages, Perello, Spadaro (2012)	SLR/ opaque	online	No	ILP	blocking ratio	Extension of previous work
[24] Peng, Nejabati, Escalona, Simeonidou (2012)	MLR / Transparent	online	No	K-shortest path	blocking ratio	Presents 3 objectives on composition: Cost-aware, Resource-aware and Impairment-aware
[25] Peng et al (2012)	SLR - MLR / Opaque	online	No	Heuristic	blocking ratio	Extension of previous work. Analices non-linear PLI
[26] Abedifar, Eshghi, Mirjalili, Mirjalili (2013)	MLR / Opaque	offline	No	PSO Meta heuristic	Cost functions	Use of PSO meta-heuristic
[27] Zhang, Shi, Vadrevu, Mukherjee (2013)	SLR-Elastic / Opaque	offline	Yes	MILP, Heuristic	Number of used links / Installed VON	Extension of previous work. Each node attached to a Datacenter with a CPU capacity. Includes path splitting and traffic grooming.
[28] Zhang, Xie, Wang, Palacharla, Sekiya (2013)	SLR / Transparent	offline	Yes	Heuristic	Max. wavelength index / load balance	Node mapping by a algorithm based on geo restrictions. In a individual request, two objectives: Minimize spans and inmie number of used wavelengths
[29] Gao and Jue (2013)	SLR / Transparent - Opaque	online	Yes	Heuristic	blocking ratio	Each node can be "transparent" or "Translucent". Considers number of transponders local add-drop and regenerators and switches.
[30] Gong, Zhao, Wen, Zhu. (2013)	Elastic / Transparent	online	Yes	Heuristic	blocking ratio	Node mapping "one-to-one", only one virtual node can be mapped on each physical node. First work on Elastic networks with node and link mapping
[31] Gong, Zhu. (2014)	Elastic / Transparent - Opaque	online	Yes	ILP / heuristics	blocking ratio and average length of longest lightpath	Proposes ILP and Heuristics for both transparent and opaque optical networks.

Figure 2: Virtual Optical Network Embedding Approaches

- [6] N. McKeown, T. Anderson, H. Balakrishnan, G. Parulkar, L. Peterson, J. Rexford, S. Shenker, and J. Turner, OpenFlow: Enabling innovation in campus networks, in Proc. SIGCOMM Computer Commun. Rev., Mar. 2008, vol. 38, pp. 6974
- [7] A. Tzanakaki, M. Anastasopoulos, K. Georgakilas, J. Buysse, M. D. Leenheer, C. Develder, S. Peng, R. Nejabati, E. Escalona, D. Simeonidou, N. Ciulli, G. Landi, M. Brogle, E. Lopez, J. F. Riera, J. A. Garcia-espin, P. Donadio, G. Parladori, and J. Jimnez, Energy Efficiency in integrated IT and Optical Network Infrastructures : The GEYSERS approach, in INFOCOM 2011 Workshop on Green Communications and Networking, April 2011, pp. 343348.
- [8] Fischer, Andreas, et al. Virtual network embedding: A survey. IEEE Communications Surveys and Tutorials (2013): 1-19.
- [9] N. M. M. K. Chowdhury, Network virtualization: State of the art and research challenges, IEEE Commun. Mag., vol. 47, no. 7, pp. 2026, Jul. 2009.
- [10] I. B. Djordjevic and B. Vasic, Orthogonal frequency division multiplexing for high-speed optical transmission, Optics Express, vol. 14, no. 9, pp. 37673775, 2006
- [11] O. Gerstel, M. Jinno, A. Lord, and B. Yoo, Elastic optical networking: A new dawn for the optical layer? IEEE Commun. Mag., vol. 50, no. 2, pp.S12S20, Feb. 2012.
- [12] Nejabati, R.; Escalona, E.; Shuping Peng; Simeonidou, D., Optical network virtualization, Optical Network Design and Modeling (ONDM), 2011 15th International Conference on , vol., no., pp.1,5, 8-10 Feb. 2011
- [13] Wei Wei; Chonggang Wang; Junqiang Hu; Ting Wang, Slice provisioning in a virtualized optical substrate network with programmable routers and ROADMs, Optical Fiber Communication - includes post deadline papers, 2009. OFC 2009. Conference on , vol., no., pp.1,3, 22-26 March 2009
- [14] Shuping Peng; Nejabati, R.; Azodolmolky, S.; Escalona, E.; Simeonidou, D., An impairment-aware virtual optical network composition mechanism for future Internet, Optical Communication (ECOC), 2011 37th

European Conference and Exhibition on , vol., no., pp.1,3, 18-22 Sept. 2011

- [15] S. Zhang, L. Shi, C. Vadrevu, B. Mukherjee, Network virtualization over WDM networks, in: Proceedings of the IEEE 5th International Conference on Advanced Networks and Telecommunication Systems (ANTS), 2011.
- [16] Abedifar, V.; Eshghi, M., A novel routing and wavelength assignment in virtual network mapping based on the minimum path algorithm, Ubiquitous and Future Networks (ICUFN), 2012 Fourth International Conference on , vol., no., pp.204,208, 4-6 July 2012
- [17] De Leenheer, M.; Buysse, J.; Develder, C.; Mukherjee, B., Isolation and resource efficiency of virtual optical networks, Computing, Networking and Communications (ICNC), 2012 International Conference on , vol., no., pp.840,844, Jan. 30 2012-Feb. 2 2012
- [18] Pages, A.; Perello, J.; Spadaro, S.; Garcia-Espin, J.A.; Riera, J.F.; Figuerola, S., Optimal allocation of virtual optical networks for the future internet, Optical Network Design and Modeling (ONDM), 2012 16th International Conference on , vol., no., pp.1,6, 17-20 April 2012
- [19] Shuping Peng; Nejabati, R.; Escalona, E.; Simeonidou, D.; Tzanakaki, A.; Anastasopoulos, M.; Georgakilas, K., Optimized PLL-aware virtual optical network composition, Transparent Optical Networks (ICTON), 2012 14th International Conference on , vol., no., pp.1,4, 2-5 July 2012
- [20] Shuping Peng; Nejabati, R.; Escalona, E.; Simeonidou, D.; Anastasopoulos, M.; Georgakilas, K.; Tzanakaki, A.; Vernitski, A., Performance modelling and analysis of dynamic virtual optical network composition, Optical Network Design and Modeling (ONDM), 2012 16th International Conference on , vol., no., pp.1,5, 17-20 April 2012
- [21] Pages, A.; Perello, J.; Spadaro, S., Planning of optical and IT resources for efficient virtual infrastructure embedding, Photonics in Switching (PS), 2012 International Conference on , vol., no., pp.1,3, 11-14 Sept. 2012

- [22] Pages, A.; Perello, J.; Spadaro, S.; Junyent, G., Strategies for Virtual Optical Network Allocation, *Communications Letters, IEEE* , vol.16, no.2, pp.268,271, February 2012
- [23] Pages, A.; Perello, J.; Spadaro, S., Virtual network embedding in optical infrastructures, *Transparent Optical Networks (ICTON)*, 2012 14th International Conference on , vol., no., pp.1,4, 2-5 July 2012 doi: 10.1109/ICTON.2012.6253704
- [24] S. Peng, R. Nejabati, E. Escalona, and D. Simeonidou, Virtual Optical Network Composition over Mixed-Line-Rate and Multiple-Modulation-Format WDM Networks, in *European Conference and Exhibition on Optical Communication, OSA Technical Digest (online) (Optical Society of America, 2012)*, paper Tu.4.D.2.
- [25] S. Peng, R. Nejabati, S. Azodolmolky, E. Escalona, and D. Simeonidou, Virtual Optical Network Composition over Single-Line-Rate and Mixed-Line-Rate WDM Optical Networks, in *Optical Fiber Communication Conference, OSA Technical Digest (Optical Society of America, 2012)*, paper OW1A.2.
- [26] Abedifar, V.; Eshghi, M.; Mirjalili, S.; Mirjalili, S.M., An optimized virtual network mapping using PSO in cloud computing, *Electrical Engineering (ICEE)*, 2013 21st Iranian Conference on , vol., no., pp.1,6, 14-16 May 2013
- [27] Shuqiang Zhang, Lei Shi, Chaitanya Vadrevu, Biswanath Mukherjee. Network virtualization over WDM and flexible-grid optical networks, *Optical Switching and Networking*, vol. 10, issue 4, pp. 291-300. November 2013
- [28] Qiong Zhang; Weisheng Xie; Qingya She; Xi Wang; Palacharla, P.; Sekiya, M., RWA for network virtualization in optical WDM networks, *Optical Fiber Communication Conference and Exposition and the National Fiber Optic Engineers Conference (OFC/NFOEC)*, 2013 , vol., no., pp.1,3, 17-21 March 2013
- [29] Chengyi Gao; Jue, J.P., Virtual optical network embedding considering mixed transparent and translucent virtual links, *Optical Fiber Communication Conference and Exposition and the National Fiber Optic*

Engineers Conference (OFC/NFOEC), 2013 , vol., no., pp.1,3, 17-21 March 2013

- [30] Long Gong; Wenwen Zhao; Yonggang Wen; Zuqing Zhu, Dynamic transparent virtual network embedding over elastic optical infrastructures, Communications (ICC), 2013 IEEE International Conference on , vol., no., pp.3466,3470, 9-13 June 2013
- [31] Long Gong; Zuqing Zhu, Virtual Optical Network Embedding (VONE) Over Elastic Optical Networks, Lightwave Technology, Journal of , vol.32, no.3, pp.450,460, Feb.1, 2014.
- [32] Yu, Yi, Rexford, and Chiang. Rethinking virtual network embedding: substrate support path splitting and migration, ACM SIGCOMM Computer Communication Review, vol.38, pp 17-29, March 2008.
- [33] Tran, P.N.; Timm-Giel, A., Reconfiguration of virtual network mapping considering service disruption, Communications (ICC), 2013 IEEE International Conference on , vol., no., pp.3487,3492, 9-13 June 2013
- [34] Gu, F.; Peng, M.; Khan, S.; Rayes, A.; Ghani, N., Virtual network re-configuration in optical substrate networks, Optical Fiber Communication Conference and Exposition and the National Fiber Optic Engineers Conference (OFC/NFOEC), 2013 , vol., no., pp.1,3, 17-21 March 2013
- [35] Ramamurthy, S.; Sahasrabudde, L.; Mukherjee, B., Survivable WDM mesh networks, Lightwave Technology, Journal of , vol.21, no.4, pp.870,883, April 2003
- [36] Saradhi, C.V.; Gurusarny, M.; Luying Zhou, Differentiated QoS for survivable WDM optical networks, Communications Magazine, IEEE , vol.42, no.5, pp.S8,14, May 2004
- [37] Habib, M.F.; Tornatore, M.; Mukherjee, B., Fault-tolerant virtual network mapping to provide Content Connectivity in optical networks, Optical Fiber Communication Conference and Exposition and the National Fiber Optic Engineers Conference (OFC/NFOEC), 2013 , vol., no., pp.1,3, 17-21 March 2013
- [38] Rahman, M.R.; Boutaba, R., SVNE: Survivable Virtual Network Embedding Algorithms for Network Virtualization, Network and Service

Management, IEEE Transactions on , vol.10, no.2, pp.105,118, June 2013

- [39] Tzanakaki, A.; Anastasopoulos, M.; Georgakilas, K., Dynamic adaptive virtual optical networks, Optical Fiber Communication Conference and Exposition and the National Fiber Optic Engineers Conference (OFC/NFOEC), 2013 , vol., no., pp.1,3, 17-21 March 2013
- [40] Meixner, C.C.; Dikbiyik, F.; Tornatore, M.; Chuah, C.; Mukherjee, B., "Disaster-resilient virtual-network mapping and adaptation in optical networks," Optical Network Design and Modeling (ONDM), 2013 17th International Conference on , vol., no., pp.107,112, 16-19 April 2013

Databases integration in grid computing applications

Paulo R. S. Ruiz ^{a1}, Haroldo F. de Campos Velho ^b, Renata S. R. Ruiz ^c and
Elton O. Ferreira ^d

^aState Technical School of São José dos Campos, SP, Brazil

^b ^cNational Institute for Space Research, São José dos Campos, SP, Brazil

^d Faculty of Technology of São José dos Campos, SP, Brazil

Abstract

Scientific applications increasingly generate an large volume of data. For this reason, are necessary new methods for manipulate these data. This work proposes the use of the integration of database by grid computing applications. Taking as example the LAG-Clima project was developed an integration of their data for facilities the distribution between the nodes of the grid.

Keywords: Databases, Web applications, Climatology, Data Science.

1. INTRODUCTION

Nowadays, a new source for understanding has emerged for the science development based on data-intensive computing, sometimes called the Fourth Paradigm [8]. Tremendous amounts of information are gathered thanks to sophisticated technologies for the observation system and computers. In this context, the technology of grid computing provides mechanisms to share and coordinate the use of several computational resources in different institutions distributed geographically, in order to create a single virtual computer capable of achieving high processing rate and storage capability [5].

Meteorological and climate studies are examples of the use of sophisticated computational tools. These have obtained considerable notoriety in recent years due to the interference of weather and climate on human activities. On the other hand, this means a huge amount of data to be stored and analysed. Today, the meteorological community has access to a giant quantity of observational data from different sources (weather stations, satellites, spacecraft, weather balloons, etc.), as well as a set of models used to generate simulated data and/or systems interpolated, employing the high performance

¹E-mail Corresponding Author: prsilvaruiz@gmail.com

computing. Therefore, there is an intense demand on data storage, with necessity of computational tools for analysis [9].

The demand for data storage is growing not only in science, but also for commercial applications. The database technology together with web applications offers to the users the possibility to store their data, allowing full manipulation, i.e., insertion, delete, update, and query of the data. Due a series of facilities, such technologies are used in meteorological and climatological applications to provide important services such as weather and climate forecast [6][11].

The goal of this work is to develop the database and the web application for the Latin American Grid for Climatology Project (LAG-Clima). The activities developed in the context are related to grid computing, for establishing a collaborative infrastructure to process and store data using computing resources for geographically distributed institutions. The research team consists of researchers, experts, and collaborators from several institutions: Servicio Meteorológico Nacional (Argentina), Group of Parallel and Distributed Processing (Informatics Institute, UFRGS), Associate Laboratory for Computing and Applied Mathematics (LAC-INPE, Brazil), Faculty of Mathematics (National University of Trujillo, Peru), Unidad de Ciencias de la Atmósfera (Universidad de la República), Dirección Nacional de Meteorología (Uruguay) and Grenoble Informatics Laboratory (LIG, France) [2].

In the LAG-Clima project, the processing is distributed among institutions, with local data storage systems. Such strategy becomes difficult sharing data among the researchers, including to spread the information for the society. Therefore, it is important to use Information Technology Resources, such as Management Systems Database and web applications, to promote the dissemination of data. This is the paper focus: a contribution for developing tools for storage and exchange data on a grid computing environment [15].

2 METHODOLOGY

The database integration is the process where several databases are transformed into only one database. which the input is a set of databases and output is a single integrated scheme [14]. For this purpose, we have used advanced database technology and web tools.

The beginnings of the database technology coming from the 70s, starting with the first file systems [16]. Such technology was to maintain digital

records allowing storage of a large volume of data. But the safe handling and administration of a database requires a set of programs able to offer this possibility to its management and especially to its users. This role is played by the Database Management System (DBMS), it is a software to become easier the tasks of definition, construction, and manipulation of databases. These systems have the ability to ensure data protection against malfunctions or failures in hardware or software, and manages the security against unauthorized access [4].

In this work, an object-relational System Manager was used: the PostgreSQL. This database environment pioneered many concepts, and such features were incorporated in commercial DBMS. The PostgreSQL is a free software, and it can be used, modified, and distributed by anyone for any purpose, from business to science. One advantage of the PostgreSQL, among others, is the full compatibility with the SQL standard [12].

The database developed follows a relational model. The model represents the data in a natural way, i.e, eliminating auxiliary structures for the database storage task. The data representation in the relational model consider data as a relation, i.e, an arrange organized into table with rows and columns, associating attributes [7].

For developing a database, it is necessary to model its structure from the data. Three steps should be observed: Conceptual Model, Logic Model and Physical model. The latter step is the actual implementation of the database, creating the entities and their attributes in DBMS adopted [13].

The task of the web application is providing access to database using a browser. Several strategies can be applied: object-oriented requirements analysis should model the real-world entities by means of object and classes. The Unified Modeling Language (UML) is a method of object-oriented design. The UML can be used for visualizing, specifying, constructing, and documenting the applications [1]. Technologies used in this step can include: Java programming language by its wide use in web applications [10]; Java Database Connectivity (JDBC) for object relational mapping [3].

3 DEVELOPMENT

The LAGClima has a grid infrastructure for climate prediction and exchange data, and they are scattered on various institutions. A database

integration is proposed into a single centralized database, where information can be accessed to users through a web application.

Firstly, a modeling of data characteristics is required. The data are classified into three types:

1) *Observational data*: are groupings of data acquisition from sensors in meteorological stations, for a 10 years period (1991-2000). A monthly average is calculated for different weather variable (pressure, temperature, precipitation, etc).

2) *Simulated and interpolated data*: Data are obtained from computer processing.

From the knowledge of the characteristics from the project data, the integrated database was modeled. The data are divided into three classes, as already mentioned: observational, interpolated, and simulated. Each class embraces weather variables: precipitation, temperature, wind, radiation, among others. Each data is associated with a period, a location, and region (geographic coordinates). The data must be considered an entity with relationships with the other entities: period, local (station and coordinates), and class. Therefore, the database will be able to store any type of weather data, and hence allow queries by location, region, or period.

A web application was developed to allow the access the central database. This feature allows all institutions has access to the integrated database. This tool allows the user to search the data by class, region, local (weather station), or time period. The selected data becomes available for download: a file to be transfered to the user computer. The queries are formulated by graphical interfaces on the browser, where parameters are collected for searching.

The use of data integration through database and web application allows the full access to the data in the integrated database. Figure 1 partially shows the web application. Figure 1a displays the Query menu, showing different types of data. Figure 1b shows the results of the search: by period and region.

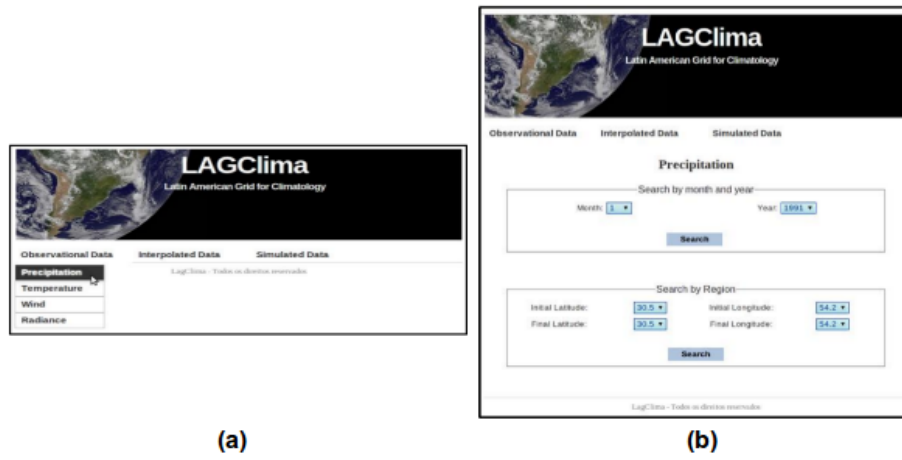


Figure 1 - Database on LAG-Clima web-site. a) Choose the type of data. b) Query result of precipitation.

4. CONCLUSIONS

The integration of databases for climate purposes was carried out. The use of relational database and consistent management systems allow efficiently track the data for the LAG-Clima project. The internet and web applications are easy way to access the project data for different users and institutions. The database integration on the grid environment provides integrity, security, and availability of data to users. Therefore, the results reported are very encouraging for the application of the mentioned technologies on grid computing applications, as reported for the LAG-Clima project.

ACKNOWLEDGMENTS: The authors like to thank the LAGClima project.

References

- [1] Booch, G, Rumbaugh, J, Jacobson, I, 2005. UML: guia do usuário. 2.ed. Rio de Janeiro: Elsevier.

- [2] Campos Velho, HF, Ruiz, RSR, Furtado, HCM, Almeida, ES, Petry, A, Navaux, POA, Maillard, N, Berri, G, Bidegain, M, Rubio, O, Richard, O, Souto, RP, 2013. Grid computing for climate processing on South America. *Ciência e Natura*, Ed. Special, p. 207-210.
- [3] Cattell, R, Hamilton, G, 1997. Jdbc database access with Java: a tutorial annotated reference. Addison-Wesley Publishing Company.
- [4] Elmasri, R, Navathe, SB, 2000. *Fundamentals of Database Systems*. 3a. Ed. USA: Addison-Wesley.
- [5] Foster, I, Kesselman, C, 2004. *The grid: Blueprint for a new computing infrastructure*, 2 ed. San Francisco, USA: Morgan Kaufmann.
- [6] Fritzsos, E, Carpanezzi, AA, Mantovani, LE, 2008. *Elaboração de um banco de dados climático para o Estado do Paraná*. Colombo: Embrapa Florestas.
- [7] Heuser, CA, 2001. *Projeto de banco de dados*. 4a Edição. Ed. Sagra.
- [8] Hey, T, Tansley, S, Tenekes, KT, Lumley, J, 2009. *The fourth paradigm: data-intensive scientific discovery*. Redmond: Microsoft Research.
- [9] Garcia, JRM, Carvalho, LSM, Camargo Jnior, H, Sanches, MB, 2006. BDC - Banco de Dados Climatológico. In: CONGRESSO BRASILEIRO DE METEOROLOGIA, 14. (CBMET), Florianópolis, SC. Proceedings... 2006. (INPE-14307-PRE/9395). <http://www.sbmet.org.br/congresso/port/index.html>. Acesso em: 30 set. 2012.
- [10] Ken, A, Gosling, J, Holmes, D, 2006. *The Java programming language*. Addison-Wesley Publishing Company.
- [11] Kozevitch, NP, 2005. *Dados meteorológicos: Um estudo de viabilidade utilizando um SGBD em plataforma de baixo custo*. Dissertação de mestrado, Curitiba-PR.
- [12] Momjian, B, 2001. *PostgreSQL: introduction and concepts*. Vol. 192. Addison-Wesley.
- [13] Navathe, SB, 1992. Evolution of data modeling for databases. *Communications of the ACM*,35(9):112-123.

- [14] Ozsú, MT, Valdúries, P, 1999. Principles of distributed database systems. 2nd edition. Ed. Englewood Cliffs: Prentice-Hall.
- [15] RUIZ, PRS, 2013. Integration of databases climatological geographically dispersed. Undergraduation report, FATEC, São José dos Campos (SP), Brazil.
- [16] Silberschatz, A, KORTH, HF, SUDARSHAN, S, 1999 Sistema de banco de dados. 3a edition. So Paulo: Makron Books.

Entrepreneurial Ecosystem: An Entrepreneurial Thematic Geoportal and Data Warehouse

Esther Hochsztain ^{a 1}, Andr maca Tasistro ^b, Mar a Messina ^a

^aFacultad de Ciencias Econ micas y de Administraci n. Universidad de la Rep blica. Uruguay

^bAGESIC Agencia de Gobierno Electr nico y Sociedad de la Informaci n. Uruguay

Abstract

Very few entrepreneurs can succeed with little outside assistance. Mostly, only a proactive perspective towards entrepreneurship is able to expand the number of businesses that start up and expand. Certainly this is a big job and many actors have to face this at one time or another. As a consequence, entrepreneurship needs a good information system. Usually a regional entrepreneurship network provides support in many ways to a set of entrepreneurs and organizations. On the other hand, most entrepreneurship projects refer to identify needs and meet them in a specific spatial context. Therefore it is necessary to link entrepreneurial with the availability of spatial data. An entrepreneurial ecosystem is proposed in this paper, composed of a thematic geoportal and a data warehouse. Also, an according framework, the flow diagram and a case study containing two fact tables are presented.

Keywords: entrepreneurship, entrepreneurial ecosystem, geoportal, spatial data infrastructure, data warehouse

1 INTRODUCTION

An entrepreneur is an individual who sees an unfulfilled opportunity and uses it to create new economic value. Nevertheless, networks and different kind of organizations are required to support entrepreneurs, such as regional entrepreneurship networks.

By the other way, spatial data infrastructure is considered as a response of society on the growing demand for spatial information, associated to the increasing relevancy of spatial information for every days functioning of states, business and citizens. As a solution, a geoportal is used for searching, visualizing, and downloading spatial data and services. Particularly, thematic geoportals are map viewers with information on a specific theme from different providers. Thus, as a global entrepreneurial ecosystem is emerging, why not think in an entrepreneurship geoportal?

In this paper we combine spatial data with business intelligence in an entrepreneurial ecosystem composed by an entrepreneurial thematic geoportal and a data warehouse.

This paper is organized as follows. First, in Section 2 a synthesis of the state of the art in entrepreneurship and spatial data infrastructures is presented.

¹E-mail Corresponding Author: esther@ccee.edu.uy

In Section 3 we introduce the entrepreneurial ecosystem proposal, followed in Section 4 by a case study. Finally, in Section 5 conclusions and future works are presented.

2 RELATED WORKS

A brief outline of the principal issues considered in the literature is presented in this section. First, entrepreneurship basic concepts are presented, followed by spatial data infrastructure, next by entrepreneurship & spatial data infrastructure and finally entrepreneurial value chain.

2.1 ENTREPRENEURSHIP

An entrepreneur is an individual who sees an unfulfilled opportunity and uses it to create new economic value. Entrepreneurship is considered as a booster for the economic growth through the diffusion of innovations and a solution to face unemployment. In the two cases (innovation and creation of one's own job), entrepreneurship refers to risk taking [16], and four pillars support entrepreneurship: entrepreneur's resource potential, market characteristics, economic organization features and public policies to create and develop business.

Very few entrepreneurs can succeed with little outside assistance. Mostly, only a proactive perspective towards entrepreneurship is able to enlarge the number of businesses that start up and expand. Certainly this is a big job and many actors have to play a part. As a consequence, entrepreneurship requires a well thought out system of support. It is well known that many people dream of becoming entrepreneurs, but seldom use or know how to access the resources needed to be able to succeed. Appropriate networks creation is therefore critical to support entrepreneurs.

A Regional Entrepreneurship Network is a set of entrepreneurs, organizations, and residents working together to make sure that entrepreneurs get the support they need to start up and flourish. A Regional Entrepreneurship System includes: a coordinated system of easily accessible technical assistance and training, local communities that value entrepreneurs and link them to appropriate services, access to appropriate capital, the formation of clusters that provide sector-specific assistance, and a process for gathering information about gaps in the system and developing policy and new services to address those gaps [9].

Most entrepreneurship projects refer to identify needs and meet them in a specific spatial context. Therefore it is necessary to link entrepreneurial with the availability of spatial data.

2.2 SPATIAL DATA INFRASTRUCTURE

Development of Spatial Data Infrastructure (SDI) is considered as a response of society on the growing demand for spatial information, associated to the growing relevancy of spatial information for every days functioning of states, business

and citizens [13]. The growing relevance demands to be able to organize and combine data across different disciplines and organizations. As a consequence Spatial Data Infrastructure refers to a complex, fuzzy an evolving concept.

Spatial Data Infrastructures are considered non-trivial for many reasons: 1) the SDI concept is ambiguous, and its understanding needs cross-disciplinary research, 2) SDIs are multi-faceted and have a reciprocal (dual) relationship with their (societal) context, 3) the development of concrete SDI initiatives has to cope with risk [2] [3].

Spatial data play an important role to recognize and transform nature. Compared with general data, spatial data has features of spatial, timeliness, multidimensional, large amount and complex spatial relationships. While spatial data is described as specific geographic location and spatial distribution of objects in real world, the non-spatial data is all the data except the spatial data [18].

Spatial Data Infrastructure aims to assist the spatial enablement of societies. One of the key characteristics of spatially enabled societies is the availability of spatial information to governments, citizens and businesses as a means of organizing their activities and information [11].

A geoportal is a crucial component of an Spatial Data Infrastructure, used for searching, visualizing, and downloading spatial data and services [15]. In particular, thematic geoportals are map viewers with information on a specific theme from different providers. The aim of the thematic geoportals is facilitating the use of geoinformation for the end user and speed up search.

In order to meet the demands of the modern information society, analyzing the space is a very important issue. Geo referenced thematic data, includes economical, demographical, educational and social conditions data, etc. As a consequence of wide access to data, published by numerous websites, information acquisition is not a problem any more. The real problem is how to transform information in useful knowledge [5].

Usually a user who searches for geographical, statistical information or who intends to spatially locate events does not expect a different form of information gathering other than a map or an atlas. Thus, the cartographic form of transfer meets the users expectations. This is one of the important prerequisites of the product usefulness. Another positive result of accessing maps in websites is related to intuitive maintenance and effectiveness of distribution of spatial information. Due to diversity of data published in geoinformation websites, a map usually plays the role of integrating particular information components. The map is also the basic element of the website composition. Next, the two issues discussed above are linked.

2.3 ENTREPRENEURSHIP & SPATIAL DATA

Discovery of the critical links used by innovation institutions in a regional economic system, is the aim of an analytical tool, as stated in [17]. Tracing interactions and identifying institutions location, conditions for each institution to

stimulate innovation and thus to participate in successful regional innovation strategies are detected. Whether and how innovation institutions at regional levels are helpful in finding combinations of regional and firm attributes to incentive innovations are analyzed. Best combinations of attributes (i.e. new product development, technologies knowledge transfer, promoting research and development) are identified and provide information for decision making about how innovative institutions can act as potential key facilitators or constructors of regional development.

As spatial determinants of entrepreneurship, quality of physical infrastructure and workforce education are the strongest factors with labor laws and household banking access also playing important roles [6]. An extensive evidence shows agglomeration economies among manufacturing industries, in particular, supportive industrial structures for input and output markets strongly linked to higher rates of local entrepreneurship.

The relationship between regional characteristics and individual entrepreneurship must be analyzed with a special focus on individual opportunity perception [14]. Based on insights from multiple disciplines its possible to investigate how regional knowledge creation, economic conditions and an entrepreneurial culture affect individual opportunity perception, which in turn affects individual start-up intentions and activity. Evidence suggests that individual opportunity perception might play an important role in the cascading down process of regional characteristics towards the individual. From a person-focused perspective, results suggest that regional characteristics which are objective may operate as background (or distal) factors in that they affect proximal predictors of entrepreneurial behavior. Objective regional characteristics may drive individual regional opportunity perception, which then drives individual entrepreneurship [14].

Innovation ecosystems have emerged as an important context for entrepreneurship [12]. Ecosystem entrepreneurs, however, face a unique set of challenges associated with the need to balance the goals and priorities set by the ecosystem leader with the goals and priorities of the new venture. In this context, analyzing the value chain in the entrepreneurial field is essential.

2.4 ENTREPRENURIAL VALUE CHAIN

Gaps on the role of operations management across the entrepreneurial value chain can be analyzed in an integrative perspective of the decisions faced by entrepreneurial firms to manage entrepreneurial uncertainty, knowledge, scalability and sustainability [10]. Resources and routines across entrepreneurial value chain is presented in Figure 1.

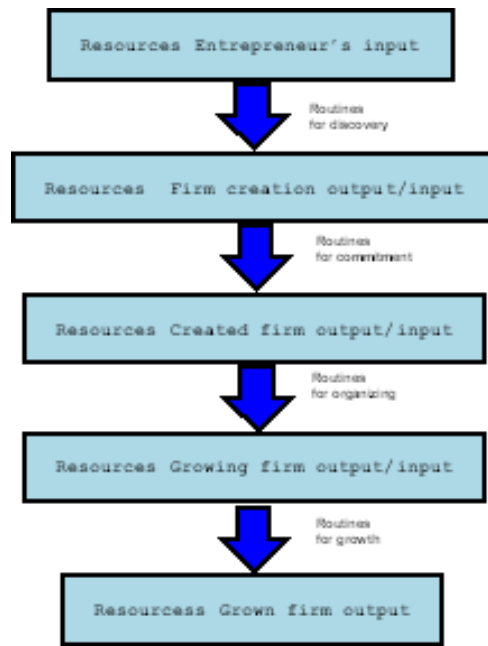


Figure 1 - Evolution of resources and routines across the entrepreneurial value chain. Adapted from [10] .

Entrepreneurial routines and resources are closely linked in a regional scope. As a consequence, an entrepreneurial regional innovation system is needed to enhance individual entrepreneurial efforts. Several regional policies aim to stimulate regional development promoting entrepreneurship. The policies applied and the entrepreneurship underlying concepts, usually differ comprising diverse mechanisms to support and stimulate entrepreneurship. A list of topics and attributes based on the dichotomies urban vs rural and centre vs periphery includes: economic environment, natural environment, social environment, human capital, settlement, accessibility and spatial distance [1].

Analytics and data based managerial solutions are evolving rapidly and being used by almost every organization. Business Intelligence analytics trends are: self service, pervasive, scalable, georeferenced and geospatial applications, clickstream crunching, cloud and respond to urgent issues [4]. The concept of analytics-as-a-service (also referred as Agile Analytics) is turning utility computing into a service model for analytics. New and improved architectures are needed to be able to process very large amount of structured and unstructured data in a very short time to produce accurate and actionable results. Different kind of users can access a virtual slice of the main data warehouse server where they can store and analyze their own data sets. Analytics-as-a-service in cloud generates economies of scale by providing many virtual analytical applications with better scalability and higher cost savings.

Having presented the related work, in the next section an inclusive entrepreneurship and geoportal proposal is presented.

3 ENTREPRENEURIAL ECOSYSTEM

A global entrepreneurial ecosystem is emerging. In this section, we introduce a web-based analytical entrepreneurial information system proposal, conformed by an entrepreneurial thematic geoportal and a data warehouse. Currently, different type of organizations, star-ups, local and government agencies accumulate, update and use large amounts of entrepreneurial spatial data. As a rule data have different formats, which don't allow their effective processing. To solve this fragmented situation, an analytical information system for entrepreneurship data querying is represented in a web-based resource named Entrepreneurial Ecosystem Thematic: GeoPortal and Data Warehouse. This kind of analytical information resource helps to ensure interoperability between different actors in the information exchange and improve the quality services provided to organizations and entrepreneurs.

The global system framework is presented in Figure 2. Requirements and resources are identified and accordingly derived to geoportal or data warehouse, as the most important form of channeling. Based on appropriate resources and requirements, geoportal and data warehouse are designed, according to the critical success factors and success metrics defined. Considering a single system composed of a geoportal and a data warehouse (instead of two separate systems), maps and data warehouse fact-tables must be in consonance.

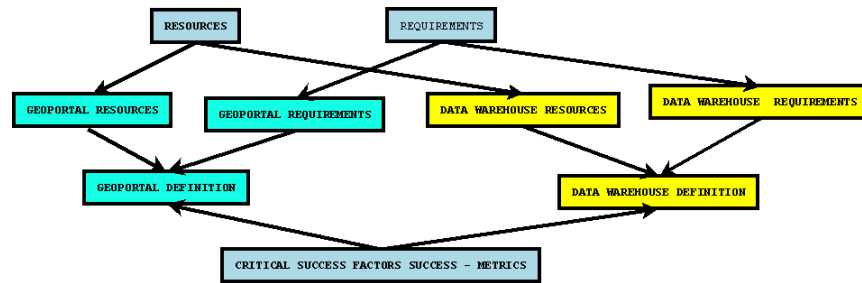


Figure 2 - Entrepreneurial Ecosystem Thematic GeoPortal and Data Warehouse Framework .

Georeferenced entrepreneurship data are visually presented using thematic maps, such as entrepreneurship organizations, entrepreneurship networks, entrepreneurship clusters, entrepreneurship resources (including, inter alia, financial, technical, education and motivation), entrepreneurs and projects registered in one or more entrepreneurship organizations.

A Data Warehouse is considered in two ways, to store and analyze: a) website navigation, and b) different entrepreneurial features.

The term clickstream denotes the path an user takes while visiting a web site. Clickstream data offer a wide range of opportunities for data analytics[7][8]. Two Clickstream Fact Tables are defined: a) Clickstream sessions fact table, and b) Clickstream pages fact table.

OLAP queries related to different entrepreneurial features are developed through Entrepreneurial organizations fact table, Entrepreneurial networks fact table, Entrepreneurship resources fact table, Entrepreneurs fact table, and Entrepreneurial projects fact table.

Figure 3 presents the system Flow Diagram. Data Capture and Preprocessing are common to both (Geoportal and Data Warehouse), ETL (Extraction, Transform and Load) are specific for Geoportal and Data Warehouse. Geoportal and Data Warehouse construction and usage analysis are set forth separately. Finally, an integrated vision is obtained through Clickstream Data Warehousing. Definitely, maps and data warehouse fact-tables must be in consonance.

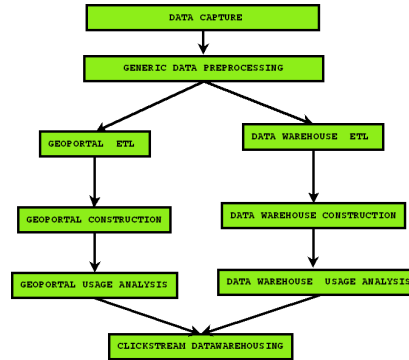


Figure 3 - Entrepreneurial Ecosystem Thematic GeoPortal and Data Warehouse Flow Diagram .

4 CASE STUDY

In this section we present the proposal prototype integrating spatial and operational data in an entrepreneurial ecosystem. As an example of the fact tables created two dimensional schemas are presented. The session data dimensional schema is presented in Figure 4. Entrepreneurship organization and thematic map dimensions are specific to this work. However, the remaining dimensions are the typical dimensions used in web server logs analysis. In the same way, usually considered clickstream facts such as time and number of pages are included.

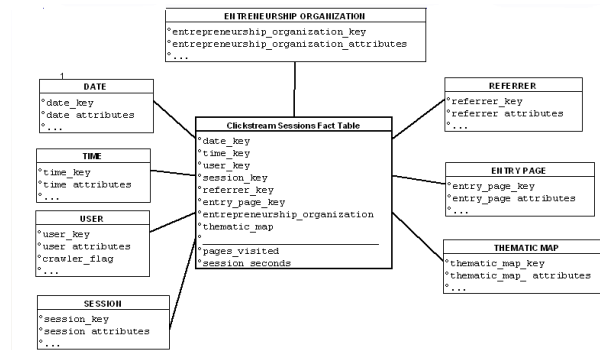


Figure 4 - Clickstream sessions fact table .

Entrepreneurial projects fact table shown in Figure 5, allows OLAP queries of budget (estimated and final) and duration (estimated and final) across date, entrepreneur, project, spatial location, financial support, entrepreneurship organization and main market

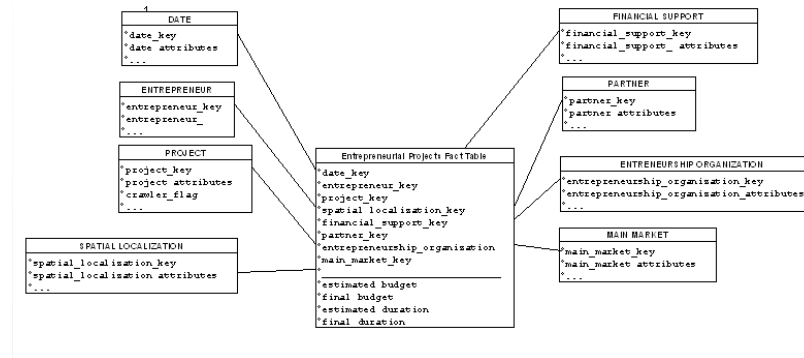


Figure 5 - Entrepreneurial projects fact table shows most required project features. .

For example, with real test data loaded in Entrepreneurial projects fact table, it was found the importance of certain factors in the success of a project.

5 CONCLUSIONS AND FUTURE WORKS

In this paper we presented an entrepreneurial Ecosystem based on an entrepreneurial Thematic Geoportal and Data Warehouse. The solution was initially a proposal adapted to Asociación de Universidades Grupo Montevideo requirements. Nevertheless, it can be easily extended to support entrepreneurs in many other regions and also promote entrepreneurship internationalization. Asociación de Universidades Grupo Montevideo (AUGM) ² is a network of public, autonomous

²<http://grupomontevideo.org>

and self-governing universities in Argentina, Bolivia, Brazil, Chile, Paraguay and Uruguay. Was born in August 1991 in response to university challenges with the aim of working for excellence, quality, relevance and fulfill the tasks required in public higher education.

For many people entrepreneurship is considered as a drug that does not fully satisfy them with a single dose. Many programs promote entrepreneurship, and make easier higher social acceptance and access to risk capital. The problem to be solved in this paper, is how to provide information to organizations to be able to better promote entrepreneurs.

With the prototype it was found that the same project was funded in several countries at the same time or at successive times. We conclude that by using the proposed Entrepreneurial Ecosystem, it will be possible to rationalize investments for these institutions.

In future works Web Usage Mining techniques will be applied to discover patterns in geoportals users navigation and Data Mining techniques will be used to discover patterns in entrepreneurship data.

References

- [1] Baumgartner, Daniel and Pütz, Marco and Seidl, Irmi, 2013. What Kind of Entrepreneurship Drives Regional Development in European Non-core Regions? A Literature Review on Empirical Entrepreneurship Research, *European Planning Studies*, Taylor & Francis, 21, 8,1095–1127 .
- [2] Black, E.D., 2010. Assessing organisational aspects of Sub-national SDIs: The case of the Balearic Islands and Catalonia, Master thesis, Delft. University of Technology. 10–13.
- [3] de Man, W.H. Erik. , 2008 The multi-faceted nature of SDIs and their assessment - dealing with dilemmas in A multi-view framework to assess SDIs, Wageningen University and Centre for SDIs and Land Administration, Crompvoets, Joep and Rajabifard, Abbas and Van Loenen, Bastiaan and Fernández, Tatiana Delgado (Eds) , Department of Geomatics, The University of Melbourne. 25-49.
- [4] Demirkan, Haluk and Delen, Dursun, 2013. Leveraging the capabilities of service-oriented decision support systems: Putting analytics and big data in cloud, *Decision Support Systems*,55, 1, Elsevier, 412–421 .
- [5] Fiedukowicz, Anna and Gasiorowski, Jędrzej and Kowalski, Paweł and Olszewski, Robert and Pillich-Kolipinska, Agata, 2012. The statistical geoportals and the cartographic added value—creation of the spatial knowledge infrastructure, *Geodesy and Cartography*,61,1,47–70.
- [6] Ghani, Ejaz and Kerr, William R and O’connell, Stephen, 2014. Spatial determinants of entrepreneurship in India, *Regional Studies*, Taylor & Francis, 48,6,1071–1089.

- [7] Hochsztain, Esther and López, Carlos and Bernabé, Miguel Angel, 2010 Anlisis de Navegacin de Geoportales, Décimo Congreso Latinoamericano de Sociedades de Estadística (XCLATSE), Argentina.
- [8] Hochsztain, Esther and Millán, Socorro and Pardo, B and Peña, José M and Menasalvas, Ernestina, 2003. A framework to integrate business goals in web usage mining, *Advances in Web Intelligence*, Springer, 28–36.
- [9] Holley, June, 2005. Building a Regional Entrepreneurship Network: A guide to action, Athens, OH: ACEnet Institute Retrieved May 9, 2014 from <http://www.networkweaver.com/wp-content/uploads/2011/12/BuildingREN.pdf> .
- [10] Joglekar, Nitin and Lévesque, Moren, 2013. The role of operations management across the entrepreneurial value chain, *Production and Operations Management*, Wiley Online Library, 22, 6, 1321–1335
- [11] Mohammdi, Hossein and Colebatch, A and Dawson, G and Ballingall, S, 2010. Intelligent Speed Assist: Spatially enabling societies, in *Proceedings of Global Spatial Data Infrastructure (GSDI) World Conference*, Singapore. 235-246.
- [12] Nambisan, S., & Baron, R. A. (2013). Entrepreneurship in Innovation Ecosystems: EntrepreneursSelfRegulatory Processes and Their Implications for New Venture Success. *Entrepreneurship Theory and Practice*, 37(5), 1071-1097.
- [13] Poslončec-Petrić, Vesna and Bačić, Željko, 2013. Interaction in Geosciences Education and Spatial Data Infrastructure development–Example Western Balkans–issues, impact and projects, 13th SGEM GeoConference on Ecology, Economics, Education and Legislation, SGEM2013 Conference Proceedings 608–619.
- [14] Stuetzer, Michael and Obschonka, Martin and Brixy, Udo and Sternberg, Rolf and Cantner, Uwe, 2014. Regional characteristics, opportunity perception and entrepreneurial activities, *Small Business Economics*, Springer, 42,2,221–244.
- [15] Tooamnian, Ara and Harrie, Lars and Mansourian, Ali and Pilesjo, Petter, 2014. Automatic integration of spatial data in viewing services, *Journal of Spatial Information Science*, 6,43-58.
- [16] Uzunidis, Dimitri and Boutillier, Sophie and Laperche, Blandine, 2014. The entrepreneur’s resource potentialand the organic square of entrepreneurship: definition and application to the French case, *Journal of Innovation and Entrepreneurship*, 3,1, Springer, 1–17.
- [17] Vaz, Eric and de Noronha Vaz, Teresa and Galindo, Purificacion Vicente and Nijkamp, Peter, 2014. Modelling innovation support systems for regional development–analysis of cluster structures in innovation in Portugal, *Entrepreneurship & Regional Development*, 26, 1-2 Taylor & Francis, 23–46.

- [18] Wang, Shuliang, 2011. Spatial data mining under Smart Earth. In Proceedings IEEE International Conference on Granular Computing (GrC), 717–722.

Simulation of Quantum Walks using HPC

Pedro C. S. Lara, Aaron Leão, Renato Portugal¹

Laboratório Nacional de Computação Científica
Petrópolis, RJ, 25651-075, Brazil.

Abstract

We describe program HiPerWalk, which is a new simulator of the main quantum walk models using high-performance computing (HPC). The simulator is able to generate the dynamics of discrete-time quantum walks and coinless quantum walks, and will be able simulate continuous-time and Szegedy's quantum walks. It has an user-friendly input and is able to use hybrid HPC architectures, which includes the main ones available nowadays. The simulator outputs the main statistics associated with the probability distribution of the quantum walk in data files and automatically generates plots. The simulator is written in open-source non-proprietary codes and employs freeware languages: Python, Neblina, Gnuplot, and OpenCL.

Keywords: Quantum computing, quantum algorithms, simulation, quantum walks, parallel programming languages.

1. INTRODUCTION

The discrete-time quantum walk model (DTQW) on the line was introduced by Aharonov *et al.* [4] and it was generalized to regular graphs in Ref. [3]. In the DTQW, the particle hops from site to site depending on the value of an internal degree of freedom, which plays the role of the coin. Quantum walks on N -dimensional lattices were studied by many authors [19, 31, 22] and display the key feature of spreading quadratically faster in terms of probability distribution, compared to the classical random walk model on the same underlying structure [5]. The DTQW was successfully applied to develop quantum algorithms, specially for searching a marked node in graphs [29, 8, 25]. There are other models of quantum walks and some of them do not use an auxiliary Hilbert space and have no coin. The

¹E-mail Corresponding Author: portugal@lncc.br

continuous-time quantum walk model introduced by Farhi and Gutman [16] and the coinless quantum walk model introduced by Patel *et al.* [23] are examples of such models. The coinless model can be used to search a marked node on two-dimensional finite lattices with the same number of steps (asymptotically in terms of the system size) compared to the coined model, with the advantage of using a smaller Hilbert space [9]. Going to the opposite direction, Szegedy's quantum walk model [30] uses the largest Hilbert space the dimension of which is the square of the dimension of the coinless model.

In this work, we describe a new high-performance quantum-walk simulator, called HiPerWalk, that can be used to obtain the dynamical evolution of the quantum walk models and can be used to calculate the main statistical distributions associated with the probability distribution. The simulator has three main parts: 1) an user interface built in Python that generate matrices and vectors (propagator and initial condition) based on the input to be used in the core of the program, 2) a core program written in the Neblina language (developed by one of us) which is able to run matrix calculations in heterogeneous HPC architectures, 3) a module that calculates the main statistical distribution and generates data files, output files, and plots. In the present version, only the DTQW and the coinless models were implemented and described.

To the best of our knowledge, this is the only simulator of its kind, except for the QWalk program [21], which simulates only DTQW on one- and two-dimensional lattices. A version of QWalk using HPC was described in Ref. [28].

2. QUANTUM-WALK MODELS

The goal of the new simulator is to generate the dynamics of the main quantum-walk (QW) models known in Literature in a generic graph. In this Section we briefly describe each one of these QW models and point out the main references. There are four models: 1) Discrete-Time Quantum Walk (DTQW), 2) Continuous-Time Quantum Walk (CTQW), 3) Szegedy's Quantum Walk, and 4) Coinless Quantum-Walk.

The Discrete-Time Quantum Walks were the first to be proposed [4] and it was successfully used to solve the problem of quantum spatial search on lattices and hypercubes. Shenvi *et al.* [29] developed a quantum search algorithm for the hypercube with time complexity $O(\sqrt{N})$, where N is the

number of vertices of the graph. This result has a quadratic gain over the corresponding classical algorithm. Ambainis et al. (AKR) [8] used a similar method to develop a quantum search algorithm in two-dimensional lattices in time $O(\sqrt{N} \log N)$ almost quadratically better than the time $O(N \log N)$ of the classical algorithm. Tulsi [32] introduced an extra qubit in the system and improved the complexity of the AKR algorithm. Ambainis et al. (ABNOR) [6] also showed how to eliminate amplitude amplification method used in the AKR algorithm by doing post-processing calculations. Moreover, Refs. [2, 17, 1] describe similar methods to many other graphs generating new efficient quantum algorithms.

The concept of Continuous-Time Quantum Walks were proposed by [15]. One of the first applications was the NAND-tree evaluation in time $O(\sqrt{N})$ developed in Ref [14]. Discrete versions of the latter were presented in [10, 7, 11] requiring time $N^{\frac{1}{2}+O(1)}$. The evaluation of minimax trees using $N^{\frac{1}{2}+O(1)}$ oracle queries was discussed in [12].

Szegedy's quantum walk model is used to obtain results in generic graphs. Szegedy [30] showed that the quantum hitting time has a quadratic gain compared to the classical hitting time for the problem of detecting whether a set of vertices is marked, in connected, regular and non-bipartite graphs. Santos and Portugal [26, 27] analyzed the search problem on the complete graph and on the cycle. With different proposals, Magniez [20] and Krovi et al. [18] developed quadratically faster quantum algorithms to find a marked vertex on ergodic and reversible Markov chains.

The Coinless Quantum-Walk model was originally described by Patel et al. [23, 24] and the application for searching on two-dimensional lattices was performed numerically. Ambainis, Portugal, and Nahimov [9] analytically proved that the coinless quantum walk in two-dimensional lattices, using the same tessellation proposed by Falk [13] has complexity $O(\sqrt{N} \log N)$. This result has the same complexity of the algorithm that uses quantum walks with coin. However, it is important to note that the coinless quantum walk needs no additional space and therefore this algorithm uses minimal memory. Here, we use Falk's method to implement this model. The evolution operator is defined by a graph tessellation. The simplest line or even-cycle tessellation is based on two sets of orthonormal vectors

$$|u_x^0\rangle = \cos \frac{\alpha}{2} |2x\rangle + e^{i\phi_1} \sin \frac{\alpha}{2} |2x+1\rangle, \quad (1)$$

$$|u_x^1\rangle = \cos \frac{\beta}{2} |2x+1\rangle + e^{i\phi_2} \sin \frac{\beta}{2} |2x+2\rangle, \quad (2)$$

which are used to define the reflection operators

$$U_0 = 2 \sum_{x=-\infty}^{\infty} |u_x^0\rangle\langle u_x^0| - I, \quad (3)$$

$$U_1 = 2 \sum_{x=-\infty}^{\infty} |u_x^1\rangle\langle u_x^1| - I. \quad (4)$$

For a N -cycle (N must be even), index x runs from 0 to $N - 1$. One step of the quantum walk is driven by the unitary operator $U = U_1U_0$.

3. SIMULATION USING HPC

The notable progress of GP-GPU architectures in recent years and the emergence of many other accelerator architectures like FPGA, IBM's Cell and Intel's MIC (Xeon Phi) indicate a strong tendency towards the heterogeneity in HPC. In this context, we use the Neblina language² to simulate QW models using parallel resources.

Neblina is a language focused on establishing a parallel computing layer requiring minimal knowledge of the user about parallel programming. For programming in Neblina, the operations are sequential independently of the underlying architecture. The Neblina interpreter sends the data to the parallel processing unit (either CPU or GPU or other) increasing productivity. This is performed transparently by using OpenCL parallel API, which accesses heterogeneous architectures. The simulation of QWs uses highly scalable matrix-matrix and matrix-vector operations that allow speedups when we use Neblina as the core program. We are interested also to obtain the statistical data of the dynamics (standard deviation, limiting distribution, mixing time and so on) of QW models. Besides simulation, the calculation of those metrics can generate large overheads in the overall processing time and some theoretical results can only be confirmed by performing simulations with large number of elements (asymptotic behavior).

Our simulation of QWs goes through three distinct major steps:

- Conversion of the input parameters into unitary operator U , which describes the dynamical evolution. These parameters can be the underlying structure (line, lattices, cycles, and others), coin operator, initial states, and so on.

²<http://www.lncc.br/~pcslara/neblina>

- Application of unitary operator U on a quantum state $|\psi\rangle$ generating vector $U^i|\psi\rangle$ for $i = \{1, \dots, T\}$ for large values of T .
- Statistical interpretation of $U^i|\psi\rangle$ for $i = \{1, \dots, T\}$. This includes the probability distribution, standard deviation, limiting distribution, and so on.

For the first we use the Python programming language that allows a high abstraction and complex data structures facilitating the process of converting input parameters into matrices and vectors. Second step is certainly the most costly one. In this step we use Neblina, which calls OpenCL to parallelize the application of matrix U on the quantum state $|\psi\rangle$ (a vector). So, this part can be performed in a GP-GPU or in a CPU multicore using the same program code. Neblina outputs files with the statistics associated with the probability distribution that are used to generate plots using Gnuplot (third step).

4. HIPERWALK: HIGH-PERFORMANCE QUANTUM-WALK SIMULATOR

HiPerWalk³ is a freeware open-source program that allows the user to perform simulations of quantum walks on graphs using HPC. The user can use the parallel resources of the computer, such as accelerator cards, multicore CPU and GPGPU to speedup the overall process without knowing parallel programming. It is under development and employs Python, OpenCL, Neblina⁴, and Gnuplot languages.

In the current version of HiPerWalk, the input text file is the main interface between the user and the simulator. The parsing process is case sensitive, and the user must take care whether the commands are typed in upper or lower case. The main input commands are:

`WALK <MODEL>` selects a quantum walk model. Currently it can be `DTQW1D`, `DTQW2D`, `COINLESS1D`, `CUSTOM`. This is a required command.

³The program can be download from <http://qubit.lncc.br/hiperwalk>.

⁴The Neblina Programming Language can be downloaded from <http://www.lncc.br/~pcslara/neblina> or from the mirror <http://qubit.lncc.br/neblina>.

DIRECTORY <NAME> defines a directory path which is used by the simulator to save the output files. This is a required command. The <NAME> must not have SPACE or TABULAR character.

GRAPH <TYPE> <SIZE> defines the graph in which the simulator will perform the walk.

GRAPH CYCLE <NUMBER_OF_VERTEX> generates an N -cycle. **GRAPH LINE** generates a line. This is a required command. <NUMBER_OF_VERTEX> must be positive integer number.

STEPS <T> defines a positive integer number that will evolve the system at time T. This is a required command. <T> must be positive integer number.

BEGINCOIN

⋮

ENDCOIN

This block defines the coin operator. The options are **HADAMARD** <N>, **FOURIER** <N>, **GROVER** <N>, which produces the Hadamard, Fourier, or Grover operators (dimension $N \times N$). A customized coin matrix can be defined by inputing each entry $a_{ij} + i b_{ij}$ as follows:

```

BEGINCOIN
  a11  b11  ...  a1N  b1N
  ⋮      ⋮      ⋮
  aN1  bN1  ...  aNN  bNN
ENDCOIN

```

BEGINSTATE

⋮

ENDSTATE

This block defines the initial state of the quantum walk.

For the coined case, the initial state has the form $|\psi\rangle = \sum_i \alpha_i |c_i\rangle |p_i\rangle$, where $\alpha_i \in \mathbb{C}$, $|c_i\rangle$ is a coin state, and $|p_i\rangle$ is a position state. Each term in the sum must be entered in a line as follow:

```

re( $\alpha_i$ )  im( $\alpha_i$ )  ci  pi

```

For example, state $|\psi\rangle = \frac{1}{\sqrt{2}}(|0\rangle + i|1\rangle)|0\rangle$ corresponds to

```
BEGINCOIN
0.70710678118654746 0 0 0
0 0.70710678118654746 0 0
ENDCOIN
```

The coinless case follows a similar pattern. If the initial state is $|\psi\rangle = \sum_i \alpha_i |p_i\rangle$, then each term in the sum produces a line with the syntax
 $\text{re}(\alpha_i) \quad \text{im}(\alpha_i) \quad p_i$

```
BEGINTESELLATION
```

```
α    φ1
β    φ2
```

```
ENDTESELLATION
```

Parameters $\alpha, \phi_1, \beta, \phi_2$ defines the unitary operator of the `COINLESS1D` model. See examples for the details.

`SIMULATION <TYPE>`, defines the simulation type: `PARALLEL` or `LOCAL`. `PARALLEL` means that the parallel architecture of the user's machine will be employed. `Neblina` and `OpenCL` are requirements and must be properly installed. `LOCAL` means that the calculation will not use parallel resources and will be performed by Python. The default value is `LOCAL`.

`PLOTZEROS TRUE` forces the simulator to save and print probabilities that are exactly zero. This command can be suppressed and the default value `PLOTZEROS TRUE` avoids to save zeros.

`PLOTS TRUE` forces the simulator to generate the graphics of the mean and the standard deviation using `Gnuplot`. This command can be suppressed and the default value avoids to create the graphics and is equivalent to `PLOTS FALSE`.

`ANIMATION TRUE` forces the simulator to save data and make a plot of the probability distribution at each time step. At the end, the simulator generates an animation file called *evolution.gif*.

`ALLSTATES <N>` forces the simulator to save the states for all time steps are multiple of `N`. If `N=1`, all intermediate states will be saved. This parameter is optional. The default is to save only the last step. The value of `N` must be a non-negative integer.

HARDWAREID <N> forces the simulator to use the *N*th processor unit (parallel device), which is described by command **neblina** -1. The default value of *N* is 0. The value of *N* must be a non-negative integer.

Comments can be introduced by putting the character **#** in the beginning of the each line.

5. EXAMPLES

In this section we show two one-dimensional examples using the coined and coinless quantum walk models. Consider two input samples. The left (right) input is an example for the coined (coinless) model.

1	WALK DTQW1D	1	WALK COINLESS1D
2	NAME DIR1	2	NAME DIR2
3		3	
4	STEPS 100	4	STEPS 50
5	GRAPH LINE	5	GRAPH CYCLE 240
6		6	
7	BEGINCOIN	7	BEGINSTATE
8	HADAMARD 2	8	1 0 120
9	ENDCOIN	9	ENDSTATE
10		10	
11	BEGINSTATE	11	BEGINTESELLATION
12	0.70710678 0 0 0	12	1.57079632 0
13	0 -0.70710678 1 0	13	2.09439510 0
14	ENDSTATE	14	ENDTESSELLATION
15		15	
16	SIMULATION PARALLEL	16	SIMULATION PARALLEL

The left column shows an input sample using the coined quantum walk on a line. The initial condition is $|\psi\rangle = \frac{1}{\sqrt{2}}(|0\rangle - i|1\rangle)|0\rangle$. The coin is the 2×2 Hadamard matrix. The right column shows an input sample using the coinless quantum walk on a cycle with 240 vertices. The required parameters for this model are $\alpha = \pi/2$, $\beta = \frac{2\pi}{3}$ and $\phi_1 = \phi_2 = 0$. The initial condition is $|\psi\rangle = |120\rangle$.

Fig. 1 shows the final probability distribution for each case generated by HiPerWalk. The simulator also produces a graph of the standard deviation.

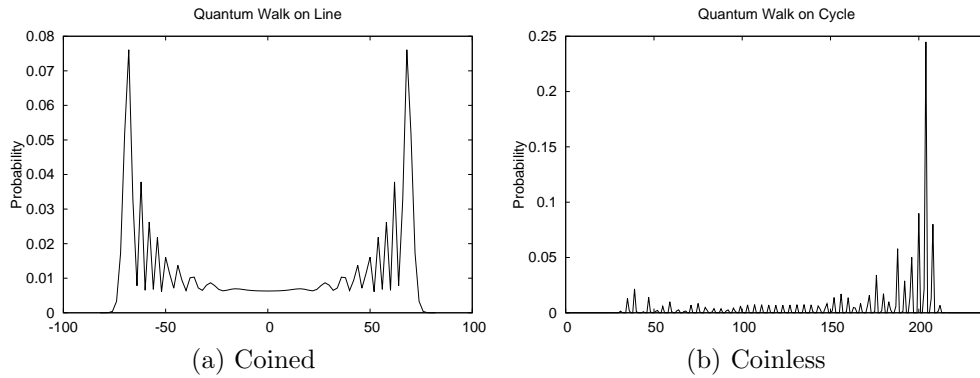


Figure 1: Probability distributions after 100 steps for the coined model (left) and after 50 step for the coinless model (right).

Fig. 2 shows the standard deviation as a function of the number of steps for left-side input (coined model). This figure uses the gnuplot fitting to find the scaling parameters of the standard deviation. From the result, one can easily verify that the standard deviation increases linearly with the number of time steps, as expected.

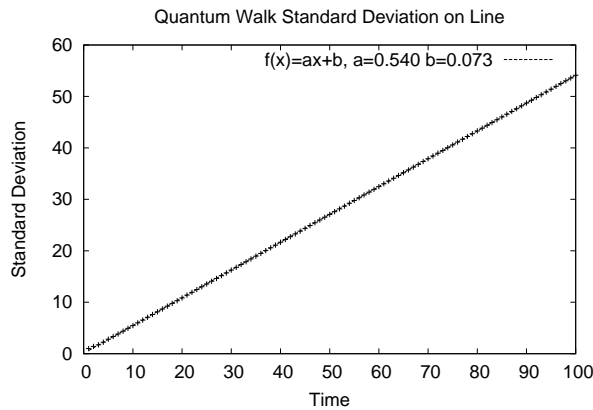


Figure 2: Standard deviation for coined model experiment.

6. CONCLUSIONS

We have briefly described a new simulator called HiPerWalk (high-perfor-

mance quantum-walk simulator), that can be used to generate the dynamics of the main quantum walk models described in Literature. Up to now, only the discrete-time coined and coinless quantum walk models have been implemented. The continuous-time and Szegedy's quantum walk models are currently being implemented.

This new simulator has two major advantages: 1) it has an user-friendly input, and 2) it is able to use hybrid HPC architectures, which include Xeon processors, Xeon Phi, Tesla cards, graphic cards, intel multi-cores, and others. The load is automatically balanced among the available processors and, to use the simulator, no knowledge of parallel programming is required.

ACKNOWLEDGMENTS: We thank CNPq, Capes and Faperj for financial support. We acknowledge the use of ComCiDis HPC structure.

References

- [1] G. Abal, R. Donangelo, M. Forets, and R. Portugal. Spatial quantum search in a triangular network, 2011. arXiv:quant-ph/1009.1422.
- [2] G. Abal, R. Donangelo, F. L. Marquezino, and R. Portugal. Spatial search on a honeycomb network. *Mathematical Structures in Computer Science*, 20:999–1009, 2010.
- [3] D. Aharonov, A. Ambainis, J. Kempe, and U. Vazirani. Quantum walks on graphs. In *Proceedings of the 33rd ACM Symposium on Theory of computing*, pages 50–59, 2000. Disponível em: arXiv:quant-ph/0012090.
- [4] Y. Aharonov, L. Davidovich, and N. Zagury. Quantum random walks. *Physical Review A*, 48(2):1687–1690, 1993.
- [5] D. Aldous and J. Fill. *Reversible Markov Chains and Random Walks on Graphs*. Monography in preparation, 1994. Disponível em: <http://www.stat.berkeley.edu/~textasciitildealdous/RWG/book.html>.
- [6] A. Ambainis, A. Backurs, N. Nahimov, R. Ozols, and A. Rivosh. Search by quantum walks on two-dimensional grids without amplitude amplification. arxiv:quant-ph/1112.3337, 2011.

- [7] A. Ambainis, A. Childs, B. Reichardt, R. Spalek, and S. Zhang. Any and-or formula of size n can be evaluated in time $n^{1/2+o(1)}$ on a quantum computer. In *Proceedings of FOCS*, pages 363–372, 2007.
- [8] A. Ambainis, J. Kempe, and A. Rivosh. Coins make quantum walks faster. In *Proceedings of the 16th ACM-SIAM Symposium on Discrete Algorithms*, pages 1099–1108, 2005.
- [9] A. Ambainis, R. Portugal, and N. Nahimov. Spatial search on grids with minimum memory. arXiv:quant-ph/1312.0172, 2013.
- [10] A. Childs, B. Reichardt, R. Spalek, and S. Zhang. Every nand formula on n variables can be evaluated in time $o(n^{1/2+\epsilon})$. Version3, arXiv:quant-ph/0703015, 2007.
- [11] A. M. Childs, R. Cleve, S. P. Jordan, and D. Yonge-Mallo. Discrete-query quantum algorithm for nand trees. *Theory of Computing*, 5(1):119–123, 2009.
- [12] R. Cleve, D. Gavinsky, and D. Yonge-Mallo. Quantum algorithms for evaluating min-max trees. In Y. Kawano and M. Mosca, editors, *Proceedings of Theory of Quantum Computation, Communication, and Cryptography (TQC 2008)*, volume 5106, pages 11–15. Springer Berlin / Heidelberg, 2008.
- [13] M. Falk. Quantum search on the spatial grid. arxiv:quant-ph/1303.4127, 2013.
- [14] E. Farhi, J. Goldstone, and S. Gutmann. A quantum algorithm for the hamiltonian nand tree. *Theory of Computing*, 4(1):169–190, 2008.
- [15] E. Farhi, J. Goldstone, S. Gutmann, and M. Sipser. Quantum Computation by Adiabatic Evolution. *ArXiv Quantum Physics e-prints*, Jan. 2000.
- [16] E. Farhi and S. Gutmann. Quantum computation and decision trees. *Physical Review A*, 58:915–928, 1998.
- [17] B. Hein and G. Tanner. Quantum search algorithms on a regular lattice. *Physical Review A*, 82(1)(012326), 2010.

- [18] H. Krovi, F. Magniez, M. Ozols, and J. Roland. Finding is as easy as detecting for quantum walks. In *Proceedings of the 37th International Colloquium Conference on Automata, Languages and Programming*, pages 540–551, 2010.
- [19] T. D. Mackay, S. D. Bartlett, L. T. Stephenson, and B. C. Sanders. Quantum walks in higher dimensions. *Journal of Physics A: Mathematical and General*, 35(12):2745, 2002.
- [20] F. Magniez, A. Nayak, P. C. Richter, and M. Santha. On the hitting times of quantum versus random walks. In *Proceedings of the Nineteenth Annual ACM -SIAM Symposium on Discrete Algorithms*, pages 86–95, 2009.
- [21] F. L. Marquezino and R. Portugal. The qwalk simulator of quantum walks. *Computer Physics Communications*, 179:359–369, 2008.
- [22] A. C. Oliveira, R. Portugal, and R. Donangelo. Decoherence in two-dimensional quantum walks. *Physical Review A*, 74(012312), 2006.
- [23] A. Patel, K. S. Raghunathan, and P. Rungta. Quantum random walks without a coin toss. arxiv:quant-ph/0506221, 2005.
- [24] A. Patel, K. S. Raghunathan, and P. Rungta. Search on a hypercubic lattice using a quantum random walk. ii. d=2. *Physical Review A*, 82(032331), 2010.
- [25] R. Portugal. *Quantum walks and search algorithms*. Springer, New York, 2013.
- [26] R. A. M. Santos and R. Portugal. Quantum hitting time on the complete graph. *International Journal of Quantum Information*, 8(5):881–894, 2010.
- [27] R. A. M. Santos and R. Portugal. Quantum hitting time on the cycle. In *Proceedings of III WECEIQ - Workshop-School of Computation and Quantum Information*, 2010.
- [28] M. Sawerwain and R. Gielerek. Gpgpu based simulations for one and two dimensional quantum walks. In A. Kwiecie, P. Gaj, and P. Stera, editors, *Computer Networks*, volume 79 of *Communications in Computer and Information Science*, pages 29–38. Springer Berlin Heidelberg, 2010.

- [29] N. Shenvi, J. Kempe, and K. B. Whaley. A quantum random walk search algorithm. *Physical Review A*, 67(052307), 2003.
- [30] M. Szegedy. Quantum speed-up of markov chain based algorithms. In *Proceedings of the 45th Symposium on Foundations of Computer Science*, pages 32–41, 2004.
- [31] B. Tregenna, W. Flanagan, R. Maile, and V. Kendon. Controlling discrete quantum walks: coins and initial states. *New Journal of Physics*, 5(1):83, 2003, quant-ph/0304204.
- [32] A. Tulsi. Faster quantum walk algorithm for the two dimensional spatial search. *Physical Review A*, 78(012310), 2008.

A New Approach of Cellular Automata Applied for Traffic Simulation

Marcelo Zamith^{a1}, Regina Célia P. Leal-Toledo^b, Esteban Clua^b

^aUniversidade Federal Rural do Rio de Janeiro

^bUniversidade Federal Fluminense

Abstract

This work introduces an innovation Cellular Automaton (CA) model applied for freeway traffic. Besides reproducing basic traffic proprieties, the proposed model herein is also capable of mimicking different drivers' style, including their fluctuation and variation. The model herein considers differentiated acceleration policy which use the concept of acceleration rate to describe the drivers nature. Furthermore, the proposed model includes a randomness in the anticipation policy. The randomness of both policy is given by *Beta* probability density function (PDF). In doing so, the CA model herein is able to describe different unpredictable behavior of drivers' styles. The simulations developed and discussed give rise to a phase diagram which resembles the fundamental real data diagram.

Keywords: drivers' style, anticipation policy, acceleration policy, cellular automaton.

1. INTRODUCTION

Vehicular traffic has grown every year due to the modern society demands by mobility, which has led to serious traffic jam problems in most big cities around the world. Traffic prediction and simulation became a hotspot research topic in different fields, being a fundamental service for the population's wellness. Scientific computational systems and efficient numerical algorithms are important instruments for dealing with this kind of problems.

Since the road saturation increases faster than its expansion, a correct comprehension of traffic flow is able to help us understand and manage the vehicular traffic motion in order to minimize the traffic effects. As a result, several mathematical models have been proposed. Louis A. Pipes [1] was

¹E-mail Corresponding Author: zamith.marcelo@gmail.com

one of first researchers in studying the traffic motion in the 1950s, which describes mathematically the vehicular motion.

Several researchers have tried to describe mathematically traffic flows and understand its bottlenecks. These models are typically classified as macroscopic or microscopic. Among the microscopic models, Cellular Automaton (CA) has been adopted with good results, due to the fact that it creates similar behavioral features of traffic vehicular motion, such as the relation of flow-density and the metastable phase [2].

In this paper we propose a Cellular Automata model applied for traffic simulation which brings an important innovation approach for the acceleration policy, taking into account an acceleration rate. Moreover, our model also considers the movement of ahead vehicle through the anticipation policy.

To model both policy acceleration and anticipation employed *Beta* probability density function (PDF) which work together with more refinement spatial discretization. This approach allows to mimic the uncertainly nature of drivers and is able to represent several realistically drivers' style. As a consequence, the proposed model allows studying how the different drivers' styles affects the global behavior of the highway, flow-density relation.

In this work some related work is reviewed in Section 2, following we describe employed variables on traffic simulation based on cellular automaton and the base model as well as its extension in Section 3. We present our proposed model in the Section 4. Finally, concluding remarks about the proposed model as well as the future work are discussed in Section 5.

2. TITLE OF THIS SECTION

The Cellular Automata (CA) is a model mathematical widely employed for describing a complex and dynamic system, such as traffic, crowd simulation, etc [3]. Its concept was presented by J. Von Neuman [4]. A theoretical systematic description of CA was developed by Wolfram [5].

CA models applied to traffic problems can describe basic properties of the traffic. They are used for representing the vehicular movement across the lattice, which represents the highway. Nagel and Schreckenberg (NaSch) [6] proposed the successful model that has been widely employed.

A well known family of these solutions is named slow-to-start. This model tries to mimic the driver inertia in returning his velocity whenever he stops. This family was introduced by Takayasu and Takayasu (T2) [7] and following several other works also tried to resemble the driver inertia [8, 9]. Despite

depicting metastable region, this family model should work with more than one probability with a different range of values, i.e., Basically, these models require a combination of more the one *uniform* probability density function. At last, metastable region relies on its initial condition: For free flow, the vehicles must be distributed uniformly by the CA lattice. On the other hand, jammed flow is represented by vehicles in jammed state on the CA lattice.

Another family of CA applied for traffic are related to those that include anticipation feature. These models resemble the continuity of drivers' movement in the next instant time. The concept adopted in this approach is that every driver considers that his vehicle in the front will move with the same velocity as in the previous time instant. The disadvantage of this model family is given by the unpredictable driver's behavior due to correct velocity definition. Emmerich et. al [10] suggests that each vehicle may adjust its velocity considering the movement of the vehicle in the front at the next time instant, but this strategy depends on flow and the results show that the flow becomes jammed prematurely, besides not reproducing metastable phase. Another strategy considers a percentage of velocity of the vehicle in the front as proposed by Larraga et. al [11], including a safety distance among vehicles. Break light models is a subset of this family, which adopts a signalize strategy [12]. Other strategy adopted by anticipation model was proposed by Lima [13], where a recursive procedure is added in order to correctly define each vehicle velocity.

3. TRAFFIC SIMULATION BASED ON CA

Probabilistic CA models employed in traffic simulation have a basic set of rules. In general, the following models extend these basic rules. The variables space and time are both discrete so, $x_i^t \in \mathbf{Z}$ and $t \in \mathbf{N}$. The highway is considered to have periodic boundary condition, i.e., the position X is the same as position $X+L$ where L is the length of the circuit. Likewise, the i^{th} vehicle is the same as the $(i+N)^{th}$ vehicle, where N is the number of vehicles.

Besides, several models adopt the spatial discretization of one cell with 7.5 meters and the time evolution scale is measured in seconds. In this case, one cell denotes one vehicle. However, others spatial discretization can be employed [12] in order to better modeling vehicles with different length (buses and trucks). The variable (v_i^t) denotes the velocity of the i^{th} vehicle at time instant t , in cells per time, while x_i^t denotes the spatial position. The

distance between two vehicles in a time instant is represented by d_i^t , and the maximum speed allowed is given by v_{max} . Finally, probabilistic character of the models describes whenever a vehicle will maintain or not its velocity, accelerating 1cell/s (7.5m/s).

In this work we introduce a novel model which is an extension of our previous work [14] and adopts a new probability function (PDF), named as the *Beta* PDF. This PDF is used to define the anticipation policy and is able to include greater flexibility to differentiated policies anticipation.

Algorithms 1 and 2 describe our base model. Our solution is explicit in time and pretends to ensure the individual correct velocity definition, considering the movement of the ahead vehicle in the anticipatory policy.

This base model is composed by two stages. In the first, velocities are defined while, in the second, positions of all vehicles are updated. The former is described by lines 2-14 and the latter is treated by line 17, both in algorithm 1. Velocity definition and position updating are independent tasks. Moreover, they are not tied to the flow direction of the simulation, thus allowing free choice of access to the data structure.

Algorithm 1 The Base Model - main algorithm

```

1: for all vehicles do
2:    $v_i^t \leftarrow \min[v_i^{t-1} + 1, v_{max}]$ 
3:    $p \leftarrow$  randomize number  $\in [0, 1]$ 
4:   if  $p \leq p_m$  and  $v_i^{t-1} > 0$  then
5:      $v_i^t \leftarrow v_i^{t-1} - 1$ 
6:   end if
7:    $\alpha_i^t \leftarrow \text{Beta}(a, b)$ 
8:    $d_{is}^t \leftarrow (x_i^{t-1} - x_{i+1}^{t-1} - 1) + [v_{i+1}^{t-1} \times (1 - \alpha_{i+1}^{t-1})]$ 
9:   if  $v_i^t > d_{is}^t$  then
10:     $v_i^t \leftarrow d_{is}^t$ 
11:   end if
12:   if  $[v_i^{t-1} \times (1 - \alpha_i^t)] > d_{is}^t$  then
13:     call Solver Vehicles' Cluster (i)
14:   end if
15: end for
16: for all vehicles do
17:    $x_i^t \leftarrow x_i^{t-1} + v_i^t$ 
18: end for

```

The anticipatory policy is composed by two steps: in the first, the driver behavior is modelled with an expectation factor of how the ahead vehicle will move in the current time instant. This is given by a random value for considering the movement of the ahead vehicle, which is produced using the PDF. In the second step, based on this perception, the driver adjusts his velocity in order to prevent a cell of CA to be occupied by more than one vehicle, which would characterize an unreal collision.

The expectation is given based on a PDF through the α parameter which represents a percentage of velocity of the ahead vehicle. The α parameter is chosen based on Monte Carlo - rejection technique [15].

Therefore, this expectation term is added to the distance between two vehicles, as described by d_{is}^t which is calculated in line 5 of algorithm 1 and line 3 of algorithm 2.

Besides that, whenever a driver notices that he will move less than the previous one could consider, he signalizes to it in order to avoid an eventual collision. Moreover, the signalization procedure is propagated for all vehicles affected by that one which move less than expected. This set of vehicles is named as a cluster of vehicles.

After defining the cluster, each vehicle of the cluster adjusts his velocity in accordance to the distance between it and its ahead one, added with a new expectation term (line 3 of algorithm 2). In this case, vehicles can move less than expected again and a new sub-cluster is built.

Line 10 of Algorithm 1 shows how the vehicles cluster is built. Algorithm 2 solves the vehicles cluster, creates the sub-clusters (line 8) and solves the sub-clusters recursively.

Algorithm 2 The Base Model - Solver Vehicles' Cluster algorithm

```

1: while vehicles do
2:    $\alpha_i^t \leftarrow \text{Beta}(a, b)$ 
3:    $d_{is}^t \leftarrow (x_i^{t-1} - x_{i+1}^{t-1} - 1) + [v_{i+1}^t \times (1 - \alpha_{i+1}^t)]$ 
4:   if  $v_i^t > d_{is}^t$  then
5:      $v_i^t \leftarrow d_{is}^t$ 
6:   end if
7:   if  $[v_i^t \times (1 - \alpha_i^t)] > d_{is}^t$  then
8:     call Solver Vehicle's Cluster (i)
9:   end if
10: end while

```

In a previous work, we employed the normal PDF in order to consider the movement of ahead vehicle. However, the so-called *Beta* is more flexible PDF can be employed to describe the randomness in the anticipatory policy due to shows an easy way to configure several different curves defined between zero (0) and one(1). Furthermore, the curves shape are symmetric or asymmetric and can assume different shapes [16].

For simulation, we adopt the same configuration of our previous work [17], where the simulated domain is in one-dimension and, the spatial discretization is given by one cell of 7.5meters, which represents one vehicle. The tests are performed with circular highways, under periodic boundary condition, with 300 cells. The maximum speed limit is 5 cells per second (135km/h).

In order to analyze the influence of *Beta* PDF, we choose three range of values, as following: the first, with $Beta(a = 1, b = 20)$, has α value close to zero, which means that the vehicles have the expectation that their ahead vehicles are going to maintain its velocity at the current time instant. The second range, $Beta(a = 4, b = 9)$, describes drivers who consider the ahead vehicle velocity with lesser probability than the previous parameters. The last one, $Beta(a = 9, b = 9)$, represents vehicles which tend to have the smallest expectation of ahead vehicle velocity. Fig. 1 illustrates the three obtained curve shapes.

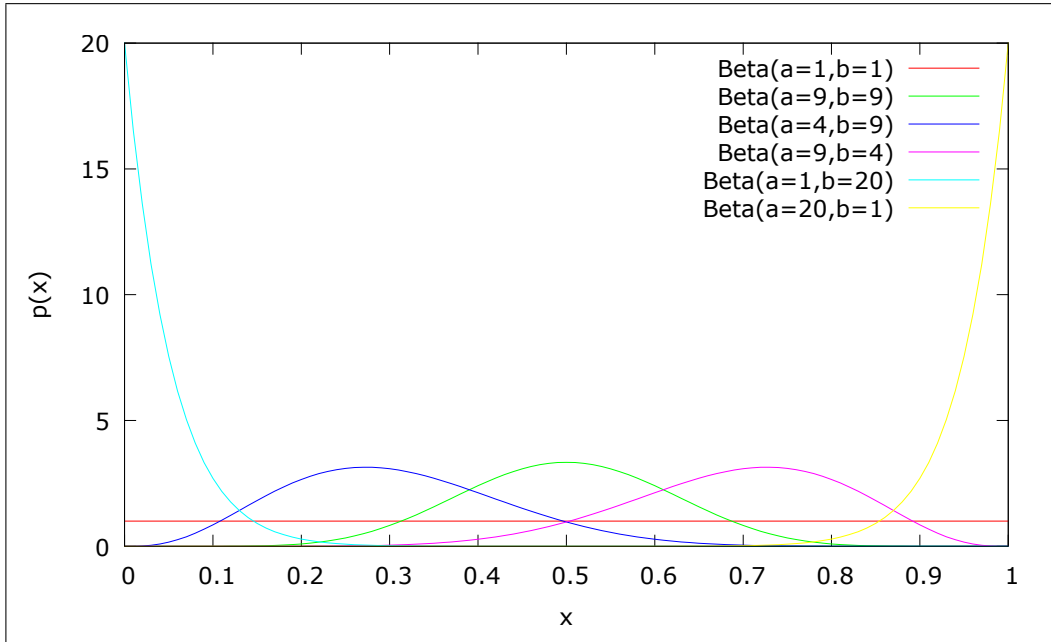
Fig. 2 shows the fundamental diagram of three curve shapes. As expected, vehicles that move farther or closer to another produce higher flow-density relation.

Employing the *Beta* FDP as an anticipation policy also produces excellent results. Furthermore, this FDP makes the model more flexible due to several other curves that can be drawn, allowing to simulate several different drivers' styles [18]. However, these results are similar to the previous one, where normal PDF in the anticipation policy was employed.

Considering the fact that, we propose a modification to the Algorithm 1, where the *Beta* PDF is also used to define the vehicles' acceleration policy, employing the concept of acceleration rate.

4. THE PROPOSED MODEL

In general, CA models applied for traffic simulation adopt the *Uniform* PDF to describe the uncertainty of drivers' styles. These models define when a vehicle is going to accelerate or not. Considering of the *Beta* PDF as

Figure 1: *Beta* curves.

mentioned in the previous section, we propose a modification for the model, where the *Beta* PDF is also applied for acceleration policy. Therefore, the use of *Beta* PDF allows the vehicles to define their acceleration rate, i.e., the vehicles are able to specify a quantity of cells they are moving at current time instant, relying on the *Beta* PDF parameters.

Besides that, in this work we also include a higher spatial refinement discretization, as suggested by [19]. Therefore, we adopt cells of 1.5meters, being a vehicle now composed by five cells. With this spatial refinement discretization combined with the curves shapes (Fig. 1), we are able to represent much more discrete values in both policy. The speed limit becomes to 25 cells per second (135km/h).

Indeed, a refined discretization allows the modeling of different rates of acceleration, i.e., a vehicle is able to increase its velocity in a range from zero to five cells per seconds (7.5m/s). Moreover, this higher discretization yields more representation of α parameter (lines 4 and 2 of Algorithms 1 and 2 respectively).

The acceleration policy is described by Eqs.:

$$\alpha = \text{Beta}(a, b) \quad (1)$$

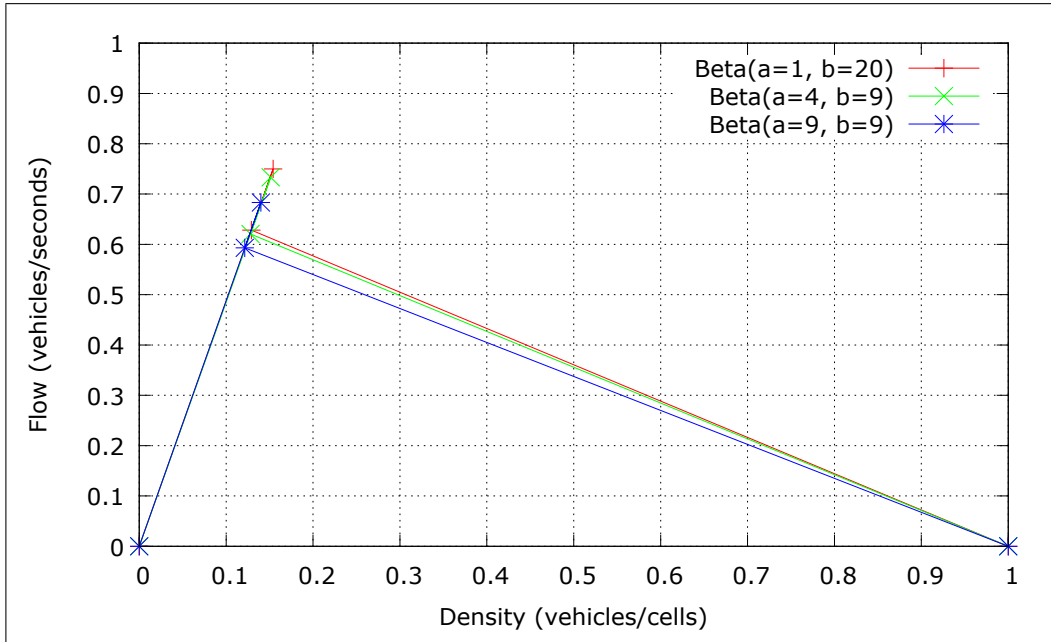


Figure 2: Fundamental diagram.

$$v_i^t = \min[v_i^{t-1} + (\delta \times (1 - \alpha)), v_{max}] \quad (2)$$

where the Eqs. 1 and 2 replace the lines 2-6 of Algorithm 1. $\delta \in [0..5]$ and represents the rate of vehicle acceleration. α is random chosen in order to determinate how much is the acceleration. Thus, the acceleration value is given by $\delta \times (1 - \alpha)$. Finally, the vehicle is limited by the the maximum speed limit of highway (v_{max}).

Additionally, a driver accelerates his vehicle in the same way he considers the movement of the ahead vehicle, i.e, the same *Beta* PDF is employed for both acceleration and anticipation policy. Therefore, when the parameter α is sorted close to 0, the driver accelerates 5cell/s (7.5m/s) in the current time instant and moves close to the ahead vehicle. Otherwise, α values near to 1 correspond to the drivers that maintain their velocity, increasing 0cell/s in the current time instant. In this case, the vehicle maintains far from the ahead one.

To validate our proposed model, the simulation executes with the same configuration of the previous simulations. Fig 3 presents the fundamental diagram of three different curves shape. While the closest is given by $Beta(a = 1, b = 20)$, $Beta(a = 4, b = 9)$ value depicts a middle and the

$Beta(a = 9, b = 9)$ models farthest.

Fig. 3 also depicts the basic features of traffic simulation independently of $Beta$ PDF employed. All developed simulations produced the three phase of traffic as well as the metastable region.

Additionally, the tests also showed that our model is robust and stable. The results reaffirm the flow theory, since the farthest drives maintain distance one to another, leaving several empty space on the highway and, consequently, making the highway jammed prematurely. This style is described by parameters $a = 9$ and $b = 9$ at the PDF. On the other hand, for the closest style, parameters $a = 1$ and $b = 20$, makes a higher value of flow-density relation [20].

The acceleration policy increases the way of simulating the traffic using CAs. Instead of defining when a driver is going to increase his velocity or not, given by the p probability in Algorithm 1 (line 3), the proposed acceleration policy determines how many cells (an acceleration rate) a vehicle is going to accelerate, similar to what is made by the real driver. Moreover, the $Beta$ PDF parameter allows to model several different drivers' styles, depending on the adopted parameters.

Likewise, all vehicles are going to increase their velocity up to the maximum speed limits or the allowed by the flow, apart from the $Beta$ PDF adopted. The farthest style consumes more time than the closest one, since the former is going to accelerate few cells per second. In contrast, the latter style accelerates almost 5 cells/s (7.5m/s) at most of the time instants.

5. CONCLUSION

We propose new CA model applied for traffic simulation explicit in time with anticipation and differentiated acceleration policy. Thus, the model herein allows to simulate different driving styles. These driving styles are given by both: anticipation and acceleration policy. The former is responsible for the driver perception in considering the ahead vehicle movement, while the latter defines how the vehicle is going to increase its velocity in the current time instant.

Therefore, the proposed model herein presented depicts an innovation acceleration policy, due to the fact that the proposed acceleration policy specifies the acceleration rate instead of dealing with when a vehicle acceler-

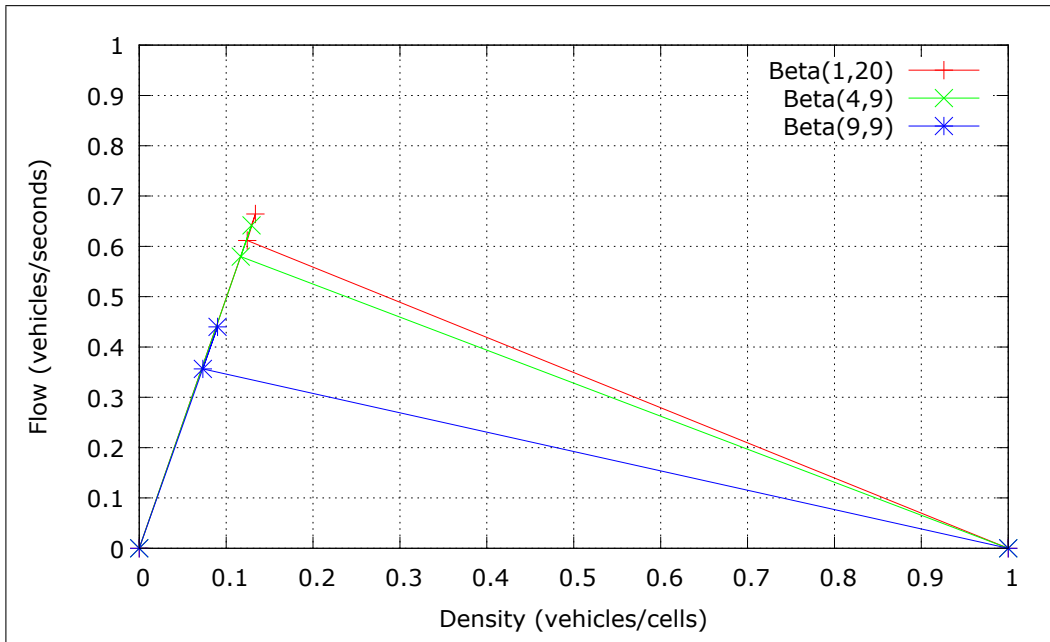


Figure 3: Fundamental diagram with refined discretization and new acceleration policy.

ates or not. In face of this, the model enriches the fundamental diagram, in both theoretical and real data.

Furthermore, the *Beta* PDF and the refinement discretization are able to resemble different drivers' styles in both policy of the model, in acceleration and anticipation policy.

Despite the proposed model represents the nature of drivers' styles, two other questions arise from this work: *i*) how many different drivers' styles exist on traffic and; *ii*) With this new acceleration policy approach, we can simplify the model.

At last, the curve shape employed describes the global highway behavior from a local interaction in according to the traffic theory [20]. In other words, how far or close the vehicles move one to another affects directly the flow-density relation. Furthermore, the fundamental diagram depicts the basic feature of traffic simulation as well as the flow-density relation in according to the driver's style.

References

- [1] L. A. Pipes. An operational analysis of traffic dynamics. *Journal of Applied Physics*, 24:274–281, 1953.
- [2] T. Nagatani. Traffic states and fundamental diagram in cellular automaton model of vehicular traffic controlled by signals. *Physica A: Statistical Mechanics and its Applications*, 8(388):1673–1681, 2009.
- [3] Y. Takai, K. Ecchu, and N. K. Takai. A cellular automaton model of particle motions and its applications. *The Visual Computer*, 11(5):240–252, 1995.
- [4] *The general and logical theory of automata*. University of Illinois Press, Urbana.
- [5] S. Wolfram. Computation theory of cellular automata. *Communications in Mathematical Physics*, 96(15-57), 1984.
- [6] K. Nagel and M. Schreckenberg. A cellular automaton model for freeway traffic. *Journal de Physique I*, 2:2221–2229, December 1992.
- [7] M. Takayasu and H. Takayasu. 1/f Noise in a Traffic Model. *Fractal 1*, 5:860–866, 1993.
- [8] K. Nishinari, M. Fukui, and A. Schadschneider. A stochastic cellular automaton model for traffic flow with multiple metastable states. *Journal of Physics A.*, 37(3101-3110), 2004.
- [9] Adam Clarridge and Kai Salomaa. Analysis of a cellular automaton model for car traffic with a slow-to-stop rule. *Theoretical Computer Science*, 411(38):3507–3515, 2010.
- [10] H. Emmerich and E. Rank. An Improved Cellular Automaton Model for Traffic Flow Simulation. *Journal of Physics A*, 234:676–686, 1997.
- [11] M E Larraga, J A del Rio, and A Schadschneider. New kind of phase separation in a ca traffic model with anticipation. *Journal of Physics A: Mathematical and General*, 37(12):3769–3781, 2004.

- [12] W. Knospe, L. Santen, A. Schadschneider, and M. Schreckenberg. Towards a realistic microscopic description of highway traffic. *Journal of Physics A: Mathematical and General*, 33(48), 2000.
- [13] B. E. Lima. Modelos micoscópios para simulação do tráfego baseados em autômatos celulares. Master's thesis, Universidade Federal Fluminense, 2007.
- [14] Marcelo Zamith, Regina Célia P Leal-Toledo, and Esteban Clua. A novel cellular automaton model for traffic freeway simulation. In *Cellular Automata*, pages 524–533. Springer, 2012.
- [15] M. KALOS and P. WHITLOCK. *Monte Carlo Methods*. Wiley-VCH, 2 edition, 1986.
- [16] M. C. Jones. Kumaraswamy's distribution: A beta-type distribution with some tractability advantages. *Statistical Methodology*, In Press, Accepted Manuscript, 2009.
- [17] Marcelo Zamith, Regina Célia P. Leal-Toledo, Mauricio Kischinhevsky, Esteban Walter Gonzalez Clua, Diego N. Brandão, Anselmo Antunes Montenegro, and Edgar B. Lima. A probabilistic cellular automata model for highway traffic simulation. *Procedia CS*, 1(1):337–345, 2010.
- [18] Arnaud Doniec, René Mandiau, Sylvain Piechowiak, and Stéphane Espié. A behavioral multi-agent model for road traffic simulation. *Engineering Applications of Artificial Intelligence*, 21(8):1443–1454, 2008.
- [19] M.E. Lárraga and L. Alvarez-Icaza. Cellular automaton model for traffic flow based on safe driving policies and human reactions. *Physica A: Statistical Mechanics and its Applications*, 389(23):5425 – 5438, 2010.
- [20] C. F. Daganzo. *Fundamentals of transportation and traffic operations*. Pergamon Press, ed. limitada edition, 1997.

Multifactor Transparent Authentication

Alcides Rivarola^{a1}, Cristian Cappelletti^a

^aFacultad Politécnica, Universidad Nacional de Asunción

Abstract

From the beginning of the Internet, web applications authentication is a real concern issue for users that need to protect personal or very sensitive information. The traditional authentication mechanism, username and password, although it may have potential vulnerabilities, till now remains the most widely used authentication method on the web.

We present the Multifactor Transparent Authentication (MFTA), a scheme that aims to increase the security of web applications authentication compared to a two factor authentication mechanism, but keeping the ease of use and the deployability challenge. It uses the user's PC as a second factor device, and checking some features of the user's PC, in the background, when authenticating. It focuses mainly on organizations where the users do not need to change their computer, or do not have the need to connect from another computer.

Keywords: Authentication, Multifactor, Login, Web, Security.

1 Introduction

The username and password till now remains the most widely used authentication mechanism on web applications. It is easy for developers to implement on a server and the users are used to it.

There are many problems with this mechanism. One of them could be the reuse of passwords by users across many web sites [3], so the compromise of one web site could lead to the compromise of other web sites. According to a study conducted by Internet security company BitDefender, over 250,000 usernames, email addresses and passwords, it finds that 75% of users had one common password for social networking and accessing their email [7, 11]. For those users who use a different password for each site, the problem is to remember all of them when there are a significant amount of sites [10]. Another problem is phishing, when Internet intruder use some scams to

¹E-mail Corresponding Author: aerivarola@gmail.com

obtain passwords and financial data [8]. These threats cause mainly financial damage, but they can also cause damage ranging from minor annoyances to real threats to life.

There are many alternatives to the traditional username and password authentication mechanism. The two factor authentication [1], the Federated login and password managers are good approaches but Bonneau evaluation framework [4] shows that none of them meet the requirements of security, usability, or deployability in practice. It is known that most of the users prefer comfort over security when it comes to authentication mechanism, thus usability is a very important issue on authentication. The schemes described before change somehow the user experience so it makes it difficult to implement within an organization.

For an organization that has a web application with valuable information, and just specific clients need to access from inside or outside the organization, none of the existing authentication mechanisms provide enough security without affecting the usability and deployability, therefore we propose the Multi Factor Transparent Authentication scheme (MFTA) which tries to deal with the issues mentioned above.

This paper is organized as follows. Section 2 presents a review of authentication methods. Section 3 describes our proposed scheme. The architecture of MFTA is presented in the Section 4. We evaluate the MFTA scheme considering the Bonneau evaluation framework [4] in Section 5. Finally, Section 6 presents the final considerations, conclusions and our work in progress.

2 Related work

In this section we examine some related work and how they attempt to address the security issues with the authentication.

THE FEDERATED LOGIN, like OpenID [2], Facebook Connect [9] and BrowserID [14], allows users to have just one account on an identity provider to which the websites consult for the validity of the user's identity. All other websites (usually called relying parties) do not ask the user to authenticate directly instead they consume identity assertions from the identity provider [6]. This could be a good approach to solve the problem of remembering many passwords by reducing to one account at the identity provider, but does not solve the original problems of passwords because people still could

use a weak password on the identity provider, and if this gets compromised then all the others websites would be too. Another challenge that this scheme face is that the identity provider may misuse personal information and the adoption of the mechanism by other websites.

TWO FACTOR AUTHENTICATION. This is possibly one of the most widely used authentication mechanism, which is defined by two of the following three factors; something the user knows (e.g. password), something the user has (e.g. phone, smart cards, tokens) [18], or something the user is (e.g. biometric, like fingerprint or voice print). The big problem with this approach is that the user always needs to carry the second factor device, if they loose or forget the device, they won't be able to login at the website. Users prefer easiness and simplicity over security [17]. or if it's intended to use something the user is, it will face the problem of deployability.

PASSWORD MANAGERS. Firefox [15], LastPass [12] and PwdHash [16], are some examples of advanced kinds of password managers that are built into browsers: they are a good choice to provide different passwords for different sites preventing phishing attacks and password sharing. These advanced password managers, however, have their own set of usability issues [5], like the fact that users no longer know the passwords for certain sites and if they forget their own password for the password manager, they could possibly lose all their information.

3 MFTA Scheme Approach

With this work we propose a variation of multiple factors authentication mechanism, but without the need of a cellphone or hardware token, for that it will use the user's PC features as a second factor for authentication.

SCOPE. The scheme is aimed at web applications, where the web application provides a service to a third party. This scheme is not general purpose, but targeted to an organization that wants to give access only to certain people belonging to a group or sector within an area or region (e.g. Country). Below are outlined the goals for this work.

- Transparent to the user. We are convinced that innovative multifactor approaches are promising, and we believe that the proposed scheme will be an asset if it is transparent to the user, which is why transparency is proposed as central axis in this work.

- Increased security through a second factor mechanism. Second factor authentication mechanisms provide an extra security to web applications, but it usually comes at the expense of usability.
- Platform independent. In order to make it useful, the scheme needs to work well on most common browsers, and be operating system independent.
- Contingency mechanism. We provide a contingency mechanism when the user needs for any reason use another computer that it is not his own.

ASSUMPTIONS. It's assumed that the user only accesses the web application from a single PC in one place, using this as a second factor device and considering that the PC does not change regularly. Access from any other PC or elsewhere that is not his is considered suspicious. We assume that the user does not change his computer regularly, nor any other feature registered. Considering that this could be implemented in a service company with very sensitive information (e.g. a bank, cooperative, credit card processing, etc), we assume that there is a security administrator that usually monitors the server for alerts. We assume that an attacker somehow obtains the user's credentials via phishing or cross site passwords reuse, and manages to successfully connect to the web application from somewhere unusual. We assume that in some cases users might use weak passwords that are easy to guess. An attacker can perform a man in the middle attack interposing between the user and the server to which user is authenticating, thus obtaining the user's credentials. We allow an attacker introduce some kind of malware (such as Keylogger) or virus and collect information and obtain the password.

4 Architecture

Our scheme uses the IP address and the user agent information as additional factors to verify the user authenticity. The scheme architecture is explained below.

When the user enters his username and password into a web application as usual, these are sent to the server along with the IP address and the user agent information. Once we have the information, the MFTA will classify the user agent information as follow: browser, operating system, device (e.g. personal

computer, smartphone, tablet, etc). The IP address will help us determine the network and from where the connection is coming. To analyze the user agent, the scheme will use the UADetector [13] library, which will provide us the information we need. We do this by using a Servlet and the function provided by the API:

```
out.append(agent.getName());
out.append(agent.getOperatingSystem().getName());
```

These features will be saved and compared with the user's PC features the next time the user signs in. As the first time the user will have no data to compare with, the scheme will automatically let the user log in and save the information that corresponds to the user's PC. For each user there would be a trusted computer list that is saved on the server, similar to what Google has, so that way it will be possible to compare user's PC features everytime the user signs in.

CONTINGENCY MECHANISM. Considering that for any reason the user needs to change his computer or some other features that our scheme registered, then it will let the user log in, and send an email to the user and the the security administrator notifying of the change in the users features.

MODES. The proposed scheme could work in two different modes, flexible and strict mode. The first one, could let the user log in from a different computer that never used before, but it will send an alert to his email with the login notification, after that, if the user don't take any action, the computer from where was logged will be included into the registered computer list. The strict mode rejects, and notify the security administrator, any user's login attempt if the user's computer is not in the registered device list, except when an user login for the first time with his computer. A new computer can also be added manually on the registered device list.

5 Evaluation

We evaluate our approach with other two approaches that are the most widely used at the moment, the passwords and Google 2 step verification, considering the usability, deployability and security metrics proposed in Bonneau evaluation framework [4]. We evaluate the flexible and strict mode of the MFTA. The table 1 shows the result of the comparative evaluation of MFTA and some others authentication mechanisms.

Scheme	Usability								Deployability				Security												
	Memorywise-Effortless	Scalable-for-Users	Nothing-to-Carry	Physically-Effortless	Easy-to-Learn	Efficient-to-Use	Infrequent-Errors	Easy-Recovery-from-Loss	Accessible	Negligible-Cost-per-User	Server-Compatible	Browser-Compatible	Mature	Non-Proprietary	Resilient-to-Physical-Observation	Resilient-to-Targeted-Impersonation	Resilient-to-Throttled-Guessing	Resilient-to-Unthrottled-Guessing	Resilient-to-Internal-Observation	Resilient-to-Leaks-from-Other-Verifiers	Resilient-to-Phishing	Resilient-to-Theft	No-Trust-Third-Party	Requiring-Explicit-Consent	Unlinkable
Passwords	n	n	y	n	y	y	s	y	y	y	y	y	y	y	n	s	n	n	n	n	n	y	y	y	y
Google 2-SV	n	n	n	n	y	s	s	s	s	n	n	y	y	n	s	s	y	y	n	y	y	y	y	y	y
MFTA flexible	n	n	y	n	y	y	y	y	y	y	s	y	n	y	y	s	s	s	n	s	s	y	y	y	y
MFTA strict	n	n	y	n	y	y	s	y	y	y	n	y	n	y	y	y	y	y	n	y	y	y	y	y	y

Table 1: Comparative evaluation of the MFTA with some others schemes. "y" means the benefit is provided, "s" means the benefit is somewhat provided, while "n" means the benefit is not provided.

USABILITY. The MFTA flexible mode scores better than the Google 2-SV and ties with the password approach. In the *infrequent-errors* the flexible mode offers the benefit because if the user changes his computer, will still be able to log in. However the strict mode won't let the user log in if he change his compute, it will need the intervention of the security administrator to add the manually the new computer to the registered device list, so we considered that the benefit is provided somewhat if the computer change is programmed.

DEPLOYABILITY. Both mode of the MFTA approach are not mature yet, so for the moment they could not provide the benefit of *mature*. We consider the benefit of *server-compatible* is provided somewhat in the flexible mode because no change need to be made to the authentication scheme on the server side, just need to gather some information. On the other hand, the strict mode does not provide that benefit because of the change that needs to be done.

SECURITY. On these metrics we can see that the MFTA, in both modes, provides a better security than passwords and the strict mode score better over Google 2-SV. We can not say the same about the flexible mode, but considering the scope of the work we believe the MFTA score well on the metrics described in the evaluation framework.

6 Conclusion

In this work we introduced the MFTA approach, which provide a better authentication mechanism for websites considering the scope proposed before. The MFTA provides usability benefit as well as conventional passwords do. At the same time it use some of the user's PC feature to provide a better security like second factor authentication do.

The fact that the user does not need to carry any device with him, provides the ease of use plays a key role in authentication, so that's why we propose the MFTA to be transparent, while increasing the security. We think that this is a viable approach and a base for other possible solutions.

References

- [1] Fadi Aloul, Syed Zahidi, and Wassim El-Hajj. Two factor authentication using mobile phones. In *Computer Systems and Applications, 2009. AICCSA 2009. IEEE/ACS International Conference on*, pages 641–644. IEEE, 2009.
- [2] OpenID Authentication. 2.0-final. *OpenID Foundation website*, 2007.
- [3] Joseph Bonneau. Measuring password re-use empirically. *Light Blue Touchpaper*, 2011.
- [4] Joseph Bonneau, Cormac Herley, Paul C Van Oorschot, and Frank Stajano. The quest to replace passwords: A framework for comparative evaluation of web authentication schemes. In *Security and Privacy (SP), 2012 IEEE Symposium on*, pages 553–567. IEEE, 2012.

- [5] Sonia Chiasson, Paul C van Oorschot, and Robert Biddle. A usability study and critique of two password managers. In *Usenix Security*, volume 6, 2006.
- [6] Alexei Czeskis, Michael Dietz, Tadayoshi Kohno, Dan Wallach, and Dirk Balfanz. Strengthening user authentication through opportunistic cryptographic identity assertions. In *Proceedings of the 2012 ACM conference on Computer and communications security*, pages 404–414. ACM, 2012.
- [7] Sabina Datcu. The limits of privacy. is this your password? <http://www.hotforsecurity.com/blog/the-limits-of-privacy-is-this-your-password-865.html>, 2010.
- [8] Anthony Elledge. Phishing: An analysis of a growing problem. *Sans Institute*, 2004.
- [9] Facebook connect. <https://www.facebook.com/help/405977429438260>, 2008.
- [10] Dinei Florencio and Cormac Herley. A large-scale study of web password habits. In *Proceedings of the 16th international conference on World Wide Web*, pages 657–666. ACM, 2007.
- [11] Christopher Hadnagy. *Social engineering: The art of human hacking*. John Wiley & Sons, 2010.
- [12] Lastpass. <https://lastpass.com/>.
- [13] Jaroslav Mallat. Uadetector. <http://user-agent-string.info/>, 2014.
- [14] Browserid. <https://login.persona.org/about>.
- [15] Firefox password manager. <https://support.mozilla.org/en-US/kb/password-manager-remember-delete-change-passwords>.
- [16] Blake Ross, Collin Jackson, Nick Miyake, Dan Boneh, and John C Mitchell. Stronger password authentication using browser extensions. In *Usenix security*, pages 17–32. Baltimore, MD, USA, 2005.

- [17] Linda Summers. Survey finds nearly half of consumers fail to upgrade software regularly and one quarter of consumers don't know why to update software. <http://blogs.skype.com/2012/07/23/intl-tech-upgrade-week/>, 2012.
- [18] Emilio Valente. Two-factors authentication: Can you choose the right one? *Sans Institute*, 2009.

Iterative Estimation for Flight Dynamic Helicopter Simulator

Ivana Y. Sumida^{a1}, Haroldo F. de Campos Velho ^a, Eduardo F.P. Luz^a,
Ronaldo V. Cruz ^b and Luiz Carlos S. Góes^b

^aNational Institute for Space Research, São José dos Campos, SP, Brazil

^bTechnological Institute of Aeronautics, São José dos Campos, SP, Brazil

Abstract

Calibration for flight simulation is parameter identification process. The process is formulated as an optimization problem, and it is solved by using a new approach named Multiple Particle Collision Algorithm (MPCA). Results show a good performance for the employed approach.

Keywords: Dynamic Flight, Parameter Identification, Multiple Particle Collision Algorithm.

1. INTRODUCTION

Flight simulators can provide a suitable alternative to simulate real flight. The applications are focused on to increase the security through the training of crew, evaluation task, and data from simulator can be used to validation and certification of aircraft systems. However, it must convey some degree of realism to the user to be effective. In the present study, a new meta-heuristics is applied, named MPCA [1], for calibrating of a dynamic helicopter flight simulator [2]. The MPCA optimization algorithm was inspired from some typical phenomena inside of nuclear reactors during the neutron travel: absorption and scattering of multiple particles.

2. CALIBRATION OF HELICOPTER FLIGHT MODEL

The equations of motion are nonlinear, but it is to derive a linear differential equations, by considering small perturbations around on an equilibrium point (represented by subscript 0). The linearized dynamical model is expressed by:

$$\frac{d}{dt} \begin{bmatrix} X_l \\ X_d \end{bmatrix} = \begin{bmatrix} A_l & C_1 \\ C_2 & A_d \end{bmatrix} \begin{bmatrix} X_l \\ X_d \end{bmatrix} + \begin{bmatrix} B_l & D_1 \\ D_2 & B_d \end{bmatrix} \begin{bmatrix} \Delta\delta_l(t - \tau) \\ \Delta\delta_d(t - \tau) \end{bmatrix} + \dot{x}_{bias} \quad (1)$$

¹E-mail Corresponding Author: ivanayoshie@yahoo.com.br

where X_l and X_d represent the longitudinal and lateral movements. Therefore, it can be expressed by:

$$\frac{dX}{dt} = AX + B\Delta\delta(t - \tau) + \dot{x}_{bias} \quad (2)$$

$$X = [\Delta u \quad \Delta w \quad \Delta q \quad \Delta\theta \quad \Delta v \quad \Delta p \quad \Delta\phi \quad \Delta r]^T \quad (3)$$

$$\Delta\delta = [\Delta\delta_B \quad \Delta\delta_C \quad \Delta\delta_A \quad \Delta\delta_P]^T \quad (4)$$

Values of interest for system identification are the elements of matrix A (stability derivatives), matrix B (control derivatives), and τ the delays associated with the aircraft response. Furthermore, the addition of tendency vector, x_{bias} , is constant and unknown. This vector is introduced in the mathematical model to represent measurement errors and noise produced by transducers and instrumentation [3]. Let $J(\Omega)$ be the cost function, given by:

$$J(\Omega) = \sum_{i=1}^n \|X_i^{obs} - X_i^{mod}(t_i, \Omega)\|_2^2 \quad (5)$$

$$\begin{aligned} \Omega = & \left(\frac{X_u}{m}, \frac{X_w}{m}, \frac{X_q}{m}, \frac{Z_u}{m}, \frac{Z_w}{m}, \frac{Z_q}{m}, \frac{M_u}{I_{yy}}, \frac{M_w}{I_{yy}}, \frac{M_q}{I_{yy}}, \frac{X_{\delta_B}}{m}, \frac{X_{\delta_C}}{m}, \frac{Z_{\delta_B}}{m}, \frac{Z_{\delta_C}}{m}, \frac{M_{\delta_B}}{I_{yy}}, \right. \\ & \frac{M_{\delta_C}}{I_{yy}}, \Delta\dot{u}_{bias}, \Delta\dot{w}_{bias}, \Delta\dot{q}_{bias}, \Delta\dot{\theta}_{bias}, \Delta u_{ref}, \Delta w_{ref}, \Delta q_{ref}, \Delta\theta_{ref}, \tau_c, \tau_b, \\ & \frac{Y_v}{m}, \frac{Y_p}{m}, \frac{Y_r}{m}, L'_v, L'_p, L'_r, N'_v, N'_p, N'_r, \frac{Y_{\delta_A}}{m}, \frac{Y_{\delta_P}}{m}, L'_{\delta_A}, L'_{\delta_P}, N'_{\delta_A}, N'_{\delta_P}, \Delta\dot{v}_{bias}, \\ & \left. \Delta\dot{p}_{bias}, \Delta\dot{\phi}_{bias}, \Delta\dot{r}_{bias}, \Delta v_{ref}, \Delta p_{ref}, \Delta\phi_{ref}, \Delta r_{ref}, \tau_a, \tau_p \right) \quad (6) \end{aligned}$$

where n is the number of measurements.

The minimum of the objective function $J(\Omega)$ – see Eq. (5) – is found by using a new meta-heuristics: MPCA, based on the canonical PCA. The MPCA uses a set with m particles, where a mechanism to share the particle information is employed. This is addressed with the blackboard, where the Best-Fitness is copy for all particles in the process. For parallel machines, a MPI (Message Passing Interface) version code was implemented [1].

The sinusoidal maneuver is represent by δ in the flight model. MPCA results take in consideration the average of 4 experiments, with synthetic experimental data. Two particles were used, under 10 iterations (exploration). The calibration with MPCA has a good agreement with real dynamics (see Fig. 1).

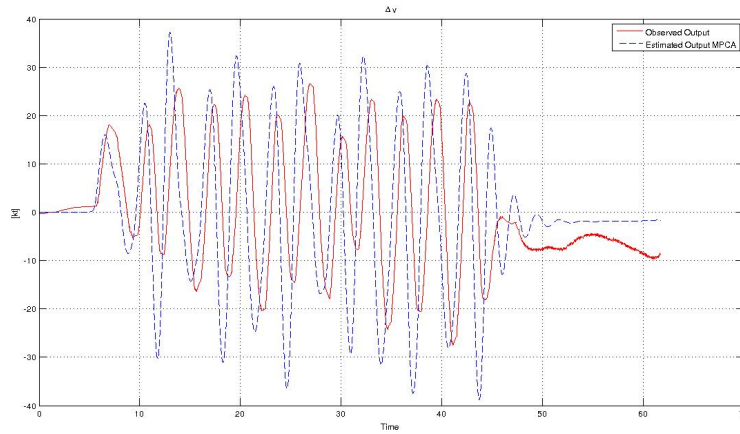


Figure 1: Lateral Velocity in Body Axis.

References

- [1] E.F.P. Luz, *Meta-heurísticas paralelas na solução de problemas inversos*, Tese de Doutorado, Instituto Nacional de Pesquisas Espaciais (INPE), São José dos Campos, (2012).
- [2] R.V. Cruz, *Desenvolvimento de um Modelo Dinâmico para Simuladores de Helicóptero*, Tese de Doutorado, Instituto Tecnológico de Aeronáutica (ITA), São José dos Campos, (2009).
- [3] M.B. Tischler, R.K. Rempfle *Aircraft and rotorcraft system identification*, AIAA Education Series, (2006).

Pervasive Monitoring of Ambulatory Hypertensive Patients and Diagnosis Support

Jorge D. Cespedes^{a1} and Cynthia Villalba^{b2}

^{a,b}Facultad Politecnica - Universidad Nacional de Asuncion (FP-UNA)

Abstract

Hypertension is the main contributor to premature cardiovascular morbidity and mortality. According to the *Panamerican Health Organization*, if uncontrolled, hypertension can cause terrible health issues such as kidney failure, myocardial infarction, among others. This work identified the main issues associated to automated hypertension diagnosis, such as technique to diagnose, attributes to take into account and data validation. It also considers issues related to monitoring of ambulatory patients, such as connectivity, mobile networks, privacy and physiological signs to monitor. We propose a novel solution by incorporating new context information to assist diagnosis, combining machine learning techniques with fuzzy logics and implementing a system entirely based on agents.

Keywords: hypertension-diagnosis, multi-agent, monitoring, pervasive.

1. INTRODUCTION

Hypertension, has been globally recognized as the main contributor to premature cardiovascular morbidity and mortality. In fact, numerous projects aim at effectively controlling the disease and expect a significant impact in health among the world population. If hypertension is properly controlled, cardiac mortality would decrease 49% while stroke mortality would decrease 62% [1]. Uncontrolled hypertension, however, according to data from *Panamerican Health Organization (PAHO)* has terrible consequences such as myocardial infarction, kidney failure, blindness and heart failure.

This work has identified two main problems based on the previously mentioned facts. Essentially, these two issues correspond to *diagnosing* the disease and *monitoring* patients who's already been diagnosed.

¹E-mail Corresponding Author: jcespedes@pol.una.py

²E-mail Corresponding Author: cvillalba@pol.una.py

Let's consider *diagnosis of hypertension* first. A clinician would follow the guides in the Joint National Committee (JNC)³ report [2], such as performing laboratory tests and measuring the patient's blood pressure at every visit to the clinic. For example, according to interviews with a hypertension specialist, the current approach to diagnose hypertension in Paraguay, is to obtain a patient's blood pressure reading and match it against any of the values appearing in table 1. However, most healthcare professionals are aware of the existence of factors causing a temporary elevation of blood pressure, misleading them to diagnose a person as a hypertensive patient. Another problem related to *diagnosis* is the classification of hypertension. For example, a patient with *Pre-hypertension* should modify its lifestyle to include a healthier one and he must be monitored regularly, because there is a chance that he will become a hypertensive patient. Other issues related are pseudo-hypertension, isolated systolic hypertension and white-coat hypertension, as [3] explains. In addition to *diagnosing* based on measurements at the clinician's office, there is also the existence of Ambulatory Blood Pressure Monitoring (ABPM), which allows to obtain several blood pressure readings and store them in the device. Normally, the equipment is worn for 24 hours and is set to measure the patient's blood pressure automatically every 15 minutes during daylight and every 30 minutes during the night. However, this isn't a hassle free method. As an example, one problem in Paraguay is that it isn't available at every clinic. If it is available, the cost of it isn't affordable for most people. Another problem is how blood pressure variability is taken into account, the current approach is to use the standard deviation but there is another method, which according to [13], better correlates blood pressure variability with cardiovascular events. A final issue is the length of the study, diagnosis could be more precise if more readings were available since, as [4] states, a 24 hours monitoring allows a clinician to obtain a patient's blood pressure more precisely, thus longer periods could be even better.

The second main issue identified, is that of *monitoring* patients. A hypertensive patient needs to avoid severe blood pressure elevations⁴ because it could lead to hypertensive emergencies⁵ or urgencies⁶. Most of the time,

³The Joint National Committee (JNC) is a committee coordinated by the National Heart, Lung and Blood Institute (NHLBI). It provides reports containing guidelines for prevention and control of hypertension.

⁴Generally, a blood pressure of 180/20 according to JNC report number 7 [2].

⁵Severe blood pressure elevation that produce damages to target organs [2].

⁶Severe blood pressure elevation that does not produce damages to target organs [2].

JNC 6 CATEGORY	SBP/DBP	JNC 7 CATEGORY
OPTIMAL	<120/80	→ NORMAL
NORMAL	120–129/80–84	↪ PREHYPERTENSION
BORDERLINE	130–139/85–89	↪ PREHYPERTENSION
HYPERTENSION	≥140/90	→ HYPERTENSION
STAGE 1	140–159/90–99	→ STAGE 1
STAGE 2	160–179/100–109	↪ STAGE 2
STAGE 3	≥180/110	↪ STAGE 2

Figure 1: Blood Pressure Classification as in [2]. Shows new categories introduced in report 7.

patients do not experience any signs of high blood pressure and they can only notice situations like these if they use the device to measure their blood pressure, or if they visit a clinic or drugstore. The former leads to two problems, it requires proactivity from the patient and it is almost impossible to detect emergencies or urgencies. Also, if users would like to keep track of their blood pressure readings, they would have to do it manually.

This work proposes a system for pervasive monitoring of hypertensive patients, using wireless sensors, and diagnosis support, which helps the clinicians along the task of diagnosing hypertension. In section 2, we present works dedicated to automated diagnosis and monitoring of patients. In section 3 we describe our proposed solution to the problems mentioned earlier in this section. Finally, section 4 presents the concluding remarks.

2. STATE OF THE ART

We will specify the programming paradigm⁷ authors chose, types of devices used as sensors and processing units, variables measured, the selected mechanism for diagnosis support and emergencies detection.

2.1. Automated Diagnosis

First, let's take into consideration works in the field of *automated diagnosis*, which implies some software assisting the clinician along the task, like [5]

⁷Programming paradigm is whether an object oriented approach was used to implement the system or an agent oriented approach.

which considers age, weight, body mass index (BMI), blood pressure and heart frequency as features. For the classification task it uses both approaches, a fuzzy expert system⁸ and a hybrid approach, a Neural Fuzzy Expert System (NFS). Whereas, [6] uses the above features but adds height, head circumference, chest circumference, waist width and gender as features. For classification, it uses Support Vector Machines⁹ trying different kernel functions¹⁰. Another work in the area of hypertension diagnosis is [7], which uses the same features as [5] and implements a NFS, allowing it to classify hypertension as stage 1, stage 2 or stage 3. In [8] authors implement a hybrid approach to achieve diagnosis, they use Case Based Reasoning (CBR) and Genetic Algorithms (GA). Other works implementing machine learning techniques to diagnose different diseases are [9] and [10], where tools such as SVMs, NFS and data mining are used. While in [11], Analytic Hierarchy Process (AHP) is used, which is a technique for analyzing complex decisions, based on mathematics and psychology.

Most of the works so far expect input data to be correct, since their only purpose is to diagnose without concerning about data gathering. There are works integrating data gathering, real time processing (more on this later) and diagnosis support, such as [12], where the author retrieves an Electrocardiogram (ECG) signal from a 3-leads portable ECG device and processes it in a smartphone, to detect a possible heart attack. Then, there is [13] in which the authors get blood pressure data from ambulatory blood pressure monitor and set thresholds for eliminating outliers. Both works are implemented with the traditional object oriented approach. For works relying on user input, we can mention [14], which operates in one of two ways to diagnose a disease, the first one called Procedural Diagnosis and the second one Heuristic Diagnosis. Procedural Diagnosis, imitates current practices and the latter uses the stored data to diagnose. It is implemented using standard passive objects. In [15], [17] and [18], agents are the core

⁸A fuzzy expert system is an expert system that uses a collection of fuzzy membership functions and rules, instead of Boolean logic, to reason about data. The rules in a fuzzy expert system are usually of a form similar to the following: if x is low and y is high then z = medium.

⁹Support vector machines (SVMs) are supervised learning models with associated learning algorithms that analyze data and recognize patterns, used for classification and regression analysis.

¹⁰Capability to project points in a higher dimensional space in order to (try to) improve data separability.

implementation objects. The first two utilize knowledge bases to diagnose certain diseases and to allow the system to learn new rules, while the third one achieves diagnosis by means of a classifier.

Some issues related to *automated diagnosis* have to do with data that should be fed to the system, in order to obtain the output desired with an acceptable precision. When the set of input data is defined, there is the problem of handling incorrect or missing data, and what technique will be applied to diagnose the patient. Most works define the features they consider to be important for diagnosis but there aren't any rules or recommendations about which ones to consider. With respect to diagnosis techniques, works could implement machine learning, rule based systems and other analysis techniques. Also, once a diagnosis technique is selected, researchers must select a tool among the many existing to apply the technique.

2.2. Patient Monitoring Systems

For works dedicated to *monitoring* patients, we consider as relevant those that can detect emergency situations. One of them is [19], which detects two physiological disorders including hypertension and hypotension, by means of blood pressure and pulse rate sensors. For emergency detection makes use of a fuzzy inference system and its implementation is entirely based on object oriented paradigm. Another one is [12] which detects possible heart attacks via a portable ECG sensor, its implementation is based on object orientation and it uses a classifier (machine learning) to detect emergencies. Then there is [20], where the authors detect emergencies by using context information via sensors installed in patients' homes and physiological data, applying fuzzy logics to identify abnormal situations. Everything is stored in some data repository along with contextual information. Some like [21] only use a smartphone as sensing and processing unit. Its authors detect falling incidents and send a Multimedia Message (MMS) to notify about the incident, a falling event is captured via the built-in accelerometer the smartphone has. It performs a real time classification using SVM and the implementation is based on passive objects. In [16], however, authors use a smartphone to receive data from a wireless blood pressure monitor only and to transmit incoming data to a server for processing. It allows to notify medical personnel about emergency situations when detected. Emergencies are detected using conditional rules.

For works implemented using agent technology, we can mention [22], that

combines wireless sensors with data mining techniques and can detect emergency situations. In [23], no wireless sensors are used, instead it notifies about emergency situations based on user input. It aims at developing a generic framework for assisting patient-physician interaction. Another approach to monitor patients is to develop a generic framework like [24], which allows any number of sensors to be attached to the patient. It can detect abnormal situations using a knowledge Base (KB).

Automated monitoring, also presents some problems. Since this work considers *monitoring* by means of sensors, lack of connectivity between these sensors and the processing device is a severe error. It was mentioned earlier that emergencies or urgencies would hardly be detected, if the patient had to manually measure its blood pressure, but it is also impossible to notify about the detected emergency to clinicians, if there aren't internet or mobile networks available. Another problem is concerned with the privacy of patients. If wireless sensors are used to monitor the patient and these sensors send their readings to a mobile processing unit, signals from patient A could be sent to patient B's mobile processing unit. Also, a mechanism to allow access to health data only to the owner or his clinician must be implemented. One final issue is defining the kind of data sensors need to provide, in order to achieve a high level of confidence in the task of monitoring a hypertensive patient. In most works, privacy issues are handled by authenticating device's MAC address when using wireless sensors and username/password authentication when users want to input data or connect to a physician. In order to overcome connectivity issues, when there is need of connecting to geographically distant devices and no internet connection available, devices would use alternative connections such as SMSs or MMSs.

3. SOLUTION PROPOSAL

This work is based on proposals such as [10], [13] and [16], where the authors use sensors like ambulatory blood pressure monitor, heart rate, oxygen, ECG, among others and a mobile phone as the base station in charged of receiving sensor data and processing those incoming signals.

Our proposal aims at the design and development of a mobile pervasive healthcare system, to seamlessly monitor hypertensive patients and provide diagnosis support. In order to monitor patients, we use a wireless blood pressure monitor, a portable 3-leads ECG sensor and an activity tracker

device. The processing unit is an ordinary android-based smartphone. In Figure 2 we can observe a graphical description of our approach.

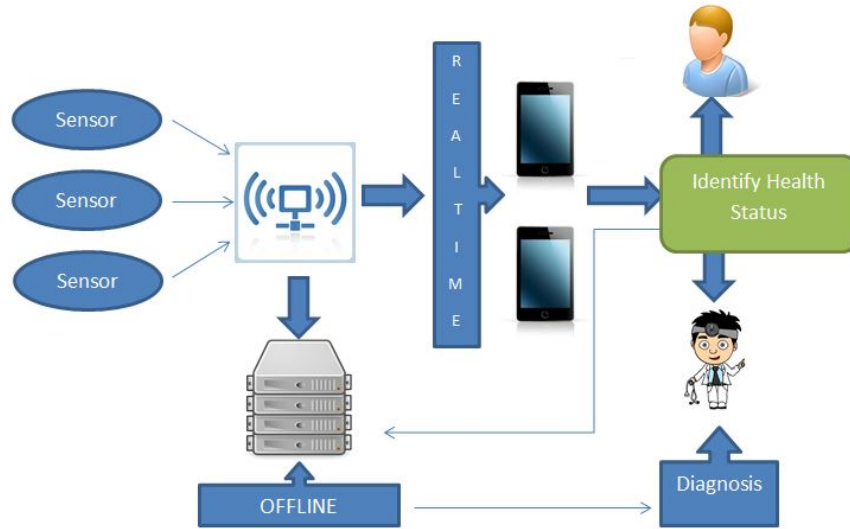


Figure 2: Graphical description of the proposed solution.

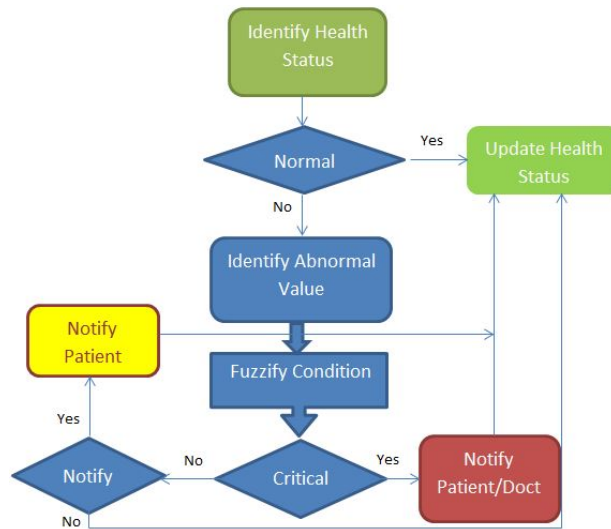


Figure 3: Analysis performed on data received from sensors.

The solution has the following behaviour. All three sensors connect to the smartphone using wireless connection and transmit the data they're sensing

to this mobile unit. The smartphone performs a real-time analysis to determine whether a patient's health status is normal or not, as shown in Figure 3. All data is submitted to a main server where sensed data is stored, labelling each record with the current health status. Real-time analysis allows to identify whether it is necessary to notify the patient, the doctor or both in case of abnormal situations, so that they can act accordingly.

The other part of the solution is related to processing stored information in the main server. We said earlier that no matter what the patient's health status is, it is stored in a central repository. This allows the system to support the clinicians in the diagnosis of hypertension. For such a task, we decided to use machine learning techniques by using *vowpal wabbit*¹¹, which is a tool implementing linear regression to achieve data classification. Besides diagnosing the disease, storing health data could be useful for further investigations in many areas and the patient has an overview of his/her blood pressure behaviour. Clinicians would also benefit from the available repository, since they have enough information to decide whether the treatment needs modifications or it should remain as currently is. Although we saw many works in *State of the art* section doing automated diagnosis, this solution proposes to include a new sensor, which is the activity tracker, allowing us to combine machine learning with partially *fuzzified* features.

The system proposed is designed using an Agent Oriented Software Engineering (AOSE) methodology which, we believe, allows a more intuitive approach because of the concept¹² based on the characteristics of agents [25] presents.

- *Reactivity*: intelligent agents has the capability to perceive their environment and respond in a timely fashion to changes in it in order to satisfy their design objectives.
- *Proactiveness*: intelligent agents are able to exhibit goal-directed behaviour by taking the initiative in order to satisfy their design objective.
- *Social ability*: intelligent agents are capable of interacting with other agents (and possibly humans) in order to satisfy their design objectives.

¹¹<http://hunch.net/~vw/>

¹²Wooldridge [25], states that an attempt to define an agent is as hard as trying to define intelligence, instead it is better to define the characteristics agents possess.

This solution requires cooperation among its components, thus it requires *social ability*. It demands *reactivity*, since components interacting with patients and doctors, need to immediately notify them when an emergency situation arises. Finally, it requires *proactivity*, to allow each component to be autonomous so that they can achieve their objectives. Therefore, it is not only naive to think of another paradigm that does not involve agents, but also counter-intuitive.

Since this is an area which hasn't been standardized yet (unlike object orientation), it is difficult to implement systems based entirely on agents. Therefore, this work is designed as one with agents as its main elements but implemented utilizing object orientation. These objects are structured to allow a multi-agent system to be built on top of them, almost in a straightforward manner, once this technology is standardized or more tools become available.

Our proposed solution tackles the problem of privacy and authentication using the device unique MAC address and prompting for username/password authentication whenever someone wants to access its health data. If a communication between the server and the smartphone isn't available due to lack of internet or mobile networks, SMSs are used to transmit the alert to server.

4. CONCLUDING REMARKS

This work has presented a solution proposal adding an extra feature for automated diagnosis, such as fuzzified user activity information. It uses machine learning techniques as some of the works mentioned in *state of the art* section, and deals with data validation to obtain reliable results following the pre-established rules approach found in some works. It is designed using an agent-oriented methodology and all of its components are structured to allow a straightforward multi-agent implementation. Issues regarding to monitoring are also taken into account, for example, an user needs to provide his username and password in order to access its own health record.

As future work is left the full implementation of the system and performing tests with patients. Those tests would allow to determine the efficiency of the system in assisting diagnosis and early detecting emergency situations. We also need to come up with a system providing user friendliness, so that users would not be reluctant to use it. Furthermore, the system needs to be robust enough when no internet connections are available.

ACKNOWLEDGMENTS: We thank Dr. Jose Ortellado for his support and all the information provided about hypertension in Paraguay.

References

- [1] Richard Lewanczuk, 2008. Hypertension as a Chronic Disease: What Can Be Done at a Regional Level?, Canadian Journal of Cardiology.
- [2] Joint National Committee, 2004. The Seventh Report of the Joint National Committee on Prevention, Detection, Evaluation, and Treatment of High Blood Pressure.
- [3] J. Berjon and F. Olaz, 1998. Diagnostico de la hipertension arterial, Anales del Sistema Sanitario de Navarra.
- [4] Eduardo Contreras and Sandra Ximena Zuluaga Martinez, 2010. Monitoreo Ambulatorio de Presion Arterial, Revista Mexicana de Cardiologia.
- [5] Das, S. and Ghosh, P.K. and Kar, S., 2013. Hypertension diagnosis: A comparative study using fuzzy expert system and neuro fuzzy system, 2013 IEEE International Conference on Fuzzy Systems.
- [6] Chao-Ton Su and Chien-Hsin Yang, 2008. Feature selection for the SVM: An application to hypertension diagnosis, Journal of Expert Systems with Applications.
- [7] Abdullah, A.A. and Zakaria, Z. and Mohamad, N.F., 2011. Design and Development of Fuzzy Expert System for Diagnosis of Hypertension, 2011 Second International Conference on Intelligent Systems, Modelling and Simulation.
- [8] Hsu, Kuang-Hung and Chiu, Chaochang and Chiu, Nan-Hsing and Lee, Po-Chi and Chiu, Wen-Ko, 2011. A Case-based Classifier for Hypertension Detection, Knowledge-Based Systems Journal.
- [9] Hanbay, Davut, 2009. An Expert System Based on Least Square Support Vector Machines for Diagnosis of the Valvular Heart Disease, Expert Systems with Applications Journal.

- [10] Fahim Sufi; Khalil, I., 2011. Diagnosis of Cardiovascular Abnormalities From Compressed ECG: A Data Mining-Based Approach, IEEE Transactions on Information Technology in Biomedicine.
- [11] Li, Qingshan and Zhang, Lihang and Chu, Hua, 2012. An AHP-Based Assessment Model for Clinical Diagnosis and Decision, Proceedings of the 4th International Conference on Artificial Intelligence and Computational Intelligence.
- [12] Joseph John Oresko, 2010. Portable Heart Attack Warning System by Monitoring the ST Segment via Smartphone Electrocardiogram Processing.
- [13] Luis J. Mena, Vanessa G. Felix, Rodolfo Ostos, et al., 2013. Mobile Personal Health System for Ambulatory Blood Pressure Monitoring, Computational and Mathematical Methods in Medicine, vol. 2013.
- [14] Dai Sheng-hui and Gui Ying and Zhu Xue Qin, 2008. Design of the Intelligent Real-Time Hypertensive Diagnosis Expert System Based on Web, Proceedings of International Symposiums on Information Processing.
- [15] Yupeng Zhang and Lee, M. and Gatton, T.M., 2009. Agent-Based Web Healthcare Systems for Real-Time Chronic Disease, Proceedings of World Conference on I-Services.
- [16] Alexander G. Logan and Warren J. McIsaac and Andras Tisler and M. Jane Irvine and Allison Saunders and Andrea Dunai and Carlos A. Rizo and Denice S. Feig and Melinda Hamill and Mathieu Trudel and Joseph A. Cafazzo, 2007. Mobile PhoneBased Remote Patient Monitoring System for Management of Hypertension in Diabetic Patients, American Journal of Hypertension, vol. 20.
- [17] Shibakali Gupta and Sripati Mukhopadhyay, 2012. Multi-Agent Based Clinical Diagnosis System: An Algorithmic Approach, International Journal of Engineering Research and Applications (IJERA).
- [18] Arus, C., Celda, B., Dasmahaptra, S. and Dupplaw, D., 2006. On the Design of a Web - Based Decision Support System for Brain Tumour Diagnosis Using Distributed Agents, Web Intelligence and Intelligent Agent Technology Workshops.

- [19] Baig, M.M. and GholamHosseini, H., 2013. A remote monitoring system with early diagnosis of hypertension and Hypotension, IEEE Point-of-Care Healthcare Technologies.
- [20] Copetti, A. and Loques, O. and Leite, J. C B and Barbosa, T.P.C. and da Nobrega, A.C.L., 2009. Intelligent Context-aware Monitoring of Hypertensive Patients, Proceedings of 3rd International Conference on Pervasive Computing Technologies for Healthcare.
- [21] Yi He, Ye Li, Chuan Yin, 2012. Falling-Incident Detection and Alarm by Smartphone with Multimedia Messaging Services, E-Health Telecommunication Systems and Networks Journal Vol. 1.
- [22] Mayuri Gund, Snehal Andhalkar and Prof. Dipti Patil, 2011. An Intelligent Architecture for Multi-agent Based m-Health Care System, International Journal of Computer Trends and Technology.
- [23] Chan, V. and Ray, P. and Parameswaran, N., 2008. Mobile E-health Monitoring: An Agent-based Approach, IET Journal.
- [24] Saleem, R.M. and Muhammad, A. and Martinez-Enriquez, A.M., 2010. Remote Patient Monitoring and Healthcare Management Using Multi-agent Based Architecture, Proceedings of Ninth Mexican Conference on Artificial Intelligence (MICAI).
- [25] Michael Wooldridge, 2009. An Introduction to MultiAgent Systems, book second edition.

CHIEM: A Centralized Health Information Exchange Model

Jesús M. Romero Riveros¹, Pablo J. López Estigarribia²,
Cynthia E. Villaba Cardozo, José L. Vázquez Noguera and Diego P. Pinto-Roa
Facultad Politécnica, Universidad Nacional de Asunción (FP-UNA)

Abstract

Electronic Health Records (EHR) contain information from health-care providers involved in a patient care. The common approach to achieve an interoperable EHR is the exchange of information between each provider by the implementation of message protocols. Traditional EHR systems are based on diverse standards, implementation languages, and information models. As consequence, EHR systems are fragmented and unable to exchange data. Data integration and interoperability are the major challenges faced by traditional EHR systems. Therefore, in this work we propose a Centralized Health Information Exchange Model (CHIEM). All healthcare providers would be able to obtain an updated and integrated EHR for a given patient by making a single request to a central system. The CHIEM architecture is cloud based, and the information model relies on archetypes that represent healthcare concepts from community defined minimum set of data (MSD). The main goal of the CHIEM is to provide a single point of request to healthcare providers, including those without an EHR system, that are interested in obtaining an integrated electronic health record of patients.

Keywords: EHR, information exchange, archetypes, cloud computing, minimum set of data, CHIEM.

1. INTRODUCTION

The technical and semantics heterogeneity among electronic health records (EHR) systems are barriers to data integration and interoperability in health-care environment. Data integration from different system sources demands a high grade of data interoperability. Most healthcare information systems persist data in proprietary formats [1].

¹jromero@pol.una.py

²pjlopez@pol.una.py

In this article, we propose a centralized interoperable architecture model named Central Health Information Exchange Model (CHIEM). Healthcare providers would be able to obtain an updated and integrated EHR for a given patient from a central system. The Central Health Information System (CHIES) is the central system in the CHIEM, it acts as an intermediary when gathering data related to a patient. The main goal of the CHIEM is to provide a single point of request to healthcare providers that are interested in obtaining an integrated electronic health record of some patient. With this approach, none of the provider should be concerned about compatibilities issues regarding heterogeneity of the EHR systems within the healthcare ecosystem.

In our proposed model, the problem is reduced to a single point communication between each EHR system and the CHIES. The model can be scalable in a long term by adapting new members to the current patient healthcare system in a transparent way. Shared information is standardized and stored in a central repository managed by the CHIES.

All standardized information stored in the CHIES central repository will be available to serve requests from all the healthcare providers. The central repository and the services provided by the CHIES are maintained in a cloud based infrastructure. This ensures availability and scalability of the system through the features offered by cloud computing. In this sense, the model is reliable with a single robust centralized architecture, rather than depending on the availability of multiple systems and services maintained by different institutions.

There are various works that treat this problem already [1, 5, 8, 10]. Our model contemplates a larger scope when considering healthcare centers without EHR systems, and bases data exchange in a standardized minimum set of data (MSD) defined in the healthcare community.

The rest of this article is organized as following. In section 2 we give a background related the proposed model. In section 3 the CHIEM is described in detail. In section 4 related works are discussed. Finally, conclusion and future works are presented in section 5.

2. BACKGROUND

In this section we will expose a background literature regarding the definition of our proposed model.

2.1. Cloud computing implication

One of the dominant paradigm in nowadays internet service is cloud computing. In [2] cloud computing is defined as a large pool of virtualized resources (hardware, development platforms and/or services). The key feature in cloud computing is that resources, such as hardware and software, can dynamically adapt their configuration based on traffic load basis. Cloud computing is often classified in three type of services: Software as a Service (SaaS), Platform as a Service (PaaS) and Infrastructure as a Service (IaaS) [2].

2.2. Information model: the two level approach

In OpenEHR standard, system implementation is unbound from the complexity of clinical information workflows and the semantic model within clinical domains. OpenEHR proposes a two level modeling approach. The first level is the information Reference Model (RM), and the second is the high level formal modeling of clinical content. Only the first level is implemented by software development [3], while the second level is achieved through definition of archetypes and templates.

Archetypes constitute an expression of semantic domains, independent of the technology, and used to guide the database schemes, software logic and GUIs definitions. Grouping archetypes conforms templates, which define particular workflows within a given institution [3]. The Reference Model defines data types and data structures to support archetypes.

2.3 Minimum Set of Data

There is a set of data considered necessary and common for users community across healthcare centers, thus standardization of this set is a priority [7]. This set is called Minimum Set of Data (MSD). The MSD is the core of health related data required by a determined group of common users, in our case, healthcare specialists. Each user group can extend or enhance the MSD according to their needs [7].

3. THE CENTRALIZED HEALTH INFORMATION EXCHANGE MODEL

The CHIEM architecture is composed by a central cloud service and multiple communication interfaces to exchange data with the involved EHR systems.

The CHIES is a central server in the cloud and has its own EHR repository (Figure 1). CHIES architecture relies on an IaaS service. IaaS provides

virtual computational resources and allows easy scalability by increasing resources as the demand of our system grows. With this cloud modality, system administrator will be able to manage each layer above the hardware infrastructure [2].

Data stored in the central repository is standardized, new EHR entries must be mapped to the CHIEM information model in order to be persisted. All services provided by CHIES are offered to the stakeholders through internet within a secure channel communication. Secure channel communication relies on HTTPS protocol. Services include interfaces to query and add information.

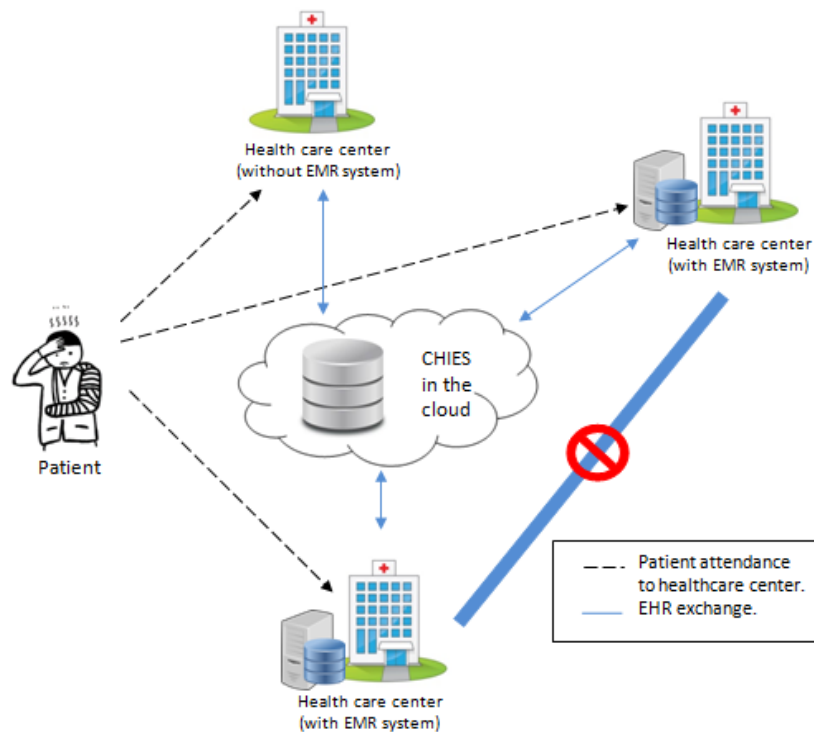


Figure 1 - CHIEM architecture based on star scheme.

Heterogeneity in EHR systems are due to the use of diverse standards, implementation languages and information models. Integration of a new member that may act as consumer/producer of information takes two steps:

1. Define the protocol to be used in the data exchange.

2. Implement CHIES interface to consume data.

In the first step, the data exchange protocol in each case should be defined. The CHIES needs to know and learn how to communicate with each EHR system. This will allow to consume data from the external EHR systems. Standardization of data to be stored in the central repository will be done in the CHIES. Moreover, when retrieving information from CHIES, EHR systems would be able to receive data in its local format.

The second step involves the implementation of the interface offered by CHIES to consume information. The services offered in CHIES to query data are generic, adapting the communication protocol according to the negotiation done with each EHR system in the first step.

Once these two requirements are met, external EHR systems would be able to start collaborating in the integration of the patients EHRs, and also consuming all EHR information stored in the central repository.

As seen in Figure 1, the CHIEM architecture is structured in a star scheme basis. CHIES is in the core of the star, and each healthcare EHR system acts as a node connected to the core.

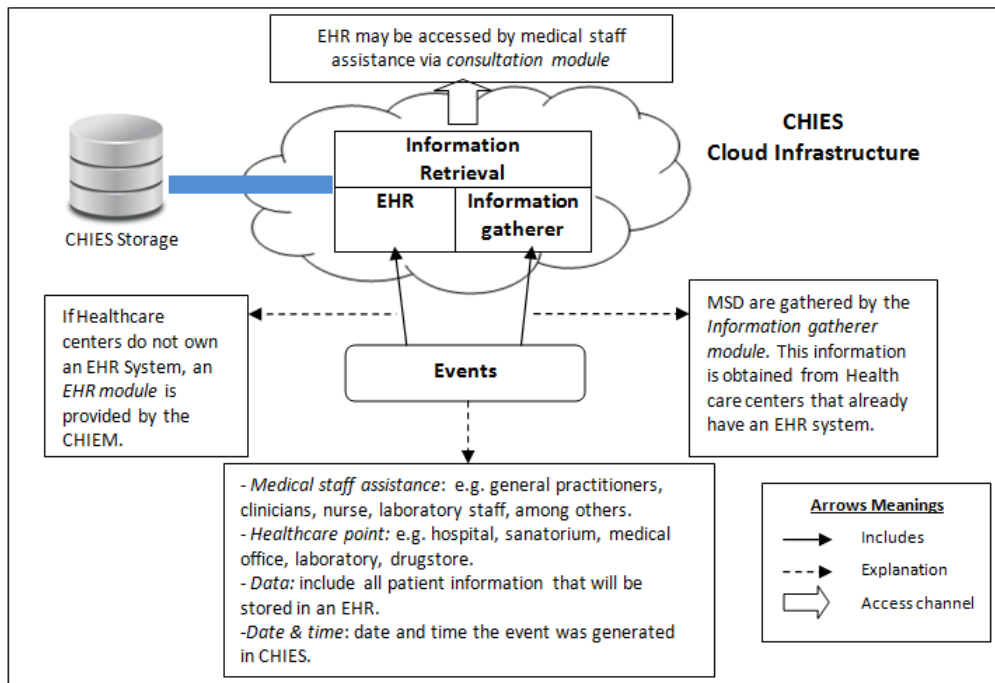


Figure 2 - CHIEM is based on event information basis.

The main advantage in this approach is that interoperability agreement among healthcare centers is not necessary. To exchange and consume patient data, just a communication channel to the central system is necessary, avoiding a peer-to-peer communication connection between each pair of healthcare centers.

An overview of the services offered in the proposed model is presented in Figure 2. The three main services are: information gatherer, retrieval and EHR. The *information gatherer* is a generic service to receive and standardize EHR data from external systems. The *retrieval* service is basically a set of REST web services that will allow external system to query data from the central repository (CHIES Storage). The *EHR* service is a web client module that allows integration of patients data from healthcare centers without an EHR system.

The proposed system is based on events. In this work we consider an event as a broad way of defining information within the CHIEM that is generated when a document needs to be stored in the central repository.

W4 [6] defines an event in terms of a four-tuple questions (who, where, what, when). Based on this approach, an event is composed by four general characteristics:

1. Author: can include to general practitioner, specialized clinicians, nurse, laboratory staff member, among others.
2. Healthcare point: may include a public or private hospital, laboratory, medical office, others.
3. Data: consists the main information to be stored in the central repository, associated with the created event. A variety of healthcare information may be held in an event. For instance, ambulatory care, clinical diagnosis, laboratory tests results, vital signs tests results are a some examples of healthcare information.
4. Date & Time: corresponds to the date and time the event was generated in CHIES.

3.1. CHIEM Modules

The CHIES core is divided in three main modules: information gatherer, information retrieval and EHR. Each of them is described below.

3.1.1. The information gatherer

The objective in this module is to gather patient information that is distributed across healthcare EHR systems. The actual scenario is that each EHR system has its own data representation and communication protocol. The CHIES consumes patients data that are based on the Minimum Set of Data (MSD) from each external system. To simplify integration of external sets of data we propose an Exchange Information Stack (see Figure 3). The Exchange Information Stack consist of five major layers. The first layer corresponds to source EHR systems. Source EHR systems are the external system running into different healthcare centers. These systems are generally a proprietary implementation with particular data representation and models [1].

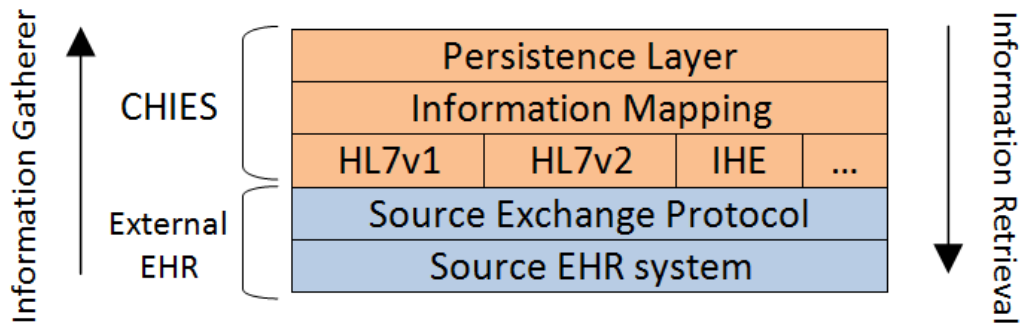


Figure 3 - Exchange information stack.

According to [11] EHR systems contemplate data exchange. Thus, it is assumed that a communication protocol is already implemented in these systems. There are many heterogeneous information models and exchange protocols that need to be integrated. The source exchange protocol layer corresponds to each external EHR implemented protocol. CHIES will be able to communicate with each protocol. A requirement to external EHR systems is that the set of data to be exchange should be aligned with the MSD established in the community. The first two layers in the exchange information stack corresponds to external EHR systems. The next three are related to the CHIES in our model.

The central system would be able to implement the necessary external protocols to communicate with each source EHR systems. This concept is illustrated in the third layer.

The main objective of the gatherer module is to integrate the recollected data. This is achieved in the *information mapping* layer. In order to obtain a repository with a homogeneous information model, integration must include standardization of data. We assume that external EHR systems to be integrated in our data scheme are adapted to the community definition of the MSD. It constitutes the basic information to be exchanged among all healthcare EHR systems. Although MSD definition may change in time, CHIEM will dynamically adapt to this changes by employing the *two level modeling* approach [3].

We base our information model in the OpenEHR standard [5]. Archetypes are defined to capture a set of data that conform healthcare concepts. Groups of archetypes are used to define more complex concepts or workflows. As the MSD varies in time, changes can be easily reflected in our model by simply modifying definitions in the archetypes. Archetypes and workflows are used to capture the semantic meaning of the stored data. None of the logic or implemented software to store data should be affected by this changes. The lower level in the two level approach is called the Reference Model (RM) and constitute the support to map the concepts within archetypes to the storage in a generic way.

Data integration is composed of three process: conformance of the MSD within each healthcare EHR system, mapping of each concept within the MSD to the archetypes and, finally, storage of archetyped concepts through the reference model (RM). This last process is performed in the *persistence* layer.

3.1.2. Information Retrieval

The *information retrieval* module purpose is to provide access to the full set of patients EHR gathered from external sources and stored in the CHIES. External EHR systems can obtain the integrated EHR of a patient by performing a single request to the CHIES information retrieval service.

The process for retrieving data from the CHIES is based in the exchange information stack (see Figure 3) in up-to-bottom direction. First of all, data is extracted from the persistence layer in the CHIES according to the request from the external EHR system. Then, the information mapping layer matches the CHIES data format to the external format and performs data exchange according to the protocol used by the external system. Finally, the response is receive in the source EHR system.

Retrieval information services will be offered via REST, URIs and HTTPS.

We will base our REST approach in the querying mechanism proposed in [9]. In [9] openEHR Reference Model objects stored in the central repository are available as resources identified by URIs. URI templates can be used to specify URI structures with variable parts as in:

https://ehr.chies/ehr:{ehr_id}/{object_id}@{version}

These paths extracted from archetypes are the basis for queries into the data. Archetype Query Language (AQL) is a declarative query language developed specifically for expressing queries for retrieving clinical data found in archetype-based EHRs. Syntax is independent of applications, programming languages, system environment, and storage models. To perform queries is necessary to first translate the clinically targeted Archetype Query Language (AQL-queries) to native storage targeted query languages (such as SQL or XQuery). Just after this, the query can be executed natively in the database. Responses are converted to the different external EHR systems representations. To enhance availability and response time, healthcare EHR systems could make a local copy of the CHIES registers, or set a cache between the CHIES and their EHR system.

3.1.3. EHR module. Cloud computing as SaaS for healthcare centers

The EHR module aims to accomplish the delivery of an EHR system service for those healthcare centers that currently do not own one, or would like to move from its current system to our service. The EHR module will be offered as a cloud computing Software as a Service (SaaS) modality. The service run entirely in the cloud, just a regular internet connection and a capable device with a internet browser would be needed to access it. New instances of the EHR module will be created for each new healthcare center client. Each healthcare center client will be able to define its own workflow by grouping available archetypes.

With the SaaS modality, healthcare centers will have an EHR system at disposal. Hence, installing a large IT infrastructure to implant this system will not be necessary for them. This will allow big savings not just in IT equipment, but also in trained employee required for the datacenter management and maintaining. Another advantage of SaaS is the shorter time to deploy the system to production. Instead of acquiring, installing and configuring an own technological infrastructure, with the cloud approach just a few steps configuration will be required to deploy the system. The SaaS

modality will facilitate the spread of EHR systems to healthcare centers that are isolated or have economic resources limitations [1, 5].

With the EHR module, data collected in these healthcare centers will already be in the standardized information model. Therefore, the mapping process is not needed. Data will be in the corresponding archetyped format, ready to be stored in the central repository through the *reference model*. The EHR web client will also implement the retrieval service interface. Thus clients are going to be able to query patients records stored in the central repository.

4. RELATED WORKS

In this section we will discuss some of the related works and proposals that pursue integrating health information of patients. A system called Lifelong Personal Health Record (LLPHR) is described in [8]. In LLPHR, clinical records are gathered through logical links to records stored in each healthcare system. The LLPHR system works as an index to obtain the distributed records across healthcare facilities in the region associated to the system. In LLPHR there is a strong dependency on external systems. Integrated EHR is accomplished by gathering the EHR pieces from each external EHR system at request time. When health professionals request to a single patients health history record via a local system in a hospital, a single request is sent to the LLPHR server. This server responds with a list of the patient EHRs links. Then, individual request are sent to each healthcare system in order to obtain the global patient EHR result. LLPHR relies directly on each healthcare system, which endanger availability. Besides, not every healthcare center will probably own an EHR system in order to share their data. CHIES tackles this issues by centralizing patient EHRs in a single robust scalable server and providing an EHR module for healthcare centers that lack an EHR system.

CHISTAR [1] is another proposed system to integrate EHR. This proposal also implements the two level approach and applies a cloud based architecture. This system uses a semantic matching to receive data from external systems [1]. Received data is not backed by any defined set of data within the community (a MSD). In CHISTAR there is not a consideration within its integration engine for potential healthcare centers that may also contribute to the patient clinical history but do not own an IT infrastructure to mount an own EHR system. We offer this feature through SaaS EHR module web client for the mentioned entities.

Other related works are discussed next. In [10] the authors propose the use of archetypes to build a semantically rich Virtual Health Records (VHR) for Clinical Decision Support (CDSS). The work in [4] demonstrates the feasibility of Semantic Web technologies for enabling interoperability between different healthcare providers, aggregating data from multiple resources and providing a medical decision support service. In [5] the author shows how an openEHR architecture based EHR system can be introduced in practical terms and how this could lead to interoperability within a emergency department. Moreover, [2] discusses the concept of *cloud computing*, and evaluates the opportunities and challenges of this computing model in the improvement of the healthcare services. Our proposal consists of a two level modeling approach with a cloud based architecture to integrate patients EHR from heterogeneous EHR systems. Moreover, our model also considers the integration of data from healthcare centers that currently do not have IT infrastructure to implement an EHR system. The exchange data is based on the MSD defined by the community.

5. CONCLUSION AND FUTURE WORKS

Interoperability of healthcare system has become a challenge to nowadays health informatics. To overcome this issue we proposed a centralized health information model. Combination of cloud computing paradigm, two level model proposed by OpenEHR and the support of community defined minimum set of data, allow the creation of a generic and scalable framework. Integration of EHR can be accomplished through a strong effort in facilitate the interoperability among external EHR systems with the centralized health information system. Our model adapts to external systems protocols and propose an EHR system module via SaaS to include patients data from healthcare centers that do not own the necessary IT equipment to mount an EHR system. Future works include a module of Personal Health Record (PHR) to allow patients to access their health record, manage privacy politics and upload of information regarding their health (e.g. blood pressure measures, weight check, among others). Privacy policies regarding patients data should be defined by patients themselves. Hence mechanism that allows patients to do it without being an overwhelming task should be investigated. Moreover, security mechanism to preserve integrity and privacy of stored data should be defined.

References

- [1] Bahga, Arshdeep, and Vijay K. Madiseti, 2013. A Cloud-Based Approach to Interoperable EHRs.
- [2] Kuo, Alex Mu-Hsing, 2011. Opportunities and challenges of cloud computing to improve healthcare services. *Journal of medical Internet research* 13.3.
- [3] Ocean Informatics, 2007. OpenEHR Release 1.0.1. Architecture Overview.
- [4] De Potter, Pieterjan, et al., 2012. Semantic patient information aggregation and medicinal decision support. *Computer methods and programs in biomedicine*.
- [5] Gok, Murat, 2008. Introducing an openEHR-based electronic health record system in a hospital. Diss. Master thesis, University of Goettingen.
- [6] Castelli, Gabriella, et al., 2009. Extracting high-level information from location data: the W4 diary example. *Mobile Networks and Applications* 14.1: 107-119.
- [7] Carrillo, Esteban, et al., 1991. Conjuntos mnimos de datos en la atencin ambulatoria. *Gaceta Sanitaria* 5.26.
- [8] F. Barbarito, et al., 2013. Implementing the life long personal health record in a regionalised health information system: The case of Lombardy, Italy, *Comput. Biol. Med.*
- [9] Sundvall, Erik, et al., 2013. Applying representational state transfer (REST) architecture to archetype-based electronic health record systems. *BMC medical informatics and decision making* 13.1.
- [10] Marcos, Mar, et al., 2013. Interoperability of clinical decision-support systems and electronic health records using archetypes: a case study in clinical trial eligibility. *Journal of biomedical informatics* 46.4.
- [11] Hyrinen, Kristiina, et al., 2008. Definition, structure, content, use and impacts of electronic health records: a review of the research literature. *International journal of medical informatics* 77.5.

A Novel Pulse Width Modulation Algorithm Based on Time Space Model

Jose A. Riveros^{a1}

^aFacultad Politecnica, Universidad Nacional de Asuncion, Paraguay

Abstract

Modulation of voltage source inverters is commonly performed using pulse width modulation (PWM) strategies. Actually, the methods widely studied and applied in the industry are derived from carrier-based or space vector schemes. Nevertheless, the development of new techniques is always a challenge in this subject. This paper introduces a new PWM algorithm for two-level three-phase variable-speed drives based on a time space approach. The duty times of the inverter legs are computed in a straightforward manner by the selection of one parameter and without the use of voltage space vector composition. Simulations results are given to demonstrate the viability of this proposal. The new technique is assessed and configured to replicate space vector schemes.

Keywords: Pulse width modulation, power electronics, three-phase drives.

1. INTRODUCTION

Control of power electronics converters has been drawn the attention of researchers, allowing the development of many device and applications such as electric vehicles, smart grids and the integration of renewable energy sources. The architecture of many high-performance AC controllers aimed to regulate either power, speed, or harmonic content requires the implementation of a modulator, which is controlled by appropriate algorithms. The main objective of this technique is to generate a pulse patterns with average-volt-second fundamental frequency component equal to an AC reference voltage. This target must be done minimising the distortion due mainly to large low-order voltage harmonics [1]. The study and development of new modulation algorithms is an interesting topic for the design of high-performance and robust AC drives [2, 3].

¹E-mail Corresponding Author: jriveros@pol.una.py

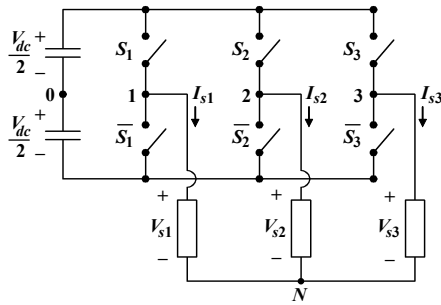


Figure 1: Schematic diagram of the two-level three-phase VSI.

The modulation methods are commonly based on pulse width modulation (PWM), which is the most utilised strategy for the control of voltage source inverters (VSIs) [1]. Carrier-based PWM (CBPWM) and space vector PWM (SVPWM) are the two schemes widely studied and applied in the industry [4]. The CBPWM structure is simple and its implementation is easy, whereas SVPWM provides better insight into the properties of three-phase drives operation at the expense of more complex algorithms [5]. New modulation strategies recently developed are limited to these two techniques applying adaptations to improve some of the performance parameters or including additional criteria [2].

This paper presents a new PWM algorithm. The technique utilises the vectorial reference voltage components to calculate the duty times of the three-phase inverter legs based on a time space model. The main contribution of this work is the development of a flexible modulation scheme that can easily operate either in continuous or discontinuous modes applying only an appropriate parameter. The paper is organised as follows. First, the model of three-phase drive is described in section 2. Then, section 3 derives the new PWM algorithm. Simulation results and comparison between the developed technique and the SVPWM are illustrated and discussed in section 4. Finally, the conclusions are summarised in the last section.

2. OVERVIEW OF THREE-PHASE DRIVES

The system under study is the two-level three-phase drive (see Fig. 1). The VSI is fed from a dc-bus with a voltage represented by V_{dc} . The phase voltages and currents are designated by V_{sk} and I_{sk} , respectively, being $k=\{1, 2, 3\}$. This topology is composed by two power switches

per leg, symbolised by S_k , and at every time only one of them must be activated (complementary switching states). These constraints allow the use of $2^3=8$ switching combinations that can be represented by a binary vector $[S_1; S_2; S_3]$ with $S_k \in \{0, 1\}$. If $S_k=1$, the upper power switch of the k -leg is ON (lower switch OFF); while the opposite case takes place when $S_k=0$ (upper switch OFF and lower switch ON). For the sake of simplicity, the effects of dead, rising and fall times are neglected in this analysis. The phase voltage set can be calculated from the switching function by means of the following matrix equation [1]:

$$\begin{bmatrix} V_{s1} \\ V_{s2} \\ V_{s3} \end{bmatrix} = \frac{V_{dc}}{3} \begin{bmatrix} 2 & -1 & -1 \\ -1 & 2 & -1 \\ -1 & -1 & 2 \end{bmatrix} \begin{bmatrix} S_1 \\ S_2 \\ S_3 \end{bmatrix} \quad (1)$$

Switching functions $[0 \ 0 \ 0]$ and $[1 \ 1 \ 1]$ synthesise null phase voltage, while combinations of $\pm V_{dc}/3$ and $\pm 2V_{dc}/3$ are achieved with the remaining switching states. The VSI model can be also represented in another orthogonal reference system using the space vector theory [1]. Then, the new three-dimensional space is characterised by the projections in one plane, namely α - β , and the z -axis using a magnitude invariant transformation depicted in equation (2), where $C_\vartheta=\cos(\vartheta)$, $S_\vartheta=\sin(\vartheta)$ and $\vartheta=2\pi/3$.

$$\begin{bmatrix} V_{s\alpha} \\ V_{s\beta} \\ V_{sz} \end{bmatrix} = \frac{2}{3} \begin{bmatrix} 1 & C_\vartheta & C_\vartheta \\ 0 & S_\vartheta & -S_\vartheta \\ 1/2 & 1/2 & 1/2 \end{bmatrix} \begin{bmatrix} V_{s1} \\ V_{s2} \\ V_{s3} \end{bmatrix} \quad (2)$$

The fundamental frequency component engages the α - β subspace, whereas the zero-sequence voltage (homopolar) is projected onto the z -axis. As result of the transformation, two zero and six different active (magnitude equal to $2V_{dc}/3$) voltage space vectors are obtained [1].

The vector components can be also computed from the switching states combining equations (1) and (2). The simplified result is detailed in the equation (3), where v_{sj} is the normalised voltage respect to $V_{dc}/2$, $v_{sj}=V_{sj}/(V_{dc}/2)$. Notice that the last row is zero because the voltage has been modelled respect to the common point. The same result is attained applying the switching states in equation (2) and it is omitted hereinafter.

$$\begin{bmatrix} v_{s\alpha} \\ v_{s\beta} \\ v_{sz} \end{bmatrix} = \frac{4}{3} \begin{bmatrix} 1 & C_\vartheta & C_\vartheta \\ 0 & S_\vartheta & -S_\vartheta \\ 0 & 0 & 0 \end{bmatrix} \begin{bmatrix} S_1 \\ S_2 \\ S_3 \end{bmatrix} \quad (3)$$

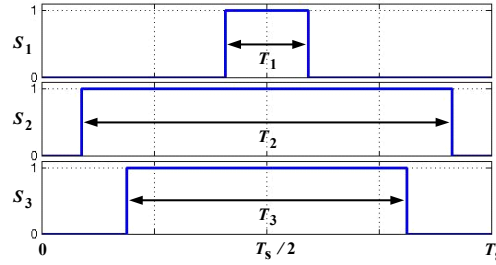


Figure 2: Symmetrical double-edge switching pattern of three-phase PWM modulation during one sampling period.

3. PWM ALGORITHM BASED ON TIME SPACE MODEL

In this paper, double-edge switching pattern (see Fig. 2) and linear modulation region are considered. The objective of modulation algorithms is to synthesise an average-volt-second fundamental frequency component equal to an AC reference voltage with the minimum low-order voltage harmonics (distortion). This is achieved using PWM techniques, which are based on the application of appropriate duty cycles T_k ($0 \geq T_k \leq T_s$) at every sampling period (T_s).

In agreement with the modulation target, during the T_s period, the average voltage value must be equal to its reference. Applying this assumption in equation (3) together with the switching pattern and being $v_{s\alpha}^*$ and $v_{s\beta}^*$ the normalised reference voltages in the α - and β -axis, respectively, the modulation law is derived in the following equation:

$$\int_0^{T_s} \begin{bmatrix} v_{s\alpha} \\ v_{s\beta} \end{bmatrix} dt = \frac{4}{3} \begin{bmatrix} 1 & C_\vartheta & C_\vartheta \\ 0 & S_\vartheta & -S_\vartheta \end{bmatrix} \int_0^{T_s} \begin{bmatrix} S_1 \\ S_2 \\ S_3 \end{bmatrix} dt \quad (4)$$

$$\begin{bmatrix} v_{s\alpha}^* \\ v_{s\beta}^* \end{bmatrix} T_s = \frac{4}{3} \begin{bmatrix} 1 & C_\vartheta & C_\vartheta \\ 0 & S_\vartheta & -S_\vartheta \end{bmatrix} \begin{bmatrix} T_1 \\ T_2 \\ T_3 \end{bmatrix}$$

The duty times T_k can be also normalised respect to T_s ($t_k = T_k/T_s$). The simplified modulation law is displayed in the equation (5).

$$\begin{bmatrix} v_{s\alpha}^* \\ v_{s\beta}^* \end{bmatrix} = \frac{4}{3} \begin{bmatrix} 1 & C_\vartheta & C_\vartheta \\ 0 & S_\vartheta & -S_\vartheta \end{bmatrix} \begin{bmatrix} t_1 \\ t_2 \\ t_3 \end{bmatrix} \quad (5)$$

The resulting system of linear equations has infinite number of solutions, but only some of them are feasible for the modulation problem. The equations and time restrictions are summarised in the following set of equations:

$$\begin{aligned}
 \pi_1 : v_{s\alpha}^* &= \frac{4}{3}(t_1 + C_\vartheta \cdot t_2 + C_\vartheta \cdot t_3) \\
 \pi_2 : v_{s\beta}^* &= \frac{4}{3}(S_\vartheta \cdot t_2 - S_\vartheta \cdot t_3) \\
 R_1 : 0 &\leq t_1 \leq 1 \\
 R_2 : 0 &\leq t_2 \leq 1 \\
 R_3 : 0 &\leq t_3 \leq 1
 \end{aligned} \tag{6}$$

The modulation problem, equation (6), is schematised in the Fig. 3 using a three-dimensional time reference frame defined by the axes t_1 , t_2 and t_3 . The restrictions R_1 , R_2 and R_3 enclose a cube (blue lines) with side length equal to 1 and placed in the first octant. The planes π_1 and π_2 are perpendicular. Furthermore, plane π_2 ($\varphi = \pi/4$ respect to t_1 - t_2 plane) is parallel to t_1 -axis and it cuts the cube in a rectangle (shadowed shape). The line r is the intersection between π_1 and π_2 planes. Moreover, r is the locus of times vectors $[t_1 \ t_2 \ t_3]$ that synthesise simultaneously the reference voltages $v_{s\alpha}^*$ and $v_{s\beta}^*$. This line also intersects the rectangle in some points which are the set of achievable solutions. Finally, the modulation problem can be simplified and modelled as a two-dimensional line. The next step is the identification of this set of solutions. It is remarkable that this model encompasses all the similar modulation techniques such as CBPWM and SVPWM.

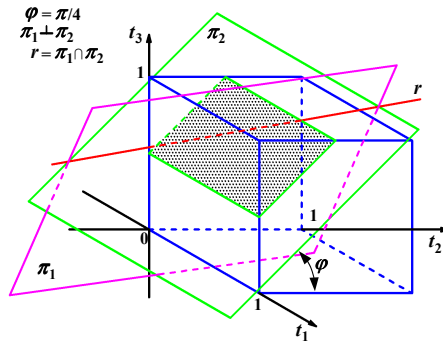


Figure 3: Scheme of the modulation problem in the time space.

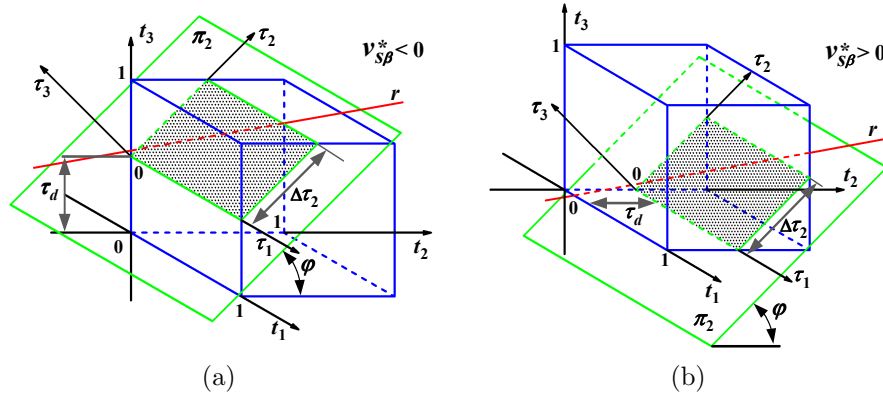


Figure 4: New reference frame τ_1 - τ_2 - τ_3 proposed in this work and possible location of the line and plane. (a) Case $v_{s\beta}^* < 0$. (b) Case $v_{s\beta}^* > 0$.

A new reference frame τ_1 - τ_2 - τ_3 is proposed in this work. The location of these axes is shown in Fig. 4. The transformation proposed (rotation plus displacement) depend on the $v_{s\beta}^*$ reference voltage sign. The two possible cases, $v_{s\beta}^* < 0$ and $v_{s\beta}^* > 0$, are illustrated in Fig. 4a and 4b, respectively. The distance between τ_1 -axis and its nearest rectangle side is represented by τ_d and it is calculated from plane π_2 equation as follow:

$$\tau_d = \frac{3|v_{s\beta}^*|}{4S_\varphi} = \frac{\sqrt{3}}{2}|v_{s\beta}^*| \quad (7)$$

Then, the developed transformations between the time reference frames according with the case (both are applicable when $v_{s\beta}^* = 0$) are defined in the next equations:

Case: $v_{s\beta}^* < 0$

Case: $v_{s\beta}^* > 0$

$$\begin{bmatrix} t_1 \\ t_2 \\ t_3 - \tau_d \end{bmatrix} = \begin{bmatrix} 1 & 0 & 0 \\ 0 & C_\varphi & -S_\varphi \\ 0 & S_\varphi & C_\varphi \end{bmatrix} \begin{bmatrix} \tau_1 \\ \tau_2 \\ \tau_3 \end{bmatrix} \quad (8)$$

$$\begin{bmatrix} t_1 \\ t_2 - \tau_d \\ t_3 \end{bmatrix} = \begin{bmatrix} 1 & 0 & 0 \\ 0 & C_\varphi & -S_\varphi \\ 0 & S_\varphi & C_\varphi \end{bmatrix} \begin{bmatrix} \tau_1 \\ \tau_2 \\ \tau_3 \end{bmatrix} \quad (9)$$

Being $C_\varphi = \cos(\varphi)$ and $S_\varphi = \sin(\varphi)$. After the application of the transformation (8) or (9), the resulting line equation is the same and it is detailed below.

$$\begin{aligned} r : v^* &= \tau_1 - C_\varphi \cdot \tau_2 \\ 0 &\leq \tau_1 \leq 1 \\ 0 &\leq \tau_2 \leq \Delta\tau_2 \end{aligned} \quad (10)$$

where, the following definitions have been used:

$$v^* = \frac{3}{4}(v_{s\alpha}^* - \frac{4}{3}C_{\vartheta}\tau_d) = \frac{3}{4}(v_{s\alpha}^* + \frac{2}{3}\tau_d) \quad (11)$$

$$\Delta\tau_2 = \frac{(1 - \tau_d)}{S_{\varphi}} = \frac{(1 - \tau_d)}{C_{\varphi}} = \sqrt{2} \cdot (1 - \tau_d)$$

It is important to highlight that only reference voltage is required to build the line r in the new subspace. Figure 5a depicts the two-dimensional resulting line and reference frame after the transformation. The line slope is always the same, while the position into the τ_1 - τ_2 plane is variable and it is defined by the pseudo-reference voltage v^* as is shown in Fig. 5b. Additionally, the domain of variable τ_2 depends on the value of $\Delta\tau_2 = f(\tau_d)$ and it makes complex the analysis. This difficulty has been overcome using the parametric equation. The line r can be defined by means of $P_1(\tau_{11}; \tau_{12})$ and $P_2(\tau_{21}; \tau_{22})$ points, see Fig. 5a, using the following relation:

$$\frac{\tau_2 - \tau_{12}}{\tau_{22} - \tau_{12}} = \frac{\tau_1 - \tau_{11}}{\tau_{21} - \tau_{11}} = \lambda \quad (12)$$

$$\frac{\tau_2 - \tau_{12}}{b} = \frac{\tau_1 - \tau_{11}}{a} = \lambda$$

From this last equation the parametric line is defined as follow:

$$\tau_1 = \tau_{11} + a \cdot \lambda$$

$$\tau_2 = \tau_{12} + b \cdot \lambda \quad (13)$$

$$\lambda \in [0, 1]$$

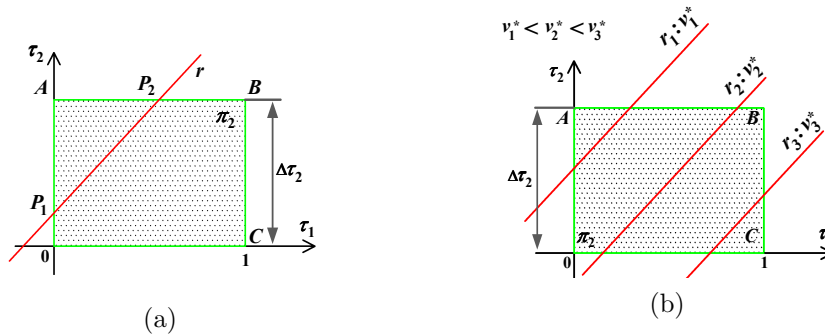


Figure 5: Line in the τ_1 - τ_2 plane. (a) Scheme of the line and its intersection. (b) Position of the line r for different values of pseudo-reference voltage v^* .

Table 1: Parametric line (13) for the different positions into τ_1 - τ_2 plane.

Position			
Range of v^*	$-(1 - \tau_d) \leq v^* \leq 0$	$0 \leq v^* \leq \tau_d$	$\tau_d \leq v^* \leq 1$
Points	$P_1(\tau_{11}; \tau_{12}) \equiv P_1(0; \tau_{12})$ $P_2(\tau_{21}; \tau_{22}) \equiv P_2(\tau_{21}; \Delta\tau_2)$	$P_1(\tau_{11}; \tau_{12}) \equiv P_1(\tau_{11}; 0)$ $P_2(\tau_{21}; \tau_{22}) \equiv P_2(\tau_{21}; \Delta\tau_2)$	$P_1(\tau_{11}; \tau_{12}) \equiv P_1(\tau_{11}; 0)$ $P_2(\tau_{21}; \tau_{22}) \equiv P_2(1; \tau_{22})$
Coordinates Eq. (10)	$P_1 : v^* = 0 - C_\varphi \cdot \tau_{12}$ $\tau_{12} = -v^*/C_\varphi$ $P_2 : v^* = \tau_{21} - C_\varphi \cdot \Delta\tau_2$ $\tau_{21} = v^* + C_\varphi \cdot \Delta\tau_2$	$P_1 : v^* = \tau_{11} - C_\varphi \cdot 0$ $\tau_{11} = v^*$ $P_2 : v^* = \tau_{21} - C_\varphi \cdot \Delta\tau_2$ $\tau_{21} = v^* + C_\varphi \cdot \Delta\tau_2$	$P_1 : v^* = \tau_{11} - C_\varphi \cdot 0$ $\tau_{11} = v^*$ $P_2 : v^* = 1 - C_\varphi \cdot \tau_{22}$ $\tau_{22} = (1 - v^*)/C_\varphi$
Coefficients	$a = v^* + C_\varphi \cdot \Delta\tau_2$ $b = \Delta\tau_2 + v^*/C_\varphi$	$a = C_\varphi \cdot \Delta\tau_2$ $b = \Delta\tau_2$	$a = 1 - v^*$ $b = (1 - v^*)/C_\varphi$

The parameter λ defines τ_1 and τ_2 for a given reference voltage. These times together with $\tau_3=0$ are applied in transformation (8) or (9) to obtain $[t_1 \ t_2 \ t_3]$. Then, the method relies on the proper selection of λ . The remaining variables of equation (13) depend on the value of v^* . Table 1 summarises the three possible cases with P_1 , P_2 and the coefficients a and b .

The developed PWM algorithm can be summarised by means of the following pseudocode:

```

For every sampling period  $T_s$  :
    Read the reference voltages  $v_{s\alpha}^*$  and  $v_{s\beta}^*$ ;
    Calculate  $\tau_d$ ,  $\Delta\tau_2$  and  $v^*$ ;
    Select the value of  $\lambda$ ;
    Calculate  $\tau_1$  and  $\tau_2$  using  $\lambda$ , equation (13) and Table 1;
    Calculate  $t_1$ ,  $t_2$  and  $t_3$  using transformation (8) or (9);
    Apply the duty times within next  $T_s$  period;
End for
    
```

In this work, the selection of λ is aimed to reproduce the continuous and discontinuous methods based on space vector approach. The proposed algorithm provides flexibility and this task can be done according with the modulation index in order to obtain the minimal distortion for a certain sampling frequency during the VSI operation [1].

Table 2: SVPWM strategies achievable with different values of λ .

λ	PWM Technique
0.5	SVPWM
0	DPWM-MIN
1	DPWM-MAX

The SVPWM techniques can be either continuous (switching pattern like the presented in Fig. 2) or discontinuous (one of the inverter legs does not switch during a sampling period). According with the value of λ used, the introduced algorithm can operate as conventional SVPWM or discontinuous methods (DPWM-MIN or DPWM-MAX) described in [1]. The pair between PWM techniques and λ values are summarised in Table 2. The traditional SVPWM is replicated using $\lambda=0.5$, while discontinuous DPWM-MIN and DPWM-MAX are reproduced with λ equal to 0 and 1, respectively. These properties confirm the flexibility of the new PWM method.

Another interesting property of modulation algorithms is the utilisation of the dc-bus [6] that can be measured with the modulation index m defined as the normalised magnitude of the reference voltage respect to $V_{dc}/2$. For instance, the SVPWM allows a maximum $m=2/\sqrt{3}=1.1547$ (15% of overmodulation). The maximum values of reference voltage achievable in the τ_1 - τ_2 by the proposed algorithm are obtained when the line r passes through the vertexes A or C , see Fig. 5. Considering the case of vertex C ($v^*=1$) and combining equations (11) and (7) the following result is obtained:

$$v^* = \frac{3}{4} \left(v_{s\alpha}^* + \frac{2}{3}\tau_d \right) = 1 \quad (14)$$

$$v_{s\alpha}^* \pm \frac{\sqrt{3}}{3}v_{s\beta}^* = \frac{4}{3}$$

Furthermore, being the reference voltage in the α - β plane defined as follow:

$$\begin{aligned} v_{s\alpha}^* &= m \cdot \cos(\omega t) \\ v_{s\beta}^* &= m \cdot \sin(\omega t) \end{aligned} \quad (15)$$

where ω is the fundamental angular frequency and t is the time variable. Then, combining equations (14), (15) and applying optimisation procedures yields a maximum modulation index $m = 2/\sqrt{3}$. Same result is accomplished

employing this analysis in the vertex A , $v^* = -(1 - \tau_d)$. Finally, the proposal achieves exactly the same dc-bus utilisation than SVPWM, which is the limit for two-level converters [6].

4. RESULTS

The presented PWM algorithm has been implemented in the Matlab environment and simulation results have been conducted to demonstrate the properties of the technique. The parameters utilised during this evaluation are shown in Table 3. The tests depict the phase voltage v_{s1} , phase voltage spectrum, duty times and switching pattern obtained. Fast Fourier Transformer (FFT) algorithm tuned to the fundamental frequency has been used to measure the phase voltage spectrum.

Figure 6 illustrates the results. The reference voltage has been fixed, while the values of λ described in Table 2 have been used. In all the cases, the algorithm shows good tracking between the instantaneous and the reference voltage values, see Fig. 6(a). The duty times applied to the leg S_1 are shown in Fig. 6(b). Notice that discontinuous methods do not switch during 1/3 of the fundamental period. Figure 6(c) depicts the resulting spectrum, which is exactly the same reported in [1] for each method as it is expected. Low-order harmonics are not synthesised and only carrier frequency along with its sideband are generated. The switching pattern resulting, Fig. 6(d), displays the continuous and discontinuous forms. Conventional SVPWM is replicated with a simpler algorithm when $\lambda=0.5$. In the DPWM-MIN, during every sampling period, one of the inverter legs is locked to the lower dc rail, $\lambda=0$. The opposite case (one leg is locked to the positive rail of the dc-bus at every T_s period) corresponds to the DPWM-MAX, which is obtained for $\lambda=1$. Other discontinuous techniques are combination of DPWM-MIN and DPWM-MAX according with reference voltage and they can also be easily replicated with the proposed PWM scheme.

Table 3: Simulation parameters.

Parameter	Unit	Value
Fundamental Frequency (f)	Hz	50
Sampling Period (T_s)	ms	0.5
Simulation step	μ s	1
Modulation Index (m)		1.1547

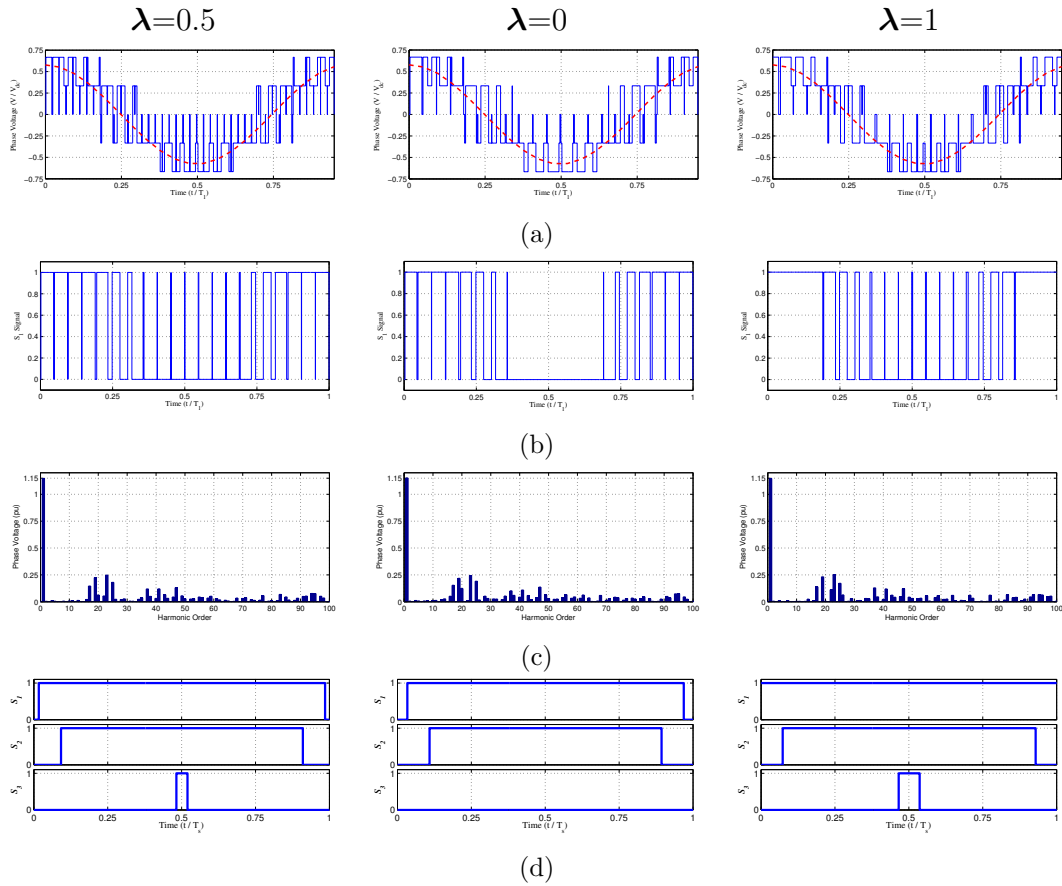


Figure 6: Simulation Results for values of λ equal to 0.5 (SVPWM), 0 (DPWM-MIN) and 1 (DPWM-MAX). (a) Reference (dashed line) and instantaneous (continuous line) phase voltage v_{s1} . (b) Duty times of S_1 leg for a fundamental period. (c) Frequency spectrum of v_{s1} phase voltage. (d) Switching pattern during one sampling period.

5. CONCLUSIONS

A new PWM algorithm had been developed in this paper. The introduced method is based on a time space model and it operates as space vector technique either in continuous or discontinuous modes by the application of an appropriate parameter. This property allows the development of a new flexible scheme to obtain minimum distortion at a certain switching frequency. Simulation results have demonstrated the

viability of this proposal. The new method shows good potential to be applied in high-performance control schemes and to be extended to other topologies of power converters such as multilevel and multiphase drives.

ACKNOWLEDGMENTS: The author gratefully acknowledge the Facultad Politecnica of the Universidad Nacional de Asuncion, Paraguay, for the financial support provided.

References

- [1] HOLMES, DG, LIPO, TA, 2003. Pulse width modulation for power converters: principles and practice, John Wiley & Sons.
- [2] DURAN, MJ, PRIETA, J, BARRERO, F, RIVEROS, JA, GUZMAN, H, 2013. Space-vector PWM with reduced common-mode voltage for five-phase induction motor drives, *IEEE Transactions on Industrial Electronics* 60(10):4159-4168.
- [3] LOPEZ, O, ALVAREZ, J, DOVAL-GANDOY, J, FREIJEDO, FD, 2008. Multilevel multiphase space vector PWM algorithm, *IEEE Transactions on Industrial Electronics* 55(5):1933-1942.
- [4] BOWES, SR, HOLLIDAY, D, 2006. Comparison of pulse-width-modulation control strategies for three-phase inverter systems, *IEE Proceedings-Electric Power Applications* 153(4):575-584.
- [5] LEVI, E, 2008. Multiphase electric machines for variable-speed applications, *IEEE Transactions on Industrial Electronics* 55(5):1893-1909.
- [6] LEVI, E, DUJIC, D, JONES, M, GRANDI, G, 2008. Analytical Determination of DC-Bus utilization limits in multiphase VSI supplied AC drives, *IEEE Transactions on Energy Conversion* 23(2):433-443.

Measurement and Monitoring System Water Level for Inland Navigation.

Ignacio Andrés Villamayor Benítez, and Norma Silva ¹,
National University of Asunción, Polytechnic School, San Lorenzo, Paraguay.

Abstract

This research was conducted with the objective of developing an electronic system for measuring and monitoring baseline water depth for river navigation. The study was carried out in the port Ita Enramada Asuncion, between the months of May 2012 and June 2013. The system features measuring sensors that collect information on the reference level of the water depth in this case the Paraguay River. Data capture is via a programmable logic controller can process analog or digital signals from the sensor and sent via wireless communication to the central monitoring station, where the logic controller may receive the same signal, decode and store the data and then display them in visual environments, located in the monitoring room, where the SCADA system on the PC, displays information on the status of all monitored variables and which states the level of water depth can be observed at each field station. The system performs autonomous measurements for reliability and security, prevent data are handled, thus achieving effective information of water depth measurement. The application of the measurement system is recommended in the vicinity of the main channel of navigation of the critical sections with corresponding signage for boaters.

Keywords: Electronic monitoring system, sensors, programmable logic controller (PLC), SCADA.

1. INTRODUCCIÓN

El Paraguay es un país mediterráneo, pues carece de costas marítimas; sin embargo posee canales de comunicación fluvial con el océano Atlántico, a través de sus ríos principales (Paraguay y Paraná)[1]. Según datos estadísticos de la Administración Nacional de Navegación y Puertos (ANNP), entidad encargada de los trabajos de mantenimiento, dragado y balizamiento

¹E-mail Corresponding Author: normasil555@gmail.com

de los ríos de nuestro país, existen pasos difíciles que traban la normal navegación del río Paraguay, acarreado grandes pérdidas económicas para el país, ya que el 85 % de del comercio exterior paraguayo depende del sistema de navegabilidad de sus principales ríos[2]. Este inconveniente es debido a que actualmente el proceso de medición y registro de variación de los niveles de agua, proceso fundamental para las acciones a tomar para determinar la condición de navegabilidad se realiza en forma manual. Este procedimiento consiste en colocada en forma vertical y perfectamente nivelada en el río una regla escalada, así al subir o bajar el nivel de agua, varia así la medición de la misma, y luego es registrado por un personal encargado. El proceso de registro se realiza completando manualmente un formulario. Luego se obtiene el dato del nivel de río y se calcula la condición de navegabilidad. En efecto, este trabajo se propone como objetivo el diseño de un sistema electronico de medición y monitoreo del nivel de referencia del agua del Río Paraguay a fin de contribuir en la disminución de crisis de navegación fluvial, reduciendo la gran incertidumbre del proceso de medición actual. Para desarrollar el trabajo se ha realizado una investigación con base en diversas fuentes bibliográficas analizando los conceptos de niveles de profundidad, patrones de diseño, y diversas tecnologías aplicables para crear dicho sistema El propósito final de este proyecto es ofrecer a los administradores del sistema portuario de navegación del Paraguay una herramienta útil que les permita ser eficientes en el sistema de monitoreo del nivel de profundidad del río Paraguay, con lo cual podrán advertir posibles problemas de navegabilidad, con un positivo impacto en la reducción del tiempo de ejecución de acciones para mejorar la navegabilidad así como en la ostensible reducción de pérdidas.

2. MÉTODOS Y MATERIALES

El montaje se realizó en dos tableros, uno ubicado en la estación de campo, que sería en la costa del río Paraguay en los puntos estratégicos y el otro tablero en la estación central de monitoreo. La medición del nivel de agua del Río Paraguay se efectúa a través de variación de presión hidrostática. Dentro de los tubos estabilizadores de oleaje son ubicados los sensores de nivel tipo sumergible que transmiten las señales de variación de presión hidrostática de forma analógica sin caída de potencial ni corriente. Las mediciones tomadas por medio del sensor sumergido en el nivel de agua del río serán transferidas al PLC, que se encargará de transformar las señales

de entrada en datos procesables para los sistemas de visualización, y por medio de ellos generar señales de alarmas cuando existan condiciones anormales en la operación. El sistema incluye dos entornos de comunicación con el usuario, uno de ellos, es un sistema SCADA instalada en una PC situada en la estación central de monitoreo y el otro es a través de una comunicación directa del usuario con el sistema de campo, con el uso de tramas GSM en caso de no ser posible con la estación central de monitoreo.

3. SISTEMA ELECTRÓNICO AUTOMATIZADO DEL SISTEMA.

Este sistema de medición y monitoreo del Río Paraguay permitirá conocer el nivel de referencia del río de navegabilidad, además proporcionará una forma de comunicación sencilla y estandarizada entre el equipo de medición y la computadora; ya que con este sistema se podrá recibir y acondicionar los datos mediante la utilización del Controlador lógico Programable y el módem TC65 con tramas GSM considerada de mayor cobertura para asegurar la comunicación [3].

Con el Controlador Lógico Programable se podrá adquirir la señal emitida por el sensor acerca del nivel de agua, y de este modo podrá realizar un sistema capaz de promediar las mediciones durante un intervalo de tiempo. Al mismo tiempo, podrá calcular un promedio del comportamiento de la variable (nivel de profundidad del río). Seguidamente, se encargará de enviar los valores a la estación remota o central para la visualización en la estación de monitoreo a través del módem TC65 guiados por tramas GSM.[4].

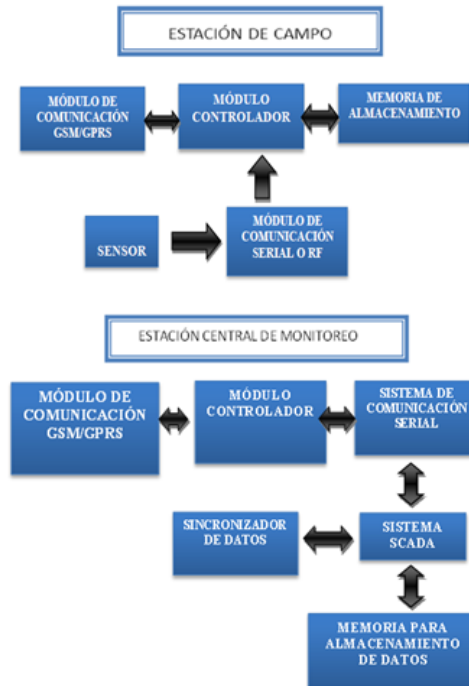


Figura 1 - Diagrama en bloque del Sistema electrónico.

4. ESTACIÓN DE CAMPO

La señal de nivel proveniente del sensor, son tratados en la estación de campo para luego ser enviados a la estación central de monitoreo a través del módulo GSM/GPRS, la misma toma 50 muestras cada 2 minutos, cada muestra es almacenada en registros internos que posee el controlador lógico programable, luego toma el promedio de las 50 mediciones realizadas conforme a los requerimientos establecidos por normas de calidad de medición. Para luego enviar el dato del promedio a la estación central de monitoreo o supervisión.

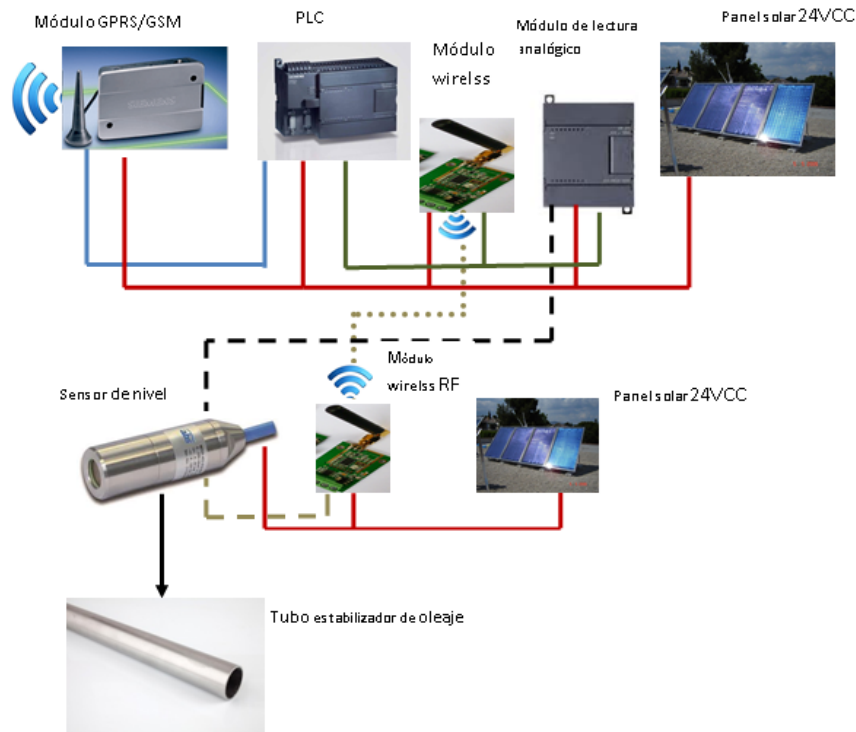


Figura 2 - Diagrama en bloques del sistema de campo.

5. ESTACIÓN CENTRAL DE MONITOREO

La señal proveniente de la estación de campo, tanto del nivel del canal y de la alarma, son recibidos en la estación central de monitoreo o supervisión.

El PLC toma los valores captados por el módulo y decodifica esa información para luego desplegarlo en una pantalla de visualización SCADA. Tiene también la posibilidad de pedido de informe de forma inmediata a la estación de campo en caso de que se precise ya la información independientemente del envío programado en la estación de campo.

Con el sistema central de monitoreo además interactúa el sistema de campo en caso de la alarma de nivel crítico de navegación, donde una vez visto la alarma el sistema central de monitoreo envía una información al sistema de campo a través de mensajes por SMS, que la situación ya ha sido

notificada y que vuelva a la condición de espera hasta que pase el nivel crítico de navegación, reiniciando el proceso de alarma, independientemente al envío del nivel del río que se realiza cada 2 minutos.

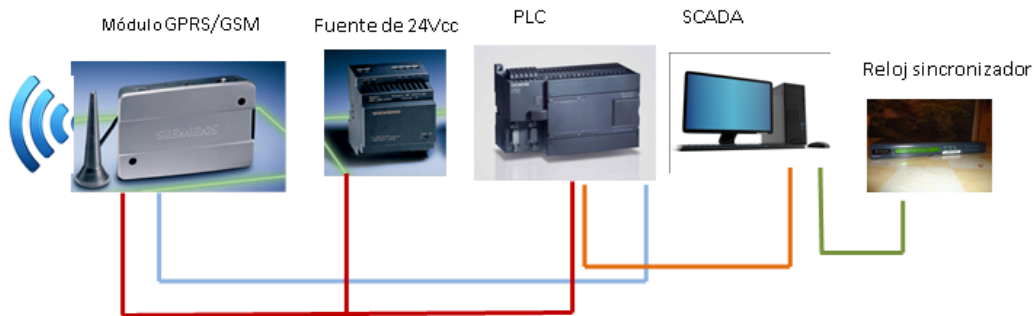


Figura 3 - Estación de central de monitoreo.

6. MUESTREO DE LA VARIABLE MEDIDA

Para realizar el cálculo del nivel de referencia del nivel del Río se toma como base el Reglamento internacional donde establece que se puede efectuar mediciones del valor patrón de forma reiterada. El número de repeticiones que asegura niveles de confianza razonable se encentra en 20 mediciones, aumentando las mediciones se reduce el margen de error. Siguiendo este método en los laboratorios acreditados y en procesos industriales cuando importa una calibración exacta.

Reglamentos ISO empleados
ISO /IEC 17025:2005
ISO 10012:2003
ISO 286 :1988
IT12 al IT18

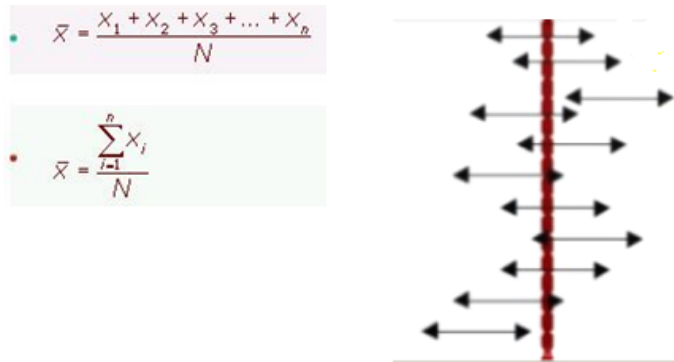


Figura 4 - Cálculo del nivel de la variable medida.

7. SISTEMA DE VISUALIZACIÓN SCADA

Con el fin de tener un registro estadístico de los datos del nivel de altura del río (m), los pedidos de aviso, alarmas y curvas de nivel del comportamiento de la variable medida, se plantea el desarrollo de un programa computacional tipo SCADA que sea capaz de tomar los datos del Controlador Programable del sistema y mostrar el valor de los mismos en una interfaz gráfica interactiva. Los datos capturados por el Controlador serán procesados y almacenados en una base de datos cada un minuto.

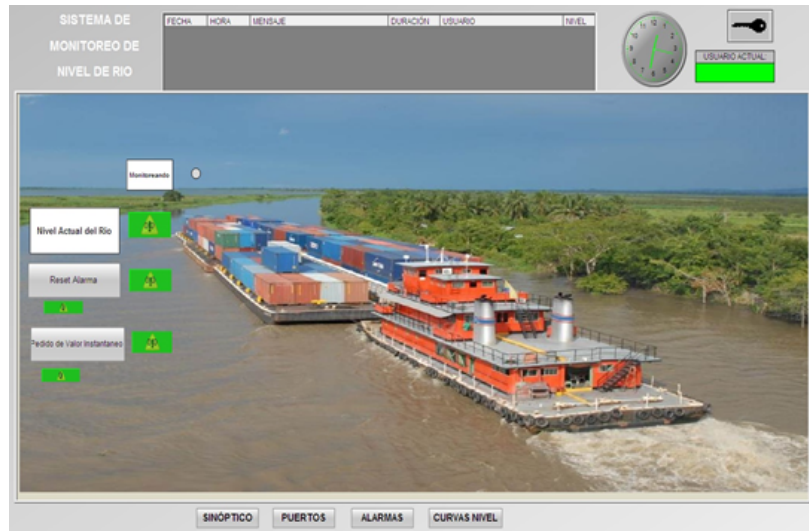


Figura 5 - SCADA pantalla principal.

Además, se cuenta con una pantalla exclusiva de la vista de todos los demás puestos que podrán ser incluidos para visualizar las operaciones de los sistemas de campo en los pasos requeridos por la ANNP para medir los niveles de ríos en los pasos críticos.

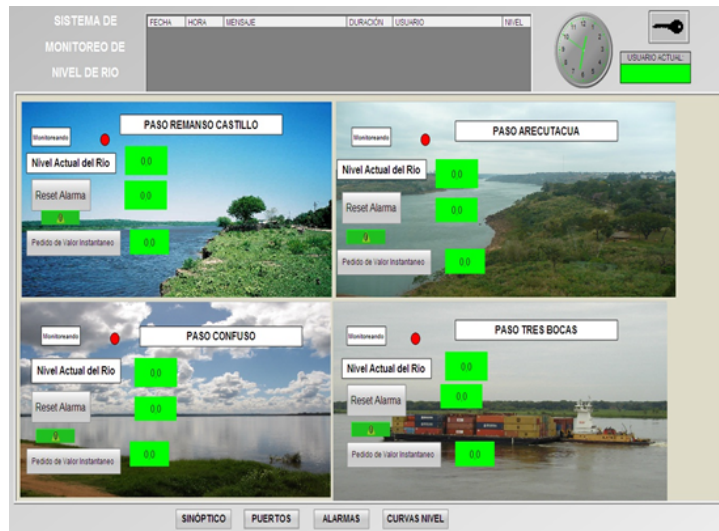


Figura 6 - SCADA. Puestos de Comunicación en diversos tramos críticos.

Las alarmas se presentan en una pantalla en forma de iconos de atención, denotando así un estado irregular del funcionamiento de alguna variable para alertar sobre los tramos críticos de navegación.



Figura 7 - Estado de alarmas del SCADA.

En la pantalla de curvas de nivel se dispondrá de un sector exclusivo mostrando el comportamiento de la variable y el valor de misma. Estos estados de alarmas se guardarán en una tabla de la base de datos con la hora y fecha de su aparición. Las alarmas podrán ser desactivadas en la pantalla una vez que el operador haya dado la notificación al sistema de la notificación aceptada.

El software del sistema, tiene la posibilidad de conectar el registro de los valores capturados a una base de datos cuyo contenido se almacena en un disco rígido a largo plazo. El Sistema también ofrece la posibilidad de visualizar el comportamiento del nivel de agua en un determinado periodo introduciendo la fecha y la hora desde cuando se quiere visualizar hasta la fecha que se desea.

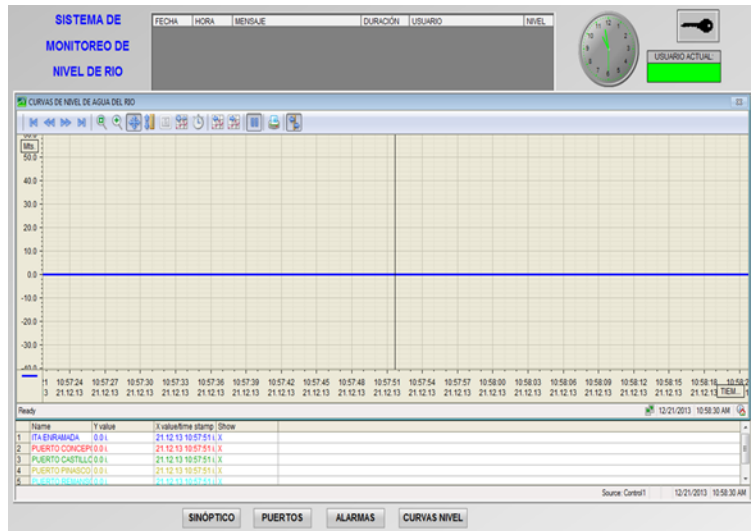


Figura 8 - Curvas de comportamiento del nivel del agua.

8. PRUEBAS Y RESULTADOS

Se verificó el correcto funcionamiento del equipo, en el puerto Ita Enramada de la ciudad de Asunción del Paraguay, en lo cual el sistema respondió correctamente arrojando resultados válidos ya que fue comparado con instrumento de medición. Los procedimientos para la validación del sistema fueron: Se calculó el punto de medición a través de una regla centimetrada, en el cual se eligió 1 metro de profundidad para comparar con los resultados que arrojó el sistema de medición.

Se instaló en tubo estabilizador de oleaje en el punto de medición a 1 metro de profundidad de agua y se introdujo el sensor en el tubo estabilizador de oleaje.

Se conectó el sensor con el sistema de medición, a través del módulo EM231 y el PLC, en el cual se pudo corroborar los datos medidos y procesados ya que arrojaban resultados válidos con un rango de error pero ya por las características técnicas del sensor.

El software de localización cumplió con los objetivos propuestos, su conexión con la estación central no presentó inconvenientes, obteniéndose los datos requeridos de manera correcta. Así como también se comprobó que su uso es

bastante sencillo para cualquier persona con conocimientos básicos de operación de computadoras.



Figura 9 - Fotografía de prueba en Itá Enramada.

9. CONCLUSIÓN

Se logro diseñar un sistema de medición y monitoreo aplicable para la medición de referencia los niveles de ríos.

La configuración de los controladores, módulos y el sensor, de manera que los datos recibidos sean las más precisas y confiables posibles.

La implementación de un software para la visualización de la variable monitoreada con una interfaz gráfica y amigable.

Se validó el funcionamiento del sistema propuesto a través de pruebas de campo y de laboratorio.

References

- [1] JARA, LUIS. 2013. GERENCIA DE NAVEGACIÓN DE LA ANNP. Nivel del río Paraguay.
- [2] El Paraguay y su ruta de navegación. Disponible en: [http://abc.com.py/nacionales/el canal de navegación Paraguay Paraná](http://abc.com.py/nacionales/el_canal_de_navegación_Paraguay_Paraná)
- [3] Módulo TC65 SIEMENS. Consultado en abril del 2013 [En línea]. Disponible en: [http://blauden.com/modem gsm siemens tc65 completo](http://blauden.com/modem_gsm_siemens_tc65_completo)
- [4] PLC s7-200 CPU 226, SIEMENS. Consultado en abril del 2013 [En línea]. Disponible en: <http://swe.siemens.com/spain/web/es/industry/automatizacion/simatic/Documents/S7200-CAT.PDF>

Energy policies in the residential sector of the Republic of Paraguay

Diana Valdéz^{a1}, Karen Balbuena ^a, Estela Riveros^a, Gerardo Blanco ^a

^aPolytechnic School - National University of Asunción, San Lorenzo, Paraguay

Abstract

Paraguay has several energy sources -both imported and domestic- to supply the energy demand of the country. Currently, the country has a large availability of domestic supply of hydropower but a low level of electricity penetration as a energy source of final use. Thus, nowadays, energy demand associated to the use for cooking food are mostly supplied by energy resources as Liquefied Petroleum Gas (LPG), charcoal and firewood; sources with low efficiency and high level of Greenhouse Gas Emissions (GHG); in addition, imported as is it is case of LPG. Taking as starting point a model based on supply and final consumption of different energy sources in the country and taking into account multiple factors (technical, economic, social and environmental) that influence on the choice of energy sources and technologies, this work analyzes energy policies at the residential sector for starting a energy transition process in Paraguay. The main objective of this research, considering the actual situation, is to analyze the impact of energy transition strategies from less efficient sources of energy (oil derivatives and biomass) to electricity (domestic, renewable and clean energy source) for residential use, including efficient electricity consumption and how it would impact in the supply of electricity. To achieve the objective was developed an integrated energy model of Paraguay on *Long Range Energy Alternatives Planning System*(LEAP©) focused on residential sector, in order to generate a energy prospective by simulating the long term behavior of the energetic matrix of Paraguay. Finally, this article seeks to analyze the implications on evolution of characterized residential demand curve on the energy supply of this sector as well as to study the environmental impact on the variation of GHG emissions.

Key words: Computational Engineering & Technological Innovation, Energy policies.

¹E-mail Corresponding Author: leti_barboza@hotmail.com

1. INTRODUCTION

In the 70s the hydroelectricity availability (clean and renewable energy source) has begun to drastically rise, by growing to values that we know today (4,650 thousand tonnes of oil equivalent), this due to the large implemented hydroelectric power plant projects at the time, as Itaipu and Yacyreta. By comparing the evolution from the 70s until 2008 [1], as far as energy is concerned, we see that the gross domestic supply of hydropower grows about 355 times (as recorded in 1970) and conversely final consumption electric power only grew by 28%.

Taking as core of this study, the high proportion of biomass consumption, in contrast to the percentage of electricity use, the biomass demand was disaggregated into final uses, determining that vast majority is for cooking food at the residential level. In addition to biomass, other energy sources are intended for cooking, among others LPG, charcoal and electricity.

We know that hydroenergy is compatible with a model of sustainable development; therefore, it should be the cornerstone of an energy policy that arises in Paraguay. This fact -combined with the heavy dependence on imported oil derivatives to meet the energy demand in Paraguay and the high percentage of fuelwood consumption- led us to identify the need to seek strategies to propose raising the penetration of clean and renewable energy such as hydroelectric sources, by replacing energy sources that either it needs to be imported and has a significant environmental impact or it has a very low efficiency rate.

These measures are aimed at reducing the negative environmental and social impact of non-clean and sustainable energy (in terms of lower emissions of GHG). Environmental benefits that entail implementing energy policies proposed in this research are discussed.

To analyze this situation at country level, was developed an energy model of Paraguay on LEAP©and assumptions scenarios that simulate how the country would behave from the energy point of view under specific study cases.

With the developed model, results under the possible scenarios of substitution and the behavior of different energy sources are analyzed, when energy policies are applied, that provide for the efficient use of energy available to the final consumer and migration to electricity.

The method of Net Present Value (NPV) is applied for the economic

analysis of the efficiency measures and substitution that have been proposed to determine the economic feasibility of the project in the long term.

2. OBJECTIVE

Analyze the impact of energy transition strategies from less efficient sources of energy (oil derivatives and biomass) to electricity (domestic, renewable and clean energy source) for residential use, including efficient electricity consumption and how it would impact in the supply of electricity.

3. JUSTIFICATION

Within this research, we analyze all energy sources that supply the energy demand of Paraguay today. For this issue, the National Energy Balance is used. From database is taken the information from 2004 to 2012 [2] these data is considered historical and provide the basis on which the baseline scenario is then projected.

The data is loaded into the LEAP©model, which is a tool used for the analysis of energy policies and assessment of climate change mitigation (GHG emissions). This model allow us a comprehensive modeling of energy consumption, production and processing resources in all sectors of a socio-economic system.

It is possible with the use of LEAP, to project a trend scenario corresponding to Paraguay's energy sector behavior (based on the historic behavior). In addition, the utilization of the LEAP provides a vision of possible future behavior of the energy matrix of Paraguay, by means of this we are able to evaluate the different proposed scenarios.

With the Paraguay model in the environment LEAP©and projected substitution scenarios we can see a range of possible future scenarios for energy, with this, we get to anticipate future situations and outline appropriate energy policies.

4. ENERGY MODEL

In the context of a prospective energy analysis, energy system model attempts to capture the behavior of a complete energy system, as a nation, city or region. Here, macroeconomic and demographic trends control the model but are exogenous variables.

We use models to reflect complex systems in a meaningful way, by organizing a large amount of information and having a consistent hypothesis to evaluate or analyze impacts on energy systems contextual framework.

Selected software

The selected Software is Long-range Energy Alternatives Planning System (LEAP©) [3]. It is a tool for modeling energy and environmental scenarios. The scenarios are based on energy balances that describe the way they consume, transform and produce energy in a given country or economy, and alternative hypotheses as population, economic development, technology, prices and other characteristics.

5. STUDIES CASE

Energy prospective

Prospective covers as many possible scenarios, which means that should cover the most likely or possible future. On this basis, the prospective study of the energy matrix of the Republic of Paraguay is made, focused on residential branch and according to three baseline scenarios that differ by population and Gross Domestic Product (GDP) growth projected [4].

Key assumptions

As key assumptions are set the time series of the macroeconomic and demographic variables or user-created variables. In the developed model, the GDP of the different sectors of the Paraguay as well as the population evolution are established.

Demand scenarios

As we know, the future is uncertain, we do not know what will happen tomorrow, but it is possible anticipate the unfolded uncertainties based on events that have already occurred and outline possible trajectories of events yet to take place. For prospective energy analysis, it was decided to outline the prospective taking into consideration three possible future scenarios, *i.e.* high demand, average demand and low demand. In each proposed scenario, key assumptions are taken, *i.e.* GDP and population evolution.

Desired Scenario 1 (ED1)

We propose two desired scenarios, based on the weaknesses identified in the residential sector to the end use of cooking. The first desired scenario called "stoves replacement" is analyzed the implementation steps for replacement of stoves in urban and rural areas. In 8% of urban households and 65% of rural households [5], the cooking is done until nowadays with firewood and other biomass. This represents approximately 521,000 households in the country. Methods of cooking with biomass ranging from open air fire, wood stove, *tatacu*, brazier among others, with an average efficiency of biomass use between 5% and 10% for the final use of cooking. These data, translated in terms of energy, for residential indicate that consumed 454 Mtoe (data from 2012), which corresponds to 25% of the biomass consumed in the country, which takes up only 5% of the energy by efficiency of end-use technology, leaving result in the loss of 95% of the energy used corresponding to 430 Mtoe. Only data from the year 2012, this represents the GHG emissions of 2,336 MtCO₂ equivalents.

Given the abovementioned data, five instruments were proposed to gradually migrate from biomass to energy sources that can have higher efficiency as LPG and electricity; in addition to the replacement of the means of cooking currently used, for using stoves more efficiency.

The first stage of substitution, contemplates the provision of residential firewood stoves more efficient since 2015 in urban and rural areas in order to reach the year 2030 to the 20% of urban households and 60% of rural households using biomass for cooking efficiently

In the second instrument, the migration from biomass cookers to LPG cookers is contemplated. It is expected that by 2030 the 20% of urban and rural households using biomass for cooking, stop using biomass for cooking and use LPG.

Third instrument is the migration of biomass to electricity, by using induction cookers. It is projected that by 2030 the 60% of the urban population and 20% of the rural population using biomass for cooking, migrate to using electricity through induction cookers.

In addition to the use of biomass migrate to other energy sources, it is contemplated the migration LPG to electricity as fourth instrument. It is expected that by 2030 the 20% of urban and rural households which use LPG for cooking would migrate to electricity.

Finally, in the fifth instrument, we propose the migration from current technologies that consume electricity to the utilization of induction for cooking. It is projected that by 2030 the 60% of urban households and 20% of

rural households using electricity for cooking, use only induction stove.

Desired Scenario 2 (ED2)

In the second scenario desired, efficiency measures and education campaigns using electricity efficiently are proposed. For the electrical use for lighting, we contemplate the 100% replacement of incandescent lamps at 2030 in urban and rural households, as well as education campaigns that encourage the energy saving culture using sunlight, and the turned off of the unused lights.

In the climatization demand, we propose the renewal of the current air conditioner technology by technologies that are designed with energy efficiency grade A.

Also, it is proposed education campaigns that include instruction of saving culture in regulating temperatures in enclosures, the turned off of the unused artifacts, among other measures. Finally, by the end use of food preservation, the replacement of 90% of old fridges for new appliances with energy efficiency grade A is proposed. In addition, education campaigns in using techniques refrigerators to prevent loss of cold are included.

6. METHODOLOGY

We develop a model representing the energy sector of the Republic of Paraguay based on the energy balance prepared by the Vice Ministry of Mines and Energy (VMME) where the primary and secondary energy offer are structured with energy transformation and energy demand.

The data are taken from the year 2004 until the last National Energy Balance (BEN) available, which corresponds to the year 2012.

Hypothesis considered

In developing the model, special attention to the final demand of the residential sector is given, considering it is in this sector where efficiency and alternative replacement measures are proposed.

The branch of residential demand was developed based on the proposal structure presented in the “*Useful Energy Balance of the Republic of Paraguay*” project, developed by the *Parque Tecnológico Itaipu* (PTI) [6].

Characterization of residential demand curve

In order to analyze the impact of the implemented instruments under the desired scenarios in national electricity grid (SIN) is necessary to characterized the hourly electricity demand in the residential sector, in order to

determine the new behavior of the hourly demand curve in order to identify potential negative impacts of implementing efficient alternative proposal on the power system network.

Characterization of residential demand are made through household surveys about their hourly consumption.

Macroeconomic impact

The economic analysis is developed from a macro approach, where the desired scenarios are presented as tools that obey energy policies established by the State. The cost of policy implementation, monitoring and enforcement thereof, are analyzed and taken into account savings by not consumed energy (electricity, firewood, LPG), savings GHG not emitted and externalities related to the efficient use of biomass. GHG savings by not issued as an externality, since Paraguay does not sell carbon credits are considered. Finally, the NPV of each instrument is estimated. A discount rate of 12% was used.

Energy Policy

Energy policy is a specification that provides the socio-economic policy framework of strategic guidelines for its formulation. It is based on a diagnosis of the situation of the energy system as a starting point, and it is considered that the socio-economic policy is aimed at finding the sustainability of development.

With the developed energy model of the Republic of Paraguay, we are able to assess the energy situation these following aspects:

- ▷ The energy sources, such as biomass, do not involve an appropriate and sustainable use of these resources. This situation can cause severe environmental damage, which are only reversible in the long-term.
- ▷ The scope of consumption, where it is visualized the low electric energy coverage for basic uses, low efficiency in end uses (between 5% and 10% for biomass), negative impacts on health and the environment due to the misuse of energy end sources (especially biomass).

These problems are diagnosed with a transverse analysis, which included the current status and operation of the energy system and a study of the historical evolution revealed dynamics, past trends and signs of change.

7. RESULTS

Table 1: Comparison of demand and savings (in thousands of tons of oil equivalent)

Scenario	High Demand		Med. Demand		Low Demand		Saving
	Dem.	Saving	Dem.	Saving	Dem.	Saving	
Tend.	1.199	–	1.100	–	1.002	–	–
ED1	735	453	681	419	620	382	38%
ED2	1.088	100	1.007	93	918	84	8%
ED1+ED2	658	530	609	491	555	447	45%

The model of Paraguay has developed on LEAP©, to validate the results, these has been compared with of BEN of VMME with LEAP©results. For different demand scenarios, we found that the energy savings under the desired scenario compared to trend scenario is 38% under the ED1, 8% under the ED2, then under the combination of both ED1 and ED2 scenarios, the overall energy savings is of about 45% compared to the trend demand scenario. The data are listed in Table 1 indicating percentage savings for each proposed scenario relative to the trend scenario.

Regarding the impact on the Residential Load Curve of SIN -for different demand scenarios- we observed that the decrements in peak hour load compared to baseline scenario and the scenarios desired applied is 12% for the ED1, 15% for ED2 and analyze both scenarios together a decrements of 22% of electricity consumption in peak load hours is presented. These data indicate that one can increase the load factor of SIN, *i.e* buying less power to supply the Paraguayan electricity market. Comparative data of electricity consumption in peak load hours for the proposed scenarios of demand and desired scenarios are detailed in Table 2, indicating the percent of decrements for each scenario.

For different demand scenarios, we observed that the reduction of GHG emissions relative to the baseline scenario and desired scenarios applied are

8% for the *ED1*, from 5% to 12% *ED2* and analyzing both scenarios together. These results are exposed in Table 3, indicating the percentage savings for each proposed scenario compared to the trend scenario.

Table 2: **Comparison of consumptions in peak load hours (Mega Watos per hour)**

Scenario	High Demand		Med. Demand		Low Demand		Saving
	Dem.	Saving	Dem.	Saving	Dem.	Saving	
Tend.	967	–	896	–	816	–	–
ED1	941	26	872	24	794	22	3%
ED2	827	140	766	130	698	118	15%
ED1+ED2	803	164	743	153	677	139	17%

Table 3: **Comparison of GHG emissions (thousands of tons of CO2 equivalent)**

Scenario	High Demand		Med. Demand		Low Demand		Saving
	Dem.	Saving	Dem.	Saving	Dem.	Saving	
Tend.	217	–	201	–	183	–	–
ED1	200	17	185	16	169	22	8%
ED2	206	11	191	10	174	118	5%
ED1+ED2	190	27	176	25	160	139	12%

Analysis of economic feasibility of implementing the proposed energy poli-

cies was conducted by the method of NPV, where the energy savings and externalities involving the migration of biomass to other energy sources such as electricity are economically quantified. In this sense, it was considered the savings by decreasing respiratory diseases, eye discomfort, burns and poisoning, as well as saving time spent cooking [7]. Investments are calculated annually according to the plan of implementation of policies and as each replacement scenario.

On Tables 4, 5 and 6 the NPVs for the investment realized in each scenario, the savings due to decreased demand and externalities for scenarios of high, medium and low demand respectively indicated, and in the last column is analyzed the NPV of each scenario, but not including externalities proposed by saving firewood each proposed scenario stage.

Table 4: NPV for high demand, discount rate of 12%, from 2015 to 2030 (millions USD)

High Demand	ED1	ED2	ED1+ED2	ED1+ED2 (withuot extern.)
Invest	(28,1)	(131,4)	(159,5)	(159,5)
Saving on electricity	16,4	58,5	74,4	74,4
Saving on LPG	15,4	54,6	69,5	69,5
Saving on Wood	19,3	1,2	19,9	19,9
Saving on GHG	8,0	6,1	84,2	–
Saving by extern.	700,4	43,1	732,2	–
NVP	731,4	32,1	811,7	4,3

Table 5: NPV for medium demand, discount rate of 12%, from 2015 to 2030 (millions USD)

Medium Demand	ED1	ED2	ED1+ED2	ED1+ED2 (withuot extern.)
Invest	(27,3)	(125,2)	(152,5)	(152,5)
Saving on electricity	16,6	55,3	70,4	70,4
Saving on LPG	14,6	51,6	65,8	65,8
Saving on Wood	18,3	1,1	18,9	18,9
Saving on GHG	7,6	5,8	79,9	–
Saving by extern.	664,5	40,9	686,2	–
NVP	693,3	128,8	768,7	3,8

Table 6: NPV for low demand, discount rate of 12%, from 2015 to 2030 (millions USD)

Low Demand	ED1	ED2	ED1+ED2	ED1+ED2 (withuot extern.)
Invest	(25,7)	(115,7)	(141,5)	(141,5)
Saving on electricity	14,6	51,6	65,7	65,7
Saving on LPG	13,7	48,1	61,4	61,4
Saving on Wood	17,1	1,1	17,7	17,7
Saving on GHG	7,1	5,4	74,8	–
Saving by extern.	621,8	38,2	642,2	–
NVP	648,5	119,6	720,4	3,4

8. CONCLUSIONS

We have developed a comprehensive energy model of the Republic of Paraguay in LEAP©. The level of disaggregation of the structure of the energy model developed allowed it possible to apply specific measures in the residential sector.

The behavior of the energy matrix of Paraguay was analyzed with different simulations and concludes that the implementation of a energy policy, that can provide an alternative to the problem of energy projected for the coming years, is necessary.

Also effective is the implementation of a culture of saving and efficient energy management in the Republic of Paraguay. Especially focused on households and representing the largest consumer of energy as VMME and model that has been developed.

It proved to be feasible awareness for sustainable energy use, and replacement of fixtures with low efficiency with higher- efficiency.

The developed model, allowed analysis for cost-effective technical and economic proposed, showing that they are cost-effective alternatives to long-term.

Besides the strengths and weaknesses of each identified energy policy even before its effective implementation, making it possible to model effective solutions to conflicts that may arise in the future.

GHG emissions were analyzed before and after the implementation of measures of substitution, resulting in the proposed instruments are effective in mitigating the greenhouse effect.

For all scenarios the NPV is positive, with an internal rate of discount of 12%, indicating that the project is profitable even without quantifying externalities.

The methodology applied in this work, can be used to make similar analysis for other demand energy sectors, like Industrial, Commercial, Government and Public street lights.

References

- [1] ROLÓN, J. 2009. Situación de la Matriz Energética en Paraguay. Soluciones para el desarrollo sostenible, Recomendaciones.
- [2] VMME, VICE MINISTERIO DE MINAS Y ENERGÍA. 2004 to 2012. Balance Energético Nacional. San Lorenzo, Paraguay.
- [3] COMMEND. 2012. LEAP software. Community for energy, environment and development. Available on: <http://www.energycommunity.org/>
- [4] VICE MINISTERIO DE MINAS Y ENERGÍA. 2007. Estudio de País: Paraguay. Aplicación del Modelo MAED del Organismo Internacional de Energía Atómica (OIEA). Proyecto Regional RLA/0/029. San Lorenzo, Paraguay.
- [5] DIRECCIÓN GENERAL DE ESTADÍSTICAS, ENCUESTAS Y CENSO. 2004 al 2009. Principales resultados de la encuesta permanente de hogares. Fernando de la Mora, Paraguay.
- [6] PARQUE TECNOLÓGICO ITAIPU, (PTI). (2013). Balance de Energía Útil de la República del Paraguay. Itaipu, Paraguay.

- [7] GARCIA-FRAPOLLI, E. (2009). Beyond fuelwood savings: Valuing the economic benefits of introducing improved biomass cookstoves in the Purpecha region of Mexico.
- [8] OLADE-CEPAL-GTZ, OLADE. 2003. Energía y desarrollo sustentable en América Latina y el Caribe, Guía para la formulacin de políticas energéticas. 1 Ed. Quito, Ecuador: OLADE.

Marginal Abatement Costs for Greenhouse Gas Emissions Reduction in Paraguay's Energy Sector: An Analysis under Uncertainty

Juan P. Nogues^{a1}

^a Universidad Paraguayo Alemana

Abstract

No country is immune to the problems and risks associated with climate change and Paraguay is no the exception. In general terms Paraguay can be considered minimally responsible for emissions and global climate change; but in turn Paraguay's economy is so inefficient with respect to its emissions of greenhouse gases (GHG) that in relative terms it can be argued that Paraguay is a highly polluting nation. For instance, in 2000, Paraguay emitted around 13.7 kg 16 of CO₂-e per dollar of GDP [1, 2] while developed countries such as France or the U.S. emitted between 0.4 to 0.6 kg CO₂-e per dollar of GDP ² - see Figure 1. This indicates that Paraguay is highly inefficient in economic output with respect to GHG emissions. The high value of emissions is mainly due to the impact from Land Use, Landuse Change and Forestry (LULUCF), which in turn is linked to urban development, energy demand for biomass and agricultural expansion. Even excluding LULUCF emissions the value remains quite high compared to many countries in the region. Countries in the region such as Argentina, Brazil, Chile, Colombia and Uruguay have an index of Kg emissions per dollar of GDP below 3.6 kg CO₂-e per dollar of GDP - which is what Paraguay emitted without LULUCF. An analysis of emissions in terms of tons per capita also shows that Paraguay emits per person more than some industrialised countries. Accounting for LULUCF Paraguay emitted about 15.7 tonnes of CO₂-e per capita while other countries of the region emitted far less in 2000. Brazil for example which has a very high rate of deforestation emitted about 12.3 tonnes of CO₂-e per capita in 2000. Excluding emissions from LULUCF Paraguay continued to be above Colombia, Costa Rica, India, Uruguay and China among others. Therefore, one could argue that per capita Paraguay is more responsible for greenhouse gas emissions,

¹E-mail Corresponding Author: juan.nogues@upa.edu.py

²Values calculated from the UNFCCC online database

and consequently climate change, than a resident in Chile, Costa Rica or China, for that particular year.

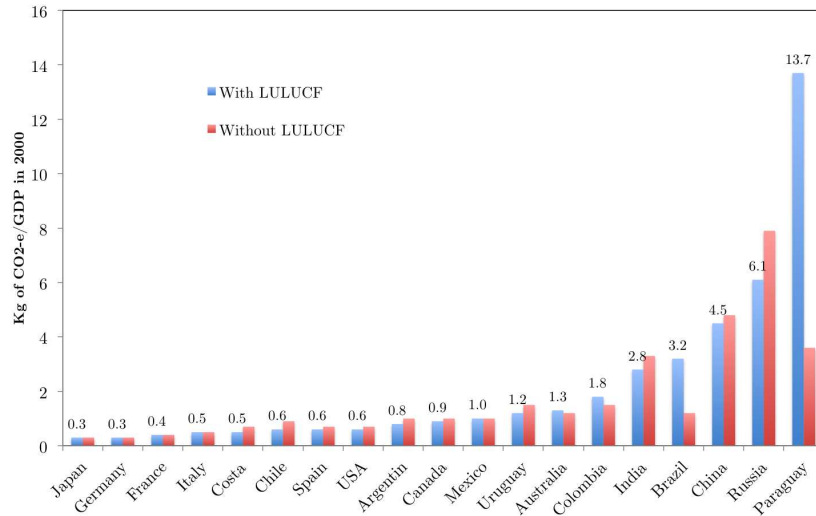


Figure 1 - CO₂-e emissions in Kg/GDP for the year 2000 for different countries. Values presented in terms of nominal GDP, with and without LULUCF emissions accounted for. Emissions from bunkers or biomass burning are not included. Values calculated from the Segunda Comunicacion Nacional [1], the IMF World Economic Outlook [2] and the UNFCCC online database.

The Energy sector of Paraguay is one of the main culprits of this inefficiency with respect to GHGs. Paraguay is largely dependent on fossil fuels for their energy consumption, although it produces clean renewable electricity to suffice almost all its Energy demand. For instance in 2011 only 15% of the energy was supplied by renewable energy (electricity) [3]. Paraguay meets its energy demand mostly with biomass derived fuels (around 48% of the energy matrix in 2011) by and petroleum derived fuels (37% of the energy demand) [3]. This type of energy matrix composition affects the efficiency factor for Paraguay, where only 37.1% of the energy consumed is used effectively [5]. Therefore, it obvious that the Energy sector of Paraguay has a lot of room for improvement regarding efficiency. It also happens that the Energy sector is composed of a variety of sub-sectors (Industry, Transport and residencial) and therefore offers a variety of technologies to solve the problem of greenhouse gases. More efficiency improvements mean a possible reduction in costs and a reduction in emissions of GHGs.

In this study, an economic evaluation of possible technologies that reduce emissions is done by considering the uncertainties in the emissions reduction factors, the costs of the new technologies and the current baseline operation. In order to calculate the economic gains/losses of certain technologies an initial baseline scenario, of the energy demands and the emissions associated, was calculated using the Long range Energy Alternatives Planning System (LEAP) model [6]. Once the baseline was determined three main technologies and policy options for Paraguay were identified: The Bus Rapid Transit (BRT) system (or Metrobus), a Biodiesel initiative to increase the mix of common Biodiesel from 1% to 5% by volume, and the adoption of efficient cookstoves in rural homes. The projections were done with the base year 2013 and ended with the 2040.

Results show that as a first order approximation, based on current consumption and the projection of the economy through 2040, Paraguay, there are at least three options that give favorable economic costs in most cases and reduce emissions significantly. Through an uncertainty analysis, based on a Monte Carlo approach, results indicate that the reductions of GHGs through a BRT system on average would be around -0.30 US\$ per ton of CO₂ reduced - without considering economic externalities such as reduction in respiratory problems and gains in time of travel. Likewise, a switch to more efficient cookstoves that use on average 50% less fuel has an average cost of -0.4 US\$ per ton of CO₂. Finally an analysis of the impact of promoting a mix of 5% BioDiesel mix with normal Diesel was done, and showed that investing in this type of mitigation would have an average cost of - 7 US\$/ per ton of CO₂.

Keywords: Greenhouse gases, Monte Carlo, Marginal Costs, Paraguay's Energy Sector

ACKNOWLEDGMENTS: The work presented here was in part financed by the Interamerican Development Bank (IDB) under research grant number RG-K1219 "Avanzando la Agenda de Investigación sobre Cambio Climático".

References

- [1] SEAM, 2011. Segunda Comunicación Nacional sobre Cambio Climático. Secretaria del Ambiente. Asunción
- [2] IMF, 2008. World Economic Outlook. International Monetary Fund. Washington D.C.
- [3] VMME, 2013. Balance Energético de la República del Paraguay. Año 2012. Ministerio de Obras Publicas y Comunicaciones.
- [4] DGEEC, 2012. Compendio Estadístico Ambiental del Paraguay 2001-2011. Dirección General de Estadística, Encuestas y Censos.
- [5] PTI-FB, 2014. Balance Energético Nacional en Energía Util de la República de Paraguay - Balance Consolidado. Itaipu-Fundación Parque Tecnológico Itaipu y Fundación Bariloche.
- [6] Heaps, C.G., 2012. Long-range Energy Alternatives Planning (LEAP) system. [Software version 2012.0056]. Stockholm Environment Institute: Somerville, MA, USA.

Part III: Poster Session

Neuro-Fuzzy Classifier for Deforestation Estimation in a Citizen Science Project

Marilyn Menecucci Ibanez dos Reis^{a1}, Adenilson Carvalho^b, Eduardo Fávero Pacheco da Luz^b, Fernando Manuel Ramos^a

^aNational Institute for Space Research, São José dos Campos, SP, Brazil

^bNational Center for Monitoring and Warning Disaster, São José dos Campos, SP, Brazil

Abstract

Brazil has the longest and most successful tropical forest-monitoring program in the world. Since 1988, the PRODES (Brazilian Amazonian Forest Monitoring by Satellite) program has been carrying detailed annual deforestation surveys in the Brazilian Amazon. PRODES uses a semi-automated procedure to perform the digital processing of TM/Landsat images. More recently, the DETER (Real Time Deforestation Detection System) program has been providing weekly alerts of deforested areas of 25 hectares or more, using MODIS (Moderate-Resolution Imaging Spectroradiometer) imagery from NASA's TERRA and ACQUA satellites. Overall, this monitoring framework, together with a free and open data policy (all software and results are available on the Web), enabled greater transparency and effectiveness in Brazil's conservation efforts, and helped the country to greatly reduce its annual forest loss in the Amazon. Unfortunately, both projects involve a costly and time-consuming inspection step of the automatic classification map by specialists, which make difficult their replication in less developed countries. Within the context above, a citizen science project called "ForestWatchers" was recently launched with the goal to involve citizens around the globe in monitoring deforestation. Using a Web interface, volunteers around the world are asked to review satellite images of forested regions, and confirm whether automatic assignments of forested and deforested regions are correct. Considering the size of the task – tropical forests cover an area of several hundred million hectares – it is crucial the development of a fast classifier that meets a twofold goal: mapping MODIS pixels into two classes ("Forest" and "Non-Forest"), and selecting the pixels to be sent to the volunteers for inspection, based on a confidence metric. Here we investigate

¹E-mail Corresponding Author: marilynmeneccuibanez@gmail.com

the use of Fuzzy Multilayer Perceptrons (FMLPs) neural networks in classification of deforestation patterns in the Brazilian Amazon, using MODIS imagery. Essentially, the MLP is a multilayer feedforward network which utilizes a supervised learning mechanism based on the setting of the parameters according to the error between the calculated and desired outputs of the network. For the FMLP learning process, we used PRODES classification maps as desired outputs. PRODES maps, which originally display five classes of land-cover, with a spatial resolution of $60m$, were resampled into the two classes (F and N) of our FMLP classifier. The spatial resolution was then reduced to $250m$, the same displayed by MODIS imagery, used as input data in the learning process. Generally, the MLP output passes through a **winner-take-all** filter that assigns 1 (one) for the winner neuron and 0 (zero) for the others. In FMLPs, outputs are mapped into the range $[0, 1]$, and refer to the degree of membership of the input pattern to each of the output classes. This allowed us to use normalized degrees of membership as a metric of confidence in the classification of each pixel, drastically reducing the volunteers task since only low confidence pixels are visually inspected by them. We tested this approach by producing a deforestation map for the State of Rondônia, in Brazil. Rondônia has an area of $237,576km^2$ (roughly, the size of Portugal), originally covered mostly by the Amazon forest. Results were compared with the corresponding PRODES deforestation map with good agreement. The use of confidence metric permitted drastically reduce the number of pixels to be inspected by the volunteers.

Keywords: citizen, science, volunteer, neural, network, fuzzy, image, satellite

CHARACTERIZATION OF THE COSMOLOGICAL NONLINEAR PATH OF SINGLE GALAXIES IN N-BODY SIMULATIONS

Diego H. Stalder D.^{a1}, Reinaldo Rosa ^a, Esteban Clua^b

^aNational Institute for Space Research, São José dos Campos, SP, Brazil

^bFederal Fluminense University, Niteroi, RJ, Brazil

Abstract

Turbulent-like behaviour is an important and recent ingredient in the investigation of large scale structure formation in the observable universe [1, 2]. Recently, an established statistical method was used to demonstrate the importance of considering chaotic advection (or Lagrange turbulence) in combination with gravitational instabilities in the CDM simulations performed from the Virgo Consortium (VC). However, the Hubble volumes simulated from GADGET-VC algorithm have some limitations for direct lagrangian data analysis due to the large amount of data and no real time computation for particle kinetic velocity along the dark matter structure evolution. We use our COsmic LAgrangian TURbulence Simulator (COLATUS) [3], based on GPU/CUDA technology, to perform gravitational Cosmological N-body simulations and tracking the particles paths. In this work we discuss the chaotic advection behavior of tracers galaxies based on the angular velocity fluctuation analysis of single particles during its trajectory to the gravitational collapse of super clusters at low redshifts.

Keywords: Turbulent-like, Cosmology, N-body simulations, GPU/CUDA

References

- [1] Caretta et al., AA doi:10.1051/0004-6361:20079105
- [2] Rosa et al., CCP doi: 10.1016/j.cpc.2008.11.018
- [3] Stalder et al., AIP doi: 10.1063/1.4756992

¹E-mail Corresponding Author: diego.s.eik@gmail.com

Automated Coronary Artery Segmentation in CTA

Federico López^{a1}, Horacio Legal ^a

^aFPUNA, Universidad Nacional de Asunción, Campus de la UNA, San Lorenzo,
Paraguay

Abstract

The main purpose of this work is to present an automated method for the segmentation of human coronary arteries from images obtained from Computed Tomography Angiography (CTA). The method consists of three separate processes that perform the following tasks: heart segmentation, blood pool segmentation, and coronary artery segmentation. This work takes advantage of the properties of the distance transform to perform the heart and coronary artery segmentation.

Keywords: Coronary Artery, segmentation, distance transform, automated, snakes, mathematical morphology

1. INTRODUCTION

According to the 2012 statistics presented in [1] the overall rate of deaths attributable to cardiovascular disease (CVD) account for about one third of the total deaths in the United States. These CVD's include high blood pressure, coronary diseases, strokes, and atherosclerosis among others. Coronary heart disease (CHD) accounts for approximately 20% of the total deaths. To evaluate heart disease, the segmentation of the coronary arteries has become an integral part of the analysis of the disease.

Several different methods to solve the problem of coronary artery segmentation have been described in literature [2] [3] [4] [5] [6] [7] [8]. In this work we divide the automatic coronary artery segmentation in three different processes: the segmentation of the heart to separate it from the lungs, the segmentation of the blood pools, and the segmentation of the coronary arteries. The segmentation of the blood pools is based on the work presented by Cline in [9]. The segmentation of the heart to separate it from the lungs is an extension of the work presented by [10] in which we take advantage of the properties of the distance transform to create a driving force for the

¹E-mail Corresponding Author: fjl@pol.una.py

deformable model. Finally, the coronary artery segmentation method presented is a modification of the work presented by Bauer [11] in which we reduce the computational complexity introduced by Gradient Vector Flow (GVF).

2. METHODS

The method for the automatic segmentation of the coronary arteries includes three main processes: the segmentation of the blood pools, the segmentation of the heart, and finally the extraction of the coronaries using a vessel filter.

The first step consists of the segmentation of the heart's blood pools. In order to do so, we start with the windowed volume. We then iterate through the whole volume in a slice by slice basis. For each slice, we first create a binary image by setting all the pixels not equal to the maximum to zero. This creates an image that contains both bones and blood pools. We then apply a hole-filling algorithm to reduce noise from the previous step. Finally, to segment the blood pools, we apply a method similar to what Cline does in [9]. The process consists of mathematical morphological erosion followed by a dilation applied to the binary image. The resulting image is a slice that only contains the blood pools and bones. We can subtract this image from the windowed image to obtain a slice without the blood pools and bones but with the coronary arteries. The process is seen in Figure 1.

The third step is performed to segment the heart from everything else (bones, lungs, etc.) in each slice. This is done to have a final image with only coronary arteries and myocardium in them. In order to do so we start with the binary volume. Again, we perform a slice by slice operation to segment the heart's contour. For each slice, the first step consists of applying a median filter for noise reduction. We then find the centroid of the image to have an initial contour that later will be deformed. The contour is found using a traditional snakes algorithm [12] [13]. The snakes algorithm contains an external energy field that will drive the initial contour (created around the centroid) to the heart's boundary. The external energy is calculated by finding the vector field that points towards the heart's border. The process is seen in Figure 2.

The final step of the process is to apply a vessel filter that is based on the work previously done by Frangi in [6] and Bauer in [4]. Unlike the work by Bauer, that uses Gradient Vector Flow (GVF) our approach consists of an

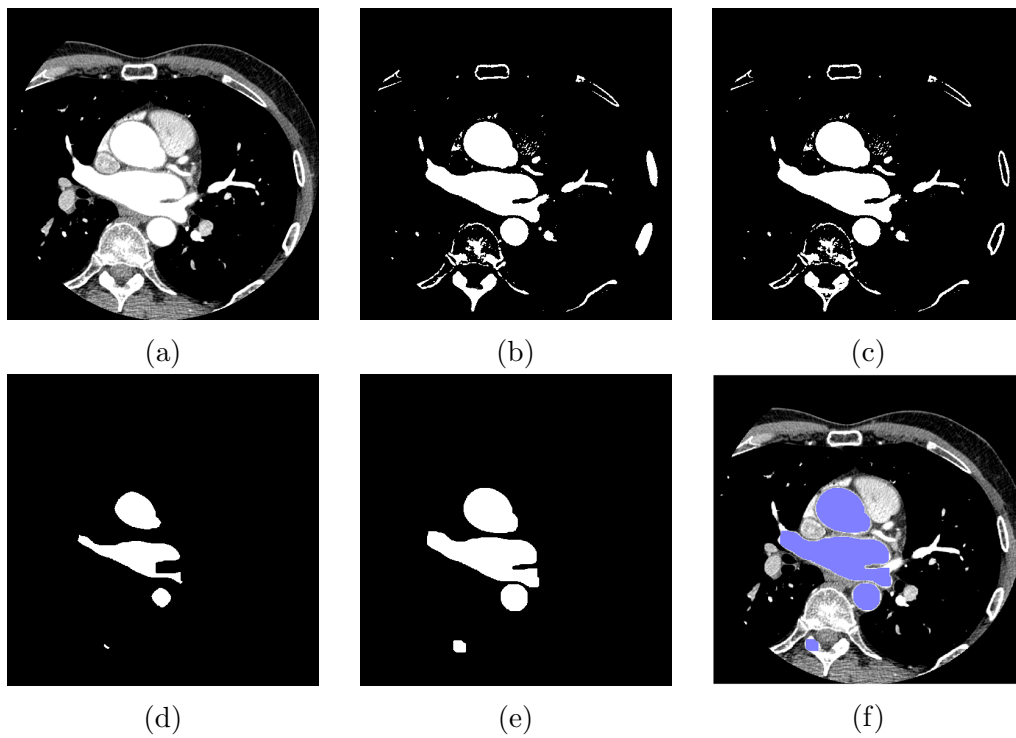


Figure 1: (a) Windowed Image I_w . (b) Binary image of hyperintense region (blood pools) I_{binbp} . (c) I_{binbp} , hole filled. (d) 3 erosions. (e) 3 dilations. (f) Results.

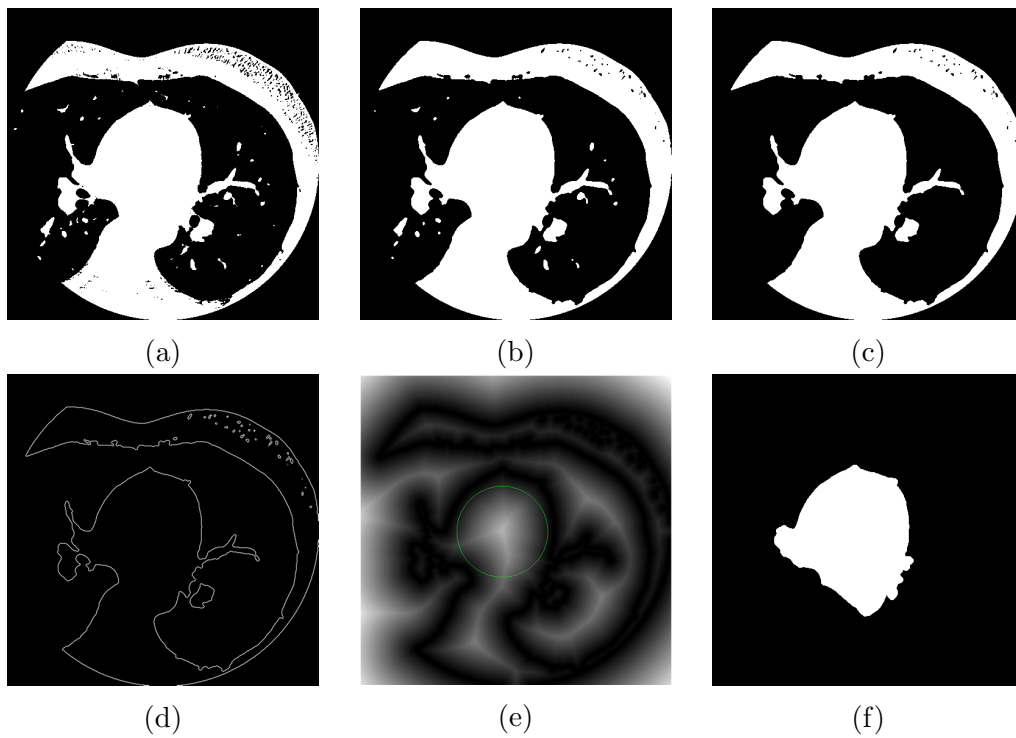


Figure 2: (a) Binary image I_{bin} . (b) Noise reduction. (c) Connected component analysis. (d) Binary image's borders. (e) Distance transform of images. (f) Results.

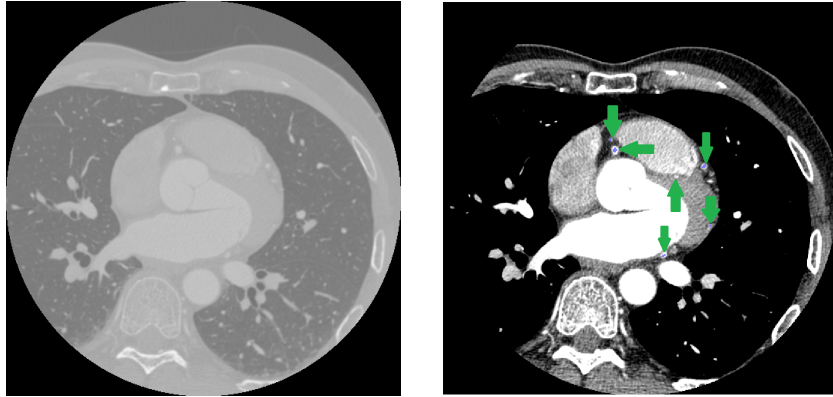


Figure 3: (a) Initial image. (b) Final image.

analysis of the second order structure of the vector field obtained using the distance transform of the magnitude of the derivative of the volume. The results are similar in the sense that they both produce vector fields that point towards the center of the vessel.

To find the vesselness of each voxel in the initial windowed volume (using Frangi's vesselness definition), we first need to calculate two different Hessian matrices. The first Hessian is calculated by first taking the normalized gradient of the input image and then constructing the Hessian using the derivative of the normalized gradient field. The second Hessian is computed by first calculating the magnitude of the first derivative of the initial volume and then calculating its distance transform. The second Hessian is then constructed by taking the derivative of this second normalized vector field. The final vessel filter response consists using Frangi's measure (for details on this calculation please refer to the cited paper) with default values on both Hessians and for each voxel choosing the greater value of the two.

The results of the calculations performed on a slice are shown in Figure 3. To the right we see the initial slice that has been windowed using the parameters in the DICOM file and to the left we see the final slice after the four steps of processing.

3. CONCLUSIONS

The objective of this paper was to implement a method to extract the coronary arteries from images obtained in CTA. By combining and modifying previously published methods, we were able to develop our own and unique

method. We chose to take advantage of the computational simplicity of the distance transform as opposed to the complexity of the GVF (Gradient Vector Flow) proposed by Bauer et al. This was a key to our process since it is used in two of the four steps that we need to segment the coronaries. In the future we plan on adding noise reduction techniques to get cleaner results.

References

- [1] Roger, Véronique L., et al. "Executive Summary: Heart Disease and Stroke Statistics—2012 Update A Report From the American Heart Association." *Circulation* 125.1 (2012): 188-197.
- [2] Diem Phuc T Banh, Iacovos S Kyprianou, Sophie Paquerault, and Kyle J Myers. Morphology-based three-dimensional segmentation of coronary artery tree from cta scans. In *Medical Imaging*, pages 65122I-65122I. International Society for Optics and Photonics, 2007.
- [3] Christian Bauer and Horst Bischof. Edge based tube detection for coronary artery centerline extraction. *The Insight Journal*, 2008.
- [4] Christian Bauer and Horst Bischof. A novel approach for detection of tubular objects and its application to medical image analysis. In *Pattern Recognition*, pages 163-172. Springer, 2008.
- [5] B Bouraoui, C Ronse, J Baruthio, N Passat, and Ph Germain. Fully automatic 3d segmentation of coronary arteries based on mathematical morphology. In *Biomedical Imaging: From Nano to Macro, 2008. ISBI 2008. 5th IEEE International Symposium on*, pages 1059-1062. IEEE, 2008.
- [6] Alejandro F Frangi, Wiro J Niessen, Koen L Vincken, and Max A Viergever. Multiscale vessel enhancement filtering. In *Medical Image Computing and Computer-Assisted Intervention MICCAI 98*, pages 130-137. Springer, 1998.

- [7] Yoshinobu Sato, Shin Nakajima, Nobuyuki Shiraga, Hideki Atsumi, Shigeyuki Yoshida, Thomas Koller, Guido Gerig, and Ron Kikinis. Threedimensional multi-scale line filter for segmentation and visualization of curvilinear structures in medical images. *Medical image analysis*, 2(2):143-168, 1998.
- [8] Andrzej Szymczak. Vessel tracking by connecting the dots. *The Insight Journal*, 2008.
- [9] Cline, H.E., Thedens, D.R., Irazrazaval, P., Meyer, C.H., Hu, B.S., Nishimura, D.G., Ludke, S.: 3D MR coronary artery segmentation. *Magnetic Resonance in Medicine* 40 (2005) 697-702
- [10] Funke-Lea, G., Boykov, Y., Florin, C., Jolly, M.P., Moreau-Gobard, R., Ramaraj, R., Rinck, D.: Automatic heart isolation for CT coronary visualization using graph-cuts. *IEEE International Symposium on Biomedical Imaging* (2006)
- [11] Bauer, C., Bischof, H.: Edge Based Tube Detection for Coronary Artery Centerline Extraction. *The Insight Journal* (2008)
- [12] Kass, M., Witkin, A., Terzopoulos, D.: Snakes: Active contour models. *International journal of computer vision* 1 (1988) 321-331
- [13] Xu, C., Prince, J.L.: Snakes, shapes, and gradient vector flow. *IEEE Transactions on image processing* 7 (1998) 359-369

Integrated system of data acquisition and monitoring of intra and peridomestic infestation of vector of Chagas disease

Luis Rodríguez^{a1}, Marcio Duarte^a, Santiago Gómez^a, Christian Schaerer^a and Antonieta Rojas de Arias^b

^a Polytechnic School, National University of Asunción, San Lorenzo, Central, Paraguay. P.O.Box: 2111 SL

^b Centro para el Desarrollo de la Investigación Científica (CEDIC/DIAZGILMedicina Laboratorial/FMB), Asunción, Paraguay.

Abstract

Chagas disease is a tropical illness that continues to exist in Latin America and exhibits high rates of infection in Paraguay. The agencies responsible for public health in Paraguay invest a lot of resources in both treatment and research to reduce this high rate of infestation [1].

In the field of research, methodologies used for field data collection in endemic areas of Chagas disease are precarious [2], resulting in stale data and the inability to make the best decision to draw up action plans against this problem.

There are currently available platforms that allow the systematic collection of data using editable graphical interfaces fitting the majority of cases. These tools are available for free but they only offer basic input functionalities and basic statistical analysis. The functionalities needed for collection of Chagas data would require the purchase of a commercial license. Analysis of historical data and comparisons of variables are also essential to have a correct diagnosis of the topic to study.

Our work helps to find an adequate solution to this problem. We use technology to facilitate the process of data collection, providing accessibility and ease to deploy a field study using digital forms. In addition, they can launch a series of analyses that help diagnose a particular situation, thus reducing the uncertainty and facilitating decision making in less time, which is essential for public health issues.

As an initial case study, we use our platform for monitoring intra and peridomestic Chagas vector infestation. The platform can be reused for another scenario where data collection and processing are required; this is achieved by employing generic data types that are

¹E-mail Corresponding Author: rodriguez.luicho@gmail.com

configurable according to the needs of each case. In addition, mobile devices with their embedded sensors and multimedia capabilities including image and sound, open up new opportunities for the data collected to provide broader and more detailed information regarding the current status of the problem under study.

Keywords: Field data acquisition, Chagas disease, real time information, mobile devices

References

- [1] Rolón, M.; Vega, C.; Román, F.; Gómez, A., Rojas de Arias, A., 2011. First Report of Colonies of Sylvatic *Triatoma infestans* (Hemiptera: Reduviidae) in the Paraguayan Chaco, Using a Trained Dog. *PLoS Negl Trop Dis* 5(5): e1026. doi:10.1371/journal.pntd.0001026
- [2] Rojas de Arias, A., Russomando, G. El control de la enfermedad de Chagas en Paraguay. 269-298. Chapter 6. In: *El control de la enfermedad de Chagas en los pases del Cono Sur de Amrica. Historia de una iniciativa internacional 1991/2001*. OPS/OMS, 2002.

Grooming-Hierarchical WDM Network Design

Alberto A. Amadeo^{a1}, Diego P. Pinto Roa^a

^a National University of Asunción

Abstract

With the increase in load and diversity type of network traffic, new architectures and optical-network design for heterogeneous speed traffic are critical issues in optical communications. In this paper we focus on the complex problem of Wavelength Division Multiplexing (WDM) Network design considering simultaneously grooming - for low speed traffic - and hierarchical - for high speed traffic- architectures using Genetic Algorithm (GA). Basically, given a network topology and a set of unicast requests with static traffic loads, the main objective is to design a grooming-hierarchical WDM network with minimum cost subject to physical layer constraint. Due to high complexity of the problem in question, the proposed GA has been implemented with different traffic packaging approaches in which the experiment indicates that the quality of solutions is highly dependent to traffic packaging strategy.

Keywords: WDM Network, Grooming Network, Hierarchical Network, Network Design, Genetic Algorithm

¹E-mail Corresponding Author: aamadeo@gmail.com

Applying Seasonality to a Discrete form of the Bass Model

Claudia Montanía^a, Santiago Gómez^a and Christian Schaerer^a

^a Polytechnic School, National University of Asunción, San Lorenzo, Central, Paraguay. P.O.Box: 2111 SL.

Abstract

In order to predict the behavior of new products as they are introduced to the market, we propose to extend the Discrete Bass model as proposed by D. Satoh to include seasonal variations and decrease prediction biases.

Some commercial products present important ups and downs in their sales during certain seasons of the year. The standard Bass model doesn't account for peaks and valleys in its prediction, yielding biased and inaccurate forecasts in those products that exhibit strong seasonality.

Research in the literature indicates that starting from a discrete model achieves greater precision when estimating the parameters of the model. Thus we extend this discretized form of the Bass model by adding seasonality, considering that the discrete form fully supports the prediction of the standard model and keeps the same parameters of innovation, imitation and market potential.

Keywords: Bass Model, Discretization, Seasonality, Parameter Estimation.

References

- [1] BASS, FRANK, 1969. A new product growth for model consumer durables, Management Science.
- [2] SATOH, DAISUKE, 2001. A discrete Bass Model and its parameter estimation, Journal of the Operations Research-Society of Japan.
- [3] PEERS, YURI, FOK, DENNIS, HANS FRANSES, PHILIP, 2010. Modelling Seasonality in New Product Diffusion, ERIM Report Series Research in Management.

Automated Monitoring of Electrical Conductivity, Humidity and Temperature of Agricultural Soil

Richard José González^{a1}, Israel Cáceres Sarubbi^a

^a Facultad Politécnica, Universidad Nacional de Asunción, Paraguay

Abstract

The Automated Monitoring of Electrical Conductivity, humidity and Temperature of Agricultural Soil, was developed with the motivation to provide an electronic tool for a faster and easier analysis of the behavior of different soil types in agricultural production, as well as the characterization and management of it during the entire growing process of grains, vegetables and fruits.

It consists in the study, design and development of a tool that makes possible the agricultural resources optimization in order to achieve a homogenization in the yield of the cultivated products. The engineering design, required researches with professors of Agronomics Sciences Faculty, looking forward to get more knowledge about the topic. The mentioned tool was possible through a combination of measurement, positioning, transmission, management and storage of technologies data. The values of electrical conductivity, soil moisture and temperature add value to the agricultural operation, if they are used to explain the variability in the crop field.

With the implementation of this system will be understood the reasons why there are huge variations in performance, which leads to a better crop management, also enhancing its performance by reducing input costs or predicting more precisely the benefits to be gained by trenching, add fertilizer, irrigation, building windbreaks or make other improvements in the yield.

Keywords: Agriculture, Soils, Electronics in agriculture, Edaphology, Soil temperature, Soil moisture, Automation

1. INTRODUCCION

The field of Precision Agriculture (PA) has had important progress in the last decades and researches about this are still in development. Due mostly

¹E-mail Corresponding Author:

to the fact that PA has become such a useful tool that allows localized management of agricultural practices, with higher products application efficiency, reducing the impact to the environment and as a consequence, it diminishes the costs of food production, which suggests improvements against conventional agricultural methods. Books like [1] offers general view about the advances and present applications about PA.

Humidity Level [2], temperature [3] and electrical conductivity level [4] [5] [6] [7] of cultivation soil that varies in time and space; in order to know the status of those levels, manual readings are performed about soil sensors [8] [9] [10] [11] [12] [13] [14] [15] [16], strategically distributed on the field.

The method's main disadvantage lies in the fact that the period of time required is too long and proportional to the field surface, another problem could be the fact that soil conditions vary with time mainly because climatic changes (rains, temperature changes, droughts, etc.) that influences on the soil measured variables.

2. OBJECTIVES

The essential objective of this work is the development of a real time monitoring system that features a remote terminal which is located in the cultivation ground which constantly sends data about the status of the variables that are studied, thanks to ZigBee transmitters [17] [18] to a computer that draws the curves and classifies chronologically the behavior of those levels in an electronic chart.

3. RESULTS ACHIEVED SO FAR

Obtaining a functional prototype which acquires information about levels of humidity, temperature and dissolved salts in the soil, and transmitted in real time to a remote monitoring central, for its statistic treatment



At the beginning, the tests performed to measure the performance and accuracy of the electronic tool prove the very reliable behavior of it, thanks to the calibrations performed to it by the recommendation of the manufacturer. The values of the studied variables obtained in the trial measurements showed no significant deviations in comparison with the values obtained by traditional methods.

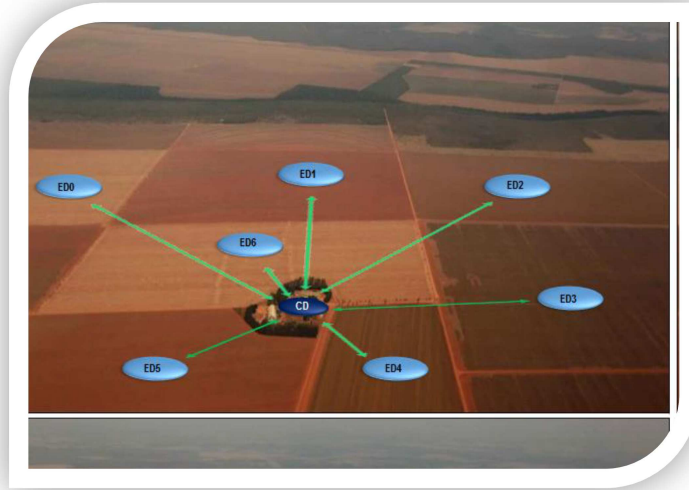
4. DEVELOPMENT AND FUTURE SCOPE

Through performed researches, errors on the traditional monitoring method could be fixed.

The tool allows obtaining automated information in real time of the status of humidity, temperature and dissolved salts levels of the soil in the cultivation field. This information constitutes support for agricultural managers.

With the implementation of the system in the field, it will be possible to make preventive and corrective actions on managing measured variables. In this way, a higher percentage of development in the harvest will be obtained.

The future aim is the implementation of a network of monitoring stations through the entire field, it will be made-up of the remote stations and the data reception center unit, in order to make possible to know the behavior of the entire field.



ACKNOWLEDGMENTS: We thank Engineer Federico Gaona for his contributions.

References

- [1] Bongiovanni, R.; Mantovani, E. C.; Best, S.; Roel, A (Eds.). 2006. Agricultura de precisión: integrando conocimientos para una agricultura moderna y sustentable. Montevideo, Uruguay, PROCISUR/IICA.
- [2] RUSSELL, E. Condiciones del suelo y desarrollo de las plantas según Russell. 1992. [online]. P. 355-386. Available on http://books.google.com.py/books/about/Condiciones_del_suelo_y_desarrollo_de_la.html
- [3] CASANOVA, E. Introducción a la ciencia del suelo. 2005. [online]. P. 147. Available on http://books.google.com.py/books/about/Introduccion_a_la_ciencia_del_suelo.html
- [4] NUEZ, F. El cultivo del tomate. 1995. [online]. P. 142. Available on http://books.google.com.py/books/about/El_Cultivo_del_tomate.html

- [5] CAPACIDAD DE INTERCAMBIO CATIONICO. [online]. Available on <http://amazoniaforestal.blogspot.com/2011/11/capacidad-de-intercambio-cationico.html>
- [6] Conductividad eléctrica. HANNA INSTRUMENTS. [online]. Available on <http://www.hannainst.es/biblioteca/>
- [7] Capacidad de intercambio catiónico. [online]. Available on <http://www.exactas.unlpam.edu.ar/academica/catedras/edafologia/practicos/capdeintcat.html>
- [8] SERNA, A. Guía Práctica de Sensores. 2010. [online]. P. 3. Available on http://books.google.com.py/books/about/Guia_practica_de_sensores.html
- [9] SOIL EC. [online]. Available on <http://www.veristech.com/products/soilec.aspx>
- [10] DOERGE, T. MAPEO DE LA CONDUCTIVIDAD ELÉCTRICA DEL SUELO. [online]. P. 2. 79 Available on http://www.logemin.com/eng/Download/pdf/39_mapeo_conductividad_electrica.pdf
- [11] DECAGON DEVICES. [online]. Available on <http://www.decagon.com/products/soils/volumetric-water-content-sensors/>
- [12] Medidas directas del contenido de agua en el suelo. [online]. Available on <http://info.elriego.com/medida-del-contenido-de-agua-en-un-suelo/text/html>
- [13] MUÑOZ, R. HIDROLOGIA AGROFORESTAL. 2005. [online]. P. 128. Available on http://books.google.com.py/books/about/Hidrologia_agroforestal.html
- [14] DECAGON DEVICES. [online]. Available on <http://www.decagon.com/products/soils/volumetric-water-content-sensors/>
- [15] PROTOCOLO DE TEMPERATURA DEL SUELO. [online]. Available on http://www.globeargentina.com.ar/guia_del_maestro_web/suelos/protocolos/prottemperaturadelsuelo.pdf

- [16] HANNA INSTRUMENTS. [online]. Available on <http://www.hannacolombia.com/productos/termometros/termometros-portatiles/termometro-termopar-tipo-k-con-microprocesador-e-impermeable>
- [17] CHÁVEZ, J. Propuesta de aplicación domiciliaria utilizando tecnología ZigBee. 2008. [online]. 106 Available on <http://revistas.utp.edu.co/index.php/revistaciencia/article/download/>
- [18] UNDERSTANDING ZIGBEE. [online]. Available on <http://www.zigbee.org/About/UnderstandingZigBee.aspx>

Applying a wire plate Electrostatic Precipitator for collection of particulate matter from burning coconut pit

Edgar M. Maqueda ^{a1}, Alfredo Renault ^b, and Norma G. Silva ^c

^{a b c}Facultad Politécnica, Universidad Nacional de Asunción, San Lorenzo,
Paraguay

Resumen

The work consists of sizing and implementation of a prototype wire plate type electrostatic precipitator for collecting particulate matter (PM) of coconut pit, and applying the method of gravimetric concentration level of the existing PM is calculated in the body issuer (fireplace), and finally compare with international quality guidelines air in relation to the same and determine their viability in this application. The evidence relating to airborne PM and its effects on public health agree reveal adverse health effects of people. The electrostatic precipitator consists of a power supply based on a flyback transformer that generates high voltage necessary to produce the electrostatic field, collectors and discharge electrodes, and an exhaust fan for introducing air into the prototype.

Keywords: Electrostatic precipitator, particulate matter, gravimetric, flyback transformer.

1. INTRODUCCIÓN

Este proyecto tiene por objetivo contribuir en la disminución de la contaminación del aire causado por las emisiones de los humos industriales a través de un Precipitador Electrostático placa-alambre aplicado a la combustión del carozo de coco. Los precipitadores electrostáticos se utilizan en la industria para limpiar los gases de combustión y los humos de los altos hornos recolectando el material particulado lo los mismos. Estos humos al ser liberados sin tratamiento alguno, contaminan el aire que respiramos causando enfermedades en las personas. El precipitador electrostático utiliza el campo eléctrico para separar las partículas de polvo de los humos que los arrastran, y captan

¹E-mail Corresponding Author: edgarmaqueda@gmail.com

partículas del tamaño de 0,01 m a 100 m con una eficiencia de más del 99 por ciento. [1]

Según una evaluación de la OMS de la carga de enfermedad debida a la contaminación del aire, son más de dos millones las muertes prematuras que se pueden atribuir cada año a los efectos de la contaminación del aire en espacios abiertos urbanos y en espacios cerrados (producida por la quema de combustibles sólidos). Más de la mitad de esta carga de enfermedad recae en las poblaciones de los países en desarrollo. [2]

2. MÉTODOS Y MATERIALES

La metodología adoptada para la determinación de la concentración del PM.

La metodología adoptada para la determinación de la concentración del PM es la gravimetría. Este método consiste en obtener la diferencia de pesos entre un filtro de PM con el contaminante recolectado y el peso del mismo filtro limpio cuyo resultado es la cantidad de material particulado recolectado en un volumen de aire determinado. La concentración del polvo o materia particulada en el aire muestreado se calcula a partir de la cantidad P, mediante la siguiente expresión:

$$C=P/V$$

Donde: C es la concentración de polvo o materia particulada en aire, en g/m³. P es la cantidad de polvo o materia particulada, en g. V es el volumen de aire muestreado, en m³. [3]

El esquema siguiente muestra el proceso propuesto para determinar el nivel de concentración del PM.



Figure 1 - Proceso para obtener el nivel de concentración del PM.

Descripción del proceso

1. Puesta en funcionamiento del PES conectada a la chimenea para recolectar el PM, durante un tiempo de 24 horas.
2. Recolección de las partículas de las placas colectoras del PES.
3. Determinación del peso del PM recolectado por el PES mediante una balanza digital.
4. Cálculo de la concentración del PM.

Normas de calidad del aire según la OMS.

Nivel de concentración del PM₁₀ = 25 g/m³ media de 24 horas.

Normas de calidad del aire para EE.UU. y MEXICO

Material particulado suspendido total (TSP), para 24 hs.

Nivel de concentración del PM = 260 g/m³. [4]

Indicador del nivel de contaminación de la atmósfera para Chile.

Establece un episodio de emergencia para PM₁₀, para 24 hs.

Nivel de concentración del PM₁₀ = 330 g/m³. [5]

La metodología del diseño del prototipo del precipitador electrostático.

La metodología del diseño del prototipo del precipitador electrostático se basó en el estudio, dimensionamiento y diseño de las partes principales del

precipitador electrostático: fuente de alimentación, electrodos colectores y de descarga.

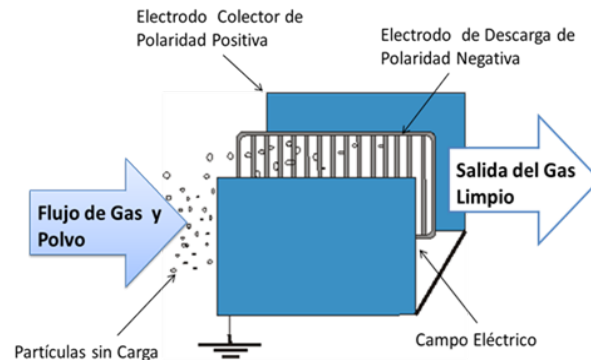


Figure 2 - Principio de funcionamiento del precipitador electrostático.

Fuente de alimentación

El estudio e investigación de la fuente de alimentación se basa en el funcionamiento de los transformadores flyback, el cual consta de las siguientes bloques: fuente de alimentación, oscilador, conmutador, protección y transformador flyback. Esta fuente posibilita obtener una tensión variable del rango de 1kV a 22kV.

Electrodos colectores

Consta de un total de tres electrodos, para su construcción se utilizó chapa galvanizada número 29 por sus características de espesor muy delgadas, su resistencia ante la corrosión, su abundancia en el mercado nacional y su bajo costo.

Electrodos de descarga

Compuesto por un total de cuatro electrodos con diez cables cada uno separados a una distancia de 6 cm unas de otras, para su construcción se utilizó alambre de acero inoxidable tipo cercado eléctrico por sus características de espesor 0,60 mm de diámetro, su flexibilidad y resistencia al tensionarlos y principalmente está preparado para manejar alta tensión y baja corriente.

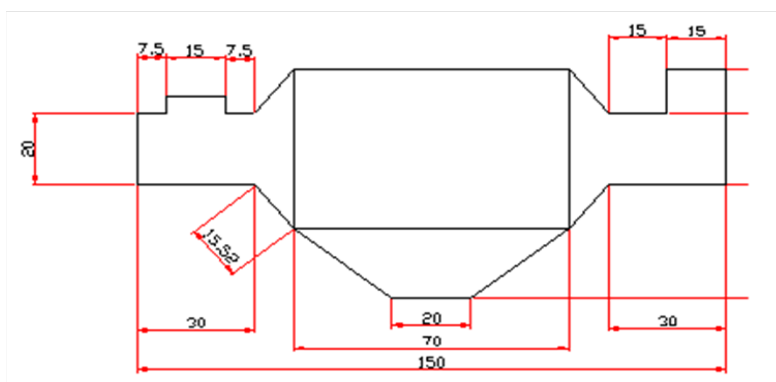


Figure 3 - Vista frontal del prototipo PES cuyas medidas están en centímetros.



Figure 4 - Imagen del prototipo de precipitador electrostático.

3. RESULTADOS

Cálculo de la eficiencia del prototipo de PES.

En la tabla 1, se observa las pruebas de laboratorio hechas para los cálculos de la eficiencia en la recolección de PM de carozo de coco. Dicha prueba fue realizada a una velocidad de flujo de aire de 3 m/s y a una tensión de 13 kV, punto de operación del prototipo donde se obtuvo la mejor eficiencia promedio de 94

Masa (g)	Mediciones de la Eficiencia (%)				
	X ₁	X ₂	X ₃	X ₄	X ₅
60	93,3	95	93,3	95	93,3
70	95,7	93	95,7	91	95,7
80	93,7	91,2	96,2	93,7	93,7

Tabla 1 - Valores de eficiencia del PES para la recolección de PM de carozo de coco.

Cálculo de validación del prototipo de PES para la reducción del PM.

Para el siguiente cálculo se realiza una simulación de una emisión de 330 g/m³ de concentración del PM correspondiente a la combustión del carozo de coco, y se aplica la metodología propuesta por el proyecto para determinar su efectividad.

Nivel de concentración de PM $C = 330$ g/m³ en 24 hs.

Caudal del PES $Q = V \cdot A$

Donde:

V = velocidad de aire dentro del PES.

A = área del ducto del PES.

$Q = 3\text{m/s} \cdot (0,20)^2 = 0,12$ m³/s

Pasamos el caudal Q a 24 hs.

$Q = 0,12 \cdot 60 \cdot 60 \cdot 24 = 10368$ m³/24 hs.

Eficiencia promedio del PES 94

Cálculo del peso equivalente de $C = 330$ g/m³

$$C=P/V ; P=C \cdot V=330\text{g}/\text{m}^3 \cdot 10368 \text{ m}^3/24 \text{ hs.} = 3,42 \text{ g}/24 \text{ hs.}$$

$$\text{PM Recolectado por el PES} = 3,42 \cdot 94$$

$$\text{PM que escapó del sistema} = 3,42 - 3,21 = 0,21 \text{ g}/24 \text{ hs.}$$

Cálculo de la concentración resultante:

$$C=P/V = (0,21 \text{ g}/24 \text{ hs})/(10368 \text{ m}^3/24\text{hs})=20,25 \text{ g}/\text{m}^3$$

4. CONCLUSIÓN

Los cálculos de rendimiento hechos al prototipo son satisfactorios, resultados que reflejan la efectividad del sistema.

Se logró validar la efectividad del sistema propuesto para la reducción de la reducción del aire donde de un lugar de concentración del PM de 330 g/m³ se redujo a 24 g/m³ ingresando dentro del nivel mínimo de exposición en 24 horas según las guías de calidad de aire de la OMS.

Referencias

- [1] FERNÁNDEZ OVIEDO ISMAEL PRIETO, 2000. Precipitadores Electrostáticos utilizados en Centrales Termoeléctricas, pp. 1-60
- [2] ORGANIZACIÓN MUNDIAL DE LA SALUD.2005. “Guías de calidad del aire de la OMS relativas al material particulado, el ozono, el dióxido de nitrógeno y el dióxido de azufre, pp. 5-21.
- [3] MINISTERIO DEL TRABAJO Y ASUNTOS SOCIALES ESPAÑA, INSTITUTO NACIONAL DE SEGURIDAD E HIGIENE EN EL TRABAJO. “Determinación de materia particulada (total y fracción respirable) en aire - Método gravimétrico”, MTA/MA-014/A88.
- [4] CENTRO DE INFORMACIÓN SOBRE CONTAMINACIÓN DE AIRE (CICA RED DE TRANSFERENCIA DE TECNOLOGÍA), para la frontera entre EE. UU. – México.

- [5] MINISTERIO DEL MEDIO AMBIENTE. GOBIERNO DE CHILE. Indicador del nivel de contaminación de la atmósfera. Índice de calidad de aire por partículas ICAP. Disponible en www.mma.gov.cl.

A numerical implementation of 2-D incompressible Navier-Stokes equations using stream function-vorticity formulation

Laura Oporto^{a1}, Christian Schaerer^b

^a Chemical School, National University of Asuncion

^b Polytechnic School, National University of Asuncion,
San Lorenzo, Paraguay. P.O.Box: 2111 SL.

Abstract

Incompressible Navier Stokes equation models a lot of processes in industry and science. Due to its importance several implementations seeking to increase the performance in its resolution have been reported in the literature [1].

In this work a stream function - vorticity formulation is used for the numerical resolution of the 2-D laminar incompressible Navier-Stokes equation. This implementation is used to solve benchmark problems, for instance the lid driven cavity flow.

The physical configuration consists of a square container filled with a fluid initially at rest. At a specific time, denoted as initial time, the lid moves with a constant velocity U , and this yields the motion of the fluid.

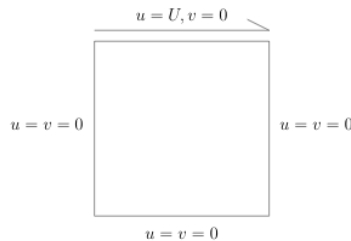


Figure 1: Problem configuration

In two dimensions, the Navier-Stokes equations can be expressed using the stream function ψ and the vorticity ω , implying the elimination of the pressure from the equations.

For a homogeneous, bi-dimensional incompressible flow, the vorticity transport equation is given by:

$$\frac{\partial \omega}{\partial t} = -u \frac{\partial \omega}{\partial x} - v \frac{\partial \omega}{\partial y} + \nu \left(\frac{\partial^2 \omega}{\partial x^2} + \frac{\partial^2 \omega}{\partial y^2} \right) \quad (1)$$

¹E-mail Corresponding Author: lauri.oporto@hotmail.es

where ω is the vorticity, defined as:

$$\omega = \frac{\partial u}{\partial y} - \frac{\partial v}{\partial x}. \quad (2)$$

Defining the stream function ψ , velocities u and v can be expressed in the form:

$$u = \frac{\partial \psi}{\partial y}, \quad v = -\frac{\partial \psi}{\partial x}. \quad (3)$$

Replacing equations (3) in (2), the Poisson equation for the stream function is obtained:

$$\frac{\partial^2 \psi}{\partial x^2} + \frac{\partial^2 \psi}{\partial y^2} = \omega \quad (4)$$

In the context of this work, equations (1) – (4) are approximated by finite differences. Forward difference is used for time and central differences for spatial derivatives.

The fluid velocity on the boundary segments are $u = v = 0$, except for the upper boundary, along which the velocity is equal to the given lid velocity $u_{wall} = U = 1$.

Initial conditions for equation (1) is the fluid is considerate to be at rest, which means $u_{i,j}^0 = 0$ $v_{i,j}^0 = 0$ in the interior points. Thus, $\omega_{i,j}^0 = 0$ and $\psi_{i,j}^0 = 0$ at the interior points.

The boundary condition for the stream function is $\psi_{wall}^k = 0$. The following figures show the stream function for $Re=100$ and $Re=700$. Equations were solved using a 51×51 grid mesh and 2500 time steps.

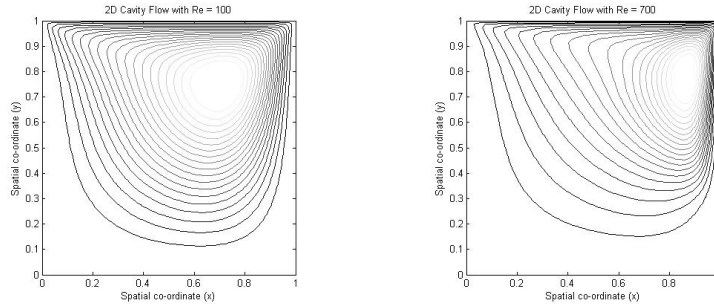


Figure 2: Driven cavity, streamlines for $Re=100$ and $Re=700$

MATLAB is used to solve the system, and the results obtained are compared to those shown in the literature [1],[2],[3]. This work is presented as a scientific initiation to determine a bachelor thesis in the field.

Keywords: stream function - vorticity, incompressible fluid, Navier Stokes equation.

References

- [1] Michael Griebel, Thomas Dornseifer, Tilman Neunhoeffler,1998, Numerical Simulation in Fluid Dynamics, SIAM.
- [2] Murli M. Gupta, Jiten C. Kalita,2005, A new paradigm for solving Navier-Stokes equations: streamfunction-velocity formulation, Journal of Computational Physics, v.207 n.1, p.52-68.
- [3] Maciej Matyka,2004,Solution to two-dimensional incompressible Navier-Stokes equations with SIMPLE, SIMPLER and vorticity-stream function approaches. Driven-lid cavity problem: Solution and visualization, Report in Computational Physics Section of Theoretical Physics, University of Wroclaw, Poland, Department of Physics and Astronomy.
- [4] Suhas V. Patankar,1980,Numerical Heat Transfer and Fluid Flows, edited in Series in Computational and Physical Processes in Mechanics and Thermal sciences.
- [5] Donan Calhoun,2001, A cartesian grid method for solving the two-dimensional streamfunction-vorticity equations in irregular regions, Courant Institute of Mathematical Sciences.

Stability command of a Tilt-rotor vehicle with a Fuzzy Logic controller

Eduardo Coronel¹, Adolfo Jara

National University of Asunción, Polytechnic School, San Lorenzo, Paraguay

Abstract

The project consists in the design, modeling and building of a two-planar rotor aircraft by the implementation of a Fuzzy Logic controller on a 8-bit microcontroller, with the use of the eFLL library [1]. The simplicity and intuitive way to apply the Fuzzy Logic control in real applications makes from it an attractive alternative to other, more complex, control systems. It has an accuracy that is at the level of the most elaborated controllers based on mathematical models. The design and simulation of the control system was implemented with the use of the Fuzzy Logic Toolbox included in Matlab®[2]. The practical fundamentals of Fuzzy Logic controllers are explained in this paper with all the analytic studies for its employment on a Tilt-rotor vehicle.

Keywords: Fuzzy Logic controller, Fuzzy Logic Toolbox, Matlab, Tilt-rotor, Aircraft, control system, eFLL, microcontroller.

1. INTRODUCTION

In the last years, there was a huge advance in the development of Unmanned Aerial Vehicles (UAV) for its uses in many civilian applications [3]. However, the development of the control system of these vehicles is not an easy task. The complex dynamics of aerial vehicles, which involves many degrees of freedom and non-linear characteristics, makes the mathematical modeling of it becomes a really headache, even for the most experimented engineers. A known control system called PID is the one usually implemented for these and for, probably, most systems that require an autonomous control. A mathematical model is, indeed, needed for the development of a PID control system [4]. Fuzzy Logic allows the treatment of information in a human like style. It can treat imprecise data, like *low temperature*, *high*

¹E-mail Corresponding Author: edamcor@gmail.com

pressure, medium height, in terms of fuzzy sets. These sets are used to associate a grade to each linguistic term (known as fuzzy memberships) and can be combined through rules to define actions. We are aware of the not need of mathematical models to control, by ourselves, the behavior of something [5], and that is the same way that a Fuzzy Logic controller works.

The main goal of the project is: design and implement a control system for the aerodynamic balance of a Tilt-rotor vehicle. The Tilt-rotor is an aircraft that generates lift and propulsion by two rotors mounted on rotating engine pods, usually at the ends of a fixed wing. The implementation of Fuzzy Logic in the control of a system like this aims to demonstrate its high control capability with few use of mathematics. This is the reason why this model of vehicle was chosen.

2. METHODS AND MATERIALS

To develop the system it was decided for the use of brushless motors for the two rotors, each one of them attached to a servo motor, which allow directional changes of the planar action of rotors. The two motors are controlled by an 8-bit PWM (*Pulse Width Modulation*) so that the throttle can be generated by the need of correction of the system. To measure the angular and altitude changes, it was decided to use an *Inertial Measurement Unit* (IMU) sensor. These values are acquired via I2C communication by a microcontroller (ATMEGA 2560), which also is in charge of the Fuzzy Logic control implementation.

3. STRUCTURE

To put in practice the Fuzzy Logic controller a Tilt-rotor system was designed. The main aspects of it are: the two "wings/arms" are made of aluminum. Few other parts, like the rotor blades, the blade protectors and other supporting components, are made of PVC (Polyvinyl Chloride) and acrylic. All the junctions are done by bolts for its easy assembly/disassembly. These materials are used for its light weight and resistance. The next image shows a 3D model of the system.



Figure 1: 3D design of the Tilt-rotor system. Image rendered in CATIA V5.

4. SYSTEM ANALYSIS AND FUZZY SET DEFINITIONS

This stage consisted in the modeling of the Fuzzy Logic controller by the definition of input and output variables. The input variables are the angular errors introduced to the system. The error variable has five fuzzy members that gives an approximation of how it changes. The number of fuzzy members depends on how much linguistic qualified information would be enough such that the Fuzzy Logic can generate the appropriate control [6]. There are two angular errors that requires control, one is introduced by changes in *pitch* axis and the other by changes in *roll* axis.

The *angular error* is the difference between the reference angle (set point) and the current measured angle:

$$e = A_{ref} - A_{act}$$

The error corrections in pitch axis is done by the planar rotation of the rotors, for this purpose, a Fuzzy Logic controller for the servo motors was designed and applied. On the other hand, by applying more thrust to one rotor and less thrust to the diametrically opposite rotor is the technique applied to make corrections on angular errors in roll axis . The generation of the appropriate thrust is, also, designed and applied with a Fuzzy Logic controller.

As viewed, there are two sets of paired actuators that need a control. For that reason, four output variables are defined. Brushless and servo motors have electronic drivers that can be commanded by PWM. However, there is a slightly difference in the commanding mode of the two motors. Brushless motors varies its speed rotation by the increase or decrease of current flow through stator. On the other hand, in servo motors, different but defined PWM values are used to make them do clockwise or counterclockwise rotations.

The Fuzzy Logic Controller generates the two PWM values for the brushless motors so the throttle of them can minimize the angular error or maintain it equal to zero. It also generates the two PWM values for the servo motors that controls the planar angle degree of the rotors.

External forces are usually getting to the system and makes it unstable, those are known as perturbations and have to be handled by the Fuzzy Logic controller. For that reason, fuzzy *Rules* are defined so they decide how to react and generate the appropriate output control signals, according to those changes that try to destabilize the aircraft [6].

The goal of the controller is to keep the Tilt-rotor vehicle horizontally, that consists to maintain the roll axis and pitch axis angular errors near to 0 degree or as minimum as possible, with 0 degree and 90 degree as reference (set point), respectively.

The *angular error* in pitch and roll axis are the two input variables of the fuzzy controller. For both input variables was defined five fuzzy memberships: Big-Negative Error (NG), Little-Negative Error (NP), Zero Error (Z), Little-Positive Error (PP), Big-Positive Error (PG). On the other hand, for the two brushless motors are defined two outputs, each one of them with five memberships: Very Slow (VS), Slow (S), Average (AV), Fast (F), Very Fast (VF). Also, for the two servo motors are defined two outputs, each one of them with five memberships: Thirty (T), Sixty (S), Ninety (N), One Hundred Twenty (HT), One Hundred Forty (HF). It is just a coincidence that the number of memberships defined for the inputs and outputs are the same, in other cases there probably will be needed more members to achieve a better control.

The ranges for each of the memberships are defined according to the quantity of divisions that the expert considers will be needed so that the system can achieve an autonomous control and according to the expectations.

The type of curves used (triangular, trapezoidal, Gaussian, etc.) and ranges varies for different systems. The type of curve widely used is the

triangular and/or the trapezoidal. For the ranges definitions, usually is used a bigger amplitude toward the farthest zones of control center and a smaller amplitude toward the desired control point.

Once all the memberships are defined, the next step is to define the *Fuzzy Rules*, which are five for each pair of motors. The rules are defined so for the same input there are two different outputs, both of them working in opposite to achieve the stability. The defined rule bases are shown next.

A. Defined rules for the two brushless motors:

Rule base	
1	if(angular error is NG) then (PWM-2 is VF And PWM-1 is VS)
2	if(angular error is NP) then (PWM-2 is F And PWM-1 is S)
3	if(angular error is Z) then (PWM-2 is AV And PWM-1 is AV)
4	if(angular error is PP) then (PWM-2 is S And PWM-1 is F)
5	if(angular error is PG) then (PWM-2 is VS And PWM-1 is VF)

B. Defined rules for the two servo motors:

Rule base	
1	if(angular error is NG) then (POS-2 is HF And POS-1 is T)
2	if(angular error is NP) then (POS-2 is HT And POS-1 is S)
3	if(angular error is Z) then (POS-2 is N And POS-1 is N)
4	if(angular error is PP) then (POS-2 is S And POS-1 is HT)
5	if(angular error is PG) then (POS-2 is T And POS-1 is HF)

5. MODELING AND SIMULATION OF THE CONTROL SYSTEM

All information described above was transmitted and loaded correspondingly to the Fuzzy Logic Toolbox included in Matlab, in order to simulate the control system [2]. The following images show the entire process.

A. Fuzzy Logic controller for the two brushless motors:

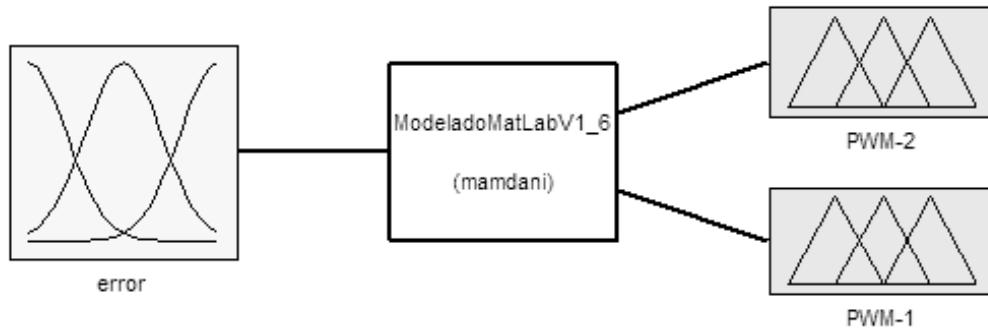


Figure 2: Definition of input/output variables and inference system.

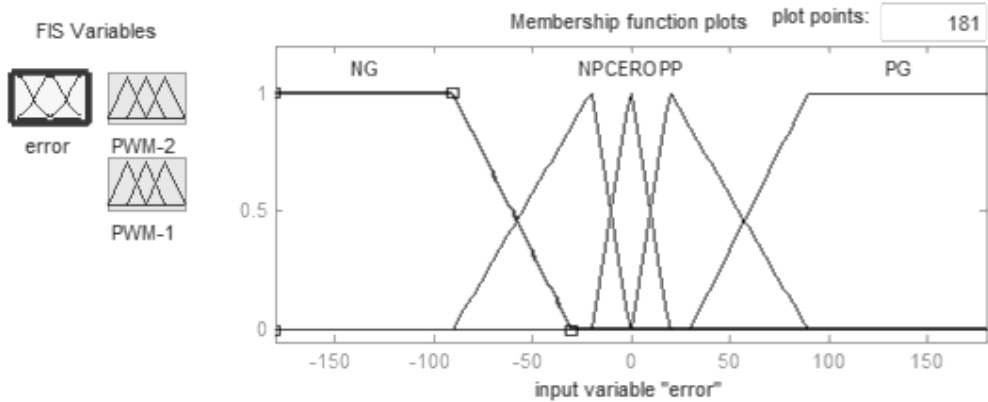


Figure 3: Definition of memberships of the input variable.

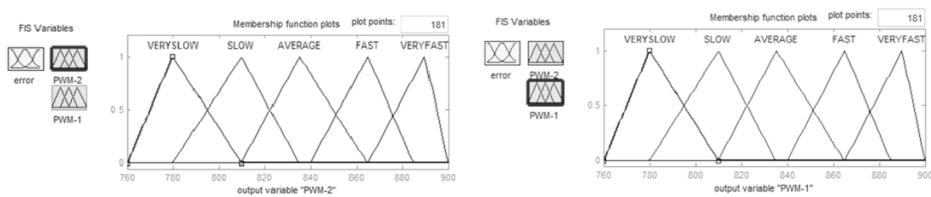


Figure 4: Definition of memberships of the output variables.

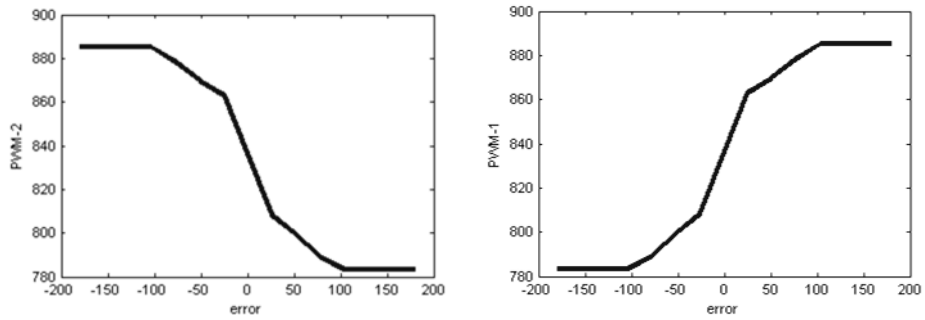


Figure 5: Simulated curves of the Fuzzy Logic controller for the two rotors.

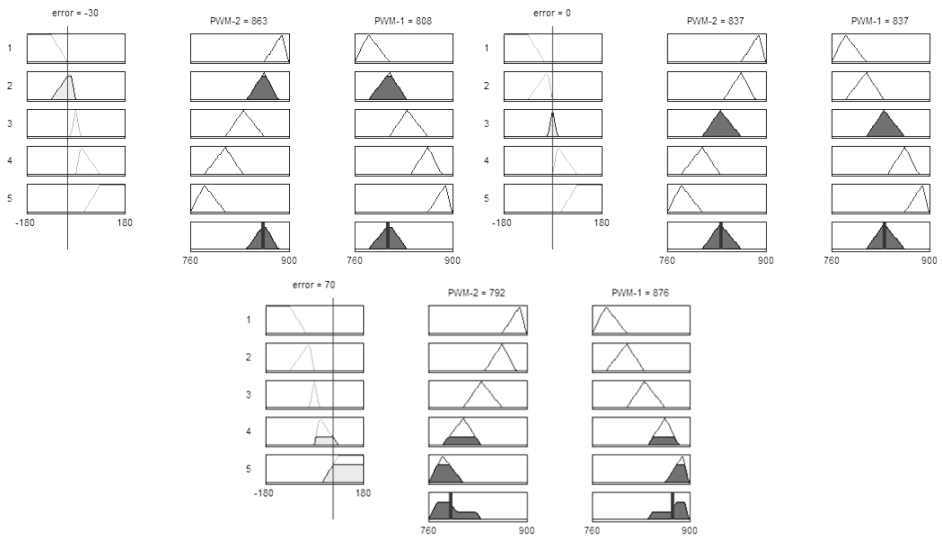


Figure 6: Output values for 3 different input values.

B. Fuzzy Logic controller for the two servo motors:

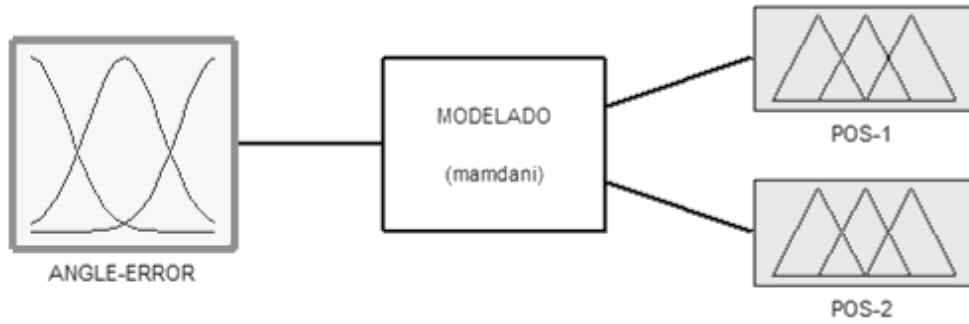


Figure 7: Definition of input/output variables and inference system.

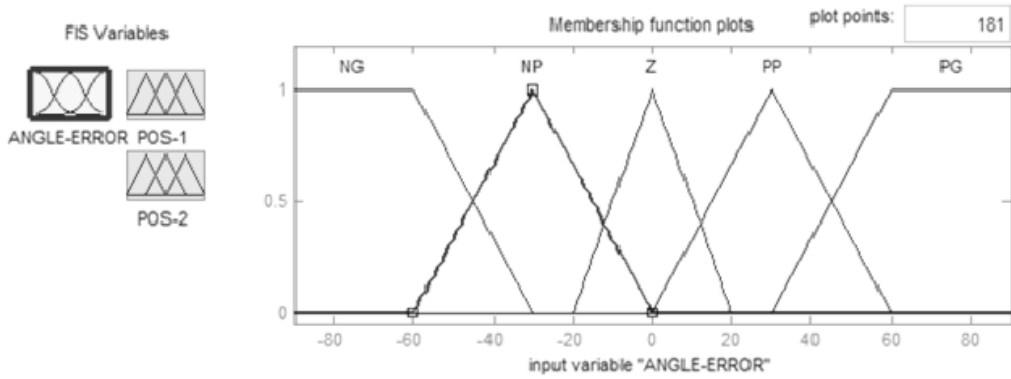


Figure 8: Definition of memberships of the input variable.

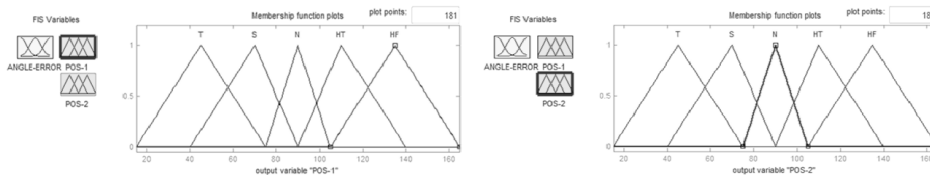


Figure 9: Definition of memberships of the output variables.

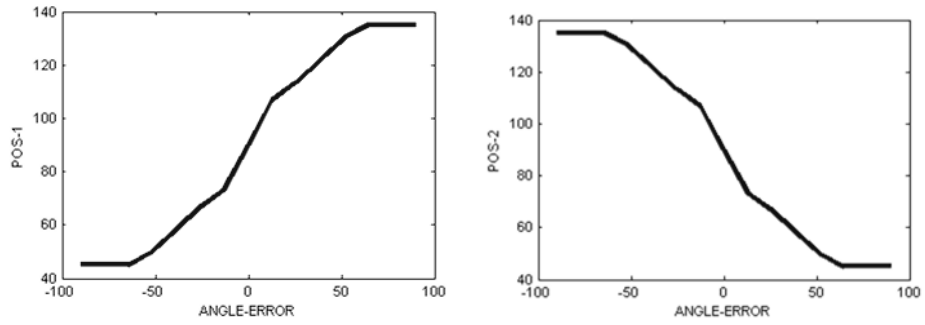


Figure 10: Simulated curves of the Fuzzy Logic controller for the two rotors.

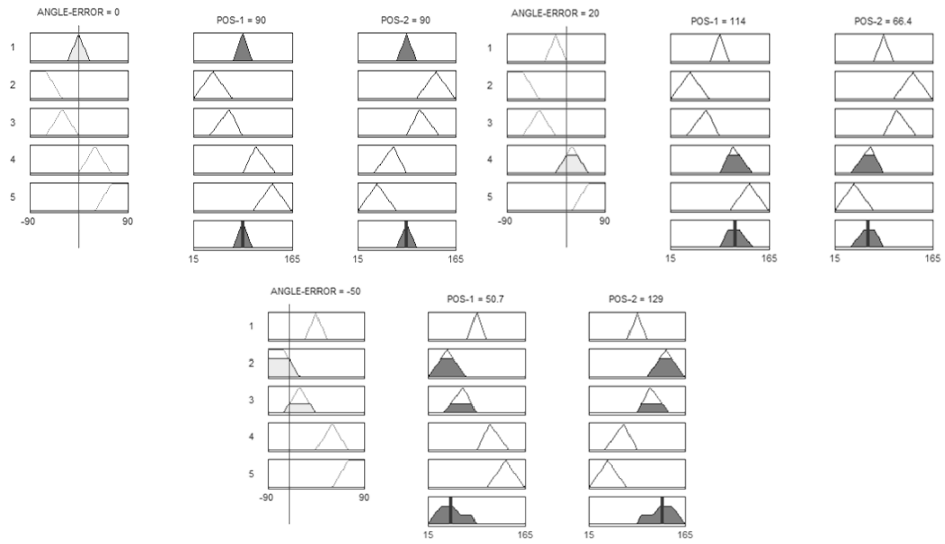


Figure 11: Output values for 3 different input values.

6. MICROCONTROLLER PROGRAMMING

The implementation of the Fuzzy Logic controller on an 8-bit embedded system (ATMEGA 2560) was possible by the use of the *Embedded Fuzzy Logic Library* (eFLL). The code is written in C++/C language with the use of the standard library "stdlib.h", for that reason it can be used in any embedded system coded in C. The main features of this library are:

A. Fuzzy memberships definition: it does not have an explicit limitation for the number of fuzzy memberships for the input(s)/output(s), neither a limitation for the number of fuzzy rules, they are just limited by the processing and storage limitations of the used microcontroller.

B. It uses the process of: maximum-minimum for the fuzzification, Mamdani [6] for the fuzzy inference and center of area (centroid) for the defuzzification.

The fuzzy control was ported to an 8-bit embedded system, which is in charge of input data reading, the application of fuzzy rules to those variables (known as *fuzzification*), and finally the *defuzzification* of the results, to generate a valid output control value in the specified ranges [7].

The pseudo-code of the control system is:

LOOP:

READ accelerometer and pressure raw data from the IMU.

COMPUTE angle and height from raw data.

DETERMINE angular errors.

GET the transformation of input values into grades of membership for linguistic terms of fuzzy sets (fuzzification).

COMBINE the facts obtained from the fuzzification with the rule base and get the fuzzy reasoning process (fuzzy inference machine).

GET the transformation from a fuzzy set to a reasonable number value (defuzzification).

SET the obtained values to the actuators.

7. ACHIEVED RESULTS

The simulation and implementation of a Fuzzy Logic controller on a Tilt-rotor aircraft was successfully achieved and the results are as expected. At

the present time, the Tilt-rotor system is under analysis to get definitive results and draw conclusions based on them.

Preliminary analysis have led to the observation of a transition time (like the observed in a classic PID control system of second order), this is barely perceptible if changes are small or medium (up to 30 degrees of angular error) and more considerable if changes are large (greater than 60 of angular error). The observed response is over-damped, reaching up to 60% of maximum over-step in the worst condition. Test:

- *Starting angle*= -90° ; - *Reference angle*= 0° ;
- *Result*= the highest position reached is approximately 50° ;
- *Maximum over-step*= $(50/90)*100\%= 55\%$;

So the system becomes unstable in the presence of large changes in short time intervals. However, if the changes are small or extended in time, it shows great accuracy and stability, without the presence of noticeable oscillations.

8. DEVELOPMENT AND FUTURE APPLICATIONS

The project shows the benefits presented by a Fuzzy Logic controller opposite a PID controller. The simplicity to define linguistic variables and the facility to transfer the knowledge into a control system, in a fast way, are the advantages that the Fuzzy Logic provides. For these reasons the goal is to expand the knowledge of this control system, so it can be implemented as a good alternative to a PID controller in all system susceptible to be automated.

9. CONCLUSION AND RECOMMENDATIONS

The versatility and simplicity to implement a Fuzzy Logic controller, applied on a complex system, has been proved. The definition of few memberships, for the inputs/outputs, and some rules were enough to develop a good and a working control system. To achieve a precise control a basic knowledge of the entire system is needed, so if you are not an expert, it is recommendable to approach a first study to know all variables that the system has, otherwise the results probably will not be as expected. For a better stability it is recommendable to define more Fuzzy memberships for the input and output variables.

ACKNOWLEDGMENTS: We thank Professor Lotfi A. Zadeh for his contributions.

References

- [1] LEMOS, MARVIN; ALVES, A.J. Robotic Research Group - State University of Piau. 2012. Recovered from:
<https://github.com/zerokol/eFLL>
<http://zerokol.com/>
- [2] JANG, ROGER; GULLEY, NED. MATLAB Fuzzy Logic Toolbox Users Guide.
- [3] VALAVANIS, KIMON. Unmanned Aircraft Systems: International Symposium on Unmanned Aerial Vehicles, UAV 08, vol. 54. Florida, USA: Springer, 2009.
- [4] OGATA, KATSUHIKO. Modern Control Engineering. 3rd Edition. Prentice-Hall. Mexico. 1998.
- [5] ROSS, TIMOTHY. Fuzzy Logic with Engineering Applications. Third Edition. Wiley. 2010. P 24.
- [6] Kasabov, Nikola. Foundations of Neural Networks, Fuzzy Systems, and Knowledge Engineering. MIT Press. Massachusetts, USA. Second printing, 1998. P 179-180, P 192-196, P 184.
- [7] M. PASSINO, KEVIN; YURKOVICH, STEPHEN. Fuzzy Control. Imprint of Addison-Wesley Longman, Inc. 1998. P 61-65.

Multiresolution analysis and robustness of a Contour-Point Signature-based human postures recognition system

Gabriela Gaona^{a1}, Javier Pérez ^a, Waldemar Villamayor-Venialbo^a,
and Christian E. Schaerer ^a

^aPolytechnic School- National University of Asuncion
P.O.Box: 2111 SL, San Lorenzo - Central - Paraguay

Abstract

A research area in Computer Vision focuses on the identification of articulated objects, and can be used in human-computer interaction. This article analyzes a new point descriptor, the Contour-Point Signature - CPS; that allows achieving a better matching of points between two figures. In addition CPS is robust to rigid traslation, scaling, rotation and independent of the origin point.

Keywords: Contour-Point Signature, Affine Transformation, Local Descriptor, Wavelet.

1 Introduction

An image \mathcal{I} is considered as a finite set of points (pixels) arranged in a matrix I of dimensions $f \times c$, where an object inside \mathcal{I} is represented by a finite subset of its contour points individualized by its coordinates $\mathcal{A} = \{a_1, \dots, a_M\}$, $a_i \in \mathbb{N}^2$.

Given the contour of a figure, the goal consists in determining the object and its groups of belonging. Hence, it is necessary a function to represent adequately the contour. This is performed by the Contour-Point Signature (CPS) introduced in [1].

2 Contour-Point Signature

The shape of a figure A is represented by a discrete set of sampled points of the object's outer contour, which will be the reference points. Based on this we adopt the following definition for the signature.

Definition 2.1. *Given a contour \mathcal{A} , whose reference points are $\mathcal{P} = \{p_1, \dots, p_N\}$, $p_i \in \mathbb{R}^2$, the Contour-Point Signature of the point p_i is given by the discrete function:*

$$f_{p_i}(j) =: \frac{1}{\|\mathcal{N}\|} |p_i - p_{\pi(j)}|, \quad (1)$$

where $\pi(j) = (i + j - 1) \pmod{N} + 1$ is a cyclic permutation, $j = 0, 1, \dots, N$, $\|\mathcal{N}\|$ is a norm and $|p_i - p_{\pi(j)}|$ is the arc-length from p_i to the others reference points.

We adopt $\|\cdot\|$ as the square root of the polygon formed by the points of \mathcal{A} . The CPS has the following properties [1]: (a) invariance to translation, (b) invariance to rotation, (c) scale invariance and (d) starting point independence.

¹E-mail Corresponding Author: gaby.lorely@gmail.com

2.1 Transformations and Correspondence between contours

Here we use the property of wavelet in performing hierarchical decomposition of functions, and apply it to the contours descriptor. This allows us to give low priority to the higher frequencies (probably noise) without losing any information of the contour [2]. Then we find the best rotation to align two contours to process subsequent transformation. We consider reference points $\mathcal{P} = \{p_1, \dots, p_N\}$ and $\mathcal{Q} = \{q_1, \dots, q_N\}$ associated to the contours \mathcal{A} and \mathcal{B} , respectively. For each $p_i \in \mathcal{P}$, seek the best match with a point $q_j \in \mathcal{Q}$.

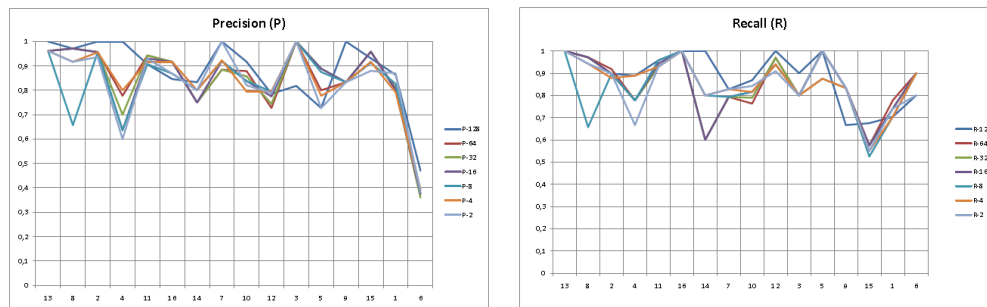
The next step is to estimate a plane transformation τ that may be used to map arbitrary points from one shape to another. For modeling the transformation, we use an affine transformation [3] $y = Tx + b$ composed of linear transformations, and translations and displacements.

Using the affine transformation above and the Definition 2.1, a dissimilarity measure is defined. Taking the contour signature matrix B defined as f_i and the contour signature matrix A' defined as g_i , where A' is the contour obtained after applying the affine transformation on a contour A , then the measure induced by the CPS is defined as $d_{CPS}(B, A') := \frac{1}{\|\mathcal{A}\|} \sum_i d(f_i, g_i)$, where $\|\mathcal{A}\|$ is a norm (root of the contour area). Analogously, we define the measure induced by the affine transformation as the equation $d_T(B, A') := \frac{1}{\|\mathcal{A}\|} \|M\|_p$, where $M = Q - PT$, $\|M\|_p = \sum_{i=1}^N \sum_{j=1}^3 |M_{ij}|$ is the sum of the elements of the array (matrix norm *Entrywise*).

3 Numerical Results

For this purpose we use the yoga video introduced in [4], which contains 16 different positions classes and a total of 428 frames.

First, we will test the system's behavior under different resolutions using wavelets. The results of precision and recall are shown in Figures 1a and 1b. Depending on the posture to compare, we can choose the resolution that is most accurate.



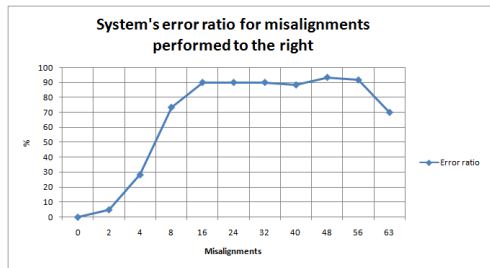
(a) System precision for different image resolutions.

(b) System Recall.

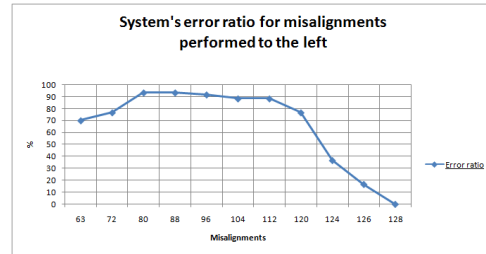
Figure 1: Results for multiple resolutions Image

Also, we tested the robustness of the proposal method when the rotation found is not the best.

To perform the experiment were selected 60 figures and having the best rotation, misalignments of all the points is performed. In Figures 2a and 2b are observed the



(a) Results for misalignments performed to the right



(b) Results for misalignments performed to the left

system's error rate. In general, a normal distribution is observed in the error ratio, and shows that the system provides some leeway to these kind of errors.

4 Conclusion

The approach presented is efficient and easy to implement, and showed robustness against errors that may occur in the process of points correspondence. A training step is important to incorporate in the process for the choice of some parameters in the recognition of postures. In addition, we remark that the proposal has feasible structure for parallel computation since each comparison between a frame and any reference posture can be made completely independently of the rest. The authors are very enthusiastic with the results obtained.

References

- [1] Waldemar Villamayor-Venialbo, Horacio Legal-Ayala, and Christian E. Schaerer. Contour-point signature: A new descriptor for matching rigid shapes with a single closed contour. In *Congresso de Matemática Aplicada e Computacional Região Sudeste*, pages 524–526, 2011.
- [2] E. J. Stollnitz, T. D. DeRose, and D. H. Salesin. Wavelets for computer graphics: A primer, part 1. *IEEE Computer Graphics and Applications*, page 2, Mayo 1995.
- [3] Serge Belongie, Jitendra Malik, and Jan Puzicha. Shape matching and object recognition using shape contexts. *Pattern Analysis and Machine Intelligence, IEEE Transactions on*, 24(4):509–522, 2002.
- [4] Xiaopeng Xi, Eamonn J Keogh, Li Wei, and Agenor Mafra-Neto. Finding motifs in a database of shapes. In *SDM*, pages 249–260. SIAM, 2007.

Implementing the Parareal method as a PETSc function

Juan José Cáceres^{ab1}, Benjamín Barán^{abc}, Christian Schaerer^a

^aLaboratorio de Computación Científica y Aplicada, Facultad Politécnica,
Universidad Nacional de Asunción, Paraguay

^bFacultad de Ciencias y Tecnología, Universidad Católica - Nuestra Señora de la
Asunción, Paraguay

^cFacultad Politécnica, Universidad Nacional del Este, Paraguay

Abstract

The Parareal method developed by Lions, Maday and Turicini proposes non trivial time discretizations to solve a partial differential equations system, that allows numeric methods approaches to obtain an approximation of the solution.

This work presents an approach that defines the solver's input and output interfaces that allows a parallel implementation in PETSc of the Parareal method using a multiple-shooting approach. The discretizations needed as input for the method are also described.

Finally, an implementation of the Parareal method with the discretizations is presented as an example of the proposal.

Keywords: Parareal, PETSc, multiple-shooting, function interfaces.

References

- [1] CÁCERES J., 2014. Implementación de un esquema de paralelización temporal utilizando PETSc. Engineering Thesis, Universidad Católica - Nuestra Señora de la Asunción
- [2] BALAY S., BROWN J., BUSCHELMAN K., EIJKHOUT V., GROPP W., KAUSHIK D., KNEPLEY M., CURFMAN MCINNES L., SMITH B., ZHANG H., 2012. PETSc users manual. Technical Report ANL-95/11 - Revision 3.3, Argonne National Laboratory.
- [3] SCHAERER C., KASZKUREWICZ E., 2001. The shooting method for the solution of ordinary differential equations: A control-theoretical perspective. *International Journal of Systems Science*, 32(8).

¹E-mail Corresponding Author: juanjocs@gmail.com

- [4] DU C., SARKIS M., SCHAEERER C., SZYLD D., 2013. Inexact and truncated parareal-in-time Krylov subspace methods for parabolic optimal control problems. *Electronic Transactions on Numerical Analysis*.
- [5] MADAY Y., LIONS J.L., TURINICI G., 2001. Résolution d'edp par un schéma en temps "pararéel". *C. R. Acad. Sci. Paris Sér. I Math.*, 332(7):661-668.

Sensitivity Analysis of a Chromium-Iron redox reaction in a batch system using PHREEQC

Luis Salgueiro^{a1}, Magna Monteiro^b, Christian Schaerer^a and Juan P. Nogues^{a2}

^a Laboratorio de Computación Científica y Aplicada, Facultad Politécnica, Universidad Nacional de Asunción, San Lorenzo, Paraguay.

^b Laboratorio de Bio-Materiales, Facultad Politécnica, Universidad Nacional de Asunción, San Lorenzo, Paraguay.

Abstract

Hexavalent Chromium (Cr(VI)) is a toxic and dangerous chemical used in several industrial processes (textile dyes, wood preservation, steel coating, among others) where effluents can pollute rivers, streams and groundwater resources. Added to this, chromium is the sixth most abundant element in the earth's crust and is registered by the U.S. EPA as a priority pollutant waste water due to its carcinogenic effects in humans and also others health problems if it's ingested in certain quantities. [1, 2].

In the treatment of groundwater and surface water contamination, numerous techniques, both physical and chemical, have been developed for the removal of chromium(VI). One of them is the use of Zero Valent Iron (ZVI), a micro scale powder of elemental iron (Fe(0)), which has been used for over 20 years [3]. The ZVI powder is generally used in the construction of filters, called permeable reactive barriers (PRB), which are mixed with sand and buried underground with the intention to immobilise contaminants as they flow through it.

One of the challenges of remediating Cr(VI) using ZVI barriers is understanding the redox chemistry between Fe(0) and Cr(VI). Therefore, one way to approach such a problem is to use numerical modeling of the chemical reactions between Fe(0) and Cr(VI). This paper presents a sensitivity analysis that provides a better understanding of the conditions - *pH*, *pe*, *concentration* - that occur by the reduction and subsequent precipitation of the chromium species. The simulations were done using PHREEQC, a computer program written in

¹E-mail Corresponding Author: lsalgueiro@pol.una.py

²Actual address: Facultad de Ciencias de la Ingeniería, Universidad Paraguayo Alemana, San Lorenzo, Paraguay.

C/C++ languages that is designed to perform a wide variety of aqueous geochemical calculations [4].

Our preliminary results show that strong reducing conditions - created by the release of electrons of the oxidation to a ferrous (Fe^{+2}) or ferric (Fe^{+3}) iron - are favorable to reduce the Chromium(VI) to Chromium(III), which is a valence state of chromium with less mobility and toxic properties. Additionally, Chromium(III) species form precipitates in the presence of iron, enabling its removal from waste water [3]. This work shows the optimal reduction and precipitation conditions that can be obtained for this redox system and which variables are significant to obtain this reduction.

The authors thank to DCI-ALA/2012/302464-AIEP/UE/Paraguay for financial support.

Keywords: Redox Reaction, hexavalent chromium, Zero-Valent Iron (ZVI), Batch system, PHREEQC.

References

- [1] GOULD, 1982. The kinetics of hexavalent chromium reduction by metallic iron, *Water Res* 16: 871 – 877.
- [2] MITRA, SARKAR, HAKRABARTI, DUTTA, 2011. Reduction of hexavalent chromium with zero-valent iron: Batch kinetics studies and rate model, *Chemical Engineering Journal* 171: 54 – 60.
- [3] U.S. Environmental Protection Agency, Zero-valent Iron Nanoparticles. Available on [http://www.epa.gov/rpdweb\\$00\\$/docs/cleanup/nanotechnology/chapter-\\$2\\$-zero-valent.pdf](http://www.epa.gov/rpdweb00/docs/cleanup/nanotechnology/chapter-2-zero-valent.pdf). Consulted in May-2014.
- [4] PARKHURST, APPELO, 2013. PHREEQC's Manual. Available on http://wwwbrr.cr.usgs.gov/projects/GWC_coupled/phreeqc. Consulted in May-2014.

A new variant of MOACS for many-objective TSP

Francisco Riveros¹, Néstor Benitez¹, Julio Paciello¹, Benjamín Barán^{1,2}

¹National University of Asuncion - UNA, Paraguay

²East National University - UNE, Paraguay

Abstract

This work proposes a comparative analysis of Multi-objective Ant Colony Optimization (MOACO) algorithms applied to a Many-objective TSP. For experimental test, TSP instances with a low correlation among objective functions were generated considering 2, 4 and 8 objectives. Hypervolume and coverage performance metrics were applied to the Pareto Fronts calculated by each algorithm in order to compare the solutions. The algorithms parameters were adjusted empirically for improving the hypervolume calculated.

Keywords: MOACO, TSP, Many-objective, Hypervolume, Coverage

1. INTRODUCTION

MOACO algorithms were traditionally used to solve multi-objective optimization problems. Past works as [1], [2] and [3] applied these algorithms to solve real world optimization problems, and can be observed that they are effectively applied to problems with 2 or 3 objectives. However, this effectiveness may be reduced when the number of objectives increases, as it happens with most evolutionary algorithms [13]. This work studies the performance of MOACO algorithms when applied to many-objective TSP considering 4 and 8 objectives, as well as 2 objectives for comparison purposes. Also, some variants of the MOACOs are proposed in order to improve considered performance metrics hypervolume and coverage.

The next sections present the many-objective TSP, the MOACO algorithms considered and the variants implemented, as well as the experimental results obtained. Finally, conclusions and future works are presented.

2. MANY-OBJECTIVE TSP

TSP can be represented as a fully connected weighted graph $G = (N, A)$, where N represents a set of nodes and A represents the set of edges that

fully connects the nodes of N . In a mono-objective case, every edge has an associated cost d_{ij} , that represents the distance between nodes $i, j \in N$. In other words, TSP can be formulated as finding the minimal distance Hamiltonian cycle, starting at an initial node, visiting each node exactly once and returning to the initial node [11]. For symmetric TSP $d_{ij} = d_{ji}$ for every pair of nodes. For the many-objective case, k cost functions are considered, having $d_{ij}^1, d_{ij}^2, \dots, d_{ij}^k$ for every edge (i, j) and the problem consists in minimizing every cost function simultaneously [12].

In the literature several bi-objective TSP instances are known (TSPLIB¹); however these benchmarks were not extended to many-objective problems with 4 or more objectives. This work proposes the resolution of many-objectives TSP problems, for this purpose instances of 2, 4 and 8 objectives instances were generated. For each instance, an adjacency matrix was generated, ensuring a low correlation among objectives. Pearson correlation coefficient [4] was used as the correlation indicator. Correlations between -1 and 0.1 were accepted, representing a reasonably low correlation or ensuring a compromise relation among objectives (contradictory objectives).

3. MOACO ALGORITHMS CONSIDERED

In this work, MOACS [1], M3AS [2] and MAS [3] were the MOACO algorithms implemented. Several tests were performed using the random generated instances against each considered algorithm. Each algorithm ran with 2, 4 and 8 objective. Every test was executed in a cost minimization context. Attending the preliminary results, MOACS was selected for parameters adjustment (see the pseudocode of MOACS below in algorithm 1). Several variants for some execution parameters as the ant count, λ distribution parameter, and the visibility impact were tested. Also, a modification of the dominance area of solutions from the Pareto Front was made, in order to verify the impact of the performance metrics according to previous works like the one by Sato et al. [5].

4. MOACO ALGORITHMS CONSIDERED

In this work, hypervolume and coverage proposed in [7] were used as performance metrics. Hypervolume considers the size of the dominance region on the objective space, and coverage compares 2 non-dominated set of

¹<http://www.iwr.uni-heidelberg.de/groups/comopt/software/TSPLIB95/tsp/>

Algorithm 1 Generic pseudocode of MOACS

```

initPheromone()
while stops criterion is not verified do
  for  $i = 1$  to  $m$  do
    ( $T = BuildSolution$ )
  end for
  if ( $Y_{know}$  was changed) then
    initPheromone()
  else
    for all ( $T \in Y_{know}$ ) do
      updatePheromone()
    end for
  end if
end while

```

solutions estimating the fraction of solutions dominated by the other set. Hypervolume combines distance, distribution and extension metrics in a single value [8]. Coverage can be used to show that an algorithm dominates other one; however, it can't quantify how better an algorithm is with respect to the other [8]. The algorithm implemented for calculating the Hypervolume is the Hypervolume by Slicing Objectives (HSO), proposed in [9].

5. EXPERIMENTAL RESULTS

This section presents experimental results obtained, and the different parameters adjustments made. All performance tests were executed on a computer with an i7 Intel processor and 8 GB of RAM over a Mac OS X. Every algorithm ran 1500 generations, 4 times foreach instance. Table 1 shows the default parameters configuration used for the MOACO algorithms.

$$p_{i,j} = \begin{cases} \frac{\tau_{i,j}^\alpha \eta_{i,j}^\beta}{\sum_{x \in J_i} \tau_{i,x}^\alpha \eta_{i,x}^\beta} & \text{si } j \in J_i \\ 0 & \text{en caso contrario} \end{cases} \quad (1)$$

5.1 Comparison of MOACO algorithms

Several tests with 2, 4 and 8 objective using MOACS [1], M3AS [2], MAS [3] and NSGII [14] were executed. In tables 2 and 3 a similar behaviour

MOACO	
Parameter	Value
Max. Generations	1500
Ant count (m)	10
Pheromones impact (α)	1
Visibility impact (β)	2
Evaporation coefficient ($1 - \rho$)	0.3
τ_0	0.1
τ_{max}	0.9
q_0	0.5
f_{max}	7782

Table 1: Algorithms parameters values, based on past works [1], [2], [3], and [15]

of all MOACO algorithms (MOACS, M3AS and MAS) can be observed in terms of hypervolume. NSGA-II shows a lower hypervolume for 2 and 4 objectives, however for 8 objectives outperforms the MOACO algorithms. In general, the hypervolume decreases when a different instance with more objectives is considered. For the MOACO algorithms, it can be observed that hypervolumes tends to 0, and the ammount of solutions tends to maximum attending to the total number of solutions generated for every ant in all generations. Thus, the computational time needed to compute the hypervolume increases considerably when applied to problems with 16, 32 or more objectives and therefore it becomes non-viable. Considering this limitation to compute the hypervolume in a reasonable time, this work limited to 8 the number of objectives. Considering the obtained results, showing a slight improvement of MOACS, it was selected as the algorithm for testing several parameters adjustments in order to increase the hypervolume obtained.

In what follows, parameters adjustments are shown, including their corresponding empirical results.

5.2 Ant count adjustment

Initially, every algorithm were executed using a constant ammount of ants $m = 10$. This parameter was modified attending to the following strategies:

	2	4	8
M3AS	0,80	0,37	0,04
MAS	0,82	0,39	0,04
MOACS	0,83	0,39	0,04
NSGA-II	0.59	0.14	0,007

Table 2: Hypervolume of evaluated MOACO algorithms

	2	4	8
M3AS	59	1204	9881
MAS	29	1094	9536
MOACS	45	1223	9617
NSGA-II	25	183	118

Table 3: Ammount of sol. for the MOACO algorithms

	2	4	8
MOACS k_1	0.80	0.38	0.04
MOACS k_2	0.81	0.39	0.04
MOACS k_3	0.82	0.38	0.04
MOACS k^2	0.82	0.37	0.04
MOACS k_{random}	0.81	0.38	0.04
MOACS $k_{constant}$	0.81	0.42	0.04

Table 4: -MOACS hypervolume for each ant count variation strategy

Multiples of the number of objectives: The number of ant used was changed to $m = k.n$, where k represents the number of objectives and $n \in \{1, 2, 3, k\}$. Thus, the number of ants will be a multiple of k .

Randomly selection of the number of ants: A random selection of the number of ants per generation was implemented, according to $m = 10 + ram$, where ram represents a number between k and k^2 , with k being the number of objectives.

Constant growth of the number of ants: A constant growth of the number of ants was implemented, according to $m = m + const$, where $const = MaxGenerationNumber / (m_0^2 - m_0)$, with m_0 being the initial number of ants. For testing purpose $m_o = 10$ was considered.

In table 4 the evolution of the hypervolume obtained for each strategy implemented and every number of objectives is shown.

As observed in table 4, neither of the proposed strategies shows a significative improvement of the hypervolume. Considering the results and for simplicity reasons, the use of a constant value $m = 10$ is proposed.

	2	4	8
MOACS <i>Dim.</i> 1%/ 15 <i>gen.</i>	0.81	0.39	0.04
MOACS <i>Dim.</i> 6%/ 100 <i>gen.</i>	0.82	0.38	0.04
MOACS <i>Dim.</i> 30%/ 500 <i>gen.</i>	0.82	0.38	0.04

Table 5: -MOACS hypervolume decreasing the impact of the visibility.

5.3 Impact of visibility

This work proposes 3 strategies for decreasing the impact of the visibility when computing a MOACO next state probability. This modification is used to guide the search based on the pheromones trails when some number of generations elapsed. The following strategies were tested:

- Reduce the impact of visibility 1 % every 15 generations.
- Reduce the impact of visibility 6 % every 100 generations.
- Reduce the impact of visibility 30 % every 500 generations.

In table 5 the evolution of hypervolume can be observed attending 2, 4 and 8 objectives and the different strategies implemented.

In this case, no significant improvement of the hypervolume can be observed, for this reason a constant value of the parameter β that weights the visibility is proposed.

5.4 Modification of the dominance region

The algorithm presented in [5] was implemented, to a contract and expand the dominance region of solutions of the Pareto Front. The dominance area was modified according to a value S_i , in the interval $[0.25, 0.7]$. In table 5 the obtained results can be observed.

In this case, neither of the modifications produces a significant improvement of the hypervolume. For this reason, this variant was also discarded.

5.5 Lambda distribution (λ)

Some adjustment in the assignment schema of the λ parameter were tested, that weighted the visibility impact considering the different objectives to optimize.

	2	4	8
MOACS $S0, 25$	0.66	0.29	0.02
MOACS $S0, 3$	0.66	0.32	0.02
MOACS $S0, 35$	0.70	0.37	0.03
MOACS $S0, 4$	0.81	0.37	0.04
MOACS $S0, 45$	0.81	0.38	0.04
MOACS $S0, 5$	0.81	0.38	0.04
MOACS $S0, 55$	0.80	0.37	0.03
MOACS $S0, 6$	0.77	0.36	0.03
MOACS $S0, 65$	0.75	0.34	0.03
MOACS $S0, 7$	0.73	0.32	0.02

Table 6: -MOACS hypervolume applying contraction and expansion of the dominance region.

In other works that solve multi-objective problems using MOACO, the λ parameter assigns, for every ant of a total of m ants, k variables $\lambda_1, \lambda_2, \dots, \lambda_k$, one for each objective. Generally, every λ_i takes one of m possible values without repeating a value assigned to other λ_j . Thus, the distribution of λ represents a k -permutation of m , that difficults the use of all possible permutations when the number of objectives is increased and the number of ants is a fixed parameterized value.

To tackle this issue, this work proposes 2 strategies: a randomly selection of the permutation of values for λ using a Tabu search [10], and a new variant denominated p-base randomly selection of λ .

5.5.1 Random distribution using Tabu search

In this approach, this work used a Tabu search with a 5 values queue. A randomly selection process is implemented to choose the permutation of λ_i to be used, where $i \in \{1, 2, \dots, k\}$, without repeating the last 5 permutations according to the Tabu search. It was tested 2 variants of λ assignment, normalized values according to the number of ants m , and without normalization.

5.5.2 P-base randomly selection

In this case, a restriction of the number of possible values that λ_i can

	2	4	8
MOACS λ <i>Tabu normalized</i>	0.73	0.28	0,02
MOACS λ <i>Tabu non normalized</i>	0.72	0.28	0,02
MOACS λ <i>run</i>	0,84	0,41	0,04
MOACS λ <i>iteration</i>	0,84	0,50	0,09

Table 7: Obtained results for the λ assignment strategies

take, was applied. Considering the objectives $f_1, f_2 \dots f_k$, for every ant an assignment of values for $\lambda_1, \lambda_2 \dots \lambda_k$ is needed. For this purpose a random value in decimal base is generated, between 0 and $p^k - 1$, where p is a parameter of the strategy that represents the number of possible values that every λ_i can take. The generated value is transformed to p base, thus, k digits are obtained, d_1, d_2, \dots, d_k , where $d_i \in \{0, 1, \dots, p - 1\}$ for all $i \in \{1, 2, \dots, k\}$. Then, the assignment is made as follows $\lambda_1 = d_1, \lambda_2 = d_2, \dots, \lambda_k = d_k$, where a value of 0 represents the minimal weight and $p - 1$ the highest. For this work $p = 3$ was used, so every λ_i can take values of 0 (low weight), 1 (medium weight) and 2 (high weight).

To evaluate this new approach, 2 variants are proposed:

- P-base assignment of λ at the start of the run.
- P-base assignment of λ at every generation (iteration).

The evolution of hypervolume can be observed in table 7. In order to get a detailed analysis, the numerical values computed for hypervolume (comparing the considered MOACS with the proposed variant, for every number of objectives) are shown in table 8. These results prove the advantage of using the proposed variant of MOACS up to 8 objectives, reflecting how the improvement in the hypervolume, compared with the considered MOACS, increases as the number of objectives do.

To reinforce the obtained results, the Pareto Front obtained by the *MOACS λ iteration* was compared to other Pareto Front using the coverage metric in both directions. In table 9 the results of coverage for 8 objectives are shown.

6. CONCLUSIONS AND FUTURE WORKS

The current work presents a comparative analysis of MOACO algorithms applied to a many-objective TSP, considering 2, 4 and 8 objectives. Several

	2	4	8
M3AS	0,80	0,37	0,04
MAS	0,83	0,39	0,04
MOACS	0,82	0,39	0,04
MOACS λ <i>run</i>	0,84	0,41	0,04
MOACS λ <i>iteration</i>	0,84	0,50	0,09

Table 8: Obtained results for the λ assignment strategies

	MAS	M3AS	MOACS
COV.(MOACS LAMBDA ITERATION, x)	0.0030	0.0018	0.0031
COV.(x , MOACS LAMBDA ITERATION)	0.0014	0.0017	0.0014

Table 9: Coverage

adjustment to different parameters were made, as the ant count, the visibility impact, the dominance region and finally the λ values assignment strategy. Analyzing the hypervolume obtained, a significant improvement when using the λ assignment per generation using the p-base proposed strategy was observed. For this reason, this strategy is recommended for the many-objective case when using MOACO algorithms.

As future works, instances of more of 8 objectives can be solved in order to validate the behaviour of the proposed λ assignment strategy. A comparative analysis against evolutionary algorithms for many-objective problems also can be implemented.

References

- [1] BARAN, B, SCHAERER, M., 2003. A multiobjective Ant Colony System for Vehicle Routing Problems with Time Windows, Proc. Twenty first IASTED International Conference on Applied Informatics, Innsbruck, Austria, pg. 97-102.
- [2] PINTO, D., BARAN, B., 2005. Solving Multiobjective Multicast Routing Problem with a new Ant Colony Optimization approach. LANC 05, Cali, Colombia.

- [3] PACIELLO, J., MARTINEZ, H., 2006, Optimización Multiobjetivo basada en Colonias de Hormigas. Teoría y estrategias de paralelización, pg. 31-44.
- [4] MURGIONDO, J., 2005. "Análisis descriptivo de datos en Educación", pg. 172-180.
- [5] SATO, H., AGUIRRE, H., TANAKA, K., 2007. "Controlling Dominance Area of Solution in Multiobjective Evolutionary Algorithms and Performance Analysis on Multiobjective 0/1 knapsack Problems".
- [6] ZITZLER, E., THIELE, L., 1998. "Multiobjective optimization using evolutionary algorithms – a comparative case study".
- [7] ZITZLER, E., THIELE, L., 1999. "Multiobjective evolutionary algorithms: A comparative case study and the strength pareto approach".
- [8] ZITZLER, E., 1999. "Evolutionary algorithms for multiobjective optimization: Methods and applications".
- [9] WHILE, L., HINGSTON, P., BARONE, L., HUBAND, S., 2006. "A Faster Algorithm for Calculating Hypervolume", IEEE Trans. on Evol. Comput., vol. 10, no. 1.
- [10] RIOJAS, A, 2005. "Búsqueda Tabú", pg. 5-9.
- [11] LAWLER, E.L., LENSTRA, J.K., RINNOOY KAN, A.H.G., SHMOYS, D. B., 1985. "The Travelling Salesman Problem", New York: Wiley.
- [12] ISHIBUCHI, H., TSUKAMOTO, N., NOJIMA, Y., 2008. "Evolutionary Many-Objective Optimization: A Short Review", Proc. of 2008 IEEE Congress on Evolutionary Computation, 2424-2431, Hong Kong.
- [13] VON LÜCKEN, C., BARAN, B., BRIZUELA, C., 2003. "A survey on multy-objective evolucionay algorithms for many-objective problems", Springer Science+Business Media, New York - 2014.
- [14] DEB, K., PRATAP, A, AGARWAL, S.,MEYARIVAN, T. "A fast and elitist Multi-Objective Genetic Algorithm: NSGA II", KanGAL, India.

- [15] KOT, K., PIETRASZKO, A., 2009. "Heuristic methods for multi-criteria combinatorial optimization", Technical Report, Akademia Gorniczo-Hutnicza (AGH), Krakow.

Viscous fingering instabilities in rectilinear porous media flow

Juan G. Zena^{a1} and Christian E. Schaerer^b

^a Engineering School, National University of Asuncion, San Lorenzo, Paraguay

^b Polytechnic School, National University of Asuncion, San Lorenzo, Paraguay

Abstract

In this scientific initiation work, we present the dynamical evolution of miscible displacements in a rectilinear flow for a two-dimensional porous medium. The phenomena is modeled using Darcy's law, the advection-diffusion equation and the continuity equation for incompressible fluids. For convenience, these equations are recast into a stream-function-vorticity formulation in order to be solved numerically. This yields a system of partial differential equations, which takes into account the spatial distribution of permeability, fluid viscosities, advection and diffusion. Numerical simulations are performed using a finite-difference scheme. The sensitivity and stability of the numerical solution to the Peclet number was mainly observed. The authors are currently motivated to correlate this results with laboratory tests of the displacement of fluid by a contaminant inflowing the porous medium.

Keywords: Computational Physics & Chemistry, Porous Media, Finite Difference, Viscous Fingering; Miscible Displacements

2. BASIC FORMULATION

Consider a two-dimensional porous medium in a horizontal rectangular domain $\Omega = [0, L_x] \times [0, L_y]$ and an incompressible fluid being injected uniformly from the left boundary with a given velocity U . The transport process is characterized by the advection-diffusion equation considering an homogeneous medium with constant permeability k . Denoting the Darcy velocity as $\mathbf{u} = (u, v)$, the basic governing equations take the form:

$$\left\{ \begin{array}{l} \nabla \cdot \mathbf{u} = 0 \\ \nabla p = -\frac{\mu}{k} \mathbf{u} \\ \frac{\partial c}{\partial t} + \mathbf{u} \cdot \nabla c = D \nabla^2 c \end{array} \right. \quad (1)$$

¹E-mail: juanguidozena@gmail.com

where D is the dispersion coefficient, $\mu = \mu(c)$ is a known function of the concentration denoting the viscosity and $k = k(x, y)$ is the permeability function. In addition to (1), some appropriate boundary and initial conditions must be imposed. The boundary conditions considered are:

$$\begin{aligned} u = U, \quad v = 0, \quad c = c_1, \quad \text{at } x = 0, \\ u = U, \quad v = 0, \quad c = 0, \quad \text{at } x = L_x, \end{aligned} \quad (2)$$

the no-flow condition at boundaries associated to $y = 0$ and $y = L_y$ of the rectangular domain:

$$\frac{\partial c}{\partial y} = 0 \quad \text{at } y = 0 \quad \text{and } y = L_y. \quad (3)$$

The initial condition has the following form:

$$\begin{aligned} u = U, \quad v = 0, \quad \forall(x, y), \\ c = c_0(x, y). \end{aligned} \quad (4)$$

3. STREAMFUNCTION-VORTICITY FORMULATION

In order to solve the equations numerically, the system of differential equations (1) is recast into the streamfunction-vorticity formulation. By introducing the streamfunction ψ and the vorticity ω in the usual way as:

$$\begin{cases} u = \frac{\partial \psi}{\partial y}, \\ v = -\frac{\partial \psi}{\partial x}, \\ \omega = \nabla \times \mathbf{u}. \end{cases} \quad (5)$$

the system of equations (1) become,

$$\begin{cases} \frac{\partial c}{\partial t} + \frac{\partial \psi}{\partial y} \frac{\partial c}{\partial x} - \frac{\partial \psi}{\partial x} \frac{\partial c}{\partial y} = \frac{1}{Pe} \nabla^2 c \\ \omega = R(\nabla \psi \cdot \nabla c) - \frac{1}{k} \nabla \psi \cdot \nabla k \\ \nabla^2 \psi = -\omega \end{cases} \quad (6)$$

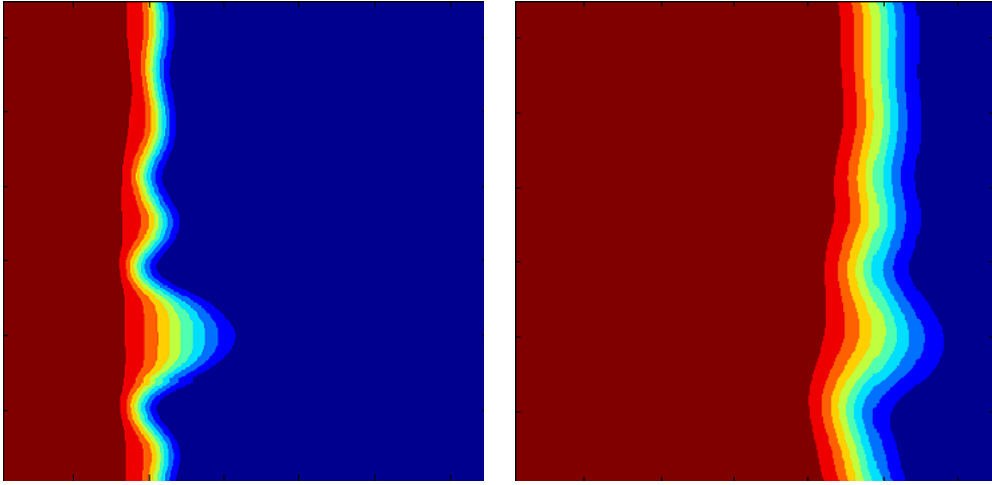


Figure 1: Initial condition and simulation results for Experiment 1 at a simulation time = 1.75×10^{-4} .

where the Peclet number Pe and the mobility ratio R are defined as:

$$Pe := \frac{1}{D} \text{ and } R := -\frac{1}{\mu} \frac{d\mu}{dc}. \quad (7)$$

4. NUMERICAL EXPERIMENTS

To solve the system (6) a central finite difference discretization of order $O(h^2)$ is used for the spatial derivatives and forward Euler discretization for the temporal derivative. The horizontal rectangular domain $\Omega = [0, L_x] \times [0, L_y]$ is used with $L_x = L_y = 1$. Two different experiments are considered.

Experiment 1. It is considered a Peclet number $Pe = 70$, $R = 1$ and $k = 1$. The mesh grid has 130×130 internal points and $\tau = 10^{-6}$ to assure the stability of the numerical method. Any other internal tolerance for the resolution of the linear system is set to $tol = 10^{-7}$. The initial condition is taken as a concentration varying from $c = 1$ and $c = 0$ passing through all values, as shown in Figure 1. Observe that the initial solution diffuses when the solution evolves overcoming the initial fingers. Hence, the fingering effect tends to disappear.

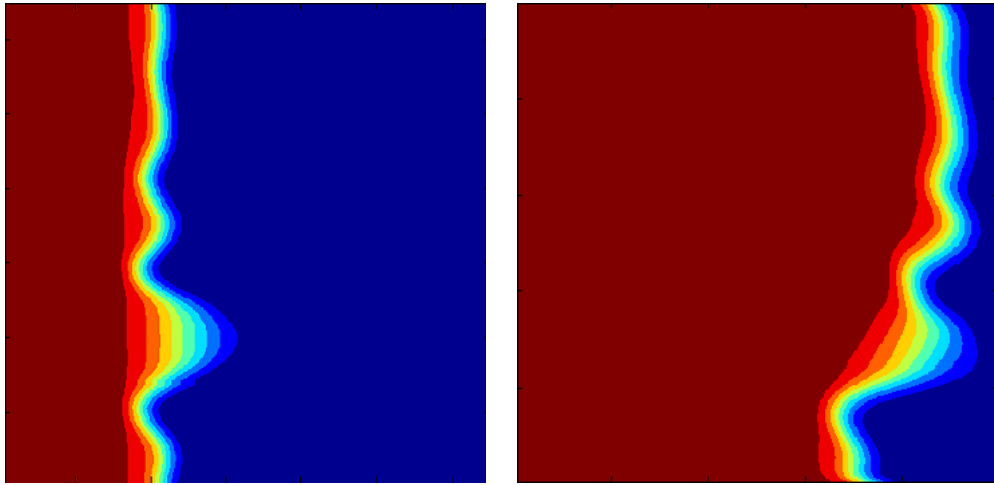


Figure 2: Initial condition and simulation results for Experiment 2 at a simulation time = 1.75×10^{-4} .

Experiment 2. It is considered a Peclet number $Pe = 300$, $R = 1$ and $k = 1$. The mesh grid has 250×250 internal points and $\tau = 10^{-6}$ to assure the stability of the numerical method. Any other internal tolerance for the resolution of the linear system is set to $tol = 10^{-7}$. The initial condition is the same as in Experiment 1. As shown in Figure 2, in this case the diffusion is not enough to overcome the fingers, so they become more accentuated when the solution evolves.

5. CONCLUDING REMARKS

In this work, a simulation modeling a flow in a rectilinear porous medium was presented. A system of partial differential equations was derived, which was solved using a finite difference scheme. It was observed that greater values of the Peclet number imply more instability events. In the preliminary results with smaller Peclet number the fingers tend to remain their form, while the solution is more sensitive with larger Peclet and certain fingers become dominant.

References

- [1] CHEN, C.; MEIBURG, E. 1998. Miscible porous media displacements in the quarter five-spot configuration. Part 1. The homogeneous case.
- [2] CHEN, C.; MEIBURG, E. 1998. Miscible porous media displacements in the quarter five-spot configuration. Part 2. Effect of heterogeneities.
- [3] DE WIT, A.; BERTHO, Y.; MARTIN, M. 2005. Viscous fingering of miscible slices. *Physics of Fluids*, 17.
- [4] PEACHMAN, D.W.; H. H. RACHFORD, JR. 1962. Numerical Calculation of Multidimensional Miscible Displacement.
- [5] SCHAEERER, C. E.; MANGIAVACCHI, N.; KASZKUREWICZ, E. Simulation of miscible flows in homogeneous porous media using a multilevel Schwarz shooting method. *Applied Mathematics and Computation*, Vol. 153, Issue 3, 2004, Pages 803 – 831.
- [6] TAN, C.T.; G. M. HOMSY. 1986. Stability of miscible displacements in porous media: Rectilinear flow
- [7] TAN, C.T.; G. M. HOMSY. 1987. Stability of miscible displacements in porous media: Radial source flow
- [8] TAN, C.T.; G. M. HOMSY. 1988. Simulation of nonlinear viscous fingering in miscible displacement.
- [9] YORTSOS, Y. C. 1990. Instabilities in displacement processes in porous media.

Superlinear Convergence for Block Conjugate Gradient using Variable Block Size Strategies

Pedro Torres^{a1}, Christian E. Schaerer^a

^aPolytechnic Faculty - National University of Asunción,
P.O. BOX: 2111 SL, Central, Paraguay

Abstract

Superlinear convergence has been observed long before on Conjugate Gradient in the solution of large sparse linear system with a single right hand side $Ax = b$, and in general on Krylov Subspace Methods. This phenomenon has studied in detail for the single right-hand-side (rhs) under two situations, first when the matrix present some special eigenvalues distributions and second when the components of initial error in the eigenvector basis has nonuniform distribution. However, very few references of this superlinear behaviour can be found for the case of Conjugate Gradient with many rhs (Block Conjugate Gradient-BCG).

On one hand, experimental observations shown important results, such as that the convergence strongly depends on the number of rhs vectors and the eigenvalue distributions of the matrix. On the other side, the BCG and in general block versions of related solvers are important for being explored in the context of new computer paradigms, due to its high ratio computation/memory access. This property makes block algorithms more competitive than single vector methods. The limit of the block size should be imposed by the underlying computer architecture. Moreover, numerical experiments show that the increase or even decrease of the block size does not contribute to accelerate this convergence, that is, depending on the eigenvalue distribution we must find the right amount of block size a each iterations. This is the subject of our study: how do we can control the superlinear convergence behaviour just varying the block sizes?.

In this work we study the convergence of a numbers of strategies for varying the block sizes. Basically we present different strategies to vary the block size, measuring the approximations to the most near invariant subspaces on each iteration and comparing each of them to the total computational cost. These strategies are tested on two groups of matrix, one artificially created and the other taken from

¹E-mail Corresponding Author: torres.pedrozpk@gmail.com

real applications. The numerical experiments show that the adaptive strategy of decreasing the block size based on the Ritz values computed on each iteration is better than the other tested strategies, resulting in a decreasing computational cost and storage for some matrix with a certain eigenvalues distribution. This results encourage the analysis and design of adaptive block algorithms.

Keywords: Superlinear Convergence, Block Conjugate Gradient, Ratio Computation/Memory access, Ritz Values.

ACKNOWLEDGMENTS: C.S. acknowledges the CONACYT-PRONII support. P.T. acknowledges the funding support of CONACYT under the contract 1698/OC-PR.

References

- [1] Simoncini, V, Szyld, DB, 2005. On the occurrence of superlinear convergence of exact and inexact Krylov subspace methods, SIAM review 47. 247-272.
- [2] Beckermann, B, Kuijlaars, ABJ, 2001. Superlinear convergence of conjugate gradients, SIAM Journal Numerical Analysis 39.300329.
- [3] Nikishin, AA, Yuremin, AY, 1995. Variable Block CG Algorithms for Solving Large Sparse Symmetric Positive Definitive Linear System on Parallel Computers, I: General Iterative Scheme, SIAM Journal Matrix Analysis 16. 1135-1153.
- [4] Ye, Q, 1996. An adaptive block Lanczos algorithm, SIAM Journal Numerical Algorithms 12. 97-110.

Allocation algorithms for dynamic partial reconfiguration on reconfigurable hardware

F. Fernández^a, J.C. Fabero^{b1}

^aFacultad Politécnica, Universidad Nacional de Asunción, Paraguay

^bFacultad de Informática, Universidad Complutense de Madrid, Spain

Abstract

The use of modern digital systems hardware designs based on the ability to dynamically reconfigure at runtime has increased dramatically during the last years. Hardware reconfigurable devices were initially employed to shorten the time to the market, allowing an accelerated design-test-debug cycle. However, with nowadays enhanced capabilities, the use of this kind of devices has spread to other applications, and now they are being employed in the design of onboard instrumentation for satellites, for example. Moreover, with the appearance of partially dynamically reconfiguration capable devices, a good planification and placement algorithm must be used in order to obtain the maximum throughput from the device. A simulator have been developed which allows the study of different task allocation strategies.

Keywords: Reconfigurable hardware, FPGA, dynamic partial reconfiguration, allocation, simulation

1. INTRODUCTION

The use of reconfigurable hardware has been spreading in the last years, although this technology appeared in 1985. However, last technological enhancements have increased the complexity and capabilities of reconfigurable devices, allowing them to compete with ASICs and general purpose processors. The FPGA is a set of hardware resources (multiplexers, logic gates, memories, flip-flops, LUTs, etc.) and a configuration memory that determines how they connect altogether in order to perform a specific task. A hardware task is a logical design with specific functionality, and stored in a file [1]. This file is called bitstream, and once it has been loaded into the configuration memory, it is ready to use. Modern FPGA allow partial dynamic

¹E-mail Corresponding Authors: fefernandezpy@gmail.com.py, jcfabero@ucm.es

reconfiguration, that is, they allow loading a bitstream into a region of the FPGA while other tasks are still executing.

2. PARTIAL DYNAMIC RECONFIGURATION

One of the main problems associated with partial dynamic reconfiguration is the fragmentation of the area in the FPGA [2, 3]. Many authors have made proposals for a solution to this problem [4, 5, 6, 7, 8]. A contribution to the solution of this problem is in [9]. The allocator maintains, among other structures, a list of vertices which defines the free area in the FPGA. When a new task is to be allocated, the allocator searches for the vertex which maximizes the adjacency. This way, the fragmentation can be minimized.

3. DYNAMIC ALLOCATION SIMULATION

To our purposes, the FPGA is considered to be divided into regions, called Minimum Allocation Region, MAR. Each MAR groups a number of CLBs, as well as communication specific hardware. The whole set of MARs conform a mesh and each MAR can communicate directly with its neighbours and route messages directed to other MARs. When a task is allocated into the FPGA, it occupies as many MARs as necessary. In the case when two tasks must communicate in order to exchange data with each other (i.e. a task needs some data generated by other task), they can accomplish this by means of the routing capabilities of the MAR structure. However, dependent tasks are not necessarily adjacent in the FPGA, so communication delays can impact global performance severely. The aim of this project is, then, to be able to compare different allocation algorithms which can take into account several factors, such as global fragmentation and communication delays. A software simulator has been implemented which allows the comparison of performance on several scenarios: the first one, when only a job composed of several dependent tasks is to be allocated; the second one, when two or more jobs are competing for the hardware resources. Also, the problem of off-line and on-line planification is to be considered. Off-line planification can be used when all jobs to be executed are known at the beginning of the execution. On-line planification, on the other hand, must be used when jobs arrive in a dynamic and unpredictable manner. Both planification strategies have been implemented into the simulator.

ACKNOWLEDGMENTS: This work was partially supported by funds

DGICT UNA - FP/01/12 and by Spanish Government research grant TIN2013-40968-P.

References

- [1] Electronic resource. <http://www.ni.com/white-paper/6983/en>
- [2] Xilinx Inc. Two flows for partial reconfiguration: Module Based and difference based, 2004. Application Note 290. <http://www.xilinx.com>
- [3] J. A. Clemente Barreira, J. L. García Casado, C. González Calvo. Implementación HW de un Gestor de ejecución para sistemas dinámicamente reconfigurables (in Spanish only). <http://www.eprints.ucm.es/9067/1/Memoria.pdf>
- [4] A. J. Acosta, J.L. Cruz Marcos, D. L. Ángeles. Diseño e implementación en lenguaje Java de un gestor de recursos de hardware reconfigurable en un entorno de red. <http://eprints.ucm.es/8966/>
- [5] B. Blodget, C. Bobda, M. Huebner, and A. Niyonkuru. Partial and Dynamically Reconfiguration of Xilinx Virtex-II FPGAs <http://citeseerx.ist.psu.edu/showciting?cid=4356857>.
- [6] I. Fernández Sánchez, Á. Morales Rodríguez, M. Salgado. Implementación de un planificador de tareas para Multitarea hardware sobre un procesador empotrado (in Spanish only) http://www.fdi.ucm.es/SI/sara_roman_06_07.doc
- [7] D. Corrales, C. Granados, R. Domínguez. Estudio de técnicas de reconfiguración parcial dinámica de FPGAs. <http://eprints.ucm.es/9283/>
- [8] I. González. 2006 UAM Dynamically reconfigurable coprocessors in FPGA-based embedded systems. 2006 UAM. <http://www.digitool-uam.greendata.es:1801/>
- [9] J. Tabero, H. Wick, J. Septién, S. Roman – A vertex-list approach to 2D HW multitasking management in RTR FPGAs <http://citeseerx.ist.psu.edu/showciting?cid=25906>

MONITORING VITAL SIGNS USING BIOMEDICAL TECHNOLOGIES BASED DEVICES RECONFIGURABLE

F. Fernndez ^a, J. Nuez ^b, L. Frutos^c

fefernandez@pol.una.py, josenu85@gmail.com,ltfrutos@pol.una.py

^aFacultad Politecnica U.N.A San Lorenzo, Paraguay

Abstract

. Using reconfigurable devices are an option in biomedical monitoring systems for vital signs featuring flexibility when designing and testing phase to optimize the final design. we presents the proyect FPGA-based system that monitors ECG biomedical signals, using signal processing for transmission wirelessly to an access point for processing and presentation of real-time signals visually receiving data presented sensors.

Keywords:Monitoring, biomedical signal, FPGA, real-time.

1. INTRODUCTION

Monitoring sensory signals is one of the most extensively studied areas in electronics. Its applications range from industrial monitoring signals , automobiles , airplanes and of course the measurement of vital signs of patients under treatment. This is very important because the average population is entering the age considered elderly which will force the state to invest more amount of equipment to meet the demands of future health . Within this discipline vital signs monitoring is critical because they are computers that have a high cost and therefore require an investment in health not only to meet the new requirements but to replace computers that are obsolete [1] [2] .

2.RECONFIGURABLE DEVICES

The FPGA is a set of hardware resources (multiplexers, logic gates, memories, flip-flops), more memory settings that determine how the different resources are connected together to perform a task. Moreover, using reconfigurable devices introduces flexibility to the period of testing and debugging

technology project required around reducing costs during this step and reducing the risk of damage to the initial prototypes. Besides the need for a system that enables data transmission distance of biomedical sensor signals in real time allows biomedical monitoring vital signs can be followed not only in the immediate vicinity where the patient but is in also in a site geographically paragraph [3] [4] [5] . optimization of the final design

3.MONITORING VITAL SIGNS

The project aims to design a system for monitoring vital signs using reconfigurable hardware to optimize the design of the project. This design will serve as a starting point to go to expand the services offered with a minimum of modifications reducing the time and cost to have a new design. In the first stage the objective is to design a wireless monitoring system that transmit vital signs of the patient to a physically separate access point.

References

- [1] Enfermedades cardiovasculares. Marzo 2013 Organizacin Mundial de la Salud <http://www.who.int/mediacentre/factsheets/fs317/es/> [visitado el 17/04/2014].
- [2] La OMS publica un atlas decisivo sobre la epidemia mundial de cardiopatas y accidentes cerebrovasculares Septiembre 2004 <http://www.who.int/mediacentre/news/releases/2004/pr68/es/> [en lnea, consultado.20/04/2014].
- [3] Digital System Design Lecture 8: Xilinx FPGAs. Amir Masoud Gharehbaghi. <http://ce.sharif.edu/courses/83-84/2/ce223/resources/root/CAD/8->
- [4] Cynthia Prez-Morris, Silvia Akamine-Serpa, Vctor Murray-Herrera , Gerard F. Santilln-Quionez, Muestra de una Seal Biomdica en tiempo real sobre un monitor VGA con resolucin 640x480. Consultado en Noviembre 2013 [en lnea]. Disponible en <http://www.iberchip.net/IX/Articles/PAP-063.pdf>

- [5] Rosada, Jaime Garca, Juan Carlos. Receptor de seales definido por software utilizando dispositivos FPGA Consultado en Enero 2014 [en lnea]. Disponible en <http://www.scielo.org.ve/pdf/uct/v10n38/art06.pdf>

Web Geographic Information System to visualize the Patiño Aquifer vulnerability to contamination

Liz Báez^a, Juan Pablo Nogues^{a b}, Cynthia Villalba^{a1}

^aLaboratorio de Computación Científica y Aplicada. Facultad Politécnica -
Universidad Nacional de Asunción.

^bFacultad de Ciencias de la Ingeniería - Universidad Paraguayo Alemana.

Abstract

The project “Mapeo de la Vulnerabilidad y Riesgo de Contaminación del Agua Subterránea del Gran Asunción” [1] evaluated the risk of contamination of the Patiño aquifer using a vulnerability and risk index that takes into account hydrogeological and anthropogenic factors. The methodology used in the above mentioned work is a modified version of the well established DRASTIC method [2]. The procedure consisted in the collection and analysis of existing geospatial data and maps, with hydrogeologic and anthropogenic information, distributed across different institutions and not available on web. The evaluation of the geospatial information acquired was used to create an initial map of the modified DRASTIC vulnerability index. This map was then calibrated, using known groundwater concentrations of nitrogen and coliforms, in order to obtain a more accurate vulnerability and the risk map. The results of the calibration were separated into three maps of risk of contamination: one for nitrogen, another for coliforms and one that mapped the overall risk, which was obtained by overlaying the first two maps. These maps can help policymaker and technicians to identify the areas with the highest vulnerability and risk of contamination, as well as set public policies regarding urban planning and environmental regulations.

The access to geospatial information of Paraguay is difficult because it is distributed throughout different institutions that do not provide a Spatial Data Infrastructure (SDI) that allows visualization, access and data distribution via the Internet. Therefore, the work presented here arises from the need to share and provide access to data, information and results obtained in the above mentioned project. This

¹E-mail Corresponding Author: cvillalba@pol.una.py

work aims to exploit the potential of information technology (IT), Geographic Information Systems (GIS) and the Open Geospatial Consortium² (OGC) standards to generate interactive maps through layers on a server, sharing data, information and georeferenced maps in a web map viewer.

The web page created allows the user to visualize spatial data in the form of maps and gives access to related project information. The results of the project are accessed through a friendly and intuitive graphical interface, which helps promote the project, identify and link people interested in the topic. The work uses the tools included in the OpenGeo Suite³: Spatial data stored in a PostGIS; layers served by WMS in GeoServer; viewer and composition of layers combining the libraries: OpenLayers, ExtJS and GeoExt.

Keywords: GIS Web, vulnerability, DRASTIC, risk of contamination, Patiño Aquifer.

ACKNOWLEDGMENT: This study was founded by the Consejo Nacional de Ciencia y Tecnología (CONACyT), under the Call CTS project, and by the Facultad Politécnica - Universidad Nacional de Asunción. In addition, it was supported by the Secretaría de Emergencia Nacional.

References

- [1] BAEZ, L, VILLALBA, C, NOGUES, JP, 2014. Mapeo de la Vulnerabilidad y Riesgo de Contaminación del Agua Subterránea del Gran Asunción, CONACyT Proyecto INV 20, Facultad Politécnica - Universidad Nacional de Asunción. Paraguay.
- [2] ALLER, L, LEHR, JH, PETTI, R, BENNETT, T, 1987. DRASTIC: A standardized system to evaluate ground water pollution potential using hydrogeologic settings, National Water Well Association/Bennett and Williams Inc, Ohio.

²<http://www.opengeospatial.org>

³<http://suite.opengeo.org/docs/latest/index.html>

A quasi-classical trajectory study of the OH + SO reaction: the role of ro-vibrational energy

J. D. Garrido^{a1}, W. A. D. Pires^b, M. A. C. Nascimento^c,
and M. Y. Ballester^b

^aCentro Interdisciplinar de Ciências da Natureza, Universidade Federal da Integração Latino-Americana-UNILA, Foz do Iguaçu, PR, 85867- 970, Brazil

^bDepartamento de Física, Universidade Federal de Juiz de Fora-UFJF, Juiz de Fora, MG 36036 330, Brazil.

^cInstituto de Química, Universidade Federal do Rio de Janeiro, RJ, 21941-909, Brazil

Abstract

A study of the OH + SO \rightarrow H + SO₂ reaction using a quasi-classical trajectory method is presented with the aim of investigating the role of the ro-vibrational energy of the reactants in the reactivity. The calculations were carried out using a previously reported global potential energy surface for HSO₂(²A). Different initial conditions with one and both reactants ro-vibrationally excited were studied. The reactive cross sections, for each studied combination, are calculated and then fitted to a capture-like model combined with a factor accounting for the recrossing effects. The Vibrational Energy Quantum Mechanical Threshold of the Complex method was used to correct for the zero-point vibrational energy leakage of the classical calculations. State specific and averaged rate constants are reported. The reactivity is affected when ro-vibrational energy of either of the reactants is changed. The present calculations provide a theoretical support for the experimental rate constant for temperatures below 550 K, but fail to account for the significant fall in the observed rate constant upon increasing the temperature above this value.

Keywords: Reactivity in gases.

ACKNOWLEDGMENTS: The authors acknowledge FAPEMIG (CEX APQ 00895/11), FAPERJ and CNPq (Projeto Pr-Sul 490252/2011-7) for financial support, Computational facilities from LCAD of the UNILA are also appreciated. WADP thanks PROPESQ/UFJF for the research grant (BIC).

¹E-mail Corresponding Author: garrido.jd@gmail.com

Application of the Hydrus model to simulate Redox reactions in a ZVI Filter.

Cristhel Leguizamón Montiel ^a, Magna Monteiro^b, Christian E. Schaerer^a and Juan P. Nogues^{a,1,2}

^aLaboratorio de Computacion Cientifica y Aplicada, Facultad Politecnica, Universidad Nacional de Asuncion, San Lorenzo, Paraguay.

^bLaboratorio de Bio-Materiales, Facultad Politecnica, Universidad Nacional de Asuncion, San Lorenzo, Paraguay.

Abstract

Simulations of contaminant transport in porous media were conducted to evaluate geochemical reactions between zero valent iron and water containing hexavalent chromium (Cr(VI)). The simulations were done using the Hydrus model [1, 2]. Hydrus is a Windows-based software that is used to simulate water flow in porous media and the subsequent geochemical reactions between species. The simulations consisted in making water flow in horizontal and vertical set ups using different boundary and initial conditions. In the first set of experiments, simulations modelled horizontal and vertical water flux in 1D using a combination of Dirichlet-Dirichlet and mixed Dirichlet-Neumann conditions. The second set of experiments replicated the initial set of experiments but considered a 2D model. The purpose of these simulations was to understand which set-ups, boundary and initial conditions result in the best conditions for removal of Cr(VI) and precipitation of Cr(III) for the design of a zero valent iron filter.

Keywords: water flow, porous media, Hydrus.

ACKNOWLEDGMENTS: The authors thank DCI-ALA/2012/302464-AIEP/UE/Paraguay Project for financial support.

References

- [1] SIMUNEK, SEJNA, SAITO, VAN GENUCHTEN, 2013. The HYDRUS-1D Software Package for Simulating the One-Dimensional

¹E-mail Corresponding Author: jpnogues@pol.una.py

²Currently at Facultad de Ciencias de la Ingenieria, Universidad Paraguayo Alemana, San Lorenzo, Paraguay.

Movement of Water, Heat, and Multiple Solutes in Variably-Saturated Media. University of California Riverside.

- [2] BALI, GUEDDARI, 2012. Simulation of water flow and solute transport in intermittent sand filter, J. of Water Supply: Research and Technology: Aqua, 61(1), 50-57.

Mechanism of reduction of Cr(VI) in presence of iron filings

Andrés Aquino¹, Silvia Aquino and Magna Monteiro

Bio and Materials Laboratory, Polytechnic School, Asuncion National University,
San Lorenzo, Paraguay

Abstract

The transformation of raw materials into final products involves a series of operations, usually produce waste and effluent to be treated for disposal. Environmental problems caused by improper waste and effluent management adversely affect either directly or indirectly on human health form. Among the compounds listed in the US E.P.A. main pollutant is chromium. Chromium exists in the environment in various chemical species, like hexavalent chromium, Cr(VI), and trivalent chromium, Cr(III), are those that stand out for their carcinogenic action and industrial importance respectively. The Cr(VI) can be reduced chemically or biologically, but greater efficiency is achieved through the chemical mechanism. Chemical redox reactions involving electron transfer and these occur simultaneously and in the same degree, therefore, the oxidation reaction is always accompanied by the reduction reaction. The reduction of Cr(VI) to Cr(III) requires the accompaniment of another redox pair, which are often commonly H₂O/O₂, Mn(II)/Mn(IV) and Fe(II)/Fe(III). The reduction of Cr(VI) by action of Fe(II) occurs in spite of not being thermodynamically favored because high concentrations of Fe(II), electrons sufficient to reduce the Cr(VI) was obtained. Under acidic conditions, the final products of this reaction would be Cr(III) and Fe(III). Considering neutral to alkaline conditions, the ultimate product would be Cr(OH)₃ and Fe(OH)₃ because of the low solubilities in this pH range and even, it is considered a mixed precipitate of both compounds.

Keywords: reduction, iron filings, Cr(VI).

ACKNOWLEDGMENTS: The authors thank DCI-ALA/2012/302464-AIEP/UE/Paraguay Project for financial support.

¹E-mail Corresponding Author: and9080@gmail.com

References

- [1] J.P. GOULD. The Kinetics of Hexavalent Chromium Reduction by Metallic Iron (1982).
- [2] Chromium (VI) Handbook. Independent Environmental Technical Evaluation Group (IETEG). Edited by J. Guertin, J. A. Jacobs, C. P. Avakian.
- [3] G. RAYNER-CANHAN. 2000. Descriptive Inorganic Chemistry. 2da. Ed Pearson Education.
- [4] FIUZA, A.; SILVA, A.; CARVAHLO, G.; DE LA FUENTE, A.; DELERUE-MATOS, C. Heterogeneous kinetics of reduction of Chromium (VI) by elemental iron. Journal of Hazardous Materials 175 (2010), p. 1042 to 1047.

Using the Kinect Sensor with Open Source Tools for the Development of Educational Games for Kids in Pre-school Age

Christian von Lucken^a, Romina Fernández V.^{a1},
^aPolytechnic School, National University of Asunción

Keywords: Kinect, pre-school education, eye-hand coordination, open source.

1. INTRODUCTION

The Kinect sensor is an input device that can recognize gestures and movements of user's hands and body. This technology allows a more natural human-computer interaction compared to traditional interaction interfaces. This sensor was designed for Microsoft's Xbox 360 console; but currently, several tools for developing PC applications with Kinect are available, including the official Kinect SDK [1] and open source tools [2].

The availability of programming tools allowed the development of many applications that explore the possible uses of the Kinect outside of gaming area. Thus, there are many works using Kinect in different fields of application, among which are robotics [3] and medicine [4].

Education is a promising area for the development of Kinect applications. In this work, we consider the development of an application with games for children in pre-school age (4-5 years). The interaction form proposed by Kinect is ideal for developing the eye-hand coordination, the ability to use simultaneously and in an integrated manner the hand and sight in order to perform an activity [5]. In the pre-school age, this ability is developed through activities and games. The proposed application is intended to be a tool for teachers to complement this aspect of the educational work. It will include educational games with content for pre-school children and will be developed using open source tools.

Currently, there are applications for teaching children, teenagers and adults based on Kinect sensor. Notable examples include language teaching [6] and education of children with disabilities [7].

¹E-mail Corresponding Author: romina.fernandez@pol.una.py

2. APPLICATION DESIGN

For the subject of the games, in this work was decided to develop activities that reinforce concepts taught in pre-school education, in the field of mathematics.

After the analysis the following games were selected:

1. Match, in which the child matches a number of objects with the corresponding numerical representation,
2. Order, in which the child orders a sequence of objects from lowest to highest, and
3. Sum, in which the child objects placed in boxes representing the addends of the addition operation and displays the numeric representations of each part of the operation.

For the development, was chosen OpenNI [2], an open source framework for developing applications with natural interaction technology based on C++.

3. EXPERIMENT

For the evaluation, the application was introduced in a classroom of ABC Children's Center, an education center for children aged up to 5 years. Guided by teachers, the kids tested the games one by one, while the others watched. The teachers explained to the children the goal of each game and helped if the kid had difficulties in the interaction. In total, 20 kids and five teachers take part. After the experience, a questionnaire was given to the teachers to evaluate its assessment of the application.

4. CONCLUSIONS

During the experience, it could be seen that the application caused a very positive impact on both students and teachers. Children showed great enthusiasm to try the games and could quickly understand what the purpose of each and how they should interact with them. Although the application had a positive reception, there are some drawbacks. For example, using Kinect requires a large space, as the projector must be placed at some distance from

the projection surface and the sensor requires a minimum distance of the player to function properly (0.8 m).

This experience let us see that technologies like Kinect have high potential in the field of education, especially in the pre-school education. Unfortunately, despite that there are mature tools for development, there isn't many alternatives for teachers according to the contents that should be teach. However, the application developed in this work is a first step towards the inclusion of Kinect and similar technologies in the educational field.

References

- [1] Kinect for Windows SDK. <http://www.microsoft.com/en-us/kinectforwindowsdev/default.aspx>
- [2] OpenNI Framework. <http://structure.io/openni>
- [3] Romero Molano, C. A., & Díaz Celis, C. A. (2011, October). Navegación de robot móvil usando Kinect y OpenCV. I Congreso Internacional de Ingeniería Mecatrónica-UNAB(Vol. 2, No. 1).
- [4] Chang, C. Y., Lange, B., Zhang, M., Koenig, S., Requejo, P., Somboon, N., ... & Rizzo, A. A. (2012, May). Towards pervasive physical rehabilitation using Microsoft Kinect. In Pervasive Computing Technologies for Healthcare (PervasiveHealth), 2012 6th International Conference on (pp. 159-162). IEEE.
- [5] Ortega, J. J., & Obispo, J. A. (2007). Manual de psicomotricidad.(Teoria, exploracion, programacion y practica), Pág 212. Ediciones La Tierra Hoy SL.
- [6] Ji, J., Yu, H., Li, B., & Zhang, H. (2013). Learning Chinese Characters with Gestures. International Journal of Information Technology, 19(1).
- [7] Christinaki, E., Triantafyllidis, G., & Vidakis, N. (2010). A gesture-controlled Serious Game for teaching emotion recognition skills to preschoolers with autism.

Mutual Information Based Medical Image Registration using Clever Optimization Algorithms

Pedro P. Cespedes^{a1}, Horacio Legal ^a and Christian Schaerer^a

^aScientific and Applied Computing Laboratory, Polytechnic School,
National University of Asuncion,
Campus Universitario, San Lorenzo, Paraguay

Abstract

Multimodal Medical Image Registration is treated as an optimization problem. Deterministic algorithms are mainly used to solve it. A drawback of the latter is that many of them are trapped in a local optimum. For multimodal registrations, one of the most popular metric approaches is the Mutual Information using deterministic optimization algorithms to compute the cost function with the mentioned problems. This work is aimed to overcome this disadvantage using three different clever optimization algorithms for the registration process, contrasted with Regular Step Descent Optimizer. Qualitative and quantitative validations of the results are satisfactory. Comparing with conventional methods the clever optimization algorithm has performed the registration of multimodal medical images with low error matching and not being stuck in local optima.

Keywords: Registration, Mutual Information, EV, EO, PSO.

1. INTRODUCTION

Image Registration (IR) is a challenge that arises in many image processing applications when several images must be aligned. We treat the particular case of the registration of medical images which can be of different modalities, Figure 1(a), (b). In this context, one of the most popular approaches is the Mutual Information based methods [1], [2]. IR is treated as an optimization problem with the goal of finding the spatial mapping that will bring the moving image into alignment with the fixed image [5]. Figure 1(c). Deterministic algorithms are mainly used to solve it, together with some stochastic ones. A drawback of the latter is that many of them become stuck in local optimum, especially in multimodal registration with several parameters [2]. This work is aimed to overcome this disadvantage using clever optimization algorithms.

¹E-mail Corresponding Author: pcespede@pol.una.py

One plus One, Particle Swarm Optimization and Extremal Optimization Algorithms [3], was tested as optimizers for the registration process, contrasted with Regular Step Descent Optimizer.

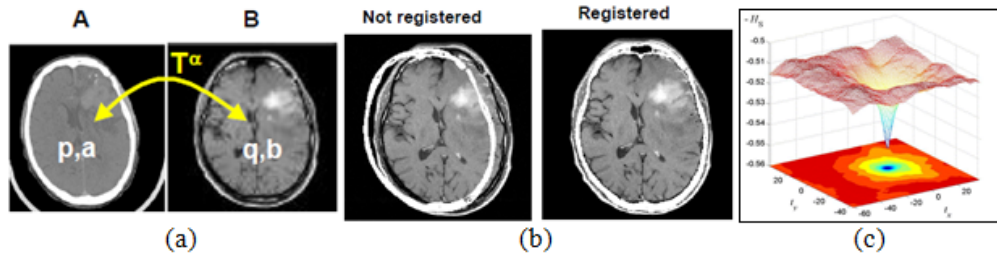


Figure 1 - (a) Goal of the Image Registration, (b) Two different modalities of brain image overlapped, before and after IR process (c) Similarity metric cost function to be optimized looking for the most suitable transformation parameters.

2. METODOLOGY

2D/2D multimodal medical image registration of tomographic CT and MRI of brain images was performed over a database of 600 2D medical images based in project RIRE²; adapting the optimization algorithms to the specific problem at hand. We used the Insight Segmentation and Registration Toolkit (ITK)³, which is a set of libraries in C++ designed for the development of registration methods [5]. Figure 2, show the ITK basic components of de registration framework: two input images, a transform, a metric an interpolator and a optimizer, represented by the next pipeline.

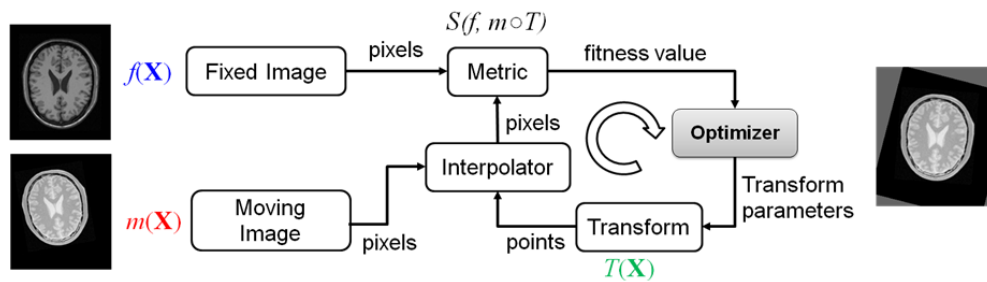


Figure 2 - ITK registration framework.

²<http://www.insight-journal.org/rire/>

³<http://www.itk.org>

3. EXPERIMENTAL RESULTS

To determine the performance of the proposed 2D/2D IR methods using clever algorithms we conducted registration experiments of CT-MRPD, CT-MRT1 and CT-MRT2 the tests was performed searching six parameters (translation (x,y) , rotation(x, y, angle) and scale). The experimental results show that the clever algorithms, combined with the MI-based metric proposed by Mattes et. al. achieve good performance in contrast to the Regular Step Descent Optimizer algorithms implemented in ITK. Table 1 and 2.

Table 1. Errors obtained using different registration Methods.

Method	Mean [mm]	Median[mm]	Max [mm]
MMI-RSG	1,26	1	1,39
MMI-IP1EV	0,74	0,41	1,12
MMI-EO	0,36	0	0,54
MMI-PSO	0,35	0,1	0,75

Table 2. % of registration success

Method	CT-MRPD	CT-MRT1	CT-MRT2
MMI-RSG	70	51	26
MMI-IP1EV	43	38	39
MMI-EO	83	62	34
MMI-PSO	79	56	38

4. CONCLUSIONS

Qualitative and quantitative validation of the results are satisfactory. Comparing with conventional methods the clever optimization algorithm have performed the registration of multimodal medical images with low error matching and not being stuck in local optima.

ACKNOWLEDGMENTS: The authors acknowledge the financial support given by CONACyT program 1698 OC/PR and the Polytechnic School, National University of Asuncion.

References

- [1] A. El-Baz, R. Acharya, A. Laine, J. Suri (Eds.), Medical Image Registration, vol. 2, Springer Science+Business Media, LLC, New York, 2011.
- [2] J. V. Hajnal, D. Hawkes, D. Hill (Eds.), Medical Image Registration, Biomedical engineering series, CRC Press LLC, New York, 2001.
- [3] J. Brownlee. Clever Algorithms: Nature-inspired Programming Recipes. Lulu, Australia, 2011.
- [4] D. Mattes, D. R. Haynor, H. Veselle, T. K. Lewellen, W. Eubank, Pet/CT Image registration in the chest using free-form deformations, IEEE Transactions on Medical Imaging, vol 22 pp. 120-128, (2003).
- [5] L. Ibanez, W. Schroeder, L.Ng, J. Cates, I. S. Consortium, The ITK Software Guide. Second Edition. Updated for ITK version 2.4, 2005. URL <http://www.itk.org>

Ant Colony Optimization applied to Microfluidic Routing Problem in DMFB

Carlos Mendoza^{a1}, Eduardo Szaran^{a2}, Diego P. Pinto-Roa^{a3},
and Carlos A. Brizuela^{b4}

^a Polytechnical School, National University of Asunción, Paraguay

^bCICESE, Ensenada, B.C., México

Abstract

Digital Microfluidic Biochips (DMFB) [1] are very promising to concurrent bioassay, like DNA analysis, recognize substances, new drugs discovery, real time toxicity detection and pathogen agents. One of the most important challenge in DMFB is the routing problem of microfluidics [2] where the movement must be scheduled in a multiplexed manner. This work addresses the microfluidics routing problem as a non-Pareto multi-objective optimization problem. For that, an Ant Colony Optimization [3] algorithm is developed to calculate the optimal routing of microfluidics considering criteria in lexicographic order as the interference between droplets, the total travel time and the number of cells used. Experimental results indicate that the proposal is promising to study the problem in question.

Keywords: Microfluidics Routing, DMFB, Ant Colony Optimization.

References

- [1] T. Mukherjee, 2005. Design automation issues for biofluidic microchips, Proc. IEEE/ACM ICCAD, pp. 463-470.
- [2] K. F. Bhringer, 2003. Optimal strategies for moving droplets in digital microfluidic systems, 7th Int. Conf. Miniaturized Chemical and Biochemical Analysis Systems (MicroTAS).
- [3] M. Dorigo, G. Di Caro, 1999. The Ant Colony Optimization Meta-Heuristic. In D. Corne, M. Dorigo, and F. Glover (Eds.), *New Ideas in Optimization*, McGraw Hill, London, UK, 11–32.

¹carlos.mendoza@pol.una.py

²eduardo.szaran@pol.una.py

³dpinto@pol.una.py

⁴cbrizuel@cicese.mx

ILP-based Mathematical Model for node failure protection in Optical Multicast Network

Miguel Brítez ¹ and Diego P. Pinto-Roa ²

Politechnical School, National University of Asunción

Abstract

Internet have experienced a large growth on traffic demand for information. Due to high capacity and low cost of Optical Networks mostly communication system migrated in this technology either in transport networks or access networks. In this massive implementation of optical networks will also accompany the flaws that are generated in nodes and/or links failures. In this paper we cover the failure of nodes whose probability of occurrence is much lower than the failure of links; but, node failure is catastrophic.

A previous study [1] proposes partial and total reconfiguration approaches to protect multicast services. The quality of solution of these approaches may not be optimum when the complexity of problem increases as the network cost and disruptions by reconfiguration objective functions are considered simultaneously.

In this paper is proposed an approach that generalizes the above particular cases [1]. A mathematical model based on Integer Lineal Programming (ILP) is defined in order to calculate optimal solution. Experimental results indicate the convenient of the proposed approach in comparison with partial and total reconfiguration strategies.

Keywords: Optical Networks, Failed Node, Reconfiguration Techniques, Integer Lineal Programming.

References

- [1] K. LUEKIJNA and C. SAIVICHIT, 2007. Multicast traffic reconfiguration in WDM network for single node failure design, The 9th International Conference on Advanced Communication Technology, IEEE, 3: 1833-1838.

¹miguel_britez@hotmail.com

²dpinto@pol.una.py

Role of type II topoisomerases in regulation of supercoiling and pre-catenation in replication intermediates of DNA

Victor Martínez^a, Jorge Cebrián^b, Maridian J. Kadomatsu-Hermosa^a, Cristina Parra^a, Alicia Castán^b, María José Fernández-Nestosa^a, Christian E. Schaerer^a, Pablo Hernández^b, Dora B. Krimer^b and Jorge B. Schwartzman^b

^aScientific and Applied Computing Laboratory. Polytechnic School. National University of Asunción. P. O. Box 2111 SL, San Lorenzo, PARAGUAY.

^bDepartment of Cellular and Molecular Biology. Centro de Investigaciones Biológicas (CSIC), Ramiro de Maeztu 9, 28040, Madrid, SPAIN.

Abstract

During replication, DNA molecules undergo topological changes that affect supercoiling, catenation and knotting. To better understand the function of the enzymes that control the topology of DNA during replication, two-dimensional agarose gel electrophoresis was used to examine a bacterial plasmid containing the replication fork stalled after replication of 60 % of the molecule and divides it in the replicated region and the non-replicated region. The DNA was isolated and treated in vitro with two type II DNA topoisomerases: topoisomerase IV (Topo IV) and DNA gyrase. The effects of these enzymes on the topology of the replication intermediates and computer simulations based on the Metropolis Monte Carlo method helped us to predict the thermodynamic stability of these molecules. Using the result of the computer simulations we obtained the potential energy curve vs. writhe to determine the enthalpy variation that can be stored in the non-replicated region. We also found the potential energy curve vs catenation number in nicked chains, to get the enthalpy variation that can be stored on the replicated region. Once we obtained the enthalpy curves for supercoiling and catenanes it was possible to guess which was the most stable conformation for an replication intermediate under the effects of both topological phenomena. This method could be useful to interpret the signals observed in two-dimensional agarose gels.

Keywords: DNA Topology, supercoiling, DNA catenation, DNA replication, DNA Topoisomerase.

References

- [1] J. B. Schwartzman, A. Stasiak, *A Topological view of replicon*. Centro de Investigaciones Biológicas (CSIC), Madrid, Spain, and Université Lausanne, Lausanne-Dorigny, Switzerland. EMBO reports vol 5, no 3, 2004
- [2] Mitchell A Berger and Chris Prior, *The Writhe of Open and Closed Curves*. UCL Mathematics Dept., Gower Street London WC1E 6BT, UK, J. Phys. A: Math. Gen. 39 (2006) 8321-8348. c 2006 IOP Publ. Ltd.
- [3] Konstantin Klenin Jörg Langowski, *Computation of Writhe in Modeling of Supercoiled DNA*. Division Biophysics of Macromolecules, German Cancer Research Center, Im Neuenheimer Feld 280, D-69120 Heidelberg, Germany Received 2 December 1999; accepted 10 April 2000
- [4] Alexander V. Vologodskii, *Conformational and Thermodynamic Properties of Supercoiled DNA*. J. Mol. Biol. (1992) 227, 1224-1243.
- [5] Frank Jülicher, *Supercoiling transition in closed DNA*. Institut für Festkörperforschung, Forschungszentrum Jülich, 52425 Jülich, Germany Physical review E. March 1994

Measurement of the Education Mobility between Generations Using Goal Programming: A Case Applied to Paraguay

Jorge L. Recalde^{a1}
and María M. López^a

^aPolytechnic School, National University of Asunción, Paraguay

Abstract

Economic growth is pertinent to present population analyses and to the prognosis of a country future. Human capital is central to a country economic and social viability. Therefore, the examination of factors such as the education of the population is an antecedent to the preparation of the work force. In this study, education level is examined. Specifically, the study examines educational intergenerational inheritance using the Shorrocks index of intergenerational educational mobility. A mathematical optimization model provides the opportunity for the practical application of the creation of estimation parameters, controlling for outliers in the regression model. The problem of parameter estimation on educational intergenerational inheritance can be stated as one of linear goal programming as Charner et al. (1977) cited in Schniederjans (1995)[4]. This procedure considers balance regression equations expressed in goals for obtaining the transition probabilities, minimizing the objective function the sum of the deviations in the formulation. In the study, the model developed was tested using aggregate data from 1990 to 2011 for Asunción and the Central State of Paraguay. The data represented primary, secondary and tertiary levels of education, reported by male and female heads of household. The findings indicated that in Asunción and the Central State, the heredity weight is statistically significant for intermediate levels of education. The greatest predictive power is attributed to the parents who did not complete high school. It appears that a parents educational achievement level predicts 46% of the variability in a childs educational achievement. Furthermore and specific to gender, a son whose father has not completed primary school has approximately 40% chance to repeat the same educational achievement level. Was obtained a $M(P)=0.89$, for the Shorrocks mobility index; a high mobility in the intergenerational transmission of education was verified. Analyzing mobility matrices built for heads of household by gender,

¹E-mail Corresponding Author: jrecalde@pol.una.py

greater inheritance is observed in the transmission of education among women heads of household and her progenitors. The Shorrocks index for male household heads was $M(P)=0.91$. In other words, for female-headed households the index indicates moderate mobility with a $M(P)=0.68$. Overall, with the support of a goal programming model, it was possible to measure one of the socio-educational indices never examined in Paraguay, Shorrocks index for intergenerational educational mobility. For the reason that the intergenerational transfer of education significantly alters the operation of production systems and much of the economic growth, this paper represents current and accurate information for making high-level decisions for public policy and socio-educational interventions.

Keywords: Educational mobility, transition matrix, goal programming, Markov chains.

References

- [1] CARDENAS, H, 2010. Desigualdad en desarrollo humano y la transmisión intergeneracional de la desigualdad educativa en Honduras, Tegucigalpa, Honduras.
- [2] IMF, JONES, M, 2005. Working Paper: Estimating Markov Transition Matrices Using Proportions Data: An Application to Credit Risk, USA.
- [3] NINA, E, GRILLO, S, ALONSO, C, 2003. Movilidad social y transmisión de la pobreza en Bogotá, Economía y desarrollo, Bogotá, Colombia.
- [4] SCHNIEDERJANS, M, 1995. Goal programming: Methodology and applications, Kluwer Academic Publishers, USA.
- [5] TORRES, T, ALLEPUZ, R, 2009. El desarrollo humano: perfiles y perspectivas futuras, Estudios de Economía Aplicada: 545-562, España.

A Quantitative Paradigm for Quality of Protection in WDM networks

Marcelo Darío Rodas Brítez^{a1}, Diego P. Pinto-Roa ^{a2}

^aPolytechnical School, National University of Asunción, Paraguay

Abstract

Currently growing web services have generated a huge need for wider transmission bandwidths. Therefore wavelength division multiplexing (WDM) networks are used commercially to exploit the capability of the optical fiber [1]. WDM networks are subject to catastrophic failure due to the high volume of information to be carried in optical fibers. Therefore, WDM networks require new capabilities such as network survivability and quality of services (QoS), which together are named as quality of protection (QoP) [2]. In the WDM network design problem, with services subject to QoP requirements, is necessary to adjust flexibly the QoP levels to variety of existing demands of connection, mainly due to lack of fairness distribution and optimal resource administration.

We propose a new paradigm for quantifying the degrees of protection service based on link-failure recovery probability. With this quantization scheme is able to generate, in a flexible way, multiple service levels according to planned service model. For optimum design of primary and backup paths is implemented a Genetic Algorithm [3] that calculates paths subject to QoP of each unicast request and considering the degrees of protection service of system. Experimental results indicate that the proposed approach is a promising solution to obtain less expensive and more fairness services than traditional protection approaches based on non-flexible QoP.

Keywords: WDM networks, Recovery Probability, Protection, Quality of Protection (QoP), Genetic Algorithms.

References

- [1] A. Somani, 2005. Survivability and Traffic Grooming in WDM Optical Networks. Cambridge University Press.

¹rodas.marcelo@gmail.com

²dpinto@pol.una.py

- [2] O. Gerstel, G. H. Sasaki, 2001. Quality of protection (QoP): a quantitative unifying paradigm to protection service grades, Optical Networking and Communications Conference, pp. 12-23.
- [3] D. E. Goldberg et al.,1989. Genetic algorithms in search, optimization, and machine learning, Addison-Wesley Reading Menlo Park, vol. 412.

Design of a Mixed-Integer Linear Programming Model for Cooperative Agricultural Production Planning, Including Inventariables Resources Managing

María M. López^{a1}
and Jorge L. Recalde^a

^aPolytechnic School, National University of Asunción, Paraguay

Abstract

Small producers of seasonal crops (e.g., vegetables and fruits), take a number of decisions to insure their productivity. For example, it is customary for them to consider matters related to type of product, crop rotation cycles, resource need and allocation. Additional complexity arises when small producers join cooperatives to lessen issues of land size, labor, production and type of crop sought by the market place. The present study reflects the design of an optimization model to plan vegetable production for small producers, with specific factors including land preparation costs, resource management, capacities and costs of production and inventory. Regarding the integrity of the model are restrictions specified as the range of usable land size, the crop rotation, the customer demand, and others. The study is sensitive to the Paraguayan context, and as such it are including the limitations in the use of refrigerated storage according to national production standards. To validate the model will be solve with a optimization software, using as parameters the technical and real data for each type of vegetables, to finally make a comparison between the actual costs and the originated with the designed model.

Keywords: Mixed-integer linear programming, optimization model, production planning, management of resources.

References

- [1] González, M, Soto-Silva, W, Acosta, L, 2012. Modelo para la planificación de cosechas en huertos de manzanas, CLAIO SBPO, Río de Janeiro, Brasil.

¹E-mail Corresponding Author: mlopez@pol.una.py

- [2] Ministerio de Agricultura y Ganadería (MAG), Cooperación Alemana al Desarrollo (GIZ), 2013. Sistemas sostenibles de producción para los principales cultivos agrícolas, hortícolas, forestales y agroforestales de la Región Centro del Paraguay, Asunción, Paraguay.

Real Time Locating System using Wi-Fi

Alberto Capli, Nora González, Claudio Barúa¹ and Cynthia Villalba
Núcleo de Investigación y Desarrollo Tecnológico, Facultad Politécnica,
Universidad Nacional de Asunción

Abstract

Inventory is the counting process, either manual, semi-automatic or automatic, of tangible goods, readily available for consumption, use, processing or sale, belonging to a company [4]. Control over it is very important for any organization as a result of fundamental part of operating costs. For this reason, many companies have automated inventory management processes in order to minimize errors in manual processes and reduce costs. However, how to obtain efficiently the accurate inventory remains a challenge.

The Real-Time Locating System (RTLS) could be used to resolve the inventory problem. These systems are used to monitor and trace objects in real time, as well as, to keep track the volume of products, automatically.

In this research, a real time monitoring system of goods using the Wi-Fi technology is proposed. The proposal allows the physical location of assets within a monitored area and, through it, perform an inventory control.

The RTLS systems involve the tags utilization (attached to objects), and reader devices that receive wireless signal from the tags, allowing them to calculate the position of objects within the monitored area. The physical surface to be controlled can be a warehouse, room, floor or block of building where are goods, which in turn could be fixed assets, commercial products or objects to be monitored by using a tag.

An architecture for RTLS was designed using Wi-Fi. The designed architecture allows to work with different Wi-Fi tags, including different brands. Each brand has its own tag application-level protocol and interacts with its own middleware through the wireless infrastructure. In turn, each middleware communicates with the RTLS server using the same protocol. The proposed architecture is able to centralize the localization in a single server without relying on a specific tag brand.

For the assets location, the so-called fingerprinting method based on Wi-Fi signal was used [5]. A fingerprint (or signal sample) is a

¹E-mail Corresponding Author: cbarua@pol.una.py

vector of signal intensities associated with the position (x,y) where the signals were recorded. The Wi-Fi fingerprinting method involves finding and storing the intensity level of the signals received from the access points (AP) in different parts of area to monitor. Stored fingerprints are then used to compare the levels of signals received by the tags, and thus estimate the position [1]. The methodology implemented in this project requires adaptation work to the environment to be monitored.

The scenario selected for the proposed RTLS is a hospital organization, which is taken as a particular case study. Specifically, we want to monitor in real time the existing medical equipments within the hospital facilities, such as: wheelchairs, stretchers, defibrillators, infusion pumps; especially valuable equipment. Determining their existence and knowing where is the nearest can define the quality of patient care, streamline service delivery and enable better management of these resources.

The tests were performed in the operating room of the first floor of Hospital de Clínicas, in an area of 39 m x 25 m (975 m^2), which has 13 rooms, plus circulation areas. Four AP were necessary to cover the area to monitor and they were configured in different channels because the AP that shares the same channel or nearby channels could cause interference [2].

The accuracy was calculated using the average Euclidean distance between the estimated location and the true position (mean distance error), while precision was obtained using the distribution of distance error between the estimated location and the true location, i.e., the cumulative probability function of the distance error as mentioned in [3].

To obtain the distance between fingerprints, 306 samples in 51 points (6 fingerprint per point) were recorded and 260 tests were performed on random location positions covering the entire area. An accuracy of 2.3 m, a physical location precision of 65% and room-level location precision of 73% was obtained. The errors were distributed between 1 m and 14 m. The room-level location precision was greater than the physical location precision because many location errors between 1 m and 5 m are in the same room as the monitored object.

The accuracy and precision obtained were considered within the limits, taking into account the size of the area (975 m^2), the room dimension (between 8 m^2 y 56 m^2), and considering other precisions and accuracies of RTLS wireless-based existing systems mentioned

in [3].

Finally, this work also serves as a starting point for further research. Some of which are listed below:

- Evaluate system performance in stressful situations.
- Improve the search algorithm used in the fingerprint method to reduce the processing time. In addition, can be introduced a variable time to calculate positioning, which will minimize the errors generated by the sudden jumps in waves intensity.
- Evaluate the proposed RTLS using other indoors location methods.

Keywords: RTLS, Wi-Fi, Access Point, Tag, Reader.

References

- [1] S. Chan and G. Sohn. Indoor localization using wi-fi based fingerprinting and trilateration techniques for lbs applications. In *Proceedings of the 7th International Conference on 3D Geoinformation*, 2012.
- [2] R. Guevara and E. Serna. Una propuesta de solución al problema de la interferencia entre redes WiFi por solapamiento de canales. *Ciencia e Ingeniería Neogranadina*, 2013.
- [3] H. Liu, H. Darabi, P. Banerjee, and J. Liu. Survey of wireless indoor positioning techniques and systems. *Trans. Sys. Man Cyber Part C*, 37(6):1067–1080, November 2007.
- [4] M. Perdomo. *Fundamentos de Control Interno*. Cengage Learning Editores, 2004.
- [5] M. Quan, E. Navarro, and B. Peuker. Wi-Fi Localization Using RSSI Fingerprinting. <http://digitalcommons.calpoly.edu/cpesp/17/>, 2010.

Theoretical study of Pirimetanil and their transformation products

G. M. Morinigo^a, A. Bisgarra^a, C. Sirtori^b, N. B. Caballero^{a1}

^a Centro Interdisciplinar de Ciências da Natureza, Universidade Federal da Integração Latino-Americana-UNILA, Foz do Iguaçu, PR 85867 970, Brazil

^b Instituto de Química, Universidade Federal do Rio Grande do Sul

Abstract

The expansion of agriculture, mainly due to the widespread use of pesticides, has contributed directly to water pollution. Pesticides generally have high chemical stability, and are usually resistant to conventional biological processes, demonstrating the necessity to develop new treatment alternatives. In this context, advanced oxidation processes (AOPs) are effective new technologies able to eliminate stable and recalcitrant compounds. Depending on the transformation during the AOP, not only the active substances must be analysed, but also the transformation products (TPs) generated during the treatment [1]. Pyrimethanil (PYR), N-(4,6-dimethylpyrimidin-2-yl)-aniline, is an anilinopyrimidine used as a fungicide in agriculture, formulated as a suspension concentrate. It has preventive and curative effect on a wide range of foliar fungal diseases. It inhibits the secretion of fungal enzymes which are necessary for avoiding infection and stopping the infection process of the pathogen; also inhibits the absorption of nutrients, development of germinative tube and therefore the growth of the fungus. Some studies have related the potential danger of PYR to an increase in liver weight. Histopathological changes in liver and thyroid have been observed in short-term toxicity studies in rats and mice [2]. The study of this compound in degradation studies is urged by its widespread use in agriculture. In order to obtain information on the structural and energetic properties of this molecule a computational study was carried out. Calculations were performed using the density functional theory with functional hybrid B3LYP, B3PW91, B98 and BH&LYP, using in all cases the basis set 6-31G (d, p) and cc-pVDZ, with the last one for analysis of neutral forms of these molecules. A similar study was carried out on the different ions, a protonated and a deprotonated forms, and fragments which can be detected in chromatographic studies in the gas phase.

¹E-mail Corresponding Author: norma.caballero@unila.edu.br

The B3LYP hybrid functional was selected as recommended in the literature for the study of gas-phase organic molecules [3]. To validate results, bond lengths and angles of the optimized structure of cypermethrin obtained from computational analysis were compared with an experimental X-ray diffraction study of the crystal structure of this molecule [4]. Structure-activity/property correlation studies, QSAR/QSPR type, were also conducted using energy parameters obtained by theoretical modeling of the structures of pyrimethanil and its main degradation products. Calculation of various physicochemical and energetic properties of these molecules allows the prediction of the primary processes of fragmentation associated with the experimental technique of mass spectrometry.

Keywords: Pyrimethanil, AOP, QSAR

References

- [1] Carla Sirtori, Ana Zapata, Sixto Malato, Ana Aguera, *Formation of chlorinated by-products during photo-Fenton degradation of pyrimethanil under saline conditions. Influence on toxicity and biodegradability*. Journal of Hazardous Materials 217 218 (2012) 217 223.
- [2] European Food Safety Authority (EFSA). *Conclusion on the peer review of pyrimethanil*. Sci. Rep. 61 (2006) 170.
- [3] Manuel, Alcam; Otilia, M; and Manuel, Yez. *Computational chemistry: A useful (sometimes mandatory) tool in mass spectrometry studies* Mass Spectrometry Reviews. 2002. Vol. 20(4) Pag. 195 - 245.
- [4] F. Baert; A. Guelzim. Acta Crystallographica. Sect. C. 1991. Vol. 47 (3) Pag. 606 608.

Theoretical Study Of Permethrin

F. J. Arias Ortiz^a, V. Lopéz Aca^b, N. B. Caballero^{a1}

^a Centro Interdisciplinar de Ciências da Natureza, Universidade Federal da Integração Latino-Americana, UNILA, Av. Tancredo Neves, 6731, Caixa Postal 2044, CEP 85866-970, Foz de Iguaçu, Brasil

^b Instituto de Investigaciones Fisicoquímicas Teóricas y Aplicadas (INIFTA), Departamento de Química, Facultad de Ciencias Exactas, UNLP, La Plata, Argentina.

Abstract

Compounds known as pyrethroids, derived from the family of pyrethrins, and are typically employed as insecticides constituents. Their high lipophilicity, relatively short lifetime in the environment and with low impact on terrestrial vertebrates have led to their wide acceptance for use as insecticides. This kind of compounds are widely used for different types of formulations for agricultural use, domestic use, public health and food preparation stages [1, 2]. In order to obtain information on the structural and energetic properties of some members of this family of molecules a computational study was carried out on permethrin. Calculations were performed using the density functional theory with functional hybrid B3LYP, B3PW91, B98 and B97-2, using in all cases the basis set 6-31G (d, p) for analysis of neutral forms of these molecules. A similar study was carried out on the different ions, a protonated and a deprotonated forms, adducts and fragments, which can be detected in chromatographic studies in the gas phase. The B3LYP hybrid functional was selected as recommended in the literature for the study of gas-phase organic molecules [3]. Calculation of various physicochemical and energetic properties of these molecules allows the prediction of the primary processes of fragmentation associated with the experimental technique of mass spectrometry.

Keywords: Pyrethroids, Permethrin, DFT

References

- [1] Damián J. G., Marino. Tesis Doctoral. *Estudio Teórico Experimental sobre Respuestas Biológicas a Compuestos Orgánicos de Relevancia Am-*

¹E-mail Corresponding Author: norma.caballero@unila.edu.br

biental. SEDICI. Repositorio Institucional de la UNLP. Biblioteca de la Facultad de Ciencias Exactas. Universidad Nacional de La Plata. 2011.

- [2] Jerome J., Schleier III, Robert K. D., Peterson, CHAPTER 3. *yrethrins and Pyrethroid Insecticides in Green Trends in Insect Control*. Pag. 94-131. Editors: Oscar Lopez, Jos G. Fernandez-Bolanos, James H. Clark and George A. Kraus. Royal Society of Chemistry. Cambridge, UK. 2011
- [3] Manuel, Alcam; Otilia, M; and Manuel, Yez. *Computational chemistry: A useful (sometimes mandatory) tool in mass spectrometry studies* Mass Spectrometry Reviews. 2002. Vol. 20(4) Pag. 195 - 245.

A Multi-objective Study of Cooperative vs Selfish Routing in WDM Networks

Baudelio Báez^{a1}, José Colbes^{a2}, Diego P. Pinto-Roa^{a3}

^aPolytechnical School, National University of Asunción, Paraguay

Abstract

The design and management of wavelength division multiplexing (WDM) network to obtain the maximum performance is essential in optical communications. In particular, wavelength converter allocation is a problem where the routing scheme –centralized or distributed– plays a critical role in the WDM network performance [1]. This work studies the benefit of a centralized routing in relation to the distributed routing in wavelength converter allocation problem considering multi-objective context. The distributed routing is based on selfish model [2] in which each connection tries to improve its blocking probability. In counterpart, in centralized routing, all connexion are calculated by a master which tries to obtain the best average blocking probability of the system, thus being a cooperative model.

For the study, we developed a multi-objective evolutionary algorithm [3] for design and management of WDM network. In the cooperative context it is proposed a pure evolutionary algorithm to calculate the converters allocation and traffic load flows at the same time. For selfish routing, an hybrid algorithm calculates the converters allocation by evolutionary process while the traffic load flow assignment that maximizes the benefit of each connection (selfish model) is performed by a simulation with the Wardrop equilibrium as stop criterion.

Both approaches are compared using the Pareto Anarchy Price measure which is a proposal of this works as generalization of Anarchy Price classic concept. Experimental results indicate when the traffic load increased, the Pareto Anarchy Price improves; however, the quality of solutions gets worse.

Keywords: WDM Networks, Wavelength Converter Allocation, Cooperative Routing, Selfish Routing, Anarchy Price, Multi-objective Optimization, Evolutionary Algorithms.

¹baudelio.baez@gmail.com

²jcolbes@pol.una.py

³dpinto@pol.una.py

References

- [1] A. Somani, 2005. Survivability and Traffic Grooming in WDM Optical Networks. Cambridge University Press.
- [2] N. Nisan, T. Roughgarden, E. Tardos, and V. Vazirani, 2007. Algorithmic Game Theory. Cambridge University Press.
- [3] C. C. Coello, G. Lamont, and D. V. Veldhuizen, Eds., 2007. Evolutionary Algorithms for Solving Multi-Objective Problems. New York: Springer.

Voronoi Tessellation for calculating local 3D densities on the environment of clusters of galaxies

Marcel Chow-Martínez^a and César A. Caretta^{a 1}

^aDepartamento de Astronomía, DCNE-CGT, Universidad de Guanajuato, Guanajuato, Gto., Mexico

Abstract

A customary problem in Astrophysics, and also in other areas, is the need for calculating punctual densities in a distribution of points. In the case we are interested in, we need to calculate local 3D densities for the environment of galaxies and clusters of galaxies. An algorithm for calculating the Voronoi Tessellation, using 3D Delaunay triangulation, was designed with this aim. Normally the 2D version of the Voronoi Tessellation can be obtained from specifically constructed software packages in different computational environments, but 3D functional versions are not easily available. The algorithm we present was programmed in a combination of *FORTRAN* language and *R* project environment. In the 3D version of the Delaunay triangulation, the Voronoi neighbours are defined as those who conform the vertices of the tetrahedron that follow the Delaunay condition, i.e., no other points in the distribution can be located inside the circumsphere that is traced by the vertices of the respective tetrahedron. The circum-center of such sphere is a vertex of the Voronoi cell for a given point, and from obtaining all those vertices for that point we are able to calculate the volume of its cell. We, then, calculated the local density as the inverse of the volume of the Voronoi cell for each of our galaxies and galaxy clusters. We also present the results of applying this methodology to the sample of 3410 galaxy clusters in the Local Universe up to a redshift of 0.15.

Keywords: Voronoi tessellation, local 3D densities, galaxies: clusters, Cosmology: Local Universe.

¹E-mail Corresponding Author: caretta@astro.ugto.mx

Two-Phase Flow Including Capillary Pressure And Buoyancy Effects: A Two-Dimensional Model To Study The Carbon Sequestration Process

Jhabriel Varela^{a1}, Christian Schaerer^b, Juan Pablo Nogues^{a,b}

^aUniversidad Paraguayo Alemana

^bFacultad Politécnica, Universidad Nacional de Asunción

Abstract

Modelling and simulation of multiphase flows in porous media haven been focus of several areas, including: enhanced oil recovery, pollution of aquifers caused by NAPL's², geological storage of carbon dioxide, absorption processes in catalytic beds, etc [1]. This poster presents a mathematical model that use the ImPES³ algorithm in order to simulate a two-phase flow in two dimensions, including heterogeneity, capillary pressure and buoyancy effects. In addition, scaling techniques are applied to analyse the influence of scales in simulations. Spatial discretization of fluid fluxes are performed using finite volume methods [2]. Finally, the results of sensitivity analysis to determine the influence of several physical parameters in the saturation front and pressure transmission of carbon dioxide in the storage process into a salty aquifer are presented [3].

Keywords: Two-phase flow, ImPES algorithm, Finite Volume Method, Carbon Sequestration.

References

- [1] CHEN, Zhangxin; HUAN, Guanren; MA, Yuanle. Computational methods for multiphase flows in porous media. Siam, 2006.
- [2] NORDBOTTEN, Jan Martin; CELIA, Michael A. Geological storage of CO₂: modeling approaches for large-scale simulation. John Wiley & Sons, 2011.

¹E-mail Corresponding Author: jhabriel.varela@upa.edu.py

²Non Aqueous Phase Liquid

³Implicit Pressure Explicit Saturation

- [3] DOSTER, Florian; KEILEGAVLEN, Eirik; NORDBOTTEN, Jan M. Multi-Phase Multi-Component Flow Including Capillary Pressure And Buoyancy: A Robust Implicit Pressure Explicit Mass Finite Volume Method.

HTTP-WS-AD: Anomaly Detector for Web Applications and Web Services

José Giménez^{a1}, Cristian Cappelletti^{a2}

^aFacultad Politécnica, Universidad Nacional de Asunción, San Lorenzo, Paraguay

Abstract

Web applications have become the most demanded systems to be developed today. This is because they have several advantages compared to traditional system models. Due to massive use of web applications they have become one of the main targets for cyberattacks. There are several types of known attacks, among which stand out XSS (Cross Site Scripting) and SQL Injection, which are still the most popular because of the effectiveness and simplicity of them.

In this paper we present HTTP-WS-AD which evaluates the effectiveness of different anomaly detection models in presence of new attacks such as HPP (HTTP Parameter Pollution) or mXSS (mutated XSS) and it includes new anomaly models for HTTP requests based on XML or JSON formats usually corresponding to Web Services and AJAX³ requests respectively.

Keywords: Anomaly Detection, Web Application Firewall, HTTP, Security, XSS, SQL Injection.

1 Proposed Work

HTTP-WS-AD is based on a transparent proxy that can be placed in front of web servers to analyze traffic, for to record requests and generate the models in the training or learning phase and to analyze requests and eventually prevent them from reaching the protected web server in the detection phase. The transparent proxy enables any web applications to be protected regardless of the used platform, and it is safer because if the attack succeeds it will only affect the proxy and not the protected application.

Figure 1 shows the architecture of our anomaly detector and evaluator. The dotted line indicates the training or learning phase. In this phase the

¹E-mail Corresponding Author: jdgimenez@pol.una.py

²ccappo@pol.una.py

³AJAX: Asynchronous JavaScript And XML

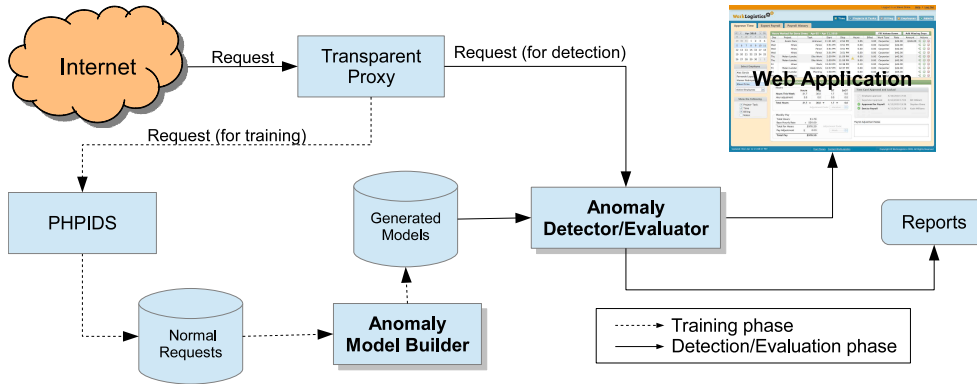


Figure 1: Architecture of HTTP-WS-AD

requests are captured by the transparent proxy. Then these requests are analyzed for a signature-based WAF named PHPIDS [1]. The reason of this step is to eliminate the requests with attack and so to obtain a clean database for training. Normal requests obtained this way are the input for the Anomaly Model Builder. This module generates the models and it saves them in the normal models database. The filled line indicates the detection/evaluation phase. In this phase the transparent proxy is switched to the Anomaly Detection/Evaluation module. In this module, requests are compared with the normal generated model. Sufficient deviation is considered an attack. Also this module generates reports about the models' effectiveness. To evaluate this effectiveness we include synthetic HTTP requests with new attacks.

The anomaly models implemented in HTTP-WS-AD are classified in three categories: a) *Parameter models*: these represent the behavior of a simple parameter (in a GET or POST request), b) *Query String models*: these evaluate the structure of all the parameters that an application receives in a particular URL. These ones evaluate the parameters set as a whole entity, and c) *Session models*: these represent user interaction and the different programs that exist in a web application.

The *Parameters Models* include these models: token, length, character distribution and structure inference [3] [4], ngram [2] and Mahalanobis distance [5]. The *Query Models* are formed for these models: attribute presence or absence and attribute order [3] [4]. In this category we include our models: the XML and JSON model. In both models we identified the order of elements in the XML or JSON format. In the learning phase the anomaly

model builder registers all observed structures (in XML or JSON format) and in the detection phase the anomaly detector tests the request structure with the normal observed structures saved in the generated models database. Finally the *Session models* include the access frequency and the invocation order [4].

References

- [1] M. Heuderich. PHPIDS, web application security 2.0. <http://phpids.org>, 2014. Access: 01/03/2014.
- [2] Kenneth L. Ingham and Hajime Inoue. Comparing anomaly detection techniques for HTTP. In *Proceedings of the 10th international conference on Recent advances in intrusion detection*, RAID'07, pages 42–62, Berlin, Heidelberg, 2007. Springer-Verlag.
- [3] Christopher Kruegel and Giovanni Vigna. Anomaly detection of web-based attacks. In *Proceedings of the 10th ACM Conference on Computer and communications security*, CCS '03, pages 251–261, New York, NY, USA, 2003. ACM.
- [4] Christopher Kruegel, Giovanni Vigna, and William Robertson. A multi-model approach to the detection of web-based attacks. *Computer Networks*, 48:717–738, Aug. 2005.
- [5] K. Wang and S.J. Stolfo. Anomalous payload-based network intrusion detection. In Erland Jonsson, Alfonso Valdes, and Magnus Almgren, editors, *Recent Advances in Intrusion Detection*, volume 3224 of *LNCS*, pages 203–222. Springer, 2004.

Energy Planning in terms of Useful Energy for the Republic of Paraguay

Enrique Buzarquis^{a1}, Javier Amattea^a, Benjamín Barán^a, Gerardo Blanco^a

^aPolytechnic Faculty - National University of Asunción

Abstract

This paper proposes the guidelines and actions to be taken in order to obtain a sustainable energy structure for the Republic of Paraguay, based on data of energy consumption behavior. This work is developed as part of the energy balance in terms of useful energy, elaborated in Paraguay for the year 2011. These data are linked to the corresponding leading variables, and consequently reflect the actual behavior of energy consumption in Paraguay.

The developed model is structured on the base of the software platform called LEAP ©(*Long-range Energy Alternatives Planning System*), where consumption sectors and energy sources employed in the Paraguayan energy system interact in a dynamical and integrated form.

This model has the advantage of being the first with these characteristics, only possible by recent data obtained in the development of the national energy matrix for the Republic of Paraguay, which was validated and structured by disaggregating data by energy consumption sectors in useful energy terms.

As main result, it is obtained the determination of critical points in the energy system, derived from the current and future energy behavior. Another important result obtained is the identification of the major consuming sectors, responsible for the emission of large amounts of greenhouse gases (GHG) and the energy sources that cause this situation.

In this work, comparisons are made among potential energy behavior scenarios through the short, medium and long term trends, using the year 2040 as study horizon. Likewise, it is analyzed the economic components of possible scenarios, in which possible energy sources substitutions are available, what is important to satisfy the energy needs and to make adjustments in the energy sectors, based on government planning proposals. It also identifies the optimal time to implement alternative measures in energy substitution for the specific

¹E-mail Corresponding Author: eburzarquis@pol.una.py

sectors of energy consumption, in order to obtain a positive effect on the sustainability of the Paraguayan energy structure.

This paper, further notes that, with a proper planning energy system, Paraguay not only can obtain a sustainable energy structure, but also with the energy model acting holistically, energy sustainability can be achieved at minimal cost and favorable to the environment. In that sense, this paper presents a model of energy behavior prospective, where the economic variables and the greenhouse emissions gases are directly linked. This model may serve as a fundamental tool to guide decision-making, and consequently pursues to contribute to sustainable development of the Republic of Paraguay.

Additionally, this paper presents the time periods in which the Republic of Paraguay will need new electric generation units, necessary to supply the domestic consumption and to guarantee energy supply.

Finally, this paper analyze the energy resources available in Paraguay and their future availability, based on the trend behavior of energy demand, in an attempt to identify possible scenarios that could generate a deficit due to indiscriminate use of energy sources from biomass.

Keywords: Republic of Paraguay, Energy Balance, Useful Energy, Energy Policy, Substitution, Greenhouse gases emissions, LEAP.

Neuro-fuzzy Approach Addressing Predictability

Pettras L. B. Santos^a, Sandra Sandri^a and Haroldo F. de Campos Velho^{a1}

^aNational Institute for Space Research, São José dos Campos, SP, Brazil

Abstract

Here we address the joint use of the Breeding method and Neuro-Fuzzy systems for predictability, described as a classification problem. The bred vectors are inputs for two Neuro-Fuzzy systems ANFIS and GUAJE, based on Takagi-Sugeno-Kang and Mamdani approaches, respectively. A better classification performance is obtained using ANFIS, but the automatic rules generated by the GUAJE are more interpretable.

Keywords: Predictability, bred vector, neuro-fuzzy.

1. INTRODUCTION

Predictability is defined as quantitative evaluations that assess prediction quality. Statistical methods are usually employed for this means but recently it has also been addressed as a classification problem [1, 4].

Lorenz strange attractor has been very widely used as a prototype of chaotic behavior [3]. It has two regimes, which could represent two possibilities in a world with only two seasons (e.g. “winter” and “summer”). Although apparently simple, in such a system it is hard to identify when a regime change will happen and how long it will last.

The Breeding method [2] is used to estimate forecast errors and is often applied in weather models (operational centers). Bred vectors are simply the difference between two model runs: the second originating from slightly perturbed initial conditions, periodically rescaled (see Fig. 1.a). The scheme based on breeding approach was employed to derive rules of thumb to classify the prediction of regime on Lorenz system [1]. In the present work, we use the breeding method and Neuro-fuzzy systems ANFIS and GUAJE [5, 6] to identify Lorenz attractor behaviour.

The model equations and comments on previous studies using bred vectors are described in the next section. Section 3 presents the results obtained with neuro-fuzzy systems, and final remarks are addressed in the last section.

¹E-mail corresponding author: haroldo@lac.inpe.br

2. PREVIOUS STUDIES

The Lorenz Model equations are given as [3]:

$$dx/dt = -\sigma x - y \quad (1)$$

$$dy/dt = -\rho x - y - xz \quad (2)$$

$$dz/dt = xy - \beta z \quad (3)$$

With $\sigma = 10, \rho = 28, \beta = 8/3$ as parameters, the resulting system is a strange attractor [3] (see Fig.1.b).

The bred-vectors algorithm is given as follows [2]; initialization step 1 is executed only once and steps 2 and 3 are repeated for each time interval (identified as a fixed number of time steps):

1. Calculate the initial perturbation $A = \delta f(x, t)$, using an arbitrary norm.
2. Add the perturbation calculated in the previous step to the basic solution, integrate the perturbed condition with the nonlinear model for a fixed number of time steps, and subtract the original unperturbed solution from the perturbed nonlinear integration

$$\delta A = \delta f(x, t + \Delta t) = f(x, t + \Delta t) - f(x, t) . \quad (4)$$

3. Measure the size $A + \delta A$ of the evolved perturbation $\overline{\delta f(x, t + \Delta t)}$, and divide the perturbation by the measured amplification factor so that its size remains equal to A :

$$\delta f(x, t + \Delta t) = \overline{\delta f(x, t + \Delta t)} \sim A/(A + \delta A) \quad (5)$$

The Breeding scheme was applied by [1] to classify the prediction of regime on Lorenz system, using as classes the size of the bred vectors, described by stars in colors red ($s(t) > 0.064$), yellow ($0.032 \leq s(t) < .0064$), green ($0 \leq s(t) < 0.032$), and blue ($s(t) < 0$). [1] proposed the use of the following rules:

- R1:** Growth rate exceeding 0.064 over eight steps with presence of one (or more) red stars, the current regime will end after it completes the current orbit.
- R2:** The length of the new regime is proportional to the number of red stars.

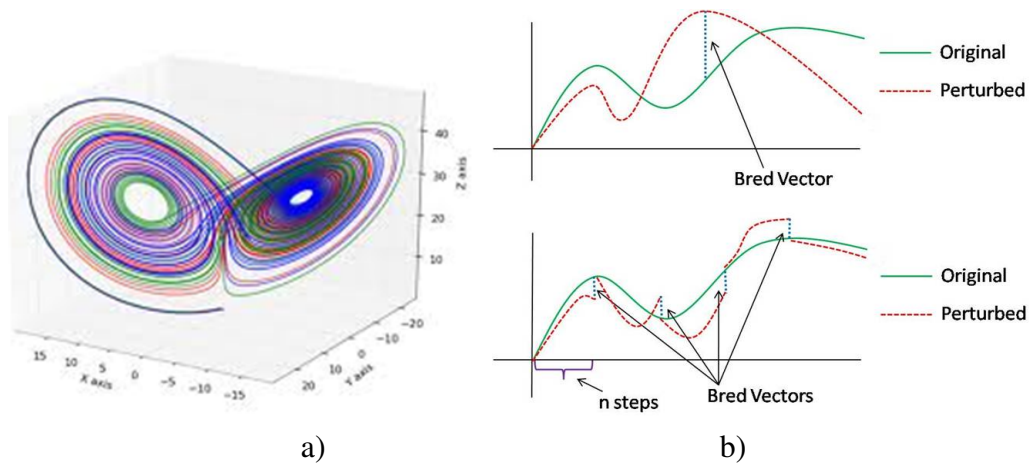


Figure 1 - a) Lorenz strange attractor and b) Breeding method.

Neuro-fuzzy systems uses a set of pairs (input, desired outputs) to derive fuzzy systems. ANFIS and GUAJE are neuro-fuzzy systems [5, 6] based on the Takagi-Sugeno-Kang (TSK) and the Mamdani approaches. Considering input variables x and y and output z , the rules in these systems are modeled as, e.g.:

ANFIS: IF x is Low AND y is High THEN z is $(px + qy + r)$,

GUAJE: IF x is Low AND y is High THEN z is Low,

where Low and High are fuzzy sets and p , q , and r are (real) constants.

3. NEURO-FUZZY CHAOTIC SYSTEMS PREDICTION

ANFIS and Guaje were applied on Lorenz attractor to determine the classes of dynamics, using as input the counts of the bred vectors size color classification and 4 dynamic classes as output: 1 (trajectory remains in the region), 2 (trajectory changes after 3 cycles), 3 (trajectory changes region and remains there from 4 up to 6 cycles) and 4 (trajectory changes region and remains there for more than 6 cycles). Tables 1 brings the result of applying ANFIS and GUAJE on Lorenz attractor, using bred vectors. Even though ANFIS presents higher accuracy with respect to GUAJE (89.81% against 77.09% of correct answers), the rules derived from Guaje are more interpretable.

ANFIS	1	2	3	4
1	143	7	1	3
2	6	87	4	1
3	0	3	14	2
4	0	0	1	3

GUAJE	0	1	2	3
0	153	1	0	0
1	47	49	2	0
2	0	9	10	0
3	0	0	4	0

Table 1: Confusion matrices (275 patterns)

4. FINAL REMARKS

We have presented the use the breeding method and Neuro-fuzzy systems ANFIS and GUAJE to classify Lorenz attractor behaviour. ANFIS produced more accurate results, but rules from GUAJE are more interpretable.

Future works include to apply the methodology to other dynamical systems, such as space weather [7]. Other investigations also include to explore a classification with more classes (precision), with possible clustering of classes, in order to have a better accuracy, for producing a good balance between precision and accuracy – searching to enhance the interpretability.

ACKNOWLEDGMENTS: Authors thank to the CAPES and CNPq, Brazilian agencies of research support.

References

- [1] Evans, E., Bhatti, N., Pann, L., Kinney, J., Peña, M., Shu-Chih, S.-C., Kalnay, E., Hansen, J., 2004. RISE: Undergraduates Find That Regime Changes in Lorenz’s Model are Predictable. *Bull. Amer. Meteor. Soc.*, vol. 85, 521–524.
- [2] Kalnay, E., Peña, M., Yang, S.-C., CAI, M., 2002. Breeding and predictability in coupled Lorenz models. *Proc. the ECMWF Seminar on Predictability*.
- [3] Lorenz, EN, 1963. Deterministic non-periodic flow. *J. Atmos. Sci.*, vol. 20, p. 130–141.
- [4] Santos, PBL, Campos Velho, HF, Cintra, R, Sandri, S, 2014. Chaotic Systems Predictability using Neuro-Fuzzy Systems and Neural Networks with Bred Vectors. In: *Recent Developments and New Directions in Soft Computing* (Studies in Fuzziness and Soft Computing – Book 317) – Editors: Lotfi

- A. Zadeh, Ali M. Abbasov, Ronald R Yager, Shahnaz N. Shahbazova, Marek Z Reformat, p. 295–315, (see also: Proc. WCONSC'2012, Baku, Azerbaijan).
- [5] Shing, J, Jang, R, 1993. ANFIS: Adaptive-network-based fuzzy inference systems. *IEEE Trans. on Systems, Man, and Cybernetics*, vol. 23, p. 714–723.
- [6] Alonso, JM, Magdalena, L, 2010. Guaje - a Java environment for generating understandable and accurate models. Proceedings of the *XV Spanish Conference for Fuzzy Logic and Technology (ESTYLF)*, p. 399–404.
- [7] Cintra, R, Campos Velho, HF, 2008. Predictability for a Chaotic Solar Plasma System. *XXIX Iberian and Latin-American Congress on Computational Methods for Engineering (CILAMCE)*, Maceio (AL), Brazil, p. 1–8.

Application of Artificial Neural Networks to Vocational Guidance

Nelson Romero^{a1}, Eustaquio Martnez ^a, and Alejandro Benítez ^a

^aFacultad Politécnica - Universidad Nacional del Este,
Ciudad del Este - Paraguay

Abstract

In order to solve the profession selection problem, a problem that affects most of the people at the time they finish their high school, artificial intelligence techniques are implemented in the development of a system capable to generate vocational recommendations. At first, a group of students from the Colegio Sembrador and the Centro Regional de Educación complete vocational tests, which are available online in a web page. Next, with the assistance of a professional, one or more vocational areas are recommended for each individual. Finally, the results of the tests and the professional recommendations are used as samples data in a procedure where the system learns and acquire, by using computational intelligence algorithms, the capability to provide recommendations automatically in future operations using as its input data nothing else but the results of the vocational tests.

Keywords: Artificial neural networks, Artificial intelligence, Personnel selection, Vocational Orientation.

1. INTRODUCTION

In most scientific areas, there are many ways for collecting data from natural complex systems [1] in order to extract data structural information and perform different kinds of analysis on them [2]. For this reason, researchers usually have a lot of data sets stored independently, occupying huge hard drive memory space, which increases with the technological advances. In this context, data systems are often composed by spatio-temporal information of one, two and three dimensions that can represent many distinct possible measurements taken from the same observed system.

Artificial Neural Networks (ANN) are a learning and automatic processing paradigm, inspired by the functioning of the nervous system of living beings. Its main purpose is the processing of information to solve problems [3].

¹E-mail Corresponding Author: nmarceloromero@fpune.edu.py

The main feature of ANN is its capability to build a system capable of solving classification and pattern prediction problems after a learning process in which the ANN receives sample data based solutions, for the problem to be modelled, which have been obtained previously. No pre-defined algorithms or models are necessary for a neural network to find the solution to a problem, only the sample data are necessary.

Considering this characteristic, this paper presents the implementation of an Artificial Neural Network capable of recommending vocational areas based on the information obtained in vocational guidance tests. The main objective of this work is to solve the problem of interpretation of the results that young people obtain from one or more vocational tests.

The implementation of neural networks is proposed because the problem of recommending vocational areas is not the kind of problem that can be traditionally programmed (it has to do with subjective opinions that are not defined by a specific model), there are only examples (vocational recommendations for a certain set of results from vocational tests applied to individuals) that the system must be able to learn and emulate [3].

1.1. Motivation

It has been decided to implement Artificial Neural Networks because they can be used in problems whit just input / output values, such as the problem to be solved. The purpose is to determine if the network is able to learn in order to become capable to offer similar vocational recommendations or at least close to those which are provided by a professional in the field of psychology.

Another motivating factor is the fact that Artificial Intelligence and Psychology have been associated in rare cases, so it is a sprawling area. The possibility of establishing a comparison between the method of vocational guidance through neural networks and the traditional psychological methods has also been an important point to be taken into account for the decision to conduct the research.

1.2. Objectives

General Objectives

To implement an artificial neural network capable of inferring an individual's vocational area based on his/her skills and/or preferences.

Specific Objectives

- To gather information about skills and preferences of individuals through psychological tests.
- To model input and output vectors (training data) from the data collected in psychological tests.
- To efficiently configure the neural network on an experimental basis.
- To obtain working results from the network.

1.3. Vocational Guidance

Vocational guidance is associated with the area of personnel selection and there are research studies that have sought to resolve such kind of problems by implementing artificial neural networks. Below are described four of them.

Personnel selection using artificial neural networks

The project was executed in 2006, in the Escuela de Ingeniera Eléctrica y Electrónica, Universidad del Valle, Cali, Colombia. The work consisted in choosing candidates who were apt to enter the Escuela Naval de Cadetes Almirante Padilla, Cartagena, Colombia. The system was based on the psychological 16-PF test, where First Order factors and the motivational distortion are extracted to be used as input to a pattern recognition algorithm that acts as a behavioral predictor. The experiment used two types of artificial neural networks, where the Multilayer Perceptron yielded a 60% effectiveness and Radial Basis Network yielded a 70% efficiency [4].

Neural network for classification of psychological profiles with Dr. RB Cattell's 16PF test applied to a student population

The aim of this study, conducted by Eng. Adolfo Gordillo in Colombia, was to detect possible conflicting personality qualities in students so as to apply the appropriate treatment according to the results obtained after the processing. The 16-PF test was used in this work where the neural network, a Multilayer Perceptron, obtained a nearly 100% effectiveness [5].

Prediction of student performance and diagnosis using neural networks

The project was carried out at the Technical University of Buenos Aires and it was aimed at the implementation of an artificial neural network with the ability to predict whether a college student would be able to approve or not a specific course, for that purpose the network used the results obtained in exams as input parameters. The type of neural network used was the Multilayer Perceptron using the Backpropagation learning algorithm with the Gradient Descent technique. The system effectiveness was of 96% [6].

Artificial neural networks for assistance in psychiatric diagnosis

In this study, which was conducted at the University of Washington, two artificial neural networks have been developed: Backpropagation Network and Kohonen Network, with the ability to classify psychiatric patients to make a diagnosis. The possible diagnoses were: schizophrenia, neurosis and normal person. At the end of the project, it was found that making a diagnosis using RNAs was more effective than using an expert system [7].

1.4. Hypothesis

It is possible to build a system capable of reproduce, with a high degree of accuracy, the process by which a professional in the field of psychology uses its knowledge and experience to analyze the results obtained by a person in one or more vocational tests and gives a vocational recommendation.

1.5. Personal Interest Test: Interest Inventory Hereford

Questionnaire of 90 questions that are numerically answered by selecting a number from 1 to 5. Each question is part of a specific area of interest, for example "play a musical instrument" is part of Music area, while "Read the classics" is a question concerning the area of Literature.

1.6. Aptitude Test: Differential Aptitude Test (DAT)

It is constituted by eight forms that contain different types of exercises, whose amount varies in each form. Unlike interest inventory Hereford, in which there is no incorrect result but only estimates of interest degrees, the answers to the exercises of the forms from the DAT test may be right or wrong [2].

2. MATERIALS AND METHODS

2.1. Materials

Hardware: Computer: Four-core processor running at 3.5 GHz (64 bits), 8 GB memory RAM DDR3, Hard disk 1 TB

Software: Technical Scientific programming language for implementing neural network Application for design and development of web sites and web applications.

2.2. Methodology

Two vocational tests were used for the development of this work: the Hereford Interest Inventory and the Differential Aptitude Test (DAT). Both tests have been made available on a website programmed in HTML [8] and PHP [9].

A total of 78 students from high schools Centro Regional of Education Dr. Jos Gaspar Rodriguez de Francia and Colegio Sembrador have completed both vocational tests accessing the website made available for the purpose.

Once all sample results were obtained from both vocational tests, and once the corresponding recommendations were made, the ANN was implemented.

The data structure established for data processing was as follows:

Input data

Vocational testing results, which include 17 items (9 Hereford test results and 8 DAT test results) standardized in numerical values between 0 and 1.

Output data

Vocational recommendations composed of four binary items, which can take values 0 or 1. Each item represents a vocational area (Physics / Mathematics, Chemical / Biological, Social Sciences, Humanities / Arts). The output value of the item determines whether the vocational area to which it refers is recommended (value 1) or not (value 0).

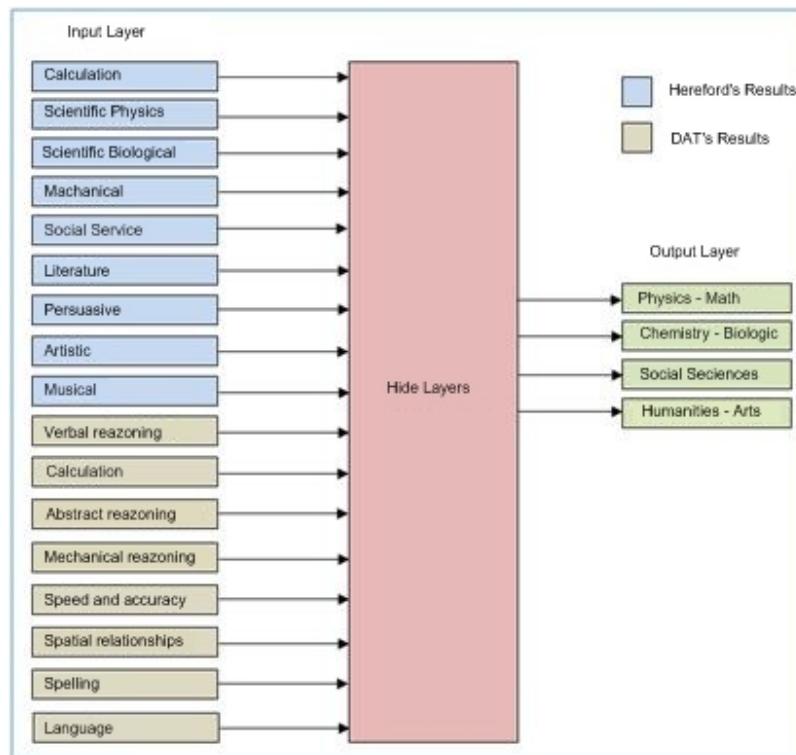


Figure 1 - Design A of the deployed Network.

The input data was designed in two ways, and the ANN was implemented using two types of structure, the first one can be seen in Figure 1, which constitutes the above mentioned design.

The second design can be seen in Figure 2, this is a structure in which the Hereford test results are obviated and only DAT test are used as input values.

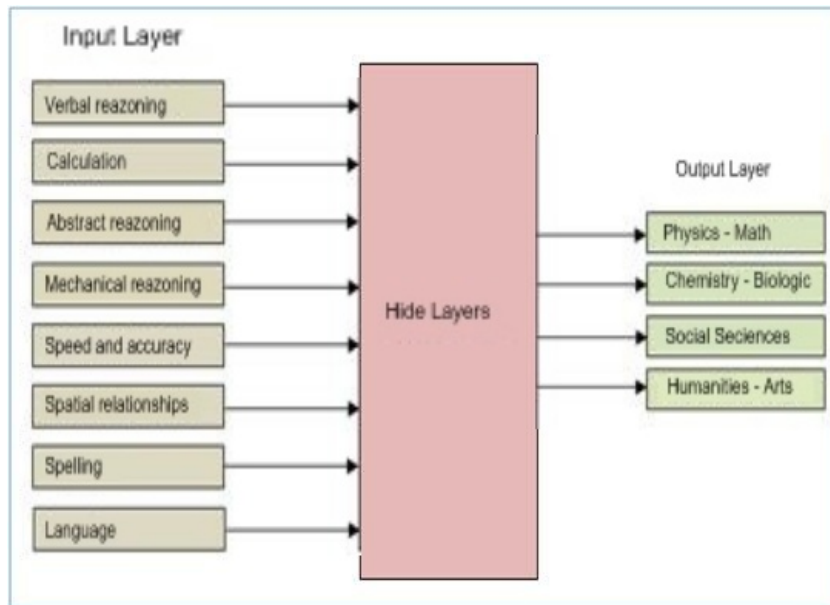


Figure 2 - Design B of the deployed Network.

Once all appropriate recommendations were made for each subject, the samples were divided into two groups: 60% for training the network and 40% for testing.

The artificial neural network has been implemented using a technical scientific programming language for both input structures seen before, and an experimental stage has been executed, which consisted in a search of a network configuration that would give the results or recommendations that were closest to those made with specialist assistance, which can be checked by contrasting the network output after processing the test data (40% of samples) with the expected output for that test data.

During the experimentation, the following parameters have been altered to obtain an acceptable effectiveness:

- Number of neurons in each layer: number of processing units in the input layer, output and hidden network.
- Number of hidden layers: the multilayer network, by definition, consists of a single layer of input neurons and a single layer of output neurons. The quantity of hidden layers may vary according to the needs of the problem.
- Activation function of each layer: is a function that is applied to the scalar product of the input vector and the weight vector of a neuron. It defines the output value of the processing unit.
- Target: the minimum expected error. The performance function used for the network was the Mean Square Error.
- Iterations: the number of times the weight vectors of the neural network are updated.
- Minimum Gradient: the minimum performance gradient.
- Maximum value for lambda (λ): λ is an adaptive value that regulates the tendency of the algorithm

The learning algorithm for all neural networks implemented is the Levenberg-Marquardt's.

To test the efficiency of different network configurations in the test process, it has been used ROC curve graphs.

3. RESULTS

The different neural network configurations where two vocational tests have been used were discarded after the experiment, for not achieving an acceptable efficiency after being trained.

The neural network with the best results is one of those that have as input the results of one single test. After the training process, the network with the best configuration has offered total of 25 (80.6%) recommendations that exactly match with those made with professional assistance, while the number of mismatched recommendations was six (19.4%).

Its ROC curve from test data can be observed in Figure 3.

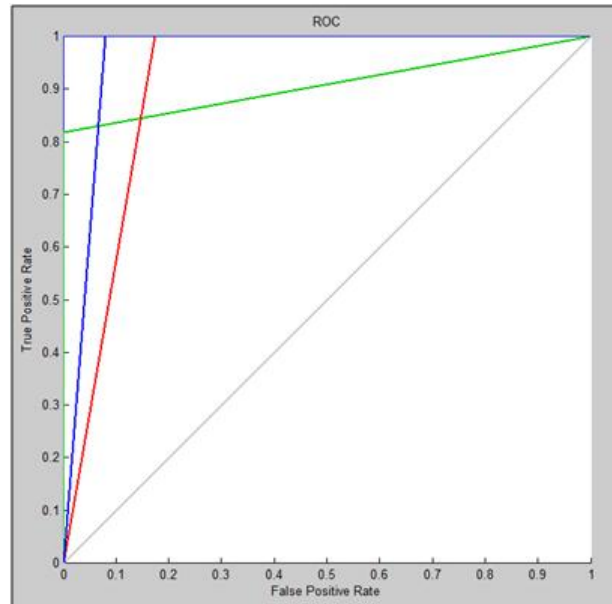


Figure 3 - ROC graph of the Network trained with the best configuration.

In a ROC graph, each curve represents the effectiveness of an output neuron of the neural network; therefore, having four output neurons, four curves are shown. The graph shows the correlation between the True Positive Rate (TPR) and the False Positive Rate (FPR). The higher the TPR and the lower the FPR, the more accurate is the output provided by that neuron. In the Figure 3, it can be perceived that in all cases the FPR is less than or equal to 0.2 and TPR is greater than 0.8. Thus, the network provides results considered acceptable.

4. DISCUSSION

ROC analysis is directly and naturally related to cost/benefit analysis in diagnostic decision making from machine learning. This applied to the studied case, implies that is possible to model and simulate subjectivity through the implementation of artificial neural networks, understanding subjectivity as an opinion or recommendation based on a personal assessment by a specialist or one that is performed with the assistance of the same one.

However, the modeling of the data that is going to be processed by the network should be made in a way that allows the input values to be closely

interrelated and that a pattern of particular output exists, a pattern that should be able to be recognized by the network during the training process, as occurred in this work with the network that has been trained using as input only the results of the DAT test.

Otherwise, it will happen what has happened when both: DAT and Hereford tests results were implemented as input values of the network, where there was no cohesion between them, as these are very different and even contradictory estimates (the first provides estimates of the skills while the other does about interest), that their combination does not lead to a pattern, ie, the input data and their results are random, which leads to the inability of the network to learn regardless of the different configurations that it can take.

The characteristics of the individuals performing the vocational tests and their results do not imply a risk of the system to erroneous recommend. However, during the training process, the conditions that the professional considers in order to give the recommendations can lead the network to learn in a wrong way and therefore not accurately recommend once it has started to do so. This would occur if the studies carried out over the samples by the professional lead to recommendations that are random or almost random. Also it would occur if the professional took a portion of the samples and make recommendations; then, after a period of time in which the recommend criteria have changed, the professional made the recommendations for the second part of the samples. In that case, the recommendations for the two parts of the sample would not be consistent with each other, leading to the network to enter in conflict in a case where it finds two identical samples or very similar to each other, but with very different outputs.

5. CONCLUSION

It has been able to implement a system capable of recommending a vocational area to the individual, after having processed his results obtained in an aptitude test. It is important to note, however, that when the system generates a recommendation, it only takes into account a number of input variables that estimate the abilities of the person to perform in determined areas in the future, but it does not cover other psychological, social, family, economic or other kind of factors, that also has direct influence on the skills used by the individual when he/she has to function in those areas.

ACKNOWLEDGMENTS: Our thanks to Prof. Alberto Rojas for his help in the translation of the article into English.

References

- [1] Anonymous, Test de Orientacin Vocacional (CHASIDE), On-line <http://www.tecnicas-de-estudio.org/general/test-orientacion.htm> 25/02/2014.
- [2] Thomas, U., Test DAT - Test de Aptitudes Diferenciales, On-line <http://www.elpsicoasesor.com/2011/03/test-dat-test-de-aptitudes.html> 25/02/2014.
- [3] Russell, S., Norvig, P. Inteligencia Artificial, Un enfoque moderno. Madrid, 2004.
- [4] Acevedo, G., Caicedo, E. and Loaiza, H., Seleccin de personal mediante redes neuronales artificiales. Revista de Matemática: Teoría y Aplicaciones, No. 14, 200.
- [5] Gordillo, A., Aplicación de una Red Neuronal para clasificación de perfiles psicologicos con el test 16PF del Dr. R. B. Cattell en una población estudiantil, On-line <http://espejos.unesco.org.uy/simplac2002/Ponencias/Inforedu/IE004%20Adolfo%20A.%20Gordillo.doc> 25/02/2014.
- [6] Cataldi, Z., Salgueiro, F. and Lage, F., Predicción del rendimiento de los estudiantes y diagnóstico usando redes neuronales artificiales, On-line <http://bioinfo.uib.es/~joemiro/aenui/procJenui/Jen2007/capred.pdf> 4/08/2014.
- [7] Zou, Y., Shen, Y., Shu, L., Wang, Y., Feng, F., Xu, K., Ou, Y., Song, Y., Zhong, Y., Wang, M., Liu, W., Artificial neural network to assist psychiatric diagnosis, On-line <http://www.ncbi.nlm.nih.gov/pubmed/8818370> 4/08/2014.
- [8] Lamarca, M., HTML, On-line <http://www.hipertexto.info/documentos/html.htm> 4/08/2014.

- [9] The PHP Group, Manual de PHP - Prefacio, On-line
<http://www.php.net/manual/es/preface.php> 26/02/2014.

Numerical simulation of plane mixing layer with exothermic chemical reaction using FEniCS libraries

Diego R. González^{a1}, Hyun H. Shin^b, Christian E. Schaerer^b

^a Chemical Science Faculty, National University of Asuncion, San Lorenzo, Paraguay

^b Scientific and Applied Computing Laboratory, Polytechnic School, National University of Asuncion, San Lorenzo, Paraguay

Abstract

The numerical simulation of second order exothermic chemical reaction in plane mixing layer is performed. The standard Galerkin finite element method is chosen to solve the problem, which is implemented in Python language using FEniCS Project libraries. The results show roll-up characteristic structures in the interface due to the velocity difference between the reactants, and also the viscosity which is function of the reactants and product concentrations contributing to the instability in the system.

Keywords: Numerical simulation, Plane mixing layer, FEniCS Project, Finite Element Method.

1. INTRODUCTION

The study of plane mixing layer is important in chemical engineering. Some applications of this kind of phenomenon are the transport and mixing of substances in chemical reactions, as combustion or pollutant transport in hydraulic channels [1]. The mixing layer is produced by the interaction of two parallel fluids streams, away from the wall with different velocities $u_2 > u_1 \geq 0$ [2]. Due to the velocity differences in the interface, the shear stress generated produces the Kelvin-Helmholtz instability [3], which is characterized by the enroled structures enhancing the momentum, heat and mass transfer.

The authors of [4] studied second order exothermic chemical reaction of type $A + B \rightarrow P$ in laminar closed channel flow in high convective conditions. They performed parametric analysis in order to study the instabilities

¹E-mail Corresponding Author: drweiberlen@gmail.com

and roll-up phenomenon. These instabilities facilitate the mass removal or promote its displacement [4].

This work is an initial part of a research dedicated to the simulation of reactive flows applied to chemical engineering. In this work, the standard Galerkin finite element method (FEM) is implemented in Python language using FEniCS Project libraries [5]. With this method, a numerical simulation of plane mixing layer with chemical reaction similar to [4], using lower parameters is performed. The use of lower parameters is due to the numerical deficiencies present in the chosen method for the convection dominated phenomena [6]. Qualitative numerical results are analysed in order to implement, in the future, others numerical methods suitable to the highly convection dominated phenomena.

In the next section, the governing equations and some details of the numerical method used are presented. In the last section, some results obtained from the simulations are shown with some final remarks.

2. GOVERNING EQUATIONS AND NUMERICAL METHODS

The problem is modeled by the Navier-Stokes equations coupled with the continuity equation for the fluid flow, the reactant and product are represented by the scalar transport equation, as well as the temperature. The exothermic reaction studied in this work is similar to the one performed in [4]. The fluid viscosity depends on the reactant, product and temperature concentrations. The mentioned equations in dimensionless form are [4]:

$$\nabla \cdot \mathbf{u} = 0, \quad (1)$$

$$\frac{\partial \mathbf{u}}{\partial t} + \mathbf{u} \cdot \nabla \mathbf{u} = -\nabla p + \frac{1}{Re} \nabla \cdot [\mu (\nabla \mathbf{u} + \nabla \mathbf{u}^T)], \quad (2)$$

$$\frac{\partial C_a}{\partial t} + \mathbf{u} \cdot \nabla C_a = \frac{1}{Re Sc_a} \nabla^2 C_a - Da e^{-\beta/(T+1)} C_a (1 - C_a - C_p), \quad (3)$$

$$\frac{\partial C_p}{\partial t} + \mathbf{u} \cdot \nabla C_p = \frac{1}{Re Sc_p} \nabla^2 C_p + 2 Da e^{-\beta/(T+1)} C_a (1 - C_a - C_p), \quad (4)$$

$$\frac{\partial T}{\partial t} + \mathbf{u} \cdot \nabla T = \frac{1}{Re Pr} \nabla^2 T + 2 Da Q e^{-\beta/(T+1)} C_a (1 - C_a - C_p), \quad (5)$$

$$\mu = \exp(R_a C_a + R_p C_p - T), \quad (6)$$

where, \mathbf{u} is the fluid velocity vector, p is the pressure and μ is the fluid viscosity; C_a and C_p are the reactant A and product concentrations, respectively, so the concentration of reactant B is $C_b = 1 - C_a - C_p$, and T is the temperature. The dimensionless numbers present in the equations are: Reynolds (Re), Schmidt (Sc), Prandtl (Pr) and Damköhler (Da); β and Q are the activation energy and heat of reaction, respectively; R_a y R_p are the viscosity ratios between reactants and product.

The problem is solved using FEniCS Project libraries [5] for the finite element method implemented in Python. The finite element used is triangular with Lagrange polynomial interpolation of degree 1 for the pressure and 2 for the rest of the variables. The velocity profile is obtained by Chorin projection method [6] and Crank-Nicholson scheme is used for the time discretization of scalar transport equations, and the source terms are set in explicit way.

Two dimensional computational mesh of 101×32 points is used to simulate the problem for a rectangular domain of $0 \leq x \leq 10$ and $-1 \leq y \leq 1$. The simulation time is set to 10 and the time step is 0.0005, which satisfy the CFL condition.

Initially, the upper half of the domain is full of the reactant A ($C_a = 1$) with temperature $T = 0$ and the lower half with reactant B with temperature $T = 1$. The reactants enter in the domain with hyperbolic tangent velocity profile with some perturbations. The reaction between reactant A and B is occurred in the interface, and is enhanced due to the instabilities generated by the velocity differences and the viscosity. The parameters used are: $Re = 1500$, $Sc_a = 0.1$, $Sc_p = 0.1$, $Pr = 7$, $Da = 0.1$, $\beta = 1$, $R_a = 2.3026$, $R_p = -1.608$.

3. RESULTS AND CONCLUDING REMARKS

The Figures 1 and 2 show the profiles of the variables studied at $t = 6.25$ and $t = 8.75$, respectively. Due to the velocity differences, roll-up structures in the interface is observed, which grows from $t = 6.25$ to $t = 8.75$.

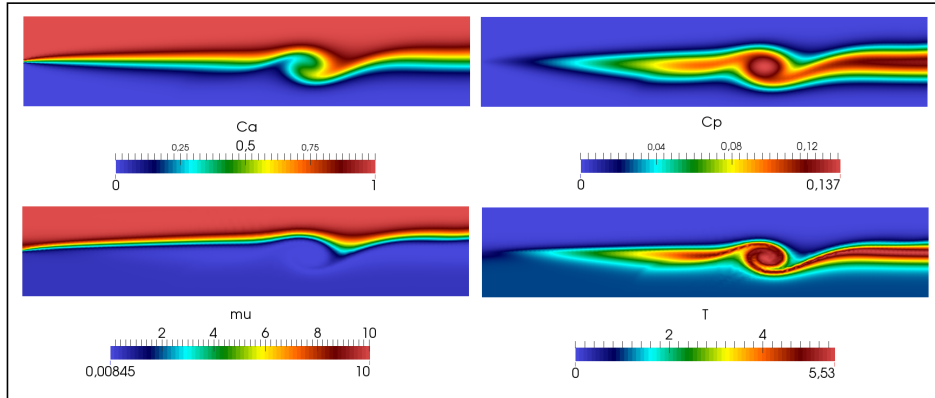


Figure 1 - Simulation at $t = 6.25$, reactant concentration A (upper left), product concentration (upper right), fluid viscosity (lower left), temperature (lower right).

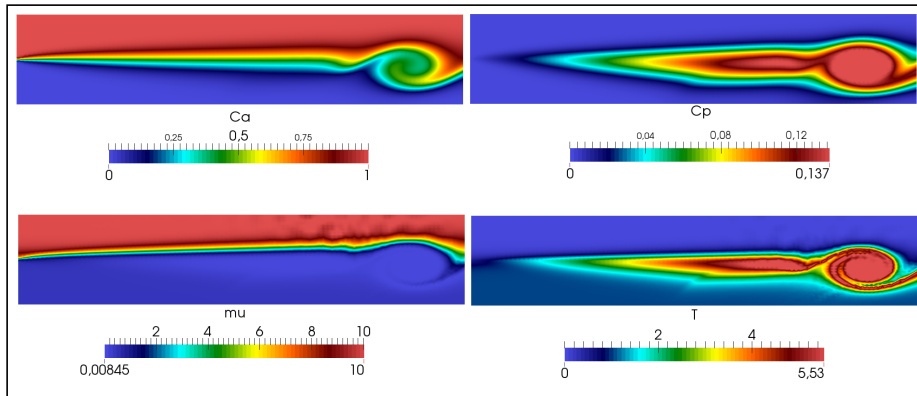


Figure 2 - Simulation at $t = 8.75$, reactant concentration A (upper left), product concentration (upper right), fluid viscosity (lower left), temperature (lower right).

The initial result obtained is promising. It is emphasized that the Schmidt numbers used are small, because of the numerical instabilities presented in convective dominated processes. Also, it should be noted that due to the first order time discretization used, high numerical diffusion is generated and restricts the appearance of roll-up structures in the interface.

Further investigation must be achieved in order to overcome the numerical instabilities, using different numerical schemes, such as, discontinuous Galerkin for spatial discretization and Adam Bashforth for the time discretization. In this way, simulations with wide range of parameters could be performed.

References

- [1] M. J. Maghrebi & A. Zarghami, DNS OF FORCED MIXING LAYER, *International Journal of Numerical Analysis & Modeling*, (2010) 7(1):173-193.
- [2] S. Pope, *Turbulent Flows*, Cambridge University Press, 2000.
- [3] P. Kundu & I. Cohen, *Fluid Mechanics*, Elsevier Science, 2010.
- [4] J. N. Kusuma, Omar K. Matar & Kirti Chandra Sahu. Numerical simulations of miscible channel flow with chemical reactions. *CURRENT SCIENCE*, VOL. 106, NO. 6, 25 MARCH 2014.
- [5] A. Logg, K. Mardal, & G. Wells. *Automated Solution of Differential Equations by the Finite Element Method: The FEniCS Book*. *Lecture Notes in Computational Science and Engineering*. Springer, 2012.
- [6] Donea, J. & Huerta, A. (2003). *Finite Element Methods for Flow Problems*. *Finite Element Methods for Flow Problems*. John Wiley & Sons.
- [7] Mason, S. D. & Rutland, C. J. (2000). Turbulent transport in spatially developing reacting shear layers. *Proceedings of the Combustion Institute*, 28(1):505-513.

Facial Recognition based on Indexed Metric Spaces

Liz J. González Brítez, Christian D. von Lüken

Facultad Politécnica, UNA, Asunción, Paraguay

Abstract

In facial recognition systems that use comparisons between a querying image and each object in the database to find a match, the recognition process tends to be increasingly slow as the number of images in the database grows. Since it is an important practical problem several works proposed alternatives to improve the scalability of these systems, as well as to provide accurate matching results. This paper presents a novel approach that combines a Principal Components Analysis algorithm with an image indexation method based on permutations. The proposed alternative optimizes the image storage and accelerates the search process to determine similarity among objects. The proposal was evaluated using the FERET (Facial Recognition Technology) database using different distance metrics.

Keywords: Facial recognition, image indexation, image similarity measure

1. INTRODUCTION

The challenge of image search in large databases for face recognition is to achieve short response time without sacrificing accuracy. Several methods have been proposed with the aim of indexing large databases, such as tree structures, approximations methods, probabilistic methods, data-independent and data-dependent hashing [2, 4]. This paper presents a technique for image indexing based on the permutations of the indexes of an array of pixel intensity that represent an image, named as Emiap. The proposed method is an alternative for the search process in databases of thousands of images. It is used here in combination with the Principal Components Analysis (PCA), that reduces the dimensionality of data. Two implementations of Emiap are proposed:

(1)Simple indexation: this implementation uses permutations to represent the order in which the elements of a set of images P are seen from

each object of the database that will be indexed. The set P is randomly selected or through a heuristic [1]. The Fig. 1a illustrates the search process. The similarity between permutations are determined using: Spearman’s Rho, Spearman’s Footrule and Kendal Tau [2]. The searched image and the resulting candidates are compared each other directly by Euclidean, Maximum, and Mahalanobis distances [1].

(2) Convex combination indexation: in this implementation similarity search is based on an Euclidean distance approximation using a convex combination [3]. The convex combination is defined by the equation $\lambda s_{(u,v)} + (1 - \lambda)\Pi_{(u,v)}$, where $s_{(u,v)}$ is the Euclidean distance between u and v , known as the magnitude part (or the symmetric part) and $\Pi_{(u,v)}$ is a metric between the permutations $\sigma_{(u)}$ y $\sigma_{(v)}$, known as the shape part [3]. The search process schematized en Fig. 1b.

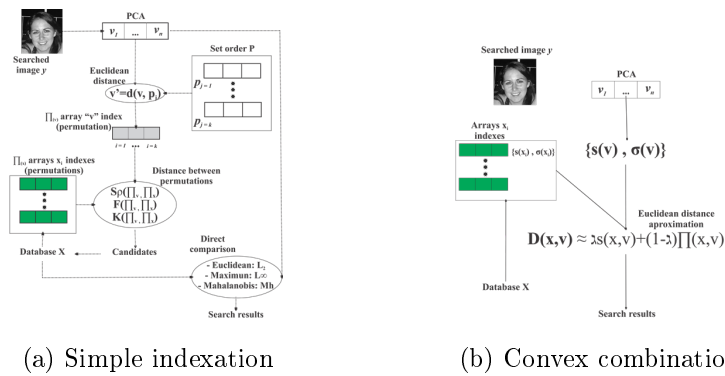


Figure 1: Search scheme with Emiap’s algorithm implementation

2. EXPERIMENTAL RESULTS

The two implementations were evaluated using the FERET database. The Fig. 2 shows the success rates obtained with the proposed implementations. These experiments show that better hit rate is reached using Kendall Tau or Spearman’s Rho as a similarity metric between permutations and Euclidean distance as similarity metric in direct comparisons among the searched image and the candidates. The Fig. 2e shows that the hit rate is higher when the heuristic is applied to the selection of the order set. The heuristic applied in this work is the minimization of the Spearman’s Rho.

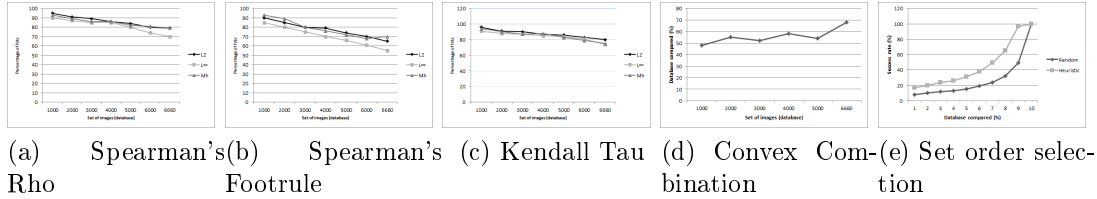


Figure 2: Success rate of Emiap implementations

3. CONCLUSION

The indexation alternative presented here facilitates the search process and the efficient match. In the simple indexing approach, only a sub-set of the database is evaluated. In the convex combination approach, the similarity is determined by the approximation of the Euclidean distance, which is calculated between the representation of the queried image and the representations of images stored in the database. Experimental results show that the proposed method, reduces the number of direct comparisons during the search process and maintains a high success rate.

References

- [1] Edgar Chavez, Karina Figueroa, Gonzalo Navarro, 2007. Indexación Efectiva de Espacios Métricos usando Permutaciones, Tesis Doctor en Ciencias.
- [2] Edgar Chavez, Karina Figueroa, Gonzalo Navarro, 2008. Effective Proximity Retrieval by Ordering Permutations, *IEEE Trans. Pattern Anal. Mach. Intell.*, 30(9):1647-1658
- [3] Omer Egecioglu. Parametric Approximation Algorithms for High-dimensional Euclidean Similarity.
- [4] Lei Zhang, Yongdong Zhang, Jinhui Tang, Xiaoguang Gu, Jintao Li, and Qi Tian. 2013. Topology preserving hashing for similarity search. In *Proceedings of the 21st ACM international conference on Multimedia (MM '13)*.

Analysis of the key parameters involved in the method of crystallization from a mixture of sucrose and steviol glycosides from *Stevia rebaudiana* Bertoni paraguayan origin

Shirley J. Duarte^{a1}, Fátima Díaz ^a, María F. Peláez^a

^aSchool of Chemical Sciences, National University of Asunción

Abstract

Currently, the food industry is progressing in the development of lower calorie sweeteners per serving compared to sugar. Some European and Latin American industries have successfully developed powder sweeteners products, composed of mixtures of sucrose and Stevia. However, the process for obtaining this product depends largely on the solubility of the raw materials and it is necessary in most of the cases a method of controlling the supersaturation of the mixture by simple instrumentation. This work consists of two parts: in the first one has been obtained the curve of the solubility of a mixture of steviol glycosides coming from leaves of *Stevia rebaudiana* Bertoni native of Paraguay and Criolla variety of priority composition in stevioside, approximately 53% and compared with existing data in the literature of other containing majority composition in Rebaudioside A, as far we know this is the first time that this curve is obtained. In the second part a crystallization process was performed by vacuum evaporation to evaluate the variation of the Brix degree of the mixture during the course of evaporation, without interrupting the vacuum applied, this method is based on the "conductivity principle" which is proportional to the content ions dissolved in a solution water. Therefore, as the mixture of sucrose and steviol glycosides it's concentrates due to the water evaporation, the Brix degree of the mixture increase and thereby; decreases the conductivity of the same. With this principle, the conductivity of the mixture is determined and corresponding to the Brix degree desired to be reached without interrupting the process. Finally the graphs of the variation of the conductivity and resistivity with the Brix degree for the mixing of steviol glycosides and sucrose are presented for the crystallization process defined. The parameters obtained in this research will provide the basis for defining the appropriate methodology for crystallization of a sugar-Stevia solution of priority composition stevioside and paraguayan origin.

¹E-mail Corresponding Author: sjoamduart@gmail.com

Keywords: Criolla variety, solubility curve, linear regression, Brix degrees, conductivity.

Influence of the Temperature of carbonization on the characteristic and efficiency of material carbonized obtained from care coconut-*Acrocomia aculeata* (Arecaceae)-

Shirley J. Duarte^{a1}, Maria B. Sarubbi ^a, Jorge Lin^a, Pedro J. Torres^b

^aSchool of Chemical Sciences, National University of Asunción

^bPolytechnic School, National University of Asunción

Abstract

This work is framed on the improvement of the efficiency use of the biomass in Paraguay. In this context, a study of the potentiality of the vegetable waste, for his efficiency use as a fuel is necessary. Actually in Paraguay, more than 60% of the energy used for thermal purposes comes from firewood, which could be cause a huge environmental impact in long term. Moreover, industrial wastes generated in large quantities of coconut shell and core of the *Acrocomia aculeata*, are used by the industries for similar purposes, with all the inefficiency that imply to burning with open fire. In the process of carbonization, the raw material, is transformed to carbon, in which is eliminated an important quantity of volatile, which correspond to hydrogen and oxygen elements on the precursor resulting in a carbonaceous skeleton with a rudimentary pore structure. This process was performed in the absence of oxygen to which it was necessary for inerting the atmosphere by injecting nitrogen at a constant flow rate and in a temperature range between 450 °C and 900 °C. Performance, the immediate analysis and calorific value was obtained. Moreover, an evaluation of the variation in the efficiency of the carbonized material was obtained with three different temperatures and different granulometries of the raw material. Based on these results, an interpolating equation was constructed, in order to predict the response variable experiment in other levels of interest. In this manner, an empirical model of the studied phenomenon was obtained. The calorific value of carbonized material obtained was compared with others fossil fuels.

Keywords: efficiency, industrial wastes, biomass, fuel, calorific value, empirical model

¹E-mail Corresponding Author: sjoamduart@gmail.com

Biodiesel production by reactive distillation: Evaluation of operating parameters using dynamic simulation

Ruth L. Garbini¹, Carlos D. Mendez

Facultad de Ciencias Químicas, Universidad Nacional de Asunción, Paraguay

Abstract

In this work the behavior of a reactive distillation column for biodiesel production using numerical simulation is studied. Modifications in the column operating parameters, specifically in feeding conditions, are introduced to assess the influence on biodiesel purity and process yield as well as the time required for the system to return to its steady state condition. The simulation results showed a linear trend of disturbances in relation to the purity and yield of reaction, producing at large, a reduction in the reactive distillation column performance during a considerable settling time where alterations in the steady state operating conditions are presented.

Keywords: Reactive distillation, biodiesel, numerical simulation.

1. INTRODUCTION

Reactive distillation is a chemical unit operation in which chemical reactions and product separations occur simultaneously in one unit. This technology has demonstrated that its application in the production of biodiesel improves overall conversion rate, unit productivity and reaction time, and produces low capital and operating costs compared to the classic combination of a reactor and separation units [1]. A large number of investigations have been reported on the implementation of RD to biodiesel production for different reagents, catalysts and column configurations through experimental works and simulations [2], but the study of the column dynamic behavior is required, where changes in the flow rate or undesired disturbances occur during transitory regimes. This motivates to evaluate, using numerical simulation, the alteration in the process under specific disturbances in the feed flow rate and the feed composition.

¹E-mail Corresponding Author: garbini.ruth@gmail.com

2. METHODOLOGY

The dynamic simulation of the RD column is performed by a code in Matlab 2012a [®] available in the literature [3] which is modified in this work for the study of the oleic acid esterification with methanol, based on the kinetic data of the reaction, the column design configuration and initial conditions calculated by the commercial simulator ProII 9.2. [®]. In this code the RD process is described by a model based on mass balances, vapor-liquid equilibrium phases, tray hydraulics, reaction kinetic data and UNIFAC thermodynamic method. The disturbances are generated by square wave pulses at regular intervals during 1 min, for variations of the following feeding conditions: total flow increase (Trial A), total flow decrease (Trial B), oleic acid increase with constant flow rate (Trial C) and oleic acid decrease with constant flow rate (Trial D).

3. RESULTS

The Figure 1 presents the biodiesel purity variation over the time for a disturbance of 15 % in the feeding conditions. Disturbances from 1 % to 13 % cause similar disturbances generated by the 15 % change, therefore, the maximum variation of the purity is shown in Figure 2.a, where a linear trend is presented. The same has been done for yield, where the minimum variation over the time is presented to all trials in the Figure 2.b. In all trials, are shown that disturbances of 1 % to 15 % in feeding conditions require settling time of 4 min to 19 min, to restore steady state condition.

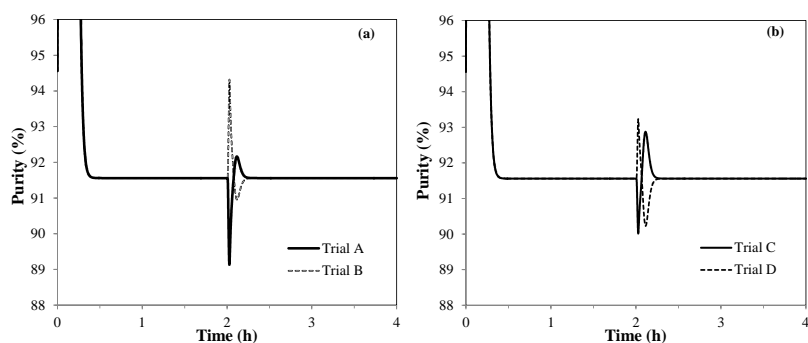


Figure 1: Purity variation over time at disturbances in feeding conditions. (a) Trial A and B. (b) Trial C and D.

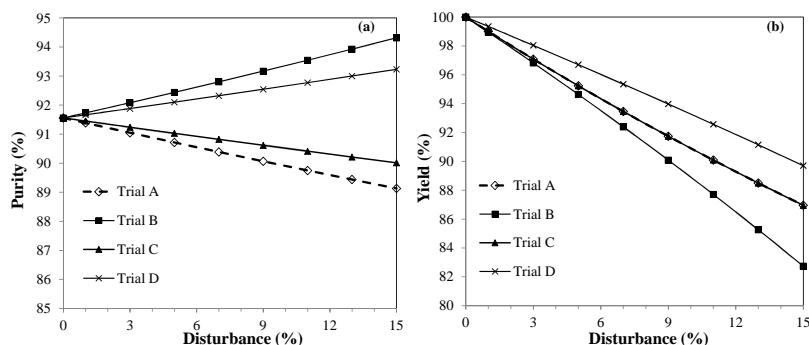


Figure 2: Alteration in column behaviour by disturbances in feeding conditions.(a) Change in biodiesel purity. (b) Change in process yield.

4. CONCLUSIONS

The introduction of disturbances during the RD column operation generates an appreciable influence on the biodiesel purity and yield, where a linear trend being observed. The simulation results showed that disturbances which reduced oleic acid flow rate produce an increase in biodiesel purity, but despite this apparent improvement process conditions a significant decrease in process yield occurs and a considerable settling time is required. These results show that a proper design of the reactive distillation column for the production of biodiesel should include efficient control strategies that maintain the column operating parameters in minimum variation ranges to offer a quality product with uniform characteristics.

References

- [1] HE B, SINGH A, THOMPSON J, 2006. A novel continuous-flow reactor using reactive distillation for biodiesel production, Transactions of ASABE 49:107-112.
- [2] KISS A, BILDEA C, 2012. A review of biodiesel production by integrated reactive separation technologies. Journal of Chemical Technology and Biotechnology 87:861-879.
- [3] HOUGE E, 2013. Reactive Distillation of Biodiesel: Modelling and optimal operation, Master Thesis, Norwegian University of Science and Technology.

Wireless Sensor Network for Aerosol Measurement

Lucas Frutos, Federico Fernandez

lfrutos@pol.una.py, fefernandez@pol.una.py

Departamento de Investigación, Postgrado y Extension
Facultad Politécnica - Universidad Nacional de Asunción

Abstract

Internet technologies, communications, ICT, convergence as well as the advances in microelectronics and miniaturization of components have enabled wireless sensor networks (WSN). One application of this technology is the environmental monitoring for air quality diagnosis. This work involves the design and implementation of a wireless sensor network to quantify the amount of particulate matter/ aerosol, indicators of air quality. The different sensor nodes or motes communicate to an access point using ZigBee wireless technology. A database store the information obtained by the different wireless sensors . A Web page displays the results of aerosols measurements by the different sensors.

Keywords: WSN, ZigBee, Aerosol measurement, Air quality.

Kaolin Pellets Processing For Slow Release Pheromone Applied To *Triatoma infestans* Capture

Silvia M. Aquino^{a1}, Maria C. Vega^b, Alexandre Antunes Ribeiro^c,
Marize Varella de Oliveira^c and Magna Monteiro^a

^aBio and Materials Laboratory, Polytechnic School, Asuncion National University, San Lorenzo, Paraguay

^bCenter for the Development of Scientific Research, Asuncion, Paraguay

^cPowder Technology Laboratory, Division of Materials Processing and Characterization, National Institute of Technology, Rio de Janeiro, Brazil

Abstract

In Latin American countries, Chagas disease is one of the troubling issues in the public health, being *Triatoma infestans*, commonly called kissing bug; it is the main vector in South America. The aim of this work was to produce and characterize porous kaolin pellets to use as slow-release devices pheromone for *T. infestans* trap. For the pellets production, a mixture of kaolin and cornstarch was uniaxially compacted, using a cylindrical die of 20 mm diameter, and sintered in air at 900°C. The cornstarch was used as a porogenic agent. Each pellet was impregnated with benzaldehyde, a pheromone substance. The pheromone release assays were carried out at two different temperatures, 29 and 39°C, in order to determine the influence of temperature on time. Furthermore, bioassays with kissing bugs were conducted for evaluating the maximum release time from the pellets. The DRX spectra showed the presence of illite and quartz phases. The FTIR results showed bands that correspond to benzaldehyde and also bands indicating the presence of benzoic acid. For the sample submitted to the assay at 39°C, the amount of pheromone released was twice the value recorded in the assay at 29°C, suggesting that at higher temperatures, there is an increase of the release pheromone. From the bioassays, it was possible to obtain promising results for both females and males kissing bugs, but not for 5th stage kissing bugs. Other parameters, which could influence on the release process will be studied in future works, like the influence of humidity, longer assays, among others.

Keywords: kissing bug, benzaldehyde, kaolin, slow release.

¹E-mail Corresponding Author: sil.mari.aqui@gmail.com

ACKNOWLEDGMENTS: 1698OC/PR program - CONACyT/Paraguay, Chemistry School/FCQUNA and CRV/CNCV/Cordoba.

References

- [1] ACOSTA, LÓPEZ, GONZÁLEZ, FERNÁNDEZ, ROJAS DE ARIAS, 2001. Perfiles isoenzimáticos de poblaciones de *Triatoma infestans* de la Región Oriental y Occidental del Paraguay 1(1):58-62
- [2] BRENER, ANDRADE BARRAL-NETO, 2000. *Trypanosoma cruzi* e Doença de Chagas.
- [3] FONTAN, GONZÁLEZ, MARTINEZ, ALZOGARAY, ZERBA, CAMPS, CORK, 2002. Attractant volatiles released by female and male *Triatoma infestans* (Hemiptera: Reduviidae), a vector of Chagas disease: chemical analysis and behavioral bioassay 39(1):191-197.
- [4] ROMAN, GÓMEZ, VEGA, ROLÓN, SÁNCHEZ, COUSIÑO, ROJAS DE ARIAS, 2010. Sensores cebados como herramienta de evaluación de re-infestación intradomiciliar por triatomíneos en comunidades indígenas del chaco paraguayo.

Describing the role of space-dependent bistability for the phenomenon of morphogenesis

Francisco J. P. Lopes^{a1}, Yuri Vilarinho^b, Eric Y. Otomo^b, Paulo M. Bisch^b

^aNúcleo Multidisciplinar de Pesquisa em Xerém, Universidade Federal do Rio de Janeiro, Duque de Caxias, Brazil

^bInstituto de Biofísica Carlos Chagas Filho, Universidade Federal do Rio de Janeiro, Rio de Janeiro, Brazil

Abstract

Pattern formation during embryonic development, or morphogenesis, is one of the most intriguing problems in biology. During this phenomenon, a sequence of processes allows a simple system, the fertilized egg, to become a mature organism. An essential step in this process is the translation of the genetic information, stored at the microscopic level of the DNA molecule, into macroscopic spatial expression patterns. These patterns precede the embryo segmentation and the tissue-organ scale of body organization. *Drosophila melanogaster*, the fruit fly, is one of the most studied systems for understanding pattern formation in biological systems. During its embryonic development, a chemical pre-pattern of gene-regulatory proteins precede the tissue differentiation that gives rise to organs and tissues. The sharp borders exhibited by these patterns are critical for separating neighboring cells into different types at the borders different tissues. To understand this phenomenon, we used a systems biology approach combining dynamical systems theory with experimental and computational techniques. We developed a diffusion-reaction model describing gene regulation at the molecular level. Our results show that space-dependent bistability plays a critical role in generating the sharp borders of the chemical pre-pattern. We show that dynamical behaviors like bistability are critical components in the flux of information from the microscopically stored genetic information to the macroscopic organization of cells and tissues.

¹E-mail Corresponding Author: flopes@ufrj.br

Authors Index

- Altbir, Dora, 108
Amadeo, Alberto, 346
Amatte, Javier, 446
Anjos, Gustavo, 17, 21, 25
Anochi, Juliana, 139
Antunes Riveiro, Alexandre, 480
Aquino Valdovinos, Andrés, 413
Aquino, Silvia, 96, 413, 480
Arias, Francisco, 436
- Báez, Baudelio, 438
Báez, Liz, 408
Balbuena, Karen, 315
Ballester, M.Y., 410
Barán, Benjamín, 121, 143, 155, 179, 189, 200, 380, 384, 446
Barua, Claudio, 431
Benítez, Alejandro, 453
Benitez Vega, Hugo R., 189
Benitez, Nestor, 384
Bevilacqua, Luiz, 3
Bisgarra, Alba, 434
Blanco, Gerardo, 315, 446
Bourgine, Paul, 9
Brassel, Daniel, 179
Brassel, Osmar, 179
Britez, Miguel Angel, 422
Brizuela, Carlos, 155, 421
Brizuela, Marcos A., 167
Buzarquis, Enrique, 446
- Cáceres Díaz, Juan José, 111
Cáceres Silva, Juan José, 121, 380
Caballero, Norma, 434, 436
Cabral Figueredo, Juan Carlos, 133
Caceres, Israel, 348
Cantero Alonso, Alcides David, 58
Capli, Alberto, 431
- Cappo, Cristian, 255, 443
Caretta, César A., 440
Carvalho, Adenilson, 333
Castán, Alicia, 90, 423
Cebrián, Jorge, 90, 423
Ceretta Nunes, Raul, 12
Cespedes, Jorge, 267
Cespedes, Pedro, 418
Chamorro Torres, Humberto, 70
Chow-Martínez, Marcel, 440
Clua, Esteban, 243, 336
Colbes, José, 438
Coronel, Eduardo, 365
Czechowski, Zbigniew, 41
- Díaz, Fátima, 473
Davalos, Enrique, 200
de Campos Velho, Haroldo F., 139, 212, 264, 448
de Rigo, Daniele, 46
De Wit, Anne, 2, 21
Duarte, Marcio, 344
Duarte, Shirley, 473, 475
Dupont, Geneviève, 4
- Encina Melgarejo, José S., 70
- Fabero, Juan Carlos, 402
Fenton, Flavio, 11
Fernández N., María José, 90, 423
Fernández, Federico, 402, 405, 479
Fernández, Romina, 415
Ferreira, Davi, 17
Frutos, Lucas, 405, 479
- Gómez, Santiago, 344, 347
Gaona Verón, Federico Augusto, 96
Gaona, Gabriela, 377
Garbini León, Ruth L., 476

- Gardel Sotomayor, Pedro Esteban, 189
Garrido, Juan D., 410
Giménez, José, 443
Goes, Luiz Carlos, 264
González Weiberlen, Diego R., 465
González, Liz J., 470
González, Richard, 348
Gonzalez Nuñez, Nora, 431
- Hernández, Pablo, 90, 423
Ho Shin, Hyun, 34
Hochsztain, Esther, 219
- Ibanez Dos Reis, Marilyn Menecucci, 333
- Jara, Adolfo, 96, 365
Juiz, Carlos, 15, 96
- Kadomatsu-Hermosa, Maridian J., 90, 423
Krimmer, Dora B., 90, 423
- López Estigarribia, Pablo José, 279
López, María, 425, 429
Lara, Pedro, 230
Laroze, David, 5, 108
Leão, Aaron, 230
Leal-Toledo, Regina, 243
Legal Ayala, Horacio, 70, 167, 337, 418
Leguizamón, Cristhel, 411
Lima, Joaquín, 179
Lin, Jorge, 475
López Aca, Viviana, 436
Lopes, Franciso J.P., 482
Lopez Bertoni, Federico, 337
Lucena, Rachel, 17, 21
Luz, Eduardo F. P., 264
- Mangiavacchi, Norberto, 17, 21, 25, 34
Maqueda Acuña, Edgar M., 354
Martín Vera, Jorge, 96
Martínez Jara, Eustaquio A., 58, 453
Martínez, Victor, 90, 423
Martinez-Mardones, Javier, 108
Mendez, Carlos D., 476
Mendoza, Carlos, 421
Messina, María, 219
Montanía, Claudia, 347
- Monteiro, Magna, 96, 382, 411, 413, 480
Moré, Luis G, 167
Morinigo, Giselle, 434
- Nascimento, M.A.C., 410
Nogués P., Juan P., 329, 382, 408, 411, 441
Nuñez, Jose, 405
- Oliveira, Elton, 212
Oliveira, Fernando A., 16
Oliveira, Gustavo, 17, 25
Oporto, Laura, 362
- Pérez, Javier, 377
Paccanaro, Alberto, 8
Pacheco Da Luz, Eduardo Fáver, 333
Paciolo, Julio, 384
Paez, Rodolfo, 189
Parra, Cristina, 90, 423
Peláez, María, 473
Pinto Roa, Diego P., 70, 167, 189, 200, 279, 346, 421, 422, 427, 438
Pires, W.A.D., 410
Pleiner, Harald, 108
Pontes, José, 17, 21, 25
Portela, Luis M., 34
Portugal, Renato, 230
- Ramos, Fernando Manuel, 333
Recalde, Jorge L., 429
Recaldre, Jorge L., 425
Renault, Alfredo, 354
Rivarola, Alcides, 255
Riveros, Francisco, 384
Riveros, José, 291
Rodas, Marcelo, 427
Rodríguez, Luis, 344
Rodriguez Aseretto, Dario, 13, 46
Rojas de Arias, Antonieta, 81, 96, 344
Romero Riveros, Jesús María, 279
Romero, Nelson, 453
Rosa, Reinaldo, 336
Ruiz de Mendarozqueta, Álvaro, 14
Ruiz, Paulo, 212
Ruiza, Renata, 212
- Saito, Miki, 111

Salgueiro, Luis, 382
Sandri, Sandra, 448
Santos, Pettras L.B., 448
Sarubbi, Maria, 475
Schaerer, Christian E., 34, 46, 90, 96, 111, 121,
133, 344, 347, 362, 377, 380, 382, 395,
400, 411, 418, 423, 441, 465
Schvartzman, Jorge B., 90, 423
Serra, Tomeu, 96
Shin, Hyun Ho, 465
Silva Ortiz, Norma G., 303, 354
Simoes Da Silva, Jose Demisio, 139
Sirtori, Carla, 434
Sotelo Torres, Pablo Hernán, 87
Stalder D., Diego H., 336
Suarez, Omar, 108
Szaran, Eduardo, 421

Tasistro, Andrómaca, 219
Thome, John Richard, 25
Torres Bobadilla, Mateo Fernando, 143
Torres, Pedro, 400, 475

Vázquez N., José L., 70, 167, 279
Valdez, Diana, 315
Varela, Jhabriel, 441
Varella de Oliveira, Marize, 480
Vega Gomez, Celeste, 96
Vega, María, 480
Vieira Cruz, Ronaldo, 264
Vilarinho, Yuri, 482
Villalba, Cynthia, 267, 279, 408, 431
Villamayor Benítez, Ignacio Andrés, 303
Villamayor V., Waldemar, 377
Viveros Vera, Roberto Andrés, 111
von Lücken, Christian, 155, 415, 470

Yael Rozenworcel, Uri Pablo, 143
Yoshie Sumida, Ivana, 264

Zamith, Marcelo, 243
Zena, Juan, 395

CCIS 2014 thanks the following volunteers

Silvia Aquino
Liz Baez
Edgar Liseras
Pedro Juan Torres
Rocío Botta
Jose Vázquez
Fabio Lopez
Martín Rafael Poletti Merlo
Adriana Canchini
Pablo Jose López Estigarribia
Luis Gerardo Medina Martinez
Adolfo R. Martinez
Cristian Rodrigo Aceval Sosa
Ester Alfonzo Delvalle
Marco Aponte
René Cristóbal Azcurra
Laura Bareiro
Merly Rossana Barrios Delvalle
Leonardo Daniel Benitez Barrios
Marcos Andres Brizuela Núñez
Leticia María Britez Ojeda
Jose Sebastian Cattaneo Martnez
Luis Fernando Delvalle
Marcelo Rafael Denis Meza
Vladimir Espinola Lezcano
Sannie Nair Figueredo Zarza
Victor Ricardo Franco Benegas
Sergio Fernández Martinez
Oscar Dennis Giménez Aguilera
Liz María Gonzalez Portillo
Jorge Luis Maidana Montiel
Sergio David Orué Tintel
Rodrigo Gabriel Santos Bacchetto
Alfredo Akira Shimosoeda Sato
José Domingo Chávez Leguizamón
Luis Guillermo Moré Rodríguez
Jesús Maria Romero Riveros
Javier Todashi Akagi Fukushima
Marcos David Tileria Palacios
Sandra Coral Ramirez

CCIS 2014

ISBN 978-85-68888-00-1



9 788568 888001



Pan-American Association
of Computational
Interdisciplinary Sciences